Prepared for:

Rijkswaterstaat Rijksinstituut voor Kust en Zee (RIKZ)

Storm Hindcasts Norderneyer Seegat and Amelander Zeegat

Report

August, 2006

H4803.11

WL | delft hydraulics

Prepared for:

Rijkswaterstaat Rijksinstituut voor Kust en Zee (RIKZ)

Storm Hindcasts Norderneyer Seegat and Amelander Zeegat

Sofia Caires, Neelke Doorn, Jacco Groeneweg and Ap van Dongeren

Report

August, 2006

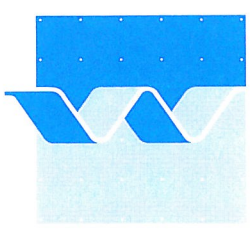

WL | delft hydraulics

WL | delft hydraulics

CLIENT:	Rijkswaterstaat, Rijksinstituut voor Kust en Zee
TITLE:	Storm Hindcasts Norderneyer Seegat and Amelander Zeegat

ABSTRACT:

In the framework of the Agreement between Rijkswaterstaat RIKZ and WL|Delft Hydraulics, RIKZ has requested the execution of a limited number of hindcasts in advance of the larger SBW project. The results of this limited set are of great importance for products of the SBW-Field Measurement project and of the International Data Exchange Project. The requested hindcasts are 2 hindcast computations for the Norderney Tidal Inlet and 5 hindcast computations for the Ameland Tidal Inlet, to be conducted with the most recent version of SWAN (v. 40.51).

The results of the computations are to be analyzed in order to make a first assessment of the model quality for the Waddenzee area. In this report it is found that the former conclusion that SWAN does not account for (enough) swell penetration cannot be made on the basis of the Norderney and Ameland measurements. There is very little swell in the data and the model does allow penetration over the shoals, which is physically correct. We also find that there are only small differences between SWAN 40.51 and SWAN 40.01 (which was used by Kaiser and Niemeyer, 2001). Like these authors we find a large mismatch in the computed and measured spectra, which we attribute to bathymetric effects (refraction), the offshore swell boundary condition and the local wind forcing and growth.

In addition, in the report the following questions are answered:

- Which data and which data format is required for future model evaluations?
- Is the quality of the Ameland Inlet data sufficient for model evaluations?
- Do the buoy locations in the Ameland Inlet need to be changed?
- Which resolution of model inputs of (time-varying) fields of wind, water level, current and bathymetry is recommended?

REFERENCES:	Request for a proposal (email ms. Zijderveld of 27 April 2006), our proposal MCI017383/H4803/avd of the same day and RIKZ commission 4500041303 of 8 May 2006.

VER	AUTHOR	DATE	REMARKS	REVIEW	APPROVED BY
1.0	Caires et al.	30/06/2006			
1.1	Caires et al.	3/7/2006	after int. review	Johan Dekker	Wiel Tilmans
1.2	Caires et al.	29/8/2006	after external rev.	Johan Dekker	Wiel Tilmans

PROJECT NUMBER:	H4803.11		
KEYWORDS:	Waddenzee, SBW, Wave boundary conditions, SWAN, hindcast, numerical modelling		
NUMBER OF PAGES:	37 + figures		
CONFIDENTIAL:	☒ YES, until October 2006	☐ NO	
STATUS:	☐ PRELIMINARY	☐ DRAFT	☒ FINAL

Contents

List of Figures

List of Tables

1 Introduction

1.1 Background

In compliance with the Flood Defences Act of The Netherlands ("Wet op de Waterkering, 1996"), the primary coastal structures must be checked every five years (2001, 2006, 2011 etc.) for the required level of protection on the basis of the Hydraulic Boundary Conditions (HBC) and the Safety Assessment Regulation (VTV: *Voorschrift op Toetsen op Veiligheid*). These HBC must be derived anew every five years and established by the Minister of Transport, Public Works and Water Management.

At this moment, there is a degree of uncertainty concerning the quality of the current HBC, in particular those for the Waddenzee. This is because they were obtained from an inconsistent set of measurements and design values (WL, 2002), while for the rest of the Dutch coast (the closed Holland Coast and the Zeeland Delta) the SWAN wave transformation model has been applied (Rijkswaterstaat, 2001).

However, there is currently insufficient confidence in the performance of the SWAN wave model in a complicated area such as the Waddenzee, so it is not yet possible to obtain reliable boundary conditions there. One of the reasons for this lack of confidence is that a previous version of the wave model provided an unsatisfactory simulation of swell penetration in an area that strongly resembles the Dutch Waddenzee (Norderneyer Seegat, see Kaiser and Niemeyer, 2001). The assumption that this observation also applies to the Dutch part of the Waddenzee must be substantiated by model verification using hindcasts on the basis of available data. This is important because measurements near the Emmapolder in Groningen have shown that swell provides a considerable contribution to the wave height, in the order of 30% (personal communication F. den Heijer, RIKZ). In addition to the swell aspects, the performance of the SWAN model should be thoroughly evaluated for Waddenzee conditions, including the effect of wave boundary conditions and input fields of bathymetry, currents, waterlevel and winds.

These concerns were the direct cause for the request from the subproject "Boundary Conditions", which is part of the main project "Strength and Loading of Coastal Structures (SBW: *Sterkte en Belasting Waterkeringen*)" to WL | Delft Hydraulics to formulate a Plan of Action (WL, 2006) in which a strategy would be determined to answer the principle question: "How do we arrive at reliable Hydraulic Boundary Conditions for the Waddenzee for 2011?" This Plan lists a sequence of activities in order to conduct this strategy. The first action to be performed is to use the latest SWAN model version and do a hindcast of available data in the Norderneyer Seegat (English: Norderney Inlet) and Amelander Zeegat (English: Ameland Inlet).

1.2 Problem statement (from RFP)

The problem statement is translated from the Dutch from the Request for Proposal (email ms. Zijderveld of 27 April 2006) with slight editorial changes.

"In the framework of the Agreement between Rijkswaterstaat RIKZ (short: RIKZ) and WL|Delft Hydraulics (short: WL), RIKZ has requested a proposal for the execution of those activities which are planned for the year 2006.

In order to avoid bottlenecks in related projects, RIKZ has requested a proposal for the execution of a limited number of hindcasts in advance of the larger project. The results of this limited set are of great importance for products of the SBW-Field Measurement project and of the International Data Exchange Project. The requested hindcasts are 2 hindcast computations for the Norderneyer Seegat and 5 hindcast computations for the Amelander Zeegat, to be conducted with the most recent version of SWAN. The precise time instants of the computations will be agreed upon at a later stage. RIKZ is responsible for providing measurements and other input data. The results of the computations are to be analyzed in order to make a first assessment of the model quality for the Waddenzee area. In addition the following questions should be answered:

- Which data and which data format is required for future model evaluations?
- Is the quality of the Amelander Zeegat data sufficient for model evaluations?
- Do the buoy locations in the Amelander Zeegat need to be changed?
- Which resolution of model inputs of (time-varying) fields of wind, water level, current and bathymetry is recommended?

The answers to these questions and the results of the hindcasts are to be given in this report."

We refer to the request for a proposal (email of 27 April 2006), our proposal MCI017383/H4803/avd of the same day and RIKZ commission 4500041303 of 8 May 2006.

1.3 Objectives of this study

The objectives of this study are three-fold:

- Gain insight into the performance of the most recent version of SWAN in the Waddenzee on the basis of hindcasts of selected storms in the Amelander Zeegat and Norderneyer Seegat.
- Determine which data and which data format are required in order to conduct accurate and efficient hindcasts.
- Evaluation of the locations of the present measuring buoys in the Amelander Zeegat.

An in-depth analysis of causes of model-data mismatches will not be made in this report. This is the subject of a number of future studies within the SBW framework.

1.4 Approach and restrictions

In order to meet the objectives the study is conducted for two tidal inlets. The SWAN computations are carried out with version 40.51, which is not an official release yet. In this version some inconsistencies in modelling combined sea-swell conditions have been removed, possibly leading to improved modelling of swell penetration.

The Norderneyer Seegat is chosen because the perceived problem of a lack of swell propagation were first noticed there (Kaiser and Niemeyer, 2001). For this inlet the model setup of Kaiser (pers. comm.) will be used and run for both the version that he used for his study (v. 40.01) and the soon-to-be-released version (v. 40.51). The intercomparison will show the difference (hopefully improvement) between the versions relative to the measured data. It is not the goal to optimize the computational results in order to match the data.

The Amelander Zeegat is chosen because it can be regarded as a representative inlet for the Dutch Waddenzee with sea and swell waves and Rijkswaterstaat has set up an extensive measuring network. The objective of the study in this inlet is to assess the performance of the soon-to-be-released version (v. 40.51) of SWAN (with default settings) without optimization (calibration of coefficients) and to perform variations in the input data, most notably the wind and current fields.

The work is divided into a number of phases for both inlets. The last two items are applicable to the Amelander Zeegat only.

1. Choice of storms and storm instants.
2. Collection of input data for those instants.
3. Set-up of the SWAN models.
4. Computations.
5. Analysis of the results.
6. Assessment of sensitivity of results to variations in current and wind field input in order to determine the required quality of the data.
7. Evaluation of the locations of the wave buoys.

1.5 Outline of the report

The report is structured as follows. In Chapter 2 the hindcast of the Norderneyer Seegat and in Chapter 3 the hindcast of Amelander Zeegat is presented. Chapter 4 contains the conclusions and answers to the questions posed in the request for proposal.

2 Hindcast of Norderneyer Seegat

2.1 Introduction

Kaiser and Niemeyer (2001) performed a hindcast of two storms, namely on 5 February 1999 (03.40 h) and on 3 December 1999 (18.30 h), in the Norderneyer Seegat using version 40.01 of SWAN. This was one of the studies on the basis of which it was concluded that the SWAN model does not compute wave boundary conditions accurate enough in an area much like the Dutch Waddenzee.

In this chapter the hindcasts of the storms considered by Kaiser and Niemeyer (2001) are redone using the latest SWAN version (unofficial release 40.51). The storm's hindcasts using versions 40.01 and 40.51 of SWAN are validated using spectra from wave measurements (obtained from dr. Ralf Kaiser, Forschungsstelle Küste Norderney). The validation results are a benchmark for the assessment of the performance of the new SWAN release (under the local conditions).

Ralf Kaiser of the Forschungsstelle Küste in Norderney, Germany, has provided us all the input data, measurements and computation results (using version 40.01) of the February storm. We have used the provided information to redo the computations of Kaiser and Niemeyer (2001) using the same settings, input (of wind, water level, bathymetry) and version 40.51 of SWAN. Unfortunately, Ralf Kaiser has no longer the input data and computation results of the December's storm presented in Kaiser and Niemeyer (2001) available. He had, however, reprocessed measurements, and improved (finer resolution) SWAN data for that storm, which he has also kindly provided us with. We have used these data to hindcast December's storm using versions 40.01 and 40.51 of SWAN.

2.2 Description of Norderneyer Seegat

The Norderneyer Seegat is situated west of the German Norderney Island in the Waddenzee; see Figure 2.1. The wave climate offshore of the inlet is characterised by waves originating mainly from Northwest, the direction from which the winds may have very long fetches, and which is also the direction from which the higher waves come.

Because of the need to design or study the reliability of the island's sea defences, such as the seawall at the northwestern shore of the island and the sea dike at its southern lee-side coast bordering the tidal flats of the Waddenzee, there are several wave measurements available in the region (see Figure 5, Kaiser and Niemeyer, 2001). These can be used in the validation of local wave hindcasts.

2.3 Storm instants

For the computations we have selected the same storms as considered by Kaiser and Niemeyer (2001). Both these storms (5 February 1999 and 3 December 1999) were from the

Northwest, with a large amount of swell energy offshore, high storm surges and strong wave breaking over the shoals of the ebb-tidal delta.

In the storm of 5th of February 1999 the conditions at 3:40 were of a water level of about 3.4 m above MSL (about 2.2 m above MHWL), a wind speed of 19 m/s from West-Northwest (290º N) and an offshore sea state with 5.97 m of significant wave height, a peak period of 14.3 s and a direction of 330º N at the spectral peak.

In the storm of 3rd of December 1999 the conditions at 18:30 were of a water level of about 3.2 m above MSL, a wind speed of 25.7 m/s from West-Northwest (290º N) and an offshore sea state with 5.94 m of significant wave height, a peak period of 13.3 s and a direction of 300º N at the spectral peak. The wind speed considered here is higher than that reported in Kaiser and Niemeyer (2001); the new value is based on recalculations of the German Weather Service for open sea conditions instead of on the wind station at Norderney (Ralf Kaiser, personal communication).

2.4 Input data

As mentioned above, the input data from Kaiser and Niemeyer (2001) was used in this study. This input data used to hindcast the storms consisted of wind and water level, bathymetry and offshore wave spectra. The wind speed, direction and water level were defined as uniform over the region considered and with values as given in the previous section.

The bathymetry used to hindcast the February storm was collected in 1995 and is available on a regular 80x80m grid. The bathymetry used to hindcast the December storm was collected in 2001 and is available on a curvilinear grid covering an area of about 33.9 km x 23.3 km and having 608x560 meshes. The main differences between the two bathymetries are in the ebb tidal delta which was shallower in December.

Offshore wave information was defined as uniform over the northern boundary in terms of (1D) spectra, independently of the water depth, based on the directional wave spectra derived from the measurements of the offshore directional waverider located at See (see Figure 2.2 and Fig 2.4). In the December storm a boundary sea state with 1m significant wave height and a mean period of 2.5 s is imposed on the entire western boundary. These values are based on the values for wave height and wave period in the tidal basin and are also imposed at the western boundary at the seaward side of the barrier island. This leads to an underestimation of the wave conditions in the vicinity of this part of the boundary, but do not affect the results in the area of interest.

There was no information on currents, so their effect is not taken into account in this study as they were not in Kaiser and Niemeyer (2001).

2.5 Model schematization

2.5.1 Grids

The domains used to model the two storms differ. For the February storm a rather restricted region is considered and computations are done using a regular and a curvilinear computational grid, as done by Kaiser and Niemeyer (2001). For the December storm a curvilinear grid covering the whole tidal basin of the Norderneyer Seegat is considered. In this study we have not assessed the effect of the domain size given the same bathymetry because the aim of this study is to compare SWAN versions for each storm.

The computational grid used to model the February storm covers a region of about 7x13 km. Figures 2.2 and 2.3 present the regular and curvilinear grids and the bathymetry computed by SWAN, respectively (recall that the bathymetry is given on a regular 80x80m grid). The grid resolution is of the order of 80 m.

The curvilinear computational grid used to model the December storm has 608x560 meshes, covers a region of about 33.9 km x 22.3 km, is bounded by the German coast in the south and has the northern boundary approximately along the -12.5 m (MSL, which is close to German Datum (Kaiser and Niemeyer, 2001)) depth contour line, see Figure 2.4. The resolution of this grid is about twice the resolution of the grid used for the computations presented in Kaiser and Niemeyer (2001) and is of the order of 50 m.

In terms of spectral resolution, for the February storm a directional resolution of 10 degrees is used and the spectra are discretized in 121 frequencies distributed logarithmically between 0.025 Hz and 4 Hz. Note that this is not the advised spacing (Van Vledder and Bottema, 2002). We have performed a reference calculation to show that the effects are minimal. For the December storm a directional resolution of 10 degrees is used and the spectra are discretized in 31 frequencies distributed logarithmically between 0.04 Hz and 1 Hz.

2.5.2 Model settings

Kaiser and Niemeyer (2001) ran the SWAN version 40.01 model in stationary mode using the default settings. Our runs were made using SWAN version 40.51 also using the default settings. Depth-induced wave breaking has been modelled according to Battjes and Janssen (1978) and the JONSWAP formulation for bottom friction (Hasselmann et al., 1973) has been applied, with a bottom friction coefficient set to 0.067 m^2s^{-3}. Also triads have been activated in order to be consistent with Kaiser and Niemeyer (2001). However, the third-generation mode default settings of SWAN version 40.51 differ from those of version 40.01. E.g. in version 40.51 the effect of triads and quadruplets are taken into account simultaneously, whereas only one of them is computed and considered in the action balance in 40.01, depending on the so-called Ursell number. A list of the modifications of SWAN since version 40.01 is available at http://130.161.13.149/swan/modifications/modifications.htm. The modifications in the numerical solvers may be relevant for the hindcasts considered here. Please note that all new

features implemented in SWAN after version 40.01 that are not activated by the default settings, such as diffraction, are not accounted for in our computations.

In version 40.51 alternative formulations for the wind generation and whitecapping are available (see Van der Westhuysen et al., 2005), solving part of the problems occurring when modelling combined sea-swell states. In all computations with 40.51 these formulations have been applied and they are activated with GEN3 WEST. In the previous versions, including 40.01, the default settings of Komen et al. (1984) are used: GEN3 KOMEN.

2.5.3 Definition of output

Directional wave spectra output is generated in the locations inside the SWAN computation grid where buoy measurements are available. For the February 1999 storm, measurements are available from the directional waveriders located at VST1, SGTNEY and RIFFGAT (see Figure 2.2). For the December 1999 storm, measurements are available from the directional waveriders located at SGTNEY and RIFFGAT and from the non-directional waveriders located at Kal, MB, Wried, Luep and Oried (see Figure 2.4). Spatial variations over the entire grid of a number of standard wave parameters are also generated as output.

2.6 Results and analysis

2.6.1 Introduction

For the February 1999 storm, Kaiser kindly provided the results of his SWAN version 40.01 computations at the buoy locations and the respective buoy measurements. He also provided the SWAN input data used by them, so that we could produce corresponding wave hindcasts using version 40.51 of SWAN. We did not redo the 40.01 computations.

For the December 1999 storm, because the original input data, settings and computational results presented in Kaiser and Niemeyer (2001), are no longer available, Kaiser provided us with input data used more recently by him to hindcast this storm. We have used these data to hindcast the storm using SWAN's versions 40.01 and 40.51. Kaiser has also provided us with buoy wave spectra measurements. However, the spectral analysis procedure used to produce these spectra differs from that used to produce the measured spectra presented in Kaiser and Niemeyer (2001). The differences have mainly to do with the use of other window characteristics and the present results should be an improvement of the old (Kaiser, pers. comm.). Consequently, there are small discrepancies between the wave spectra we will present here and those presented in their paper.

In the following subsections, we start analysing the results by presenting the wave fields resulting from our computations using SWAN version 40.51 and then compare our hindcast at the buoy locations with those of Kaiser and Niemeyer (2001) (February 1999 storm) or our computations using SWAN version 40.01 (December 1999 storm) and the respective buoy measurements, in the same way as presented in Kaiser and Niemeyer (2001).

Before proceeding we would like to point out that, in both storms the boundary wave spectra contain almost the same amount of energy, but for the February 1999 storm the energy is concentrated at a slightly lower frequency and waves come more from the North (cf Figures 2.7a and 2.8a). The wind direction is the same, but the wind speed in the December 1999 storm is about 35% larger (25.7 m/s) than that used to model the February 1999 storm (19 m/s). In terms of modelling, the grid used to model the December's storm is finer than that used to model the February's storm and the offshore boundary wave conditions are better defined on the December's storm, since the grid north boundary coincides with the measurements depth isoline (note the depth variations on the north boundary of the February's storm grids, Figures 2.2 and 2.3). On the other hand, the frequency resolution used in the February's storm computations about 2.5 times finer than that used in the December's storm computations.

2.6.2 Fields

February 5, 1999; 3:40 hr

The results of the 5th February 1999 3:40 hindcasts are shown in Figures 2.5a-c, which present spatial maps of the significant wave height, mean wave period and peak wave period fields computed using the regular and the curvilinear grid.

Overall, differences between the results using a regular or a curvilinear grid are small. The highest differences occur in the western portion of the domain in a region where boundary effects are still present, mainly because no incoming waves are defined on the western boundary of the domain, and because parts of Juist are inundated in the regular grid computations (a region not covered by the curvilinear grid). Another region where differences between the computations using the different grids can be seen is in the channel west of the tip of the Norderney Island (esp. in Fig 2.5c).

In terms of spatial variation of the wave field, there is a strong wave energy dissipation by depth induced breaking over the ebb-tidal delta from offshore up to the 8 m depth line, with the significant wave height decreasing to below 3 m (cf. Fig 2.2 and Fig 2.5a). For water depths lower than 8 m, the wave pattern west of the deep channel on the tip of the Norderney Island differs from that east of that channel. The significant wave height in the channel is lower than west of it over the shoals. This occurs because most of the low frequency waves reaching the channel are refracted out of the channel, mostly to the coast and dissipated. This effect can also be observed in the mean wave period and peak period plots (cf. Fig 2.5b and 2.5c): these periods have smaller values in the channel than on the tidal flats because long period waves are more susceptible to refraction than short period waves. Therefore the results are sensitive to the schematisation of the channel (compare panels of Figures 2-5c.

On the tip of the Juist Island there is also a lot of refraction towards the coast, but low frequency wave energy still penetrates into an area just south of the island (the red shaded area around "Loc 1"). This is further illustrated by Figure 2.9, showing the spectral energy distribution in Loc1.

December 3, 1999; 18:30 hr

The different panels of Figures 2.6a-c present spatial maps of the significant wave height, mean wave period and peak wave period fields of the simulation of the storm of 3rd December 1999 18:30 computed using SWAN version 40.51.

In terms of spatial variation of the wave field, as for the February 1999 storm, there is a lot wave energy dissipation by depth induced breaking over the ebb-tidal delta from offshore up to the 8 m depth line, with the significant wave height decreasing to below 3 m. However, at lower water depths, there is much more dissipation of low frequency waves north and in the mouth of the inlet. As described in section 2.3 the waterlevel for the December storm was 20 cm lower than for the February storm. Some of the extra energy dissipation can be explained by the differences in bathymetries used to hindcast the two storms, the ebb tidal delta and northwest of Norderney are shallower in the bathymetry used to hindcast the December's storm (compare Figure 2.4 with the lower panel of Figure 2.3). The mean wave period and peak period plots (Figures 2.6b-c) show that, contrary to February 1999 storm, almost no low frequency waves penetrate into the inlet.

2.6.3 Measured and modelled buoy data comparison

February 5, 1999; 3:40 hr

Figure 2.7a presents the wave spectra measurement at the buoy location See, which was applied on the north boundary of the computational grids. The spectra contains a lot of swell energy (frequencies below 0.08 Hz), which comes from a more northerly direction than the wind sea waves in the spectrum.

Table 2-1 presents the measured and the computed wave parameters at the VST1, SGTNEY and RIFFGAT buoy locations, as well as the relative errors of the computed parameters compared to the measured counterparts. Figures 2.7b-d present the measured and the computed wave spectra. Overall, we can say that there are no significant differences between the results using version 40.01 or version 40.51 of SWAN. Differences between the computation results using a regular (in Table 2-1 denoted as 'rg') or a curvilinear grid ('cg') are also not significant and of the same order of magnitude as the differences between the results using different versions of SWAN.

Table 2-1: Measured and hindcasted wave parameters for the storm of 5/2/1999, 3:40. The wave parameters were determined by integrating over the finite frequency domain with f_{low} = 0.04 Hz and f_{high} = 0.60 Hz.

	H_s (m)	H_s error (%)	T_{m01} (s)	T_{m01} error (%)	T_p (s)	T_p error (%)
VST1						
measurements	2.89		8.00		12.50	
SWAN 40.01 rg	2.75	-4.8	6.34	-20.8	14.50	16.0
SWAN 40.51 rg	2.69	-6.9	6.32	-21.0	14.50	16.0
SWAN 40.01 cg	2.83	-2.1	6.33	-20.9	14.50	16.0
SWAN 40.51 cg	2.74	-5.2	6.40	-20.0	14.50	16.0
SGTNEY						
measurements	1.35		4.21		5.00	
SWAN 40.01 rg	1.32	-2.2	3.79	-10.0	3.75	-25.0
SWAN 40.51 rg	1.29	-4.4	3.71	-11.9	4.83	-3.4
SWAN 40.01 cg	1.38	2.2	3.71	-11.9	3.75	-25.0
SWAN 40.51 cg	1.33	-1.5	3.66	-13.1	4.83	-3.4
RIFFGAT						
measurements	0.90		3.29		4.55	
SWAN 40.01 rg	0.75	-16.7	2.77	-15.8	3.30	-27.5
SWAN 40.51 rg	0.78	-13.3	2.83	-14.0	3.30	-27.5
SWAN 40.01 cg	0.75	-16.7	2.77	-15.8	3.30	-27.5
SWAN 40.51 cg	0.73	-18.9	2.83	-14.0	3.44	-24.4

At the VST1 location, offshore of the northwestern beach of Norderney (see Figure 2.2), the computed and measured waves compare rather well in terms of significant wave height, but there are clear discrepancies between the data in terms of the energy distribution per frequency and of the mean wave direction of the low frequency waves, which could be due to the bathymetry schematisation (Fig. 2.7b). The computed spectra can be described as double peaked which is probably due to the triad formulations in SWAN, whereas in the measured spectrum the energy is more concentrated around the mean wave period. The computed spectra overestimate the energy around 0.07 and 0.15 Hz. The directions which SWAN computes are consistent up to about 0.2 Hz. For higher frequencies, the new version produces consistently more northerly directions. Comparing Figures 2.7a (See) an 2.7b (VST1) we notice that SWAN keeps the peak position and shape of the boundary spectrum in tact, while in the measurements we notice more low and high frequency components around the peak.

The SGTNEY buoy is located at the edge of the tidal channel, south of the tip of the Norderney Island. There is a rather good correspondence between the computed and measured spectra for frequencies above 0.2 Hz (Fig. 2.7c). For lower frequencies the location and amplitudes of the peaks of the measured and computed spectra differ. The peak around 0.08 Hz is better reproduced in the new version, the energy in the frequency range from 0.1 to 0.2 Hz is underestimated by both versions and grid types. There is a mismatch of about 30 degrees in the computed and measured mean wave direction in the most energetic region of the spectra, between 0.2 and 0.3 Hz. This is probably due to the schematization of the bathymetry which has a resolution of about 80 meters, which is too coarse to accurately describe the channel walls. The errors in the computed wave parameters relative to the

measured ones are virtually the same, except for T_p which compares rather well for version 40.51.

At the RIFFGAT location both the measurements and the computations show that the offshore swell component (with a frequency of about 0.08 Hz) is not present anymore (Figure 2.7d). However, the spectra computed by SWAN underestimate the wave energy measured for frequencies between 0.18-0.25 Hz. The discrepancies in the spectra are also clear in the differences between the computed and measured mean wave period and peak period (cf. Table 2-1). The mean wave direction of the SWAN spectra for frequencies of about 0.15 Hz has a discrepancy of about 10 degrees from the measured mean wave direction per frequency. The difference between the measured and computed spectra at RIFFGAT is most likely due to the fact that at SGTNEY already the computed wave directions are more northerly than the measured ones. These northerly waves will then not reach RIFFGAT to the east, also because of the relative low resolution of the bathymetry. This emphasizes the necessity of accurate wave boundary conditions for the directions and a high resolution bathymetry.

In addition, the computations were performed without current fields, which also have an effect as will be shown in the next chapter for the Amelander Zeegat.

As mentioned in Section 2.5.1, the effect of performing the calculations with a frequency resolution close to the advised value of 0.1 (54 frequencies) instead of that used in the computations (0.04, 121 frequencies) is minimal. Figure 2.7e present the computed spectra at RIFFGAT using both frequency resolutions. As the figure shows the differences in results are minimal, the relative differences in the computed H_s and T_{m01} are of less than 0.2%.

December 3, 1999; 18:30 hr

The various panels of Figure 2.8 present the wave spectra measurements available from the December storm. Note that at the Kal, MB, Wried, Luep and Oried locations no wave direction measurements are available. Figure 2.8a shows the spectrum measured at the See location and which was used as boundary condition in our hindcasts of this storm. Table 2-2 presents the measured and the computed wave parameters at the buoy locations.

Table 2-2: Measured and hindcasted wave parameters for the storm of 3/12/1999, 18:30. The wave parameters were determined by integrating over the finite frequency domain with f_{low} = 0.04 Hz and f_{high} = 0.60 Hz.

	H_s (m)	H_s error (%)	T_{m01} (s)	T_{m01} error (%)	T_p (s)	T_p error (%)
Kal						
measurements	0.90		3.18		4.00	
SWAN 40.01	1.09	21.1	3.00	-5.7	3.62	-9.5
SWAN 40.51	1.14	26.7	3.04	-4.4	3.62	-9.5
MB						
measurements	1.11		3.47		3.80	
SWAN 40.01	1.25	12.6	3.15	-9.2	3.62	-4.7
SWAN 40.51	1.32	18.9	3.27	-5.8	4.03	6.1
Wried						
measurements	1.23		3.83		4.60	
SWAN 40.01	1.26	2.4	3.27	-14.6	4.03	-12.4
SWAN 40.51	1.30	5.7	3.32	-13.3	4.03	-12.4
STGNEY						
measurements	1.45		4.05		5.00	
SWAN 40.01	1.44	-0.7	3.67	-9.4	4.03	-19.4
SWAN 40.51	1.51	4.1	3.81	-5.9	4.49	-10.2
RIFFGAT						
measurements	1.10		3.18		3.40	
SWAN 40.01	1.04	-5.5	3.06	-3.8	4.03	18.5
SWAN 40.51	1.05	-4.6	3.12	-1.9	4.03	18.5
Luep						
measurements	1.11		3.47		4.50	
SWAN 40.01	1.19	7.2	3.14	-9.5	3.62	-19.6
SWAN 40.51	1.25	12.6	3.24	-6.6	4.03	-10.4
Oried						
measurements	1.14		3.64		3.90	
SWAN 40.01	1.36	19.3	3.45	-5.2	4.49	15.1
SWAN 40.51	1.38	21.1	3.46	-5.0	4.49	15.1

We will now compare the wave spectra computed by the different SWAN runs and the measured wave spectra. We start by the western buoy locations. At the Kal location (Figure 2.8b) SWAN overestimates the measured wind sea, but the peak and shape of the spectrum agree. Also the penetration of swell at Kal is underestimated but it should be mentioned that the energy levels in the measured swell are rather low here. Further into the Waddenzee, SWAN underestimates the energy at the peak of the wind sea spectrum at the MB location (Figure 2.8c) and underestimates the energy at the peak and slightly the peak period of the wind sea spectrum at the Wried location (Figure 2.8d). At all these location the computed SWAN spectra have a high frequency tail containing more energy than those of the measured spectra. The swell at MB is reasonably predicted but is too low at Wried. The computed wave directions differ for frequencies smaller than 0.15 Hz.

In the eastern part of the tidal basin, at the SGTNEY buoy location (Figure 2.8e), SWAN underestimates the wave energy for frequencies between 0.1 and 0.2 Hz and overestimates for frequencies between 0.2 and 0.3 Hz. There is a rather good correspondence between the

high frequency tails of the measured and computed spectra, except for the dip in the measured spectrum at 0.22 Hz.

At the RIFFGAT buoy location the correspondence between the measured and the computed wave spectra is quite good (Figure 2.8f). Note that in the February's storm the computed SWAN spectra compared rather poorly with the measurements for frequencies between 0.18-0.25 Hz at this location (cf. Figure 2.7d and Figure 2.8f). In this storm the most energetic part of the spectrum starts from 0.2 Hz in both the measurements and the hindcasts.

At the Luep location (Figure 2.8g), almost at the eastern tip of the channel southwest of the Norderney Island, SWAN predicts a wind sea younger that the one measured and, as was the case at Wried location, hindcasts a high frequency tail stronger than the one measured.

Finally, at the Oried location (Figure 2.8h) SWAN overestimates the measured wind sea.

From these buoy comparisons, we can conclude that there are only small differences between the results using version 40.01 and version 40.51 of SWAN. Generally SWAN version 40.51 computes wind sea with slightly more energy and in some cases a rather older wind sea (higher peak period) than SWAN version 40.01. The amount of swell energy is higher in the results of SWAN version 40.51 than in those of version 40.01 but not by much. Consequently, the underestimation of the wave period T_{m01} is smaller with SWAN 40.51 than with SWAN 40.01. The former version predicts higher values for the significant wave height.

2.7 Discussion and conclusions

Kaiser and Niemeyer (2001) performed a hindcast of storms in the Norderneyer Seegat using version 40.01 of SWAN and compared those with a number of buoy directional spectra measurements in the region. We have repeated the same exercise using version 40.51 of SWAN, reanalysed the results and also presented spatial fields of the main wave parameters.

Kaiser and Niemeyer (2001) have concluded that SWAN behaves rather well in this basin apart from the underestimation at mid-frequencies (0.18-0.25 Hz) wave energy on the lee side of the Norderney Island (RIFFGAT buoy) in the February 1999 storm. For the other storm the agreement is much better. Overall they conclude that there is too much energy going through the inlet directly to the German coast and too little wave energy penetration to the lee side of the Norderney Island compared to the measurements. They suggest as possible causes for the SWAN underperformance a poor resolution of (the details of) the bottom topography and the neglect of diffraction in the model.

We have found only small differences in SWAN hindcast using version 40.01 or 40.51 in the buoy locations considered. However, our interpretation of the results is slightly less positive than that of Kaiser and Niemeyer (2001). The computed significant wave heights are extremely accurate, but in terms of spectral form we find that the shape of the spectra estimated by SWAN in some cases compares rather poorly with the measurements. The bathymetry of the regions considered is rather complex, with a number of shoals and a

rather deep channel. The shoals and channel can change the form of the spectra considerably, producing multiple peak spectra. In such a situation a good representation of the bottom profile and wave direction at the boundary is important for a successful hindcast of the wave spectra.

The results presented by Kaiser and Niemeyer (2001) have been interpreted as evidence that SWAN has problems in reproducing low energy penetration in an inlet. This can, however, not be concluded from our and Kaiser and Niemeyer's results. For the VST1 and STGNEY buoy locations, the buoy measurements considered in the validation of these storm hindcasts are of wind sea dominated sea states, which contain only a rather negligible amount of low frequency wave energy. Furthermore, SWAN hindcasts of the February 1999 storm South of the Juist Island do show low frequency energy penetration, which can be verified in the peak period field presented in Figure 2.5c and in the spectrum at the location marked as "Loc 1" in the figure, which is presented in Figure 2.9.

It should be noted that the greater penetration of low frequency energy into the inlet in the February 1999 storm relative to the December 1999 storm in SWAN computations is not due to the differences in the bathymetry used to hindcast each of the storms, but to the storm characteristics (boundary wave spectra, cf. Figures 2.7a and 2.8a). This can be verified in Figures 2.10a-c which present spatial maps of the wave parameters of February's storm computed using the grid and bathymetry used to model the December 1999 storm (Figure 2.4).

On the other hand, the differences in the bathymetries used in the two storms result in rather significant differences in the computed wave spectra. Figures 2.11a-c present the spectra of February 1999 storm as measured by buoys and computed by SWAN's version 40.51 using two different grids and bathymetries: a) the regular grid and bathymetry presented in Figure 2.2 (grid a) and b) the grid and bathymetry presented in Figure 2.4 (grid b). In the computations using the bathymetry and grid of December 1999 storm (grid b) there is more swell energy and less wind sea energy at the buoy locations than in those using the bathymetry and regular grid of February 1999 storm.

The hindcasts have been performed without currents. As the hindcasts of the Amelander Zeegat will show, this can have a significant effect. In future hindcasts the current input (taken from a separate model) should be included.

We have so far refrained from commenting on the quality of the wave measurements. Waverider buoy measurements are considered to be very accurate and we have regarded them as 'sea truth'. Note, however, that the buoy's positioning information is often rather inaccurate. The buoys considered in these studies are located in regions with rather large bathymetry gradients, where the wave spectrum varies significantly with the location, and where currents are present. Thus, the accuracy with which the measurements considered here depict the sea state at the measurement locations, depends strongly on the accuracy of buoy location information.

In conclusion, we find that:

- There are small differences in the results using SWAN version 40.01 and 40.51 with some improvement in the low-frequency part of the spectrum.

- SWAN's estimates of the integral wave height are good, the periods are fair but the computed and measured spectra do not agree well for most buoy locations, especially in locations in the tidal basin far away from the inlet gorge.

- This underperformance is due to the quality of the bathymetry, the accuracy of the offshore wave conditions and the local wind growth (which is a combination of input and modelled physics). The most determining factors for a successful hindcast are therefore the inputs rather than the modelled physics.

- We find no evidence that swell does not penetrate into the inlet. Swell energies are very small in most of the measuring locations, and the SWAN period fields show that low frequency energy does penetrate over the shoals in the vicinity of the inlet (where there happen to be no measuring locations).

3 Hindcast of Amelander Zeegat

3.1 Introduction

The Amelander Zeegat is located between the Dutch barrier islands Terschelling and Ameland (Figure 3.1). The inlet consists of a main channel (the "Borndiep") with local depths of more than 20 m and a secondary channel on the western side of the inlet with bottom depths up to 6 m. The main Borndiep channel is highly instrumented with wave buoys. The locations of the available wave buoys, wind and water level stations are shown in Figure 3.2. The upper panel shows the offshore wave buoys (ELD and SON; diamonds) and the wind stations (Texelhors, Vlieland and Terschelling; triangles), whereas the lower panel shows the available wave buoys in the inlet (circles) and the water level stations (Terschelling and Nes; triangles). Wave data have been collected for a number of years. RIKZ (2004) and Svasek (2005) have written a data report for the storm seasons 2003/2004 and 2004/2005, respectively. In these studies four storms are identified:

- 20-22 Dec 2003
- 7-9 Feb 2004
- 1-3 Jan 2005
- 7-9 Jan 2005

In this chapter, we will select three instants in which the situation is near-stationary in terms of wind and water level, and with low current velocities (slackwater conditions). In addition we will select two instants with stationary wind conditions but with maximum flood and ebb currents, so as to assess their influence. The chosen storms will be hindcasted using SWAN version 40.51 and the results compared with measurements. In order to be consistent with future Hydraulic Boundary Conditions (Dutch: Hydraulische Randvoorwaarden, HR) computations we have chosen to use the permanent offshore ELD and SON buoys as boundary conditions rather than the most offshore temporary buoy AZB11

3.2 Selection of storms and instants

In the present hindcast study the objective is to assess the performance of the most recent SWAN version in this inlet. We will limit ourselves to situations in which the model assumptions are met and in which there is a likelihood of swell penetration into the inlet, since this aspect is of primary concern to Rijkswaterstaat.

We will consider the three latest storms identified in the studies mentioned about. For each of the storms we have chosen an instant when the following conditions are satisfied:

- high water levels (for which long waves penetrate strongest into tidal basin)
- slackwater (or minimum currrents) conditions
- near-stationary conditions in the peak of a storm (in terms of winds, waterlevels and currents).

An analysis of the two reports yielded the following storm instants : 8 Feb 2004 (22.20 h), 2 Jan 2005 (12.00 h) en 8 Jan 2005 (18.00 h) which satisfy these assumptions.

For the 1-3 Jan 2005 storm we will also hindcast an instant with a near-maximum ebb current and a near-maximum flood current. This storm is characterized by a period of 24 hours in which the wind speed and direction were nearly constant. The maximum water level occurs on 2 Jan at 13.00 hrs. This is halfway the 24-hr wind-stationary interval. The maximum flood current and the maximum ebb current around this instant are estimated (based on maximum gradients in the measured water level at Nes) to occur at about 10.00 h and 17.00 hr., respectively. The flow conditions will be used to assess the effect and sensitivity of currents on the wave conditions.

3.3 Input data

3.3.1 Wind

During the February 2004 storm wind measurements have been conducted at the wind station near the island of Terschelling. For the January 2005 storms no wind data was available at the wind station at Terschelling but at the following stations near the Amelander Zeegat instead: Texelhors and Vlieland. See Figure 3.2 for the locations of these wind stations.

The wind measurements at the locations Terschelling, Texelhors and Vlieland are shown in Figure 3.3. The figure shows the time series of the wind speed (solid line) and the wind direction (dotted line) in nautical convention. In the upper panel the wind at Terschelling during the February 2004 storm is shown. The second and third panel show the wind measurements in Texelhors and Vlieland during the first and second January 2005 storm respectively.

During the February 2004 storm the wind is westerly during the first day (February 7) with wind speeds up to 12 m/s. On February 8 at 01:00 hr and at 21:00 hr the wind speed reaches its maximum value (14 m/s). The wind turns to a north-westerly direction. During the chosen instant at 22.20 hr both the wind direction and the wind speed are more or less constant. The value of the wind speed at the chosen instant approximately coincides with the value measured during the storm peak.

During the first January 2005 storm the wind is south-westerly at first but on the second day (January 2, 2005), as the wind speed increases, the wind direction turns to a more westerly oriented wind. The wind speed and direction is more or less constant in a time span around the chosen instants at 12.00 hr (near HW slack), at 10.00 hr (flood tide) and at 17.00 hr (ebb tide). The value of the wind speed at the chosen instants is slightly lower than the value measured during the storm peak.

Although not constant, the variation in the wind direction is less for the second January 2005 storm compared to the other two storms. During this storm the highest values of the wind speed are measured (up to 22 m/s). The storm has its peak between 10:00 and 12:00 hr,

which is approximately 7 hours before the selected instant at 18:00 hr. Directions are westerly.

Model wind fields from the Dutch Meteorological Institute (KNMI) atmospheric HIgh Resolution Limited Area Model (HIRLAM) were available for all storms. These wind fields, which have a spatial resolution of about 11 km, were used both to check the value of the wind in the computations with a uniform wind and for the additional computation with a varying wind field. On the basis of a comparison between the HIRLAM data and the wind data at the wind stations it followed that for the January 2005 storm the wind speed and direction measured at the location Vlieland is representative for the Waddenzee.

During the February 2004 storm the wind comes from a north-westerly direction (the North Sea area). For this storm with this direction, it is assumed that the local HIRLAM wind field gives a better representation of the wind in the computational domain than the wind measured in the wind station at Terschelling. The wind as computed with HIRLAM is more or less uniform on the North Sea side of the barrier islands. Therefore, this HIRLAM wind is chosen as the representative wind instead of the wind measured in the wind station Terschelling and is imposed as a spatially uniform wind field in the SWAN computation.

Table 3-1 shows the wind data that are used in the computations with a uniform wind field.

Table 3-1 Wind conditions used in SWAN computations with uniform wind.

date	time	wind speed [m/s]	wind direction [°N]	source
2004-02-08	22:20hr	15	326	HIRLAM
2005-01-02	10:00hr	17	274	Vlieland
2005-01-02	12:00hr	18	280	Vlieland
2005-01-02	17:00hr	17	273	Vlieland
2005-01-08	18:00hr	19	270	Vlieland

At 12:00hr on January 2, 2005 the storm is also modelled with a spatially varying wind field. The wind field is derived from the HIRLAM data. Figure 3.4 shows the HIRLAM wind field at 09:00hr, 12:00hr and 15:00hr respectively. The spatial resolution is 0.125 degrees longitude and 0.0833 degrees latitude (approx: 11 km x 11 km). Figure 3.4a shows the entire North Sea area, while Fig. 3.4b is zoomed in on the Waddenzee.

Fig. 3.4b shows that the wind is more or less stationary between the 09:00 and 15:00 hr in the area of interest. The HIRLAM wind field at 12:00hr is used in the computation. The wind data is interpolated to a rectilinear grid covering the whole area of interest (nearshore part of the North Sea and the Waddenzee). The dimensions of this grid are 180 km x 120 km, with a mesh size of 5 km by 5 km. The origin (X, Y) of the grid is (70 km, 540 km) in RD coordinates.

The errors in the wind direction, caused by projecting the latitude-longitude grid on a Cartesian grid, are less than 1 degree and therefore considered negligible.

3.3.2 Water level

Two water level stations are located in the area of interest: one at the North Sea side of the island of Terschelling and one at the Waddenzee side of the island of Ameland (Nes). The tidal wave traverses from the west to the east with a phase lag of about 1 hour between Terschelling and Nes.

In Figure 3.5 time signals of the measured water level in station Terschelling (blue) and Nes (red) are shown. The solid black lines show the storm instants that are chosen. These are the slackwater instants and the instants of (near maximum) flood and ebb current speed. The figure shows that the phase lag between the two stations is approximately 1 hour.

The water level in Nes is taken as representative for the computations with a uniform water level. The mean tidal range at Nes is approximately 2.5 m.

Table 3-2 shows the water level data in the two water level stations.

Table 3-2 Water level in stations Terschelling and Nes.

date	time	water level Nes [m w.r.t. N.A.P.]	water level Terschelling [m w.r.t. N.A.P.
2004-02-08	22:20hr	2.54	1.90
2005-01-02	10:00hr	1.04	1.29
2005-01-02	12:00hr	2.07	1.50
2005-01-02	17:00hr	1.34	0.36
2005-01-08	18:00hr	2.29	1.60

3.3.3 Current

At the maximum flood and ebb instants on January 2 (10:00 hr and 17:00 hr respectively) computations were performed using the circulation model WAQUA by RIKZ. The results have been provided to us. The computations were performed on a curvilinear flow grid with an approximate resolution near the Amelander Zeegat of 50 – 100 m in flow direction and 100 – 200 m perpendicular to the flow direction. With this resolution the current field in the main channel is assumed to be accurately modelled.

Figures 3.6, 3.7 and 3.8 show the current field half an hour before maximum flood (09:30 hr; Figure 3.6), at maximum flood (10:00 hr; Figure 3.7) and half an hour after maximum flood (10:30 hr; Figure 3.9). The upper panel shows the magnitude of the current and the lower panel shows a vector plot of the current direction (on every 10^{th} grid cell). Figures 3.9, 3.10 and 3.11 show the corresponding water level fields at 09:30 hr, 10:00 hr and 10:30 hr

respectively. The figures show that the water level difference between the North Sea side of the barrier islands and the Waddenzee is approximately 30 cm during maximum flood. The current velocity reaches values up to 2 m/s in the channels. The differences between the current fields at 09:30 hr and 10:30 hr are low, whereas the water level strongly increases in this time interval, indicating that the instant of 10:00 hr is indeed the instant of near maximum flood current speed with a somewhat lower water level than at 10:30 hr.

Figures 3.12, 3.13 and 3.14 and Figures 3.15, 3.16 and 3.17 show the current and water level field respectively near maximum ebb current speed. The maximum ebb current speed is approximately 1.1 m/s.

Since the WAQUA domain does not cover the whole Waddenzee only the computations on the nested grids 2, 3 and 4 are performed with a spatially varying current and water level field. To do so the WAQUA data is interpolated to the three nested grids used in SWAN (to be defined later). Since the resolution of the WAQUA grid is lower than the resolution of the SWAN computational grids and there are no coinciding grid points, the data needs to be extrapolated near the landboundaries and the grid cells that are dry during the computations. For the current field this is unproblematic. Near the landboundaries and the dry cells the magnitude of the current decreases to zero anyway, so it does not make a real difference whether the current velocity is zero due to interpolation or whether an exception value is given (and hence the current velocity is equal to zero as well). Therefore, the current data is interpolated where possible and an exception value is given at grid cells where the water level could not be based on the WAQUA data.

For the water level, extrapolation is less straightforward. In grid cells where the water level is not specified SWAN assumes a water level equal to zero. If the same procedure as the one for the current would be followed, the water level would drop from a certain value computed with WAQUA, which is usually not equal to zero, to zero. Based on the water level measured in Nes, the water level is approximately 1.0 m (10:00 hr) and 1.34 m (17:00 hr) so neglecting this extrapolation effect would result in errors of more than 1.0 m (10:00 hr) or 1.34 m (17:00 hr) locally. Although the drop in the water level would probably affect the wave characteristics only locally, these boundary effects are to be minimized as much as possible. Therefore, a realistic value needs to be specified at grids cells where WAQUA data is not available. For that purpose the values in the dry points have been replaced by a threshold value, which is set equal to the highest computed value, and to interpolate the WAQUA data to the SWAN grids afterwards. The threshold value was chosen equal to 1.45 m and 1.10 m for the water level field at 10:00 hr and 17:00 hr respectively, based on the maximum water levels observed in the WAQUA computations. This way the maximum ‘water level drop’ at the boundaries is less than 10 cm. For the computation at 10:00 hr the threshold value is equal to 1.45 m and for the computation at 17:00 hr the threshold value is equal to 1.1 m.

In order to investigate the effect of the resolution of the WAQUA computations, two different sets of water level and current fields are generated. The first is based on the aforementioned WAQUA data, using all the data point. A second set of water level and current fields has been generated by using an artificial ‘coarse’ WAQUA grid. I.e., instead of using all the WAQUA data points, every 3^{th} point was used only, resulting in a resolution near the main channel of 150 – 300 m in flow direction.

3.3.4 Bathymetry

The depth configuration is based on the following sources of information:

- the most recent available depth configuration from the Dutch "Kuststrookmodel" (fine grid).
- 'vaklodingen 2005' at Borndiep.

The depth data supplied by RIKZ is visualized in Figure 3.18a and Figure 3.18b. Figure 3.18a shows the bathymetry of the Kuststrookmodel and Figure 3.18b shows the bathymetry derived from the "vaklodingen" at Borndiep. These "lodingen" (soundings) are available on a 20 m x 20 m grid.

3.3.5 Offshore wave information

At the offshore locations ELD (Eierlandse Gat) and SON (Schiermonnikoog Noord) wave measurements have been obtained with directional waveriders. The processed data of these buoys, available at 60 minute intervals, was supplied by RIKZ. For application in this study these data have been converted into wave boundary conditions for the SWAN model.

For the location SON the time series were not complete. Only for the first January 2005 storm the wave data from this buoy was available.

For the actual computations, wave data from 60 minutes earlier (*i.e.*, one process interval) than the instant used for the verification of the wave model results in the inlet were imposed as wave boundary conditions. This duration roughly corresponds to the time delay of the waves propagating from the location of the offshore wave buoys to the area of interest.

Figure 3.19, 3.20, 3.21 and 3.22 show time series of the wave parameters H_{m0}, T_p, T_{m02}, T_{m01} and the direction in ELD and SON (when available) for the February 2004, the first and the second January 2005 storm respectively. Although the T_{m01} is not available directly from the buoy data, it can be derived from the general relation between T_{m01} and T_{m02}, assuming a JONSWAP spectrum. For an analytic JONSWAP spectrum with $\gamma = 3.3$ the following relation holds: $T_{m01} = 1.0732\ T_{m02}$. We have included the derived quantity T_{m01} because it is used in the calibration. The instants are indicated with black lines.

Figure 3.20 and 3.21 show that the wave conditions in ELD and SON are comparable. The wave period in SON is slightly higher. The storm travels from west to east, having its peak at ELD some hours before it reaches SON.

3.4 Model schematization

3.4.1 Grids

The computations in the Amelander Zeegat are conducted on one curvilinear grid and four nested rectilinear grids, see Figure 3.23a for the curvilinear grid and the location of the offshore wave buoys, Figure 3.23b for the location of the nearshore wave buoys and Figure

3.23c for the location of the nested grids. The "outside" grid (gridCL) is derived from the "Kuststrookmodel". For all of these grids separate bottom files have been constructed, with a fine resolution when the resolution of the computational grid is fine. For all of these bottom files the 'vaklodingen' at Borndiep form the basis. Outside the Borndiep area the bathymetry from the "Kuststrookmodel" was used.

Figures 3.24 – 3.27 show the bathymetry of the nested grids. The first nested grid is a coarse rectilinear grid with a mesh size of 100 m x 100 m, covering the whole Amelander Zeegat and extending some 30 km into the North Sea. The computation on this grid provides boundary conditions for both grid2 and grid3. For grid3 the boundary conditions could be provided either by the computation on grid1 or the computation on grid2. Since grid1 can also provide information on the westerly waves, generated locally in the Waddenzee, nesting in grid1 will result in more accurate boundary conditions for the computation on grid3. A reference computation (not shown) was made to verify that along the northern boundary the difference between using grid1 or grid 2 as boundary conditions for grid 3 was minor. On the basis of these arguments we chose to use the boundary conditions provided by the computation on grid1.

Boundary conditions for grid4 are provided by the computation on grid3. The three grids grid2, grid3 and grid4 have a resolution of 20 m x 20 m. In Table 3.3 the definition of the grids is given in terms of origin (X0, Y0), number of grid points (Nx, Ny), size (Lx, Ly) and rotation.

Table 3-3 Computational grids

grid code	X0 [km]	Y0 [km]	Nx [-]	Nx [-]	Lx [km]	Ly [km]	rotation [deg]	boundary conditions
gridCL	N.A.	N.A.	160	390	N.A.	N.A.	N.A.	ELD/SON
grid1	141.	589.	560	430	56.	43.	12	gridCL
grid2	163.5	603.	500	500	10.	10.	12	grid1
grid3	164.	595.	600	400	12.	8.	12	grid1
grid4	174.	597.	550	400	11.	8.	12	grid3

The boundary conditions for the offshore (curvilinear) grid are derived from the wave buoy data at Eierlandse Gat (ELD) and Schiermonnikoog Noord (SON), indicated in Figure 3.23a. At the two locations at the offshore boundaries which are closest to SON and ELD parametric JONSWAP spectra are imposed. SWAN interpolates at boundary grid points in between these two points. Towards the corners of the offshore boundary the spectra are extrapolated constantly. Since wave information in SON is missing for the February 2004 storm and the second storm in January 2005, the parametric spectrum based on the ELD data is uniformly imposed at the entire offshore boundary.

The parametric JONSWAP spectrum at the boundary is given in terms of the significant wave height H_{m0}, mean wave period T_{m01}, mean wave direction, directional spreading and the peak enhancement factor γ.

The boundary conditions are tuned such that the computed wave parameters H_{m0} and T_{m01} in locations ELD and SON are within 4% (target) of the measured wave parameters. For normal fetch-limited waves the default value of γ is 3.3. However, it was found that for the February 2004 storm and for the 10:00 hr instant during the first January 2005 storm the measured spectrum at ELD was better reproduced with a value of γ equal to 1 (Pierson-Moskowitz spectrum). For the other instants the value of γ was equal to the default value of 3.3.

The resulting wave conditions are shown in Table 3-4 (ELD) and Table 3-5 (SON). The tables show per wave parameter, the value of the imposed wave (at the boundary), the measured value, the computed value and the relative difference between the measured and computed value (at the measurement locations). The differences are larger than the target value of 4%, especially for the wave period. This is due to the fact that the calibration of the wave parameters at ELD and SON was performed on the outside grid (grid CL) with an unintended model setting of the Komen formulation for wind-generation and white-capping instead of Van der Westhuysen settings. This error could unfortunately not be fixed in time for all calculations. The differences will be noticeable on the outer delta where the influence of the sea conditions is large, and not inside the Waddenzee where the wave field is dominated by local processes. Note that the wave direction and directional spreading have not been tuned. The same values for the mean wave direction and directional spreading as measured in ELD and SON are imposed as boundary condition.

Table 3-4 Wave conditions at offshore wave boundary (comparison with measured wave data in ELD).

date	**time [hr]**	Hm0 [m]				Tm01 [s]				γ [-]	Dir [°N]	Spr [°N]
		imposed	measured	computed	difference	imposed	measured	computed	difference	imposed	computed	computed
20040208	22:20	6.3	5.5	5.2	4.8%	7.8	8.4	7.9	5.8%	1	315	34
20050102	10:00	5.3	4.9	4.8	1.7%	7.2	7.6	7.3	4.4%	1	288	33
20050102	12:00	4.5	4.7	4.6	2.4%	7.1	7.6	6.9	9.2%	3.3	292	33
20050102	17:00	3.2	4.3	4.2	1.7%	8.1	7.5	6.9	8.0%	3.3	289	35
20050108	18:00	6.7	6.0	5.5	8.5%	7.5	8.0	7.5	7.2%	3.3	276	33

Table 3-5 Wave conditions at offshore wave boundary (comparison with measured wave data in SON).

date	time [hr]	Hm0 [m]				Tm01 [s]				γ [-]	Dir [°N]	Spr [°N]
		imposed	measured	computed	difference	imposed	measured	computed	difference	imposed	computed	computed
20040208	22:20	6.3	-	4.8	-	7.8	-	8.6	-	1	326	29
20050102	10:00	6.0	4.8	4.5	6.9%	7.3	7.9	7.9	9.3%	1	301	28
20050102	12:00	5.0	5.0	4.6	7.4%	8.0	8.0	7.9	11.0%	3.3	301	28
20050102	17:00	4.9	4.8	4.4	7.4%	8.7	8.2	8.1	10.2%	3.3	305	30
20050108	18:00	6.7	-	4.6	-	7.5	-	7.8	-	3.3	293	27

3.4.2 Spectral resolution

The spectral resolution is related to the largest and smallest wave periods measured at the offshore buoys and the buoys in the Amelander Zeegat. The smallest wave periods are measured at buoys AZB51 and ABZ52. The minimum wave period over all storms is $T_{m-1,0}$ = 3s (see timeseries of $T_{m-1,0}$ in RIKZ, 2004 for the February storm and in Svasek, 2005 for the two January storms in 2005). As a rule of thumb we apply $f_{high} = 3\ T_p$, which gives f_{high}=0.85 Hz. For the lower frequencies we concluded from the measurements (especially at offshore buoys AZB11 and AZB12) that there is some energy density measured at 0.03 Hz and that the peak of the swell waves is near 0.08 Hz. As lower boundary for the frequency domain we therefore used f_{low} = 0.03 Hz. Aiming at a frequency resolution of 10%, 35 frequency bins have been considered. A directional resolution of 10 degrees is used.

The spectral resolution is applied for all computations (for all storms and in situations with and without currents and uniform or spatially varying wind field). The settings for the frequency and directional resolution are comparable to the advised settings by Alkyon (2003). They found that the default setting are sufficient, i.e. 10 degrees directional resolution, f_{low} = 0.03 Hz, f_{high}=0.8 Hz and a frequency resolution of 10%.

3.4.3 Model settings

As for the hindcasts in the Norderneyer Seegat most of the model settings have been set to the default values. Depth-induced wave breaking has been modelled according to Battjes and Janssen (1978) and the JONSWAP formulation for bottom friction (Hasselmann et al., 1973) has been applied, but instead of the default bottom friction coefficient of 0.067 m^2s^{-3} the bottom coefficient was set to 0.038 m^2s^{-3}, which is the advised value for long period waves. Also triads have been activated. The non-default formulation suggested by Van der Westhuysen et al. (2005) for wind-generation and whitecapping, which is only available in the presently applied SWAN version 40.51, has been used instead of the default formulations for wind input of Komen et al. (1984) and for whitecapping dissipation of Hasselmann (1974).

The action balance equation in SWAN is solved iteratively. Zijlema en Van der Westhuijsen (2005) have shown that the standard convergence criterium in SWAN is not always satisfactory. The standard criterium is the so-called 2%-criterium. This means that in more than 98% of the (wet) grid points the critrium is fulfilled that the relative change in both the significant wave height and the mean wave period T_{m01} from one iteration to the next is less than 2%. In this study the 1%-criterium is applied, as suggested by Zijlema en Van der Westhuijsen (2005).

3.4.4 Definition of output

Four forms of output are generated:

- spatial distribution of the wave parameters H_{m0}, $T_{m-1,0}$, T_{m02} , T_p, mean wave direction (MWD) and directional spreading (DSpr) on the whole computational domain;
- integral wave parameters at the locations of the wave buoys in the Amelander Zeegat;
- 1D and 2D wave spectra at the buoy locations;
- six different rays of output locations: two along the coast of Ameland and Terschelling, one ray through the main channel, connecting the different wave buoys, one through the side channel and two connecting the inlet with the main land (see Figure 3.81).

3.5 Results and analysis

3.5.1 Introduction

We have hindcasted the above defined storm instants using the settings and data described above. Recapping, we have performed a total of 10 hindcasts. In total 5 storm instants were chosen: 8/2/2004 22:20, 2/1/2005 10:00, 12:00 and 17:00, and 8/1/2005 18:00. We shall refer to these storm instants as Storm 1, Storm 2 SW (Slack Water), Storm 2 FS (Flood Stage), Storm 2 ES (Ebb Stage) and Storm 3, respectively. The 2/1/2005 10:00 and 17:00 instants correspond to maximum flood and ebb, respectively, the other instants correspond to slackwaters. At each of these instants a hindcast was performed using spatially uniform water levels and winds fields and no currents. At the 2/1/2005 12:00 instant there was an extra hindcast carried out using the HIRLAM wind fields, and at the 2/1/2005 10:00 and 17:00 instants there were extra hindcast carried out using WAQUA fine and coarse resolution water level and current fields. In Table 3.6 we have synthesized the spatially uniform input water levels (WL), wind velocities and directions (U_{10} and θ_w), and offshore wave boundary conditions imposed in the SWAN computations (based on wave parameters measured at ELD and SON).

Table 3-6 SWAN spatially uniform input water levels, wind velocities and directions, and offshore wave boundary conditions (from ELD and , if available, SON).

				boundary cond ELD			**boundary cond SON**		
	WL (m NAP)	U_{10} (m/s)	θ_w (ºN)	H_{m0} (m)	T_{m01} (s)	MWD (ºN)	H_{m0} (m)	T_{m01} (s)	MWD (ºN)
Storm 1	2.54	15	326	6.3	7.8	315	6.3	7.8	315
Storm 2 SW	2.07	18	283	4.5	7.1	299	5.0	8.0	304
Storm 2 FS	1.04	16	278	5.3	7.2	293	6.0	7.3	296
Storm 2 ES	1.34	18	282	3.2	8.1	290	4.9	8.7	308
Storm 3	2.29	19	265	6.7	7.5	274	6.7	7.5	274

The results of the computations are presented in various plots.

- Similar to the previous chapter, the results are presented in spatial maps, showing the spatial distribution of the different wave parameters over the four nested grids (grid1, grid2, grid3 and grid4). The following wave parameters are presented: H_{m0}, T_{m-10}, T_{m02}, T_p, MWD (mean wave direction) and DSpr (directional spreading). All figures have three parts: a, b and c. Part a contains maps of Hm0 (upper panel) and $T_{m-1,0}$ (lower panel), part b contains maps of T_{m02} (upper panel) and T_p (lower panel), and part c contains maps of MWD (upper panel) and DSpr (lower panel).
- Scatter plots have been generated for a qualitative statistical comparison. These scatter plots contain comparisons of the significant wave height H_{m0}, the mean wave periods T_{m02} and T_{m-10} and the peak period T_p. Although the computations were performed on a spectral range of 0.03 Hz – 0.85 Hz, the spectral moments that are required to determine the significant wave height and the mean wave periods are determined by integrating over the finite frequency domain with f_{low} = 0.03 Hz and f_{high} = 0.50 Hz. This was done in order to compare the computed wave parameters with the measured wave parameters on the same frequency range.
- 1D- and 2D-spectral plots. The former show a comparison between the measured and the computed spectral densities. 2D-spectral information of the wave buoys was not available and so the 2D-spectral plots do not contain a comparison between the measured and the computed spectral densities.

These plots are analysed in the following subsections. Concluding remarks are given in section 3.7.

3.5.2 Convergence of computations

As explained in Section 3.4.3 the action balance equation in SWAN is solved iteratively. In this study the 1%-criterium is applied, as suggested by Zijlema en Van der Westhuijsen (2005). The maximum number of iterations is set to 50. Figures 3.28 – 3.29 show the iteration behavior of the wave parameters H_{m0} and T_{m01} as a function of iteration number in the ten buoy locations, both in terms of the convergence of the absolute values of the wave parameters and in terms of relative error compared to the obtained solution in the final iteration.

In Figure 3.28 the iteration behavior of the computed wave parameters is shown for storm 2 SW (Slack Water), based on the computation with the HIRLAM wind field. Figure 3.29 shows the iteration behavior of the wave parameters for storm 2 ES (Ebb Stage) with the water level and current field derived from the fine WAQUA grid. The results in the buoy locations AZB11 and AZB12 show the convergence on grid 1, whereas the results in the buoy locations AZB21/AZB22/AZB31/AZB32, AZB41/AZB42 and AZB51/AZB52 show the convergence on grid 2, 3 and 4 respectively. Since the data is derived from computations on different grids, the number of iterations is not the same for all buoys.

Both Figure 3.28 and Figure 3.29 show that the wave parameters converge. Inspection of the values of the relative error, expressed as the relative difference between the value after each iteration and the value at the final iteration, shows that the relative error approaches zero. For both storms the relative errors in significant wave height and mean wave period, comparing the values at the last and one-but-last ieteration, is less than 0.5% at all buoy locations. For these storms we conclude that the solution in the buoy locations has converged. Since we considered storms with a varying wind field or with an ebb current, we expect that for situations with a uniform wind field and without current converged solutions at the buoy locations have also been obtained.

3.5.3 Fields

February 8, 2004; 22:20 hr (Storm 1)

Figures 3.30 – 3.33 show the spatial variation of the hindcast wave parameters for Storm 1, computed on each of the grids, respectively. Note that the white spots in these and other field plots are locations where the bottom level is higher than the water level (drying).

The figures show a strong decrease in the wave height. At the North Sea side of the barrier islands the wave height is more than 5 m, whereas the maximum values in the main channel is less than 2 m. This radical decrease is especially visible in Figure 3.31a, which shows the spatial distribution of the wave height on grid2. This grid covers the main part of the Amelander Zeegat. The strong decrease in wave period also indicates that a lot of the offshore swell is dissipated before reaching the inlet into the Waddenzee. There is however still some swell penetrating the inlet, west of the channel.

There is less wave energy crossing the inlet on the east side because a lot of energy is dissipated on the shoal offshore of the channel and also a lot of the waves reaching the shoal refract to the coast. Thus, although the water depth west of the channel is lower than the water depth in the main channel, the wave height in the former is in general higher than the wave height in the latter.

January 2, 2005; 12:00 hr (Storm 2 SW)

Figures 3.34 – 3.37 show the spatial variation of the hindcast wave parameters for Storm 2 SW, computed on each of the grids, respectively. Figures 3.38 – 3.41 show the same information for the computation with a spatially varying wind field, based on the HIRLAM data.

Concentrating first on the results of the computations using a spatially uniform wind field, the pattern of the spatial variation of the wave parameters is similar to what was computed for Storm 1. Recall that, comparing with this storm, the significant wave height and mean wave period at the boundary for Storm 1 are higher and the waves are from a more northerly direction as is the imposed wind velocity, but the wind speed is lower; the water level is about 0.5 m higher (cf. Table 3.6). Consequently, on the Storm 1 computations wave heights and periods outside the inlet are higher and there is more low frequency wave energy penetrating the inlet than in this storm. Inside the inlet (grid 4) the wave conditions are wind dominated and because of the higher wind speeds and longer fetch lengths the wave heights and periods computed for this storm are higher than in Storm 1.

The differences between the computation with a uniform wind field and the computation with a spatially varying wind field are very small. The largest differences are observed at the North Sea side of the barrier islands. From these results we can conclude that wind fields can, as we did, be considered spatially uniform at this instant, and that small wind velocity variations in space do not affect the wave fields significantly.

January 8, 2005; 18:00 hr (Storm 3)

Figures 3.42 – 3.45 show the spatial variation of the hindcast wave parameters for Storm 3, computed on each of the grids, respectively. Compared to the above discussed storms, the boundary waves imposed on this storm are similar to those imposed in Storm 1 (although a bit more from the West) and the forcing wind velocity similar to that used in Storm 2 SW. Consequently, the hindcast wave field on the North Sea side of the barrier islands is quite similar to that for Storm 1—besides for the smaller periods, and the wave field inside the inlet is quite similar to the Storm 2 SW hindcast.

January 2, 2005; 10:00 hr (flood stage) and 17:00 hr (ebb stage) (Storm 2 FS and ES)

We will now present the hindcast results for flood and ebb strength. For each storm instant three hindcasts were performed:

- uniform water levels and no currents,
- WAQUA fine grid water levels and current fields;
- WAQUA coarse grid water levels and current fields.

Comparisons of the different results allows us to draw conclusions about the effect of currents on the SWAN computed waves and the importance of having spatially varying fields available and what resolution such fields should have. Recall that because WAQUA data is not available for the whole grid1 domain, the WAQUA fields were only used in the small domain computations (on grid2, grid3, grid4).

We start by analysing the maximum flood hindcasts. Figures 3.46 – 3.49 present spatial distribution of wave parameters computed using a uniform water level and no current field. Compared with the previously presented storms there is much more dissipation of wave energy by depth-induced breaking in the North Sea (recall the lower water level used in these hindcasts). H_{m0} drops below 4.8 m already when waves cross the 27.5 m depth isoline and there is less wave energy crossing the inlet. The amount of wave energy on the islands North Sea coast and in the inlet is rather low and the peak switches to a higher value in these

regions. The spatial pattern of the computed MWD and DSpr is also very similar to that computed for the other storm instants.

Figures 3.50 – 3.52 present the spatial distribution of wave parameters of Storm 2 FS, which are computed using the fine resolution WAQUA data. Figures 3.53 – 3.55 present the spatial distribution of the differences between the wave parameters computed using the high and the low resolution WAQUA data. Comparing the computations with uniform water level and no currents with those using spatially varying high-resolution WAQUA water level and current fields we can say that:

- In grid2 (located in the inlet mouth) H_{m0}, T_{m-10}, $T_{m02,}$ hindcast using the WAQUA data are lower than those without considering the data. The WAQUA fields have no effect on the MWD and DSpr hindcasts.
- In grid3 it is clear to see that there is much less energy crossing the east end of the inlet in the computations using the WAQUA data. Consequently the hindcast of H_{m0} and mean periods is lower in the grid3 and grid4 (located in the sheltered area of the barrier islands) computations using WAQUA data. Again, the WAQUA fields have no effect in the MWD and DSpr hindcasts.

The differences found in the computations with and without the inclusion of the WAQUA data are as expected since a parallel current in the same direction as the waves (cf Figure 3.7 [lower panel] and 3.50c/3.53c [top panel]) has a decreasing effect on the wave height and the wave period. The opposite should occur by an opposing current. This is more prominent in the tidal channel, where the variation in current across the channel causes additional refraction out of the channel. This affects longer periods more than short periods.

Figures 3.56 – 3.59 present the Storm 2 ES spatial distribution of wave parameters computed using an uniform water level and current field. The boundary conditions imposed in the Storm 2 ES computations are the milder of all the storm instants considered. The results of the computations using a uniform water lever and no currents show that the wave height decreases steadily from offshore, as it approaches the barrier islands. The spatial pattern of the mean period, MWD and DSpr hindcast is rather similar to those of Storm 2 SW.

Figures 3.60 – 3.62 present Storm 2 ES spatial distribution of wave parameters computed using the high resolution WAQUA data. Taking into account the (opposing) current the wave heights and the mean wave periods increase. Also the directional spreading in the grid2 domain slightly increases. The changes in wave heights and periods are lower than those computed for the maximum flood instant. This can partly be explained by the fact that the magnitude of the ebb current is lower than the magnitude of the flood current. The values of H_{m0} in the channel are up to 0.2 m higher when computed using the WAQUA data instead of uniform water levels and no currents. And the respective T_{m-10} and T_{m02} values are up to 0.5 s higher.

Figures 3.63 – 3.65 present the spatial distribution of the differences between the wave parameters computed using the high and the low resolution WAQUA data for Storm 2 ES. In both storm instants the effect of the resolution of the WAQUA grids is not significant. The differences between wave parameters are quite small. The only significant difference is in the peak period in a small number of locations where the spectra is double peaked with very

similar levels of energy in both peaks. Small changes in the energy level at the peaks may cause the peak period to change.

3.5.4 Model/data comparison

There is a total of 10 waverider buoys located around the Amerland inlet. The buoy reference names are: AZB11, AZB12, AZB21, AZB22, AZB31, AZB32, AZB41, AZB42, AZB51, and AZB52. The buoy with subsequent reference numbers (e.g.: AZB21 and AZB 22) are located in the close vicinity of each other, see Figure 3.2 where the black dots denote the main buoys (AZB*x*1) and the red dots denote the backup buoys (AZB*x*2). Some of these buoys are directional waveriders but we have only received 1D spectra measurements from RIKZ. There are some missing measurements in the storm instants considered here. For Storm 1 measurements are available from the AZB11, AZB21, AZB31, AZB41 and AZB51, buoys and for the remaining storm instants from the AZB11, AZB12, AZB31, AZB32, AZB41, AZB42, AZB51, and AZB52 buoys. Figures 3.66 – 3.75 show scatter plots of the measured and computed wave parameters and Figures 3.76 – 3.81 comparisons between the computed and measured spectral densities. The SWAN computed 2D spectra at the buoy locations are available on the attached CD-ROM. The hindcasts at the buoy locations are the results of different grid computations. At the AZB11, AZB12, AZB21 and AZB22 locations the results come from the grid1 computations, at the AZB31 and AZB32 locations from the grid2 computations, at the AZB41 and AZB42 locations from the grid3 computations, and at the AZB51 and AZB52 locations from the grid4 computations.

February 8, 2004; 22:20 hr (Storm 1)

Figure 3.76 shows the comparison between the measured and computed spectra for Storm 1. Starting from the furthest offshore location (AZB11) the compute SWAN spectrum compares rather well with the measurements for frequencies above 0.15 Hz, but underestimates the low frequency energy and the peak period. At the AZB21 location the SWAN computed spectrum is double peaked whereas in the measured spectrum the energy is distributed more evenly in frequency. There is some overestimation of swell energy by SWAN. At the AZB31 location SWAN overestimates the spectral wind sea energy. At the AZB41 location the measurements show only very low energy levels, whereas SWAN computed a wind sea with a significant wave height of about 1 m. At AZB51 SWAN reproduces the high frequency tail of the spectrum rather well, but overestimates the energy at frequencies lower than 0.3 Hz and the peak period. The scatter plots presented of Figure 3.66 show that in terms of integral wave parameters the hindcasts and measurements compare rather well, besides for the wave heights overestimation by the model in the AZB41 and AZB51 locations.

January 2, 2005; 12:00 hr (Storm 2 SW)

Figures 3.67 and 3.68 show the scatter plots and Figures 3.77a,c show the spectral comparisons between the measurements and the hindcasts using spatially uniform and the HIRLAM wind fields for Storm 2 SW. The differences between the computational results using the different wind fields are minimal. The comparisons in terms of wave parameters are good, but the spectral comparisons are rather poor. At the AZB11 and AZB12 locations the computed swell energy is underestimated and concentrated at a higher frequency than measured. At the AZB31 and AZB32 location the SWAN spectra are very similar, but at the

AZB32 location more swell energy is measured than at the AZB31 location. SWAN underestimates the amount of swell energy at the AZB32 location (possibly due to the underestimation already noticed in AZB11/12) and overestimates the amount of wind sea energy at the AZB31 location. Again at the AZB41 and AZB42 locations SWAN spectral hindcasts are very similar and severely overestimate the measured energy at the peak of the spectra. At the AZB51 and AZB52 location both the measurements and the hindcasts are of wind sea only and H_{m0} is higher in the former than in the latter location. In both locations SWAN overestimates the sea state severely, but reproduces the high frequency tail rather well. The corresponding computed mean directions per frequency (Figures 3.77b,d) show there are only negligible differences in direction between the results for the uniform wind field and those for the HIRLAM wind fields.

January 8, 2005; 18:00 hr (Storm 3)

Figures 3.69 shows the scatter plots and Figure 3.78 shows the spectral comparisons between the measurements and the hindcasts for Storm 3. In this storm the measured swell energy is lower than in the previous storm (Storm 2 SW), but the wind sea energy levels are higher. The agreement between this hindcast and measurements is better for wind sea than for the previous storm, especially at the AZB42, AZB51 and AZB52 locations the measured spectra is rather well reproduced by SWAN. Note that Storm 2 is just before HW and Storm 3 at HW or just after HW. This means that the current conditions are slightly different with Storm 3 more at slackwater and thus producing better results.

January 2, 2005; 10:00 hr (Storm 2 FS)

Figure 3.70-3.72 shows the scatter plots and Figures 3.79a,c show the spectral comparisons between the measurements and the hindcasts for Storm 2 FS. At the AZB11 and AZB12 buoy locations SWAN strongly underestimates the peak energy of the spectrum. Recall that there are no computations with WAQUA fields at these locations. At the AZB31 and AZB32 buoy locations, as was the case in the previous storms, the measured and the computed spectra are double peaked. SWAN underestimates the spectral energy for frequencies lower than 0.3 Hz and overestimates for higher frequencies. The differences between the results of SWAN computations with or without the WAQUA fields is minimal at the AZB31 and AZB32 locations, with the computations without WAQUA fields reproducing the measured high frequency tail better. At the AZB41, AZB42, AZB51 and AZB52 buoy locations the measurements show very low energy levels (similar to what was measured at location AZB41 in Storm 1), as was the case in the previous storms, SWAN computations using uniform water level and no currents severely overestimate the measured wind sea spectrum. The results of the computations using the WAQUA fields show less overestimation and a better correspondence between the shape of the measured and the computed spectra. It should be noted that currents are fairly strong, which may affect the quality of the buoy measurements as well. The corresponding computed mean directions per frequency (Figures 3.79b,d) show there are only negligible differences in direction for the case of a fine and coarse WAQUA grid but the differences are large between the cases with and without currents. The swell waves are seen to refract out of the channel at the flood stage and becoming more westerly. The high-frequency waves become more aligned with the flow.

The plots show no differences between the results of the computations using WAQUA data on a fine or a coarse grid.

January 2, 2005; 17:00 hr (Storm 2 ES)

Figures 3.73-3.75 show the scatter plots and Figures 3.80a,c show the spectral comparisons between the measurements and the hindcasts for Storm 2 ES. Contrary to what happened for the other storm instances considered, at the AZB11 and AZB12 buoy locations SWAN reproduces the measured spectra rather well. In this storm the correspondence between the measured and computed H_s at ELD is also rather good, which shows how important a good definition of the boundary wave conditions is. Again, recall that there are no computations with WAQUA fields at these locations. Again, at the AZB31 and AZB32 buoy locations the measured and the computed spectra is double peaked. The SWAN computations without currents reproduce the measured spectra reasonably well, but the high frequency tail of the computed spectra contains more energy than the tail of the measured spectra. The computations taking the WAQUA data into account reproduce the measured local wind sea part of the spectrum better. At the AZB41, AZB42, AZB51 and AZB52 buoy locations SWAN overestimates the measured wind sea spectrum. The computations taking the ebb current and varying water level into account reproduce the measured local wind sea part of the spectrum slightly better, but severely overestimate the wave energy at frequencies lower than 0.3 Hz at the AZB52 location. The corresponding computed mean directions per frequency (Figures 3.80b,d) show there are only negligible differences in direction for the case of a fine and coarse WAQUA grid but the differences are large between the cases with and without currents. The swell waves are seen to refract towards the centre of the channel at the ebb stage and becoming more northerly. The directions of the high-frequency waves only show minor differences (esp. considering the low energy content).

3.5.5 Rays

In order to better describe the variation of wave energy from the North Sea into the Waddenzee a few rays were defined across the inlet and along the channels. The rays are presented in Figure 3.81. Figures with the wave parameter variation along the defined rays are provided in the attached CD-ROM. Figure 3.82 presents 1D spectral plots of the Storm 2 SW hindcasted spectra at different rays locations across the inlet (the considered locations are also presented in the Figure). Figure 3.82 panels clearly shows that, in terms of wave characteristics, the inlet can be divided in 2 parts: the west and the east part. In the western part the flats just south of the inlet throat and west of the channel are an attractor of swell through refraction and swell seems to penetrate over these flats rather than through the channel. The penetration is stopped when the water depth is too small and the swell waves are dissipated through bottom friction or breaking. In the eastern part the propagating spectra are double peaked with much less swell energy that in the western locations and with the amplitude of the swell and wind sea peaks varying with the location. The location in the centre of the channel is the location where less swell energy is hindcast.

3.6 Answers to questions posed in RFP

Which data and which data format is required for future model evaluations?

We have found from the above that the results are influenced by the input conditions in the following descending order of importance: bathymetry, offshore boundary conditions, current field, wind field, waterlevel field. Besides the inputs we require validation buoy data from locations in the inlet.

The bathymetry data which was required was adequate and in a format which could be cast into a SWAN format. For the hindcast, we require the high resolution which was provided but this caused some problems with the pre-processing program QUICKIN because of the number of data points. This is more a concern of the program than of the data.

The offshore boundary conditions at the model boundary are derived from the offshore stations SON and ELD. Of those stations we did not have the measured spectra but only the integral wave height and period parameters. From those parameters we needed to reconstruct a spectrum. Rather, for future hindcasts we would require the offshore measured 2D-spectra. In addition we would recommend a verification buoy offshore of the inlet at a depth of about 20 meters because the permanent stations ELD and SON are too far west and east of the inlet.

The current and waterlevel fields provided from the WAQUA model are also in the right format and could be coupled to SWAN without any problem. The provided water level and current fields were smaller than the model domain, which meant that these fields needed to be extrapolated. This gave some problems with respect to the water levels at the land boundaries. As the results show, the effect of the spatial water level variation is small, and the current field could be provided with the coarser resolution. However, we don't recommend that because in the future detail in the fields might be of importance. The fact that the coarse and fine current fields give similar results implies that even further refinement of the current field is not necessary.

The HIRLAM format in which the wind field was provided was adequate and could be coupled with SWAN without a problem. However, in the results we see only a small difference when using a uniform or spatially-varying wind field for the simple reason that over the area of interest the HIRLAM results do not vary too much. This lack of variation is inherent to the size of meteorological depressions which are larger than the Amelander Zeegat.

For validation purposes the hindcast effort requires buoy data in the inlet. The DONAR format was not usable because we did not have the necessary conversion software. After the conversion was made by RIKZ, the provided data including the meta information was adequate. The quality of the data from the existing buoys is adequate. There is an ongoing concern about the behavior of the buoys in conditions with strong currents. Also, there was some missing data so the data collection could be more robust.

In addition, for a better verification future hindcasts would benefit from measuring locations of wave data

- offshore of the inlet in order to verify and control the input conditions which are critical;
- just landward of the throat of the inlet on the flats to verify the penetration of swell over the flats due to refraction;
- near the mainland dikes and the leeside of the islands in order to verify the end effect of physical processes which occur in the inlet channels and on the flats. In the end these are the areas most relevant for the sea defences.

Is the quality of the Amelander Zeegat data sufficient for model evaluations?

As described above, the quality of the data is sufficient. However, there is concern about the behaviour of the buoys in conditions with strong currents. For the safety assessment and design of sea defences data are also required on the flats near the dikes of the mainland and the southern side of the islands.

Do the buoy locations in the Amelander Zeegat need to be changed?

The buoys are presently located at the (most often the eastern) edges of the channel (Fig. 3.2). This is necessary in order to avoid conflict with other uses of the channel such as navigation channels. However, the spatial distributions (Figures 3.30 – 3.65) show large gradients of the wave heights and periods over the channel edges (which is not surprising). There are also strong variations in the current fields at those locations. For hindcasting purposes the buoys have not been placed at optimal locations.

The shipping lanes (provided by RIKZ and shown in Fig. 3.83) appear to be on the eastern side of the channels, which is where the buoys are located as well. One could consider to move the buoys to the west, preferably more in the middle of the channel.

The spacing of the buoys along the length of the channels appears to be in order. The measurements capture the changes in spectral shape.

As mentioned above, besides buoy locations in the inlet channel, future hindcasts require measurement locations just offshore of the inlet, on the flats just south of the inlet and near the sea defenses.

Which resolution of model inputs of (time-varying) fields of wind, water level, current and bathymetry is recommended?

As described above, the provided wind field resolution is adequate. The water level and current fields could be provided at a coarser grid but we do not recommend it. The present WAQUA resolution is adequate and does not need to be refined. It would be an improvement to provide WAQUA data for a larger area. The present resolution of the

bathymetry is adequate. It is important to use up-to-date (relative to the time instant of the hindcast) data, especially in morphodynamically active regions such as the ebb tidal delta and the inlet throat.

3.7 Conclusions

From the analysis of the hindcasts in the Amelander Zeegat the following conclusions can be drawn:

- As was the case for Norderney, there is no evidence of swell penetration to the Waddenzee region east of the channel, neither in the measurements nor in the hindcasts.

- The flats just south of the inlet throat and west of the channel are an attractor of swell through refraction. Swell seems to penetrate over these flats rather than through the channel. The penetration is stopped when the water depth is too small and the swell waves are dissipated through bottom friction or breaking.

- It is important to have a good definition of the swell wave boundary conditions. The discrepancies found between the measured and computed spectra at the AZB11 and AZB12 locations and the low-frequency peak in AZB31 and AZB32 can be explained by the errors already found close to the boundaries. However, the boundary conditions do not reach the remaining buoy locations and therefore do not influence the quality of the hindcasts there.

- During maximum flood the computations including WAQUA data (currents and waterlevel) lead to results that compare better with the measurements than those without currents. At maximum ebb SWAN overestimates the measured wave energy inside the inlet and the inclusion of WAQUA data, although not solving the problem completely, reduces the overestimation of energy at frequencies higher than 0.3 Hz..

- The variations in the WAQUA water level fields are not enough to justify the differences between the SWAN results using uniform water level and no currents, or spatially varying WAQUA water level and current fields. Therefore, the observed differences must result from the inclusion of current fields in the computations.

- In all the hindcasts SWAN results compare well with the wind sea measured in the Waddenzee. Although often overestimating the low-frequency wave energy, it does reproduce the measured high-frequency tail of the spectra rather well. The good reproduction of the high-frequency tail is also valid for the other buoy locations.

- For the instants we considered the wind fields can be considered spatially uniform, since the spatial wind velocity variations do not affect the wave fields significantly.

- The provided data format and resolution of the input bathymetry, current-, water level- and wind fields are adequate. The quality is adequate as well, except for a concern about the performance of the buoys in currents.

- The present locations of the buoys on the channel edges is not optimal for the purpose of hindcasting because of the large local gradients in the hydrodynamics (wave height, period, current). We recommend relocation to the middle of the channel.

4 Conclusions and recommendations

In this section the conclusions of the Norderneyer Seegat and Amelander Zeegat are repeated and overall conclusions are drawn:

4.1 Norderneyer Seegat

- There are small differences in the results using SWAN version 40.01 and 40.51 with some improvement in the low-frequency part of the spectrum.

- SWAN's estimates of the integral wave height are good, the periods are fair but the computed and measured spectra do not agree well for most buoy locations, especially in locations in the tidal basin far away from the inlet gorge.

- This underperformance is due to the quality of the bathymetry, the accuracy of the offshore wave conditions and the local wind growth (which is a combination of input and modelled physics). The most determining factors for a successful hindcast are therefore the inputs rather than the modelled physics.

- We find no evidence that swell does not penetrate into the inlet. Swell energies are very small in most of the measuring locations, and the SWAN period fields show that low frequency energy does penetrate over the shoals in the vicinity of the inlet (where there happen to be no measuring locations)

4.2 Amelander Zeegat

- As was the case for Norderney, there is no evidence of swell penetration to the Waddenzee region east of the channel, neither in the measurements nor in the hindcasts.

- The flats just south of the inlet throat and west of the channel are an attractor of swell through refraction. Swell seems to penetrate over these flats rather than through the channel. The penetration is stopped when the water depth is too small and the swell waves are dissipated through bottom friction or breaking.

- It is important to have a good definition of the swell wave boundary conditions. The discrepancies found between the measured and computed spectra at the AZB11 and AZB12 locations and the low-frequency peak in AZB31 and AZB32 can be explained by the errors already found close to the boundaries. However, the boundary conditions do not reach the remaining buoy locations and therefore do not influence the quality of the hindcasts there.

- During maximum flood the computations including WAQUA data (currents and waterlevel) lead to results that compare better with the measurements than those without currents. At maximum ebb SWAN overestimates the measured wave energy inside the

inlet and the inclusion of WAQUA data, although not solving the problem completely, reduces the overestimation of energy at frequencies higher than 0.3 Hz..

- The variations in the WAQUA water level fields are not enough to justify the differences between the SWAN results using uniform water level and no currents, or spatially varying WAQUA water level and current fields. Therefore, the observed differences must result from the inclusion of current fields in the computations.

- In all the hindcasts SWAN results compare well with the wind sea measured in the Waddenzee. Although often overestimating the low-frequency wave energy, it does reproduce the measured high-frequency tail of the spectra rather well. The good reproduction of the high-frequency tail is also valid for the other buoy locations.

- For the instants we considered the wind fields can be considered spatially uniform, since the spatial wind velocity variations do not affect the wave fields significantly.

- The provided data format and resolution of the input bathymetry, current-, water level- and wind fields are adequate. The quality is adequate as well, except for a concern about the performance of the buoys in currents.

- The present locations of the buoys on the channel edges is not optimal for the purpose of hindcasting because of the large local gradients in the hydrodynamics (wave height, period, current). We recommend relocation to the middle of the channel.

4.3 Recommendations

From the above conclusions we can recommend the following:

- The present hindcast study should be followed up with a detailed analysis (including sensitivity runs) of the presently hindcast storms which includes the following aspects:
  - effect of the specification of swell boundary conditions (esp. direction),
  - effect of the bathymetry,
  - balance of local wind growth due to wind input and wind formulation in SWAN and friction,
  - triads,
  - effect of currents at high water.

- As the calculations show that the effect of currents is important. With respect to the Amelander Zeegat, they should be measured in the field (preferably in the channels) in order to validate the phase and magnitude of the WAQUA-calculated currents. With respect to the Norderneyer Seegat, current fields are presently not available and should be included in future studies. This involves the construction of a local current model for that area.

- Validate SWAN with a physical model experiment of the penetration of swell in a schematized tidal inlet system which consists of a barrier island, a curved inlet channel and tidal flats. This could be a new experiment if such a study has not been done before.

- Relocation of the measurement buoys to areas with less gradients in the hydrodynamic properties and extension of the measurement network with stations on the flats near the inlet, near the sea defenses and just offshore of the inlet.

- Use other type of instrument to validate buoy measurements under strong currents.

- A future activity in the SBW project is the formulation of a generic hindcasting procedure. The experiences obtained in the current study should be used in this activity.

- Similarly, the measured data, the model set-up and inputs should be used in the calibration and validation tools to be developed next year in the SBW project.

References

Battjes, J.A. and J.P.F.M. Janssen, 1978: Energy loss and set-up due to breaking of random waves, Proc. 16th Int. Conf. Coastal Engineering, ASCE, 569-587.

Hasselmann, K., 1974: On the spectral dissipation of ocean waves due to whitecapping, *Bound.-layer Meteor.*, **6**, 1-2, 107-127

Hasselmann, K., T.P. Barnett, E. Bouws, H. Carlson, D.E. Cartwright, K. Enke, J.A. Ewing, H. Gienapp, D.E. Hasselmann, P. Kruseman, A. Meerburg, P. Müller, D.J. Olbers, K. Richter, W. Sell and H. Walden, 1973: Measurements of wind-wave growth and swell decay during the Joint North Sea Wave Project (JONSWAP), *Dtsch. Hydrogr. Z.* Suppl., vol. 12, A8

Kaiser, R. and H. D. Niemeyer, 2001: Analysis of directional spectra in shallow environment, *Proc. 4th Int. Symp. WAVES*, 944-952.

Komen, G. J., S. Hasselmann and K. Hasselmann, 1984: On the existence of a fully developed wind-sea spectrum, *J. Phys. Oceanogr.*, **14**, 1271-1285.

Rijkswaterstaat, 2001: Hydraulische Randvoorwaarden 2001 voor het toetsen van primaire waterkeringen. (Hydraulic Boundary Conditions Book). Den Haag.

RIKZ, 2004: Meetcampagne Amelander Zeegat stormseizoen 2003-2004. Meetverslag van twee noordwesterstormen. Werkdocument RIKZ/OS/2004.129w, Oktober 2004.

Svasek, 2005: Meetverslag Amelander Zeegat stormseizoen 2004-2005. Rapport Svasek Hydraulics cg/05449/1356, December 2005.

Van der Westhuysen, A. J., M. Zijlema and J. A. Batjes, 2004: Improvement of the numerics and deep-water physics in an academic version of SWAN, *Proc. 29th Int. Conf. Coastal Engng.*, ASCE, **1**, 855-865.

Van der Westhuysen, A. J., M. Zijlema and J. A. Batjes, 2005: Saturation-based whitecapping dissipation in SWAN for deep and shallow water. Submitted to Coastal Engng.

Van Vledder, G.Ph. and M. Bottema, 2002: Improved modelling of nonlinear four-wave interactions in shallow water. *Proc. 28th Int. Conf. Coastal Engng.*, ASCE, 459-471.

WL 2002: Kwaliteit randvoorwaardenboek en kwaliteit SWAN. WL|Delft Hydraulics Report H4061, Januari 2002.

WL 2006: SBW Plan of Action on the boundary conditions for the Waddenzee. WL|Delft Hydraulics Report H4750, April 2006.

Zijlema, M., and A.J. van der Westhuysen, 2005: On convergence behaviour and numerical accuracy in stationary SWAN simulations of nearshore wind wave spectra, Coastal Engineering, Vol. 52, 237-256.

A SWAN inputfiles

For one Norderney case (storm February 1999) and one Ameland case (Storm January 2, 2005, 12.00hr, uniform windfield) the SWAN inputfile used in this project have been listed here. For the Amelander Zeegat only the input file for grid 3 is given.

A.1 Norderneyer Seegat

```
$*************HEADING*************************************************
$
PROJ 'Riffney' '9901' $d
$
$ 1999,   mit TRIAD (standard),  mit Quad, Standardauflösung
$ wie Riffney 9901 aber mit geaenderter NUM ACCUR
$
$ 05.02. 03:36  (Wind aus 290) Sturmflut; geaendert von 330 zu 340 (Swan-Konv)
$ wie 9901c aber nach Sued verlaengertem Modellgebiet
$ (gleich n pkte; +1000m)
$************MODEL INPUT*********************************************
$
SET level=3.39 CARTESIAN
$
CGRID REG 67000. 55800. 287. 7720. 12640. 84 158 CIR 36 0.025 4 120
$
INPGRID BOTTOM 65899. 48922. 0. 211 164 80. 80.
READINP BOTTOM -1. 'NYO1995.BOT' 6 4  FORM 8
$
WIND 19 340
$
BOUNDSPEC SIDE N CONSTANT FILE 'spt050299.txt'
$
NUM ACCUR 0.02 0.02 0.02 98.0 15
$
GEN3 WESTH
TRIAD
FRIC JONS
$
$************ OUTPUT REQUESTS ************************
$
FRAME 'grobErg' 69100. 56300. 287. 6600. 9600. 33 48
$
POINT 'SEE'    74045 57907
POINT 'VST1'   75331 54278
POINT 'SGTKAL'  73071 51162
POINT 'SGTNEY'  75607 51855
POINT 'RIFFG'  77212 52205
POINT 'divpnts' FILE 'divpnts.txt'
$
$************************** BLOCK UITVOER ****************************
$
BLOCK 'COMPGRID' NOHEAD 'NieuweUitvoer\Block\riffney9901d.mat' XP YP DEP HS RTP TMM10
TM01 TM02 FSPR DIR DSPR WLENGTH
$
$********************* AREA*************************************************
$
TABLE 'grobErg' NOHEAD 'riffney9901_g.txt' XP YP DIR PDIR TDIR
TABLE 'COMPGRID' NOHEAD 'riffney9901_f.txt' XP YP DEP HS TM01 RTP QB WLEN DISSIP
$
TABLE 'SEE'    FILE 'riffney9901d_SEE.txt'      HS TM01 RTP DIR PDIR WLEN
TABLE 'VST1'   FILE 'riffney9901d_VST1.txt'     HS TM01 RTP DIR PDIR WLEN
TABLE 'SGTKAL' FILE 'riffney9901d_SGTKAL.txt'   HS TM01 RTP DIR PDIR WLEN
```

```
TABLE 'SGTNEY' FILE 'riffney9901d_SGTNEY.txt'   HS TM01 RTP DIR PDIR WLEN
TABLE 'RIFFG'  FILE 'riffney9901d_RIFFG.txt'    HS TM01 RTP DIR PDIR WLEN
TABLE 'divpnts' FILE 'riffney9901d_divpnts.txt'  HS TM01 RTP DIR PDIR WLEN
$
$********************* 1D-SPECTRUM ***************************************
$
SPECOUT 'SEE'    SPEC1D ABS 'riffney9901d_SEE.SPT'
SPECOUT 'VST1'   SPEC1D ABS 'riffney9901d_VST1.SPT'
SPECOUT 'SGTKAL' SPEC1D ABS 'riffney9901d_SGTKAL.SPT'
SPECOUT 'SGTNEY'  SPEC1D ABS 'riffney9901d_SGTNEY.SPT'
SPECOUT 'RIFFG'   SPEC1D ABS 'riffney9901d_RIFFG.SPT'
SPECOUT 'divpnts' SPEC1D ABS 'riffney9901d_divpnts.SPT'
$
$********************* 2D-SPECTRUM ***************************************
$
SPECOUT 'SEE'     SPEC2D ABS 'riffney9901d_SEE.SP2'
SPECOUT 'VST1'    SPEC2D ABS 'riffney9901d_VST1.SP2'
SPECOUT 'SGTKAL'  SPEC2D ABS 'riffney9901d_SGTKAL.SP2'
SPECOUT 'SGTNEY'  SPEC2D ABS 'riffney9901d_SGTNEY.SP2'
SPECOUT 'RIFFG'   SPEC2D ABS 'riffney9901d_RIFFG.SP2'
SPECOUT 'divpnts' SPEC2D ABS 'riffney9901d_divpnts.SP2'
$
COMPUTE
HOTFILE 'riffney9901d.hot'
STOP
$
```

A.2 Amelander Zeegat (grid 3)

```
$******************************** HEADING ************************************
$
$
PROJ '20050102-1200' '3'
$
$      Runid:  'SBW'
$    Lev:   2.29
$
$
$************************************ MODEL INPUT ****************************
SET LEVEL = 2.29 MAXERR = 3 NAUT
$
$ Definitieve rooster en bodem
CGRID REGULAR 164000. 595000. 12. 12000. 8000. 600 400 SECTOR 130 80 31  0.03 0.85 35
$
INP  BOTTOM  164000.  595000. 12. 599 399  20.  20. EXC -999.0
READ BOTTOM  1. 'bottom\grid3.bot'  IDLA=3 NHEDF=0 FREE
$
$************************************ BOUNDARY CONDITIONS ********************
$
$BOU NEST  'Bcond\grid3_20050102a.RVW'
BOUNDSPEC   SEGMENT   XY   164000.   595000.   162336.70   602825.19   VAR   FILE   0.
'Bcond\grid3_20050102a.RVW'
BOUNDSPEC  SEGMENT  XY  162336.70  602825.19  172802.89  605049.81  VAR  FILE  1189.
'Bcond\grid3_20050102b.RVW'
$
$************************************ PHYSICA ********************************
$
GEN3 WESTH
QUAD
TRIAD
BREAKING 1. 0.73
FRICTION JONSWAP CFJON=0.067
$
$ wind Vlieland
WIND 18.0  280.
$
```

```
$****************************** NUMERIEKE PARAMETERS ******************************
$
NUM ACCUR 0.01 0.01 0.01 99. STAT MXITST=50
$
$****************************** NEST ***********************************************
$
NGRID 'nest'   174000.  597000.  12. 11000.  8000.  550 400
NEST  'nest'  'Bcond\grid4_20050102.RVW'
$
$****************************** DEFINITIE VAN UITVOERPUNTEN ***********************
$
POINTS 'PNT2' FILE 'Points\boeien_AZG2005.pnt'
$
$****************************** DEFINITIE VAN UITVOERRAAIEN************************
$
POINTS 'RAY1' FILE 'Rays\geul.pnt'
POINTS 'RAY2' FILE 'Rays\geul_vasteland1.pnt'
POINTS 'RAY3' FILE 'Rays\geul_vasteland2.pnt'
POINTS 'RAY4' FILE 'Rays\ameland_ray.pnt'
POINTS 'RAY5' FILE 'Rays\terschelling_ray.pnt'
POINTS 'RAY6' FILE 'Rays\nevengeul.pnt'
POINTS 'RAY7' FILE 'Rays\boeien_AZG2004.pnt'
$
$ ****************************** BLOCK UITVOER  *********************************
$
BLOCK 'COMPGRID' NOHEAD 'Block\grid3_20050102.mat' LAYOUT 3 XP YP DEP HS RTP TMM10
TM01 TM02 FSPR DIR DSPR WLENGTH TPS DHSIGN DRTM01
$
$ ****************************** TABEL UITVOER ******* ***************************
$
TABLE   'PNT2'    HEAD 'Table\grid3_20050102.tab'        XP YP DEP HS RTP TMM10 TM01
TM02 FSPR DIR DSPR WLENGTH TPS DHSIGN DRTM01
TABLE   'RAY1'    HEAD 'Table\Ray1_grid3_20050102.tab'  XP YP DEP HS RTP TMM10 TM01
TM02 FSPR DIR DSPR WLENGTH TPS DHSIGN DRTM01
TABLE   'RAY2'    HEAD 'Table\Ray2_grid3_20050102.tab'  XP YP DEP HS RTP TMM10 TM01
TM02 FSPR DIR DSPR WLENGTH TPS DHSIGN DRTM01
TABLE   'RAY3'    HEAD 'Table\Ray3_grid3_20050102.tab'  XP YP DEP HS RTP TMM10 TM01
TM02 FSPR DIR DSPR WLENGTH TPS DHSIGN DRTM01
TABLE   'RAY4'    HEAD 'Table\Ray4_grid3_20050102.tab'  XP YP DEP HS RTP TMM10 TM01
TM02 FSPR DIR DSPR WLENGTH TPS DHSIGN DRTM01
TABLE   'RAY5'    HEAD 'Table\Ray5_grid3_20050102.tab'  XP YP DEP HS RTP TMM10 TM01
TM02 FSPR DIR DSPR WLENGTH TPS DHSIGN DRTM01
TABLE   'RAY6'    HEAD 'Table\Ray6_grid3_20050102.tab'  XP YP DEP HS RTP TMM10 TM01
TM02 FSPR DIR DSPR WLENGTH TPS DHSIGN DRTM01
TABLE   'RAY7'    HEAD 'Table\Ray7_grid3_20050102.tab'  XP YP DEP HS RTP TMM10 TM01
TM02 FSPR DIR DSPR WLENGTH TPS DHSIGN DRTM01
$
$ ****************************** SP1 UITVOER ************************************
$
SPEC 'PNT2' SPEC1D 'Spec1d\grid3_20050102.sp1'
SPEC 'RAY1' SPEC1D 'Spec1d\Ray1_grid3_20050102.sp1'
SPEC 'RAY2' SPEC1D 'Spec1d\Ray2_grid3_20050102.sp1'
SPEC 'RAY3' SPEC1D 'Spec1d\Ray3_grid3_20050102.sp1'
SPEC 'RAY4' SPEC1D 'Spec1d\Ray4_grid3_20050102.sp1'
SPEC 'RAY5' SPEC1D 'Spec1d\Ray5_grid3_20050102.sp1'
SPEC 'RAY6' SPEC1D 'Spec1d\Ray6_grid3_20050102.sp1'
SPEC 'RAY7' SPEC1D 'Spec1d\Ray7_grid3_20050102.sp1'
$
$ ****************************** SP2 UITVOER ************************************
$
SPEC 'PNT2' SPEC2D 'Spec2d\grid3_20050102.sp2'
SPEC 'RAY1' SPEC2D 'Spec2d\Ray1_grid3_20050102.sp2'
SPEC 'RAY2' SPEC2D 'Spec2d\Ray2_grid3_20050102.sp2'
SPEC 'RAY3' SPEC2D 'Spec2d\Ray3_grid3_20050102.sp2'
SPEC 'RAY4' SPEC2D 'Spec2d\Ray4_grid3_20050102.sp2'
SPEC 'RAY5' SPEC2D 'Spec2d\Ray5_grid3_20050102.sp2'
SPEC 'RAY6' SPEC2D 'Spec2d\Ray6_grid3_20050102.sp2'
SPEC 'RAY7' SPEC2D 'Spec2d\Ray7_grid3_20050102.sp2'
```

```
$
$ ************** TEST UITVOER VOOR MEETLOCATIES ***********************************
$
TEST 1 0 POINTS XY &
161240.  613520.  &   $ AZB11
164990.  614010.  &   $ AZB12
167200.  610400.  &   $ AZB21
167610.  610400.  &   $ AZB22
169380.  607320.  &   $ AZB31
169450.  607110.  &   $ AZB32
171340.  604400.  &   $ AZB41
171500.  604250.  &   $ AZB42
174290.  601500.  &   $ AZB51
175600.  600820.  &   $ AZB52
PAR 'Par\grid3_20050102.par'
$
COMPUTE
$
HOTFILE 'Hot\grid3_20050102.hot'
$
STOP
```

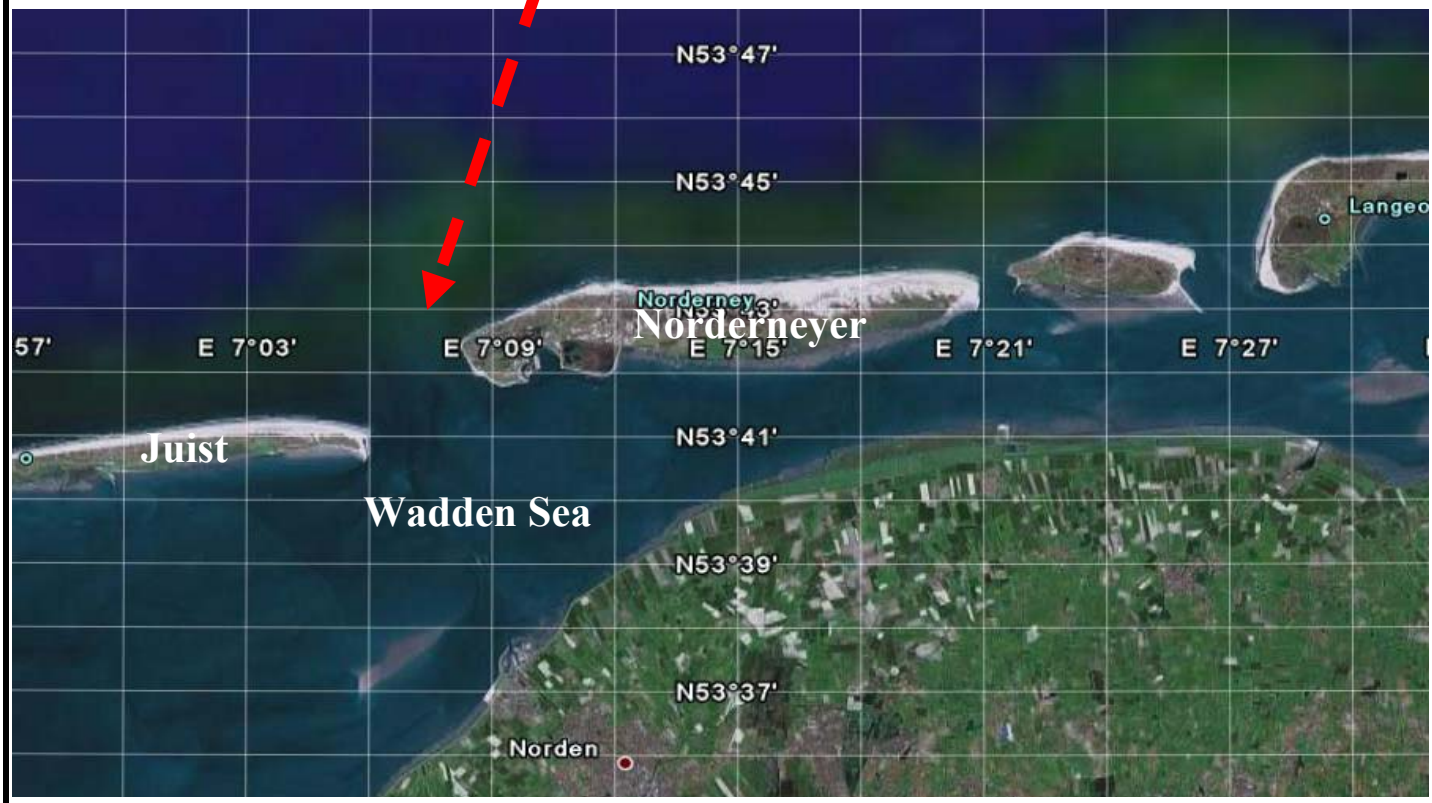

General and detailed aerial views of the Norderney area		
WL | Delft Hydraulics	**H4803**	**Fig. 2.1**

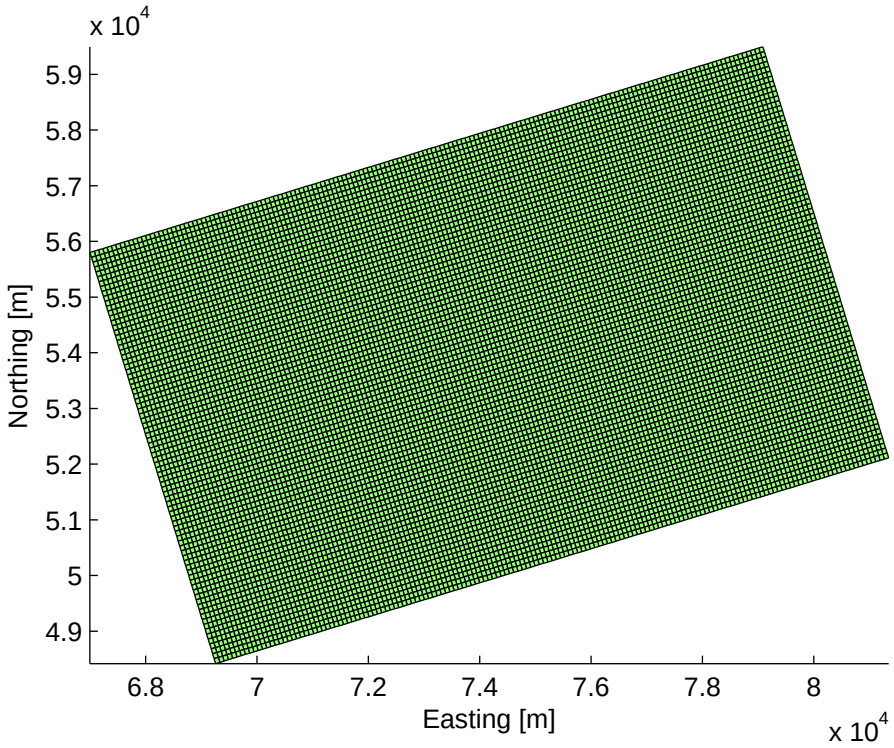

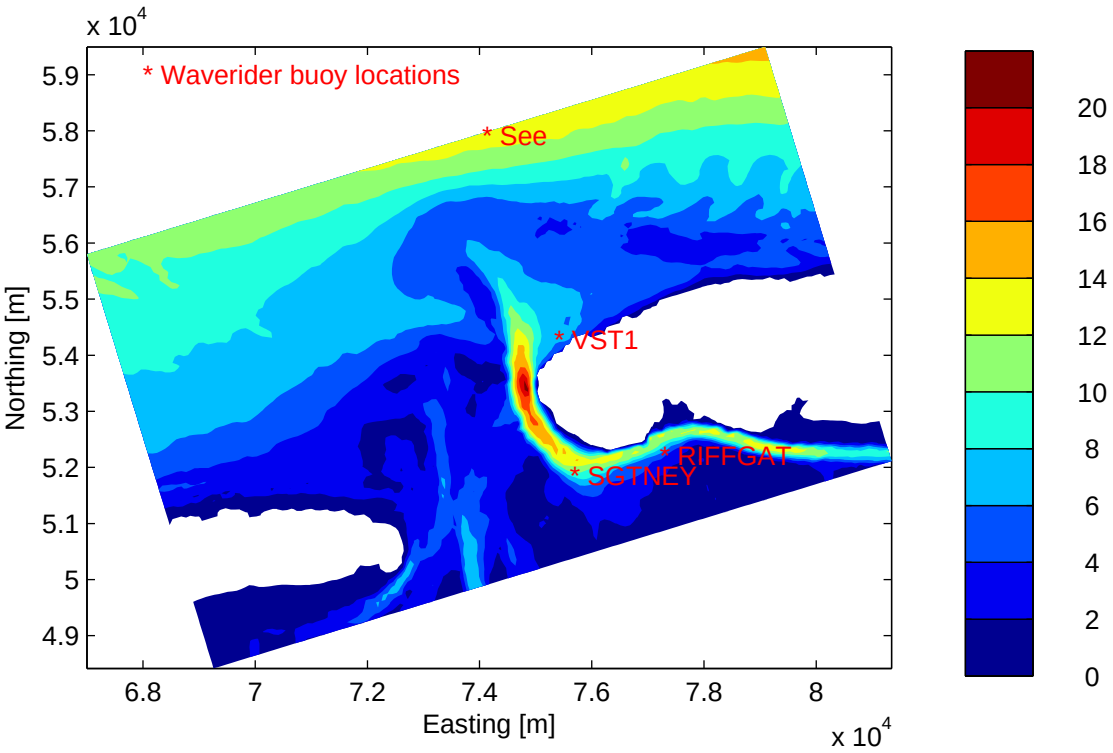

Top panel: Regular grid Bottom panel: Bathymetry (in metres below MSL) and buoy locations	5 Feb 1999	
	Norderney	
WL | DELFT HYDRAULICS	H4803	Fig. 2.2

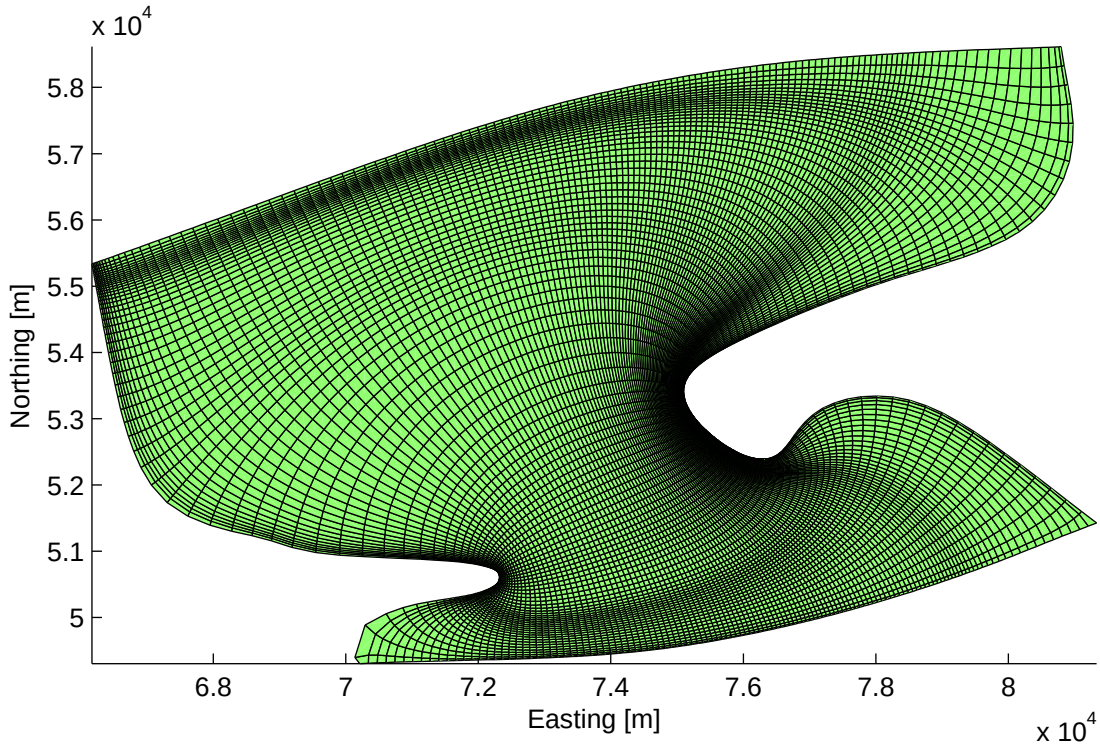

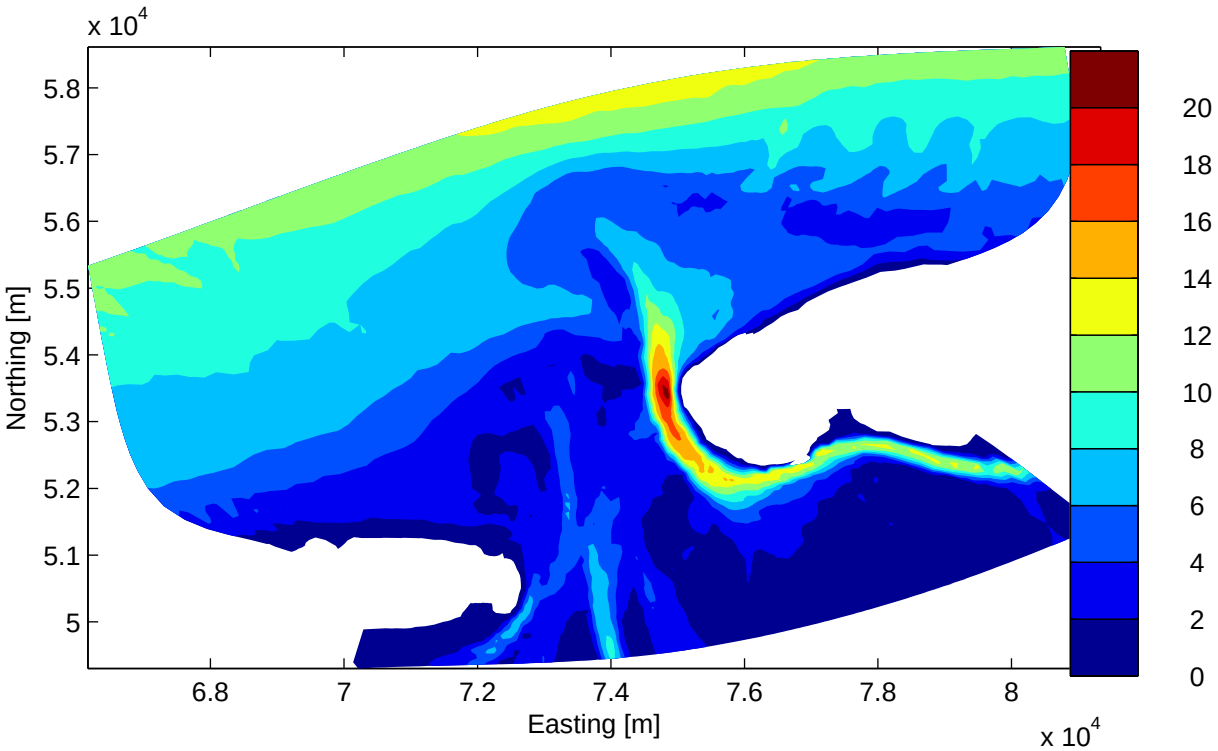

Top panel: Curvilinear grid Bottom panel: Bathymetry (in metres below MSL)	5 Feb 1999	
	Norderney	
WL | DELFT HYDRAULICS	H4803	Fig. 2.3

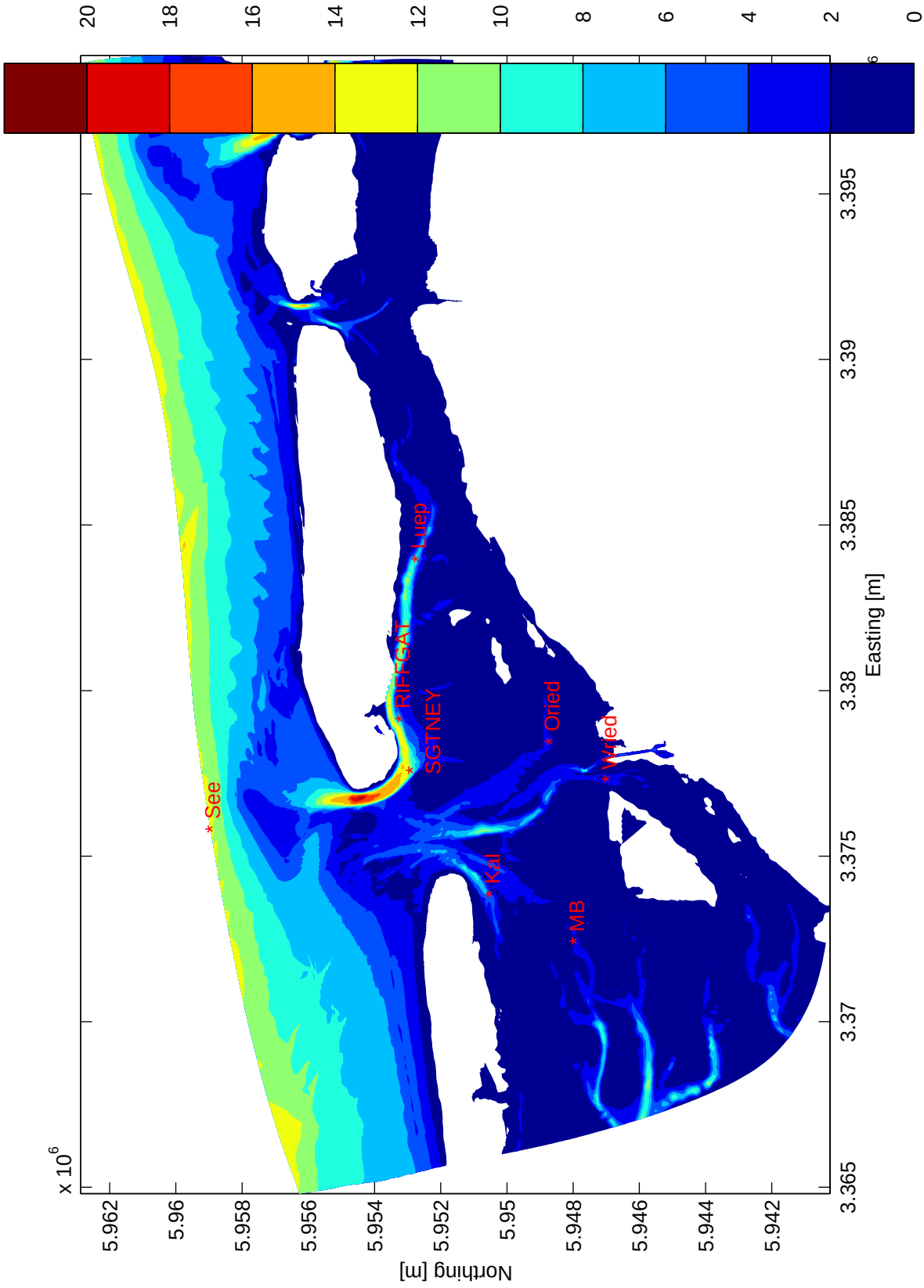

Bathymetry (in metres below MSL) and buoy locations	3 Dec 1999	
	Norderney	
WL | DELFT HYDRAULICS	H4803	Fig. 2.4

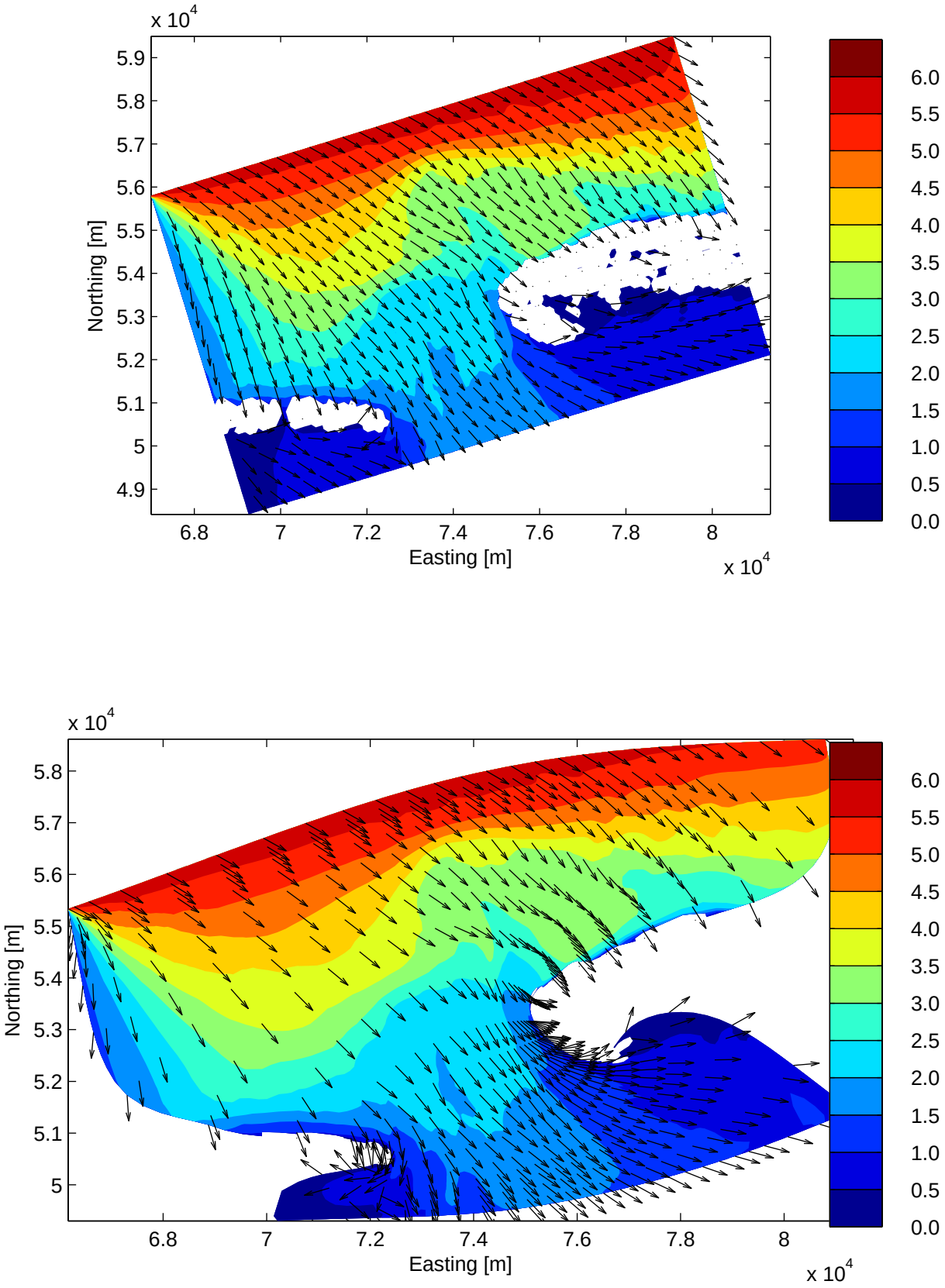

Significant wave height (m) Top panel:Regular grid; Bottom panel: Curvilinear grid	5 Feb 1999	SWAN 40.51
	Norderney	
WL | DELFT HYDRAULICS	H4803	Fig. 2.5a

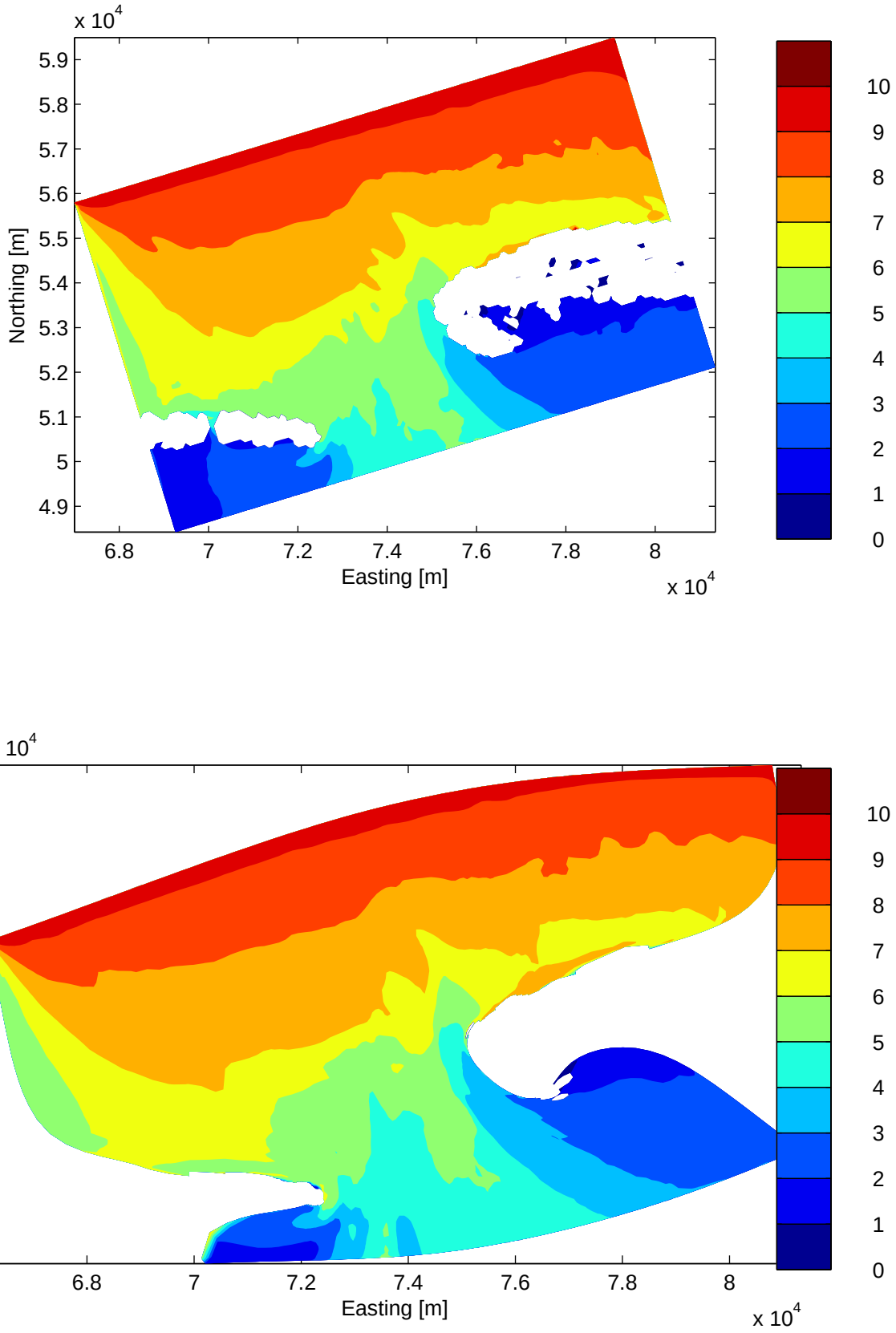

Mean wave period (T_{m01}, s) Top panel:Regular grid; Bottom panel: Curvilinear grid	5 Feb 1999	SWAN 40.51
	Norderney	
WL | DELFT HYDRAULICS	H4803	Fig. 2.5b

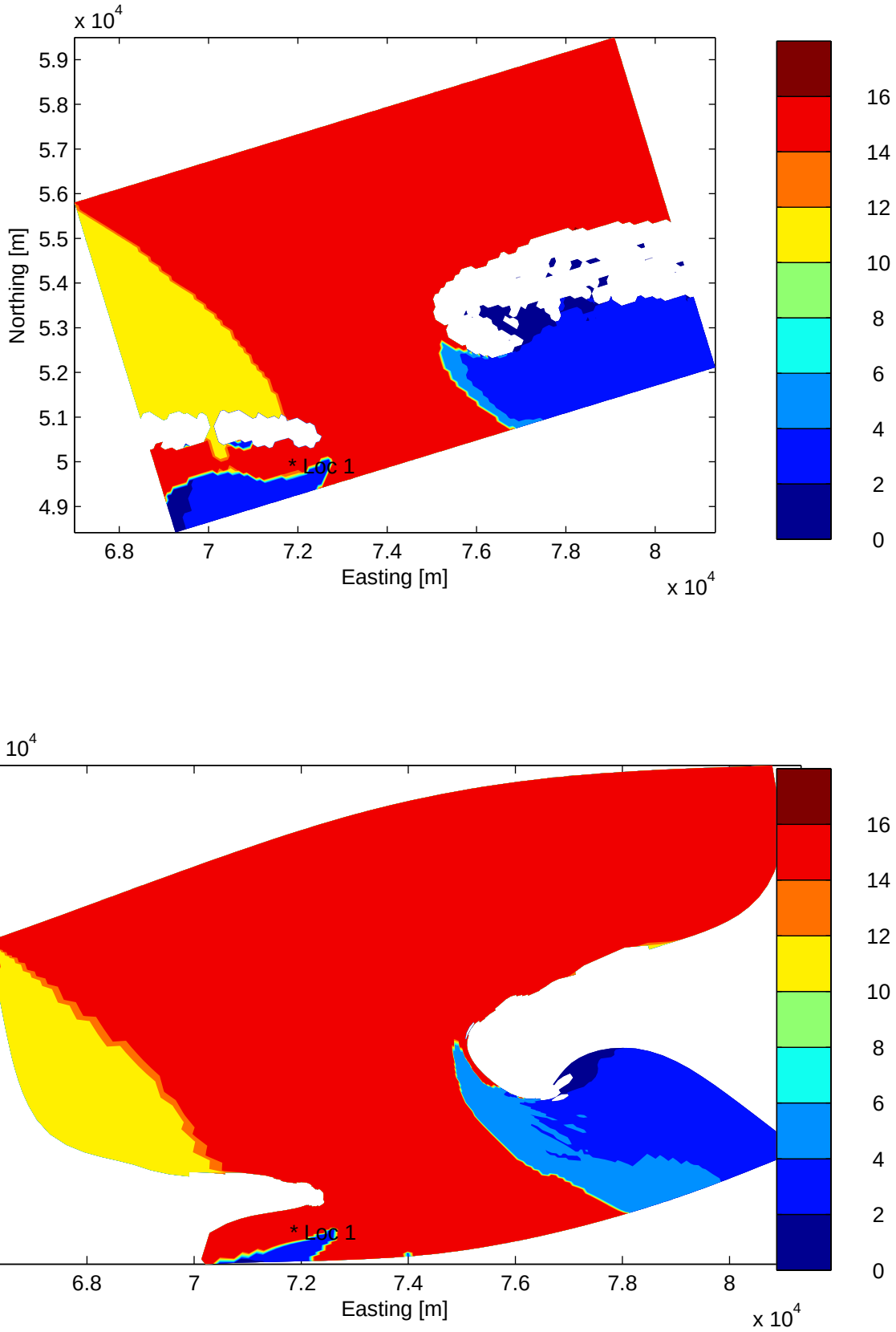

Peak period (s) Top panel:Regular grid; Bottom panel: Curvilinear grid	5 Feb 1999	SWAN 40.51
	Norderney	
WL | DELFT HYDRAULICS	H4803	Fig. 2.5c

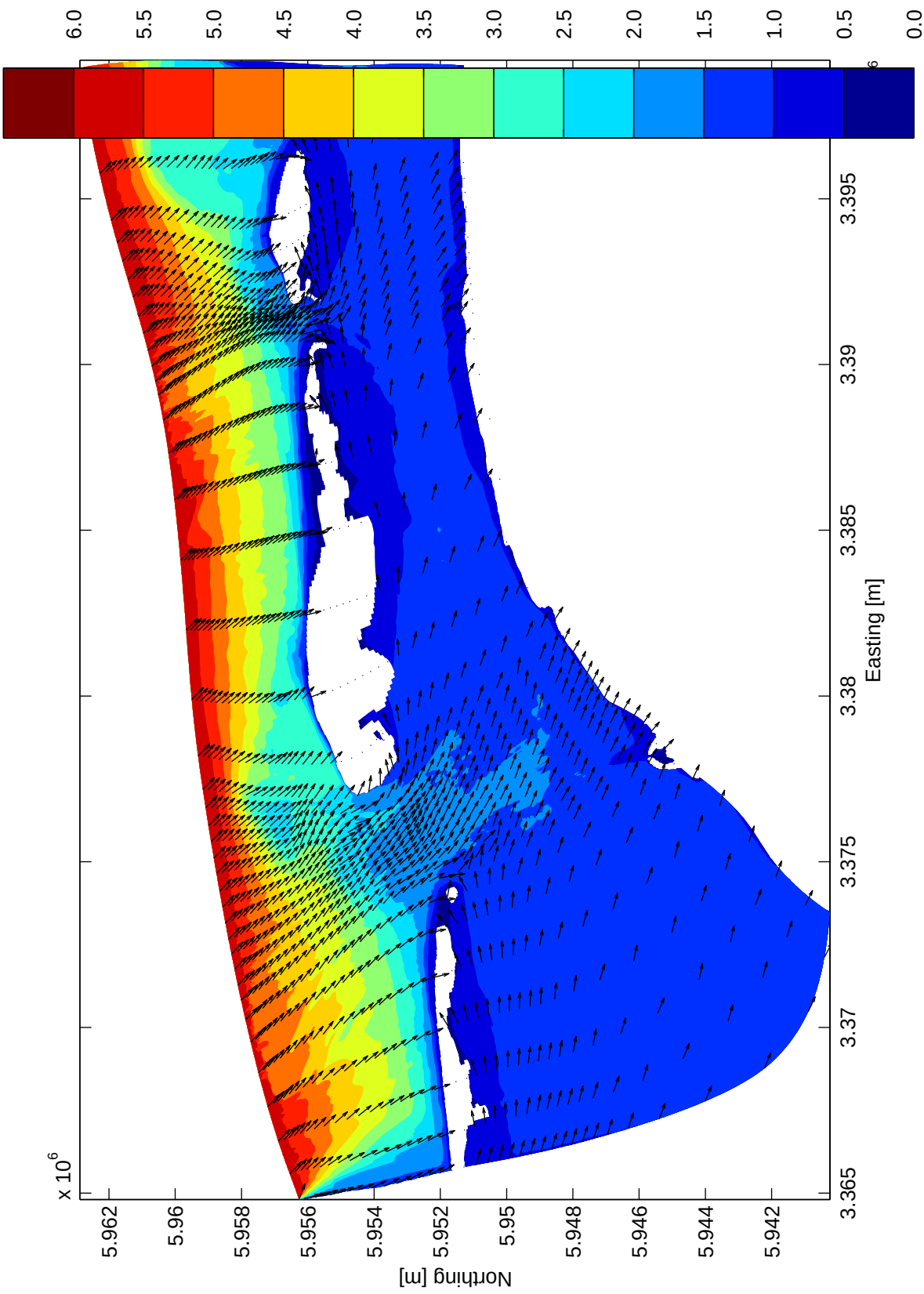

Significant wave height (m)	3 Dec 1999	SWAN 40.51
	Norderney	
WL | DELFT HYDRAULICS	H4803	Fig. 2.6a

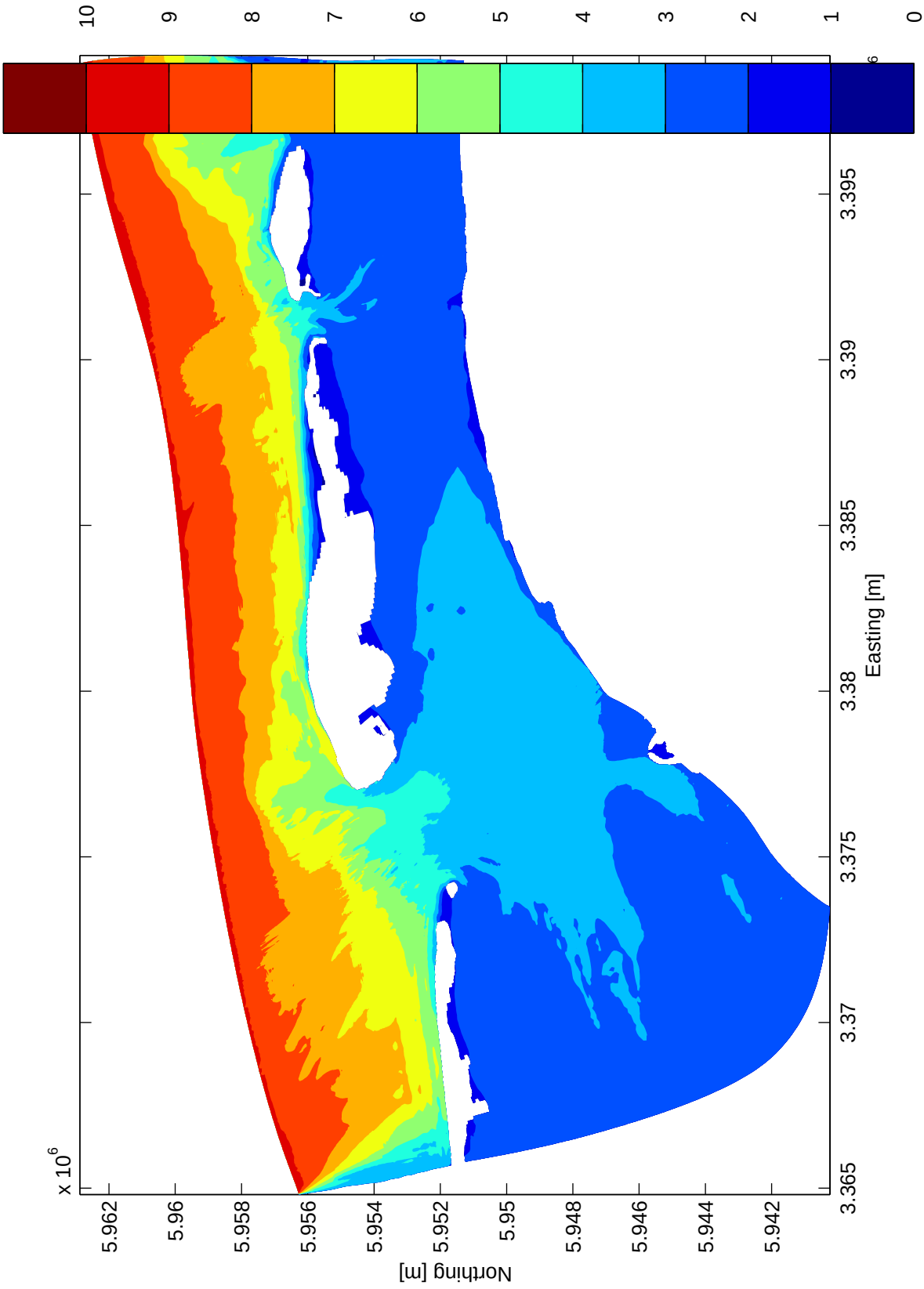

Mean wave period (T_{m01}, s)	3 Dec 1999	SWAN 40.51
	Norderney	
WL | DELFT HYDRAULICS	H4803	Fig. 2.6b

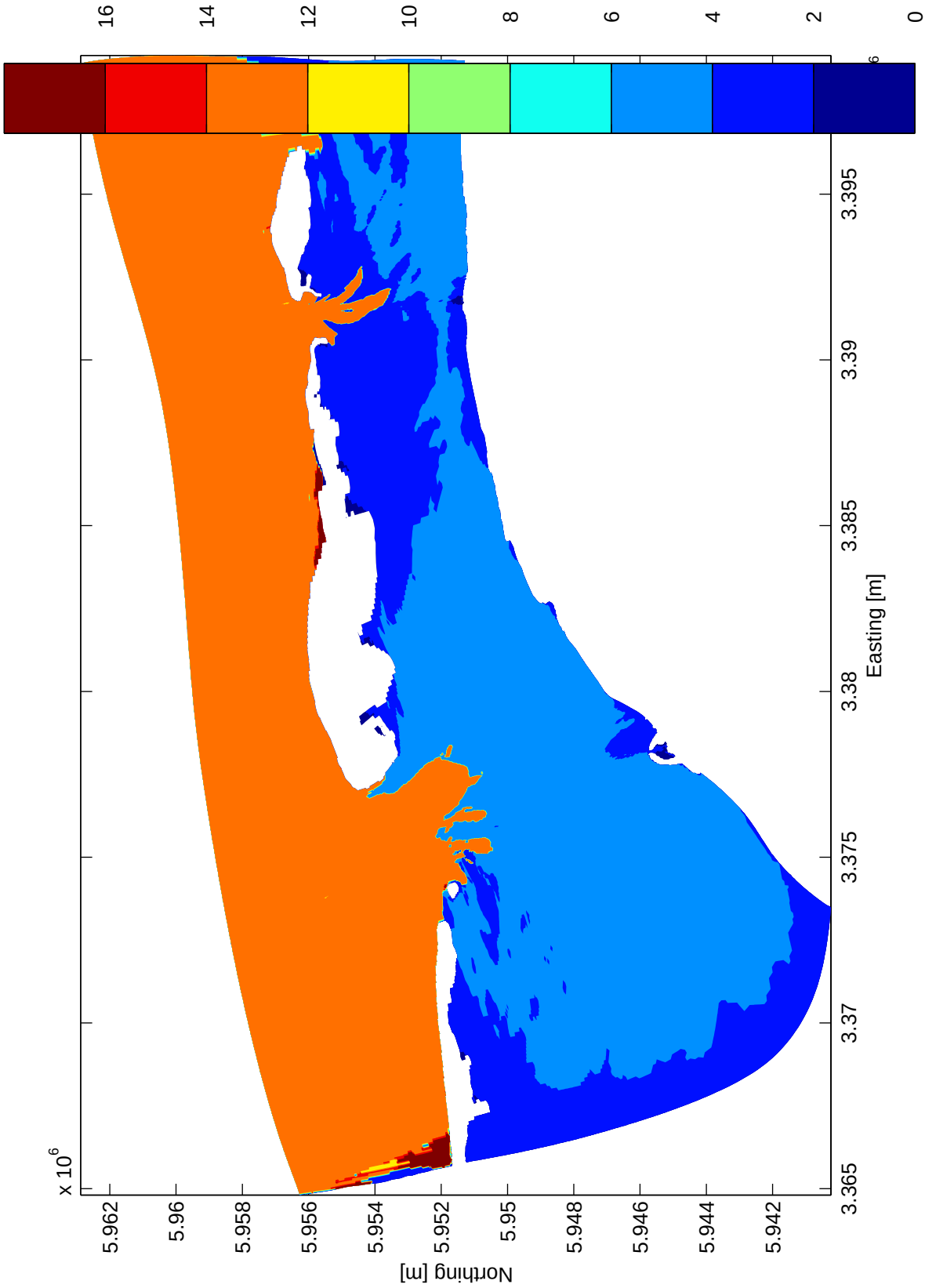

Peak period (s)	3 Dec 1999	SWAN 40.51
	Norderney	
WL | DELFT HYDRAULICS	H4803	Fig. 2.6c

See, 5 Feb 1999 3:40		
	Norderney	
WL | DELFT HYDRAULICS	H4803	Fig. 2.7a

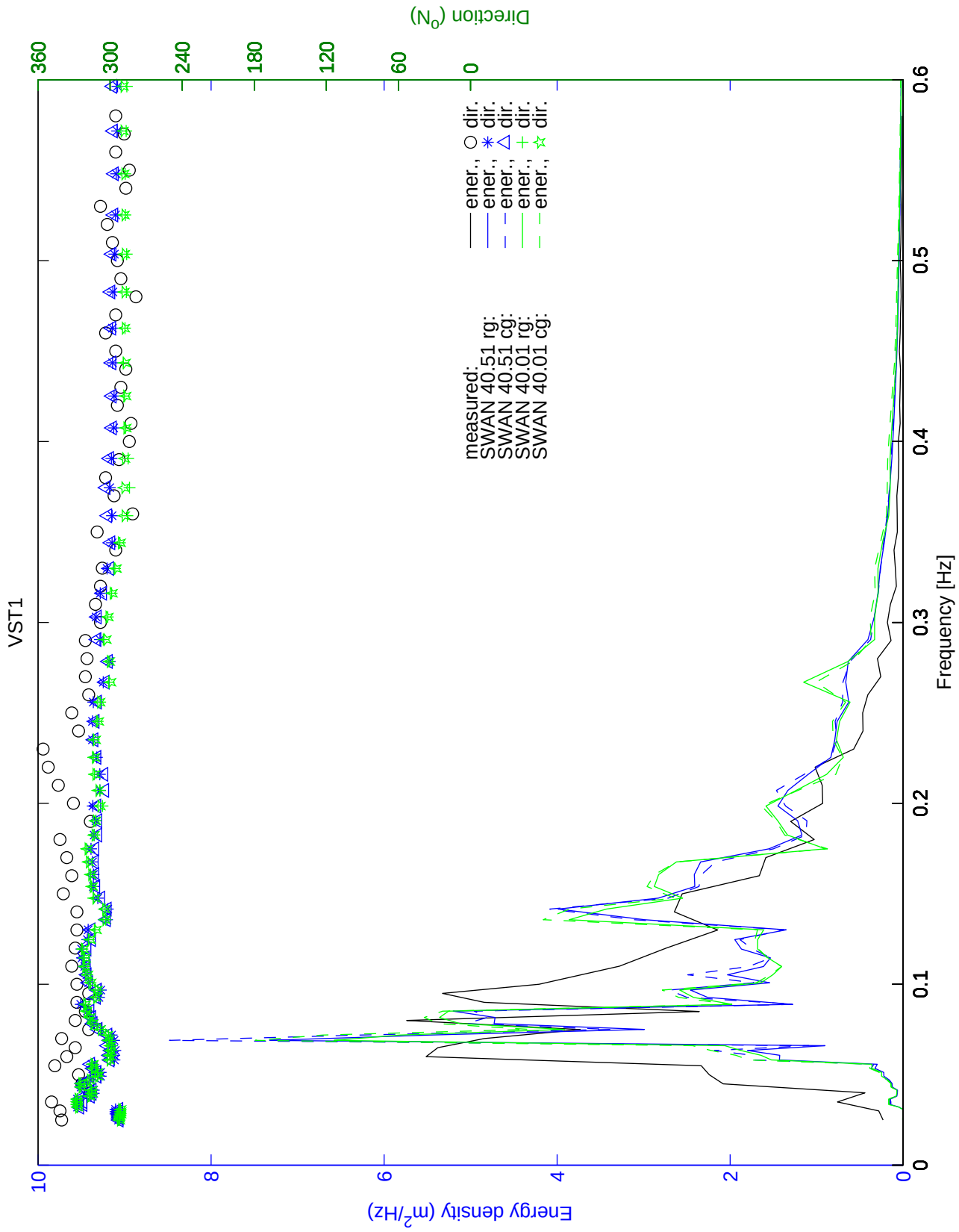

VST1, 5 Feb 1999 3:40		
	Norderney	
WL | DELFT HYDRAULICS	H4803	Fig. 2.7b

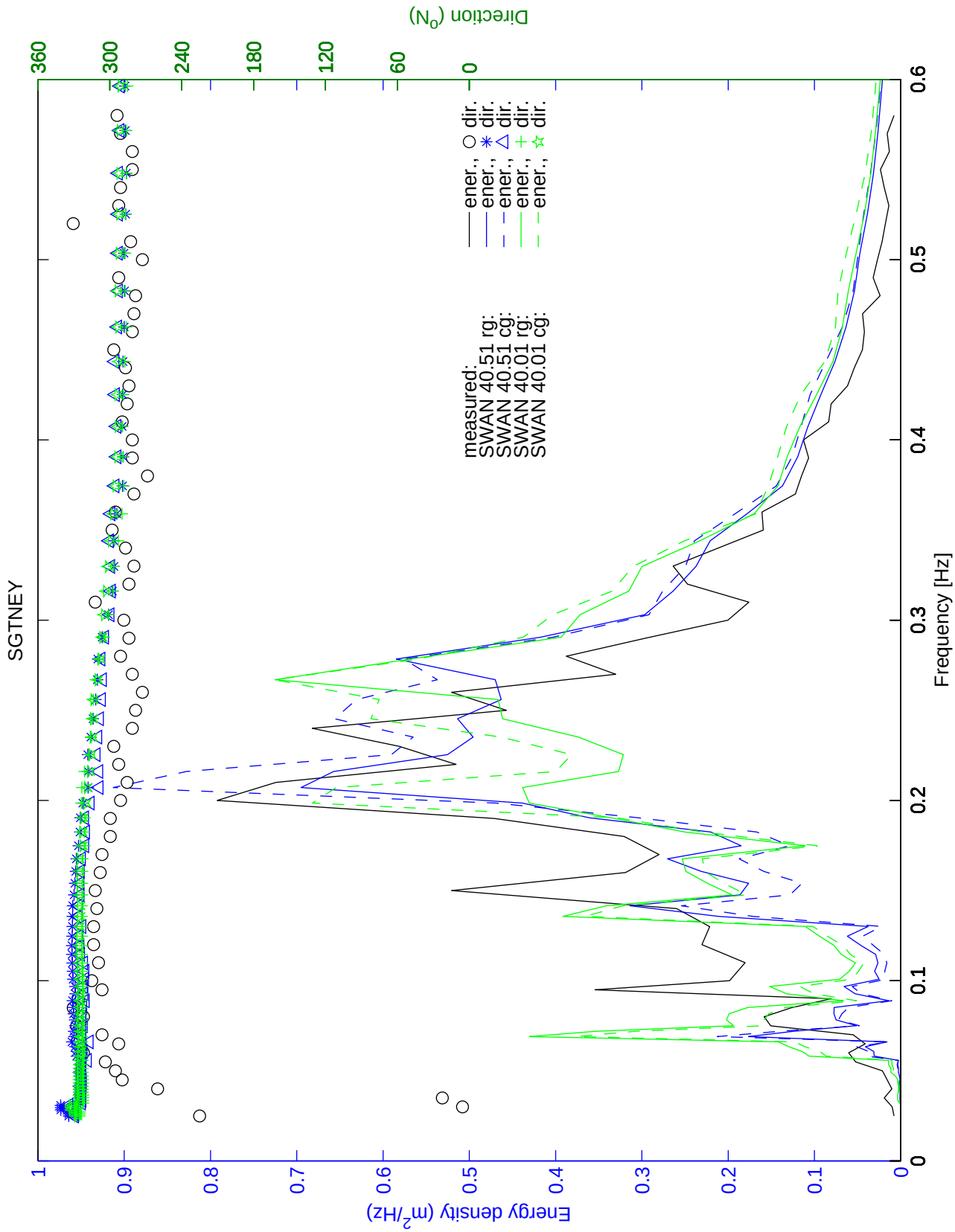

SGTNEY, 5 Feb 1999 3:40		
	Norderney	
WL | DELFT HYDRAULICS	H4803	Fig. 2.7c

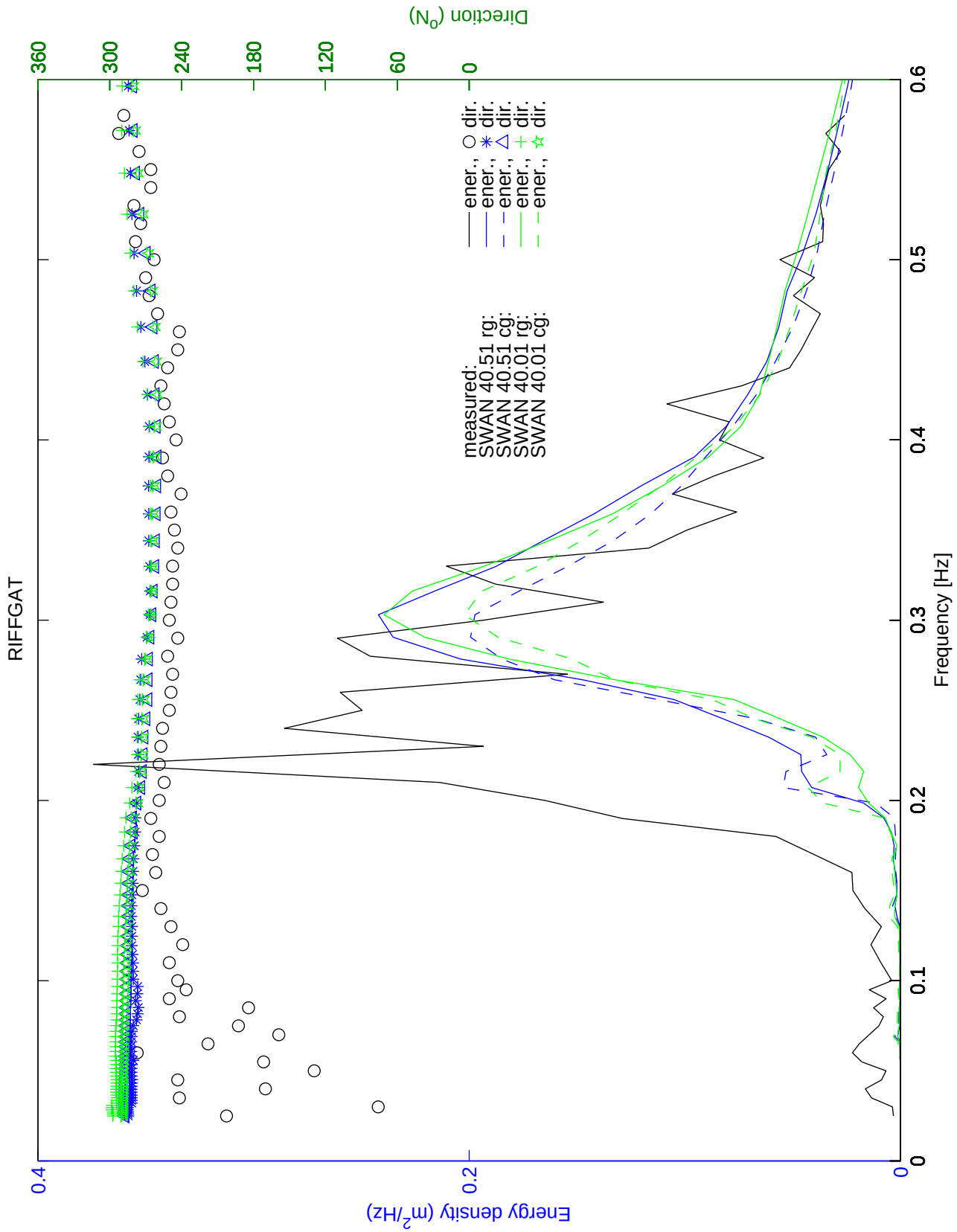

RIFFGAT, 5 Feb 1999 3:40		
	Norderney	
WL | DELFT HYDRAULICS	H4803	Fig. 2.7d

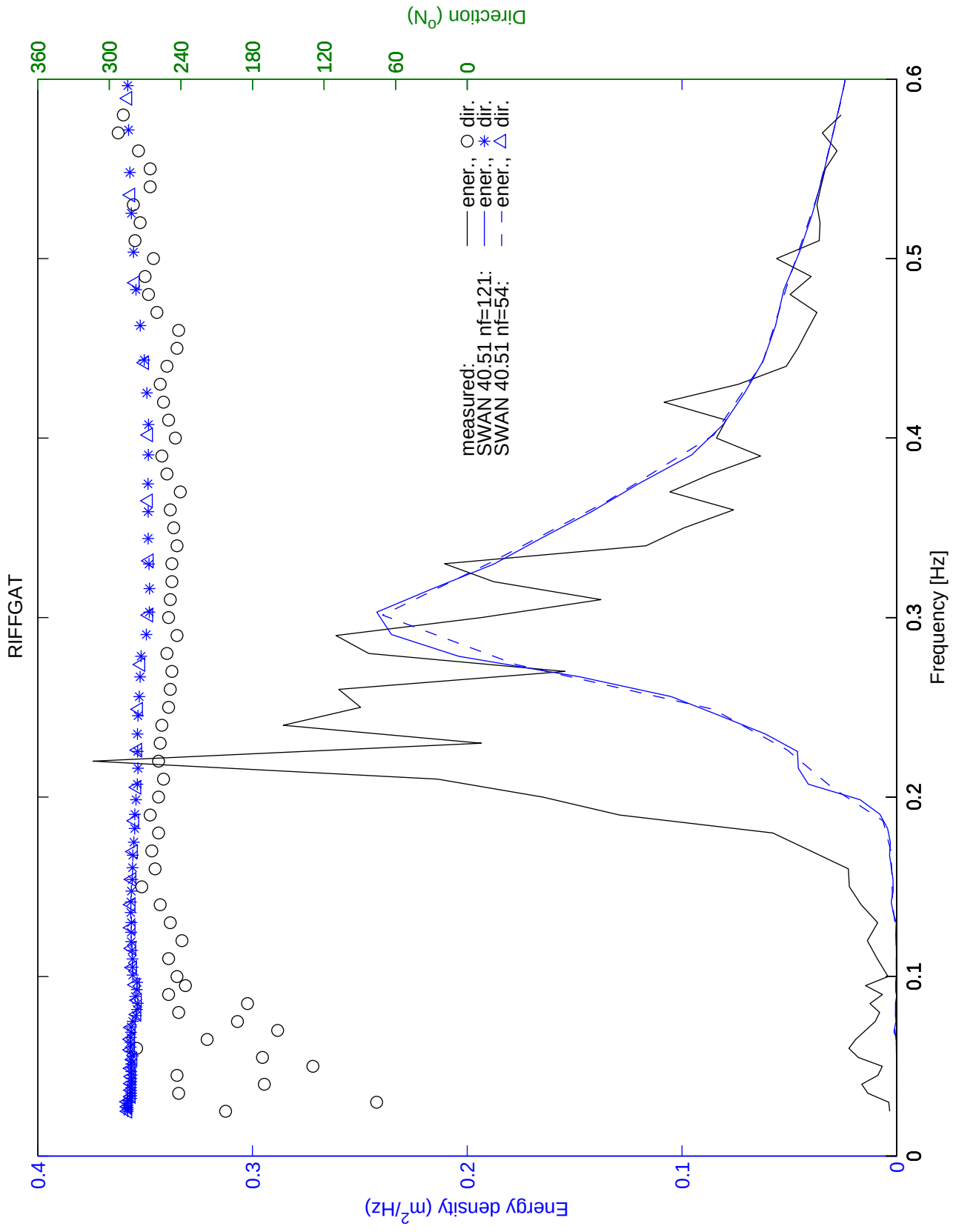

RIFFGAT, 5 Feb 1999 3:40		
	Norderney	
WL | DELFT HYDRAULICS	H4803	Fig. 2.7e

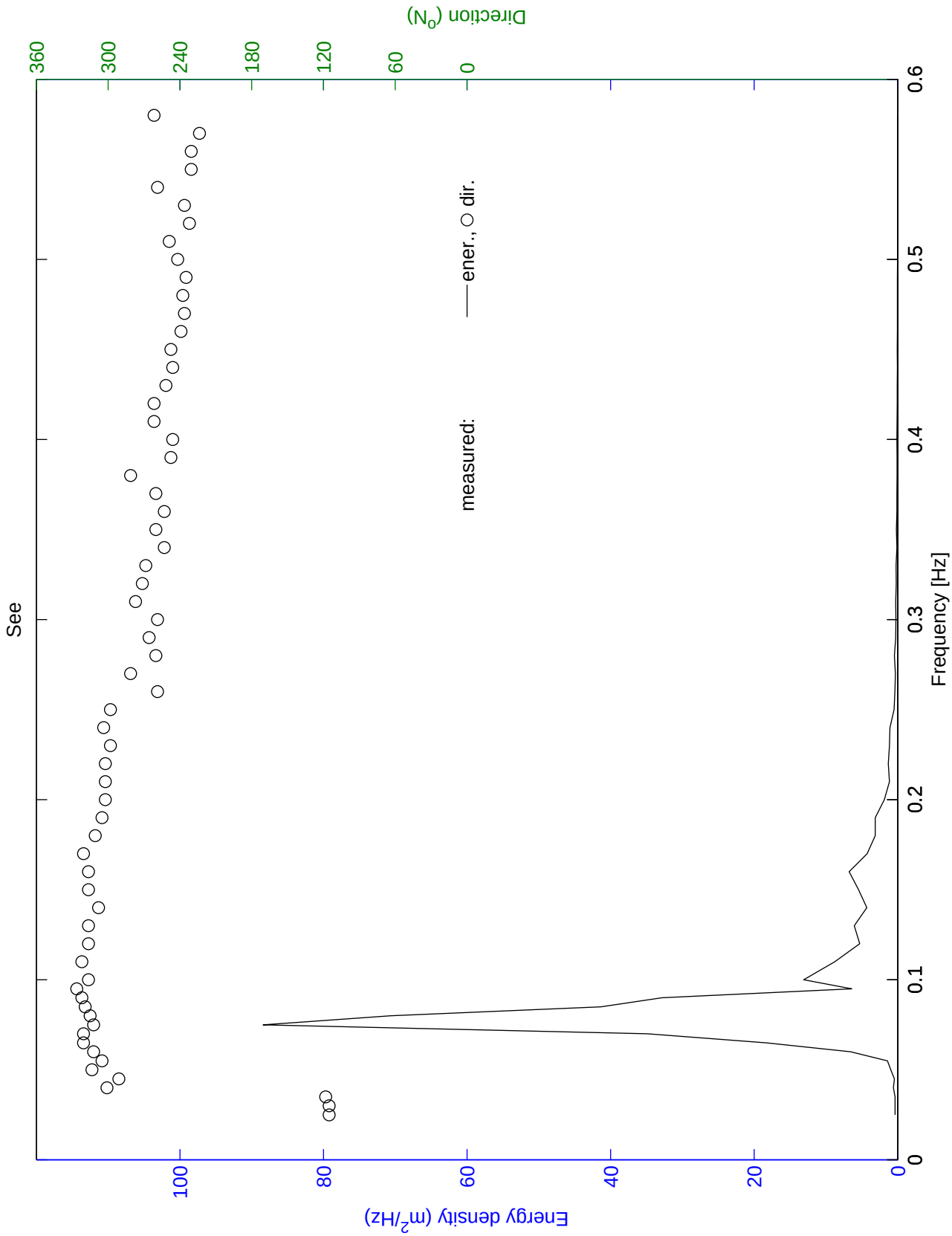

See, 3 Dec 1999 18:30		
	Norderney	
WL | DELFT HYDRAULICS	H4803	Fig. 2.8a

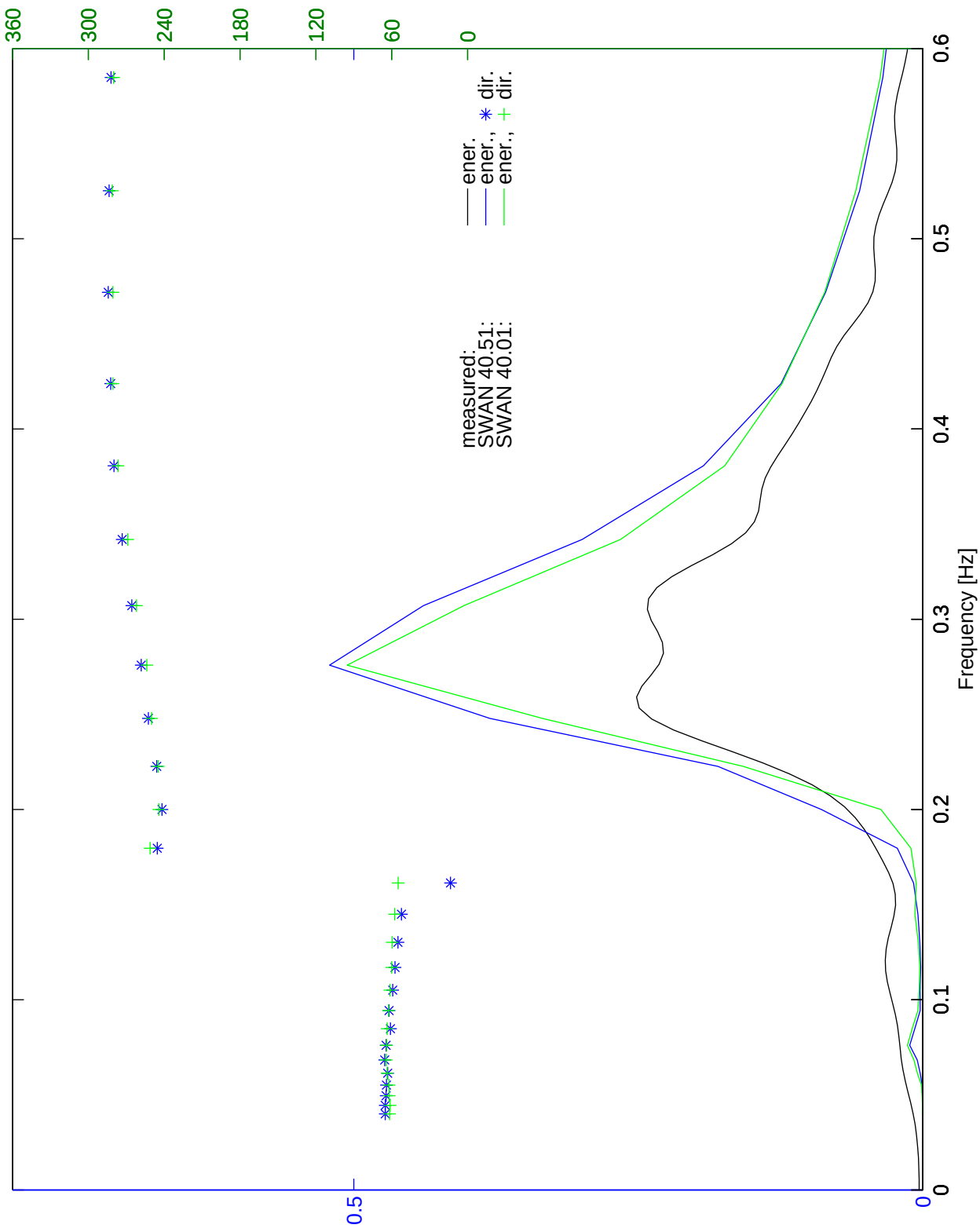

Kal, 3 Dec 1999 18:30		
	Norderney	
WL | DELFT HYDRAULICS	H4803	Fig. 2.8b

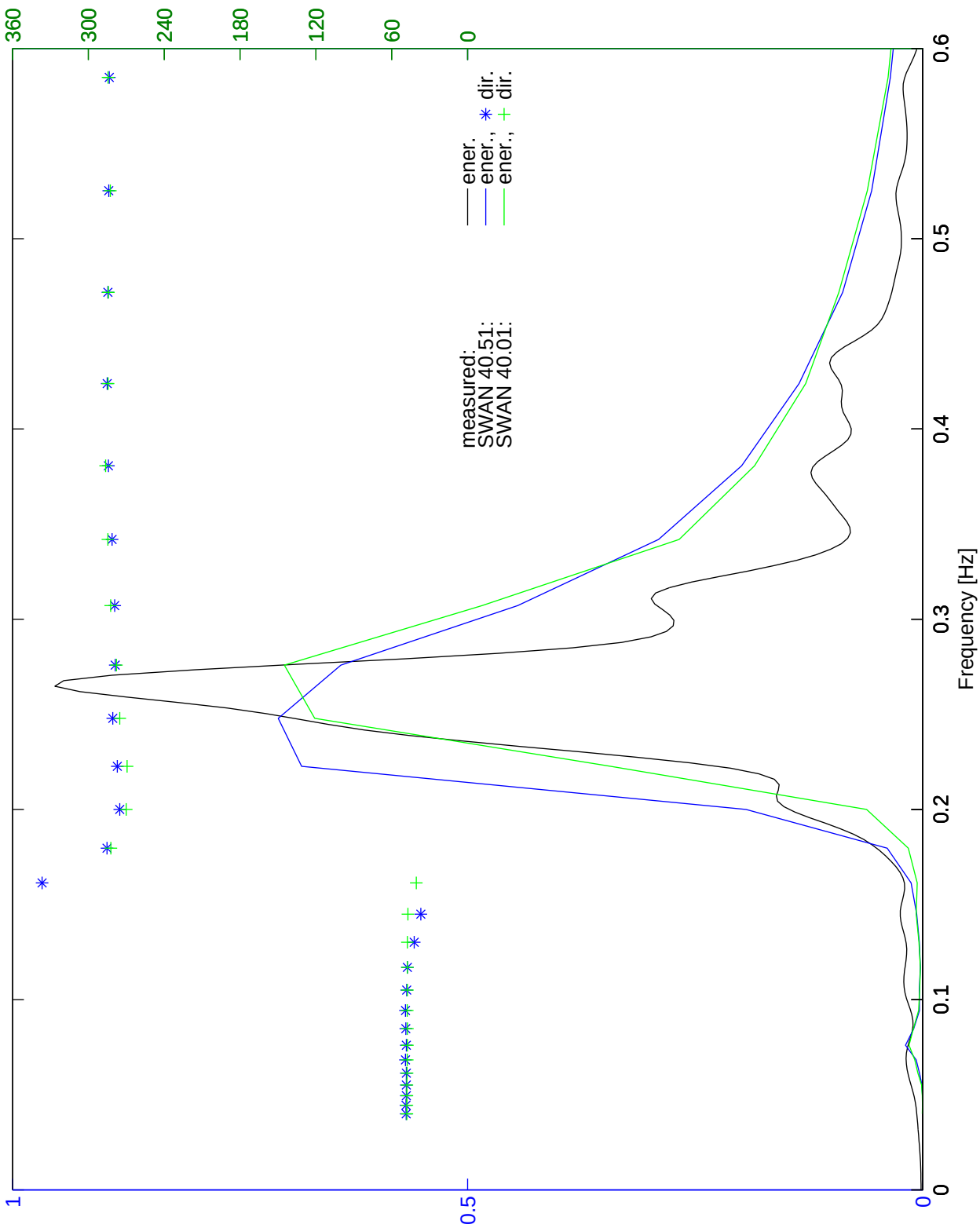

MB, 3 Dec 1999 18:30		
	Norderney	
WL | DELFT HYDRAULICS	H4803	Fig. 2.8c

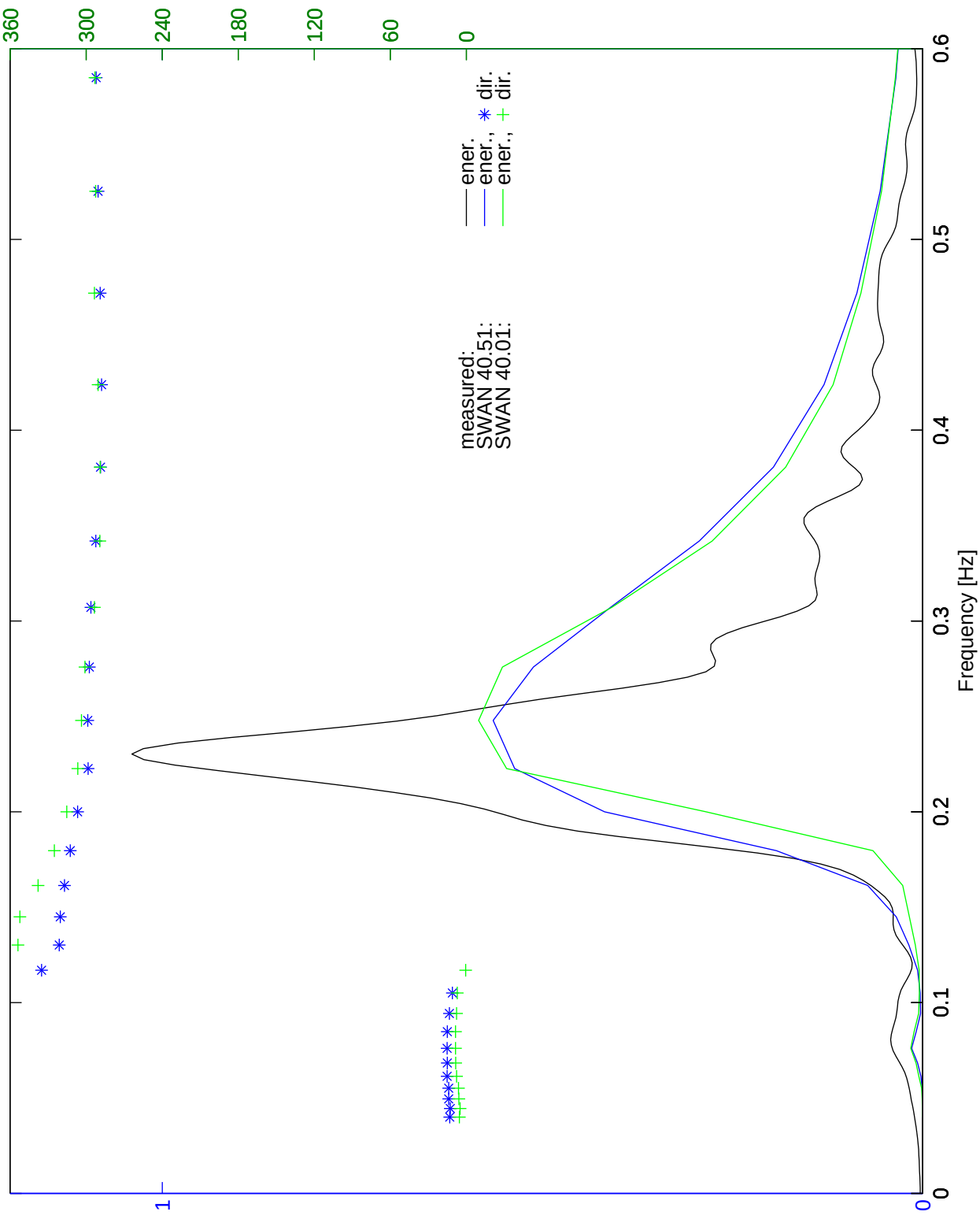

Wried, 3 Dec 1999 18:30		
	Norderney	
WL | DELFT HYDRAULICS	H4803	Fig. 2.8d

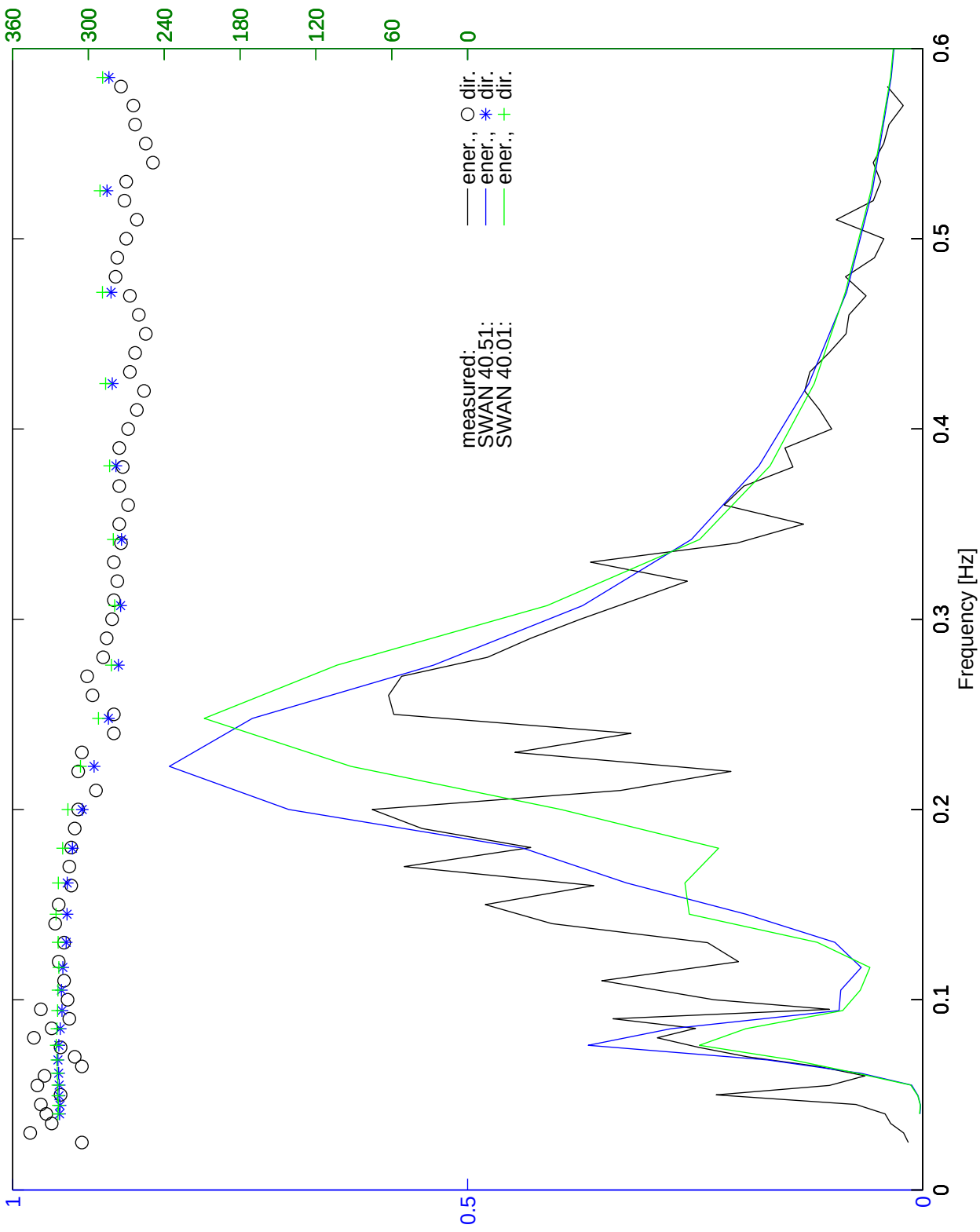

SGTNEY, 3 Dec 1999 18:30		
	Norderney	
WL | DELFT HYDRAULICS	H4803	Fig. 2.8e

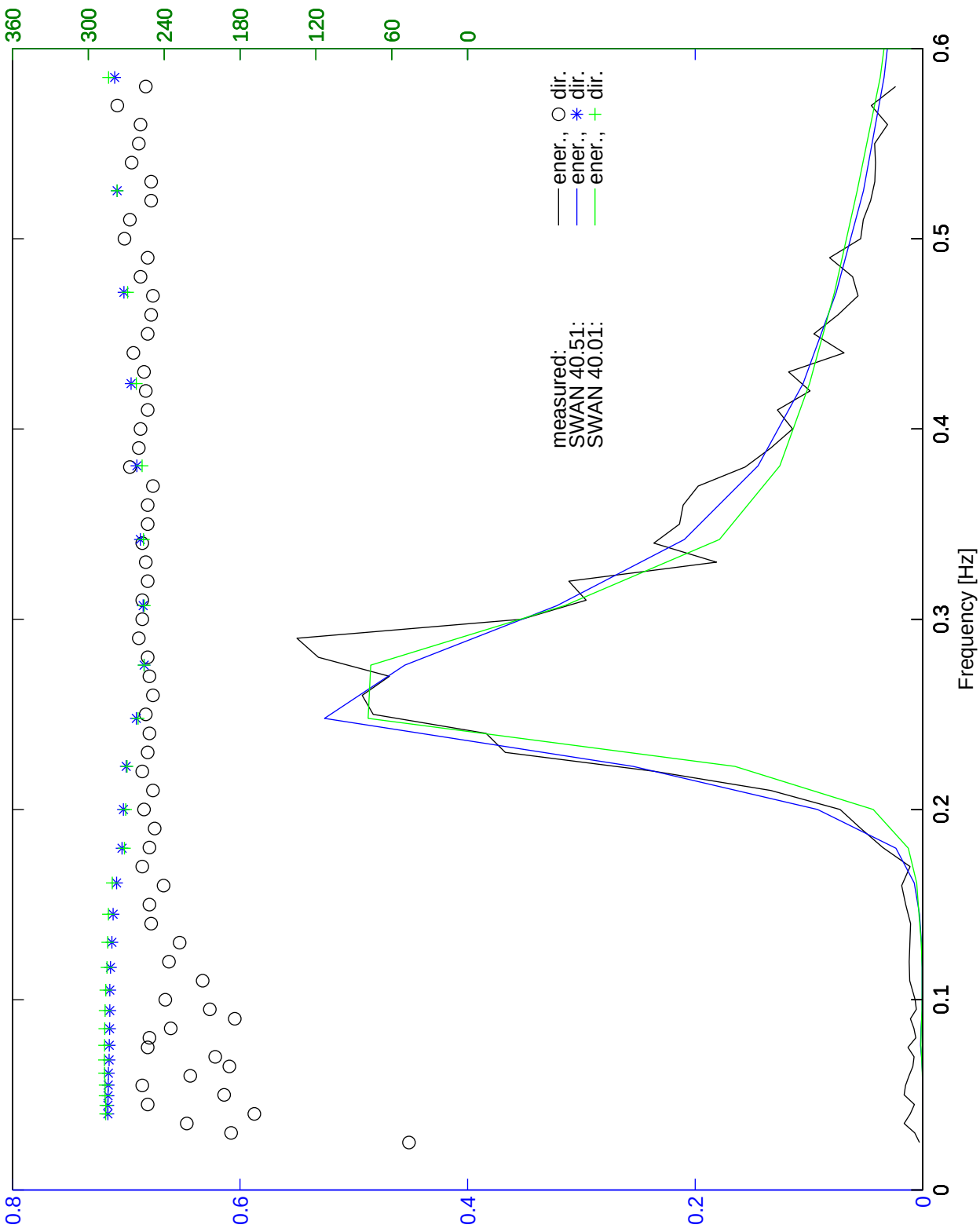

RIFFGAT, 3 Dec 1999 18:30		
	Norderney	
WL | DELFT HYDRAULICS	H4803	Fig. 2.8f

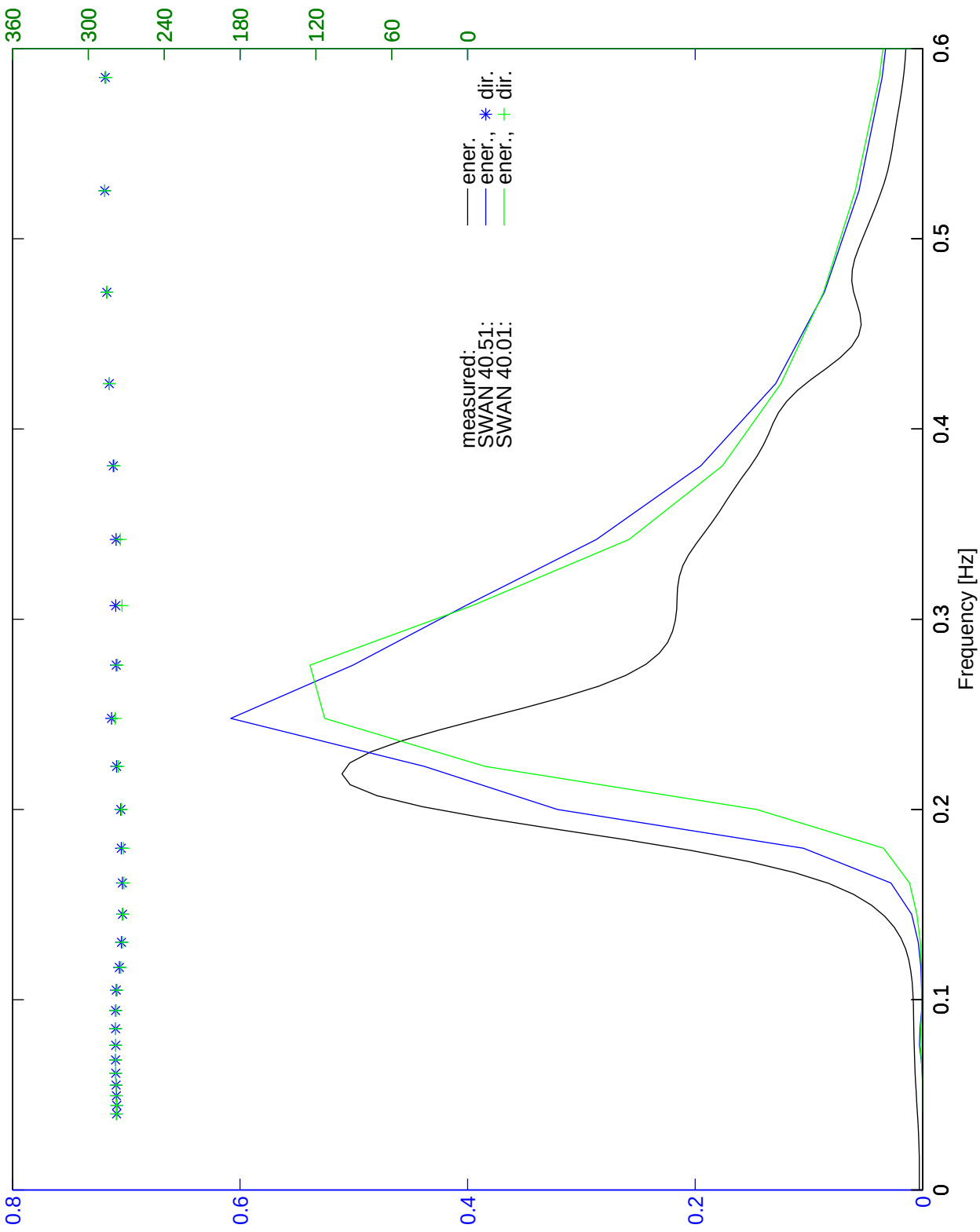

Luep, 3 Dec 1999 18:30		
	Norderney	
WL | DELFT HYDRAULICS	H4803	Fig. 2.8g

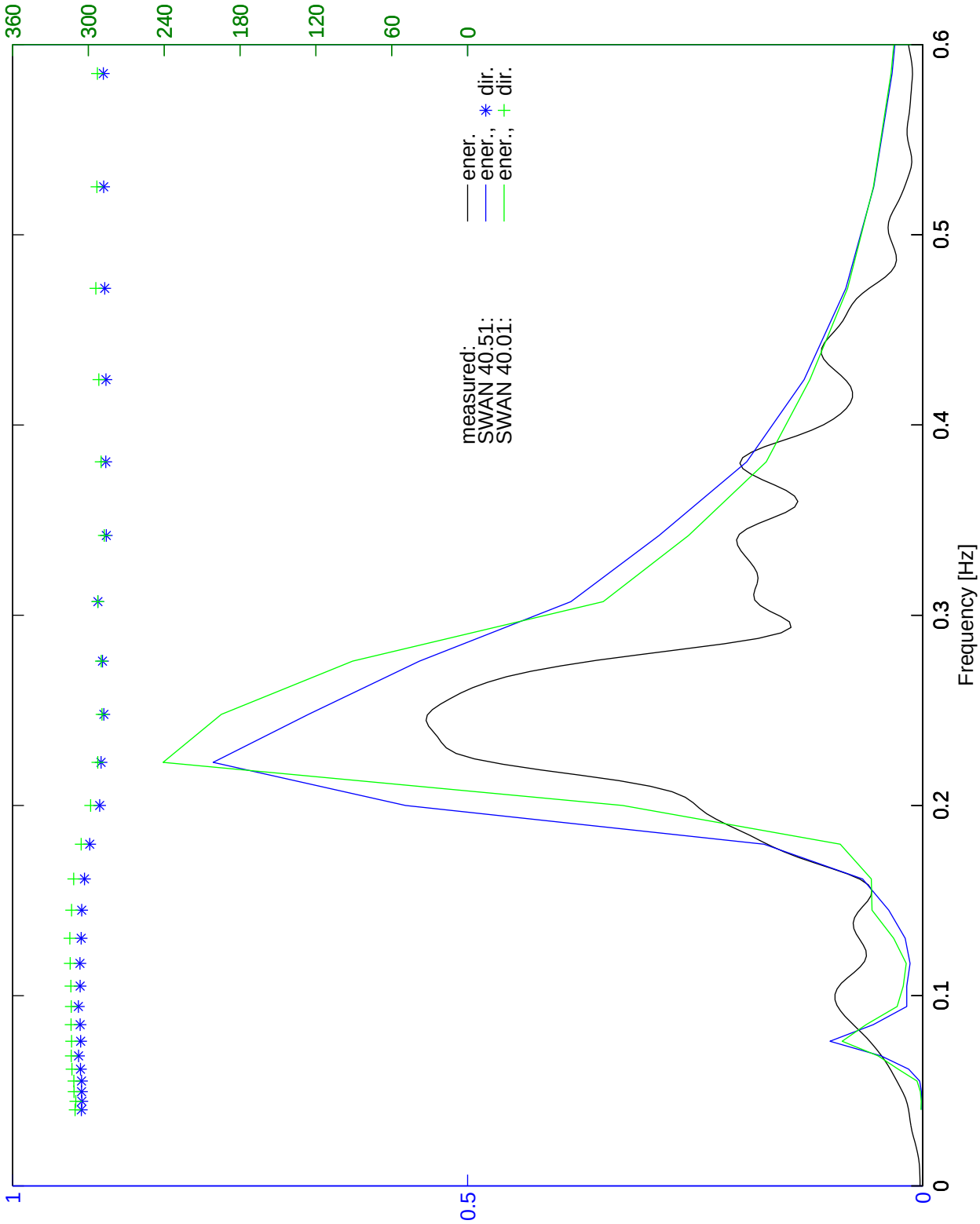

Oried, 3 Dec 1999 18:30		
	Norderney	
WL | DELFT HYDRAULICS	H4803	Fig. 2.8h

Loc 1, 5 Feb 1999 3:40		
	Norderney	
WL | DELFT HYDRAULICS	H4803	Fig. 2.9

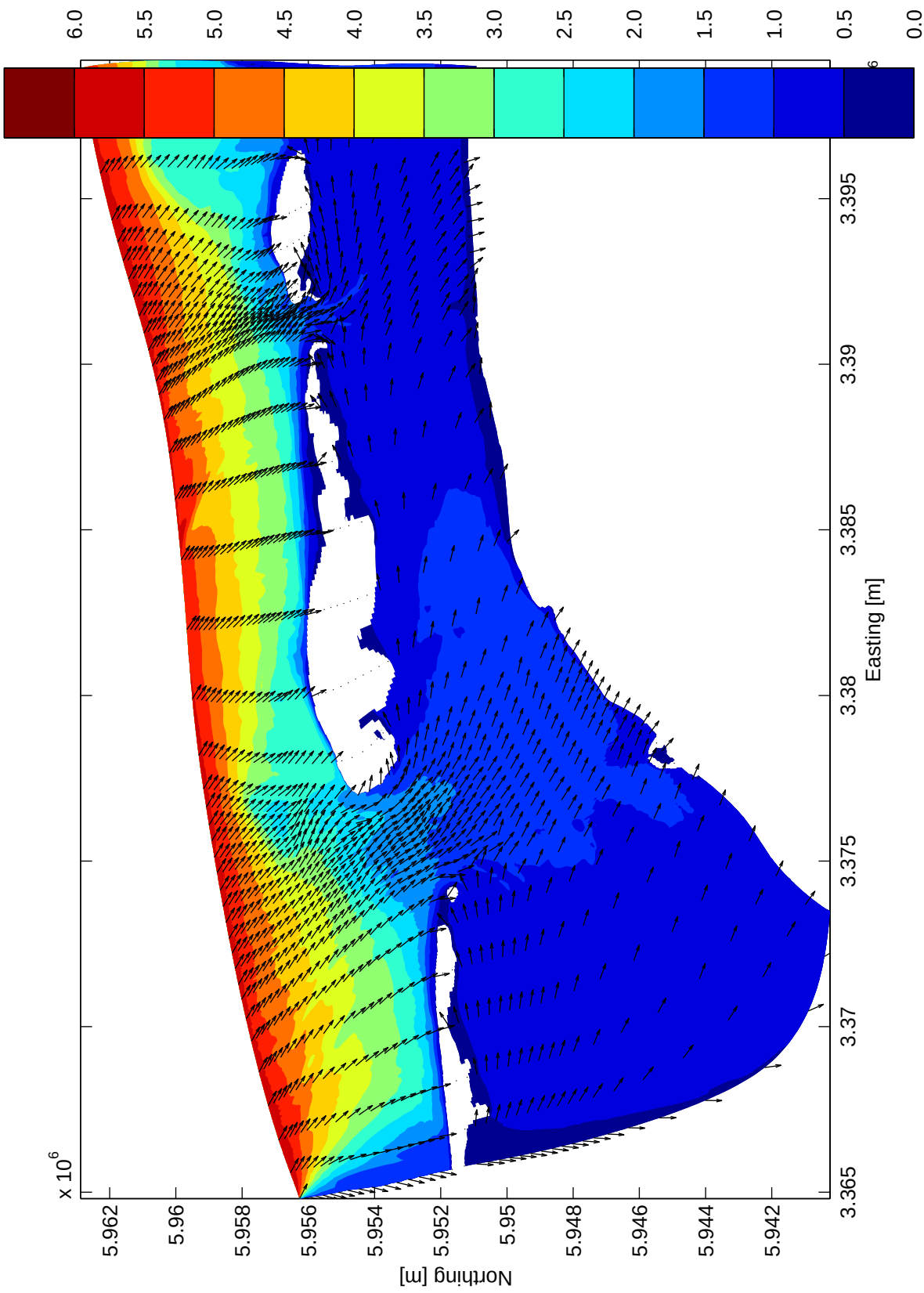

Significant wave height (m)	5 Feb 1999	SWAN 40.51
	Norderney	
WL | DELFT HYDRAULICS	H4803	Fig. 2.10a

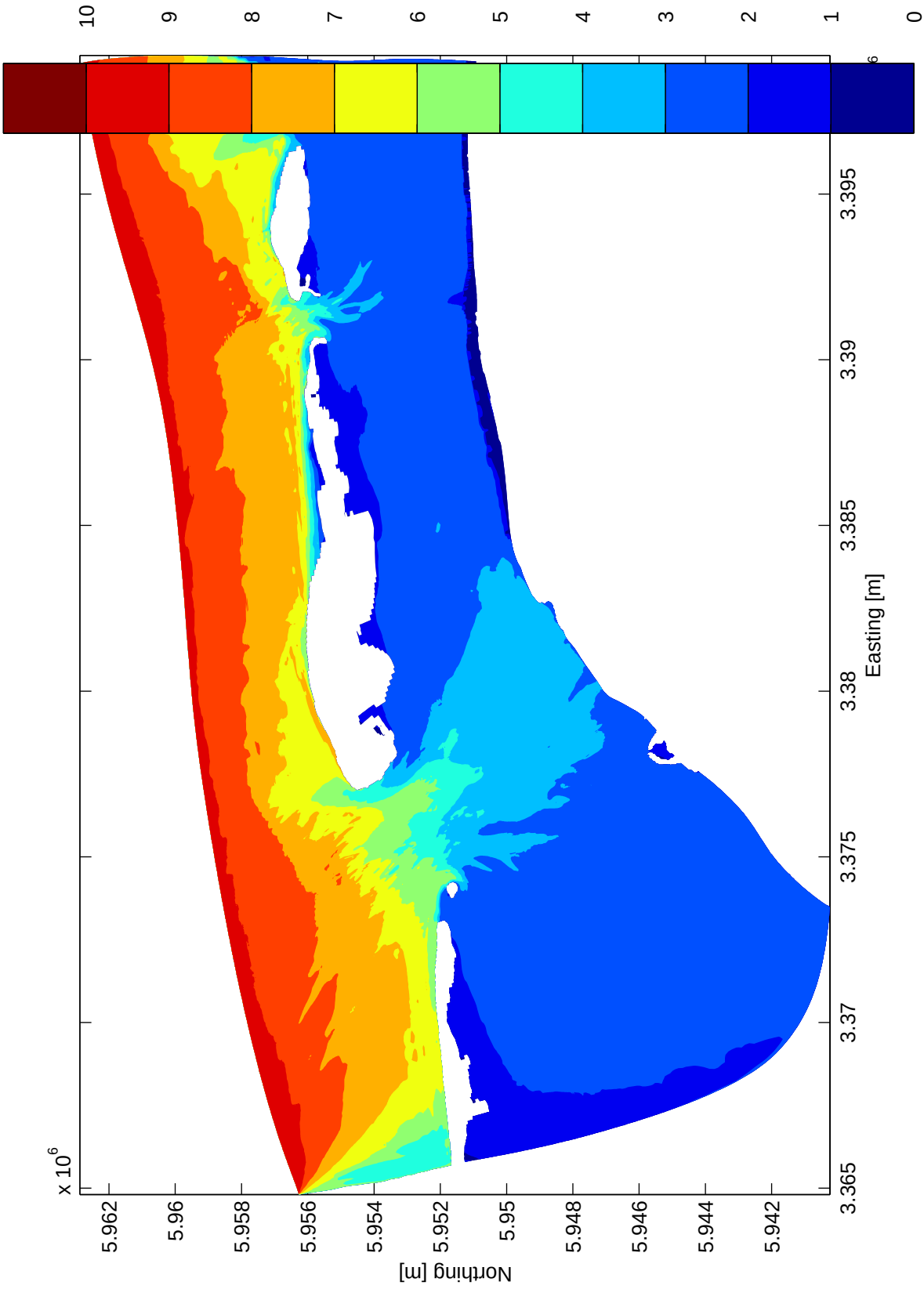

Mean wave period (T_{m01}, s)	5 Feb 1999	SWAN 40.51
	Norderney	
WL | DELFT HYDRAULICS	H4803	Fig. 2.10b

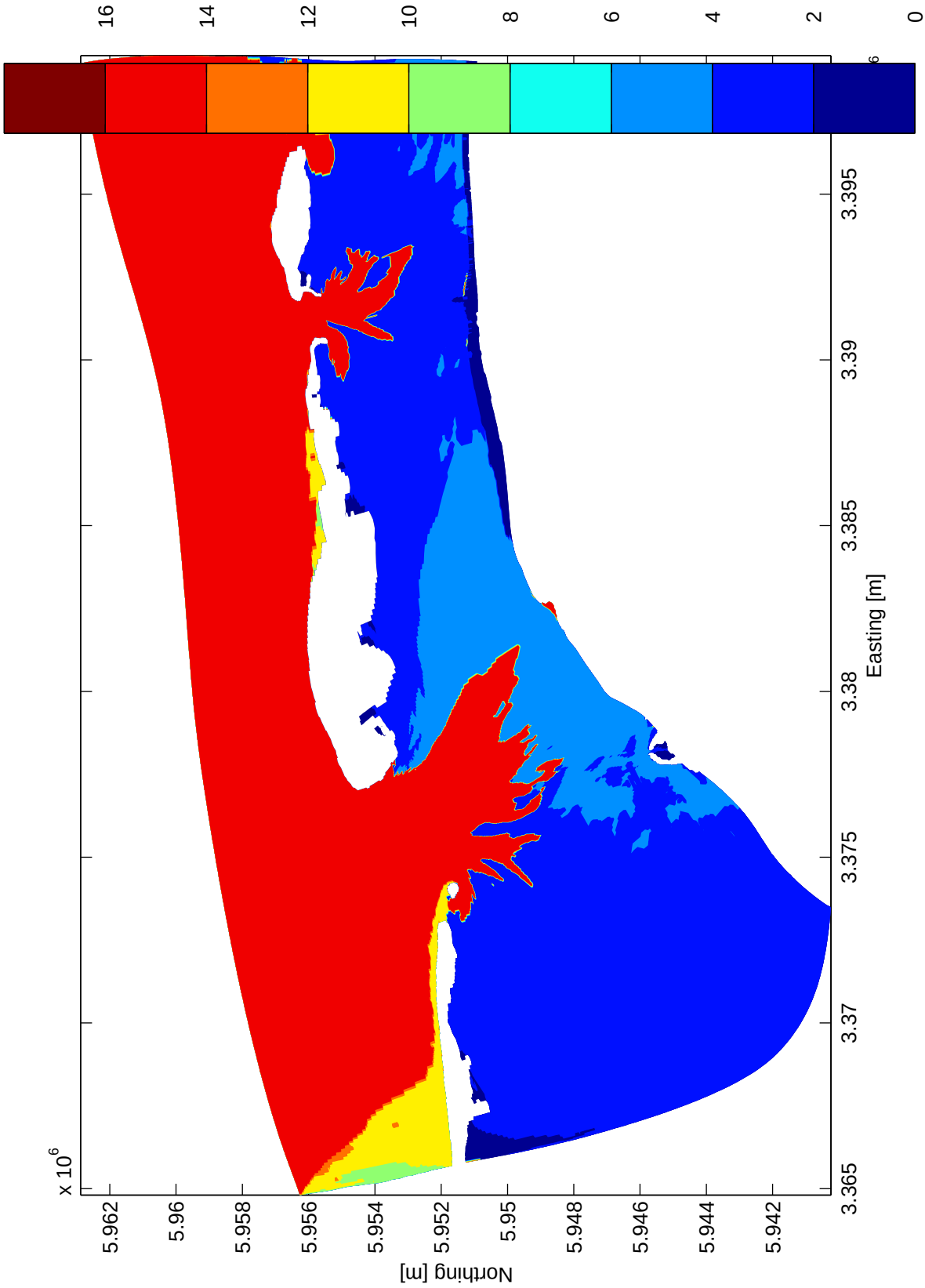

Peak period (s)	5 Feb 1999	SWAN 40.51
	Norderney	
WL | DELFT HYDRAULICS	H4803	Fig. 2.10c

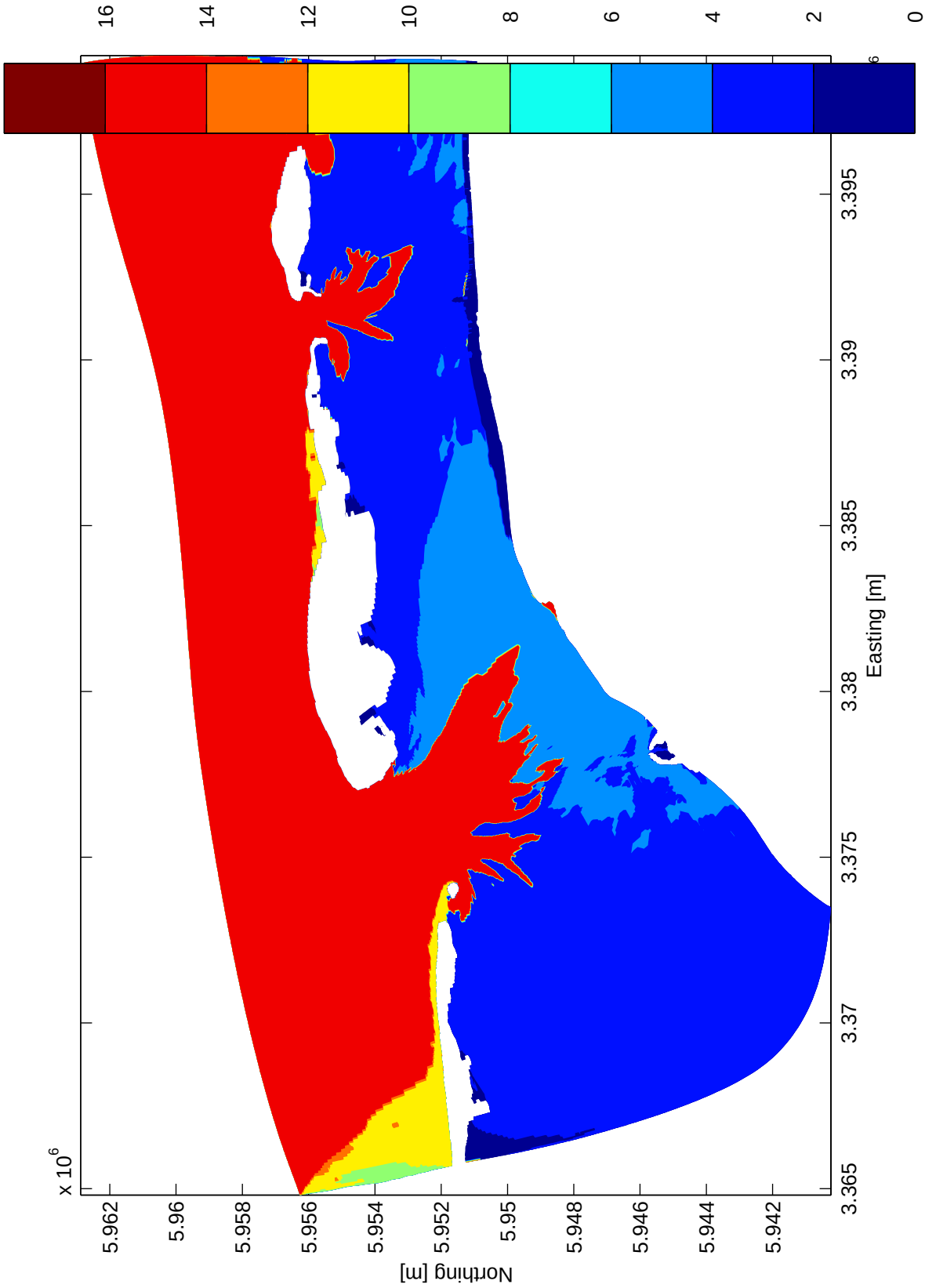

Peak period (s)	5 Feb 1999	SWAN 40.51
	Norderney	
WL | DELFT HYDRAULICS	H4803	Fig. 2.10c

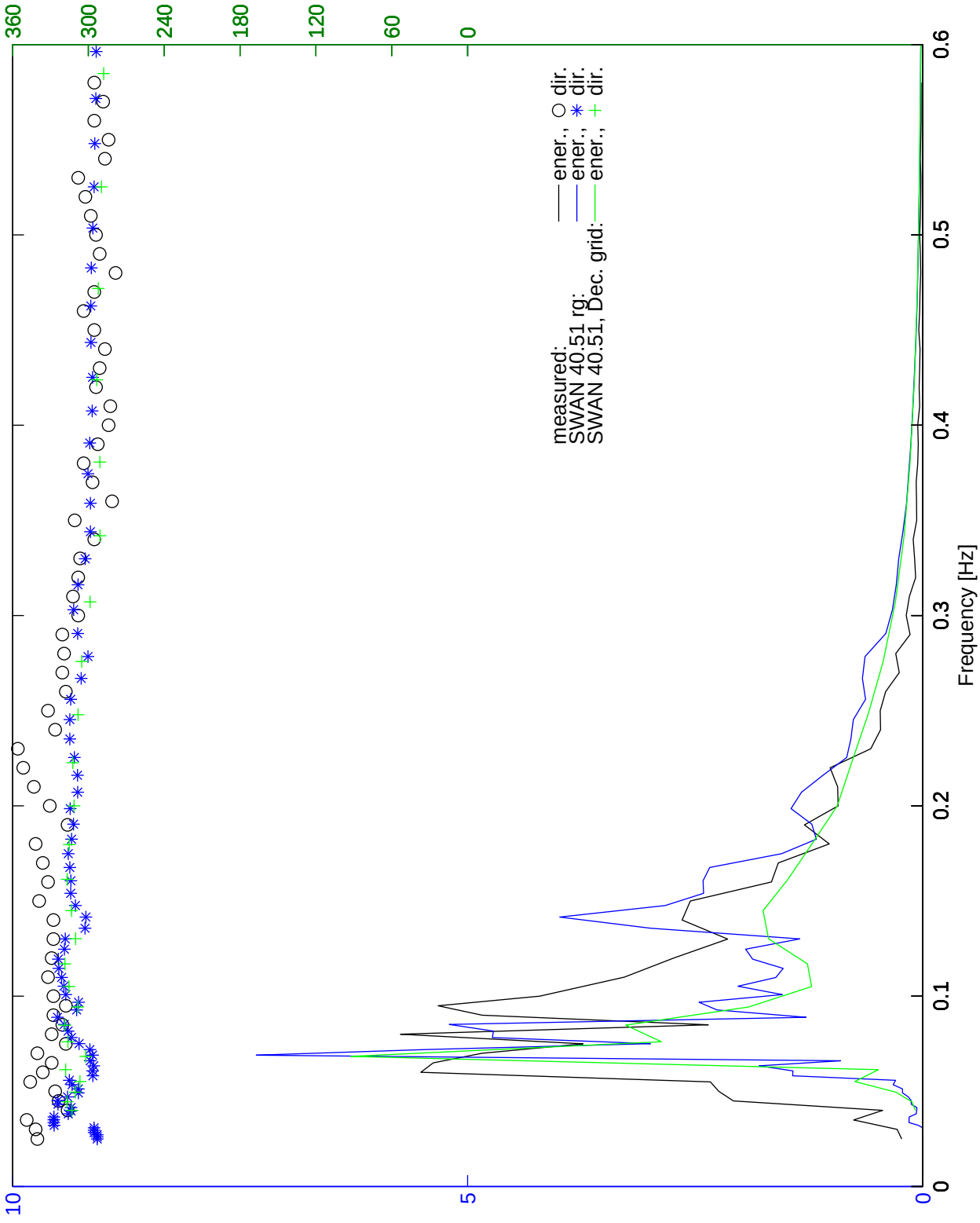

VST1, 5 Feb 1999 03:40		
	Norderney	
WL | DELFT HYDRAULICS	H4803	Fig. 2.11a

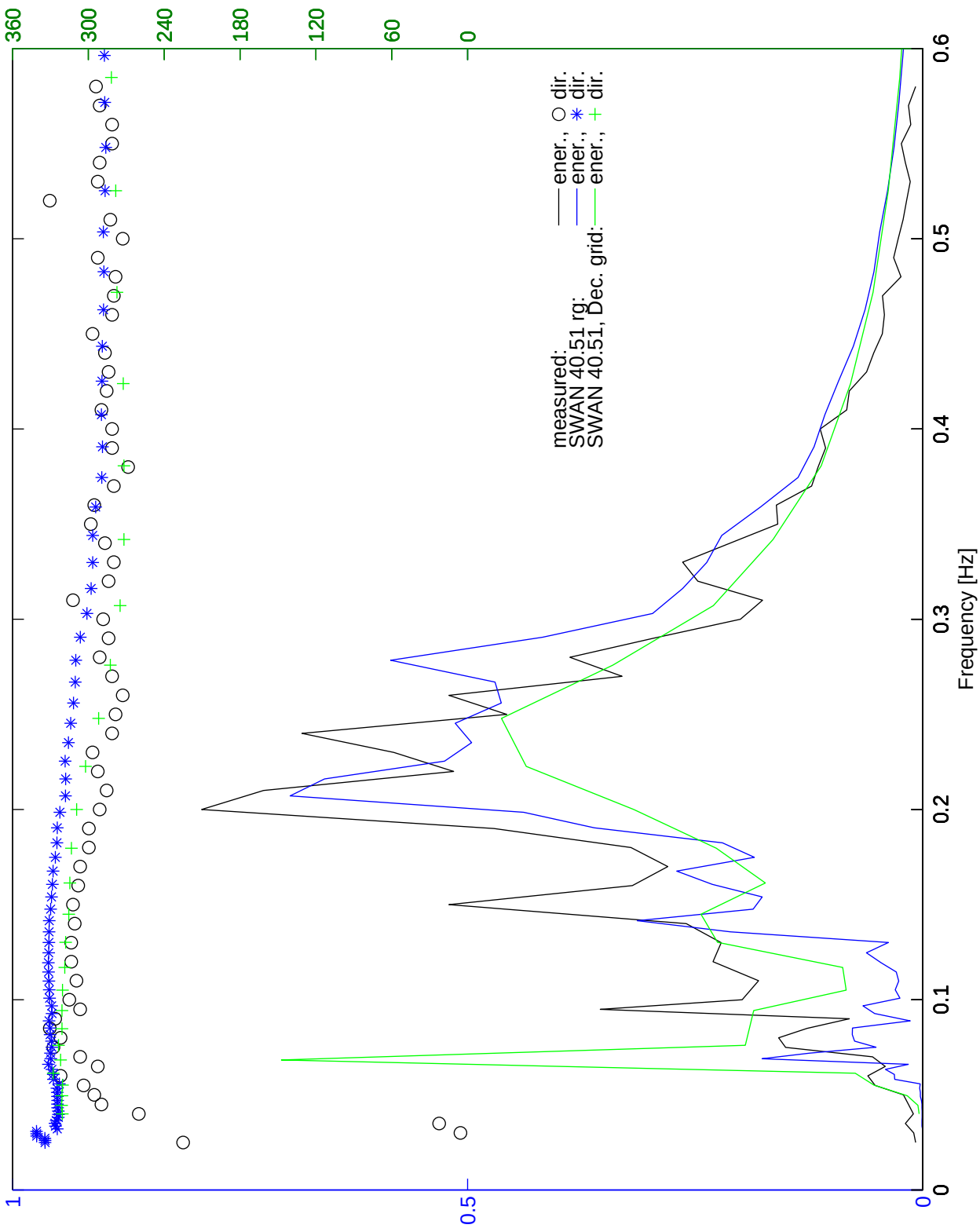

SGTNEY, 5 Feb 1999 03:40		
	Norderney	
WL | DELFT HYDRAULICS	H4803	Fig. 2.11b

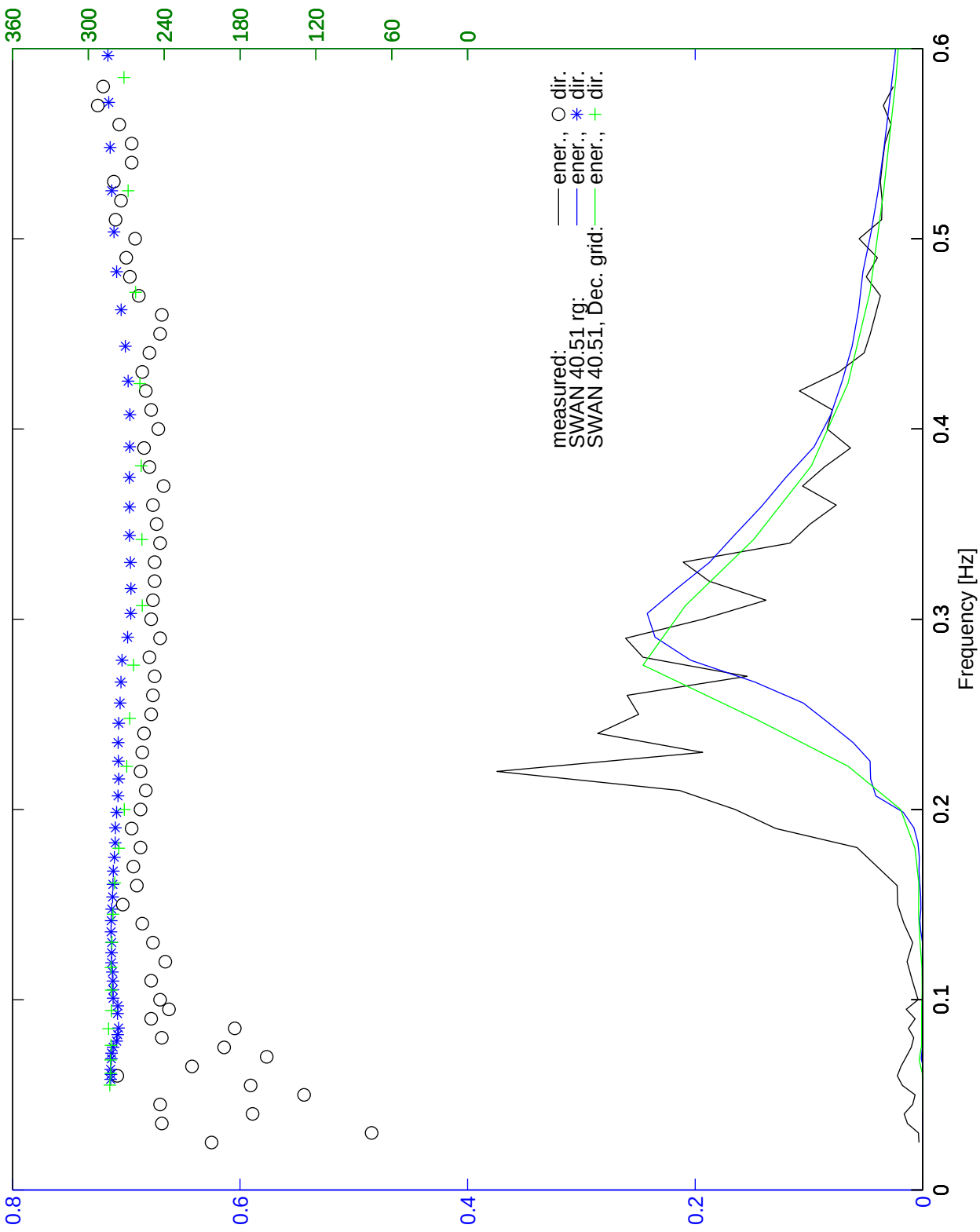

RIFFGAT, 5 Feb 1999 03:40		
	Norderney	
WL | DELFT HYDRAULICS	H4803	Fig. 2.11c

Plan view of Amelander Zeegat		
WL | DELFT HYDRAULICS	H4803.11	Fig. 3.1

Offshore wave buoys and wind stations

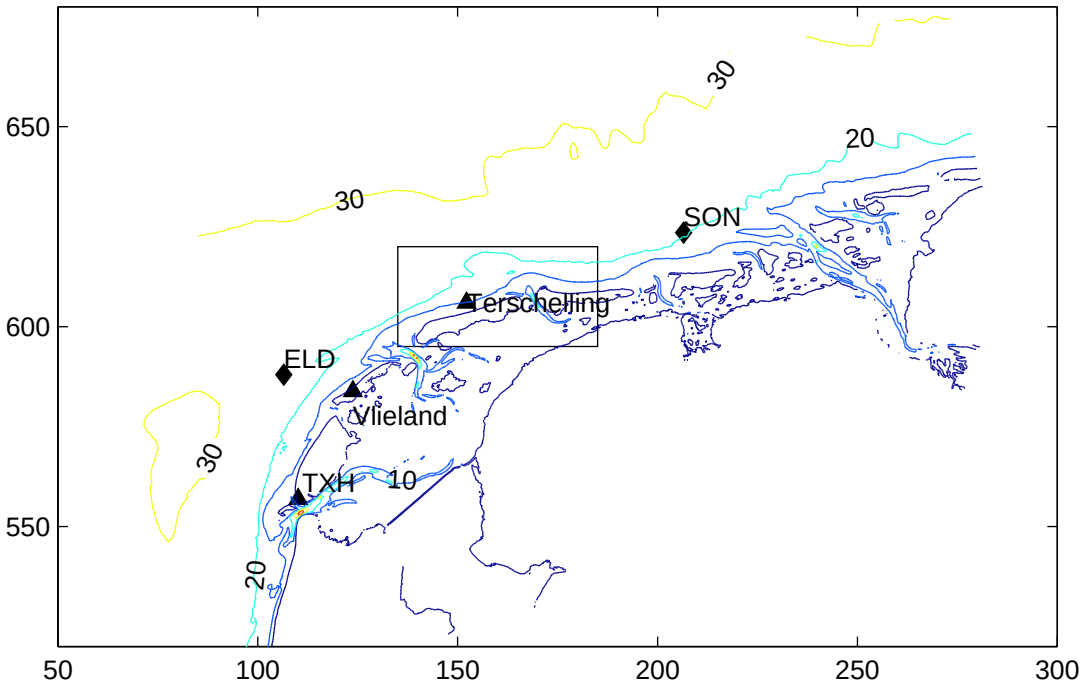

Nearshore wave buoys and water level stations

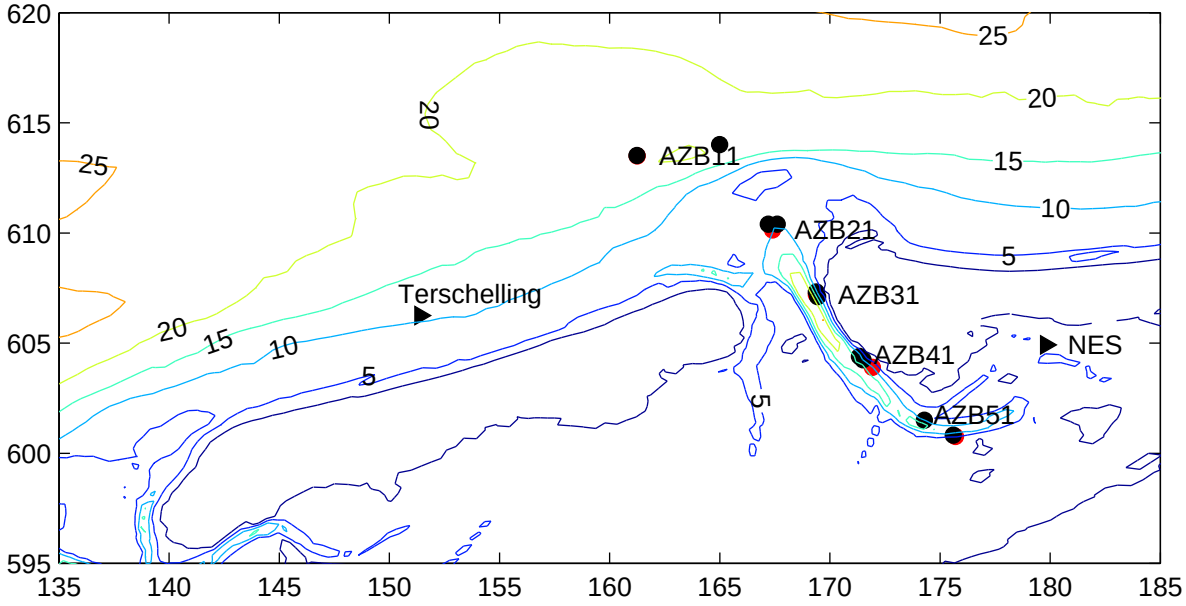

Location of measurement stations (water level, wind and waves)		
	Hindcast Amelander Zeegat	
WL | DELFT HYDRAULICS	H4803.11	Fig. 3.2

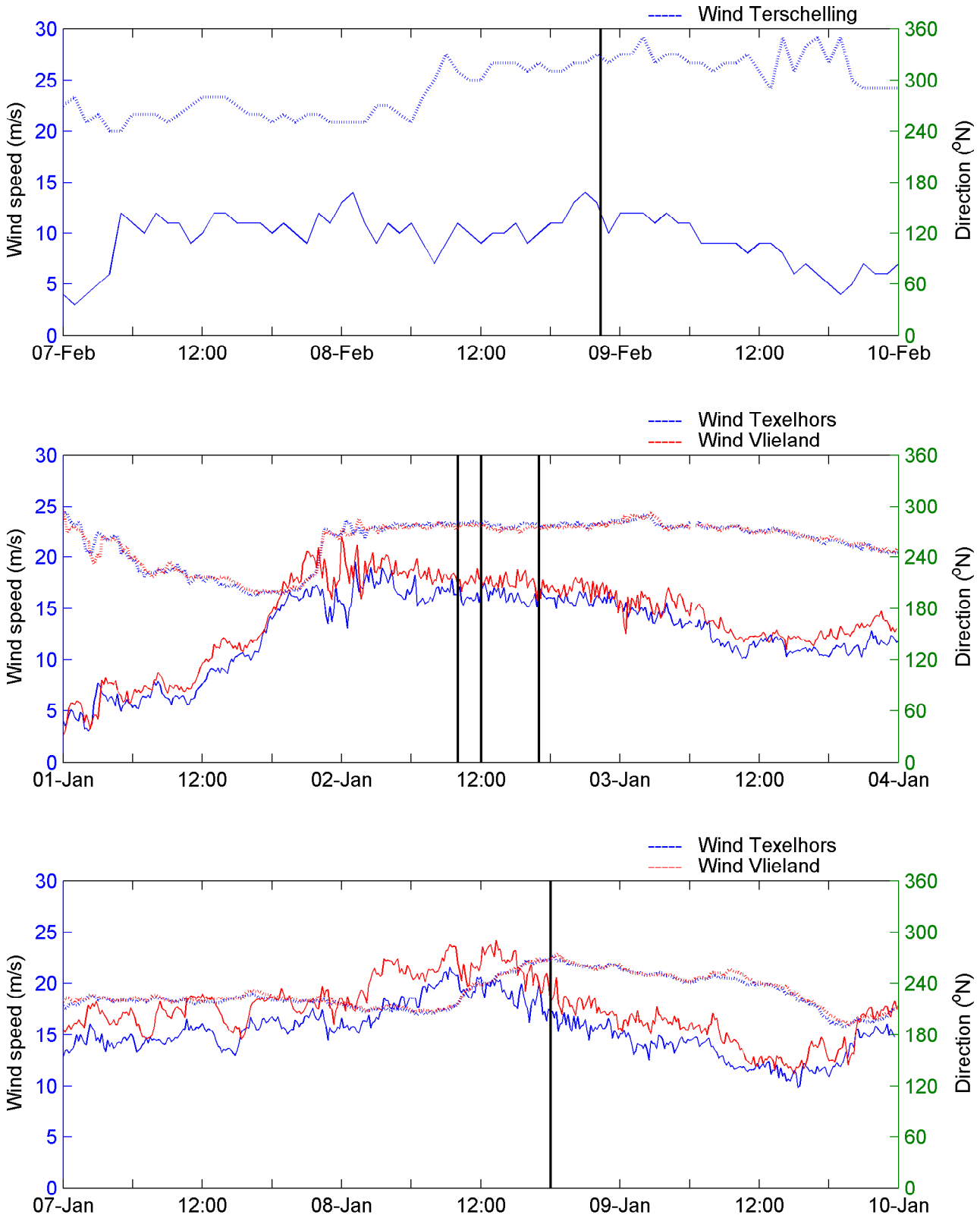

Time series of wind speed (solid line) and direction (dotted line) in stations Terschelling, Texelhors and Vlieland		
	Hindcast Ameland Inlet	
WL | DELFT HYDRAULICS	H4803.11	Fig. 3.3

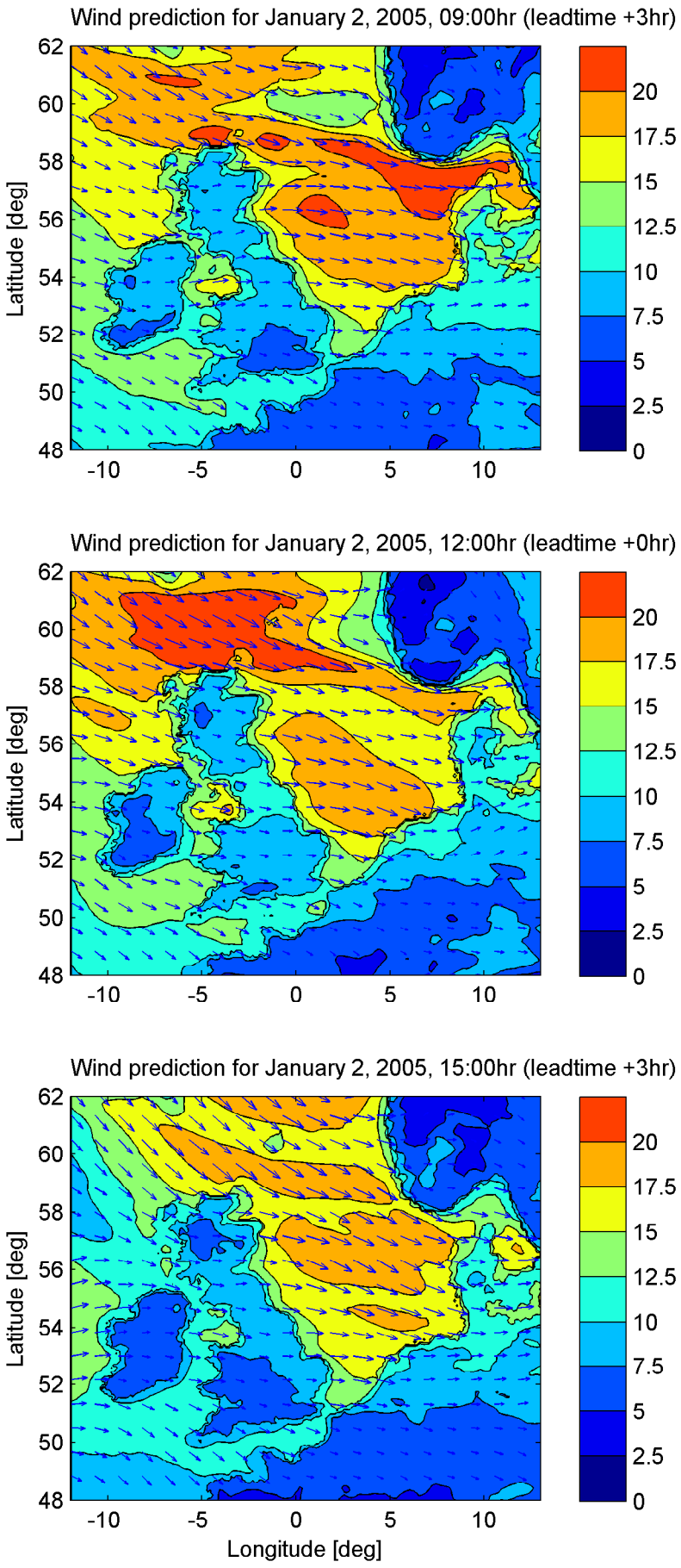

HIRLAM wind fields on January 2, 2005 at 09:00hr, 12:00hr and 15:00hr respectively

Hindcast Ameland Inlet

WL | DELFT HYDRAULICS

H4803.11

Fig. 3.4a

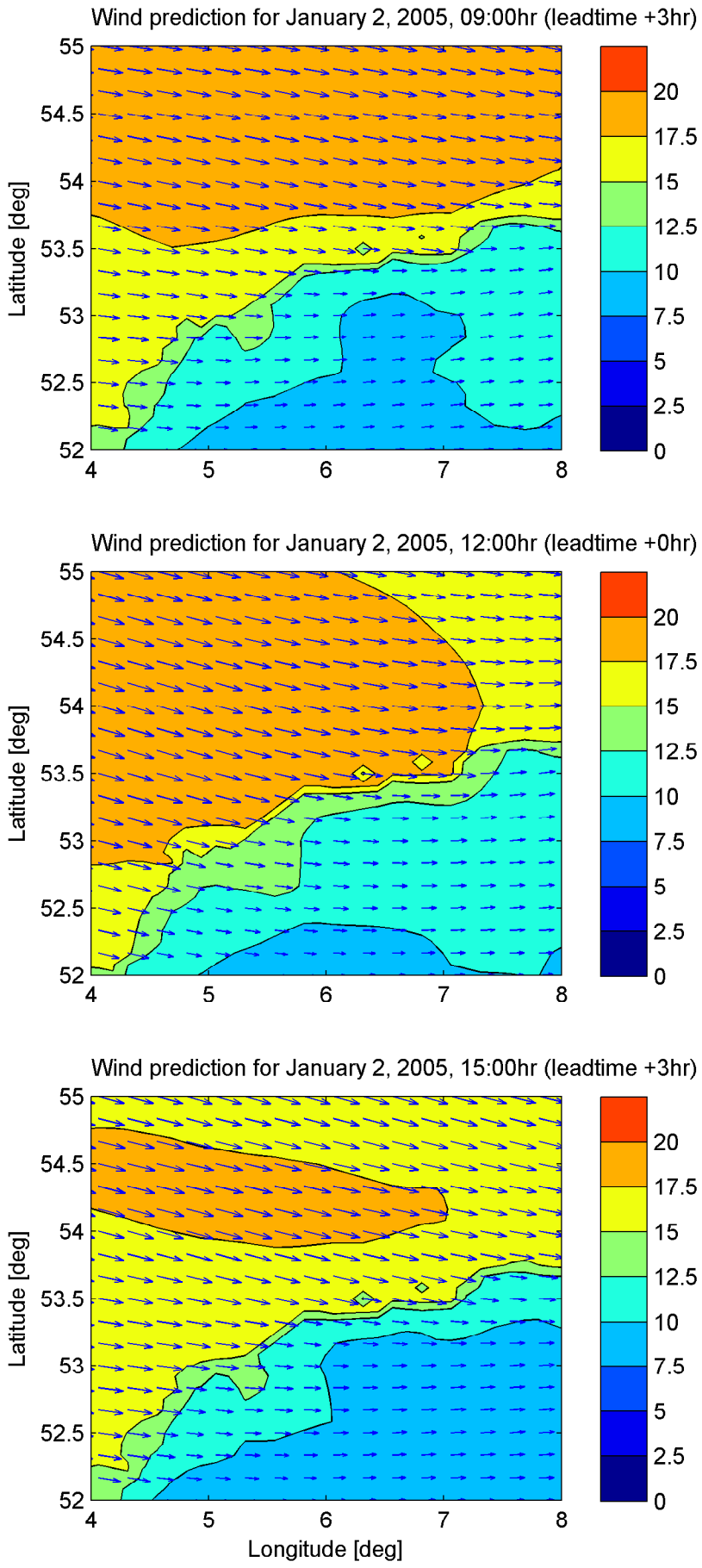

HIRLAM wind fields on January 2, 2005 at 09:00hr, 12:00hr and 15:00hr respectively (zoomed in on Waddenzee Area)

Hindcast Ameland Inlet

WL | DELFT HYDRAULICS

H4803.11

Fig. 3.4b

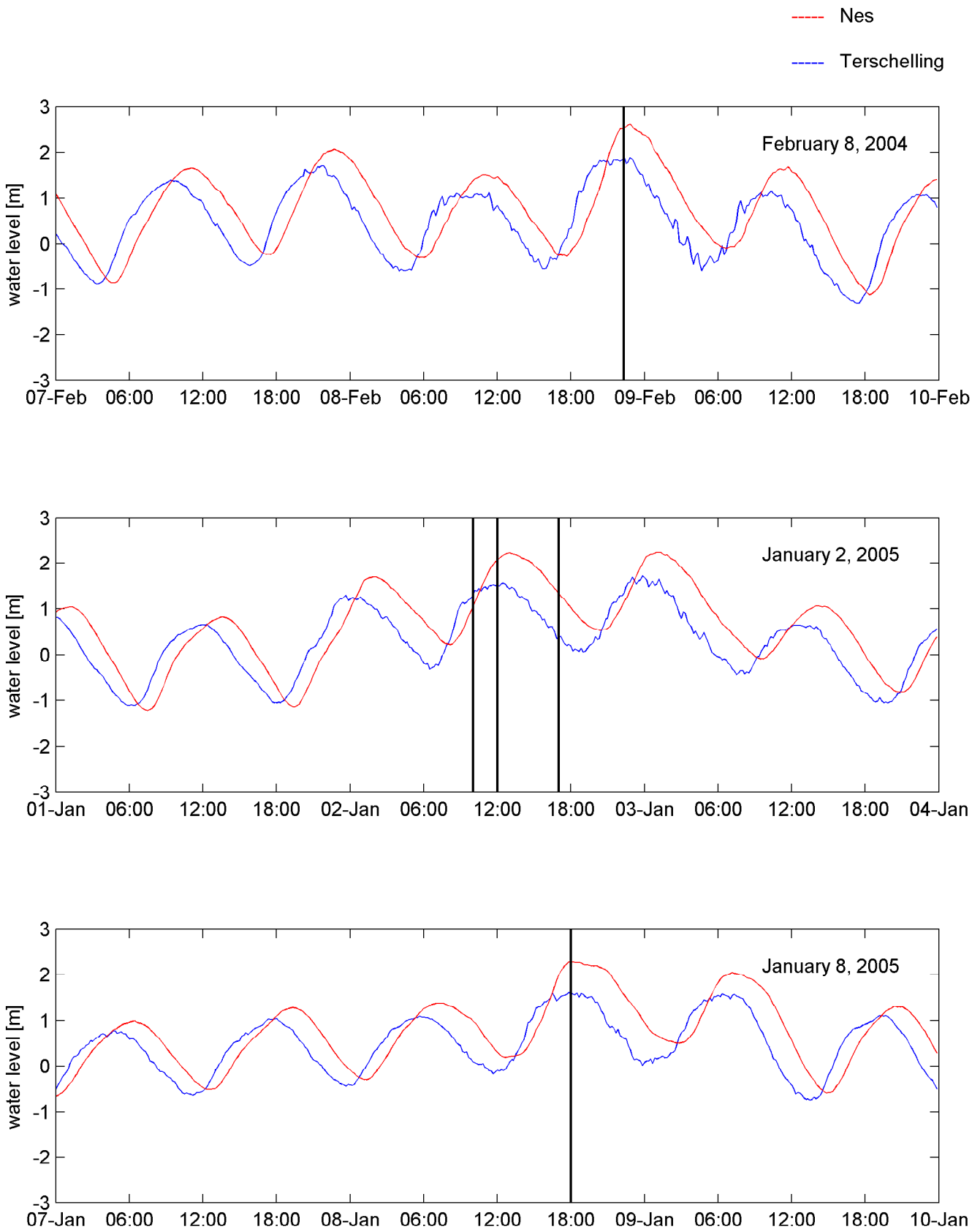

Time series of water level in stations Terschelling and Nes		
	Hindcast Ameland Inlet	
WL | DELFT HYDRAULICS	H4803.11	Fig. 3.5

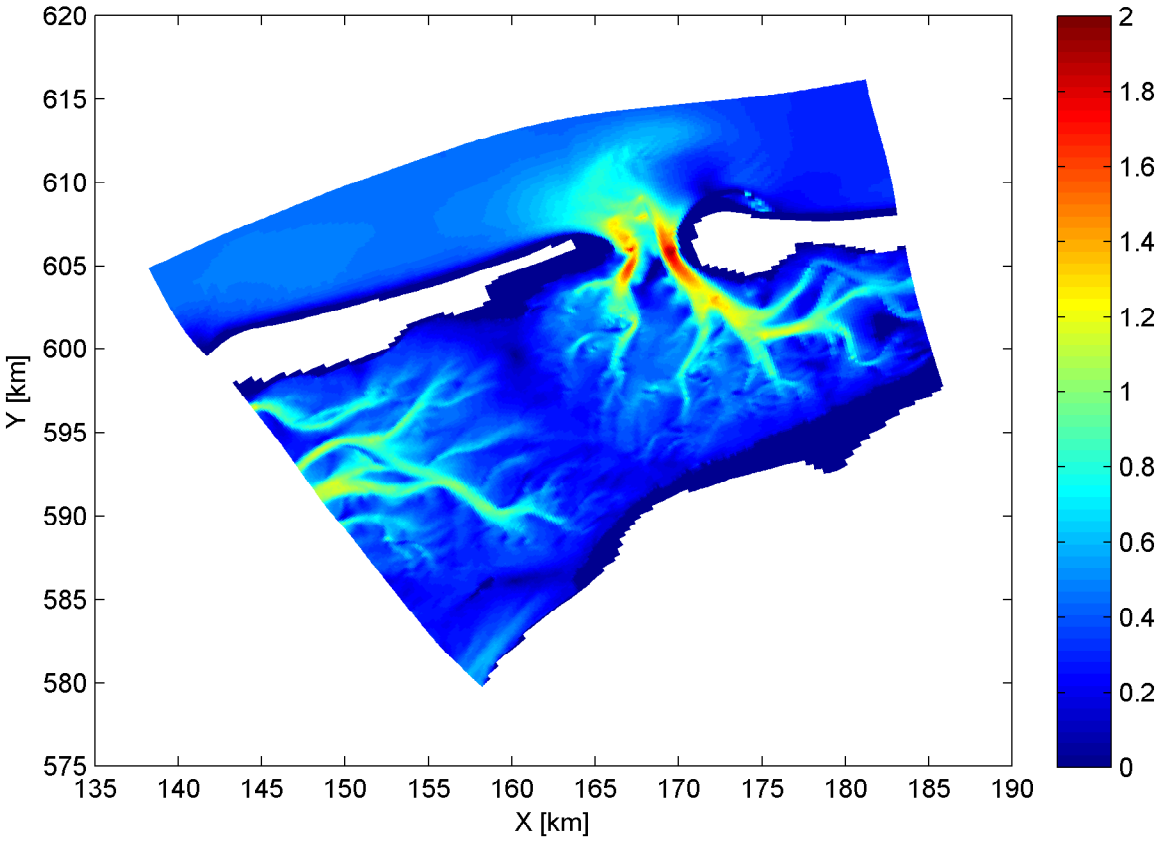

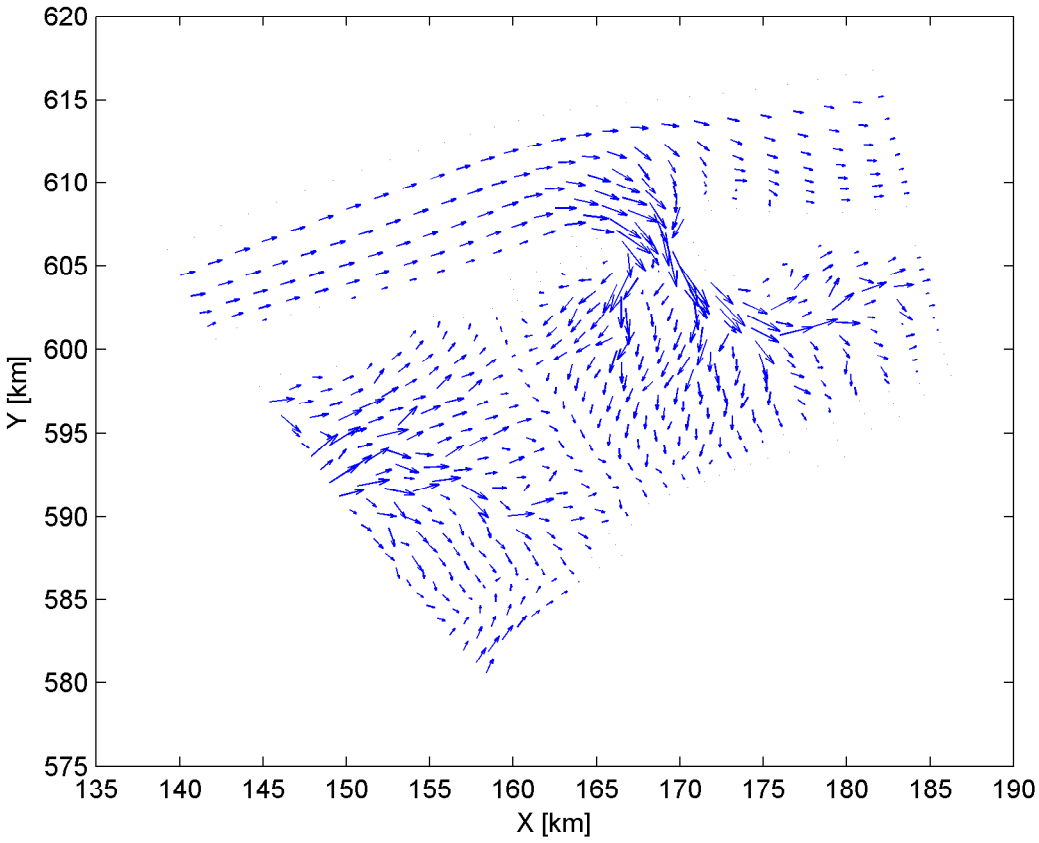

Spatial distribution of magnitude (upper panel) and direction (lower panel) of current velocity, based on WAQUA computation	20050102	09:30hr
	Hindcast Ameland Inlet	
WL | DELFT HYDRAULICS	H4803.11	Fig. 3.6

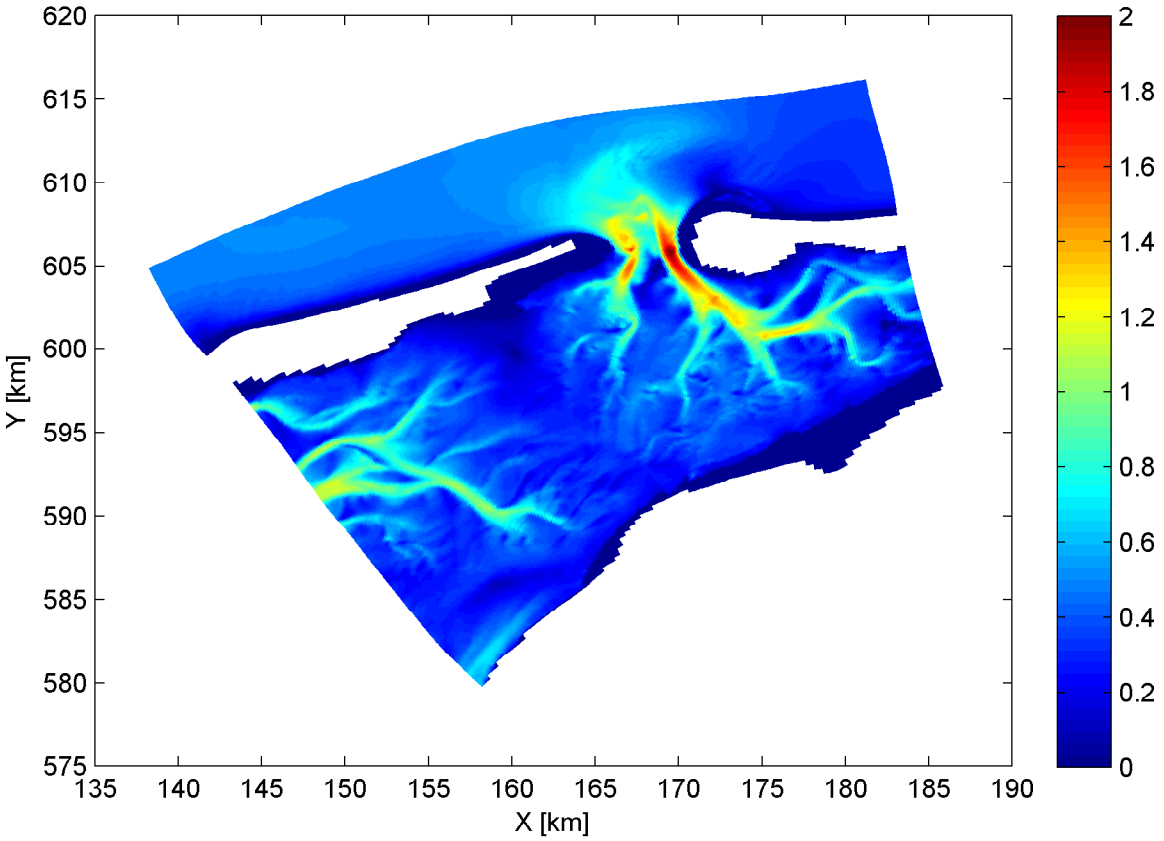

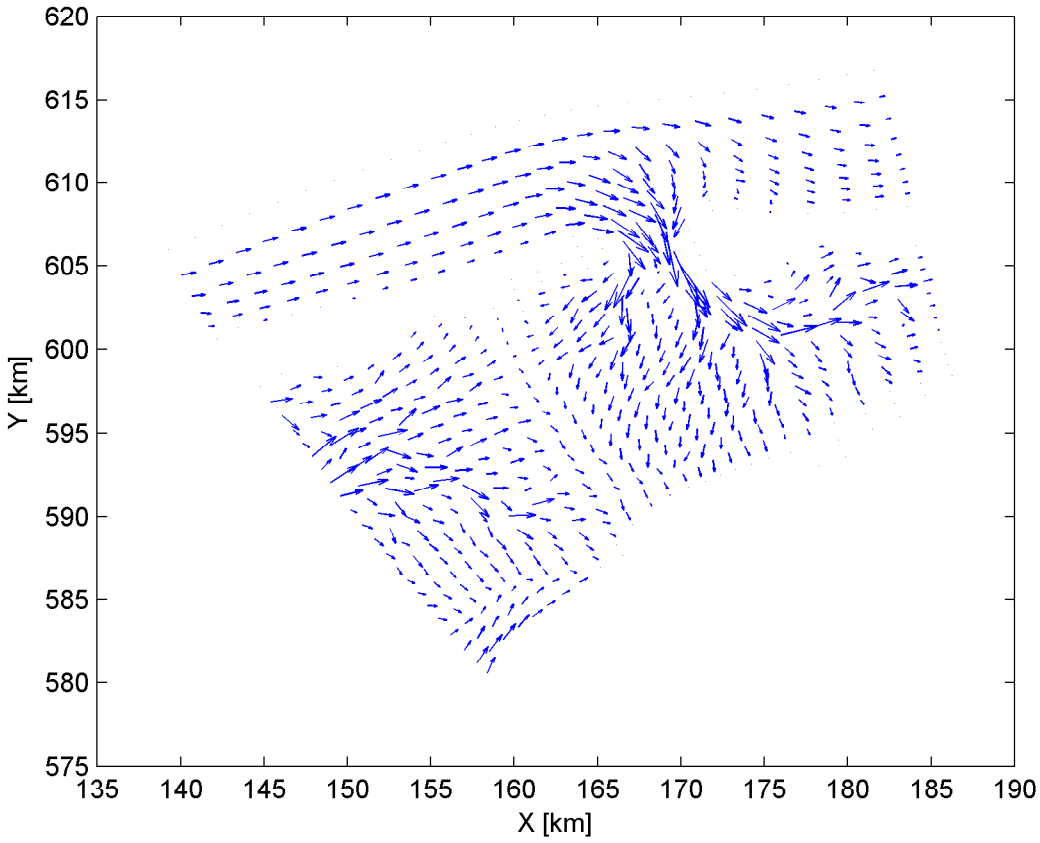

Spatial distribution of magnitude (upper panel) and direction (lower panel) of current velocity, based on WAQUA computation	20050102	10:00hr
	Hindcast Ameland Inlet	
WL | DELFT HYDRAULICS	H4803.11	Fig. 3.7

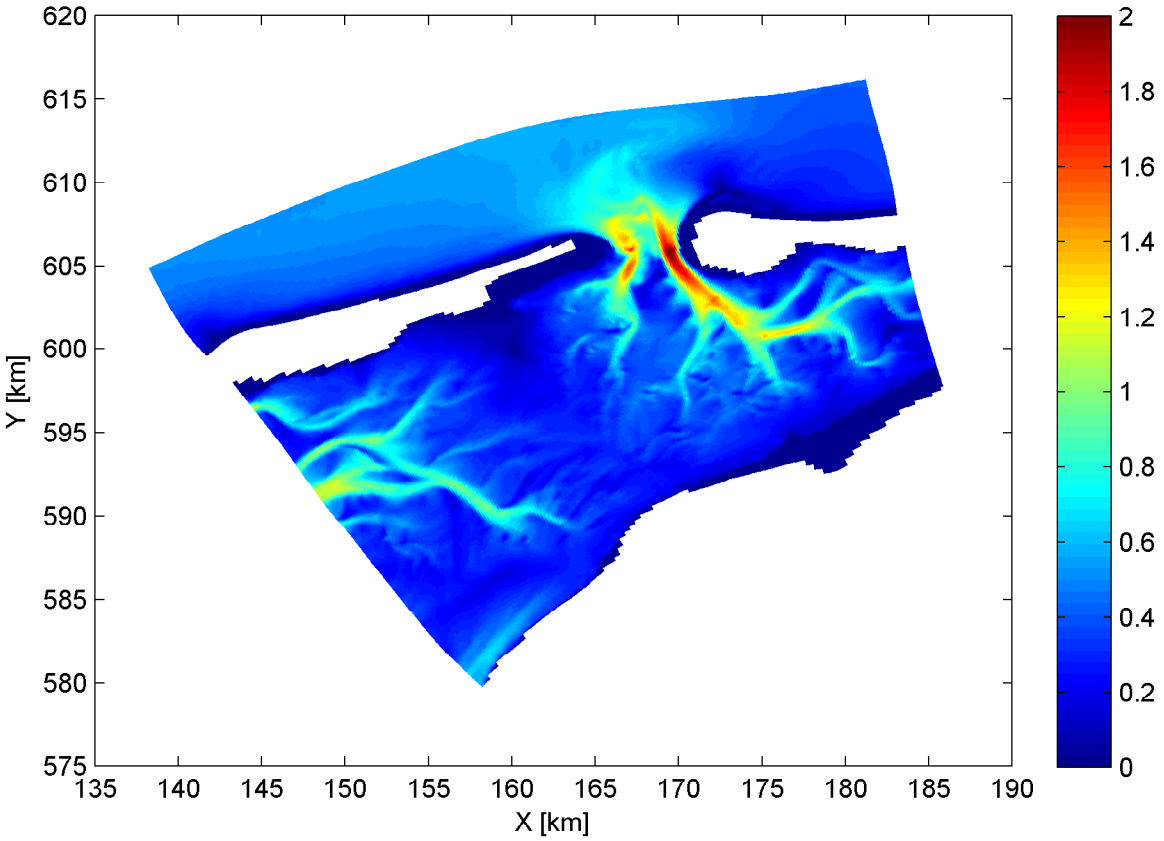

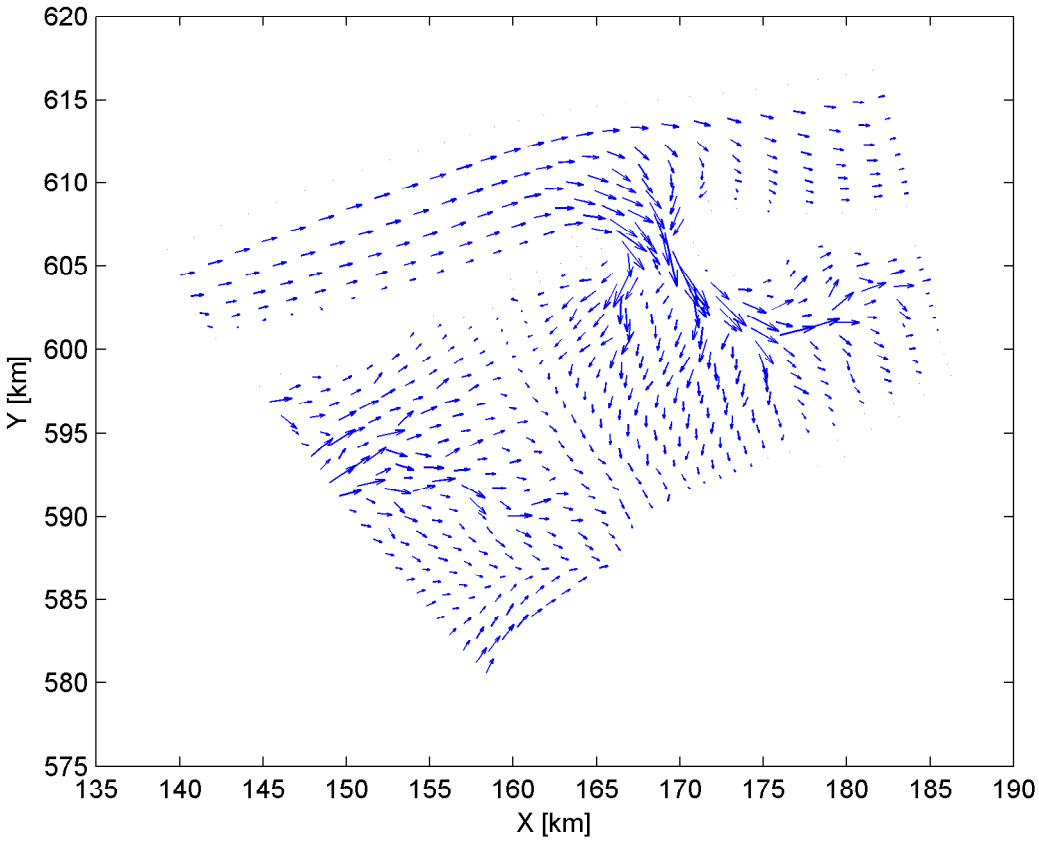

Spatial distribution of magnitude (upper panel) and direction (lower panel) of current velocity, based on WAQUA computation	20050102	10:30hr
	Hindcast Ameland Inlet	
WL | DELFT HYDRAULICS	H4803.11	Fig. 3.8

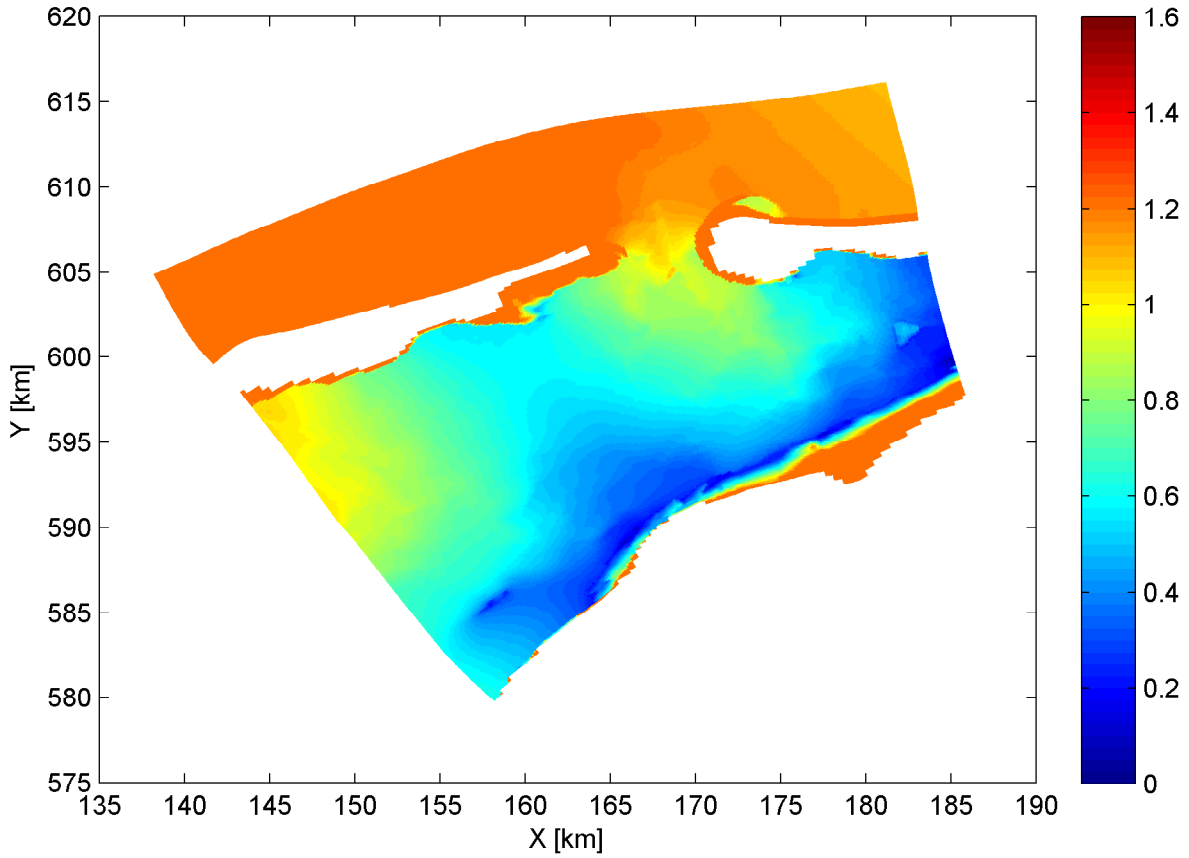

Spatial distribution of water level based on WAQUA computation	20050102	09:30hr
	Hindcast Ameland Inlet	
WL | DELFT HYDRAULICS	H4803.11	Fig. 3.9

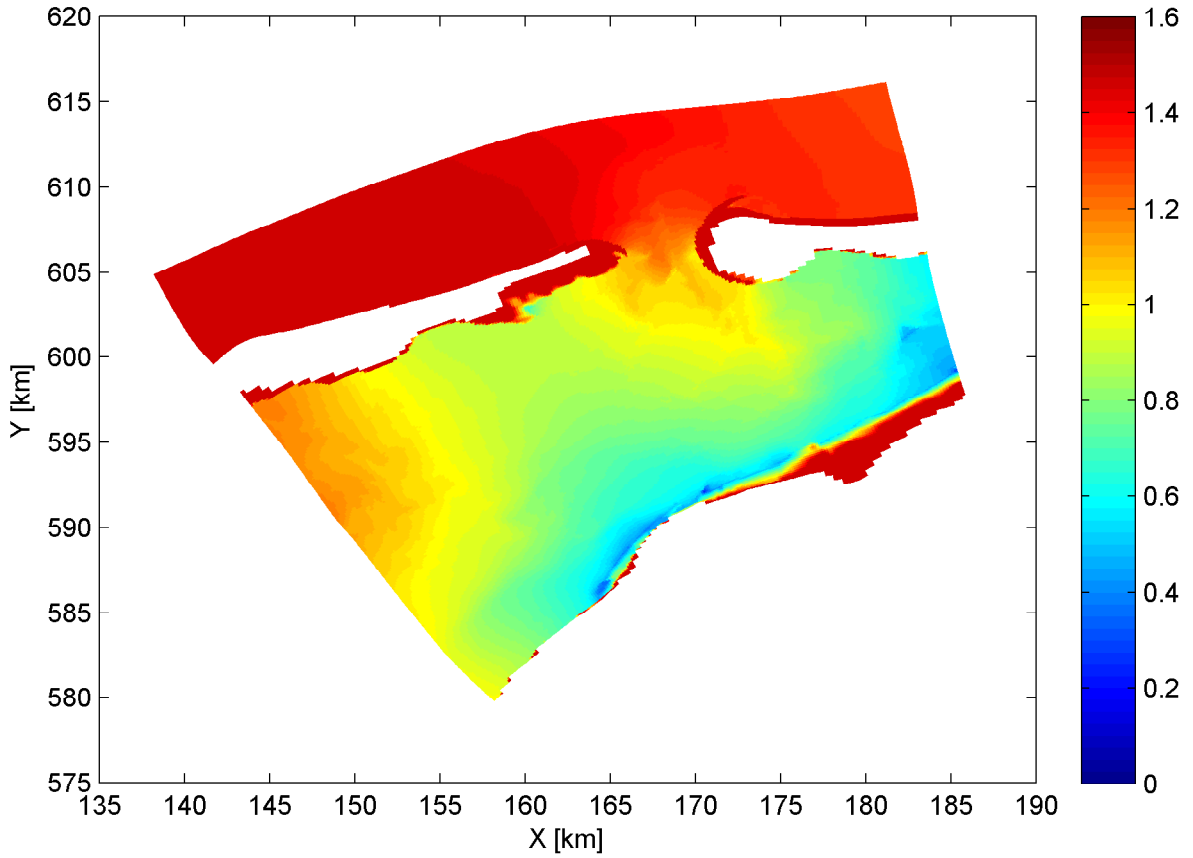

Spatial distribution of water level based on WAQUA computation	20050102	10:00hr
	Hindcast Ameland Inlet	
WL | DELFT HYDRAULICS	H4803.11	Fig. 3.10

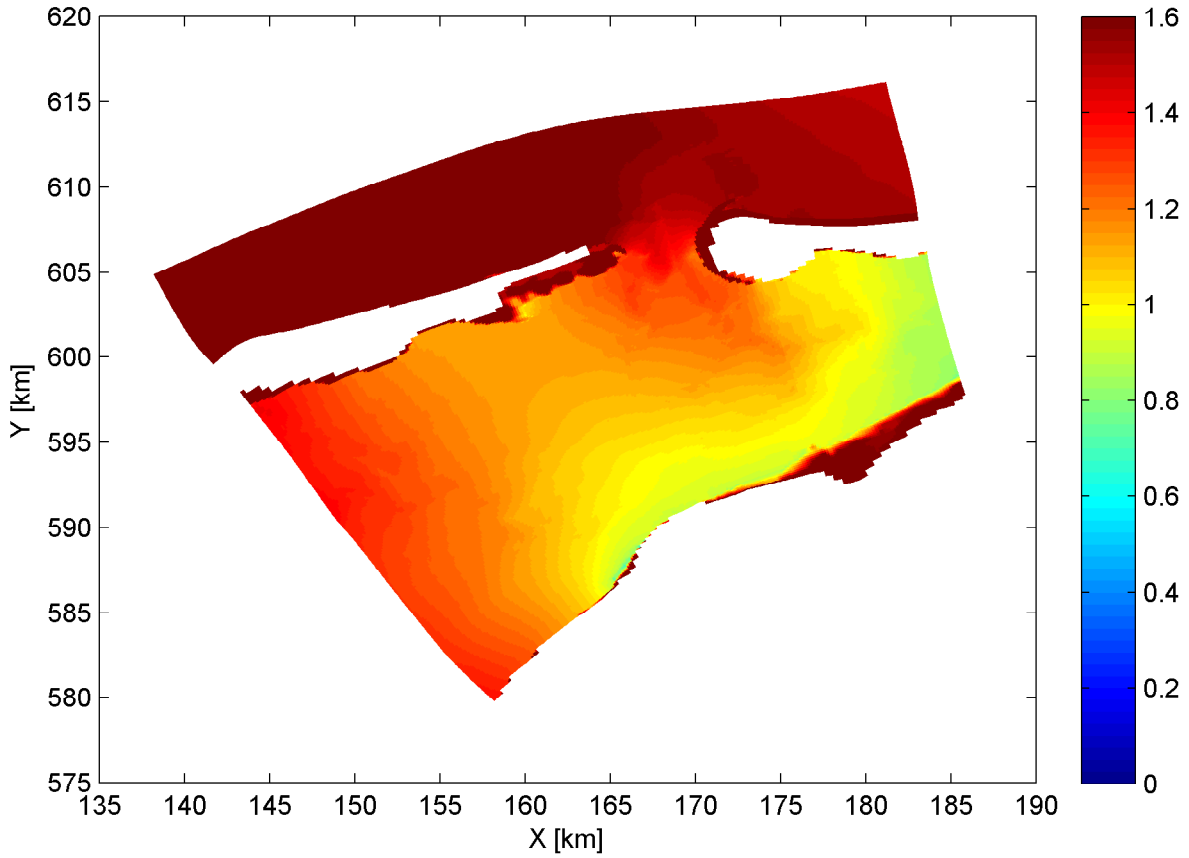

Spatial distribution of water level based on WAQUA computation	20050102	10:30hr
	Hindcast Ameland Inlet	
WL | DELFT HYDRAULICS	H4803.11	Fig. 3.11

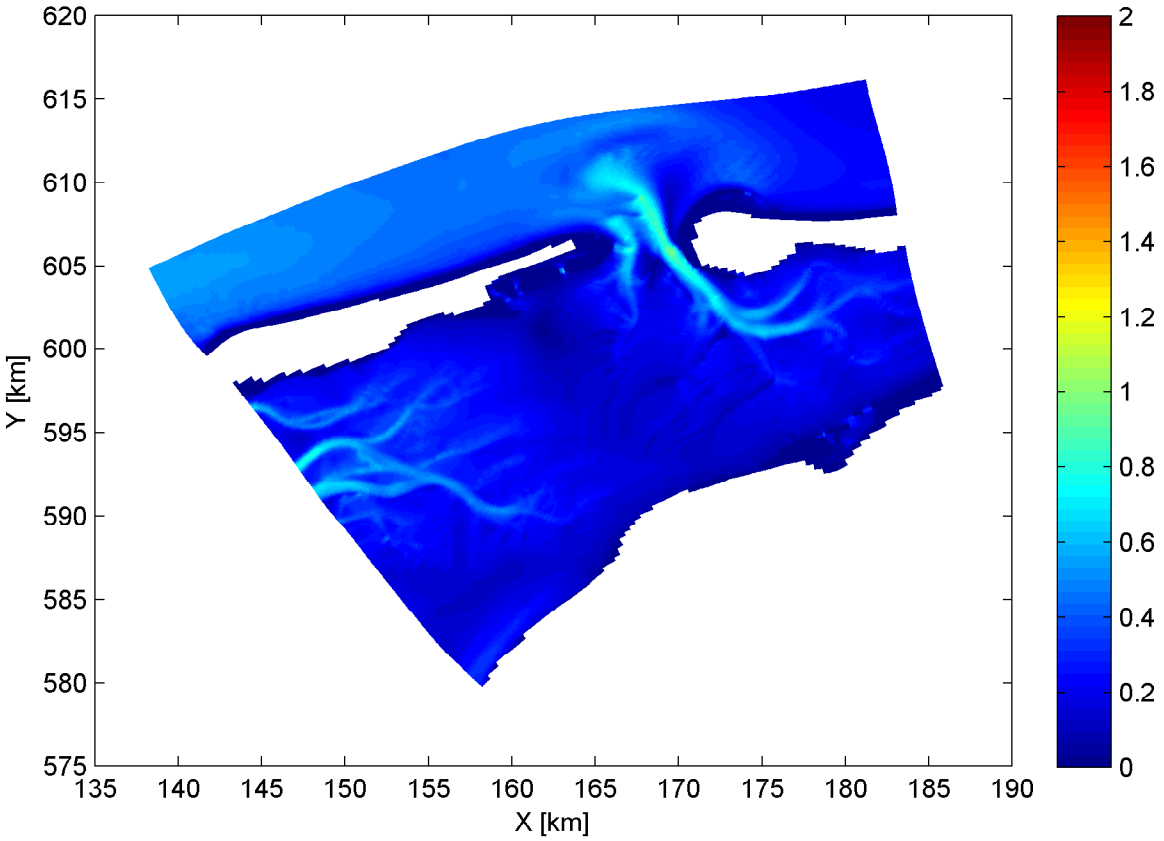

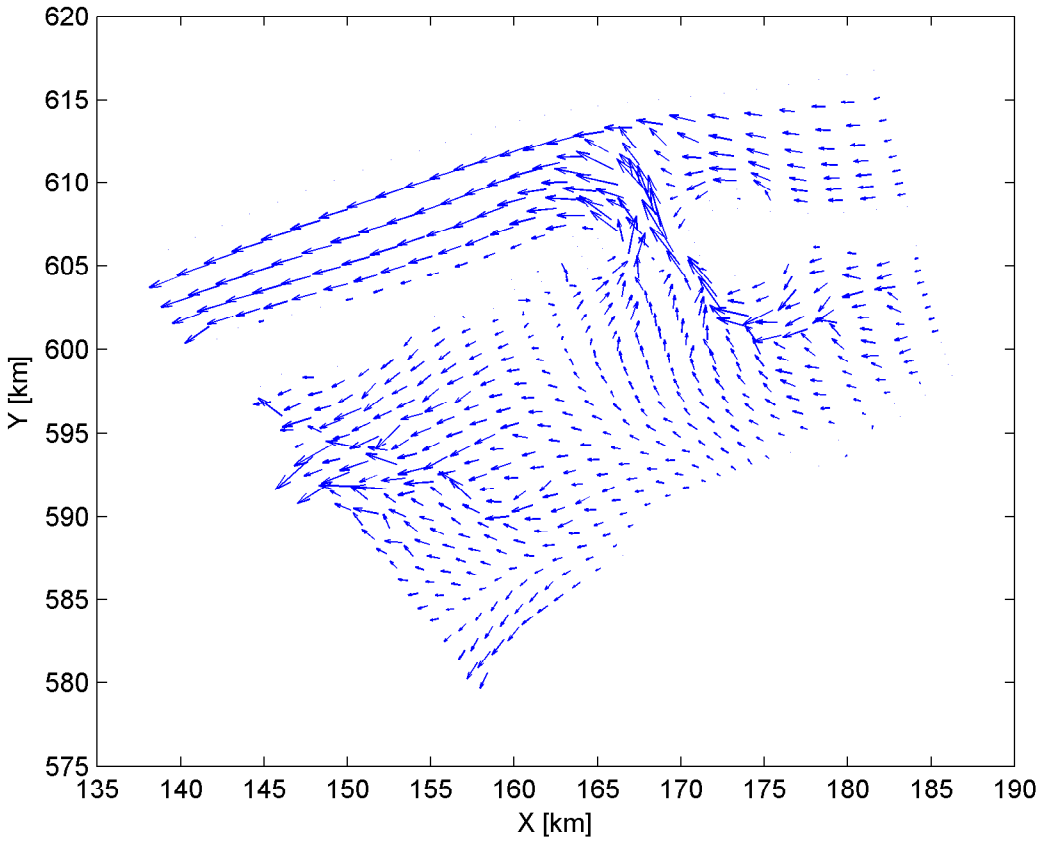

Spatial distribution of magnitude (upper panel) and direction (lower panel) of current velocity, based on WAQUA computation	20050102	16:30hr
	Hindcast Ameland Inlet	
WL | DELFT HYDRAULICS	H4803.11	Fig. 3.12

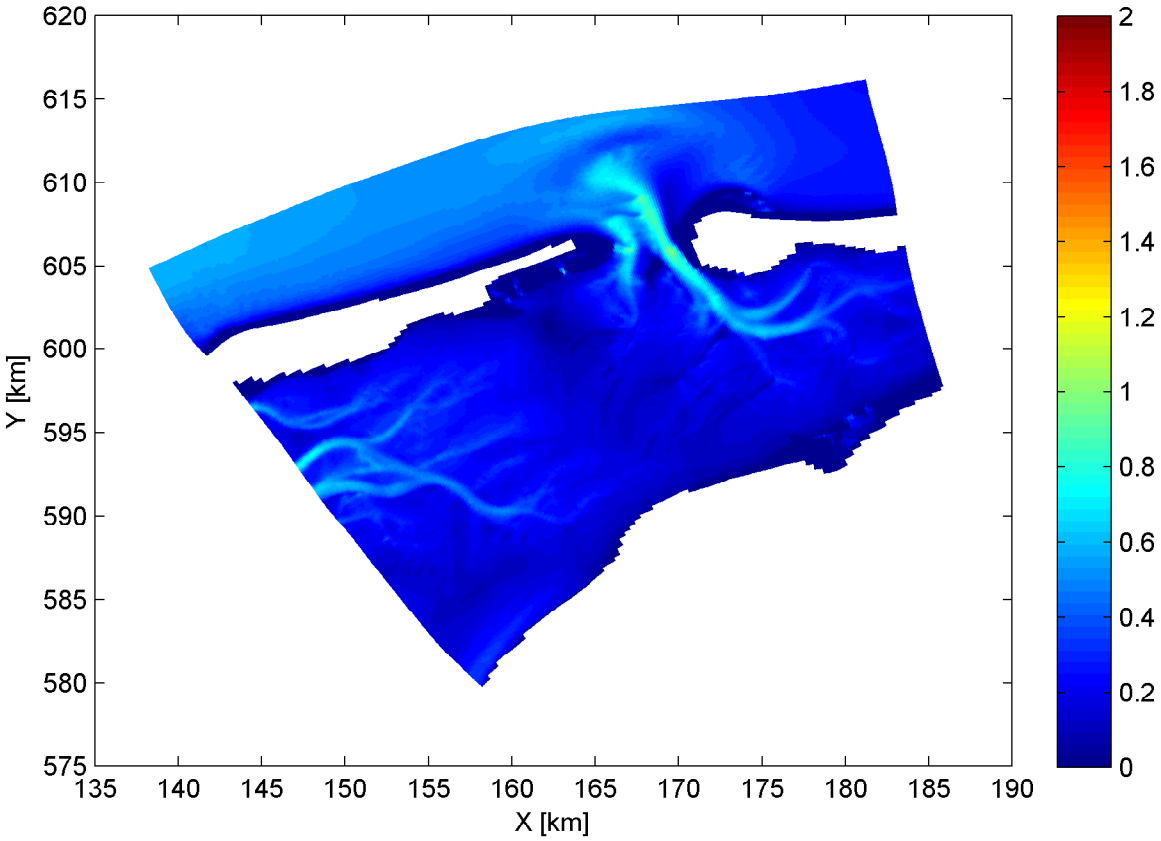

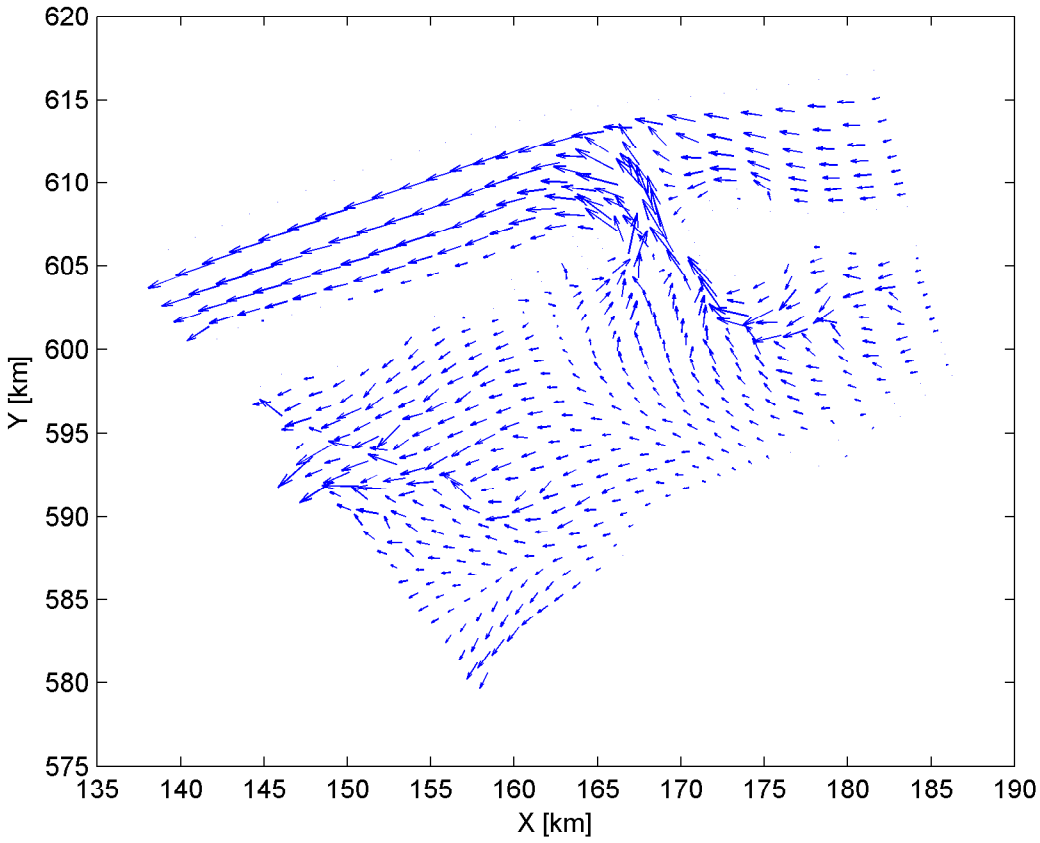

Spatial distribution of magnitude (upper panel) and direction (lower panel) of current velocity, based on WAQUA computation	20050102	17:00hr
	Hindcast Ameland Inlet	
WL | DELFT HYDRAULICS	H4803.11	Fig. 3.13

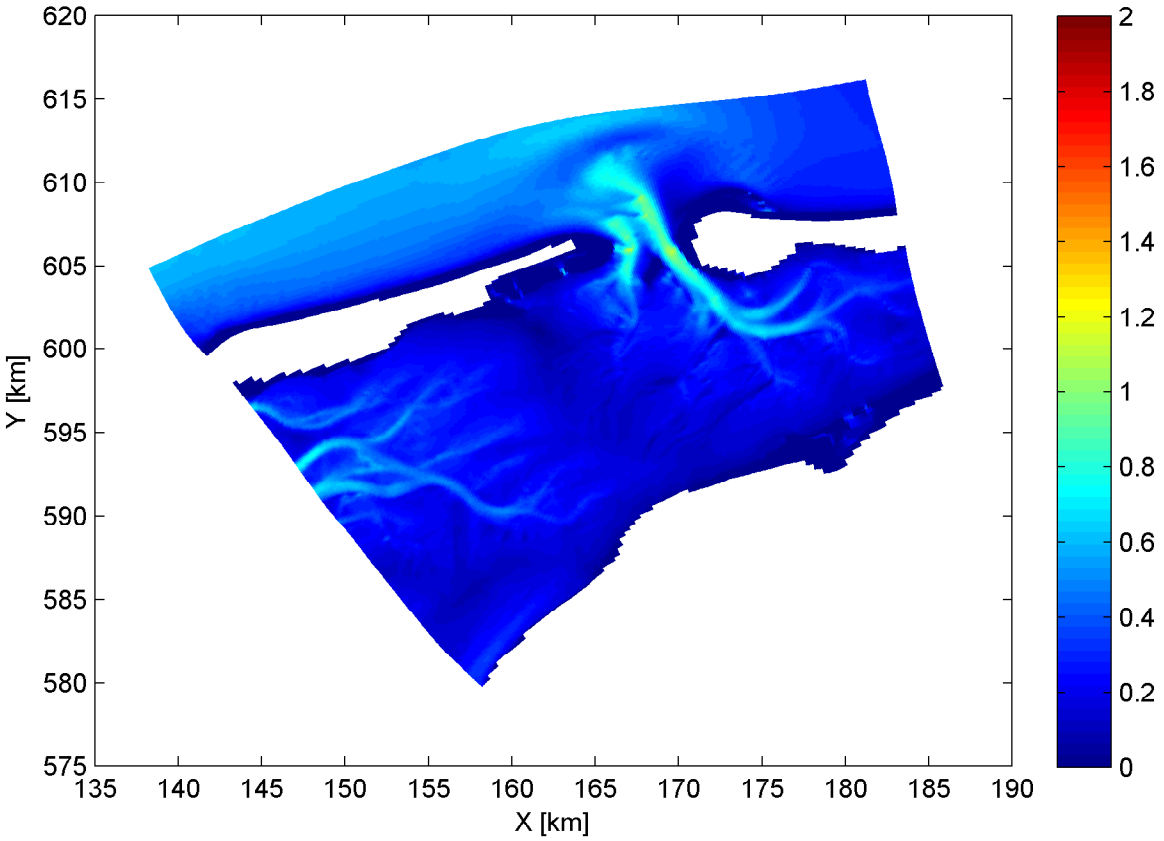

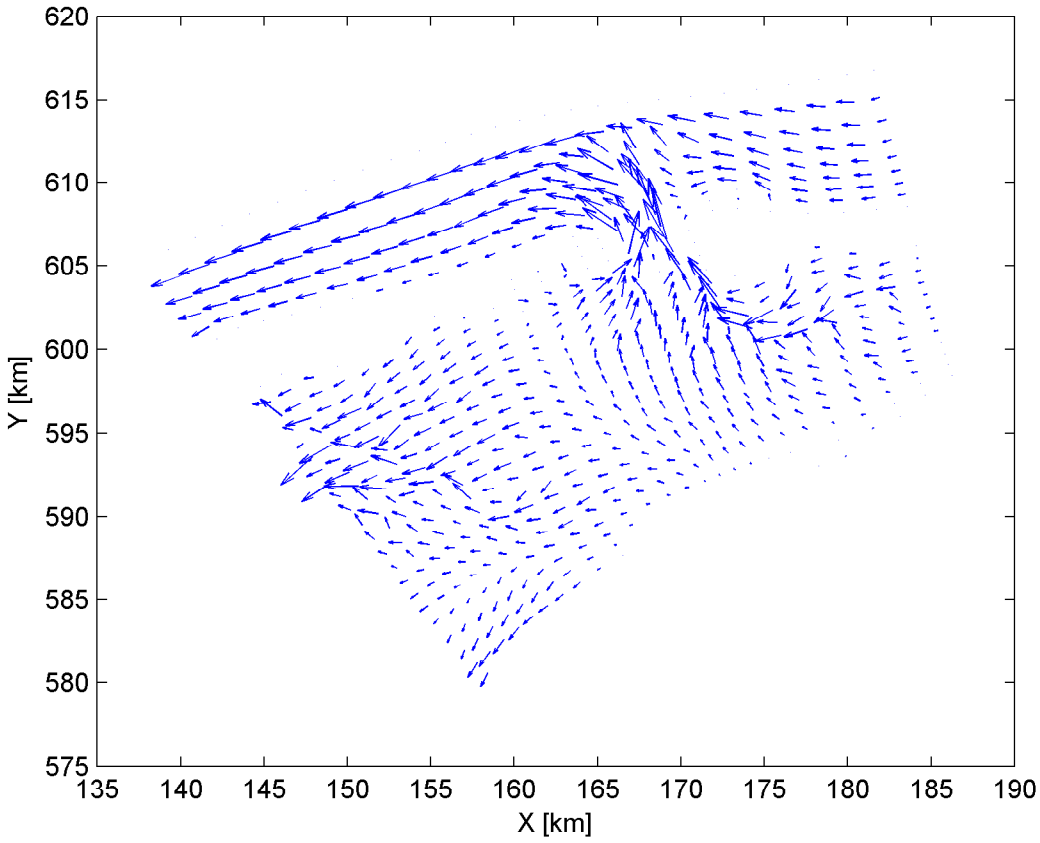

Spatial distribution of magnitude (upper panel) and direction (lower panel) of current velocity, based on WAQUA computation	20050102	17:30hr
	Hindcast Ameland Inlet	
WL | DELFT HYDRAULICS	H4803.11	Fig. 3.14

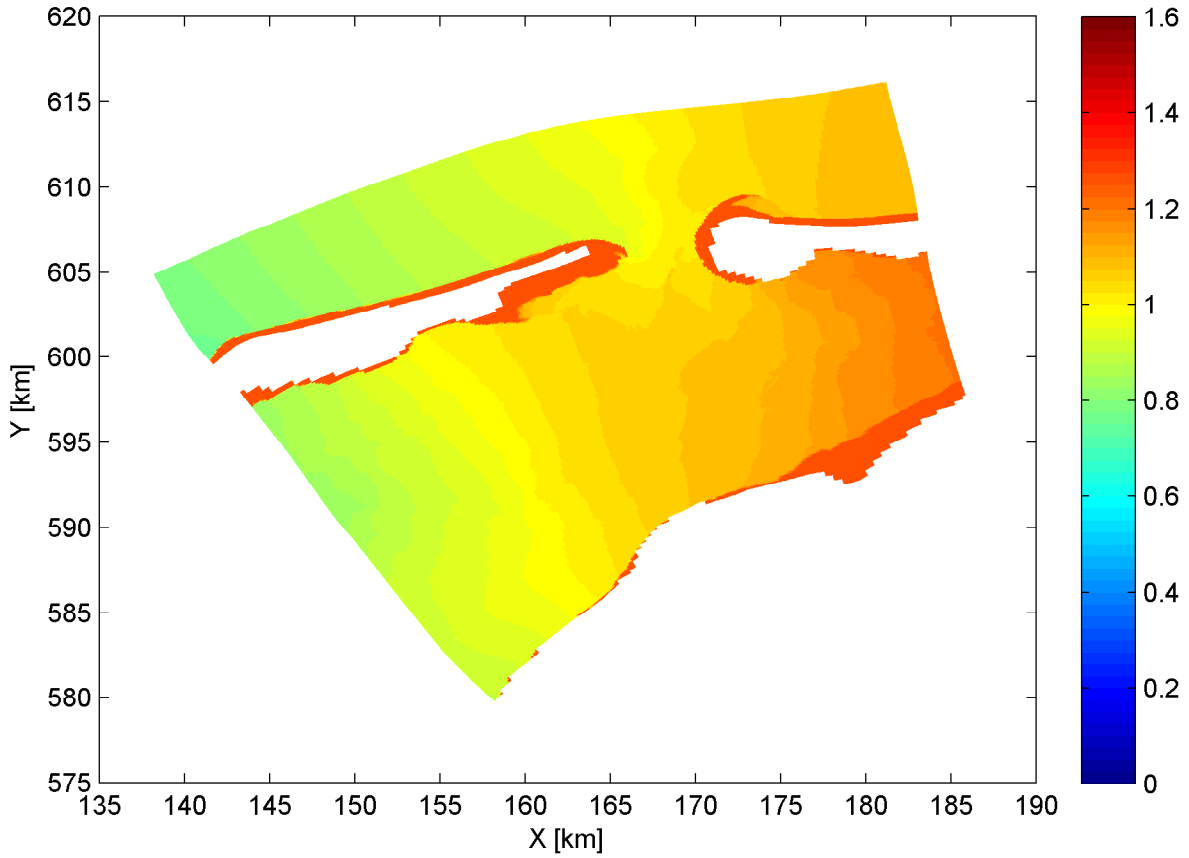

Spatial distribution of water level based on WAQUA computation	20050102	16:30hr
	Hindcast Ameland Inlet	
WL | DELFT HYDRAULICS	H4803.11	Fig. 3.15

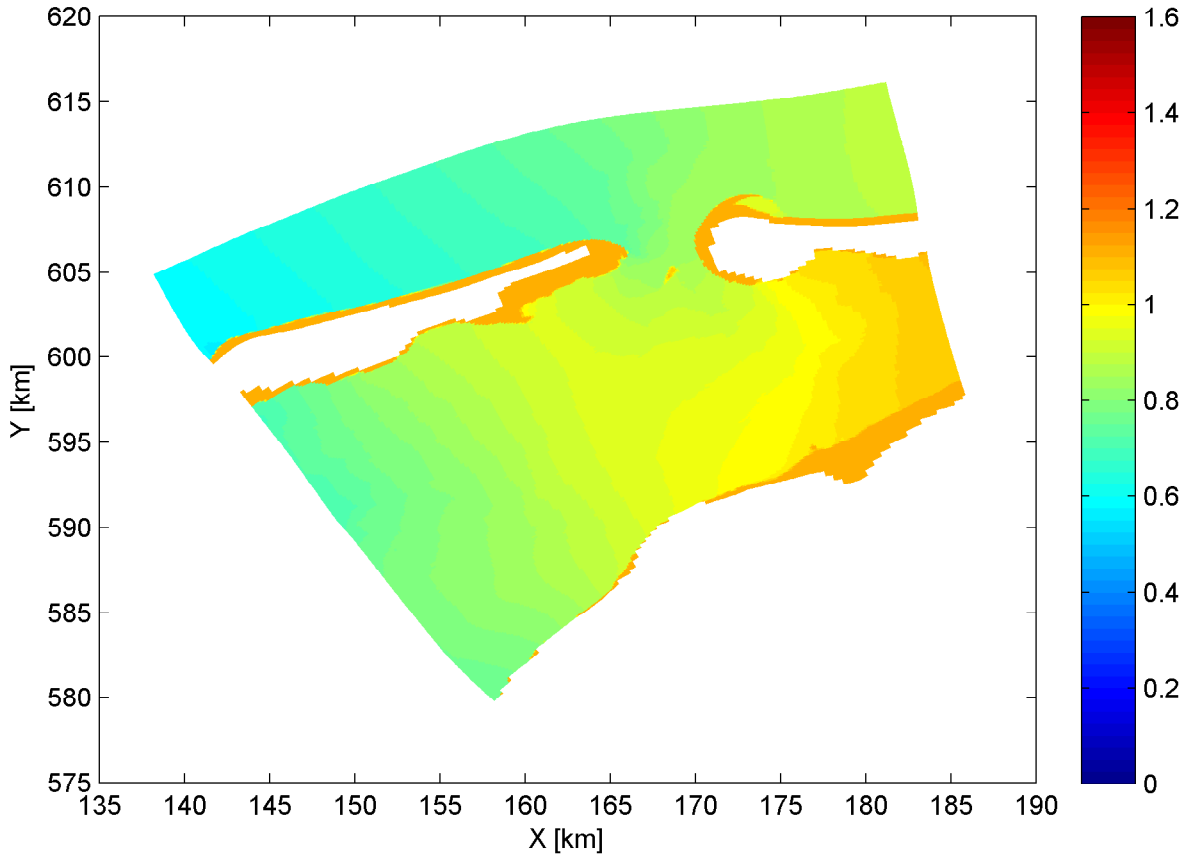

Spatial distribution of water level based on WAQUA computation	20050102	17:00hr
	Hindcast Ameland Inlet	
WL | DELFT HYDRAULICS	H4803.11	Fig. 3.16

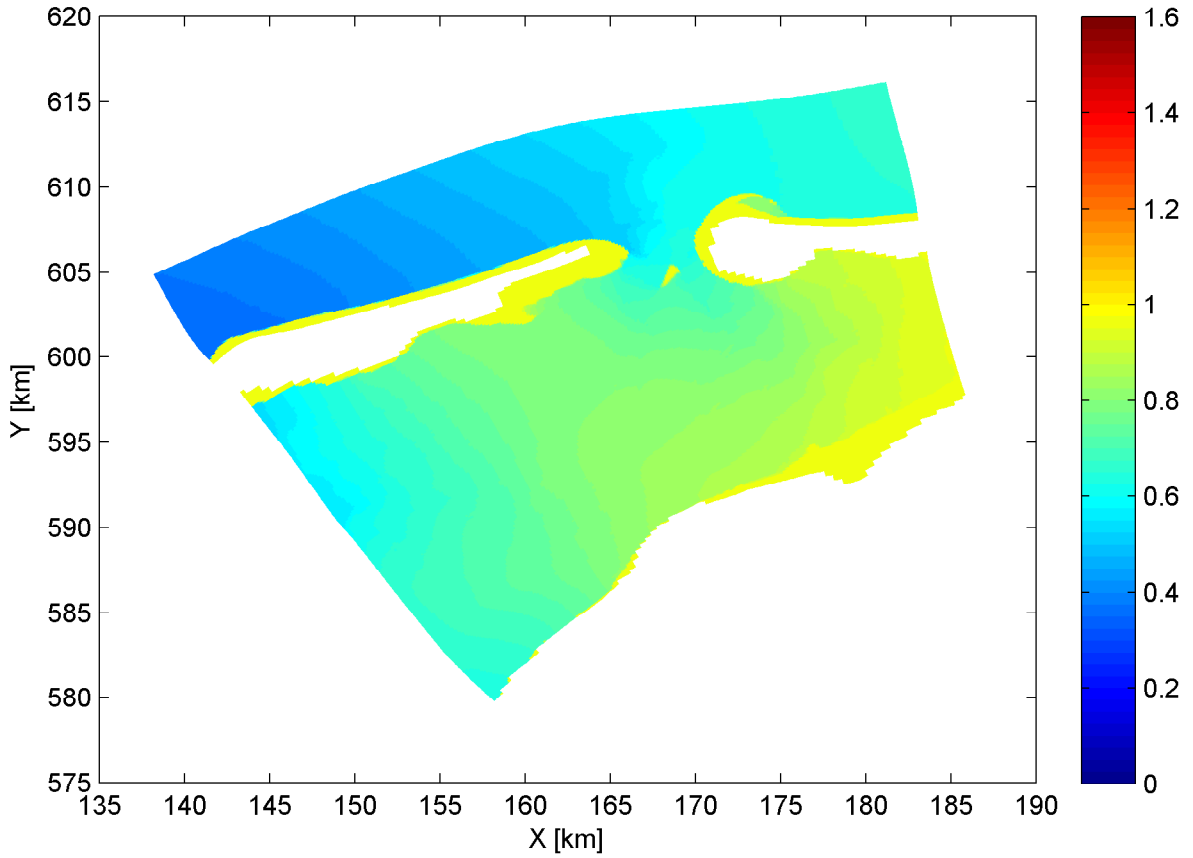

Spatial distribution of water level based on WAQUA computation	20050102	17:30hr
	Hindcast Ameland Inlet	
WL | DELFT HYDRAULICS	H4803.11	Fig. 3.17

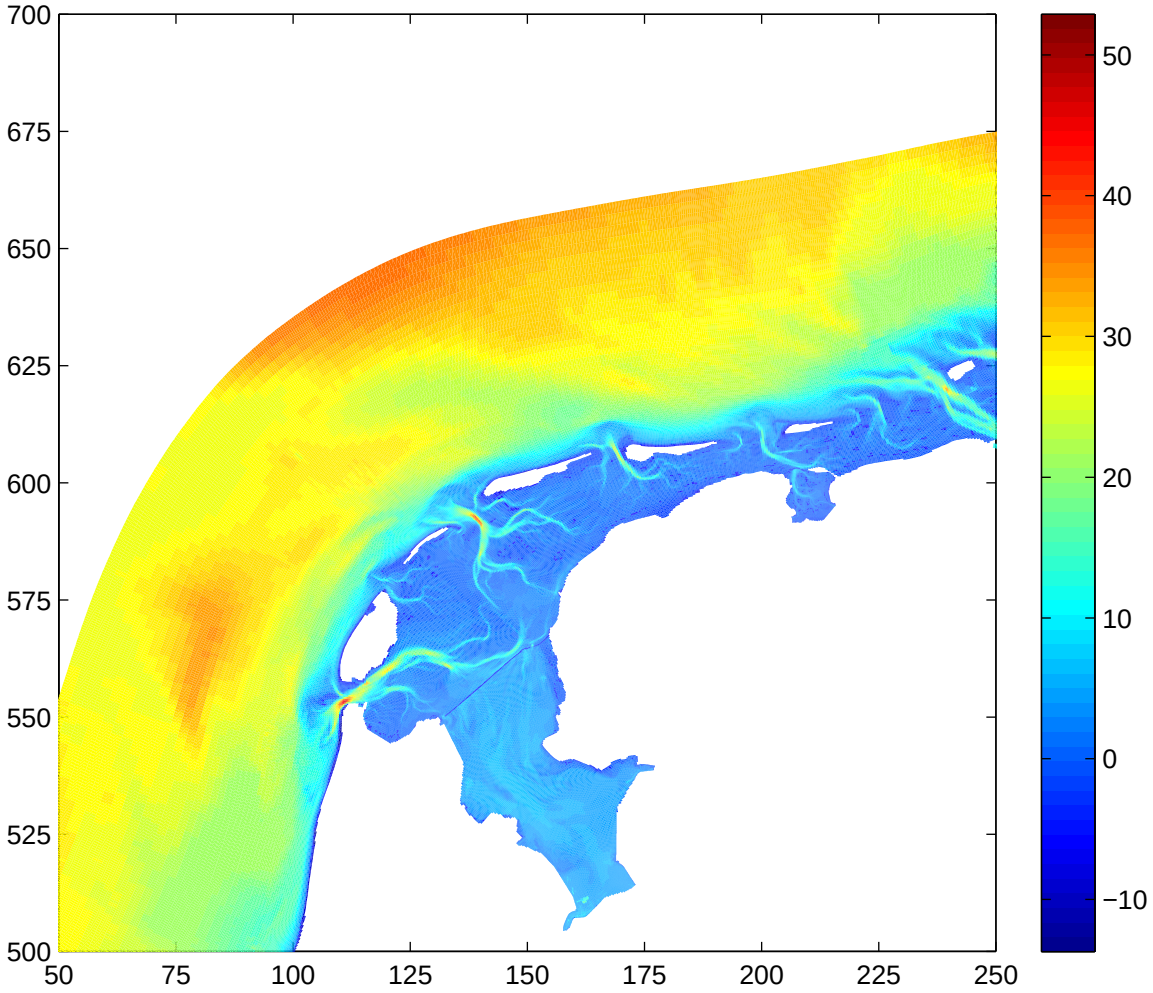

Bathymetry of Kuststrookmodel; depth in [m]		
	Hindcast Ameland Inlet	
WL | DELFT HYDRAULICS	H4803.11	Fig. 3.18a

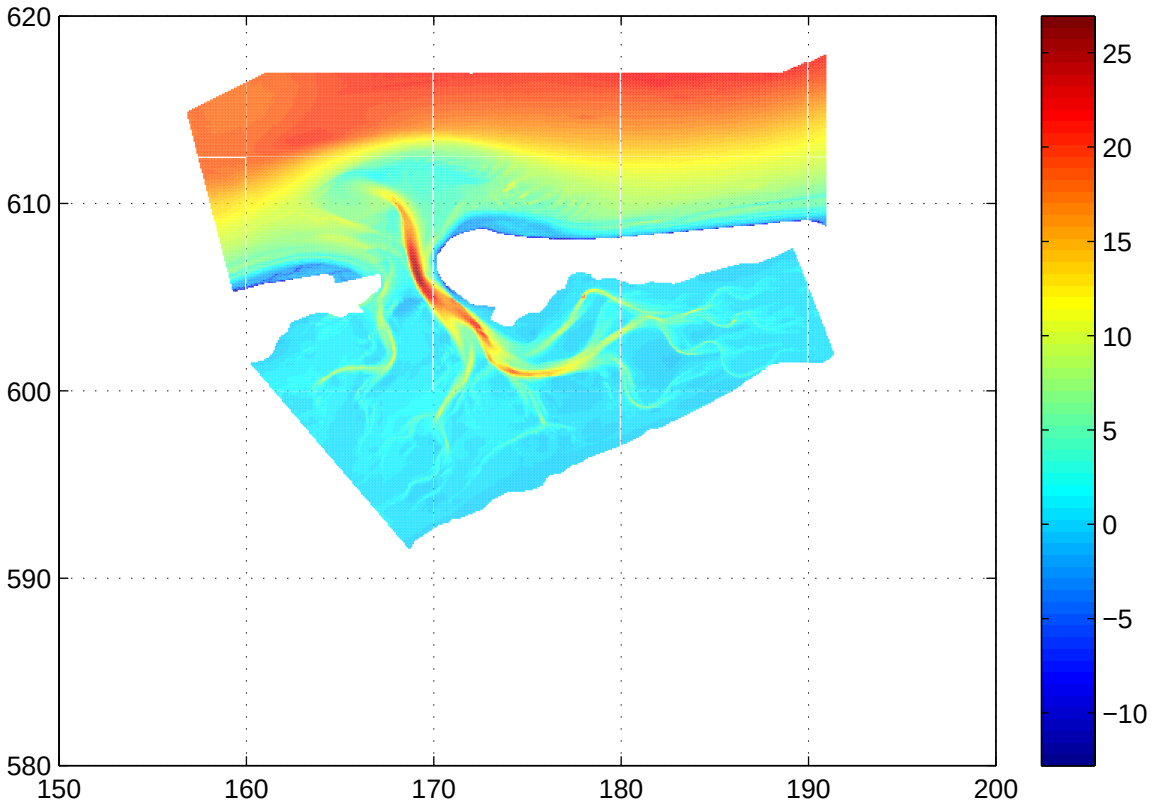

Vaklodingen (soundings) Borndiep 2005		
	Hindcast Amelander Zeegat	
WL | DELFT HYDRAULICS	H4803.11	Fig. 3.18b

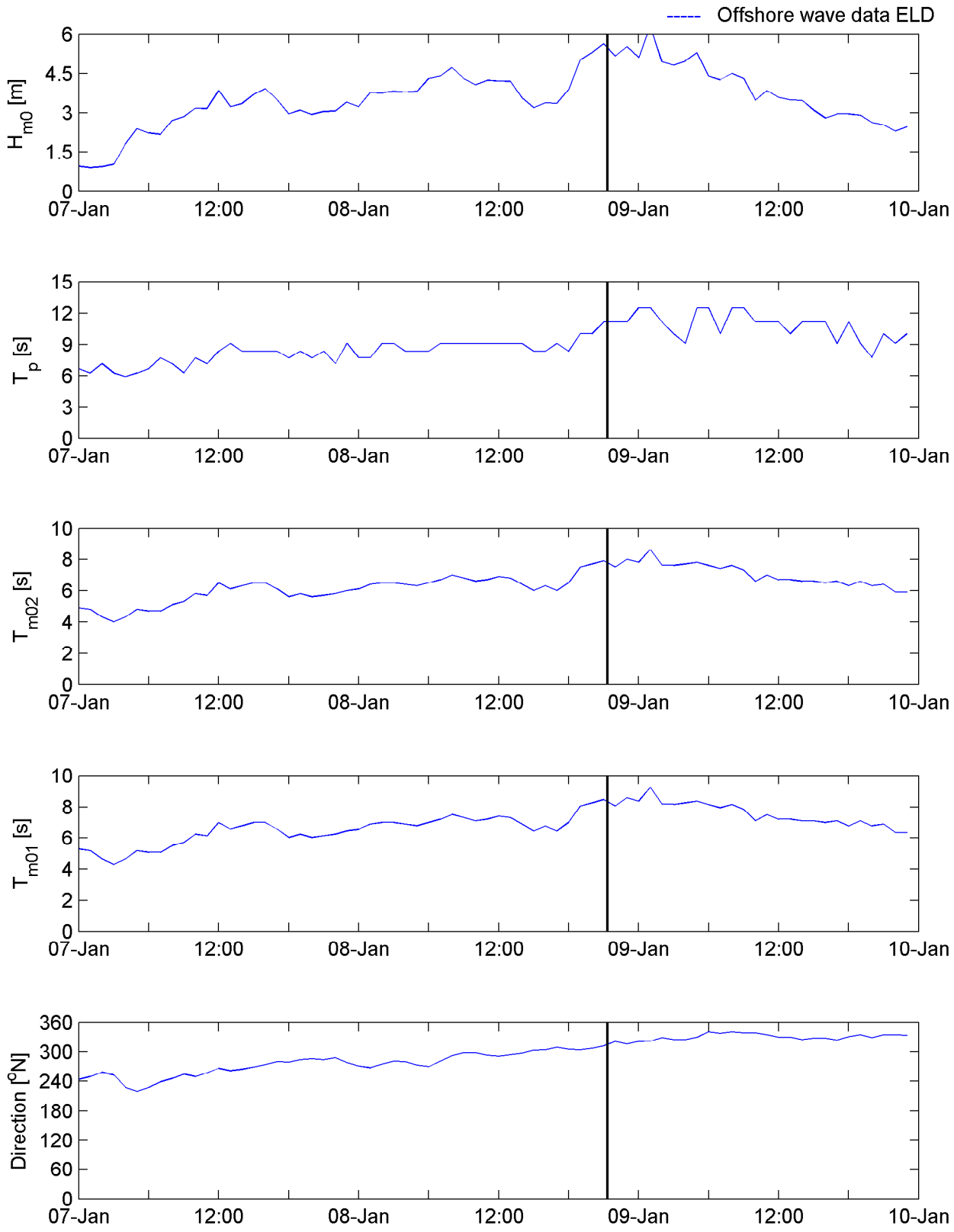

Offshore wave data at ELD	20040208	
	Hindcast Ameland Inlet	
WL | DELFT HYDRAULICS	H4803.11	Fig. 3.19

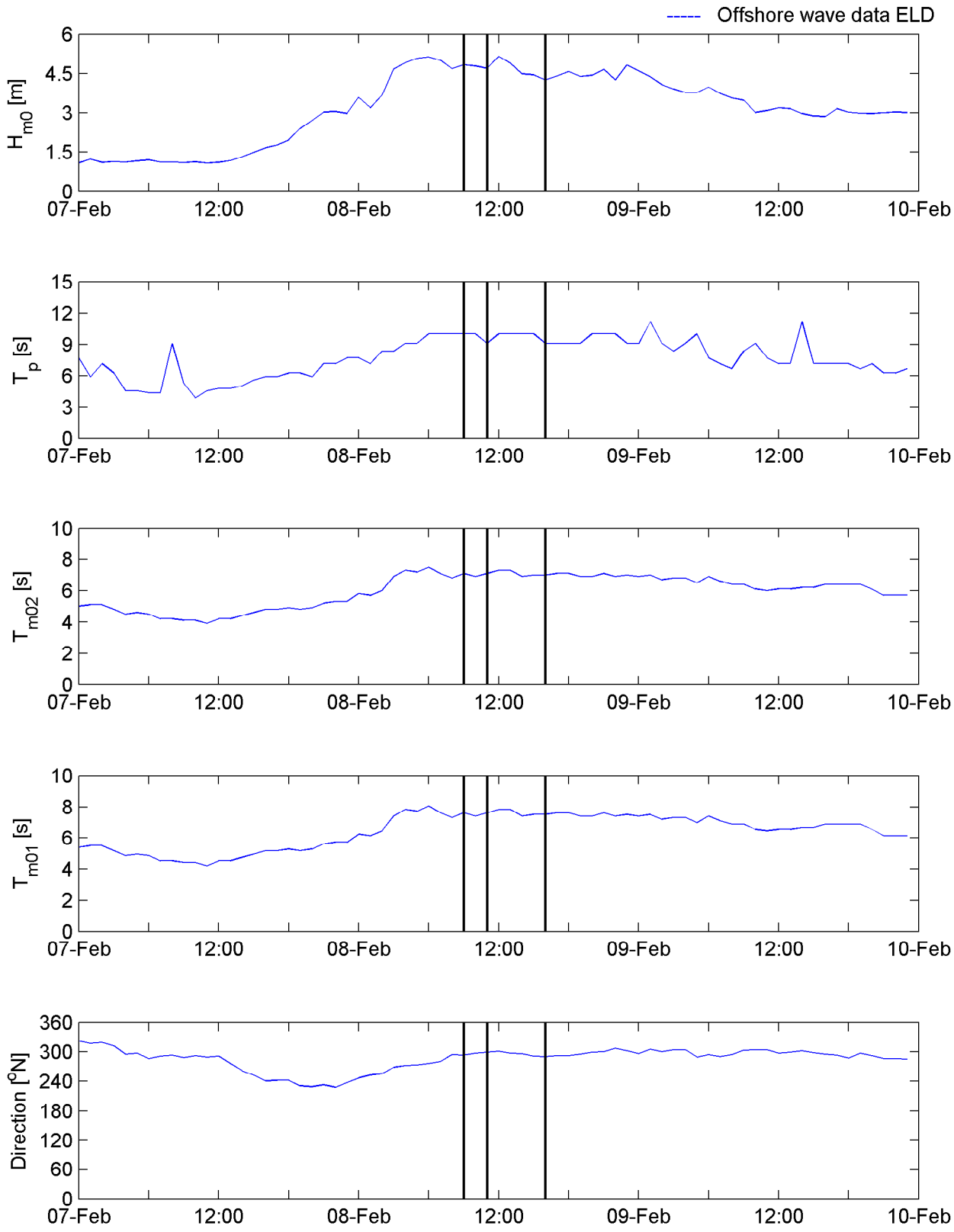

Offshore wave data at ELD	20050102	
	Hindcast Ameland Inlet	
WL | DELFT HYDRAULICS	H4803.11	Fig. 3.20

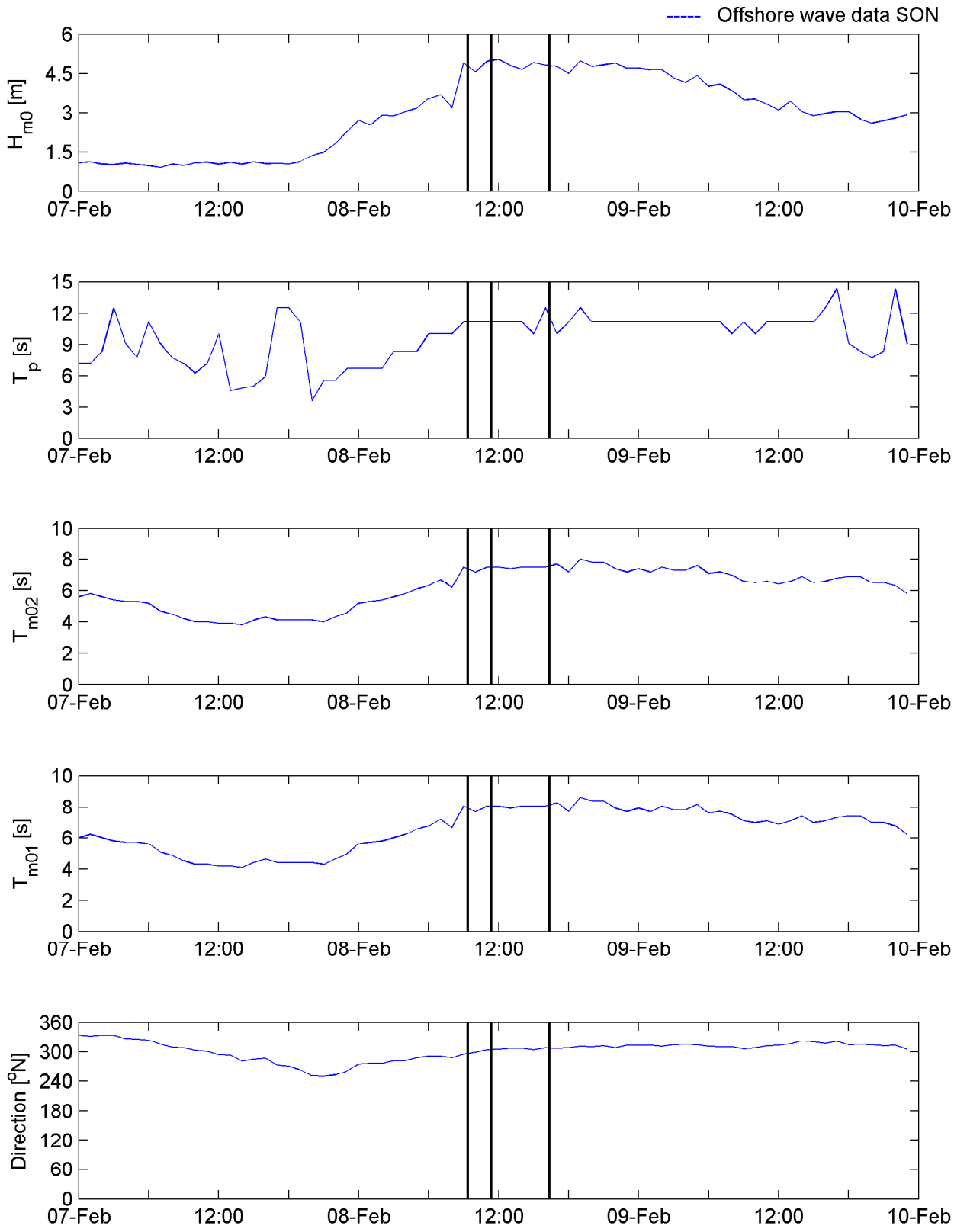

Offshore wave data at SON	20050102	
	Hindcast Ameland Inlet	
WL | DELFT HYDRAULICS	H4803.11	Fig. 3.21

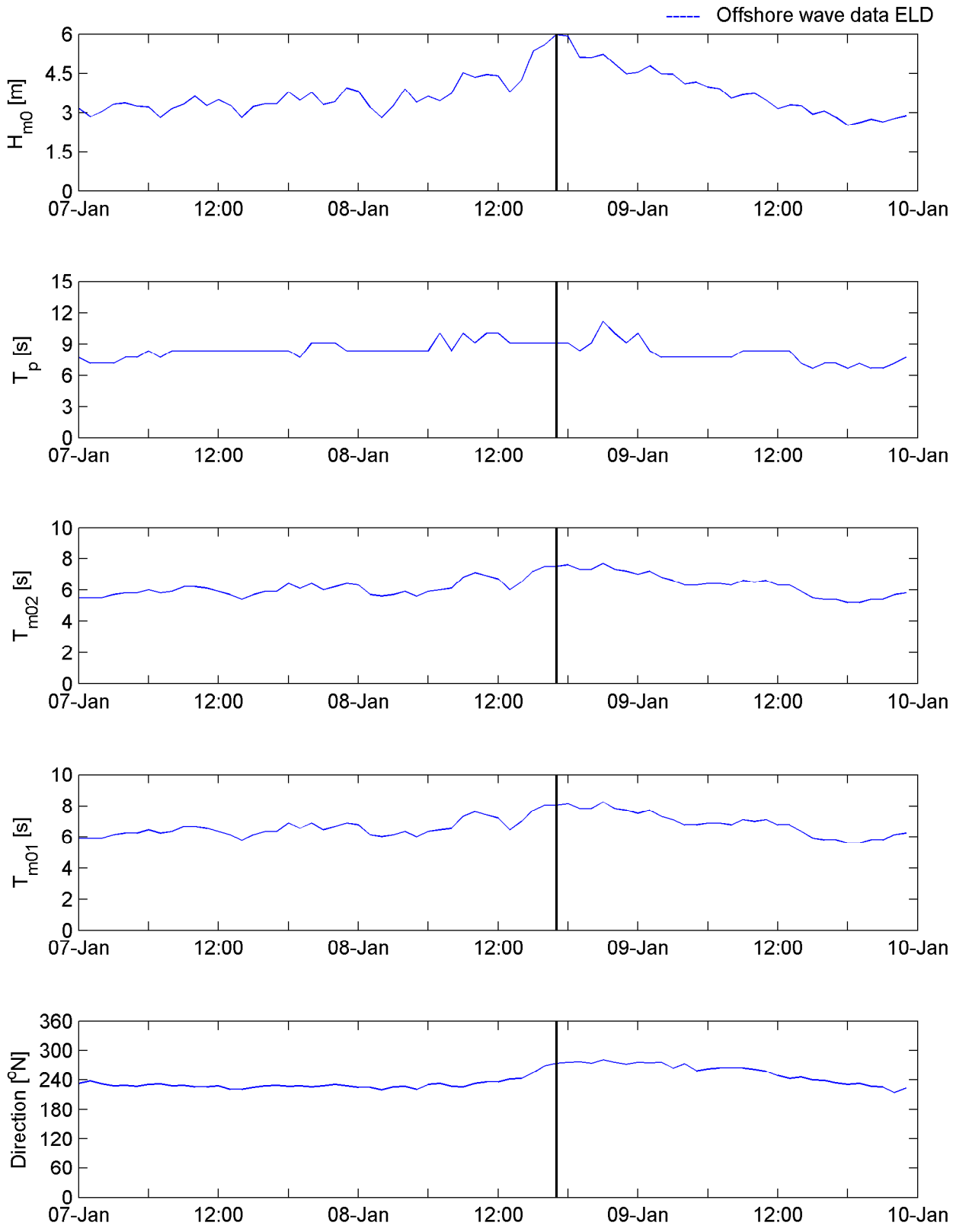

Offshore wave data at ELD	20050108	
	Hindcast Ameland Inlet	
WL | DELFT HYDRAULICS	H4803.11	Fig. 3.22

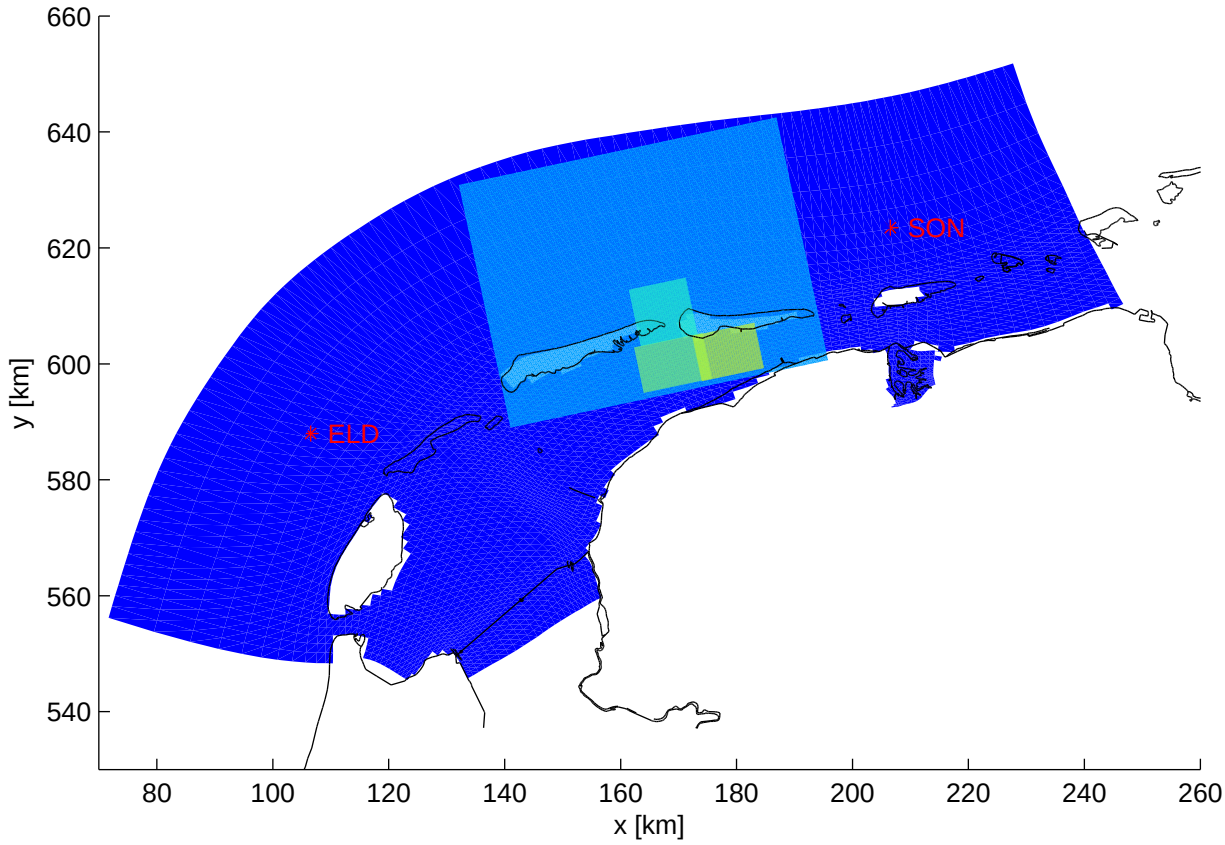

Curvilinear ("outside") and nested grids and location of offshore wave buoys		
	Hindcast Ameland Inlet	
WL | DELFT HYDRAULICS	H4803.11	Fig. 3.23a

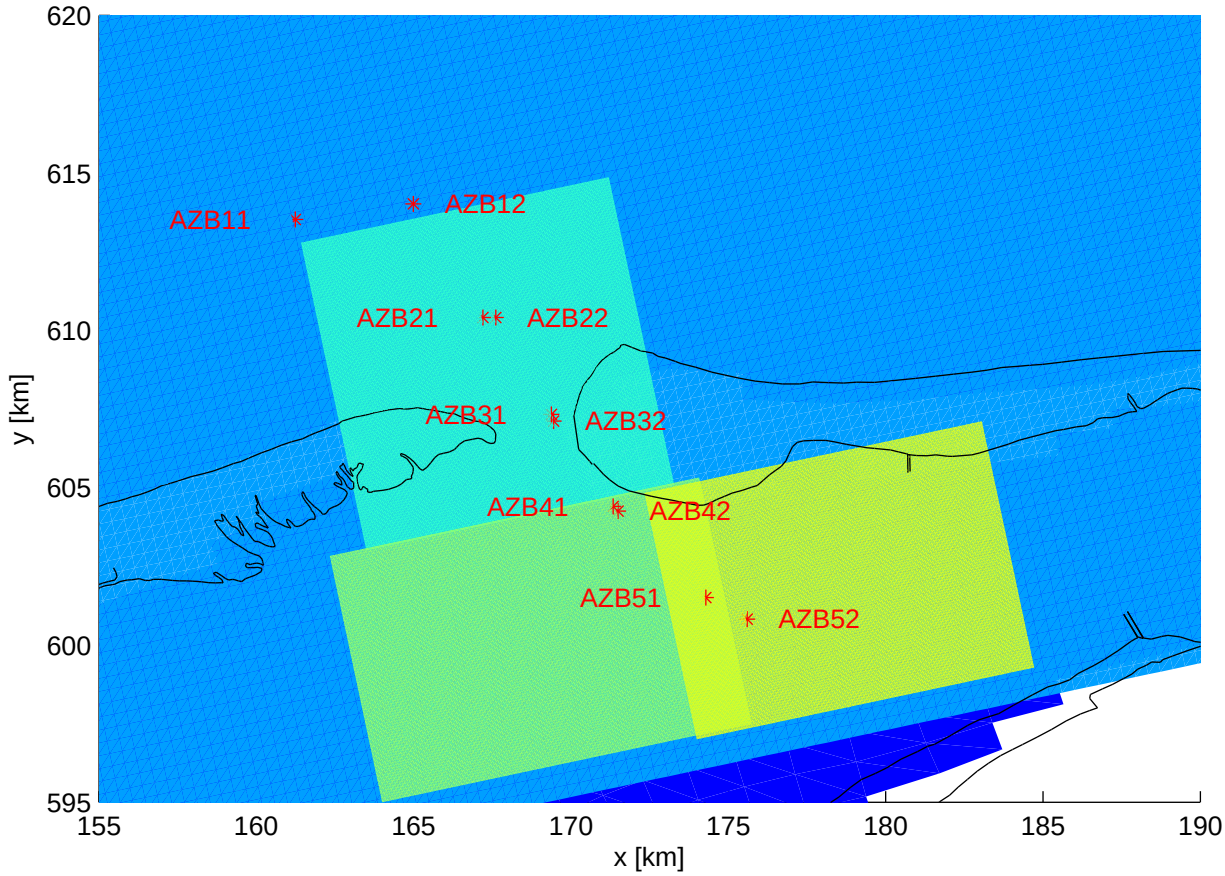

Location of wave buoys in Ameland inlet		
	Hindcast Ameland Inlet	
WL | DELFT HYDRAULICS	H4803.11	Fig. 3.23b

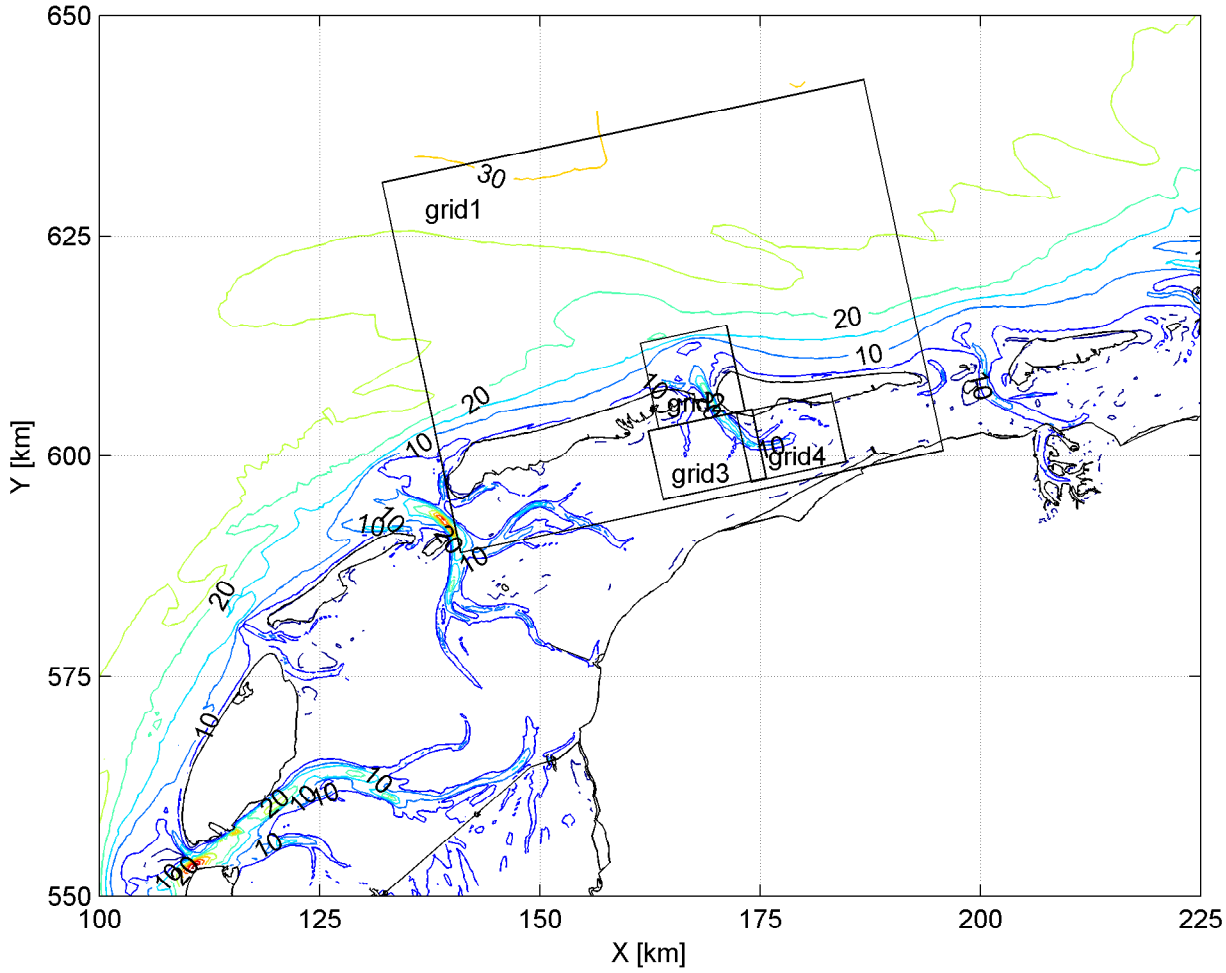

Nested grids		
	Hindcast Ameland Inlet	
WL | DELFT HYDRAULICS	H4803.11	Fig. 3.23c

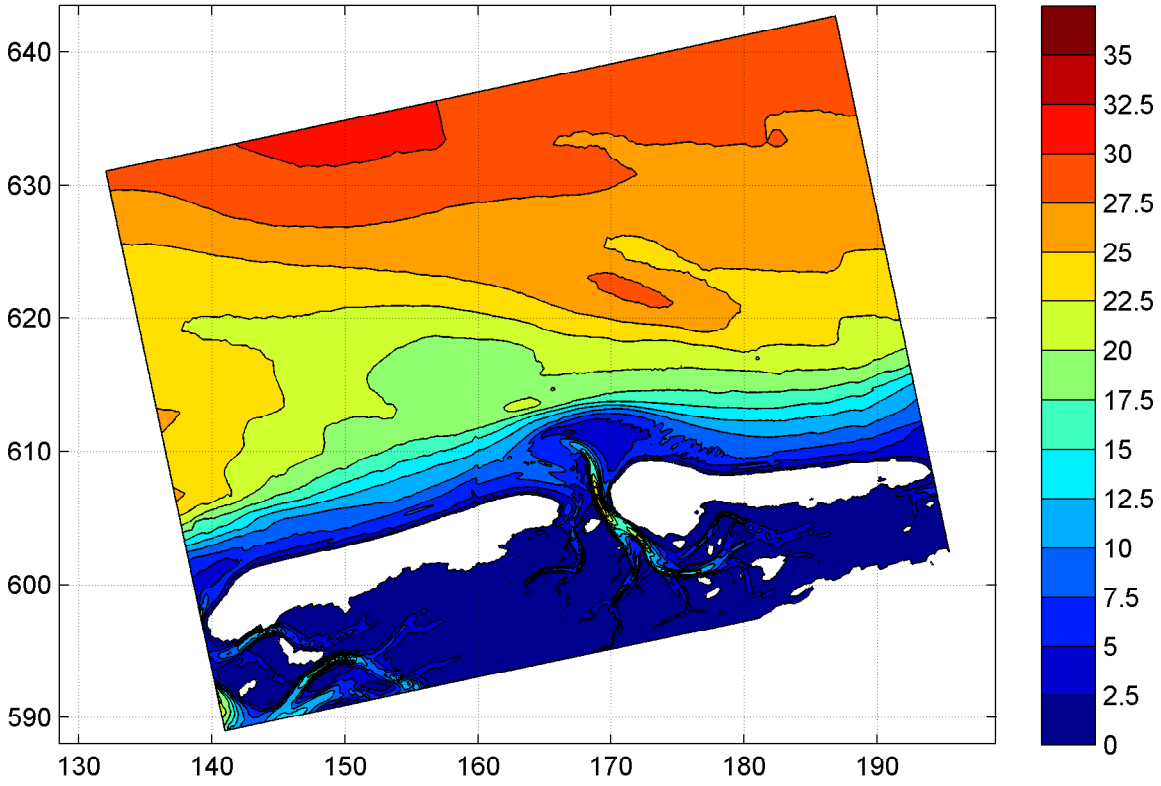

Bathymetry grid 1		
	Hindcast Ameland Inlet	
WL | DELFT HYDRAULICS	H4803.11	Fig. 3.24

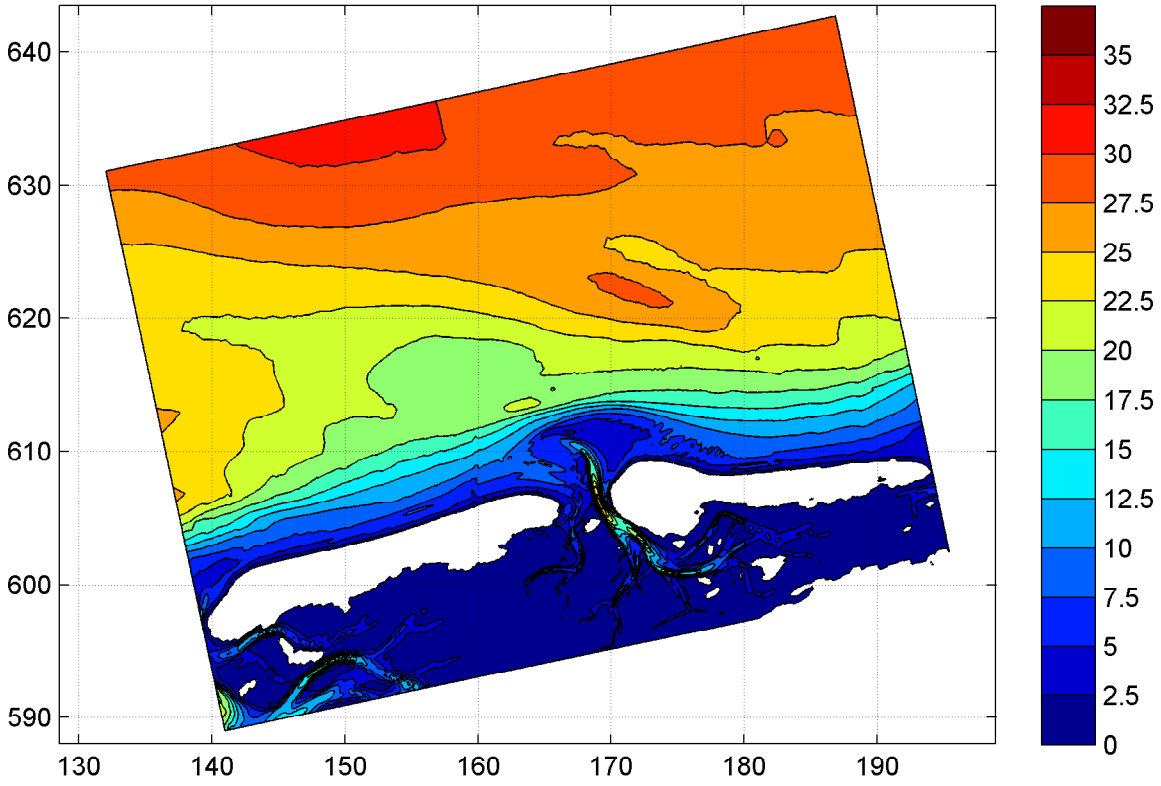

Bathymetry grid 1		
	Hindcast Ameland Inlet	
WL | DELFT HYDRAULICS	H4803.11	Fig. 3.25

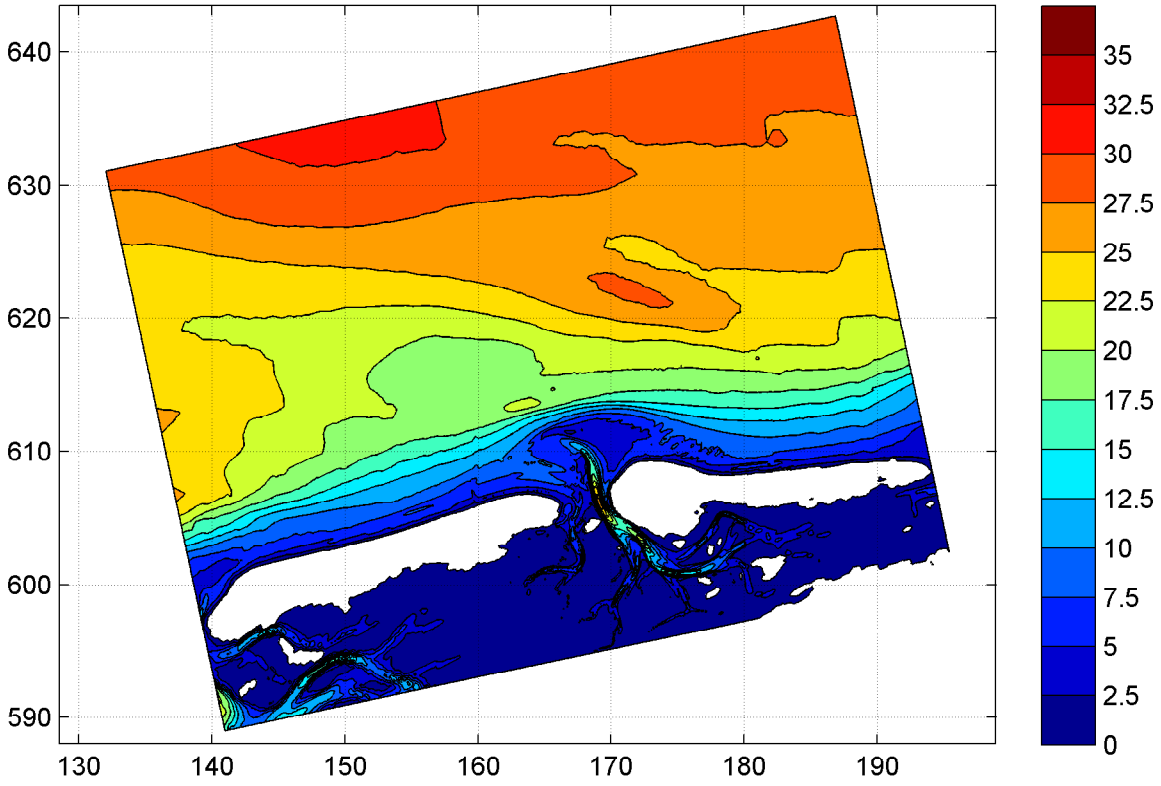

Bathymetry grid 1		
	Hindcast Ameland Inlet	
WL | DELFT HYDRAULICS	H4803.11	Fig. 3.26

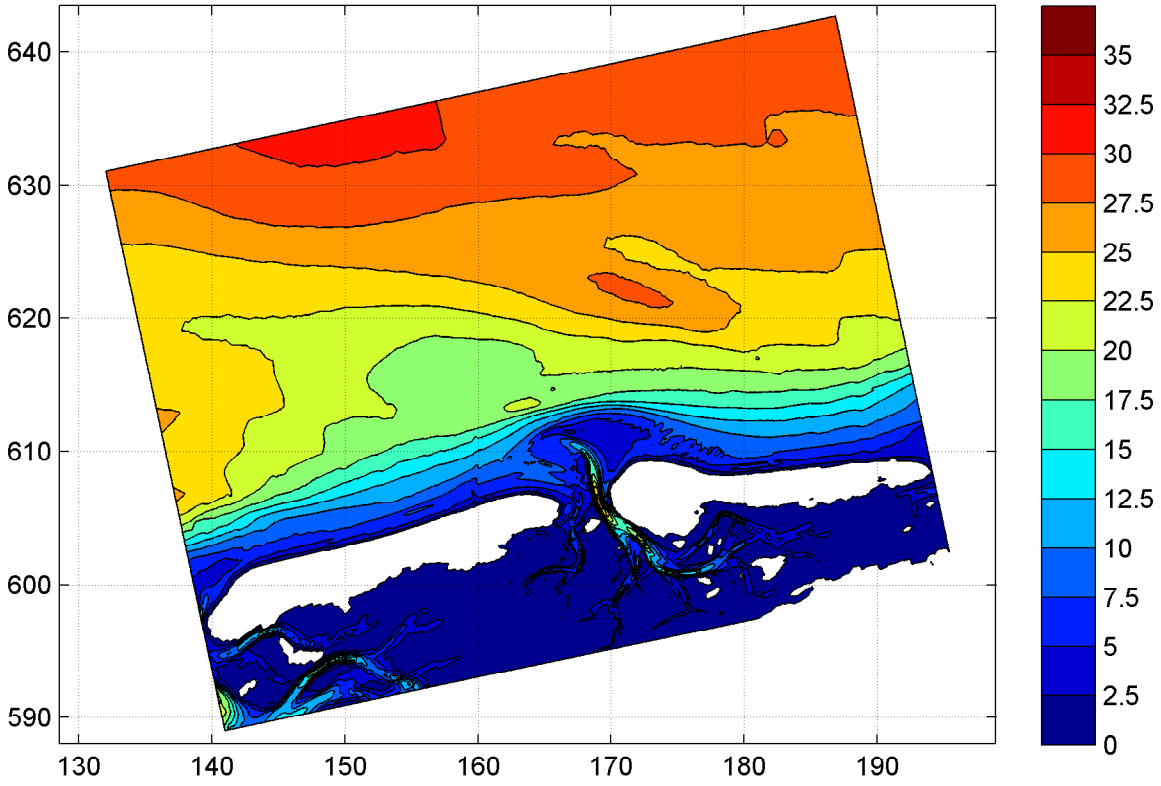

Bathymetry grid 1		
	Hindcast Ameland Inlet	
WL | DELFT HYDRAULICS	H4803.11	Fig. 3.27

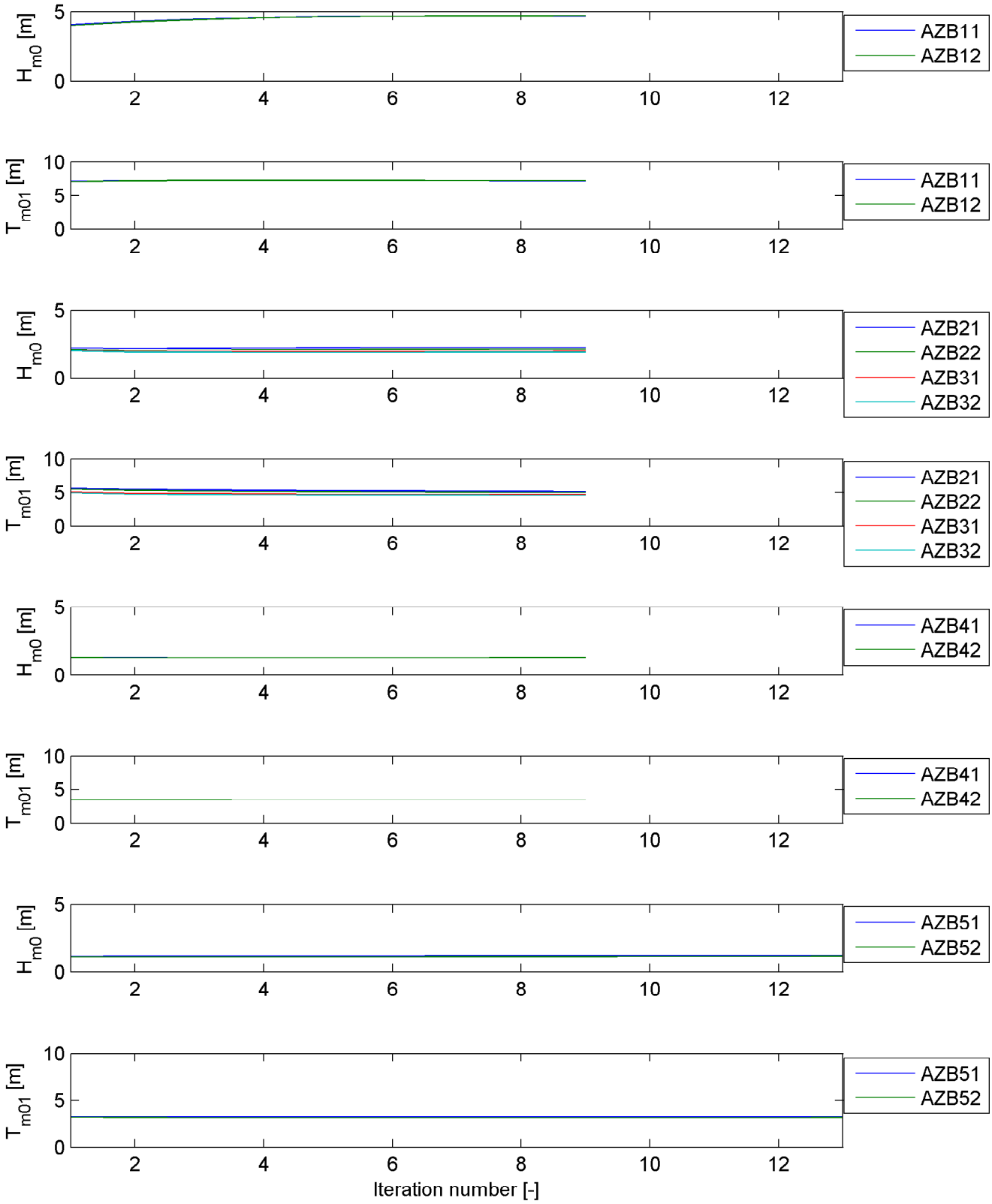

Convergence of wave parameters at all buoy locations for January 2, 2005 at 12:00hr; HIRLAM wind field	12:00hr	20050102
	Hindcast Ameland Inlet	
WL | DELFT HYDRAULICS	H4803.11	Fig. 3.28a

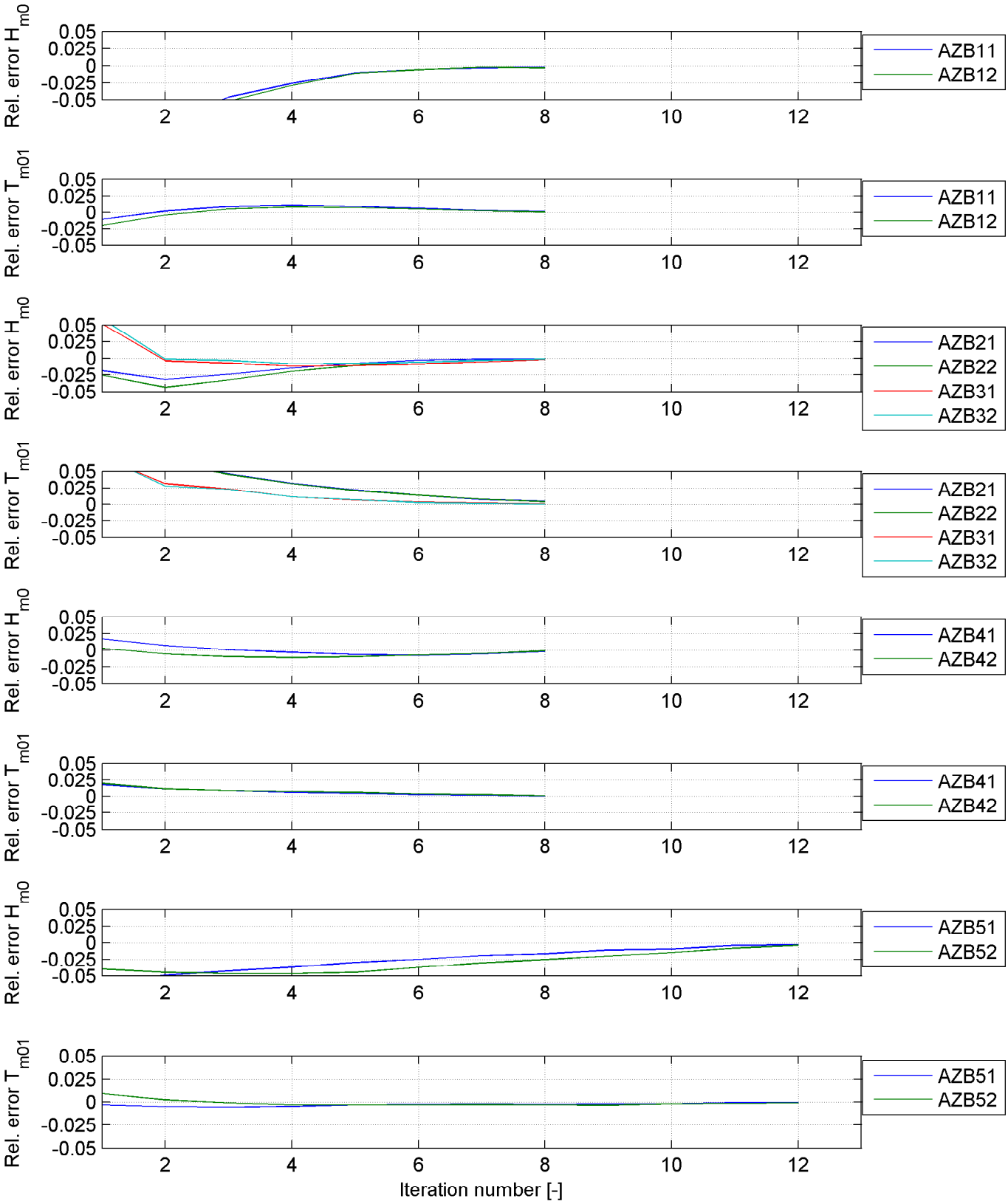

Relative error of wave parameters at all buoy locations for January 2, 2005 at 12:00hr; HIRLAM wind field	12:00hr	20050102
	Hindcast Ameland Inlet	
WL | DELFT HYDRAULICS	H4803.11	Fig. 3.28b

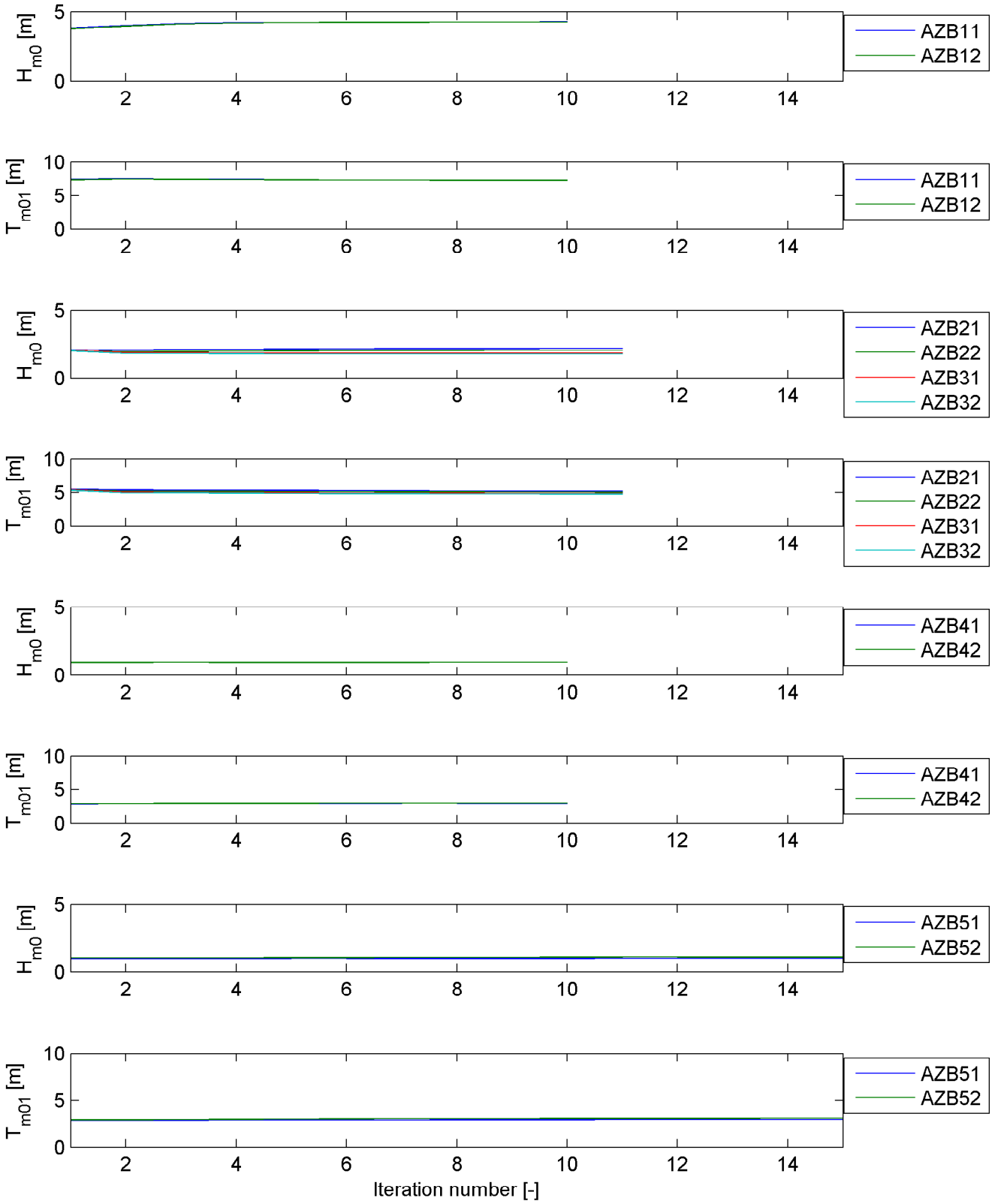

Convergence of wave parameters at all buoy locations for January 2, 2005 at 17:00hr; WAQUA water level and current field	17:00hr	20050102
	Hindcast Ameland Inlet	
WL | DELFT HYDRAULICS	H4803.11	Fig. 3.29a

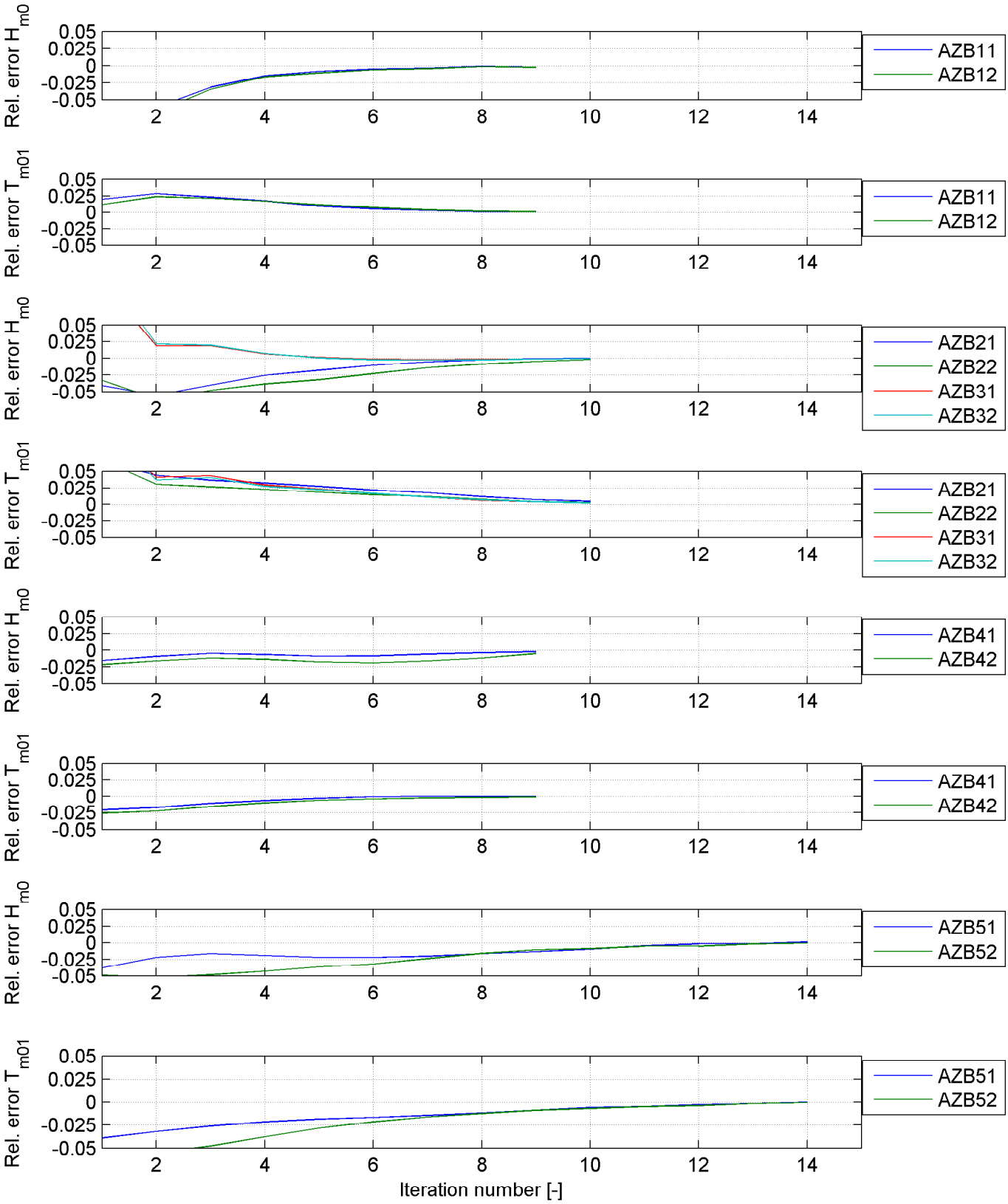

Relative error of wave parameters at all buoy locations for January 2, 2005 at 17:00hr; WAQUA water level and current field	17:00hr	20050102
	Hindcast Ameland Inlet	
WL | DELFT HYDRAULICS	H4803.11	Fig. 3.29b

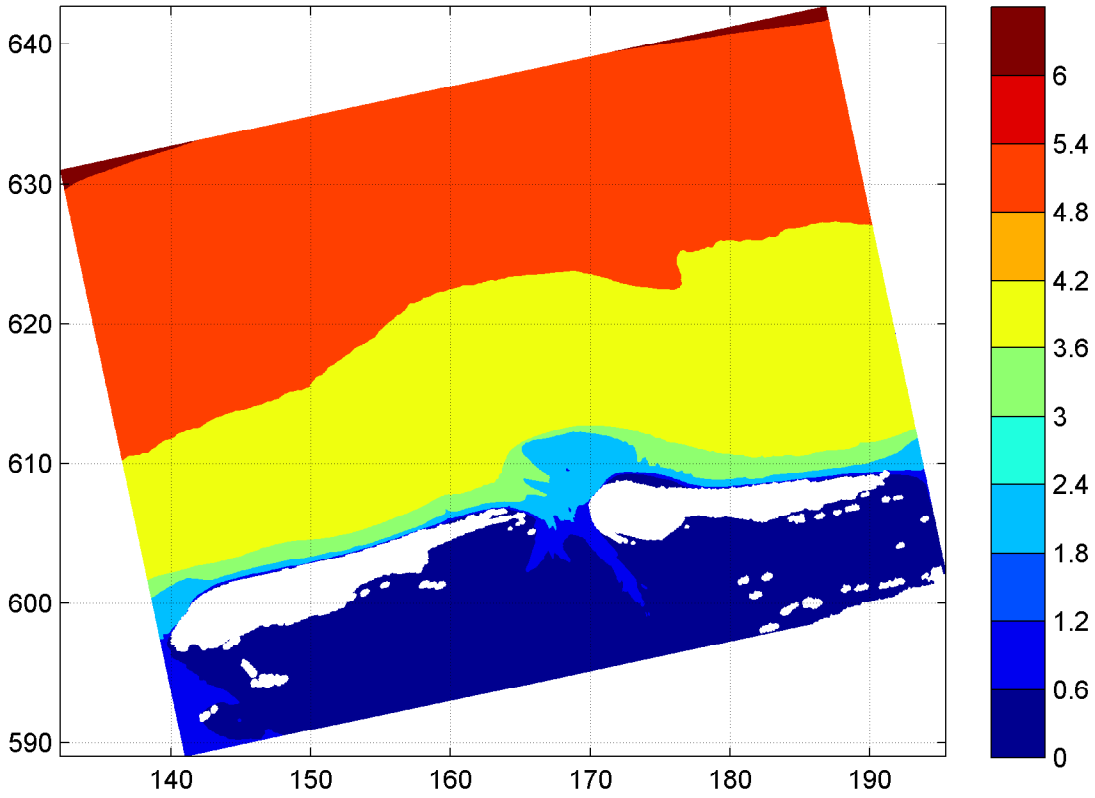

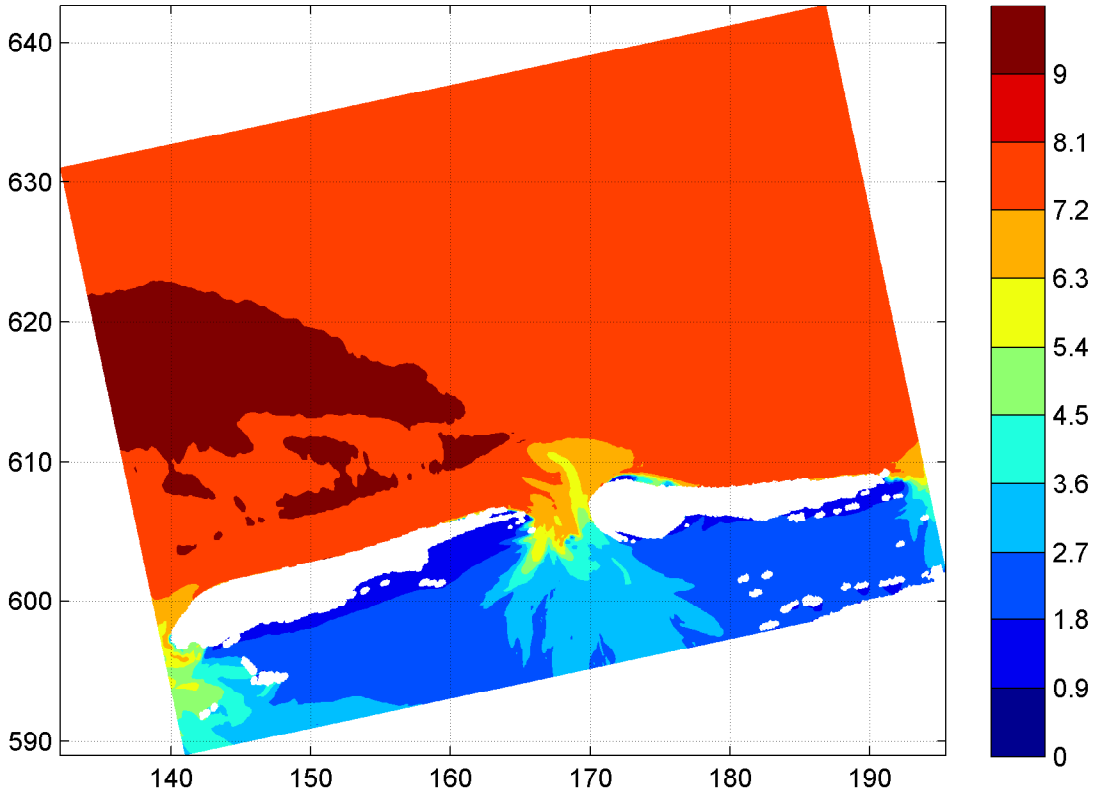

Spatial distribution of wave height H_{m0} [m] (upper panel) and wave period $T_{m-1,0}$ [s] (lower panel) on grid1	20040208	22:20hr
	Hindcast Ameland Inlet	
WL | DELFT HYDRAULICS	H4803.11	Fig. 3.30a

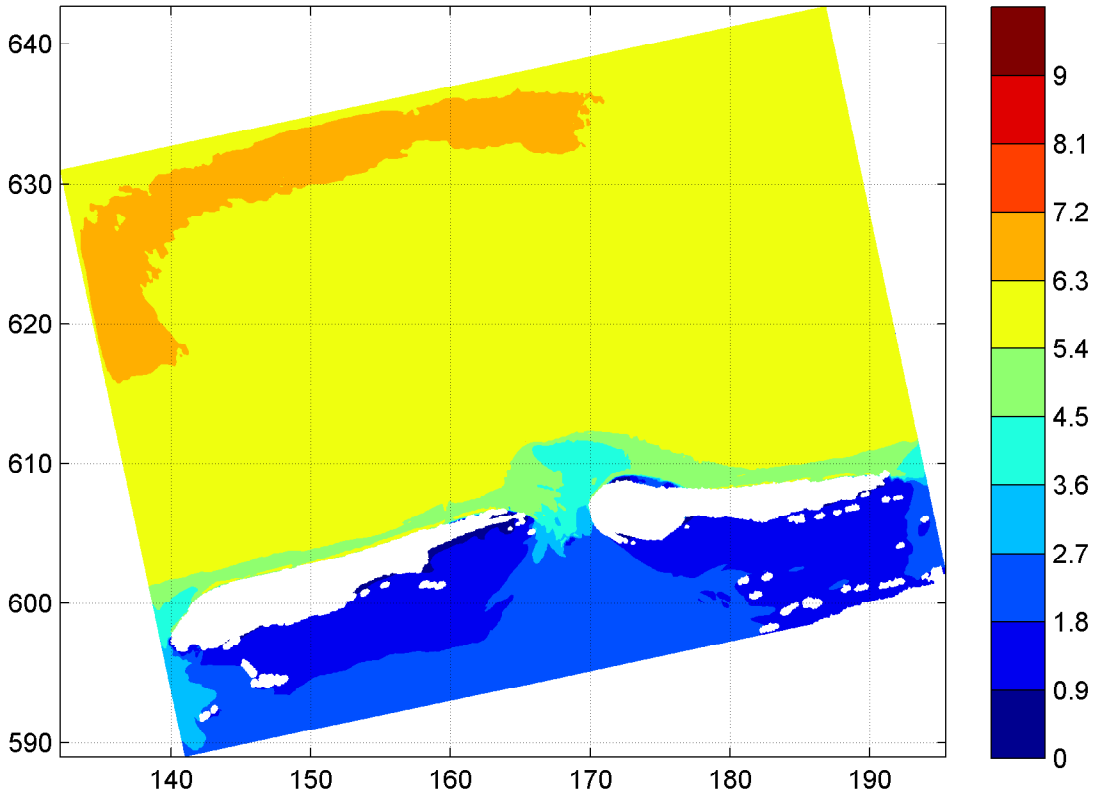

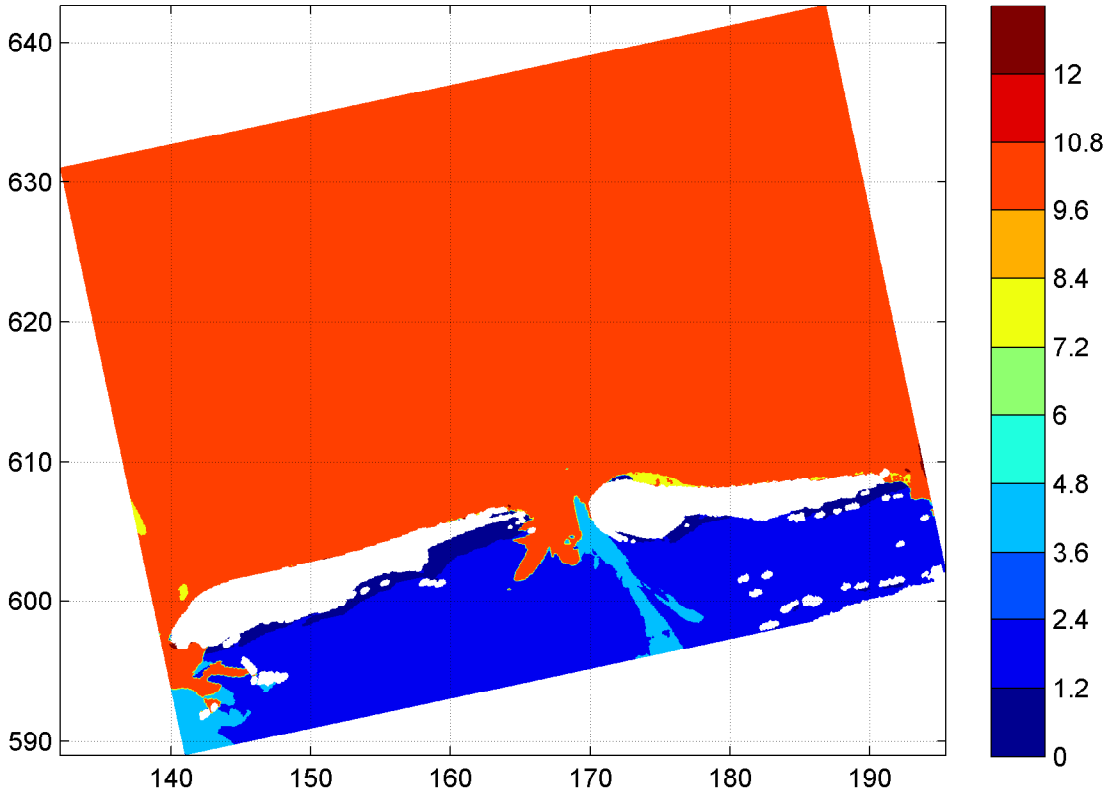

Spatial distribution of wave period T_{m02} [s] (upper panel) and wave period T_p [s] (lower panel) on grid1	20040208	22:20hr
	Hindcast Ameland Inlet	
WL | DELFT HYDRAULICS	H4803.11	Fig. 3.30b

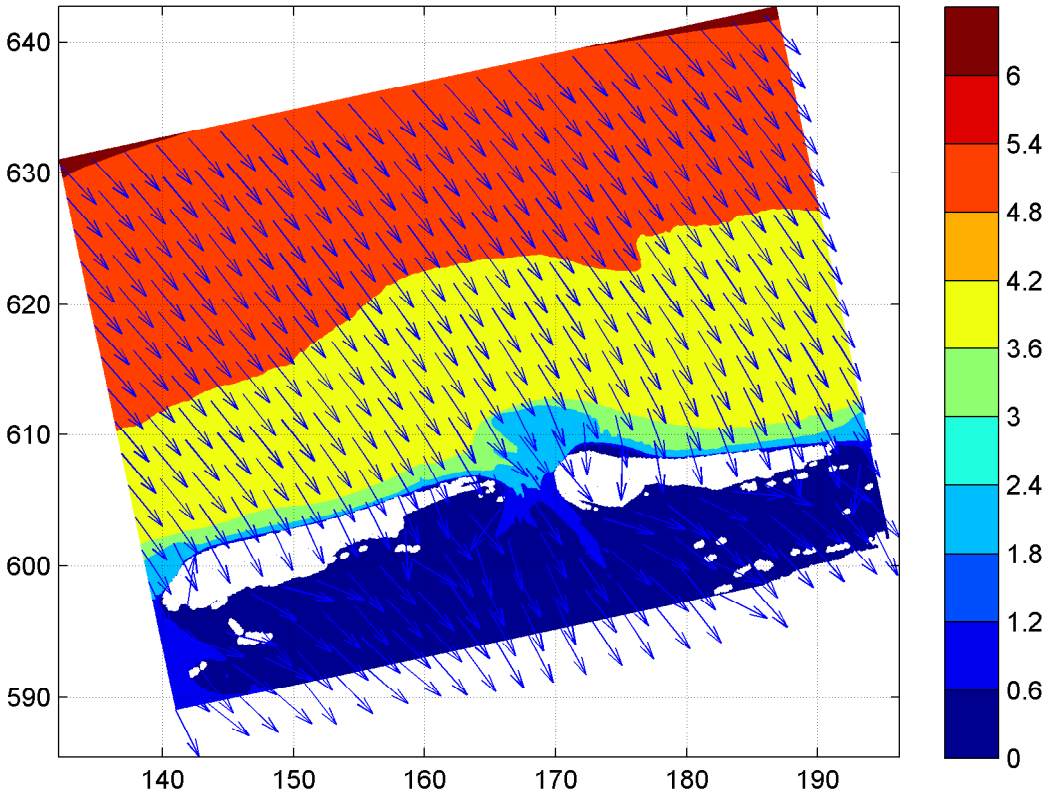

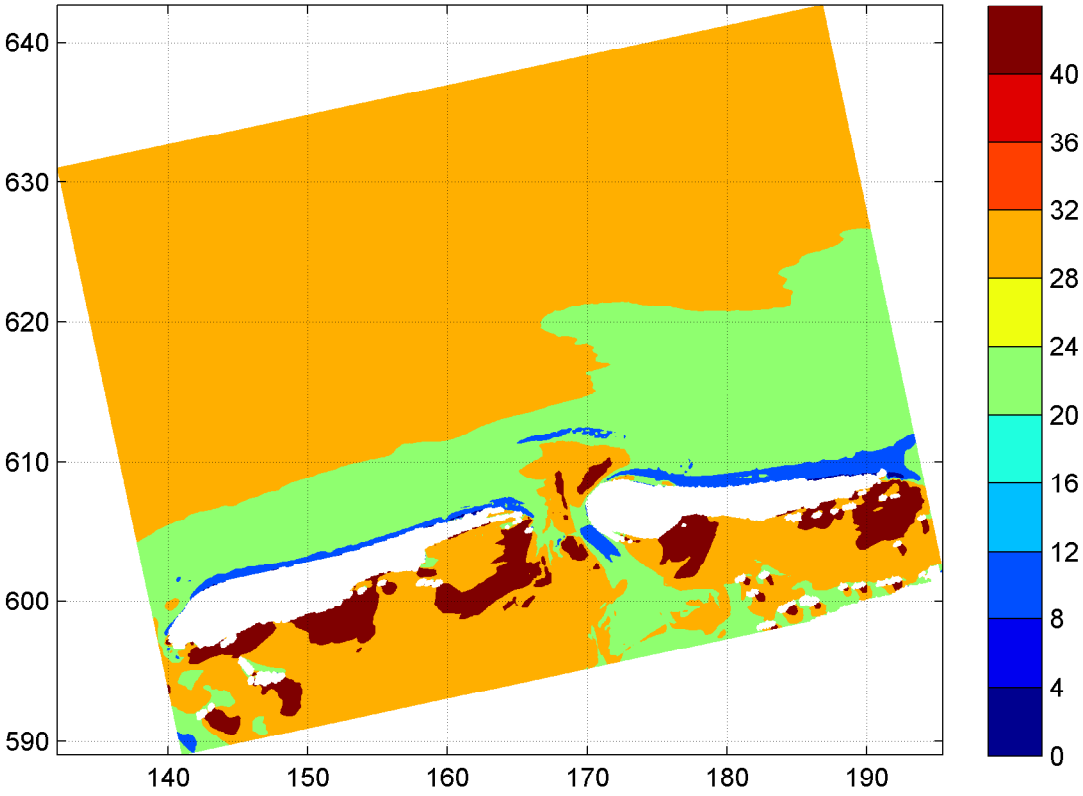

Spatial distribution of wave height [m] and mean wave direction (upper panel) and directional spreading [°] (lower panel) on grid1	20040208	22:20hr
	Hindcast Ameland Inlet	
WL | DELFT HYDRAULICS	H4803.11	Fig. 3.30c

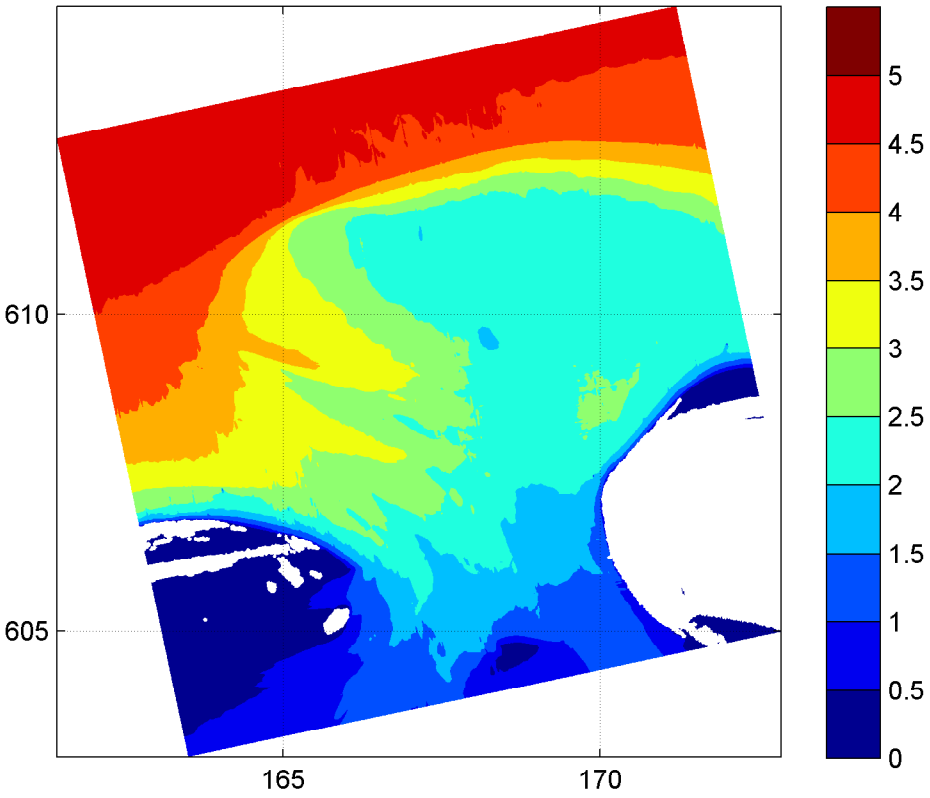

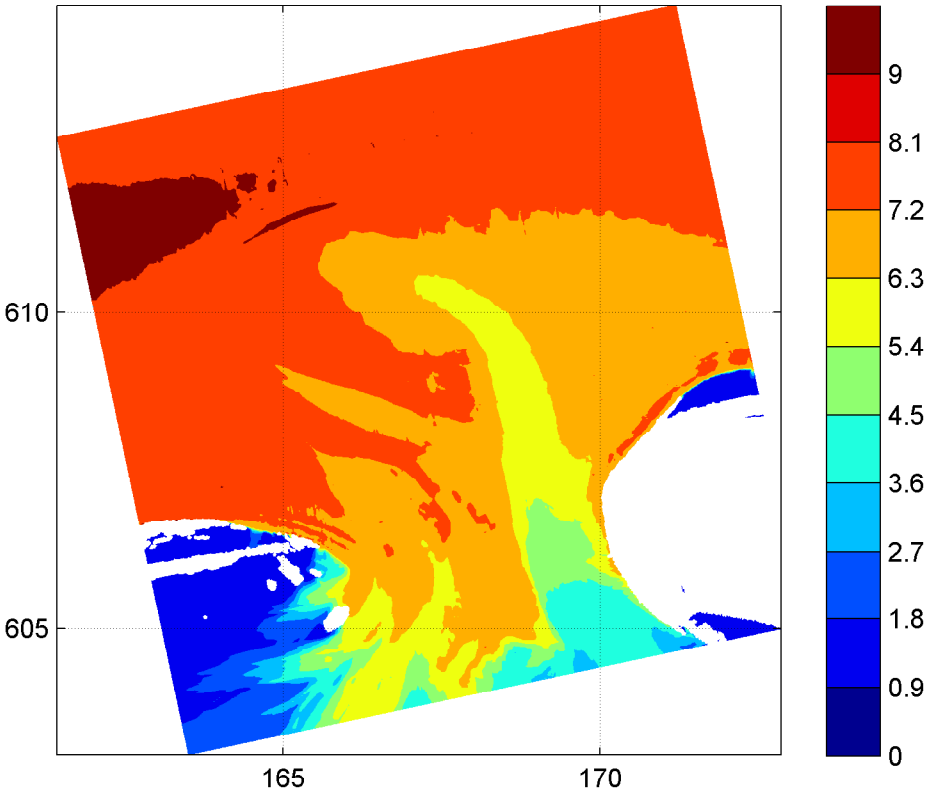

Spatial distribution of wave height H_{m0} [m] (upper panel) and wave period $T_{m-1,0}$ [s] (lower panel) on grid2	20040208	22:20hr
	Hindcast Ameland Inlet	
WL | DELFT HYDRAULICS	H4803.11	Fig. 3.31a

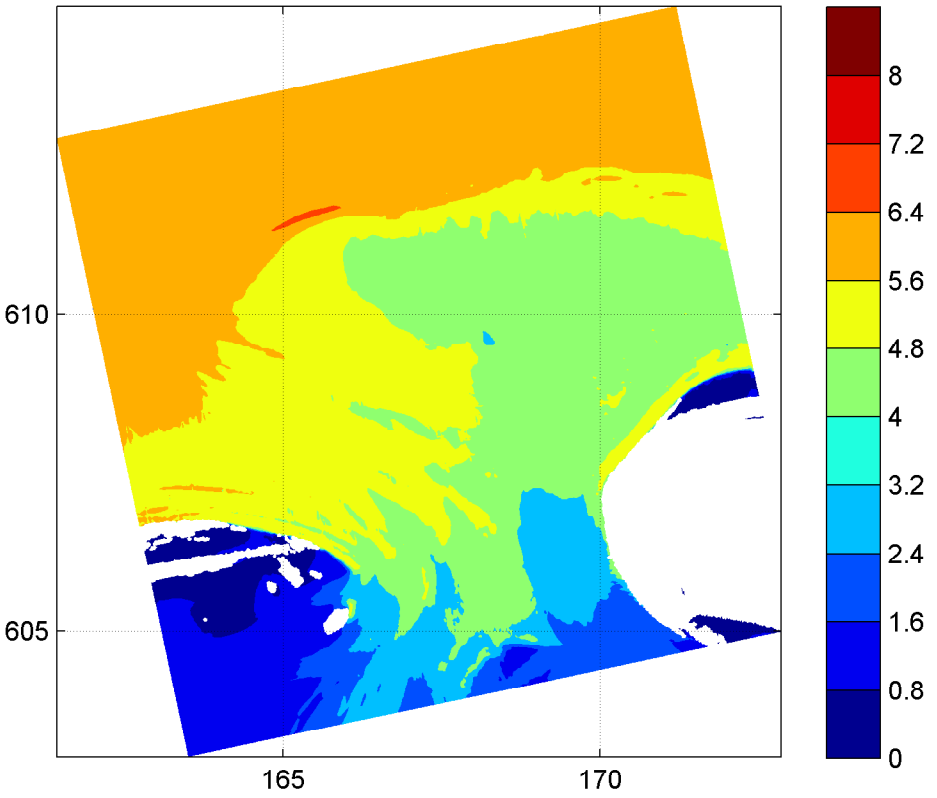

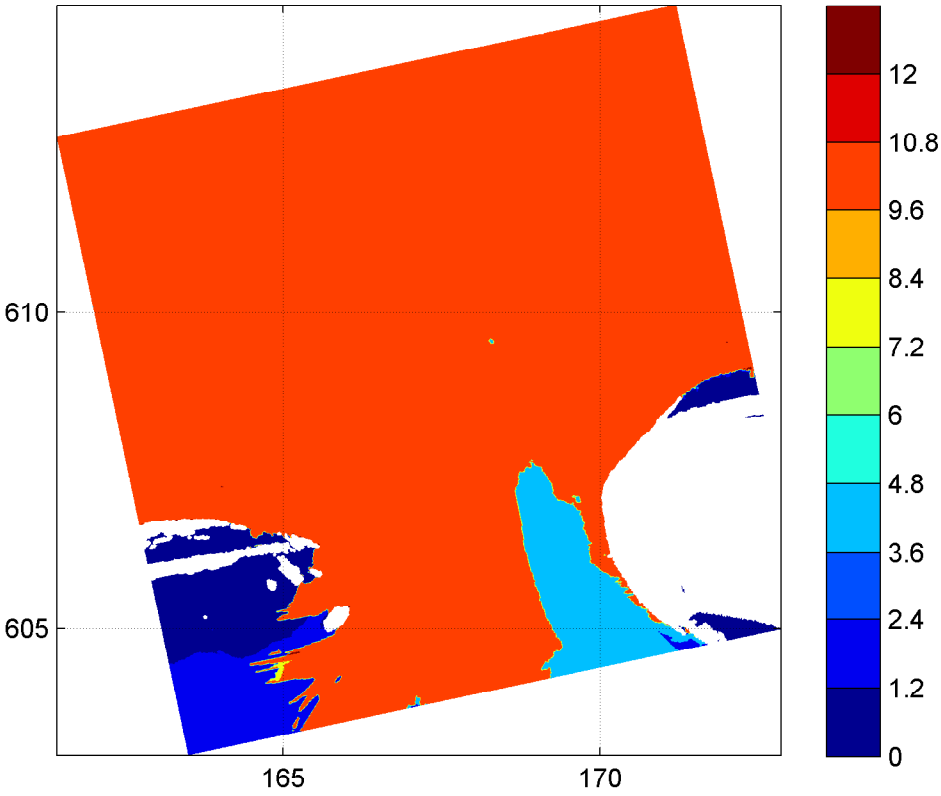

Spatial distribution of wave period T_{m02} [s] (upper panel) and wave period T_p [s] (lower panel) on grid2	20040208	22:20hr
	Hindcast Ameland Inlet	
WL | DELFT HYDRAULICS	H4803.11	Fig. 3.31b

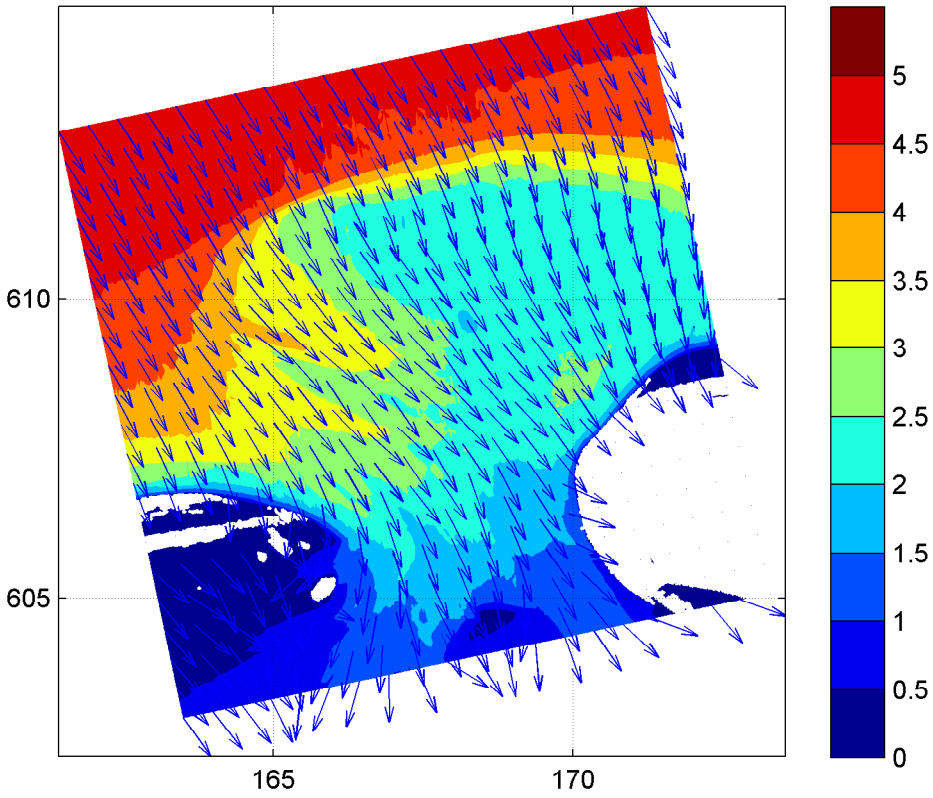

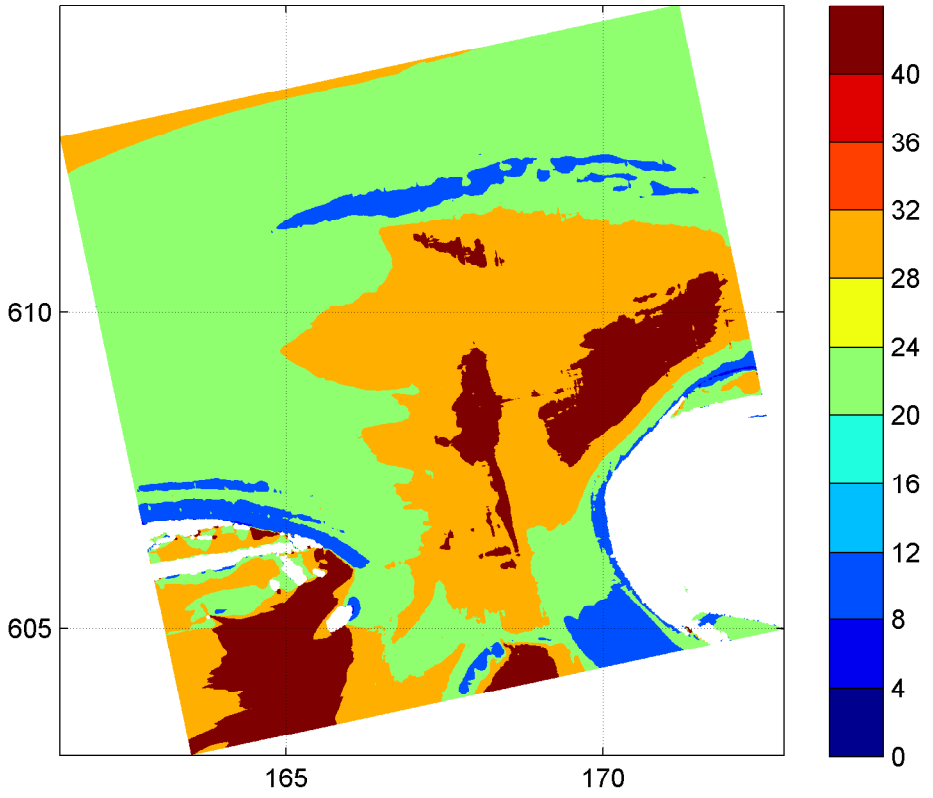

Spatial distribution of wave height [m] and mean wave direction (upper panel) and directional spreading [°] (lower panel) on grid2	20040208	22:20hr
	Hindcast Ameland Inlet	
WL | DELFT HYDRAULICS	H4803.11	Fig. 3.31c

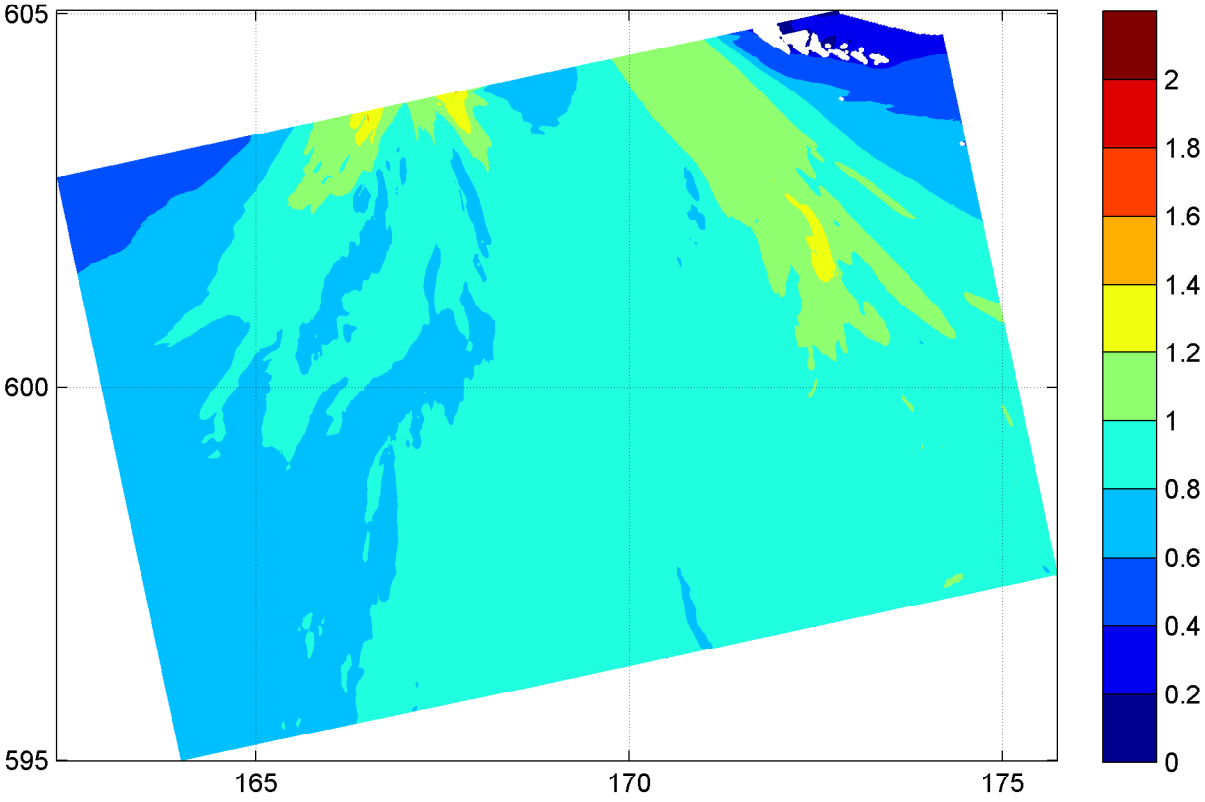

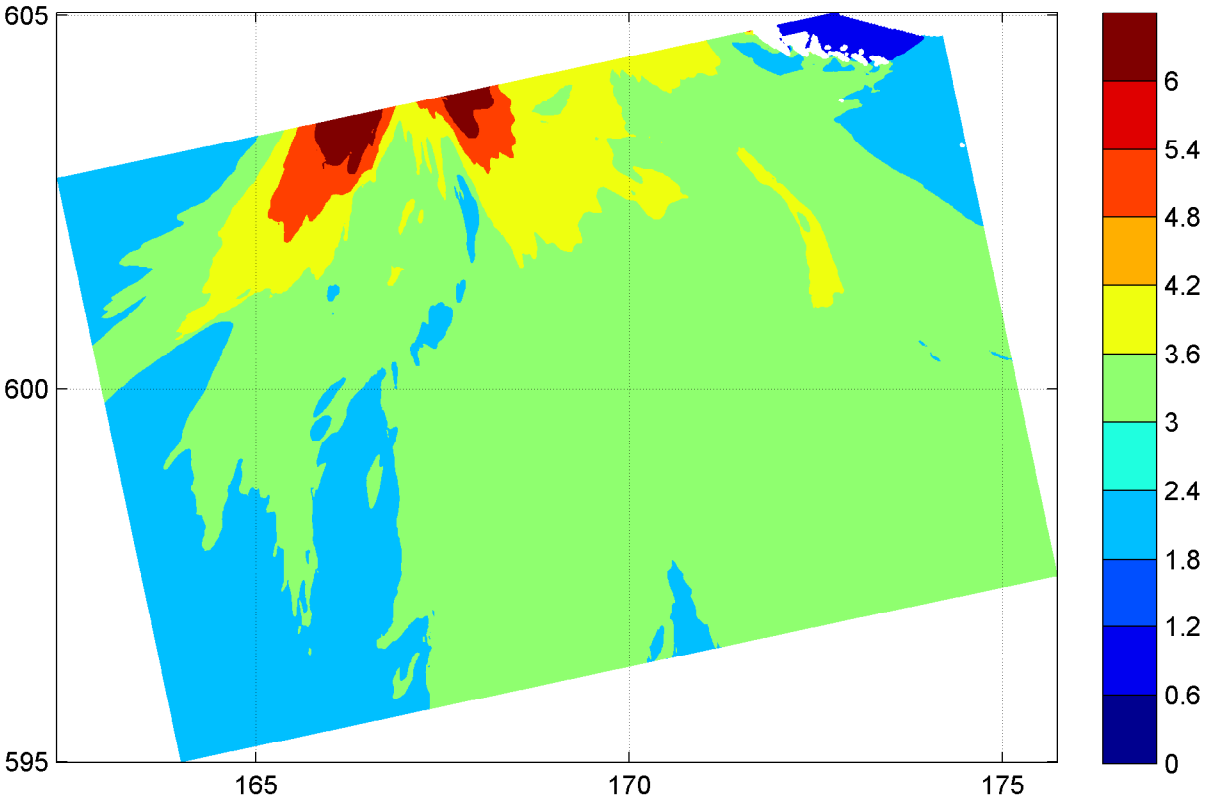

Spatial distribution of wave height H_{m0} [m] (upper panel) and wave period $T_{m-1,0}$ [s] (lower panel) on grid3	20040208	22:20hr
	Hindcast Ameland Inlet	
WL | DELFT HYDRAULICS	H4803.11	Fig. 3.32a

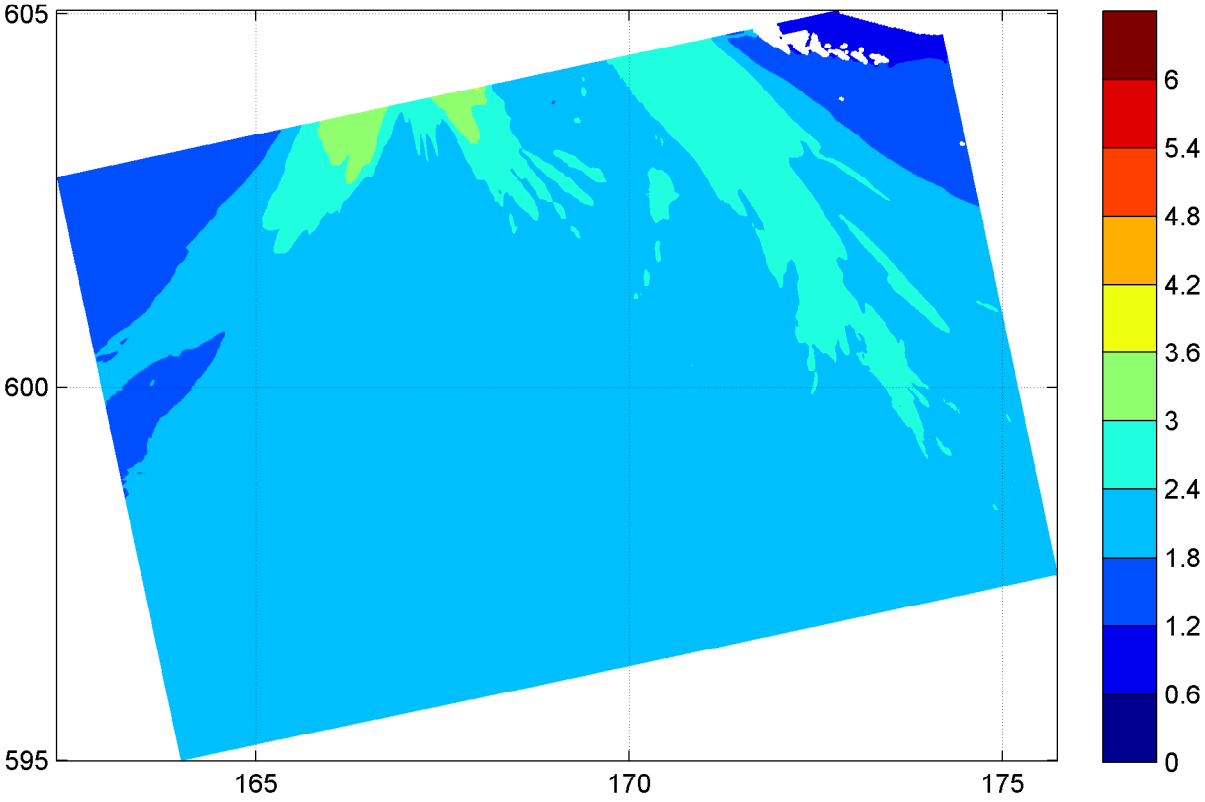

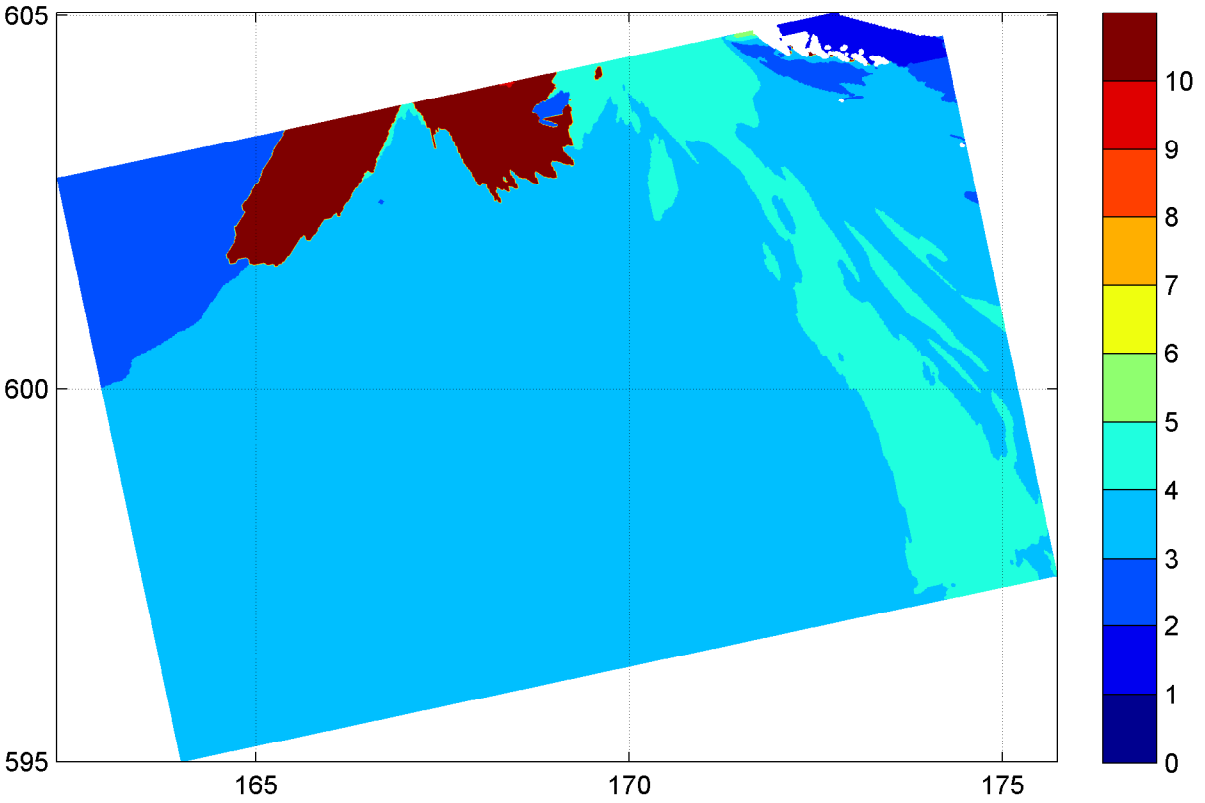

Spatial distribution of wave period T_{m02} [s] (upper panel) and wave period T_p [s] (lower panel) on grid3	20040208	22:20hr
	Hindcast Ameland Inlet	
WL | DELFT HYDRAULICS	H4803.11	Fig. 3.32b

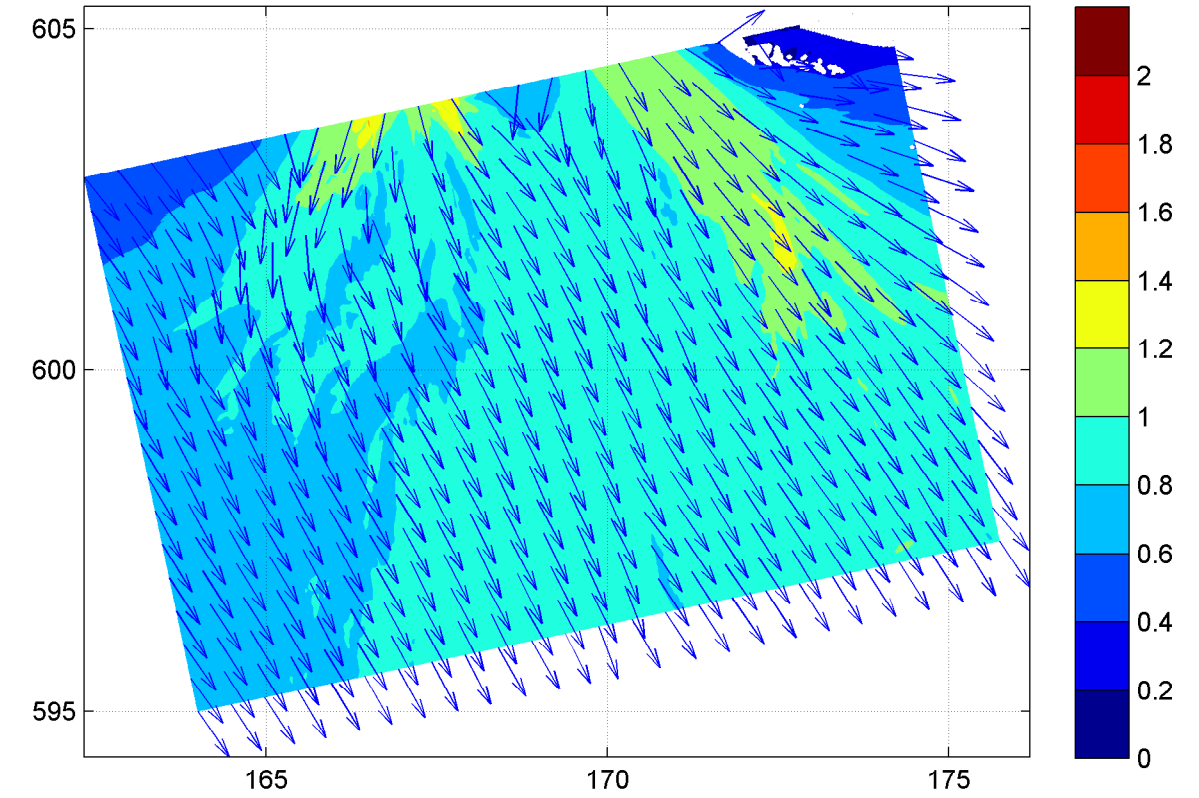

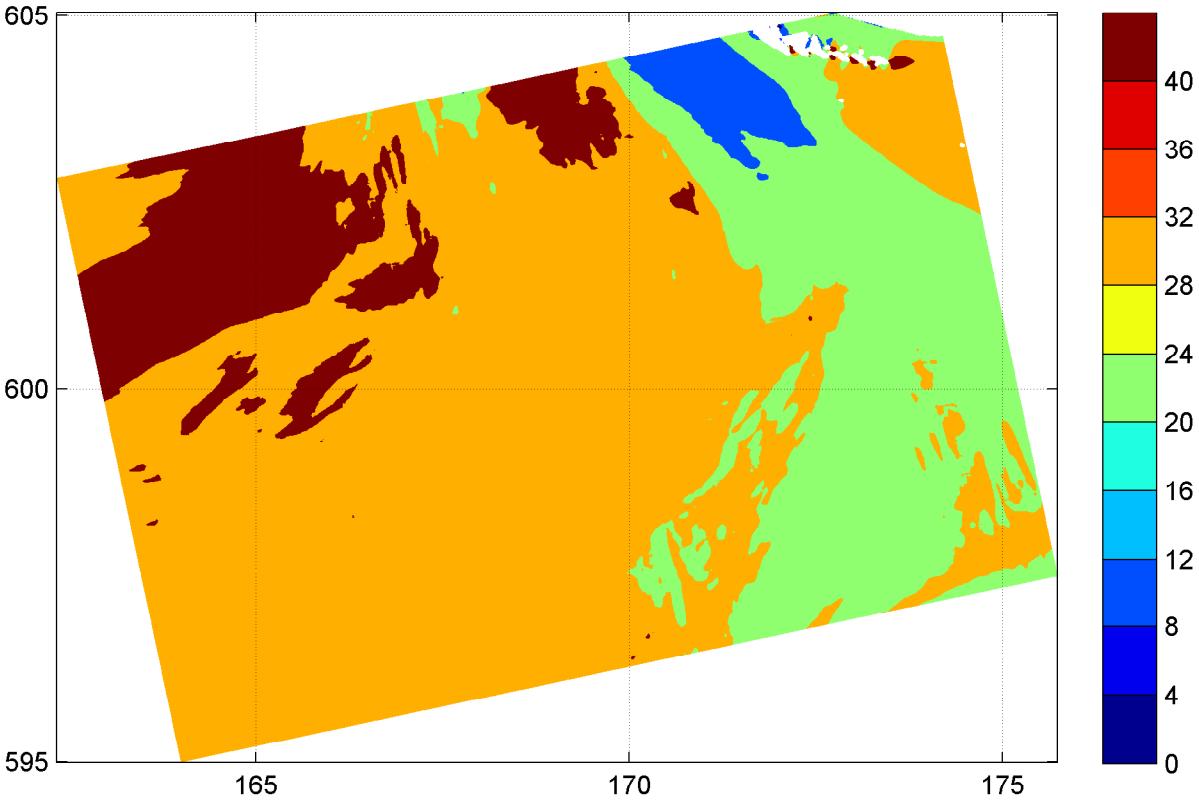

Spatial distribution of wave height [m] and mean wave direction (upper panel) and directional spreading [°] (lower panel) on grid3	20040208	22:20hr
	Hindcast Ameland Inlet	
WL | DELFT HYDRAULICS	H4803.11	Fig. 3.32c

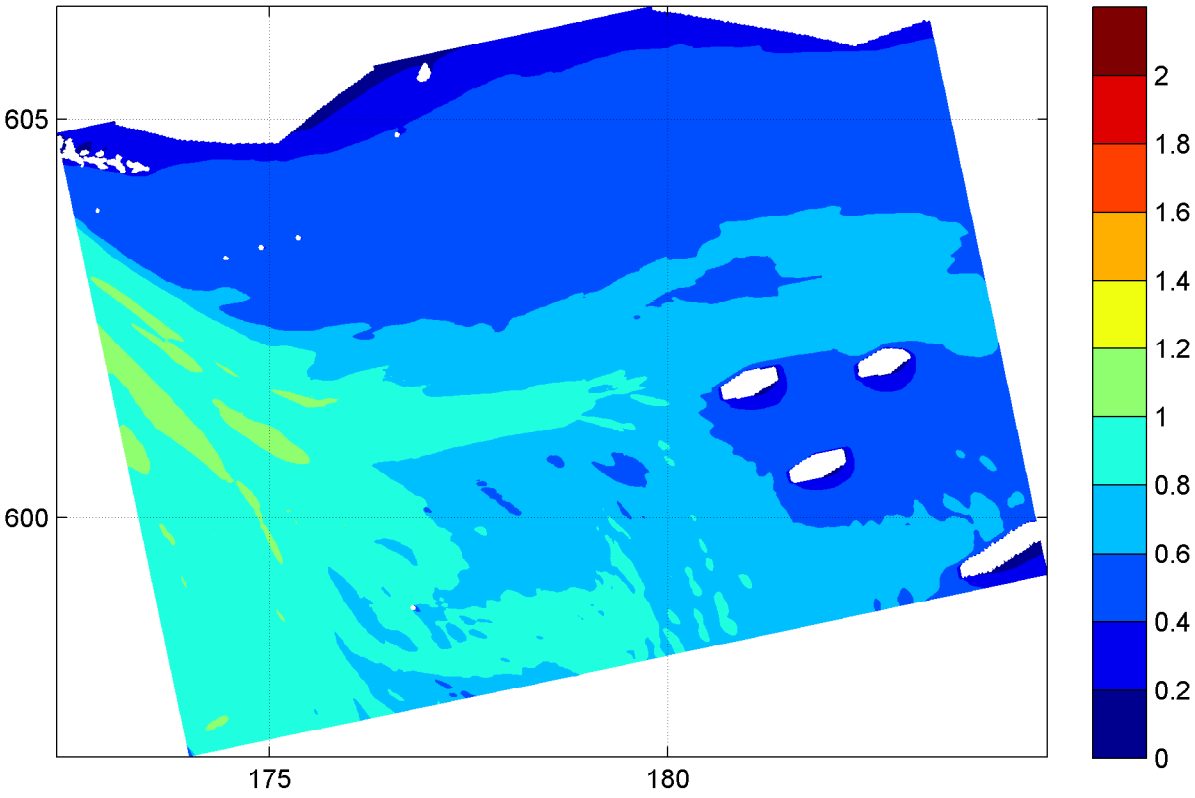

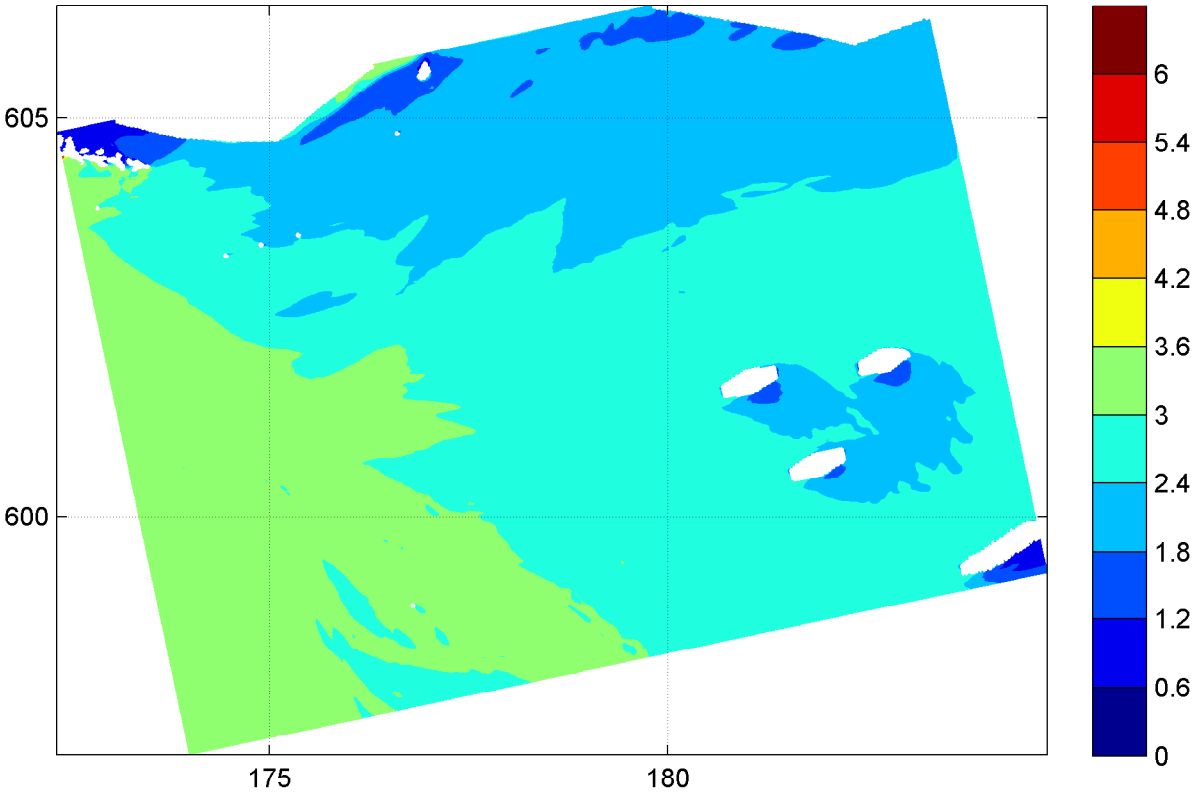

Spatial distribution of wave height H_{m0} [m] (upper panel) and wave period $T_{m-1,0}$ [s] (lower panel) on grid4	20040208	22:20hr
	Hindcast Ameland Inlet	
WL | DELFT HYDRAULICS	H4803.11	Fig. 3.33a

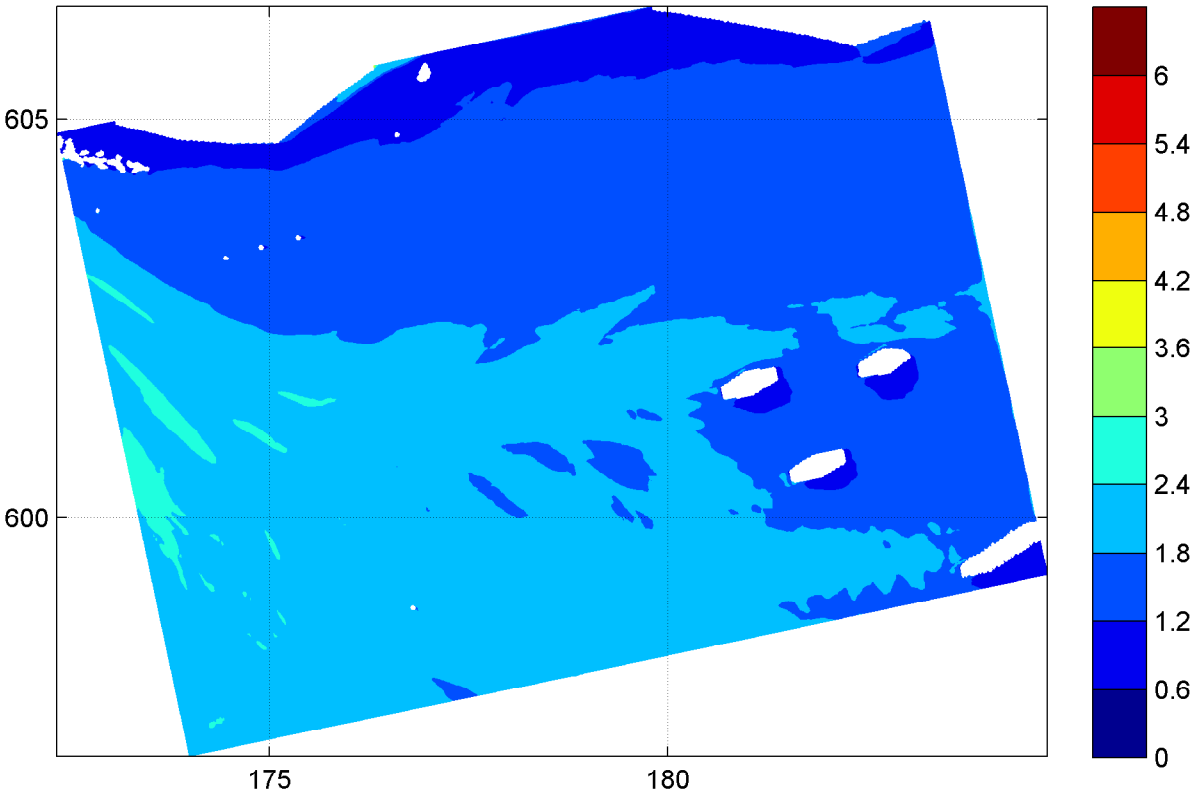

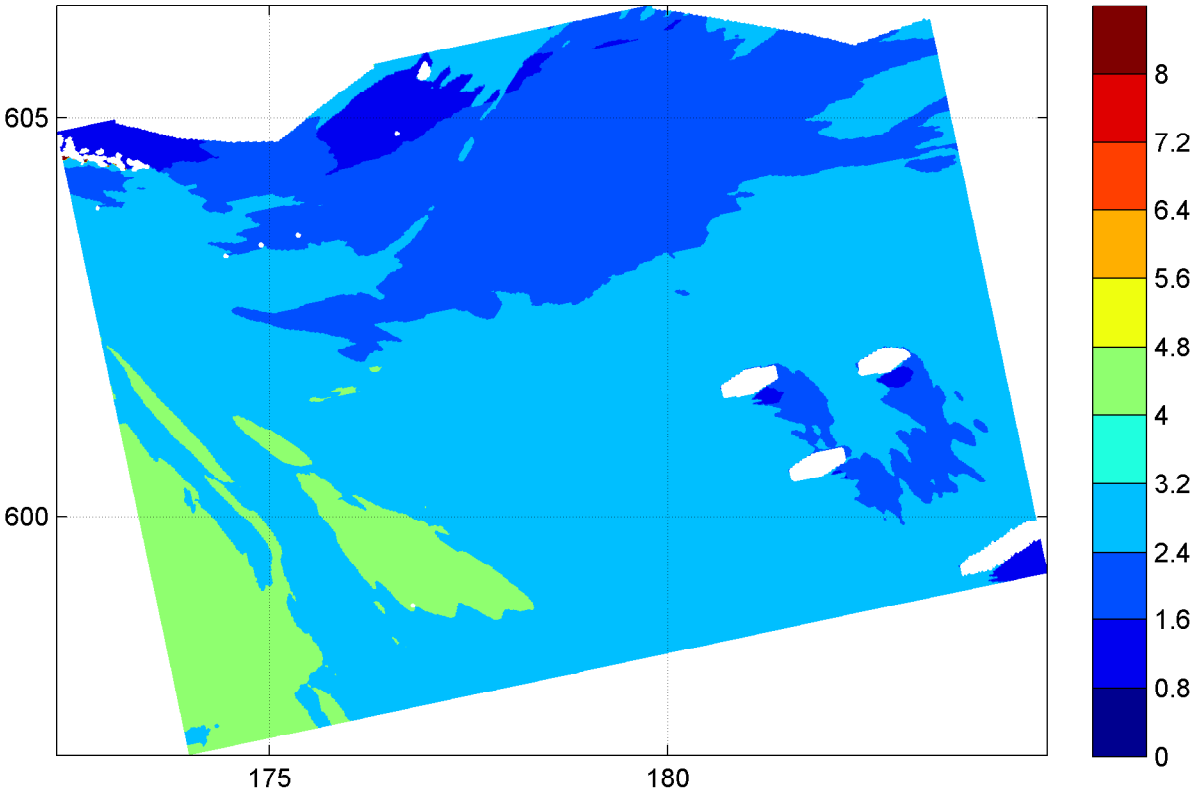

Spatial distribution of wave period T_{m02} [s] (upper panel) and wave period T_p [s] (lower panel) on grid4	20040208	22:20hr
	Hindcast Ameland Inlet	
WL | DELFT HYDRAULICS	H4803.11	Fig. 3.33b

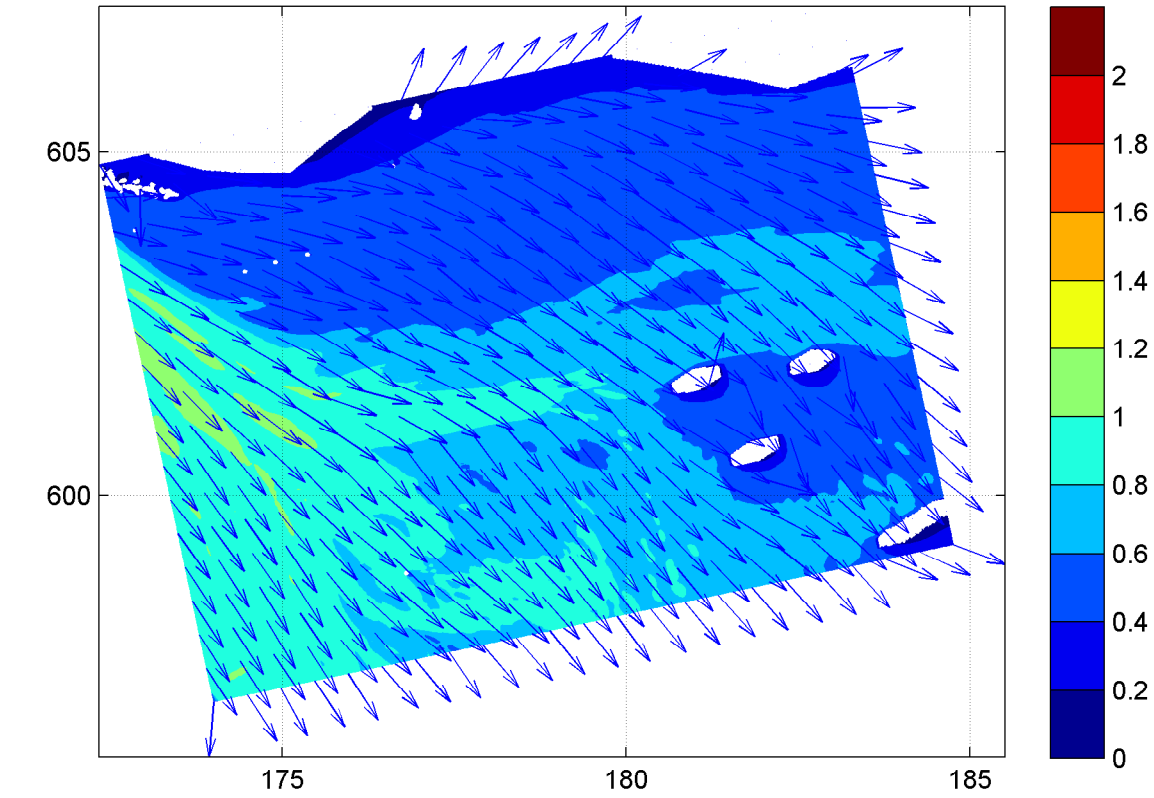

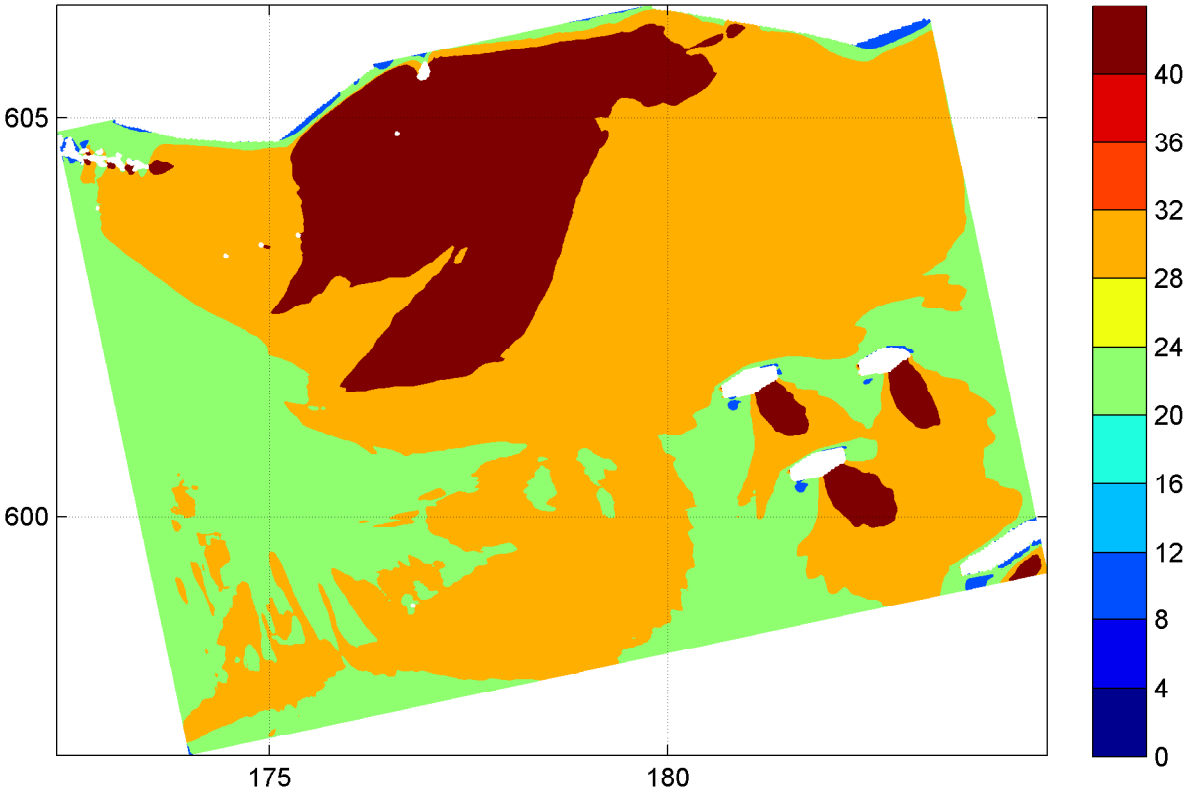

Spatial distribution of wave height [m] and mean wave direction (upper panel) and directional spreading [°] (lower panel) on grid4	20040208	22:20hr
	Hindcast Ameland Inlet	
WL | DELFT HYDRAULICS	H4803.11	Fig. 3.33c

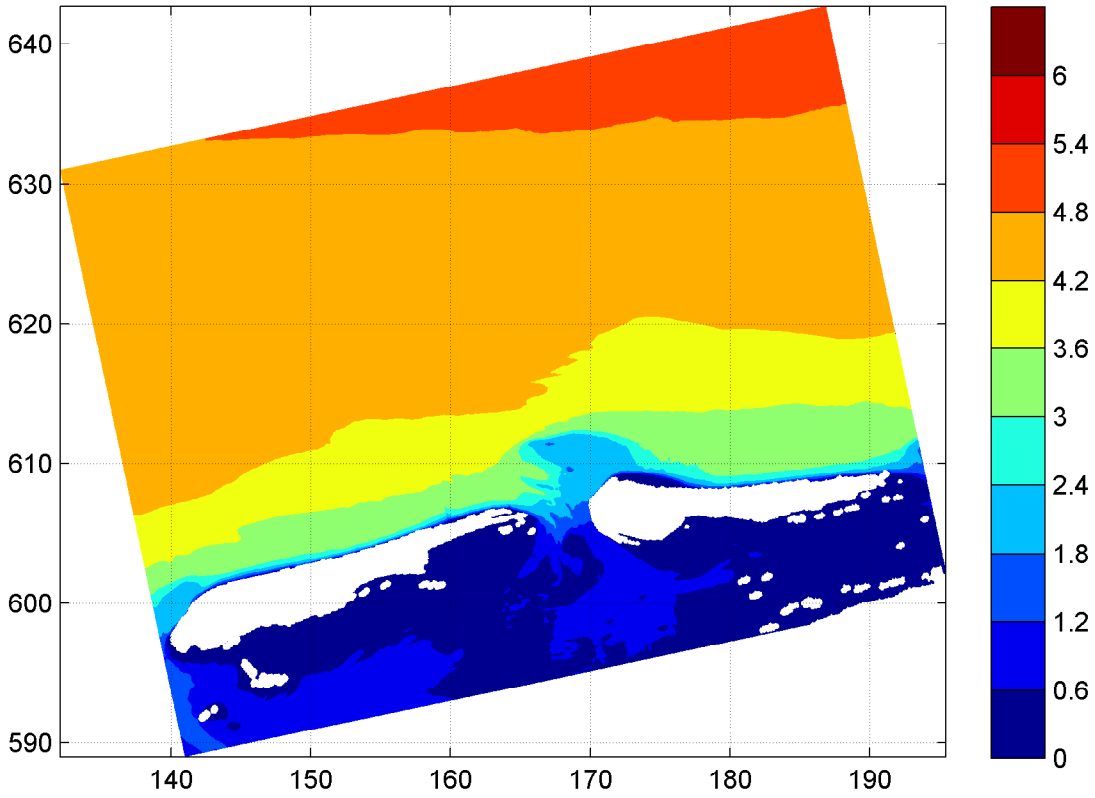

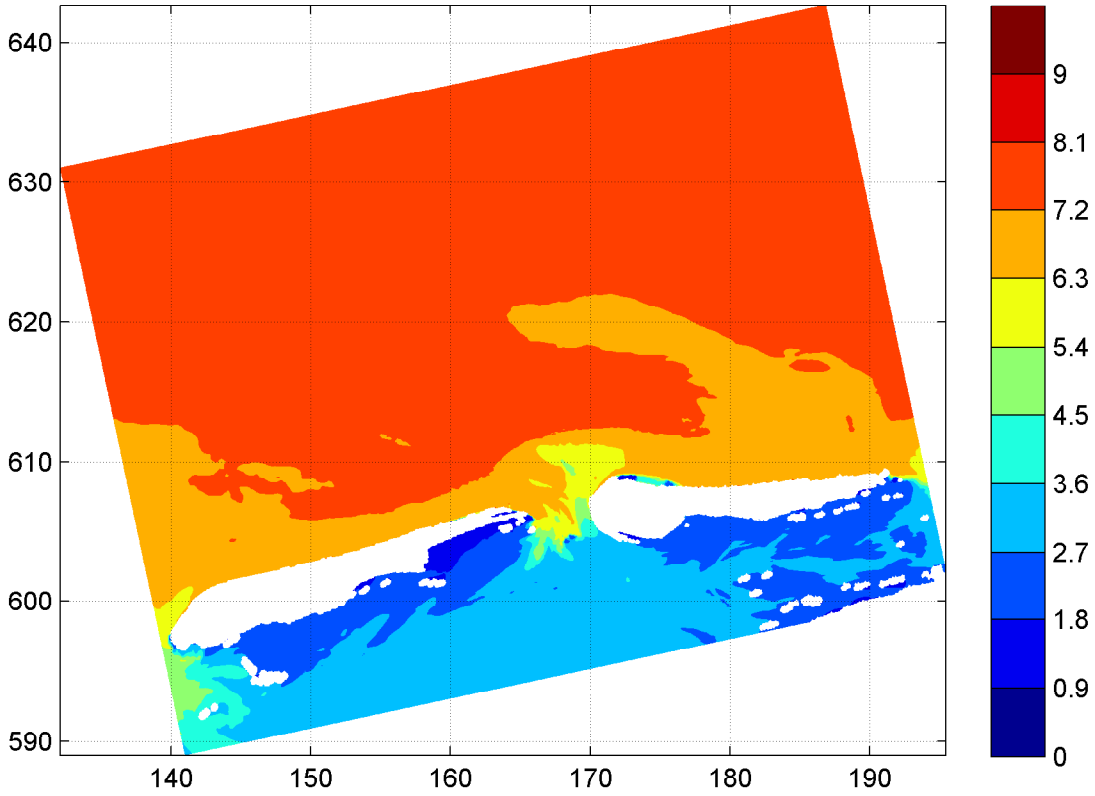

Spatial distribution of wave height H_{m0} [m] (upper panel) and wave period $T_{m-1,0}$ [s] (lower panel) on grid1 uniform wind field	20050102	12:00hr
	Hindcast Ameland Inlet	
WL | DELFT HYDRAULICS	H4803.11	Fig. 3.34a

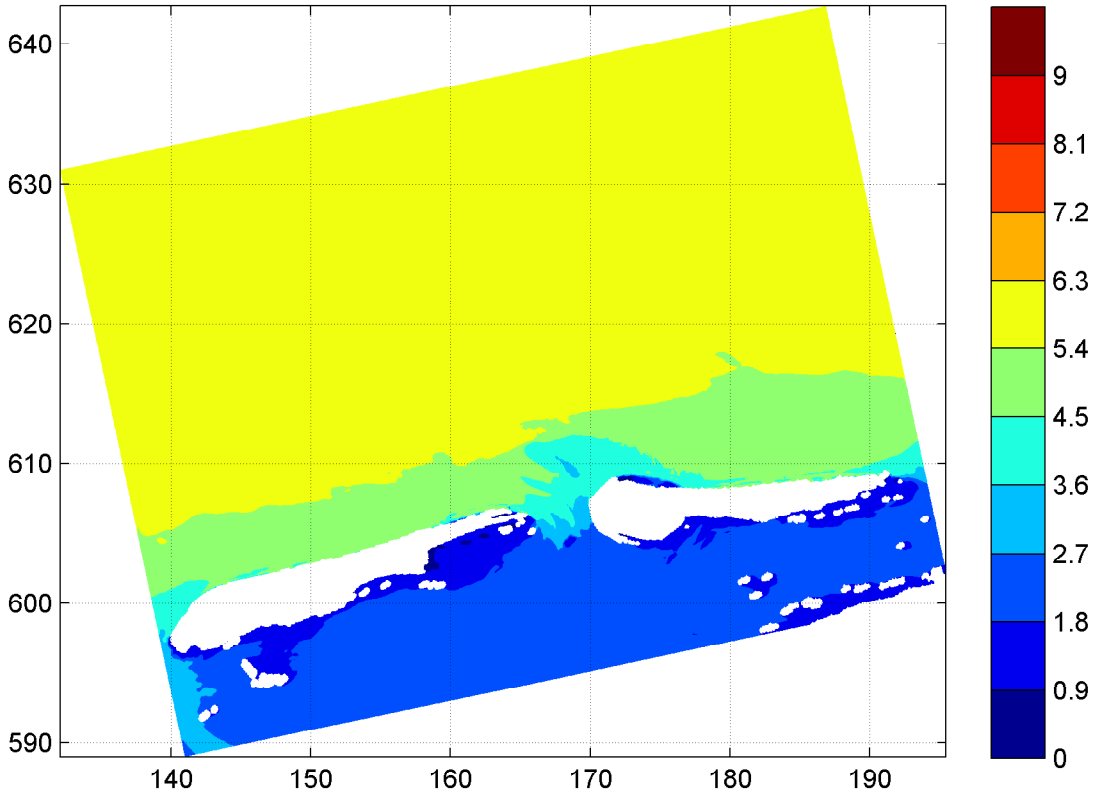

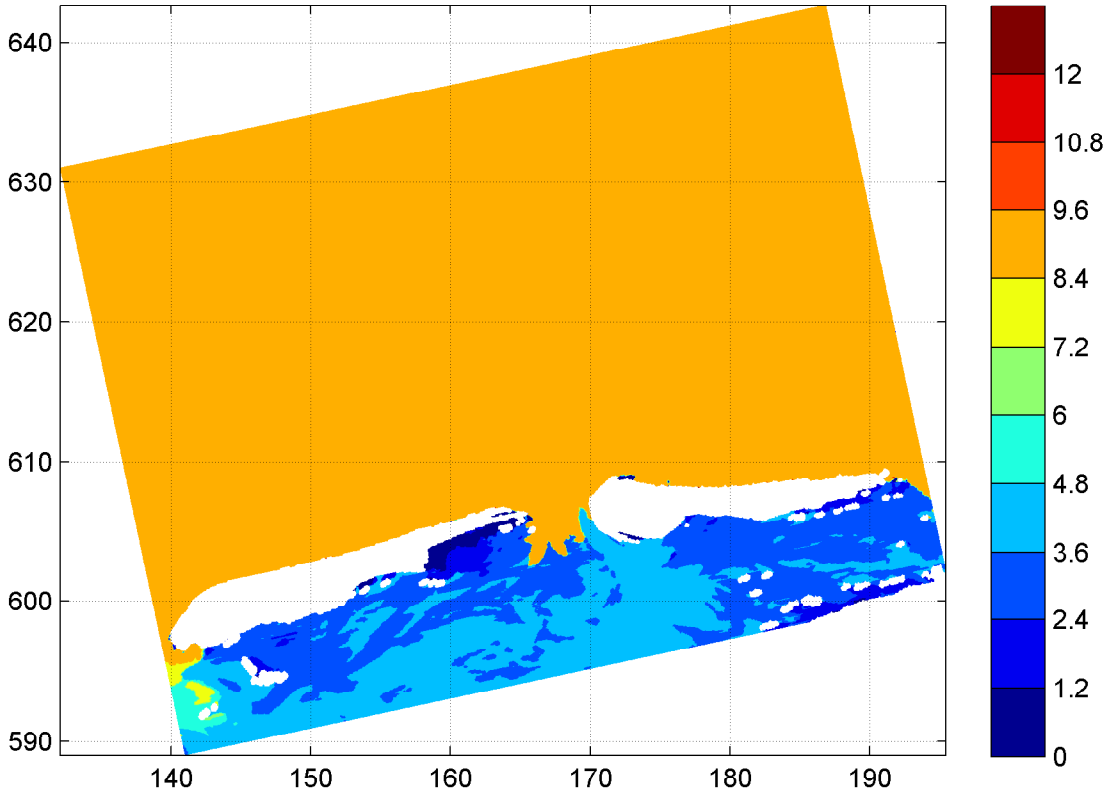

Spatial distribution of wave period T_{m02} [s] (upper panel) and wave period T_p [s] (lower panel) on grid1 uniform wind field	20050102	12:00hr
	Hindcast Ameland Inlet	
WL | DELFT HYDRAULICS	H4803.11	Fig. 3.34b

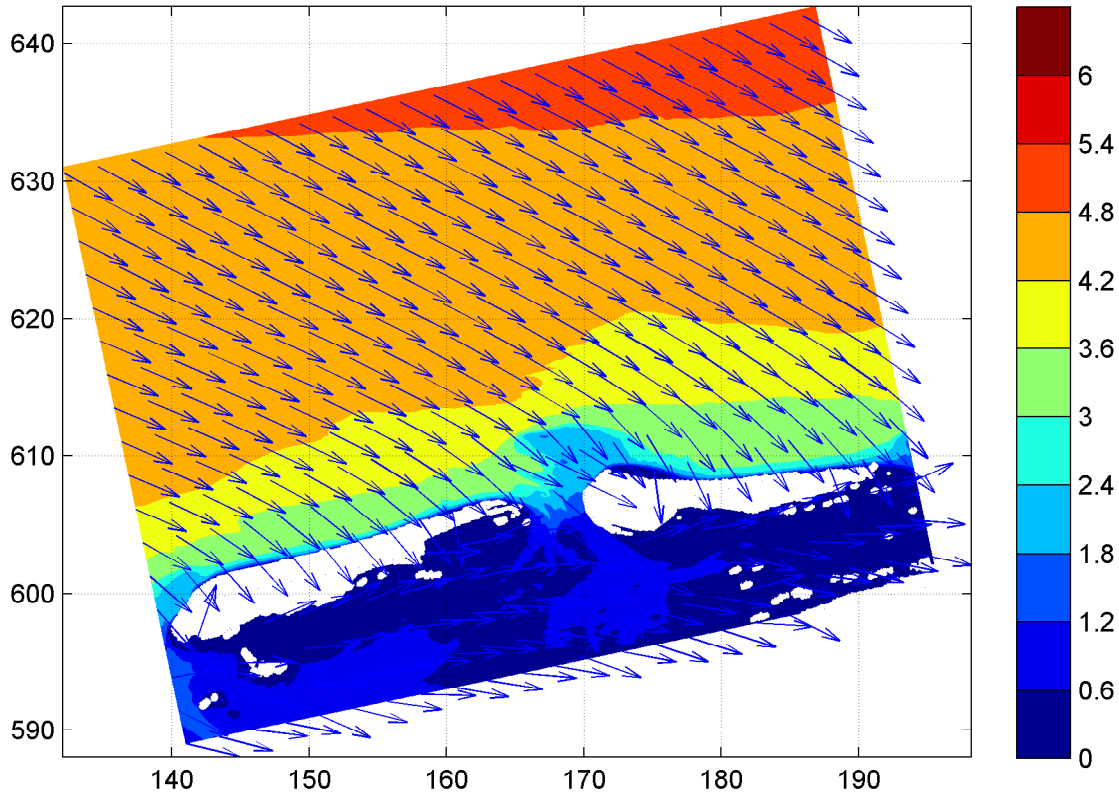

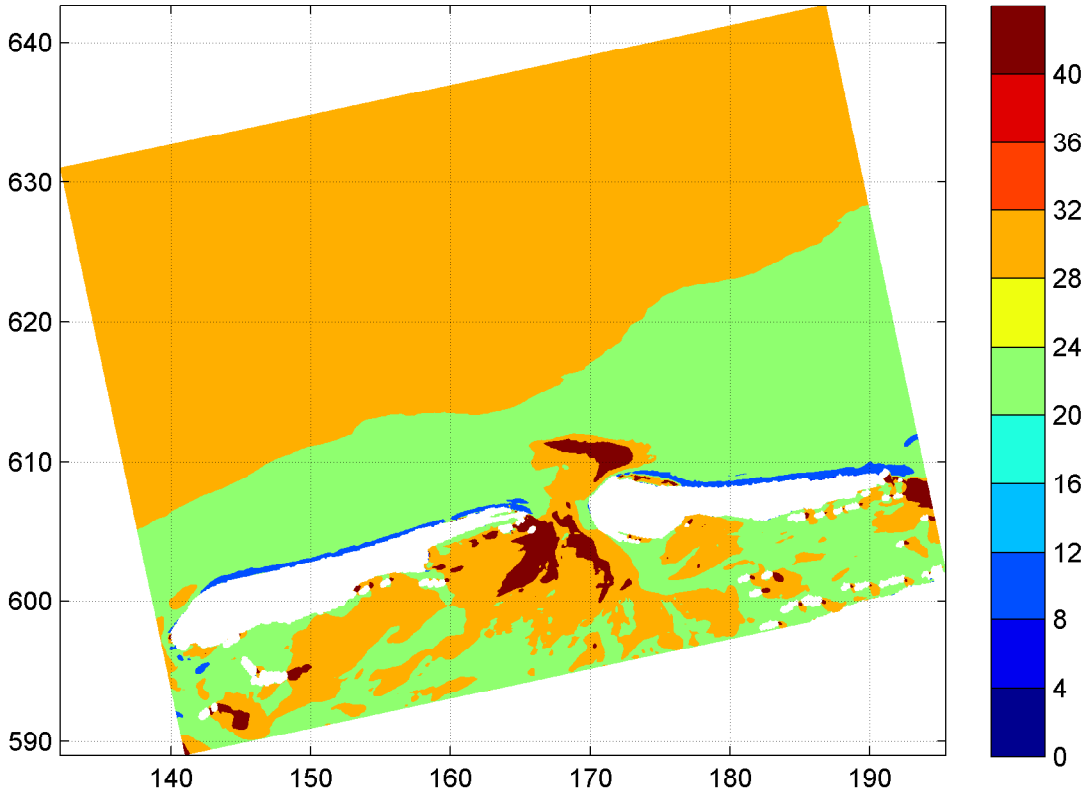

Spatial distribution of wave height [m] and mean wave direction (upper panel) and directional spreading [°] (lower panel) on grid1 uniform wind field	20050102	12:00hr
	Hindcast Ameland Inlet	
WL | DELFT HYDRAULICS	H4803.11	Fig. 3.34c

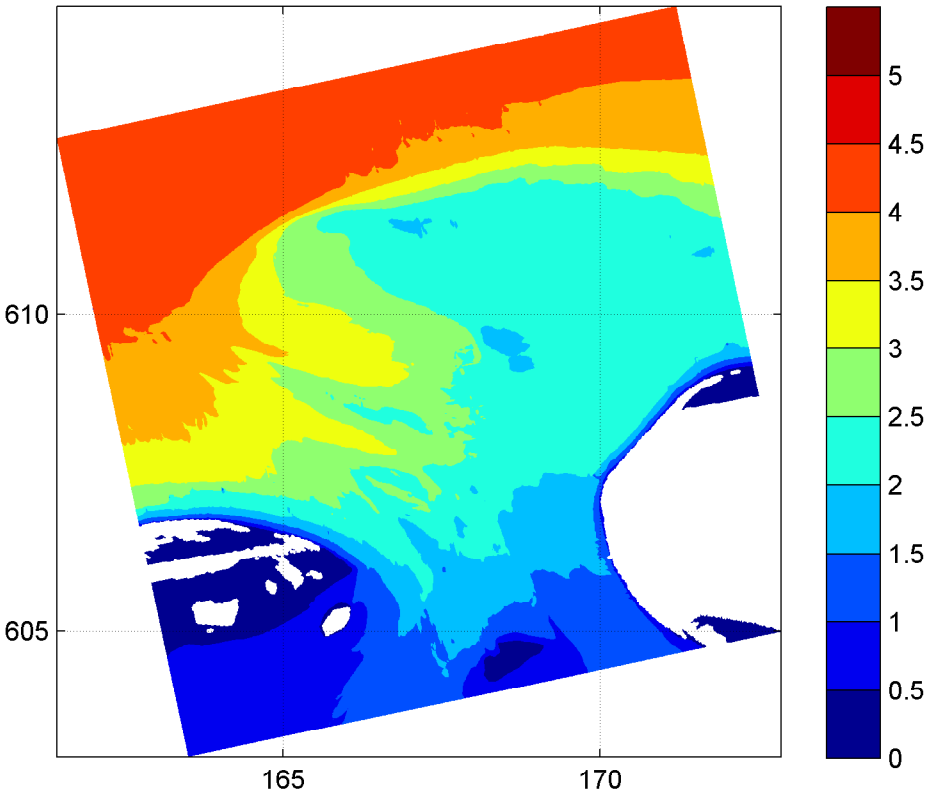

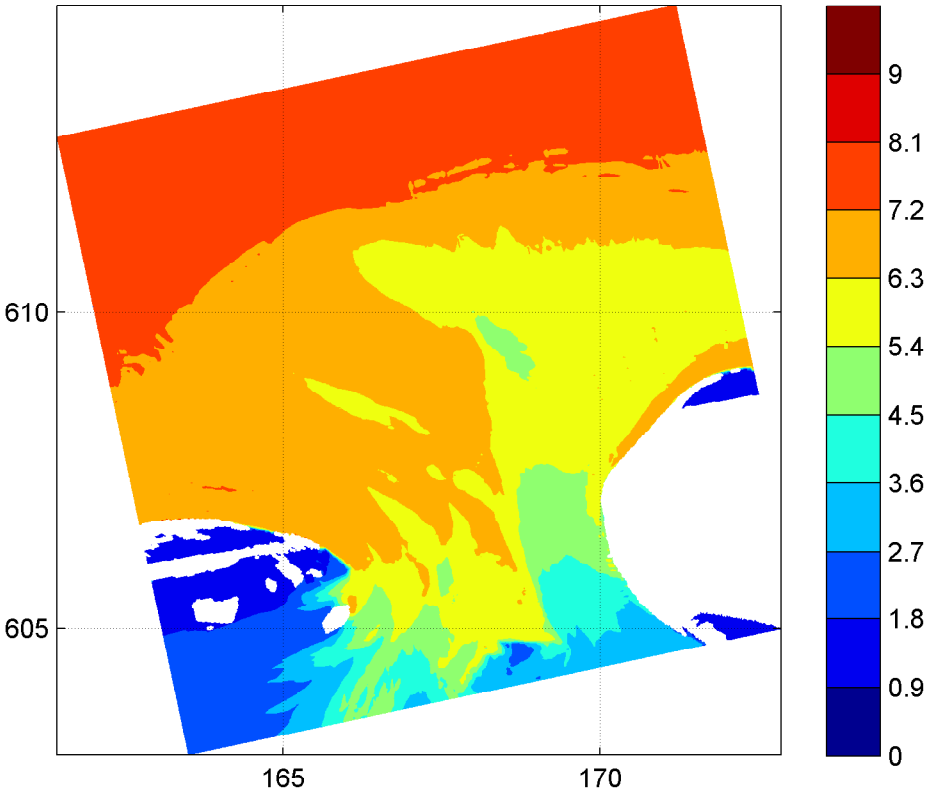

Spatial distribution of wave height H_{m0} [m] (upper panel) and wave period $T_{m-1,0}$ [s] (lower panel) on grid2 uniform wind field	20050102	12:00hr
	Hindcast Ameland Inlet	
WL | DELFT HYDRAULICS	H4803.11	Fig. 3.35a

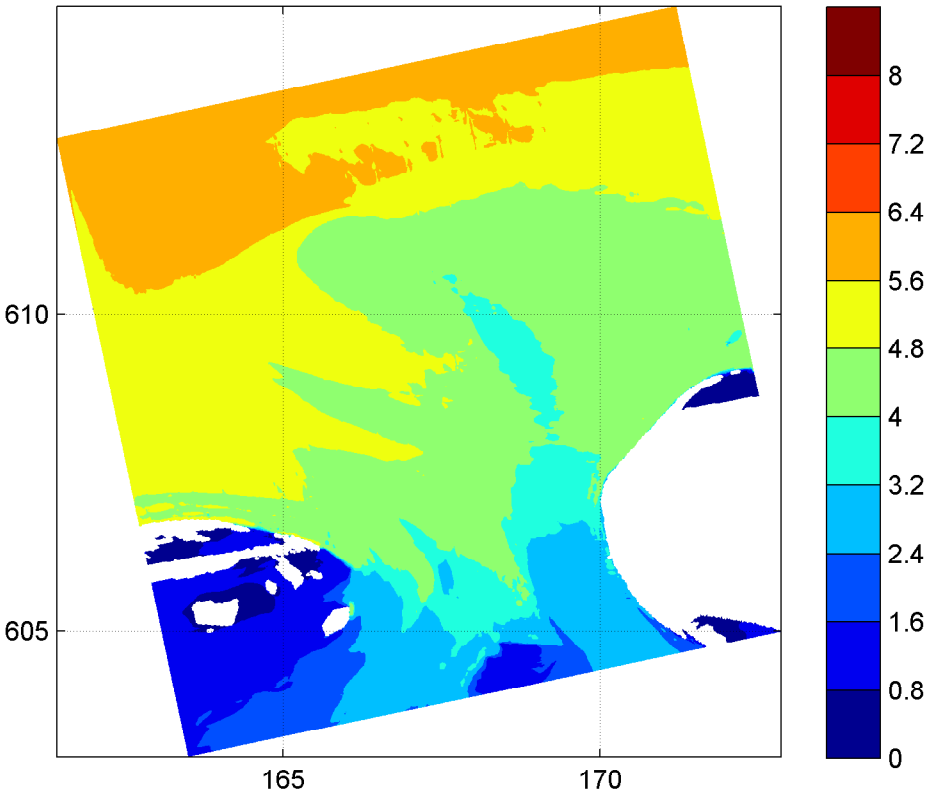

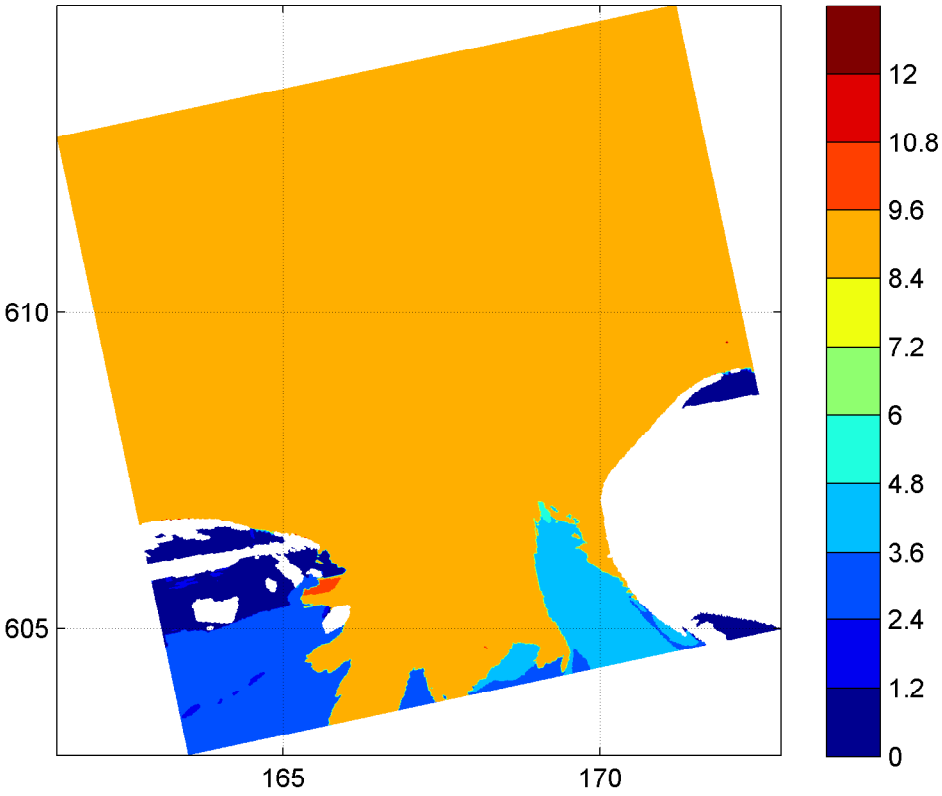

Spatial distribution of wave period T_{m02} [s] (upper panel) and wave period T_p [s] (lower panel) on grid2 uniform wind field	20050102	12:00hr
	Hindcast Ameland Inlet	
WL | DELFT HYDRAULICS	H4803.11	Fig. 3.35b

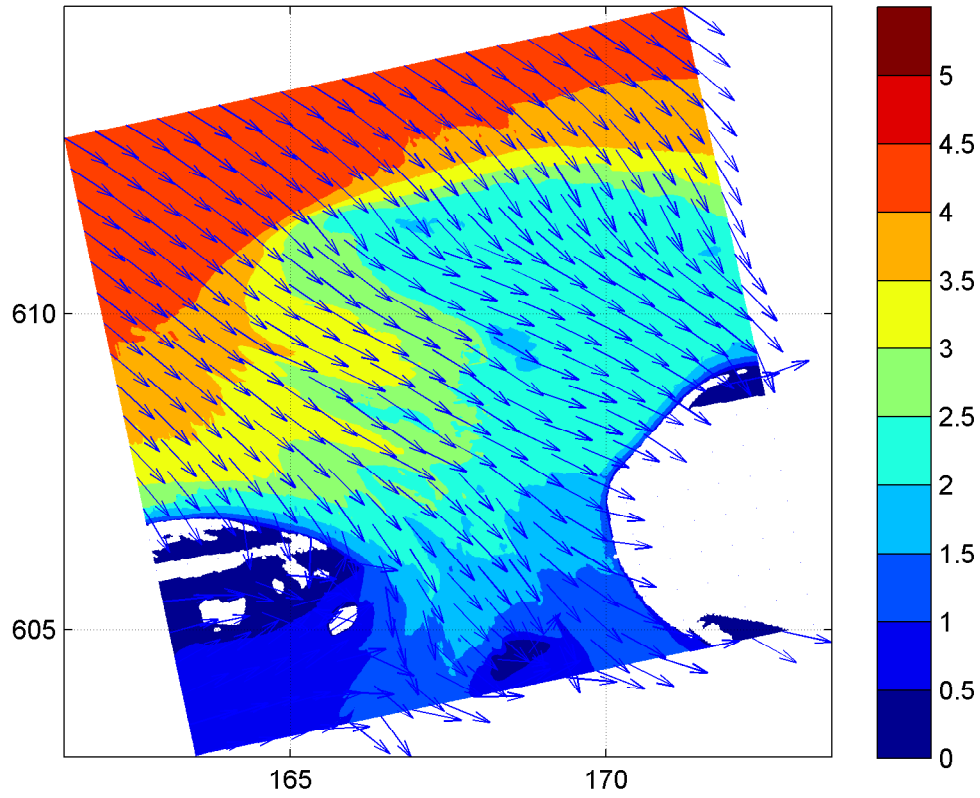

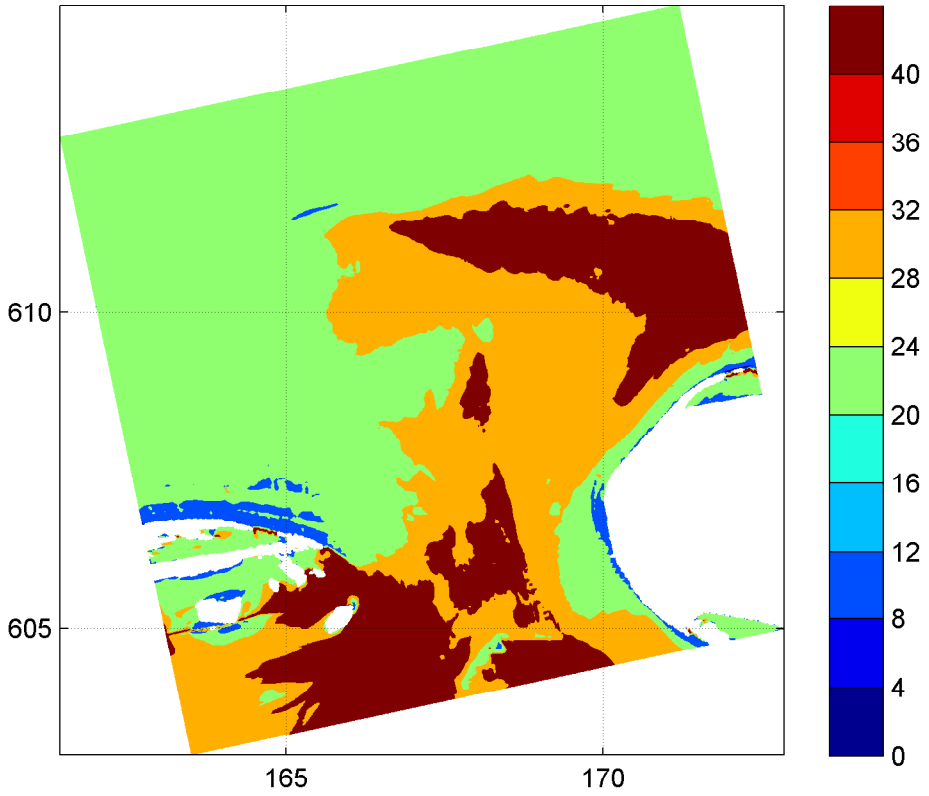

Spatial distribution of wave height [m] and mean wave direction (upper panel) and directional spreading [°] (lower panel) on grid2 uniform wind field	20050102	12:00hr
	Hindcast Ameland Inlet	
WL | DELFT HYDRAULICS	H4803.11	Fig. 3.35c

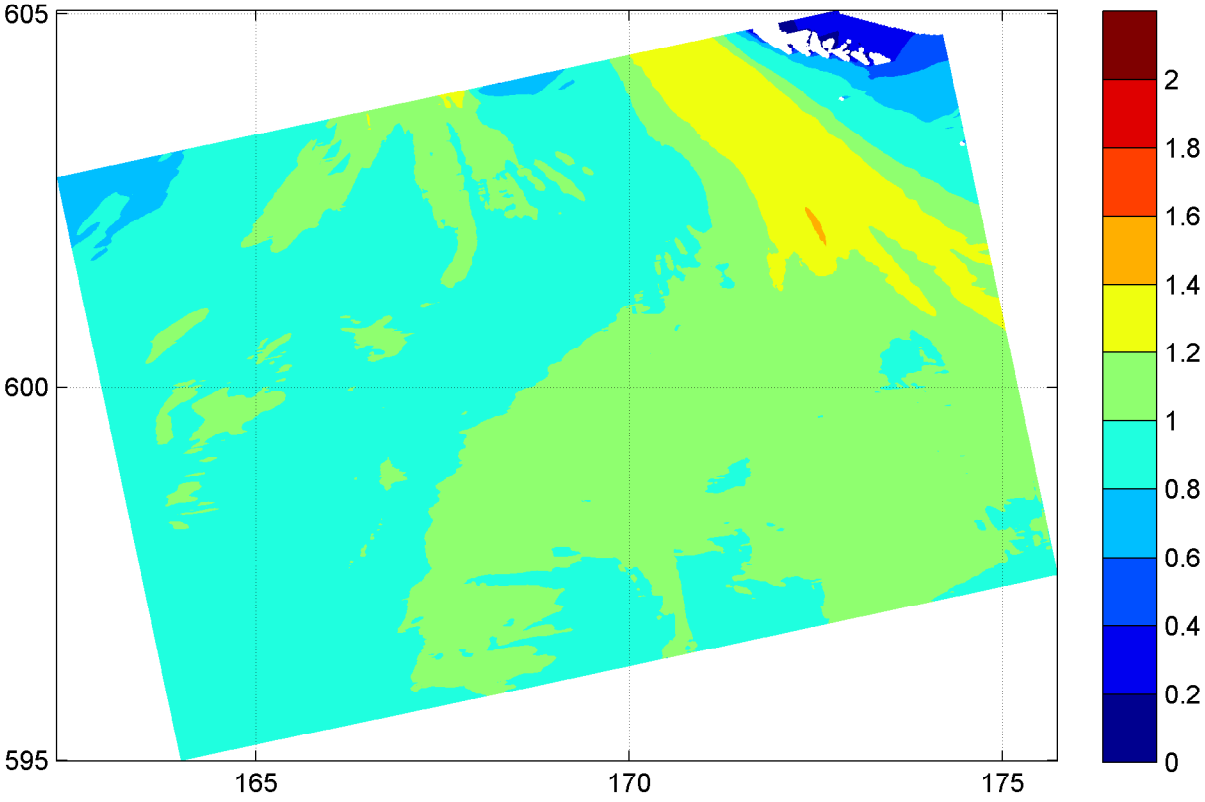

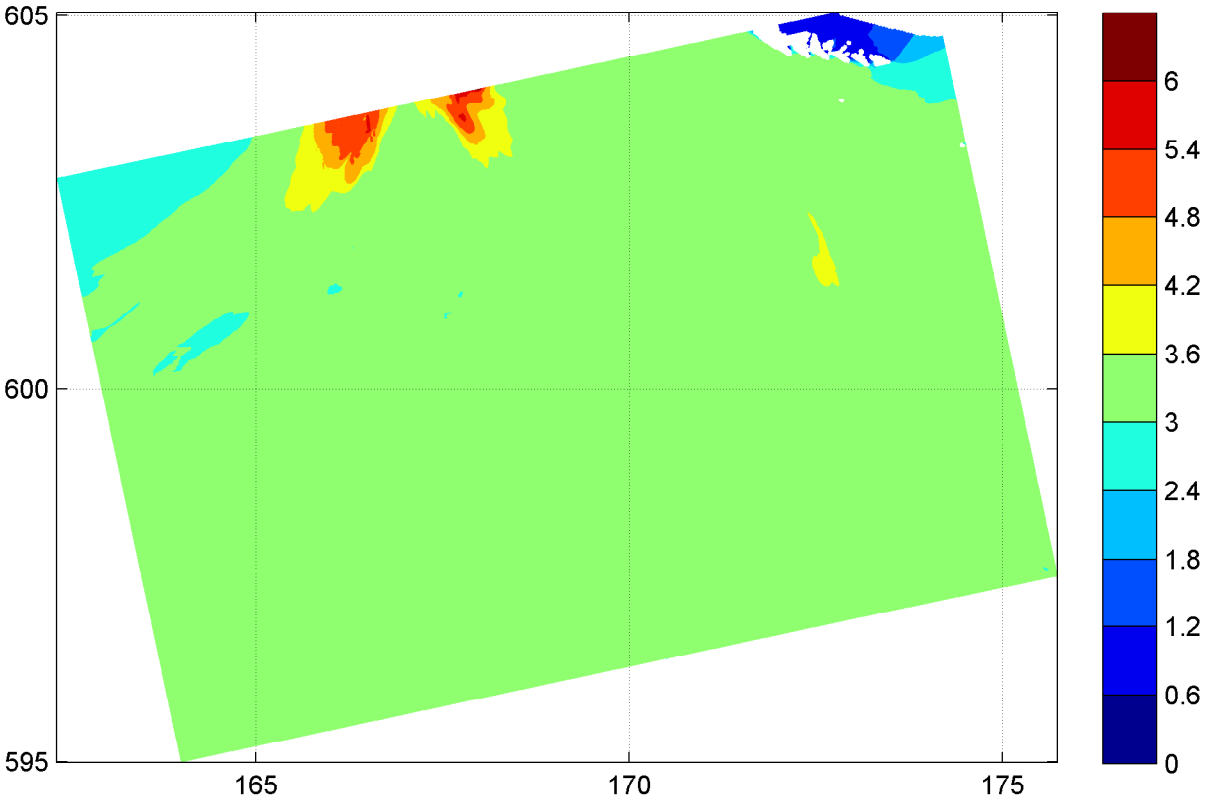

Spatial distribution of wave height H_{m0} [m] (upper panel) and wave period $T_{m-1,0}$ [s] (lower panel) on grid3 uniform wind field	20050102	12:00hr
	Hindcast Ameland Inlet	
WL | DELFT HYDRAULICS	H4803.11	Fig. 3.36a

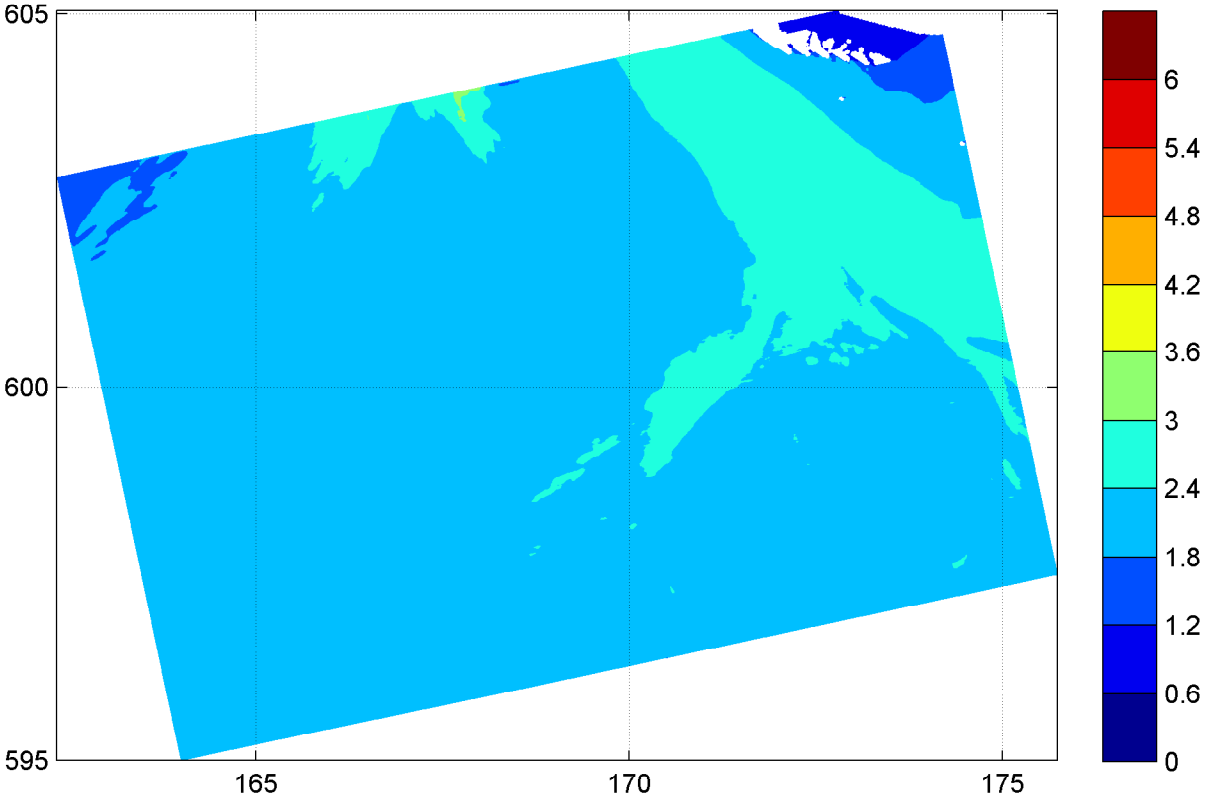

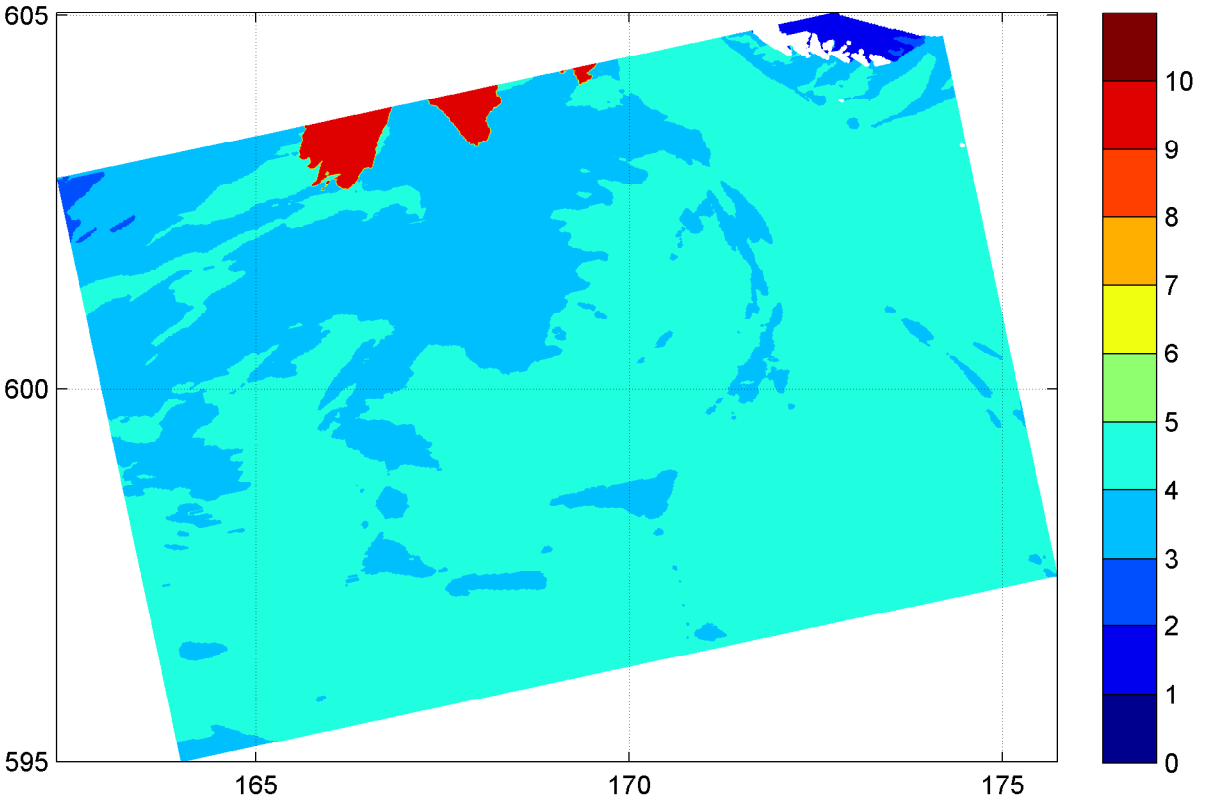

Spatial distribution of wave period T_{m02} [s] (upper panel) and wave period T_p [s] (lower panel) on grid3 uniform wind field	20050102	12:00hr
	Hindcast Ameland Inlet	
WL | DELFT HYDRAULICS	H4803.11	Fig. 3.36b

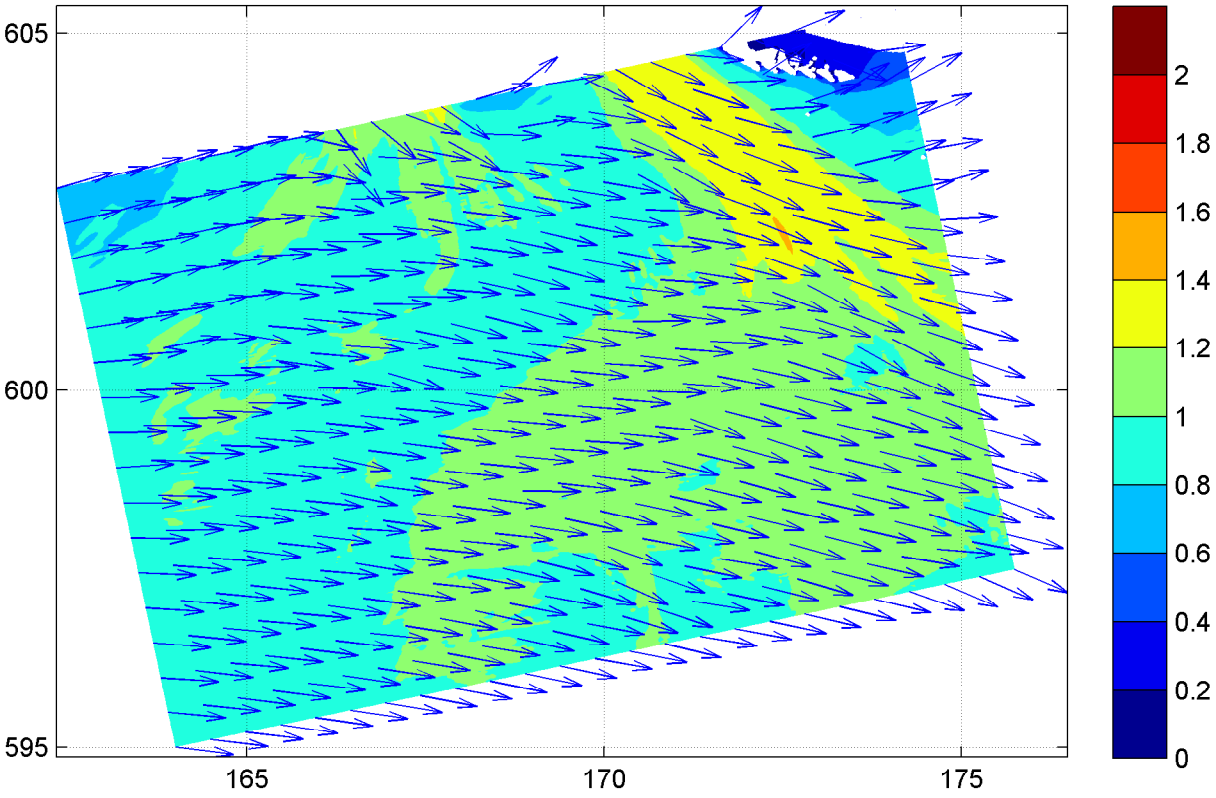

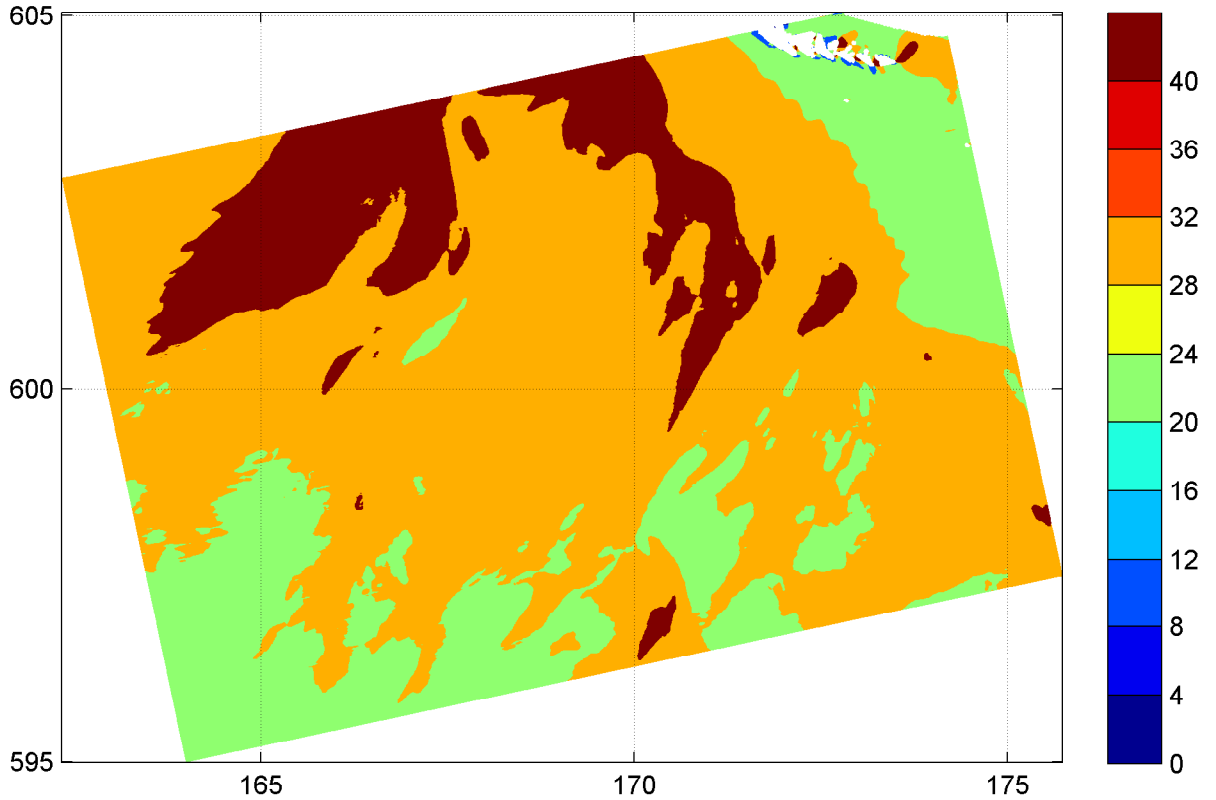

Spatial distribution of wave height [m] and mean wave direction (upper panel) and directional spreading [°] (lower panel) on grid3 uniform wind field	20050102	12:00hr
	Hindcast Ameland Inlet	
WL | DELFT HYDRAULICS	H4803.11	Fig. 3.36c

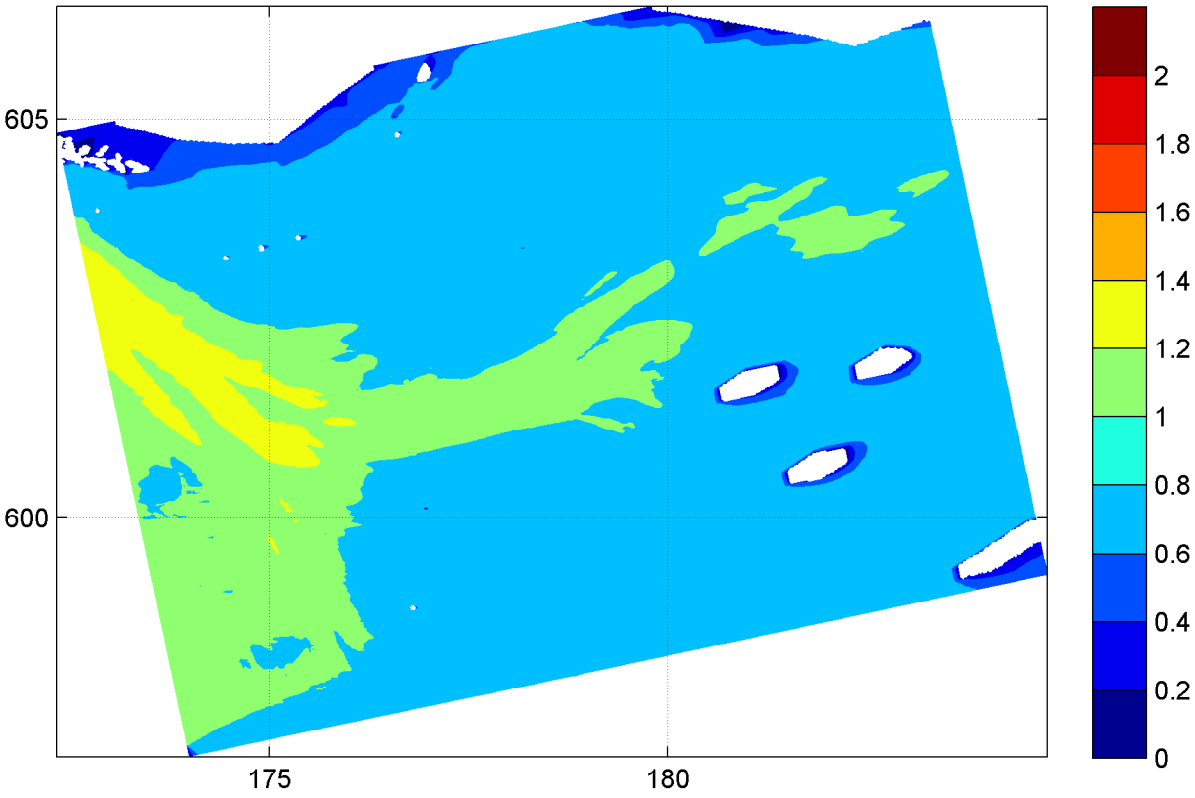

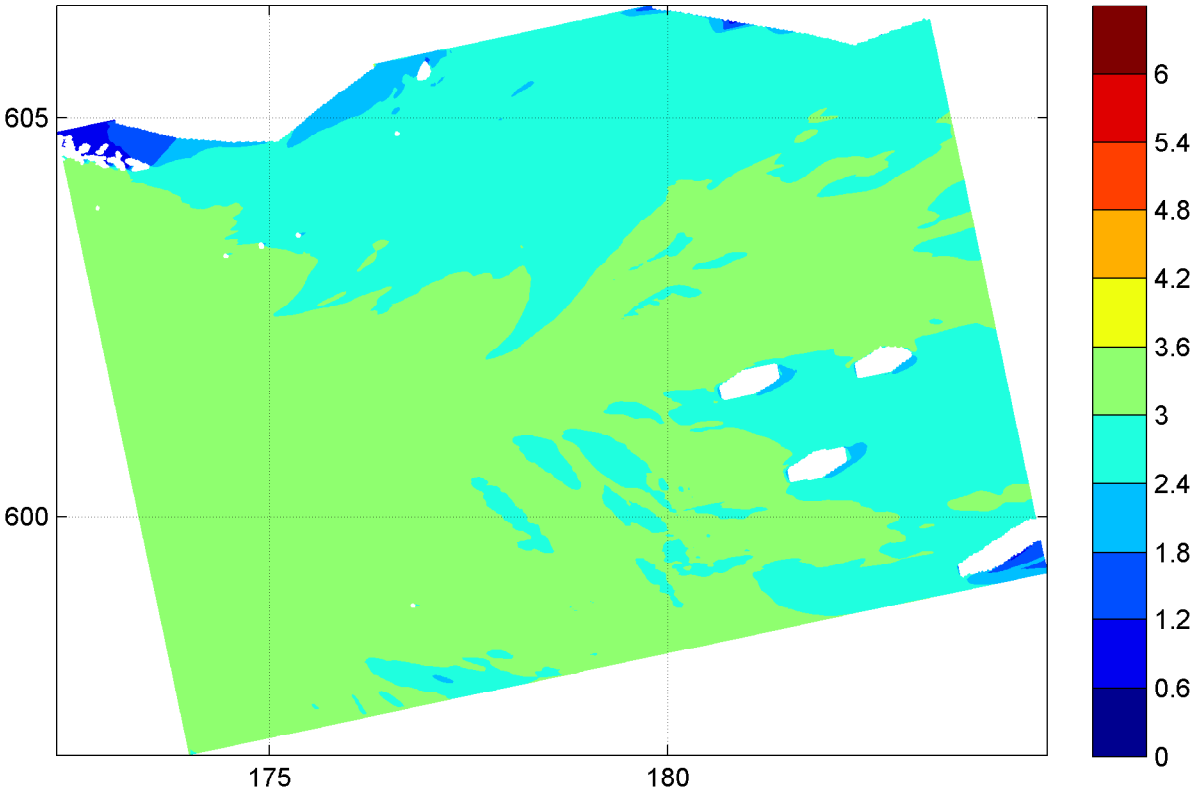

Spatial distribution of wave height H_{m0} [m] (upper panel) and wave period $T_{m-1,0}$ [s] (lower panel) on grid4 uniform wind field	20050102	12:00hr
	Hindcast Ameland Inlet	
WL | DELFT HYDRAULICS	H4803.11	Fig. 3.37a

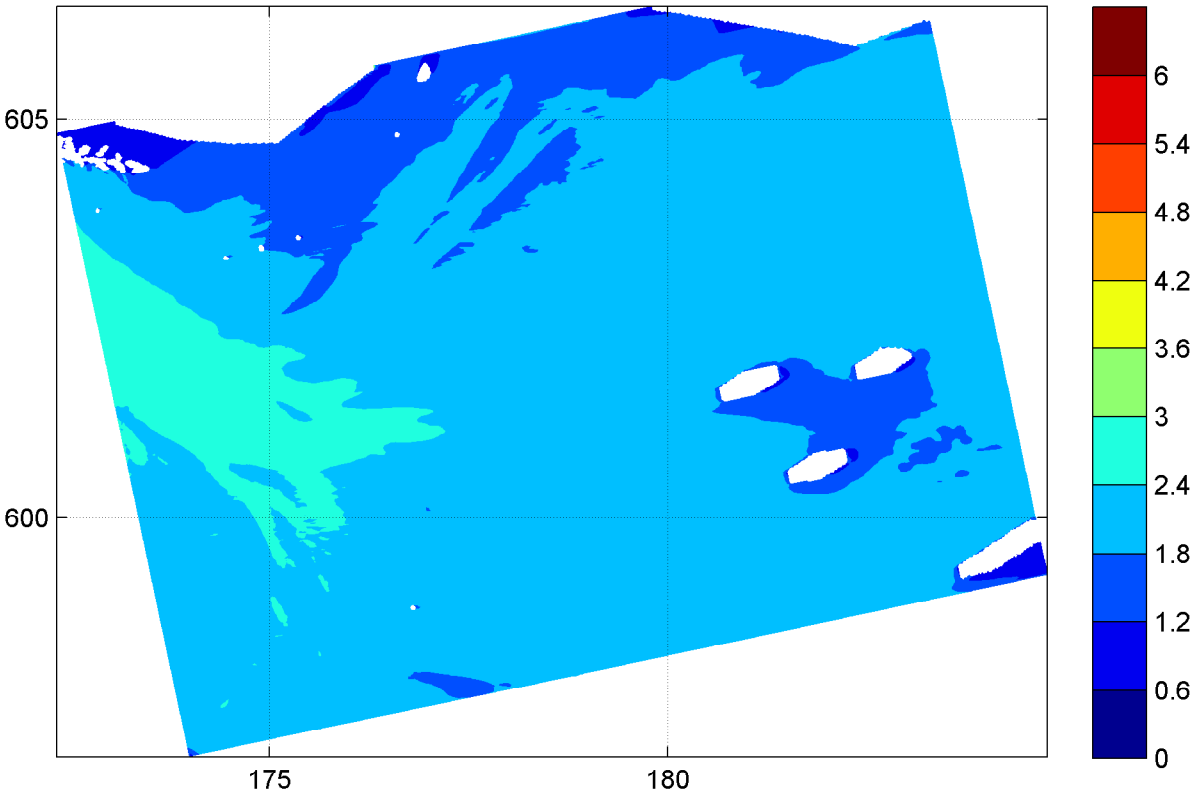

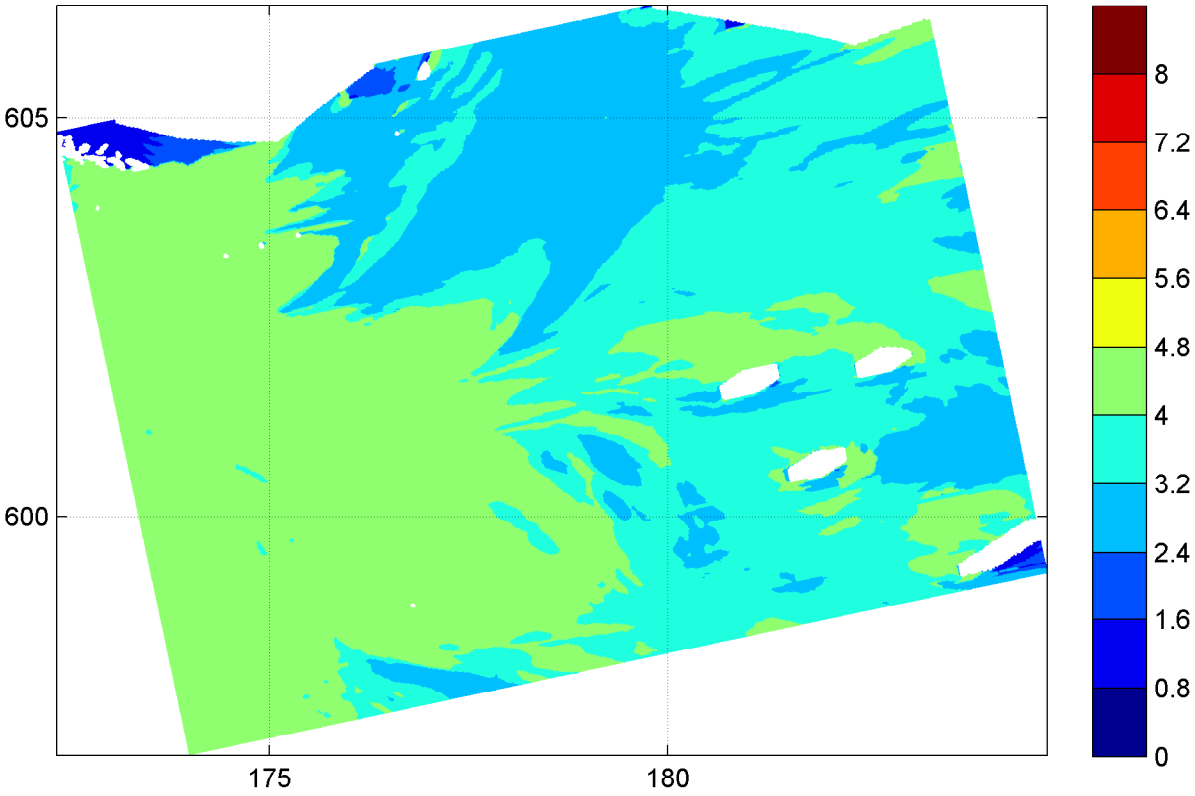

Spatial distribution of wave period T_{m02} [s] (upper panel) and wave period T_p [s] (lower panel) on grid4 uniform wind field	20050102	12:00hr
	Hindcast Ameland Inlet	
WL | DELFT HYDRAULICS	H4803.11	Fig. 3.37b

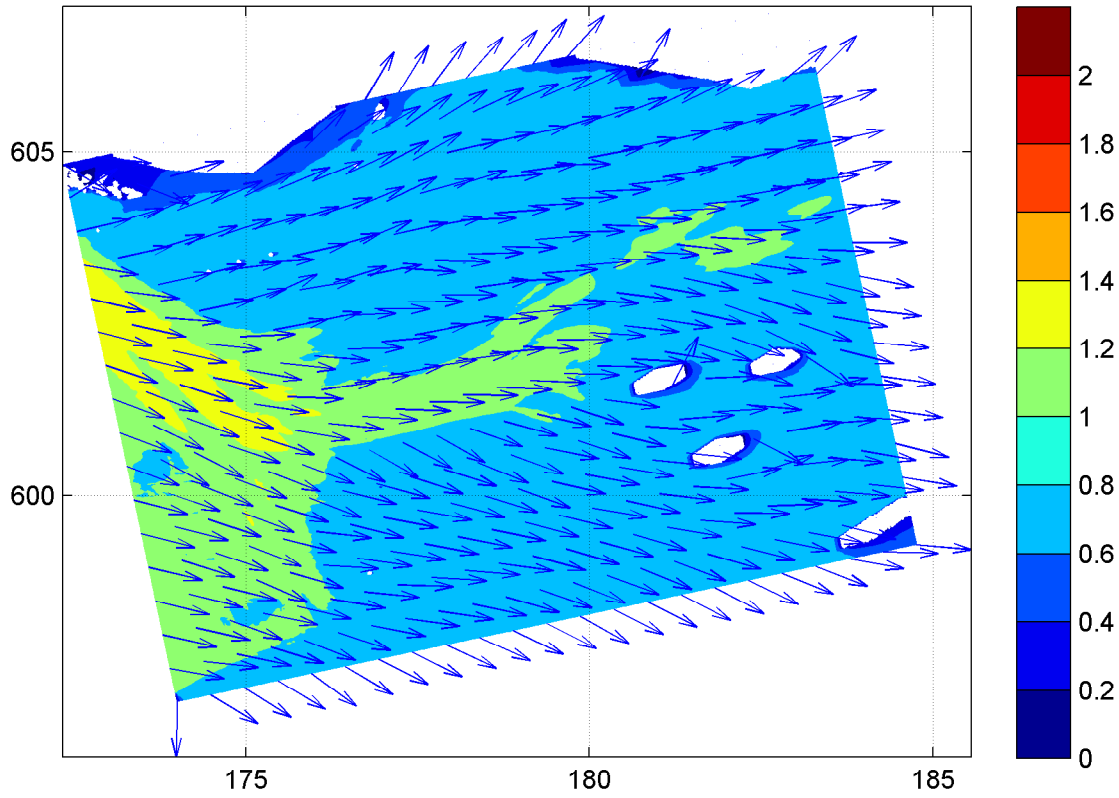

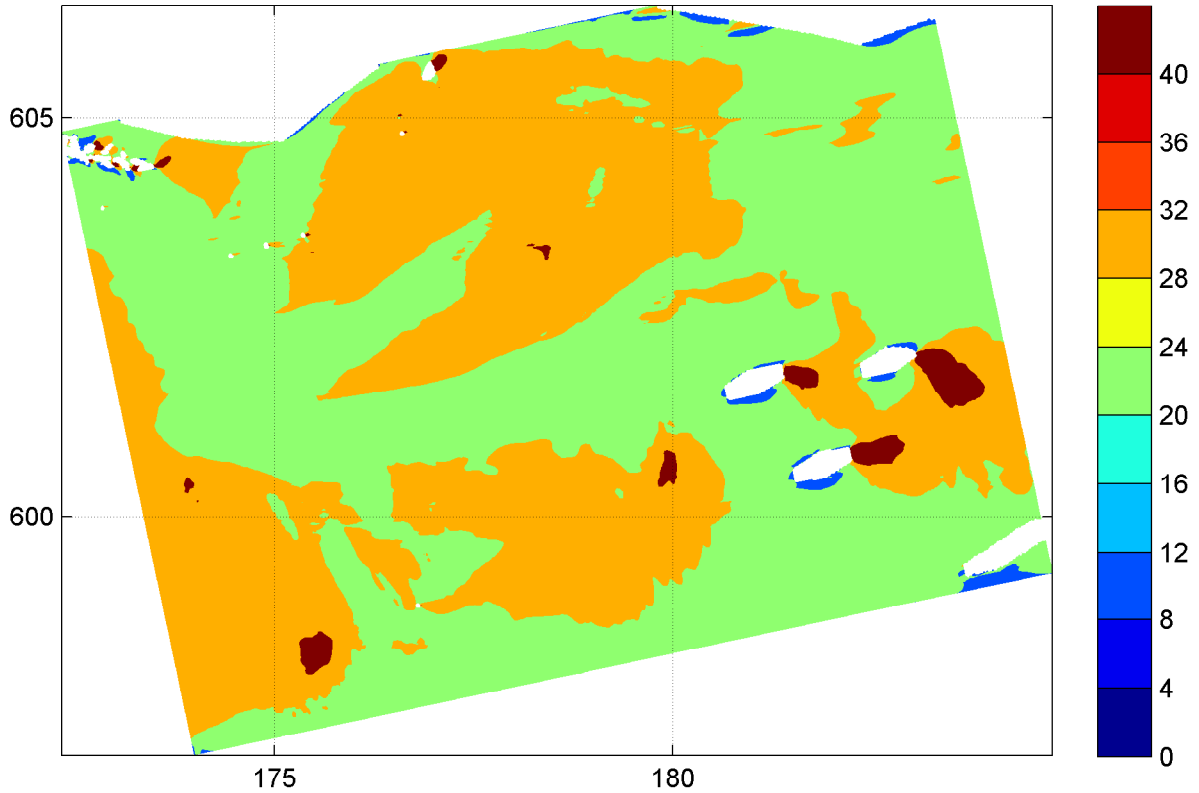

Spatial distribution of wave height [m] and mean wave direction (upper panel) and directional spreading [°] (lower panel) on grid4 uniform wind field	20050102	12:00hr
	Hindcast Ameland Inlet	
WL | DELFT HYDRAULICS	H4803.11	Fig. 3.37c

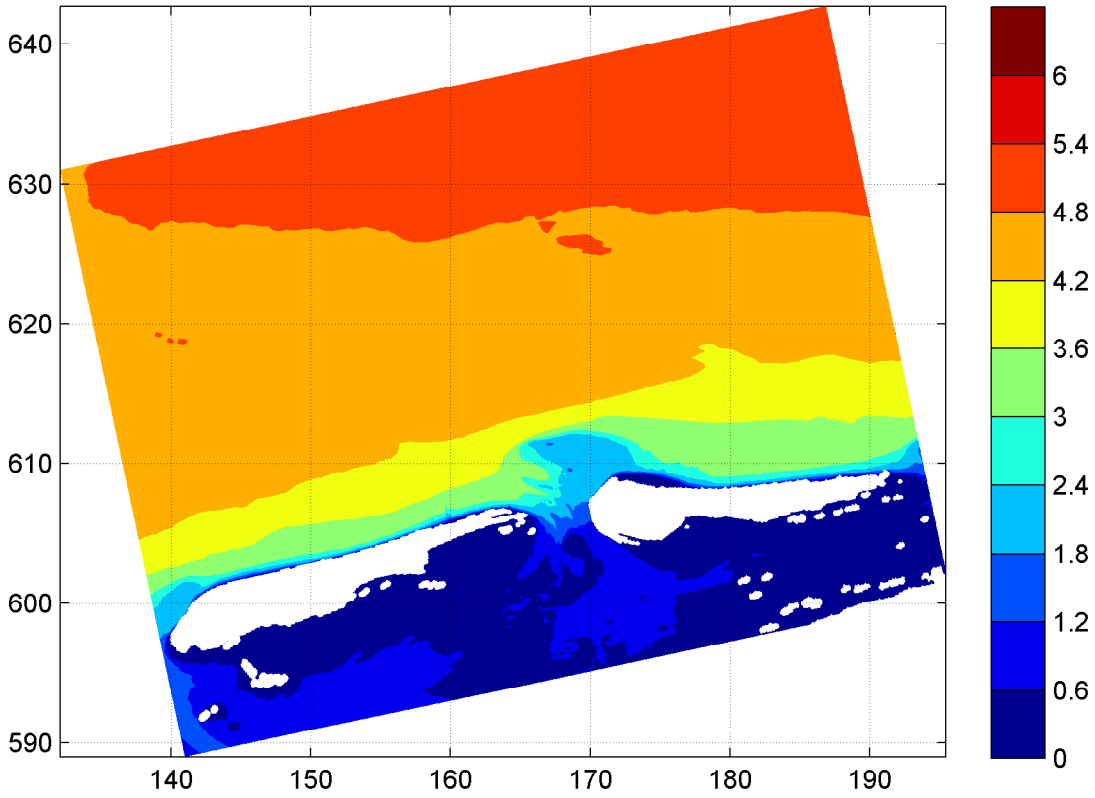

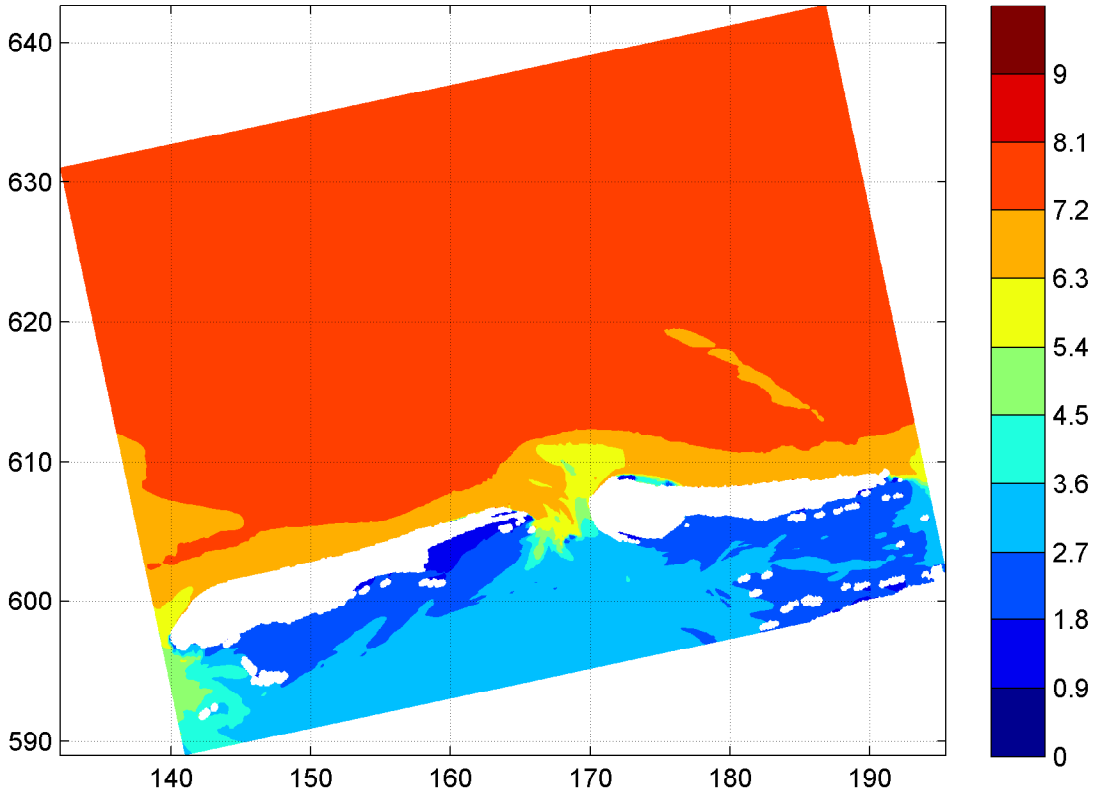

Spatial distribution of wave height H_{m0} [m] (upper panel) and wave period $T_{m-1,0}$ [s] (lower panel) on grid1 HIRLAM wind field	20050102	12:00hr
	Hindcast Ameland Inlet	
WL | DELFT HYDRAULICS	H4803.11	Fig. 3.38a

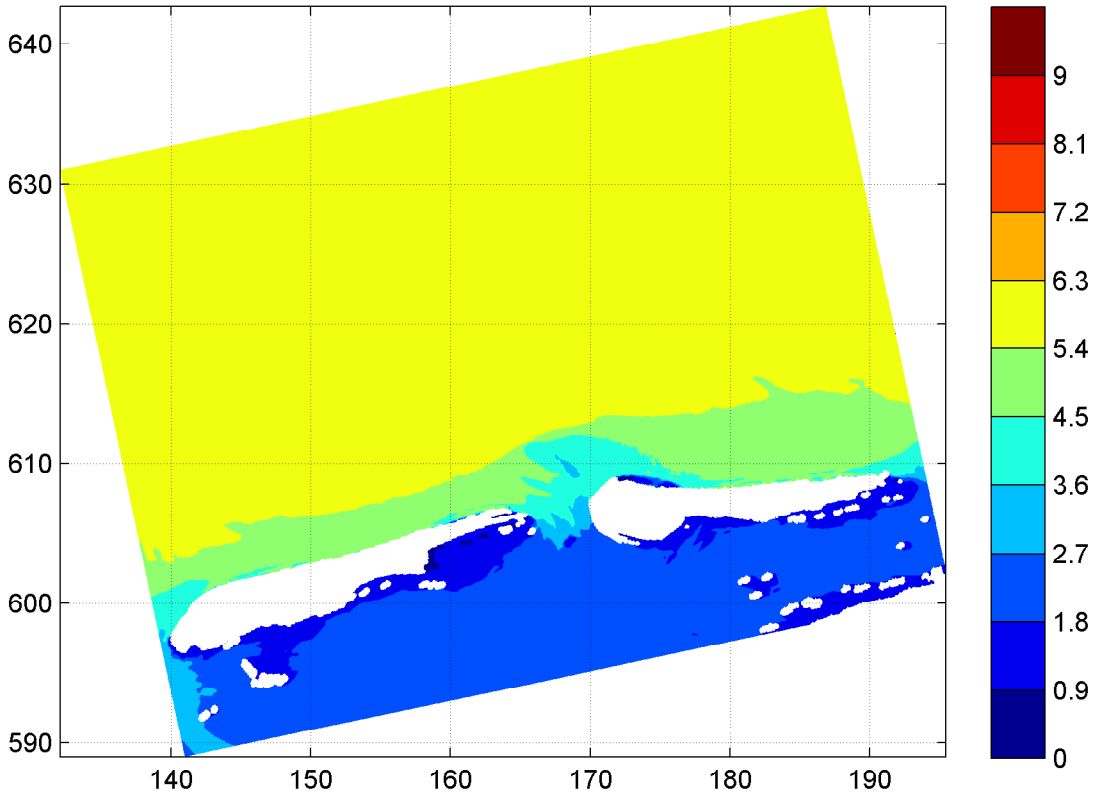

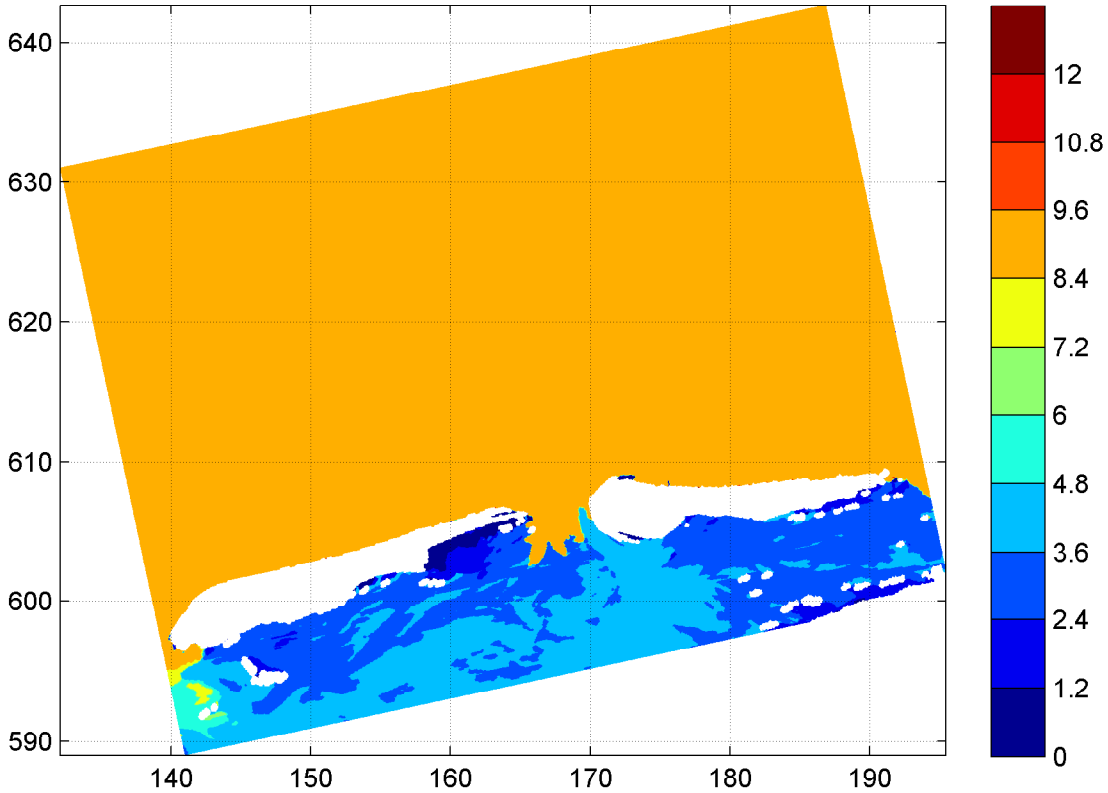

Spatial distribution of wave period T_{m02} [s] (upper panel) and wave period T_p [s] (lower panel) on grid1 HIRLAM wind field	20050102	12:00hr
	Hindcast Ameland Inlet	
WL | DELFT HYDRAULICS	H4803.11	Fig. 3.38b

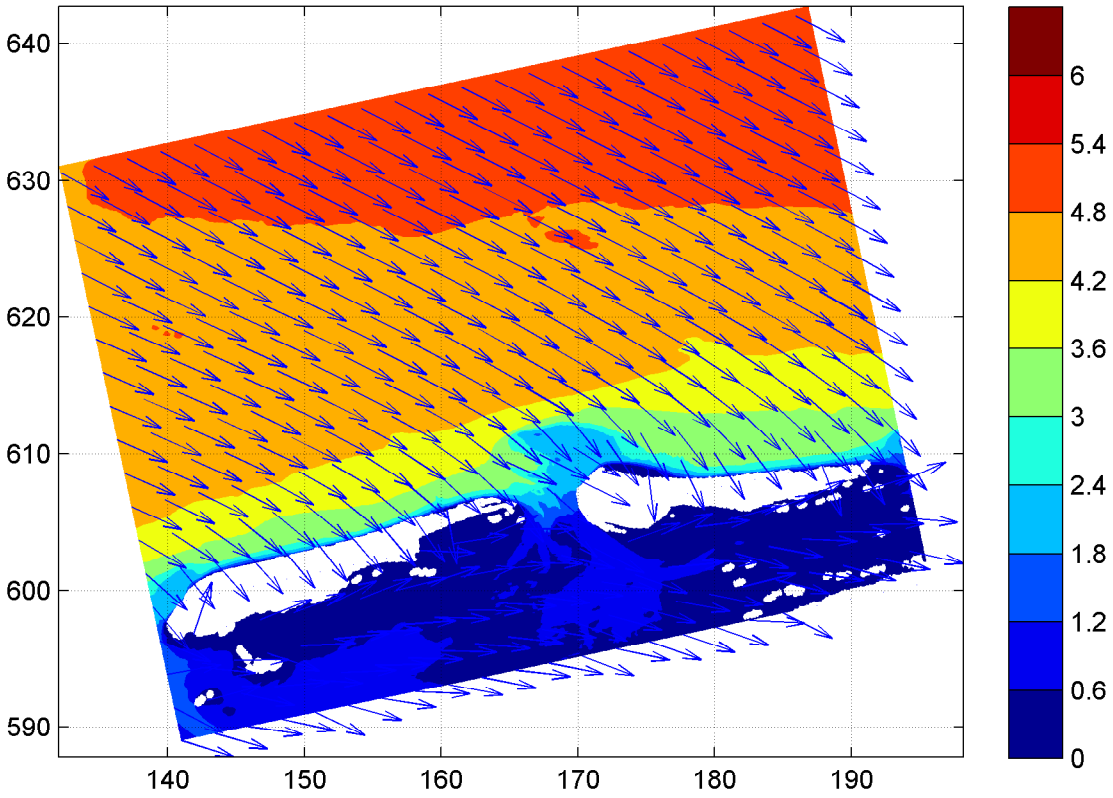

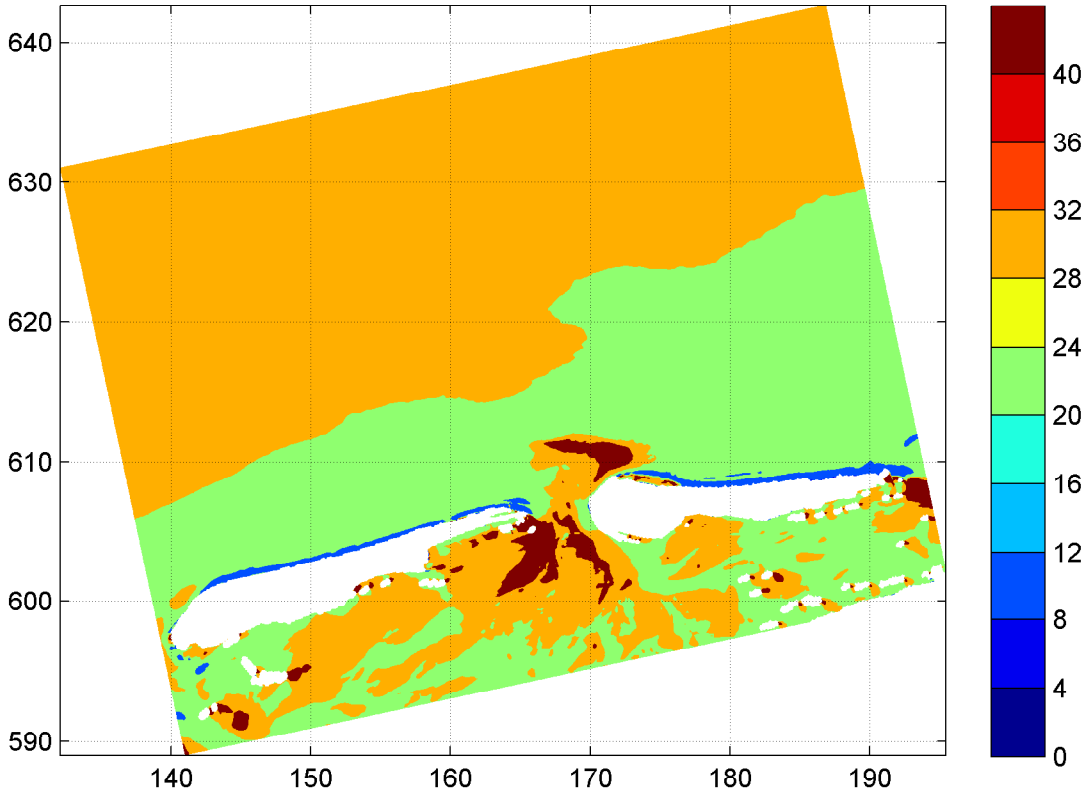

Spatial distribution of wave height [m] and mean wave direction (upper panel) and directional spreading [°] (lower panel) on grid1 HIRLAM wind field	20050102	12:00hr
	Hindcast Ameland Inlet	
WL | DELFT HYDRAULICS	H4803.11	Fig. 3.38c

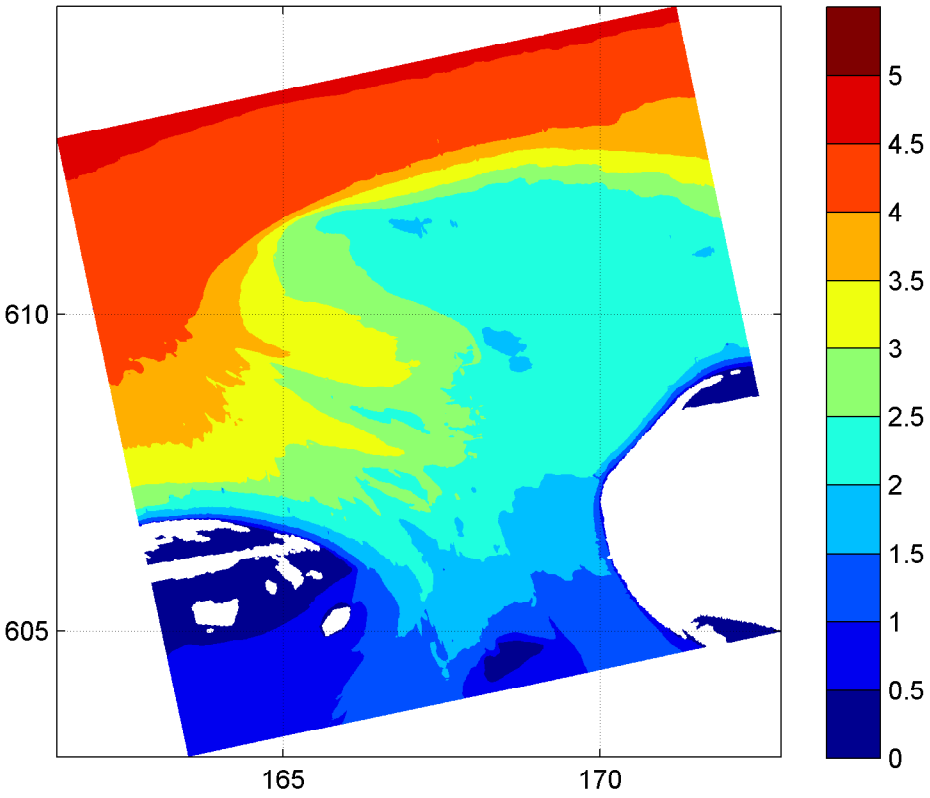

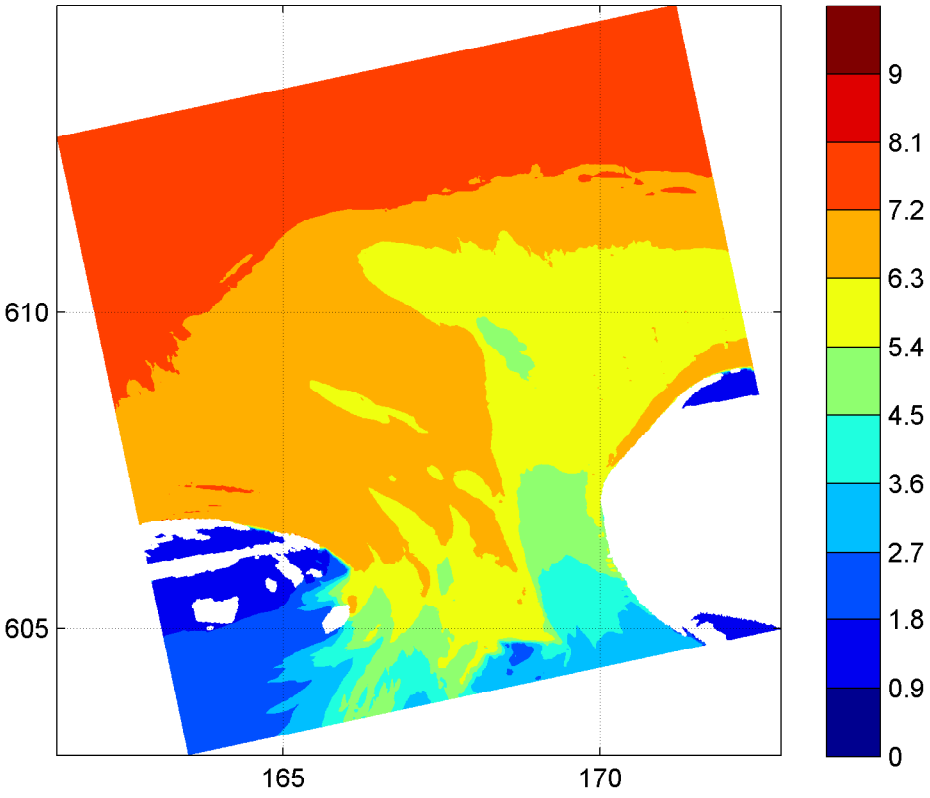

Spatial distribution of wave height H_{m0} [m] (upper panel) and wave period $T_{m-1,0}$ [s] (lower panel) on grid2 HIRLAM wind field	20050102	12:00hr
	Hindcast Ameland Inlet	
WL | DELFT HYDRAULICS	H4803.11	Fig. 3.39a

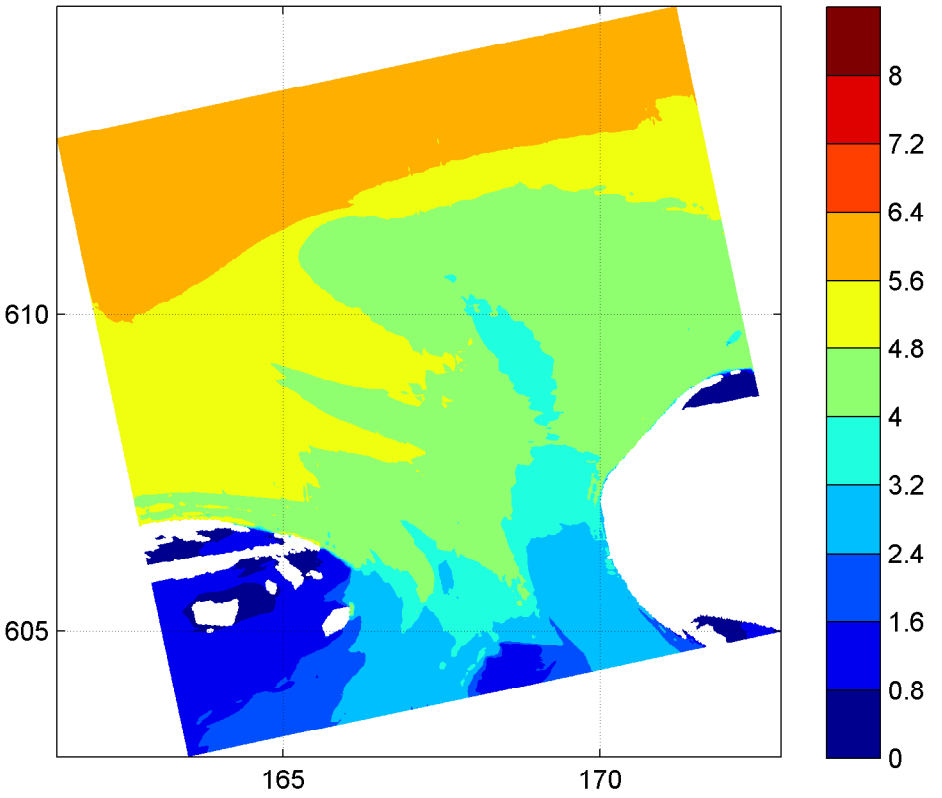

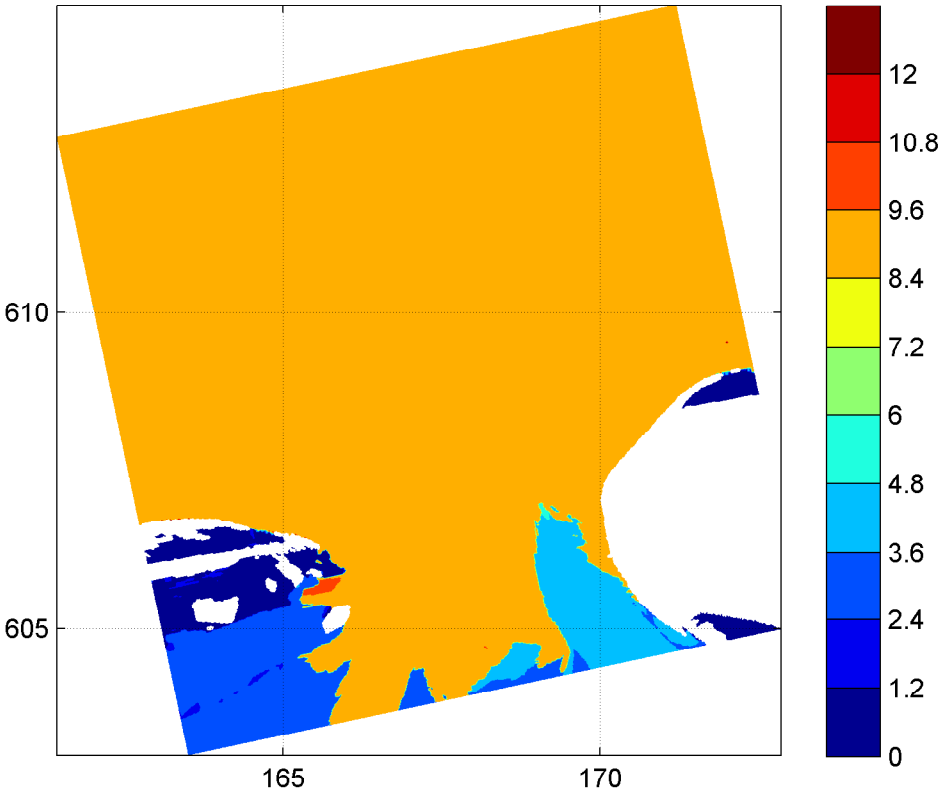

Spatial distribution of wave period T_{m02} [s] (upper panel) and wave period T_p [s] (lower panel) on grid2 HIRLAM wind field	20050102	12:00hr
	Hindcast Ameland Inlet	
WL | DELFT HYDRAULICS	H4803.11	Fig. 3.39b

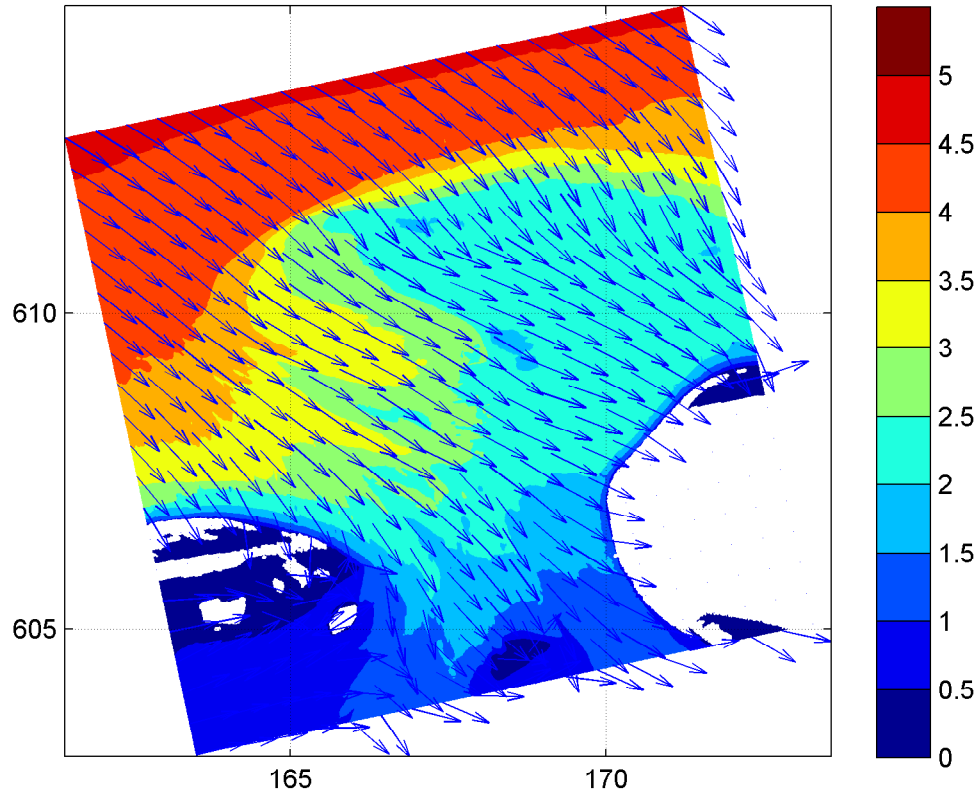

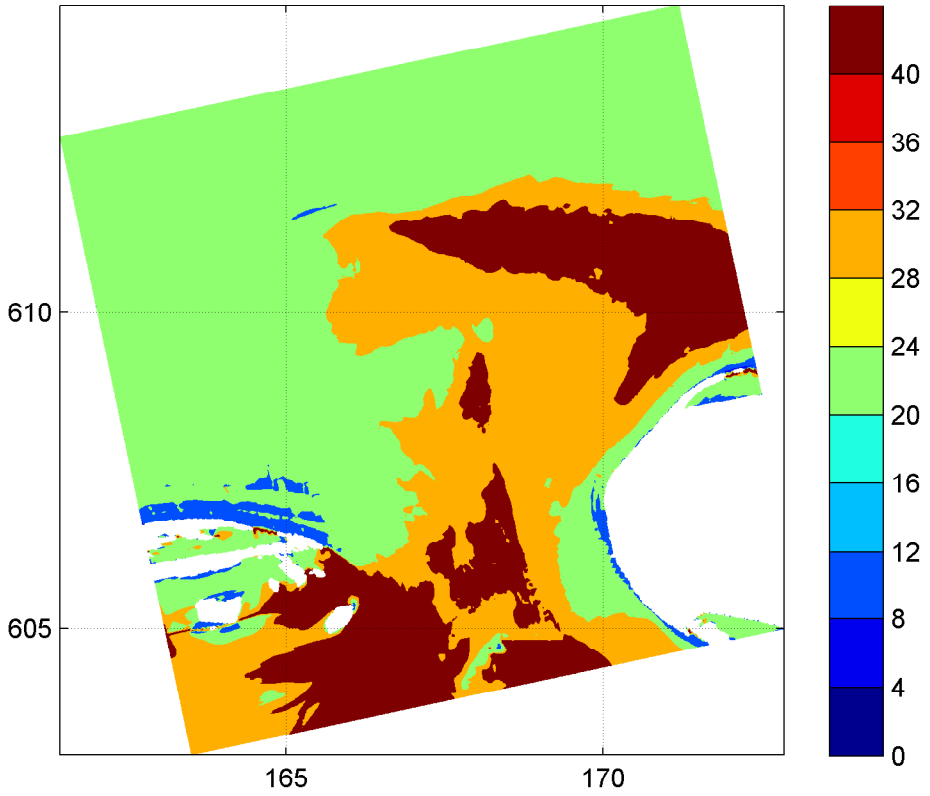

Spatial distribution of wave height [m] and mean wave direction (upper panel) and directional spreading [°] (lower panel) on grid2 HIRLAM wind field	20050102	12:00hr
	Hindcast Ameland Inlet	
WL | DELFT HYDRAULICS	H4803.11	Fig. 3.39c

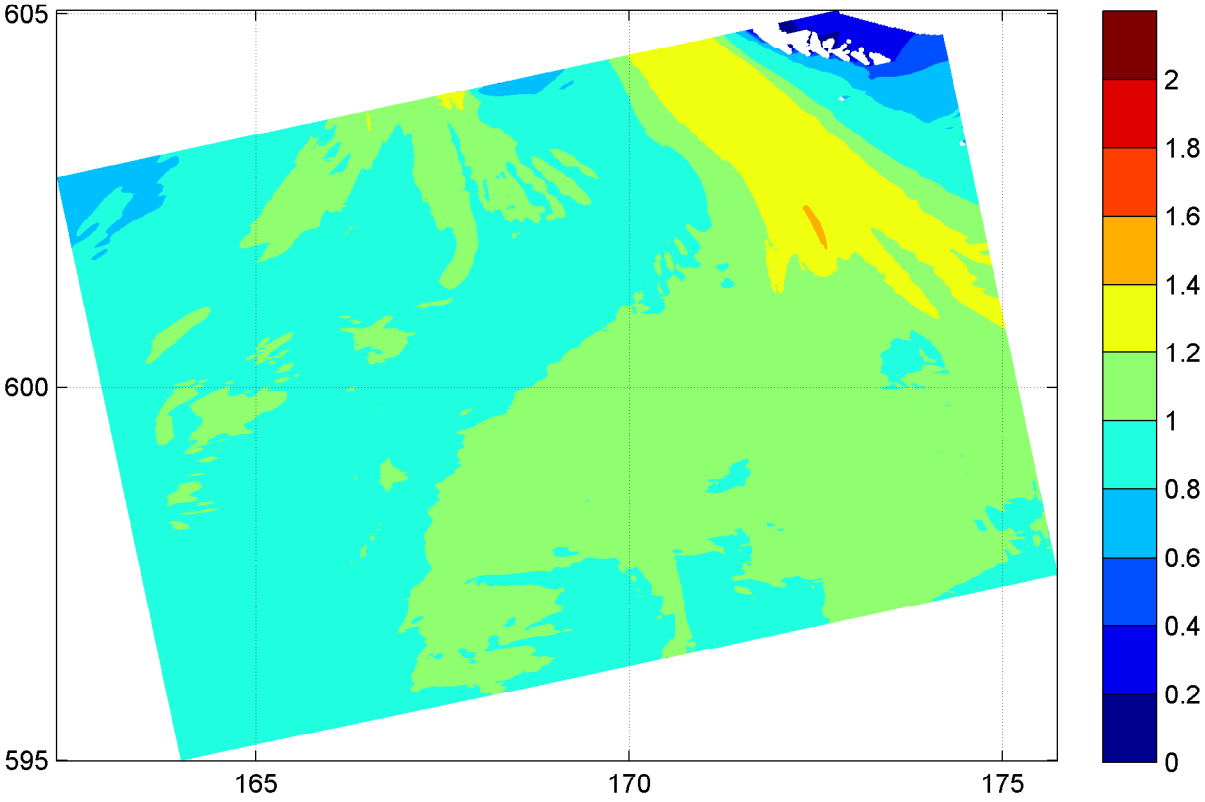

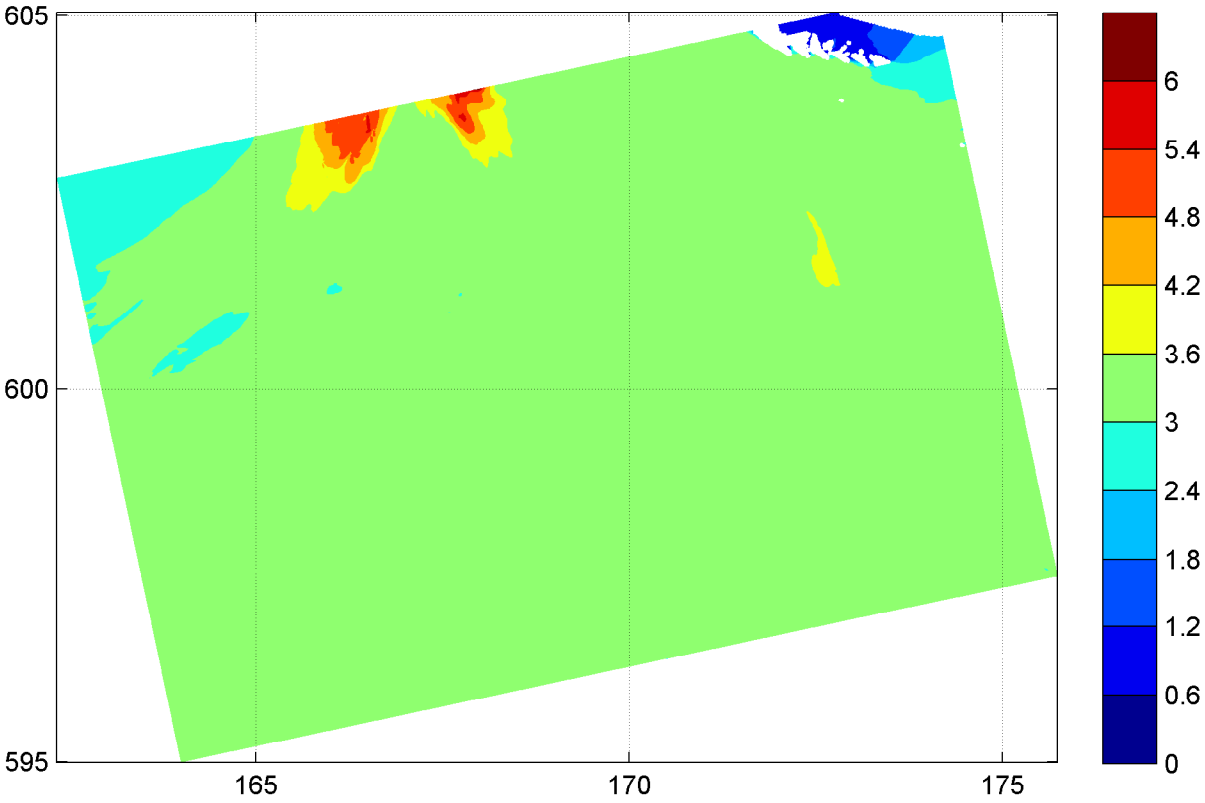

Spatial distribution of wave height H_{m0} [m] (upper panel) and wave period $T_{m-1,0}$ [s] (lower panel) on grid3 HIRLAM wind field	20050102	12:00hr
	Hindcast Ameland Inlet	
WL | DELFT HYDRAULICS	H4803.11	Fig. 3.40a

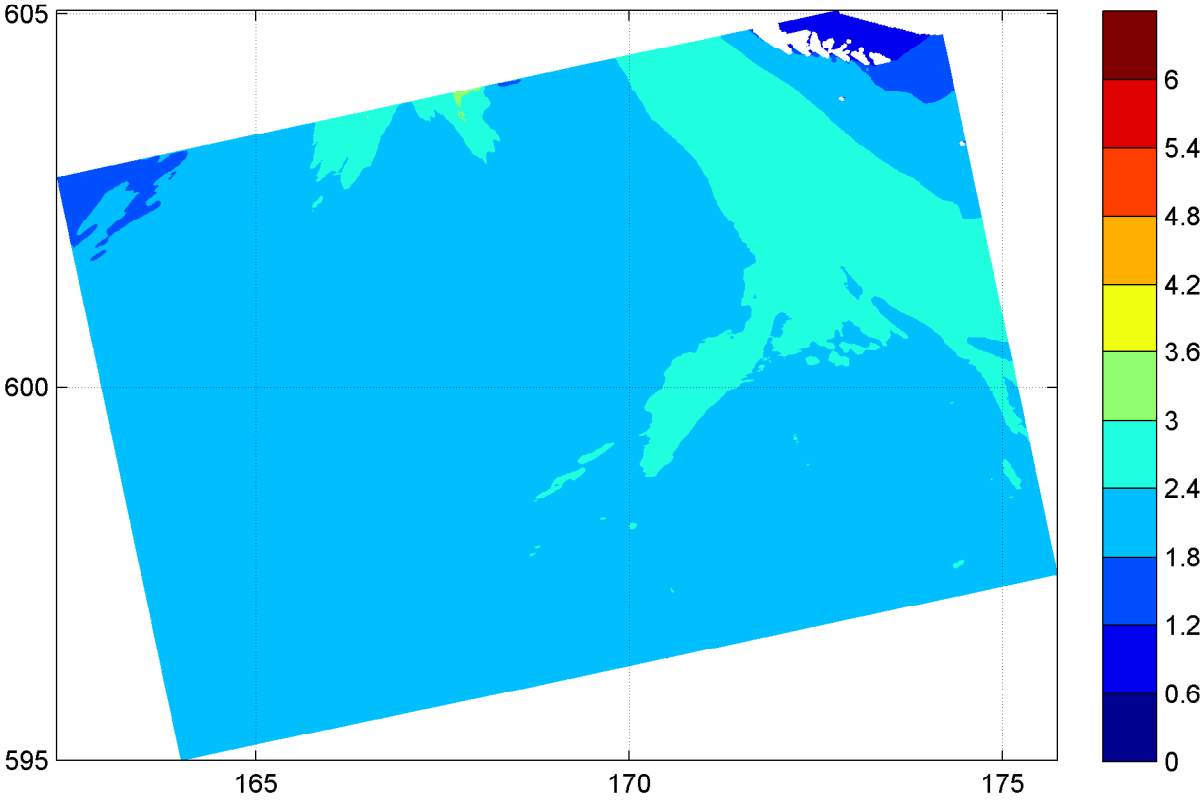

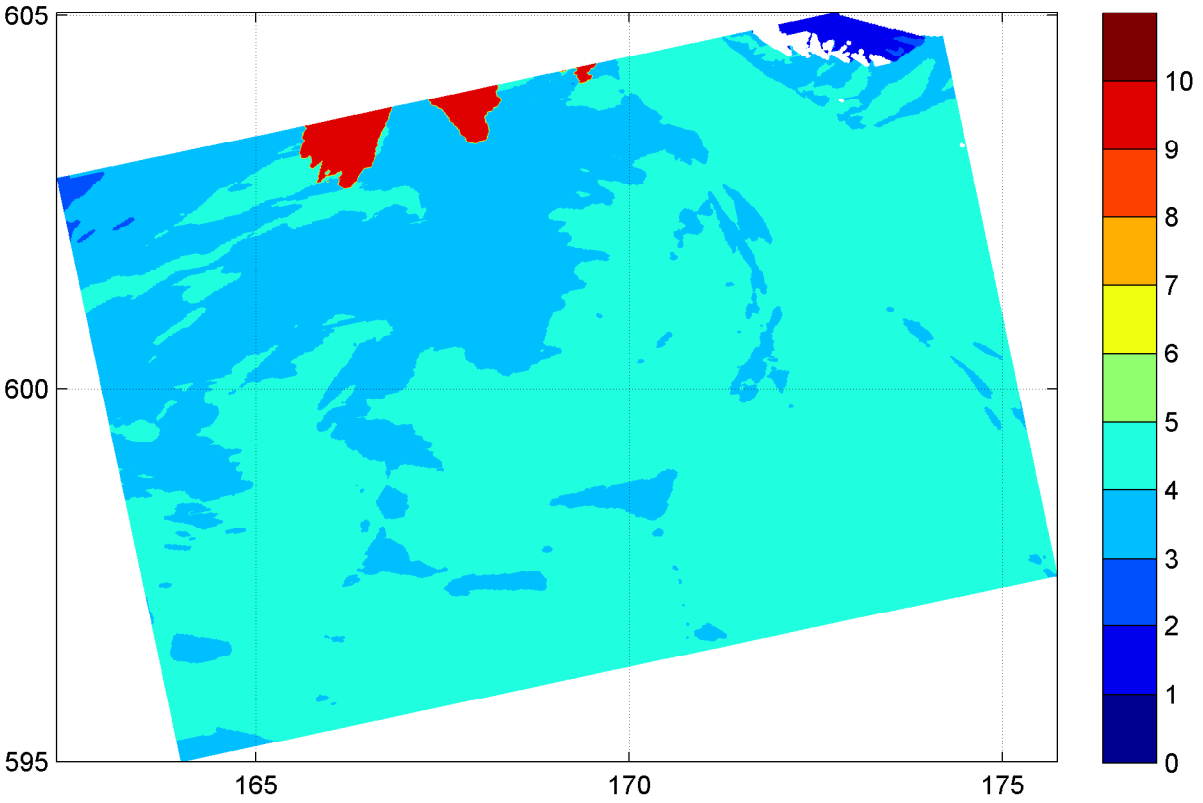

Spatial distribution of wave period T_{m02} [s] (upper panel) and wave period T_p [s] (lower panel) on grid3 HIRLAM wind field	20050102	12:00hr
	Hindcast Ameland Inlet	
WL | DELFT HYDRAULICS	H4803.11	Fig. 3.40b

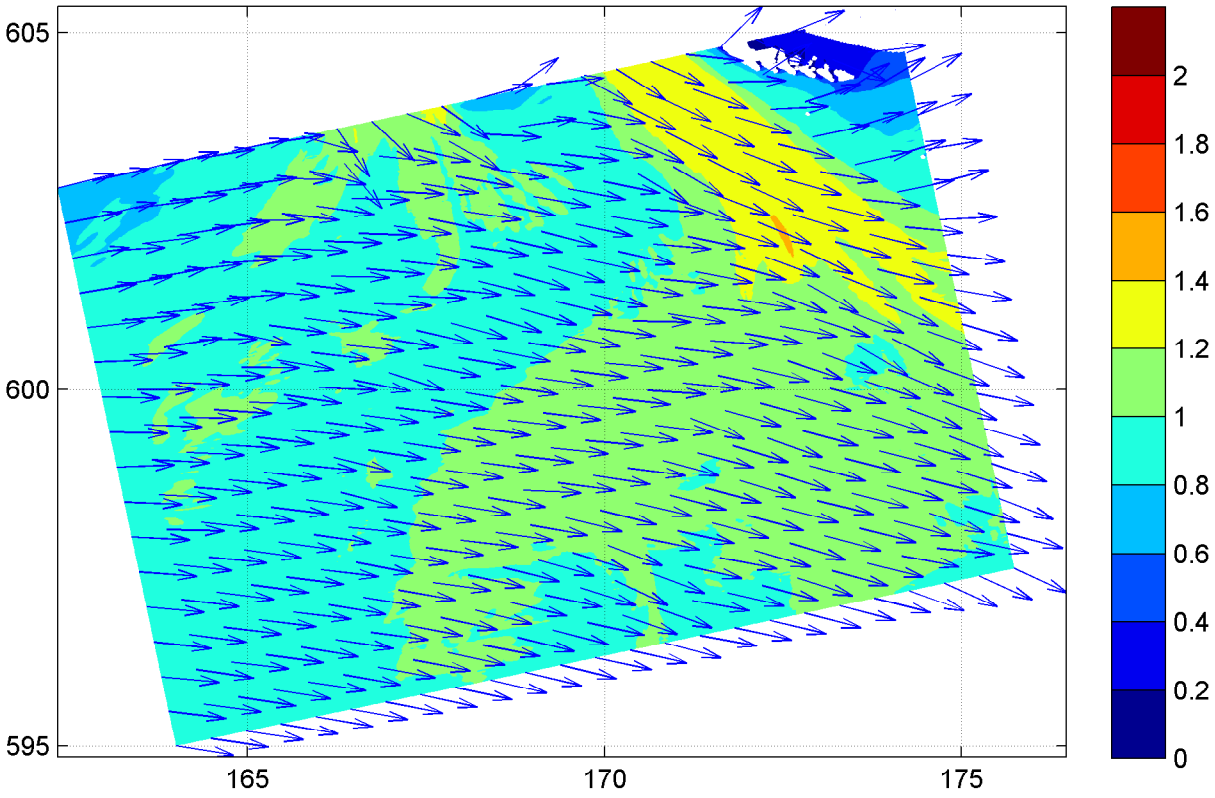

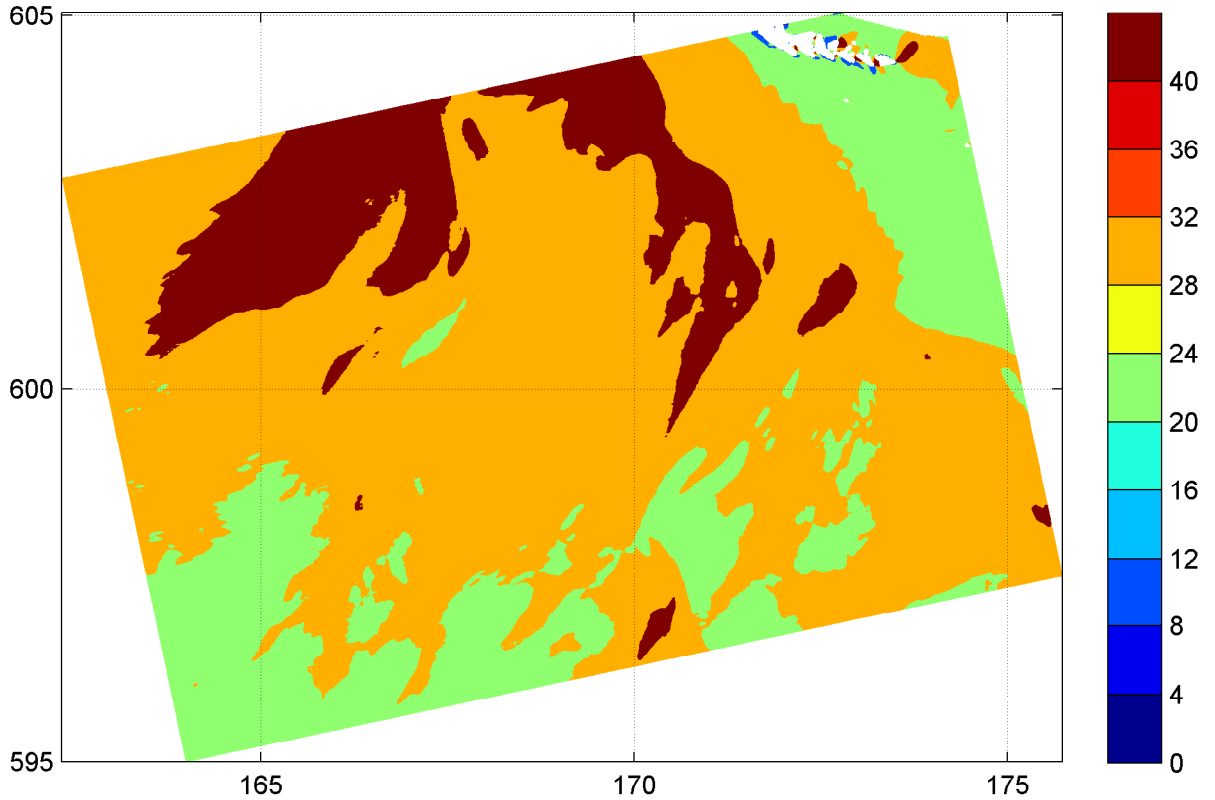

Spatial distribution of wave height [m] and mean wave direction (upper panel) and directional spreading [°] (lower panel) on grid3 HIRLAM wind field	20050102	12:00hr
	Hindcast Ameland Inlet	
WL | DELFT HYDRAULICS	H4803.11	Fig. 3.40c

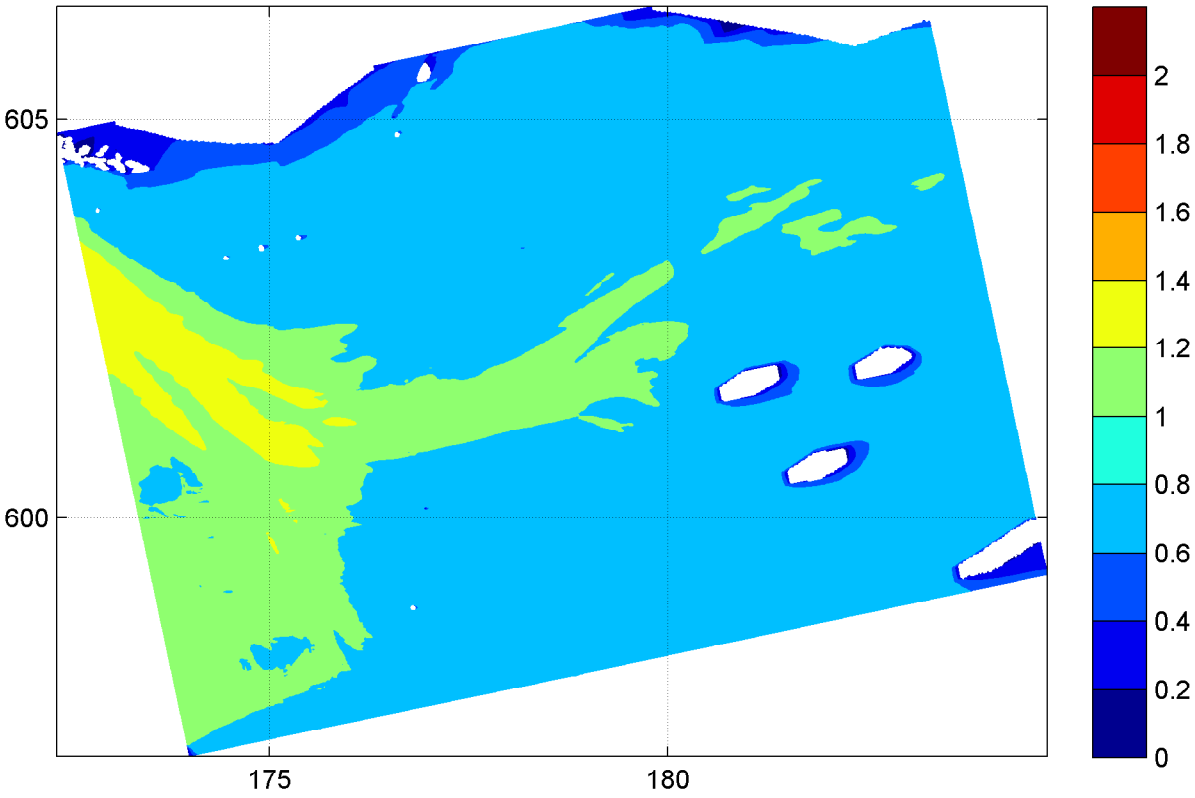

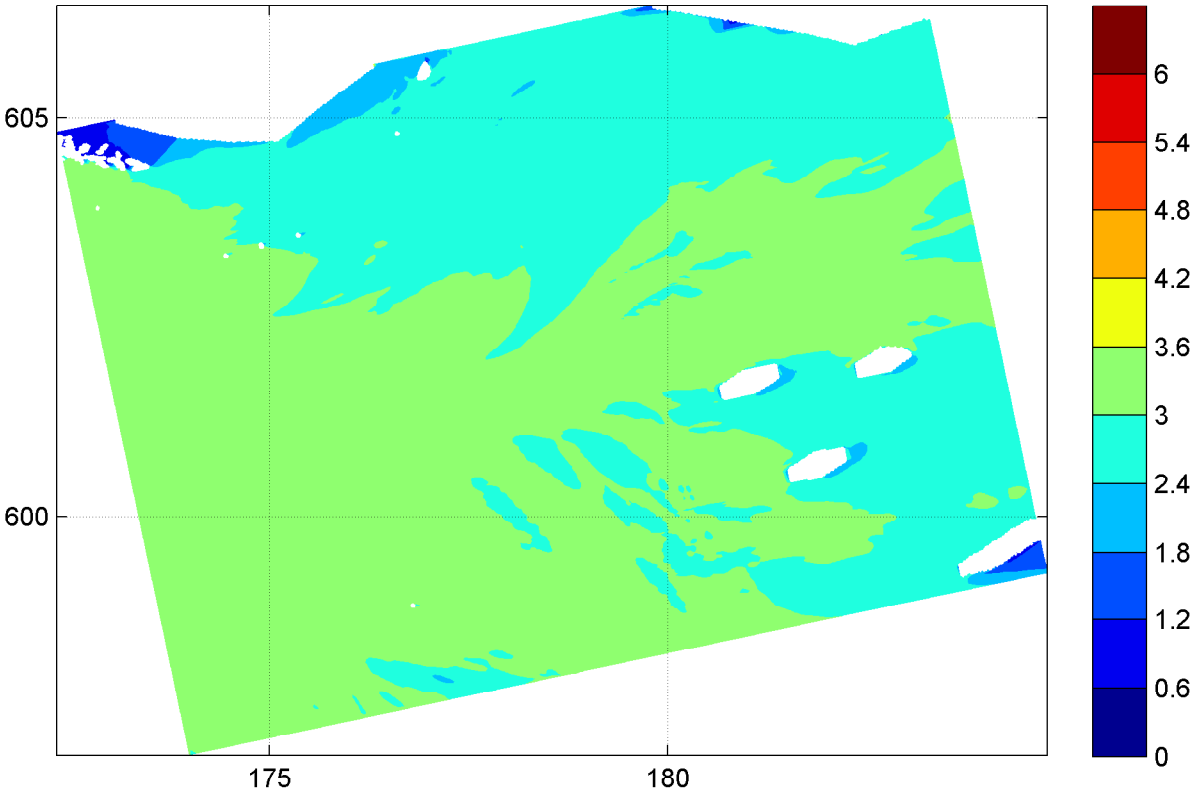

Spatial distribution of wave height H_{m0} [m] (upper panel) and wave period $T_{m-1,0}$ [s] (lower panel) on grid4 HIRLAM wind field	20050102	12:00hr
	Hindcast Ameland Inlet	
WL | DELFT HYDRAULICS	H4803.11	Fig. 3.41a

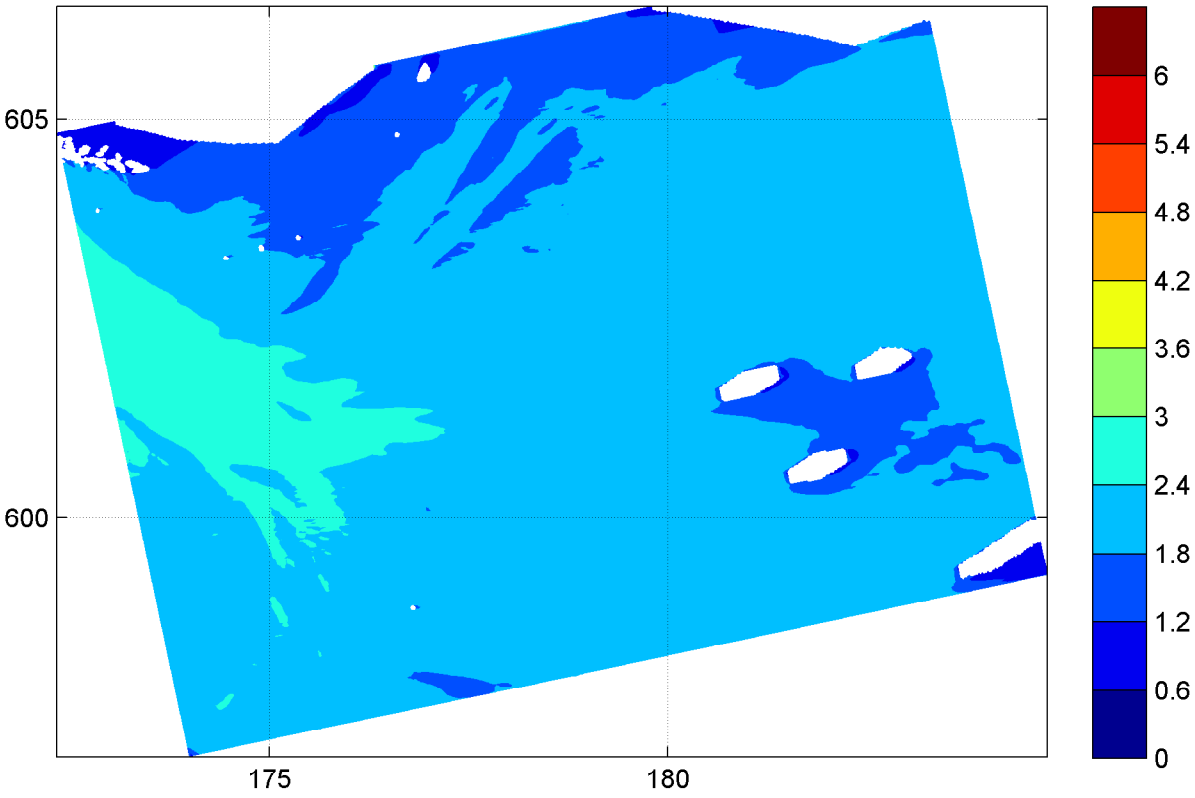

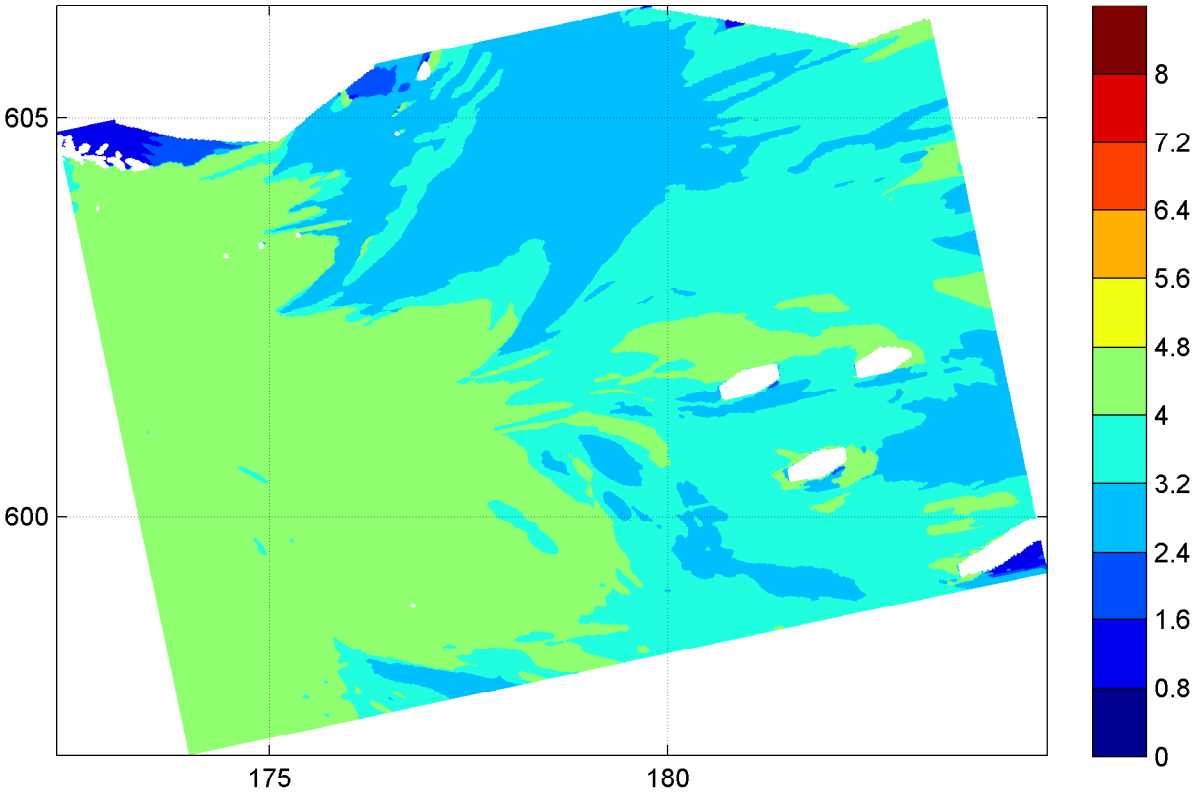

Spatial distribution of wave period T_{m02} [s] (upper panel) and wave period T_p [s] (lower panel) on grid4 HIRLAM wind field	20050102	12:00hr
	Hindcast Ameland Inlet	
WL | DELFT HYDRAULICS	H4803.11	Fig. 3.41b

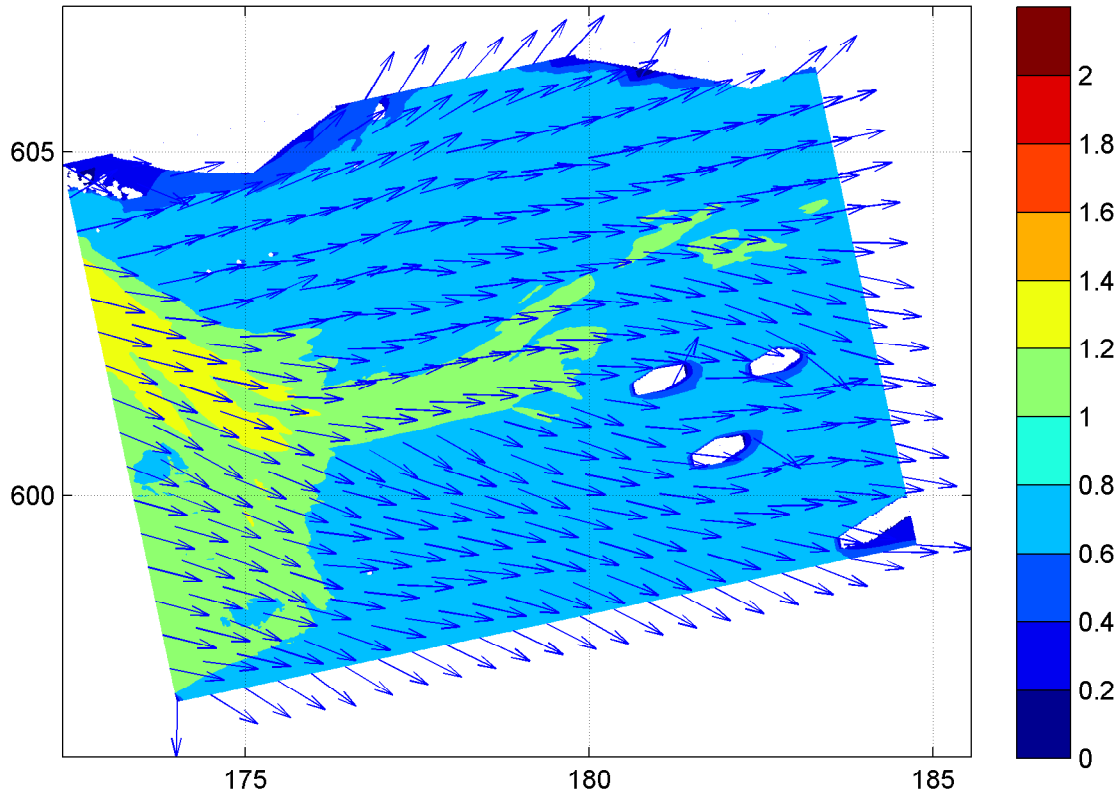

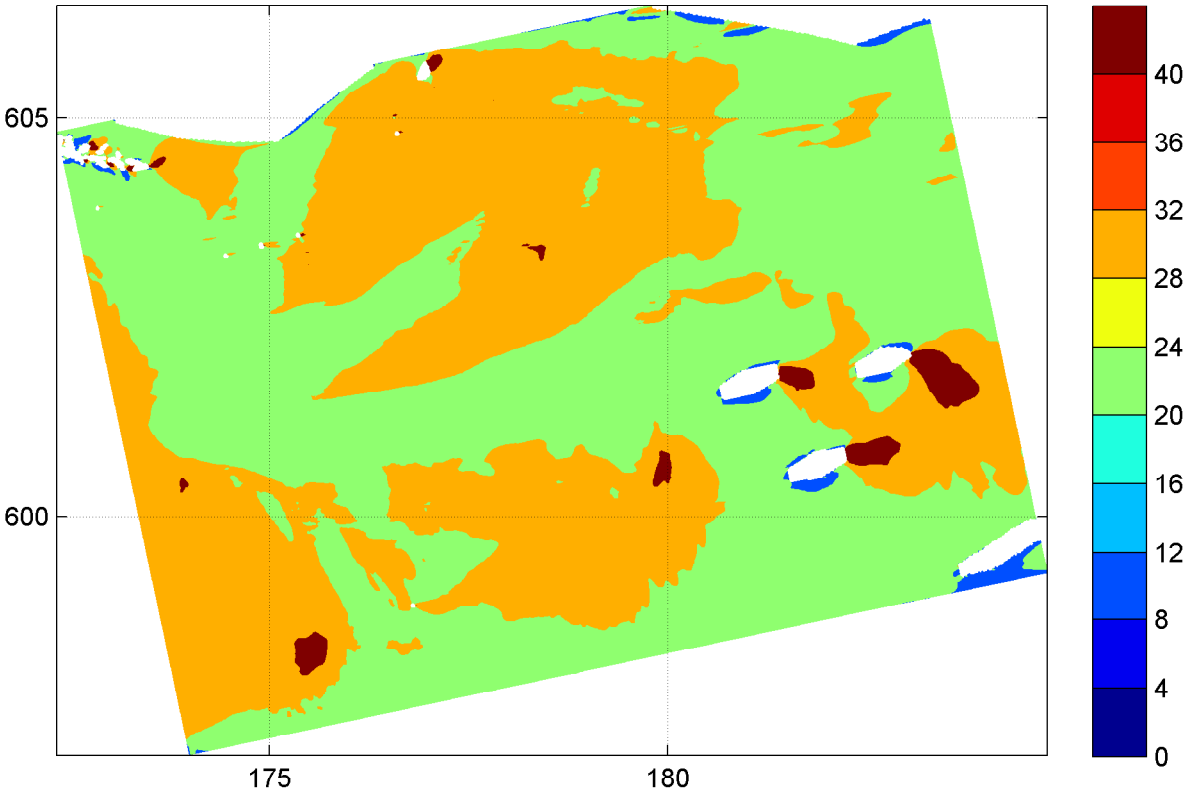

Spatial distribution of wave height [m] and mean wave direction (upper panel) and directional spreading [°] (lower panel) on grid4 HIRLAM wind field	20050102	12:00hr
	Hindcast Ameland Inlet	
WL | DELFT HYDRAULICS	H4803.11	Fig. 3.41c

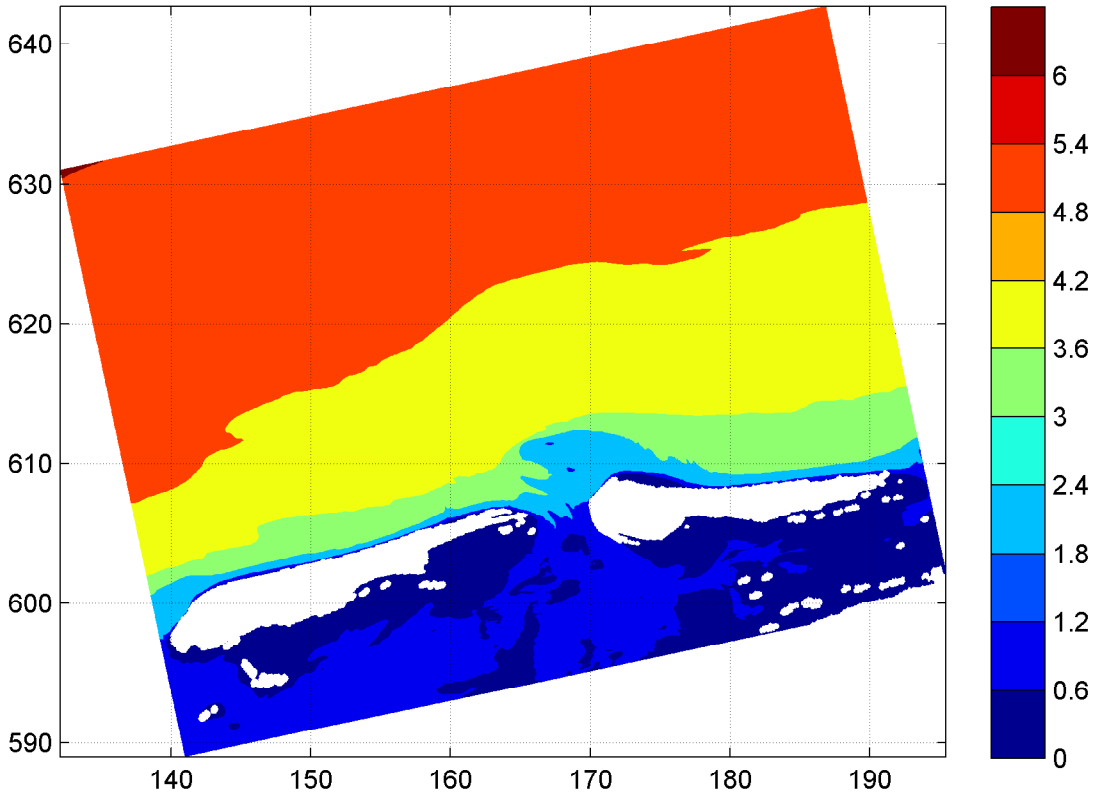

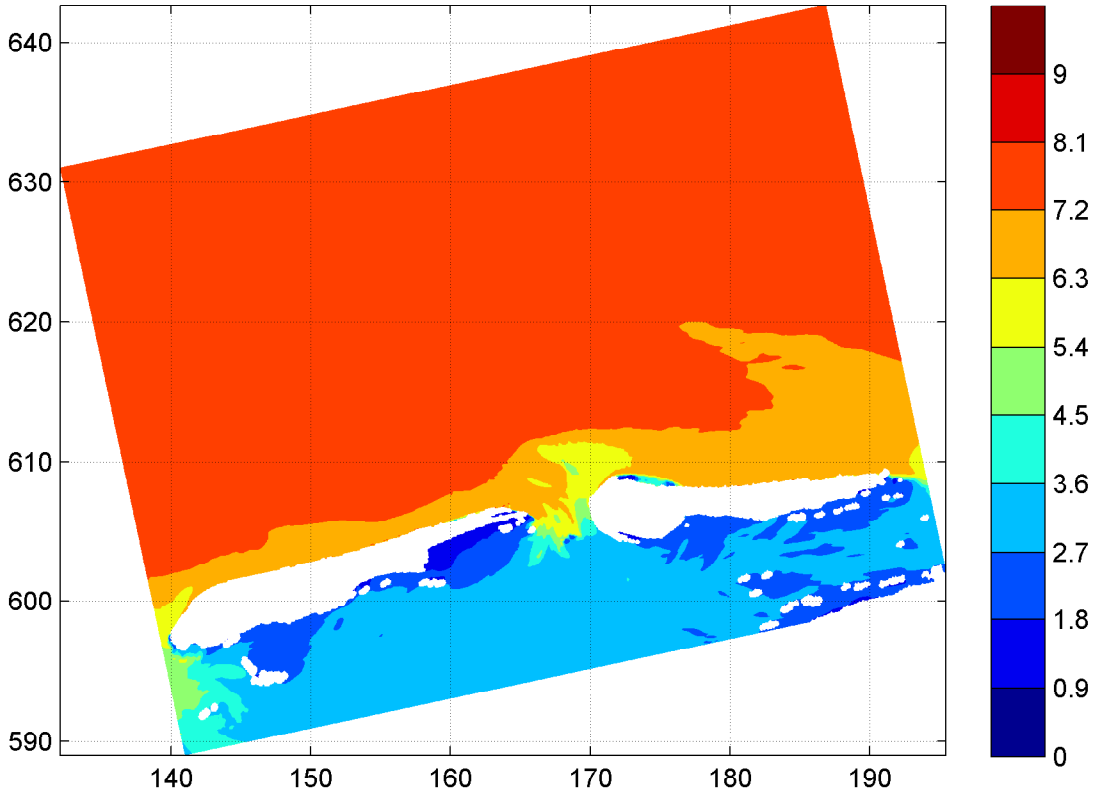

Spatial distribution of wave height H_{m0} [m] (upper panel) and wave period $T_{m-1,0}$ [s] (lower panel) on grid1	20050108	18:00hr
	Hindcast Ameland Inlet	
WL | DELFT HYDRAULICS	H4803.11	Fig. 3.42a

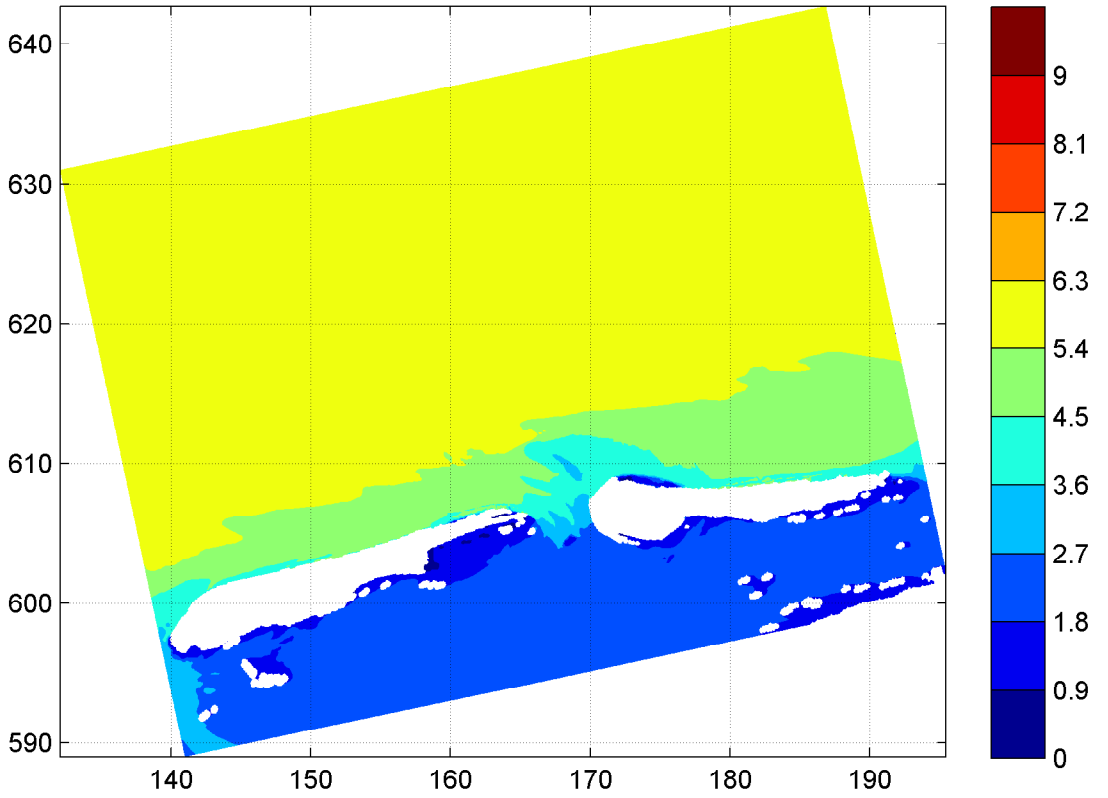

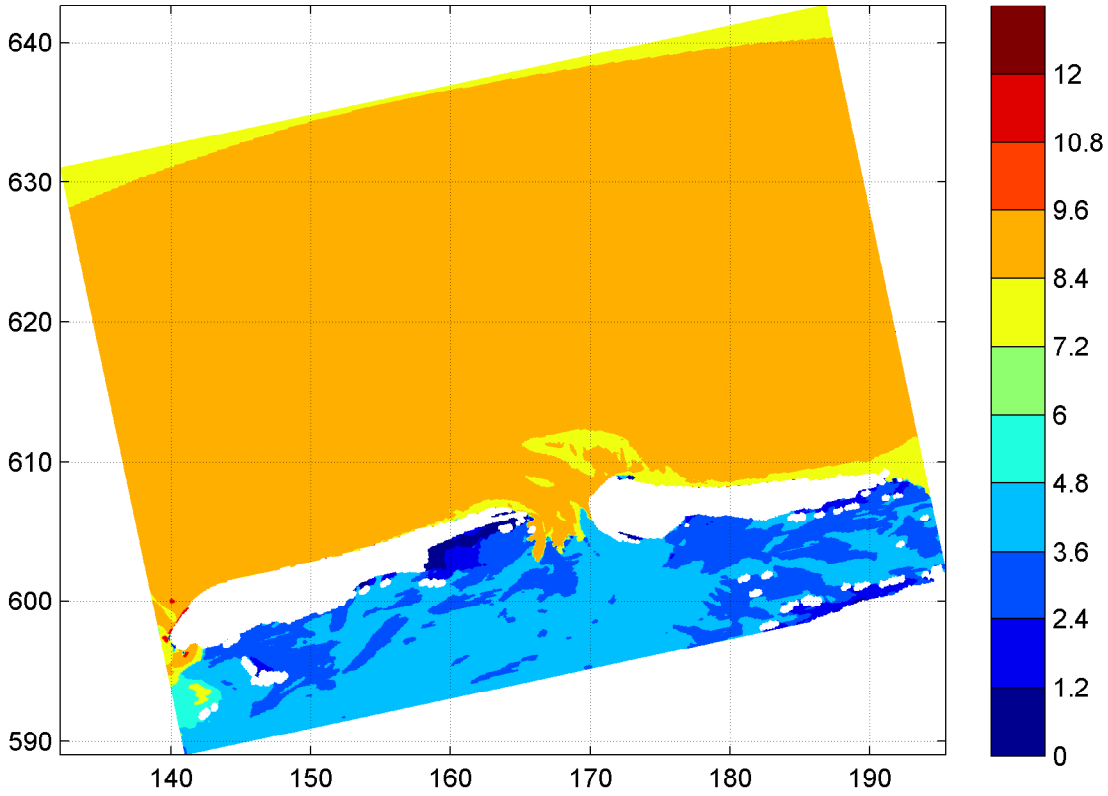

Spatial distribution of wave period T_{m02} [s] (upper panel) and wave period T_p [s] (lower panel) on grid1	20050108	18:00hr
	Hindcast Ameland Inlet	
WL | DELFT HYDRAULICS	H4803.11	Fig. 3.42b

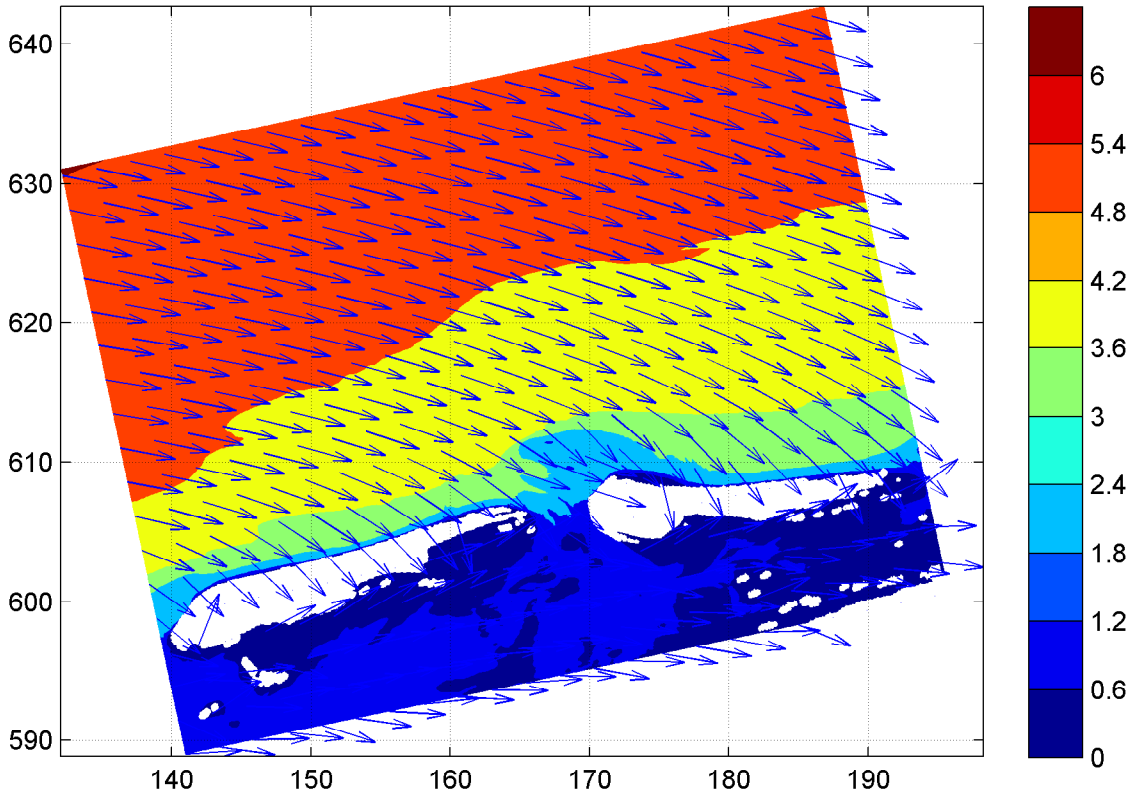

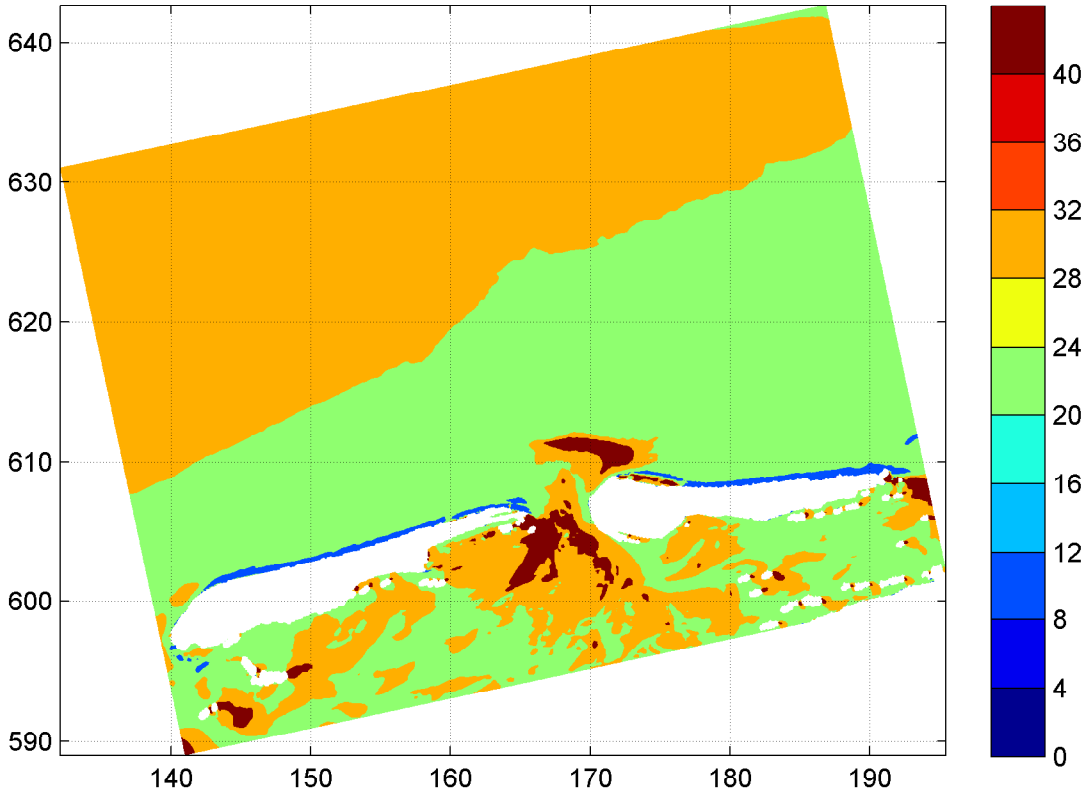

Spatial distribution of wave height [m] and mean wave direction (upper panel) and directional spreading [°] (lower panel) on grid1	20050108	18:00hr
	Hindcast Ameland Inlet	
WL | DELFT HYDRAULICS	H4803.11	Fig. 3.42c

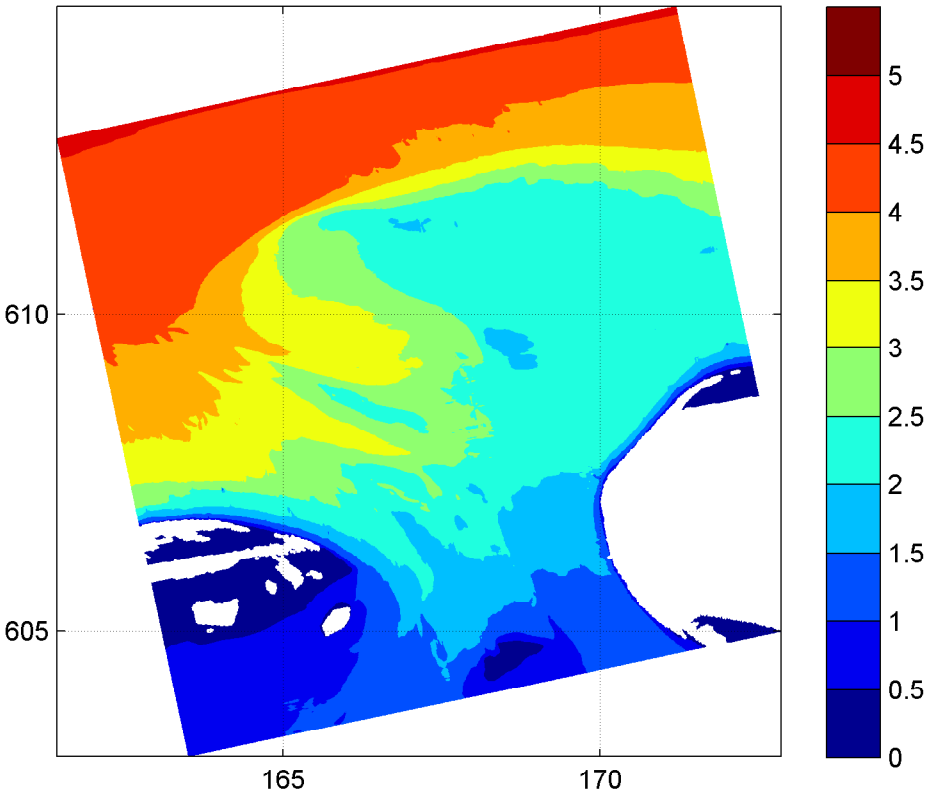

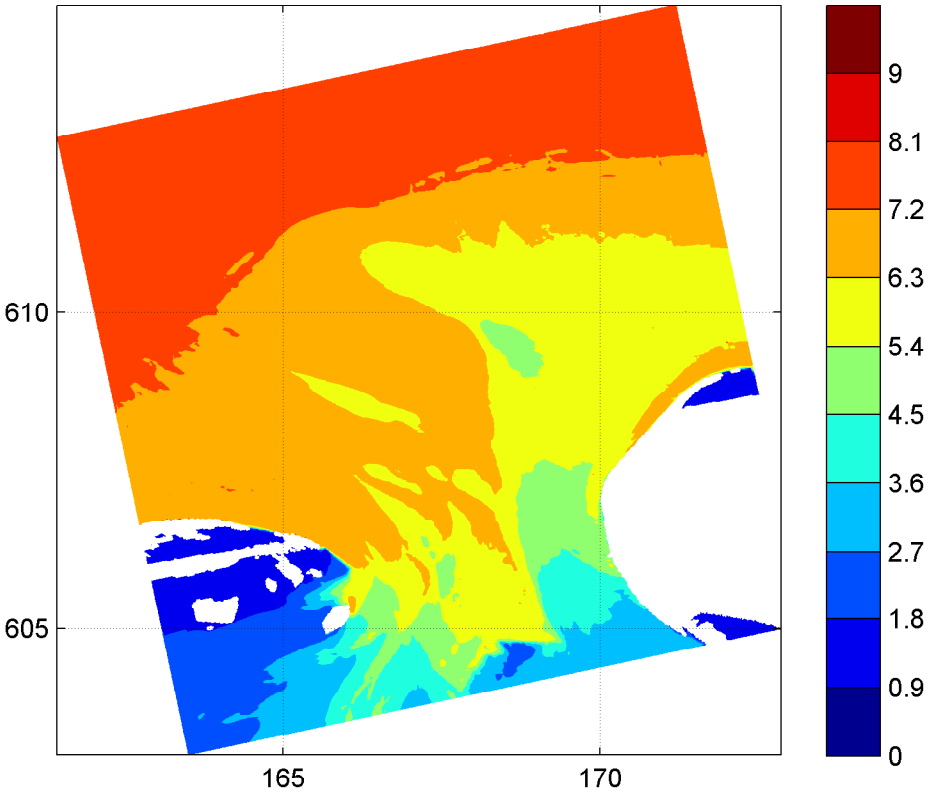

Spatial distribution of wave height H_{m0} [m] (upper panel) and wave period $T_{m-1,0}$ [s] (lower panel) on grid2	20050108	18:00hr
	Hindcast Ameland Inlet	
WL | DELFT HYDRAULICS	H4803.11	Fig. 3.43a

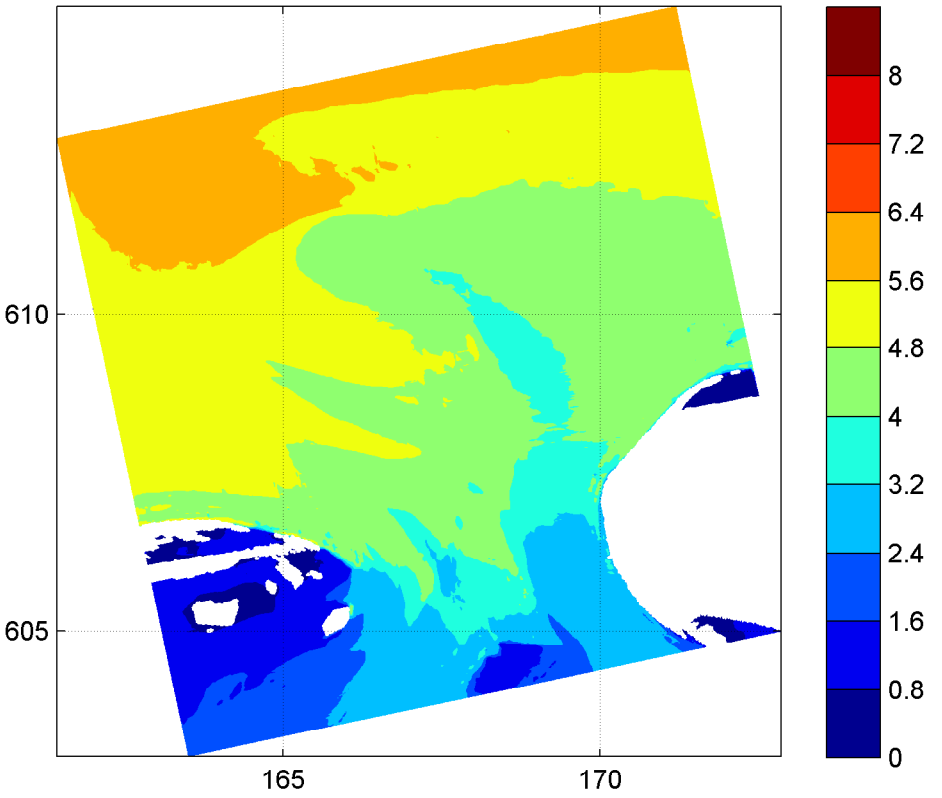

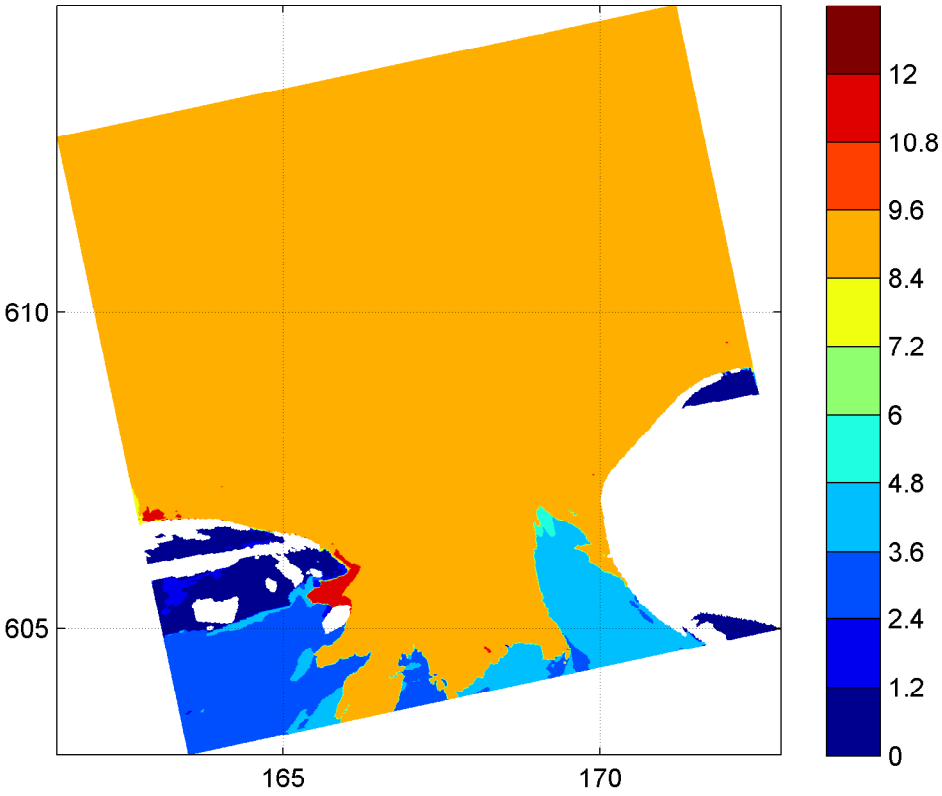

Spatial distribution of wave period T_{m02} [s] (upper panel) and wave period T_p [s] (lower panel) on grid2	20050108	18:00hr
	Hindcast Ameland Inlet	
WL | DELFT HYDRAULICS	H4803.11	Fig. 3.43b

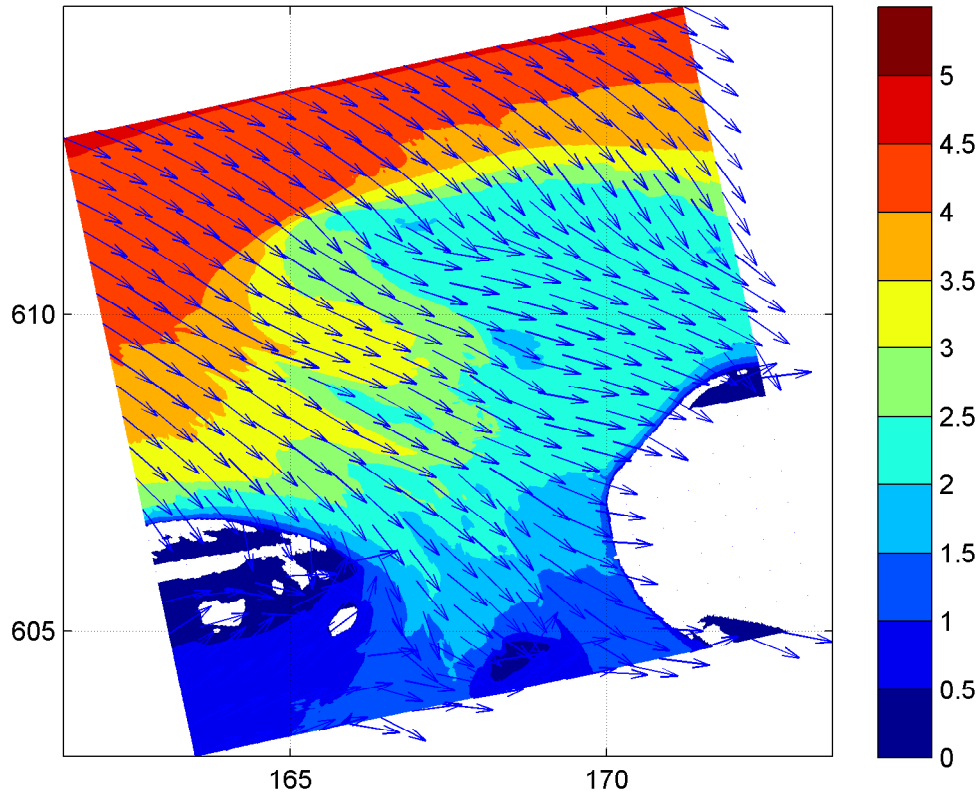

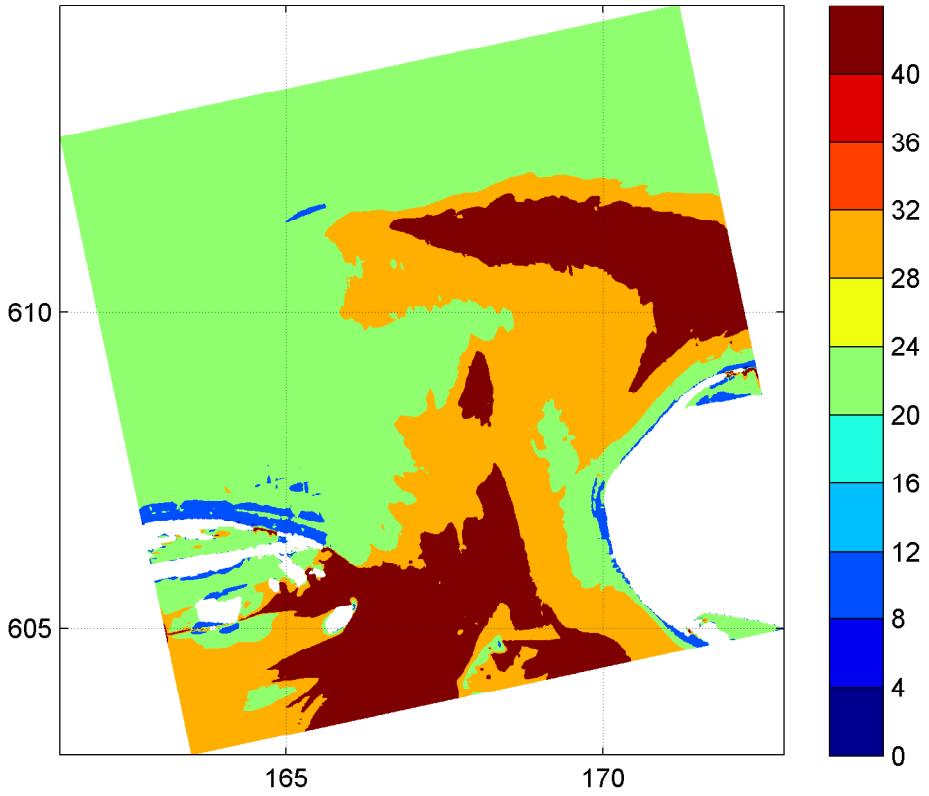

Spatial distribution of wave height [m] and mean wave direction (upper panel) and directional spreading [°] (lower panel) on grid2	20050108	18:00hr
	Hindcast Ameland Inlet	
WL | DELFT HYDRAULICS	H4803.11	Fig. 3.43c

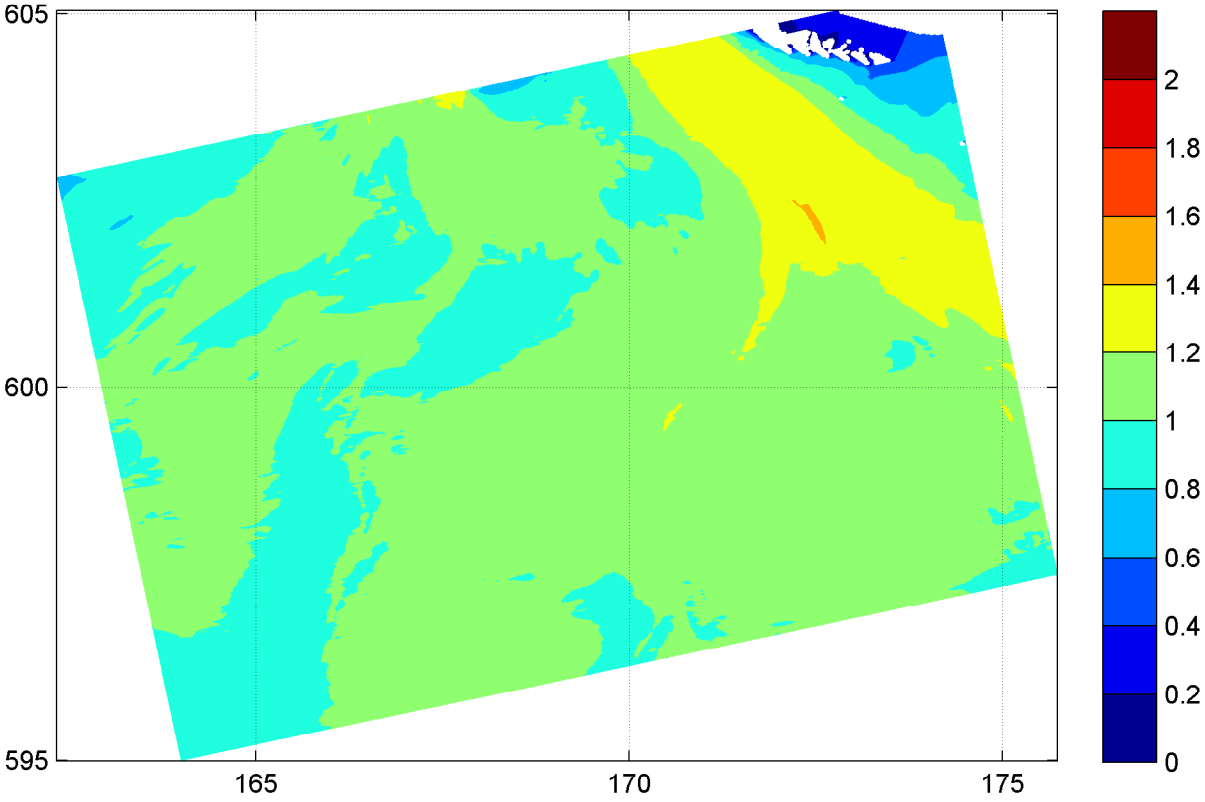

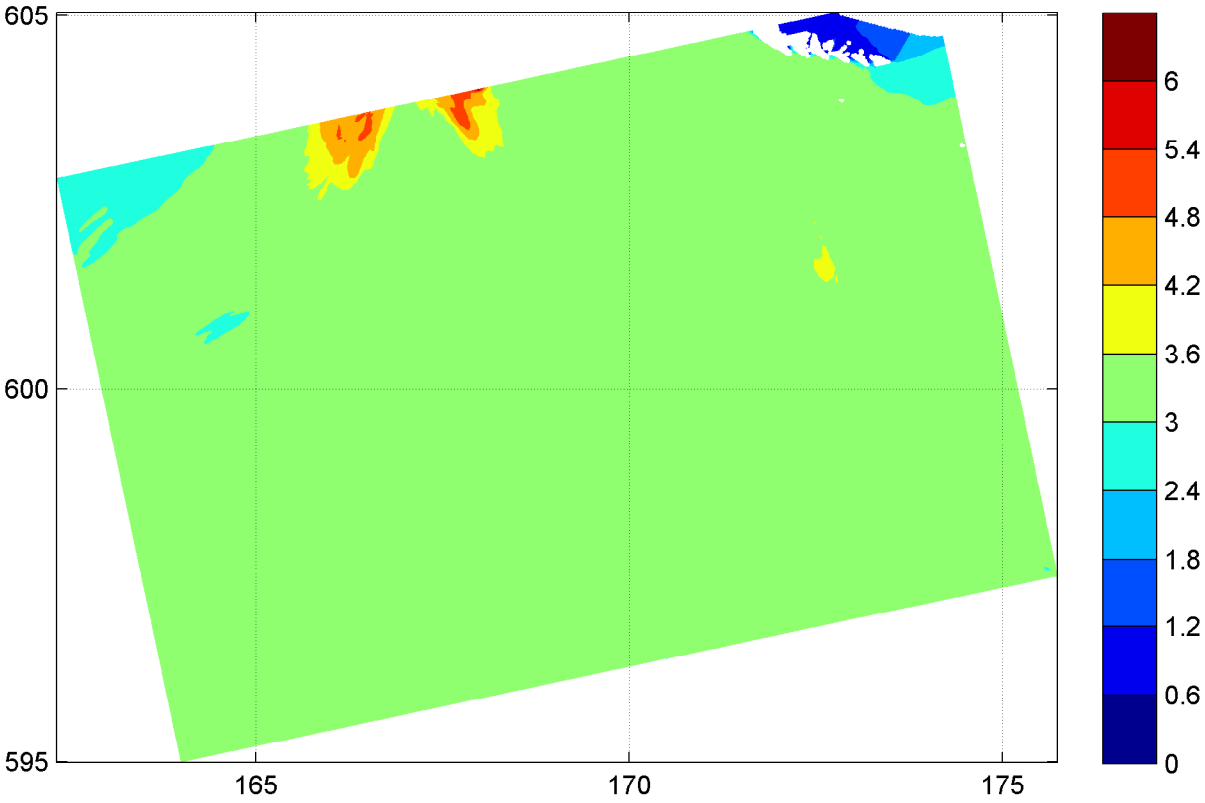

Spatial distribution of wave height H_{m0} [m] (upper panel) and wave period $T_{m-1,0}$ [s] (lower panel) on grid3	20050108	18:00hr
	Hindcast Ameland Inlet	
WL | DELFT HYDRAULICS	H4803.11	Fig. 3.44a

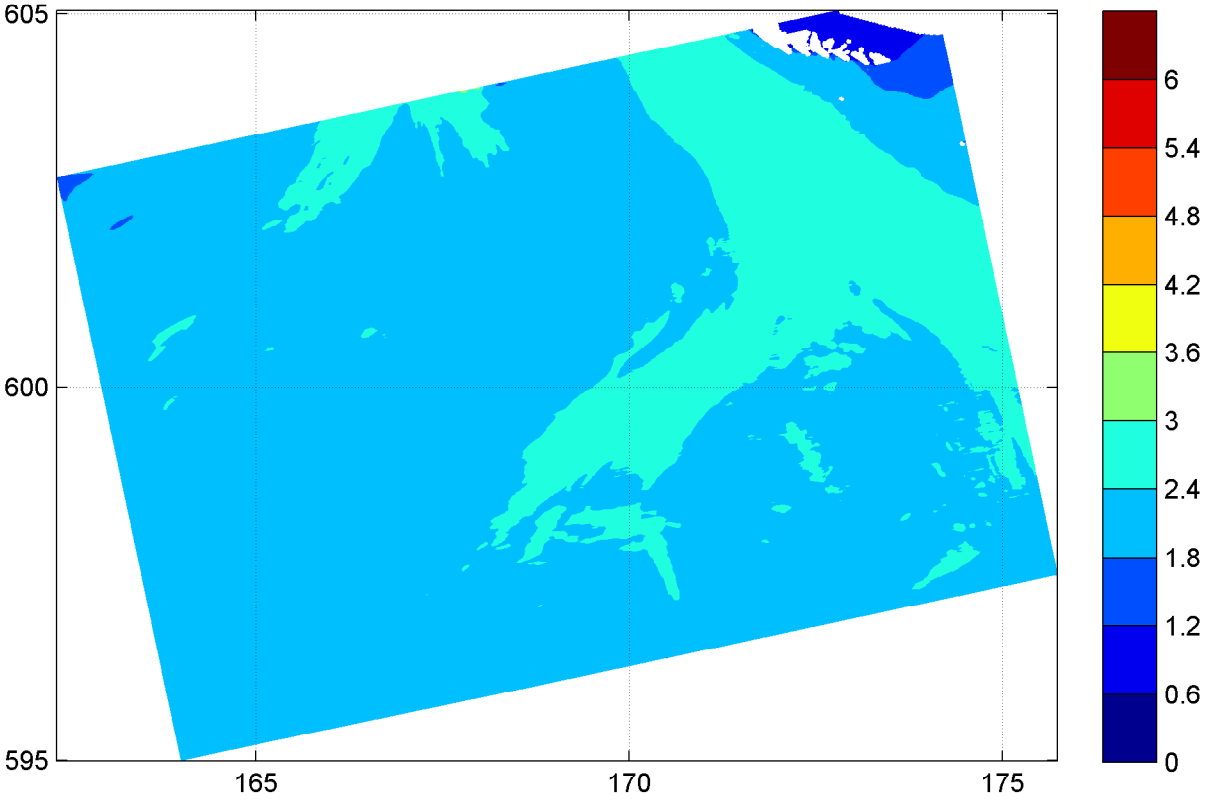

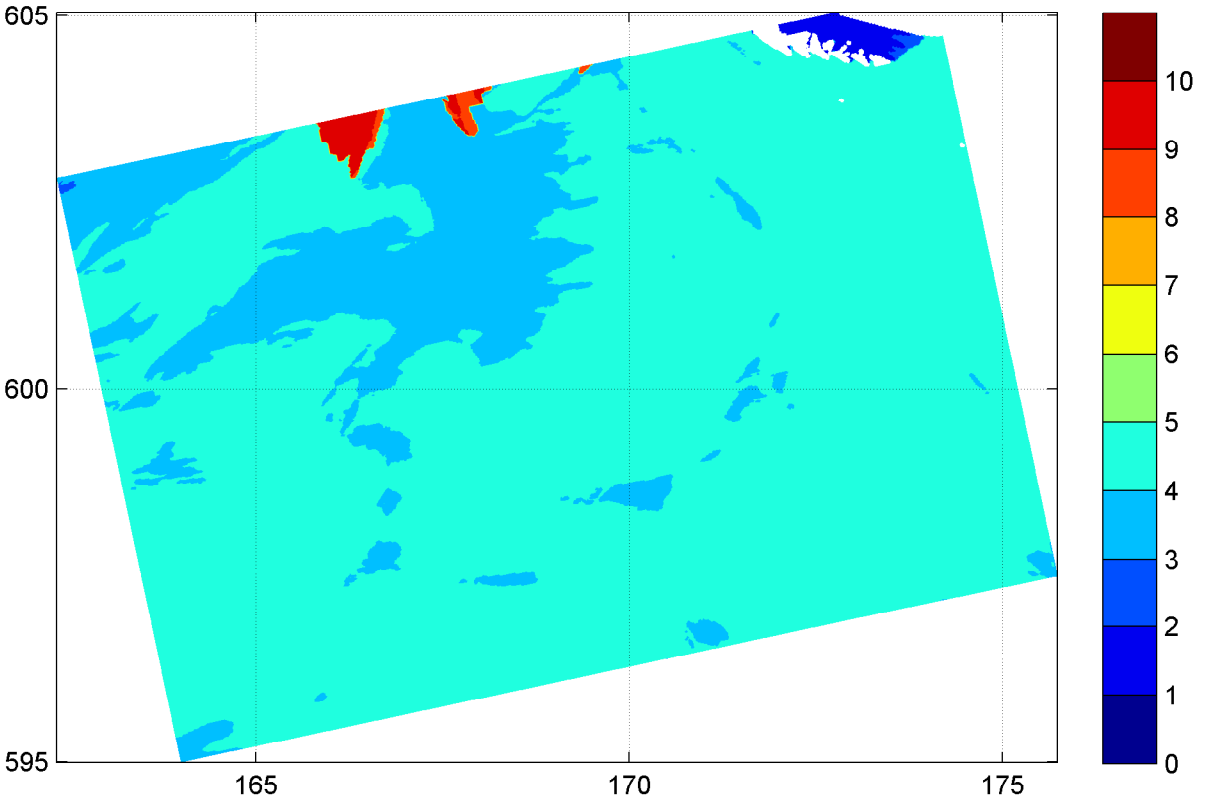

Spatial distribution of wave period T_{m02} [s] (upper panel) and wave period T_p [s] (lower panel) on grid3	20050108	18:00hr
	Hindcast Ameland Inlet	
WL | DELFT HYDRAULICS	H4803.11	Fig. 3.44b

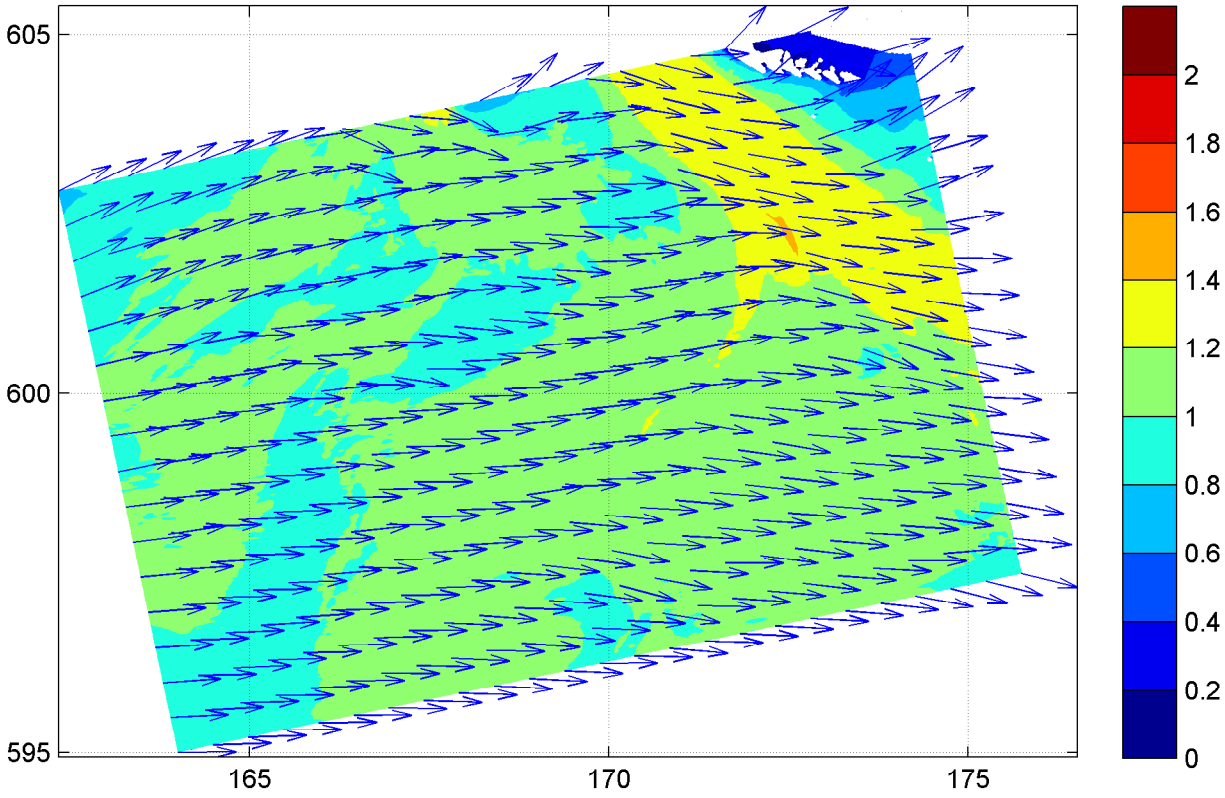

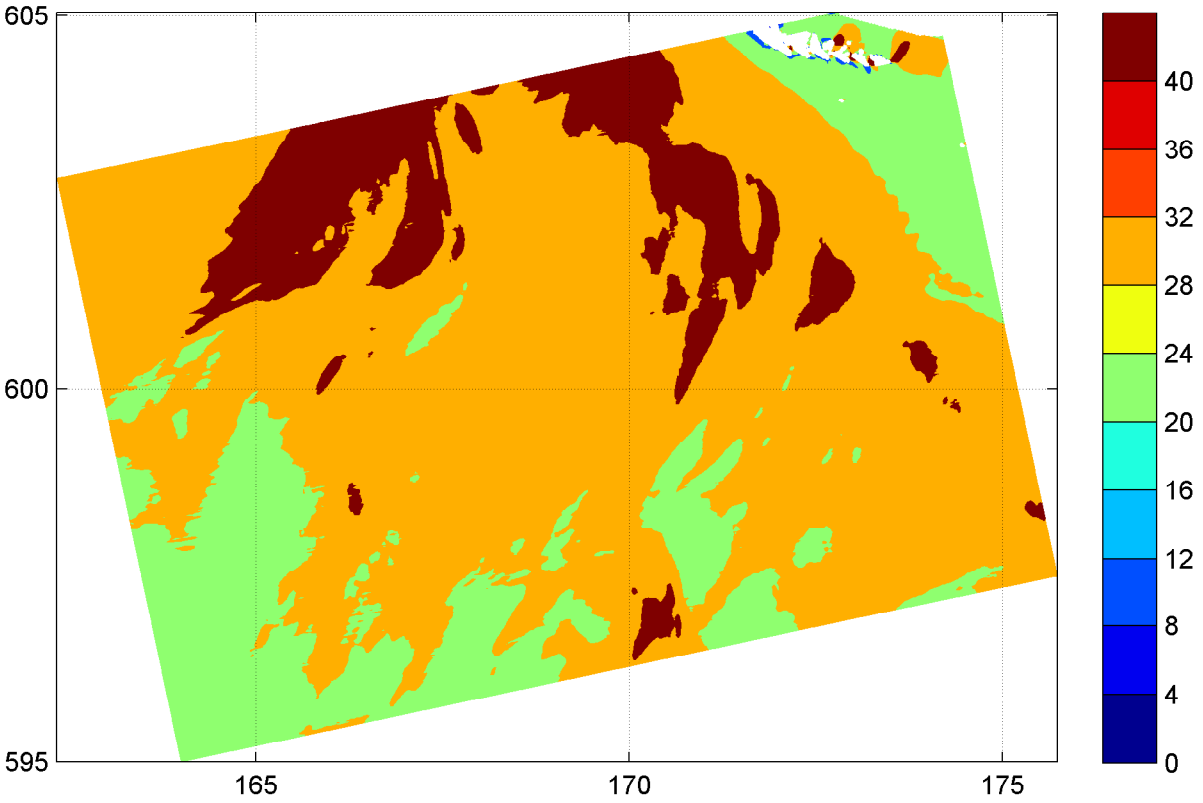

Spatial distribution of wave height [m] and mean wave direction (upper panel) and directional spreading [°] (lower panel) on grid3	20050108	18:00hr
	Hindcast Ameland Inlet	
WL | DELFT HYDRAULICS	H4803.11	Fig. 3.44c

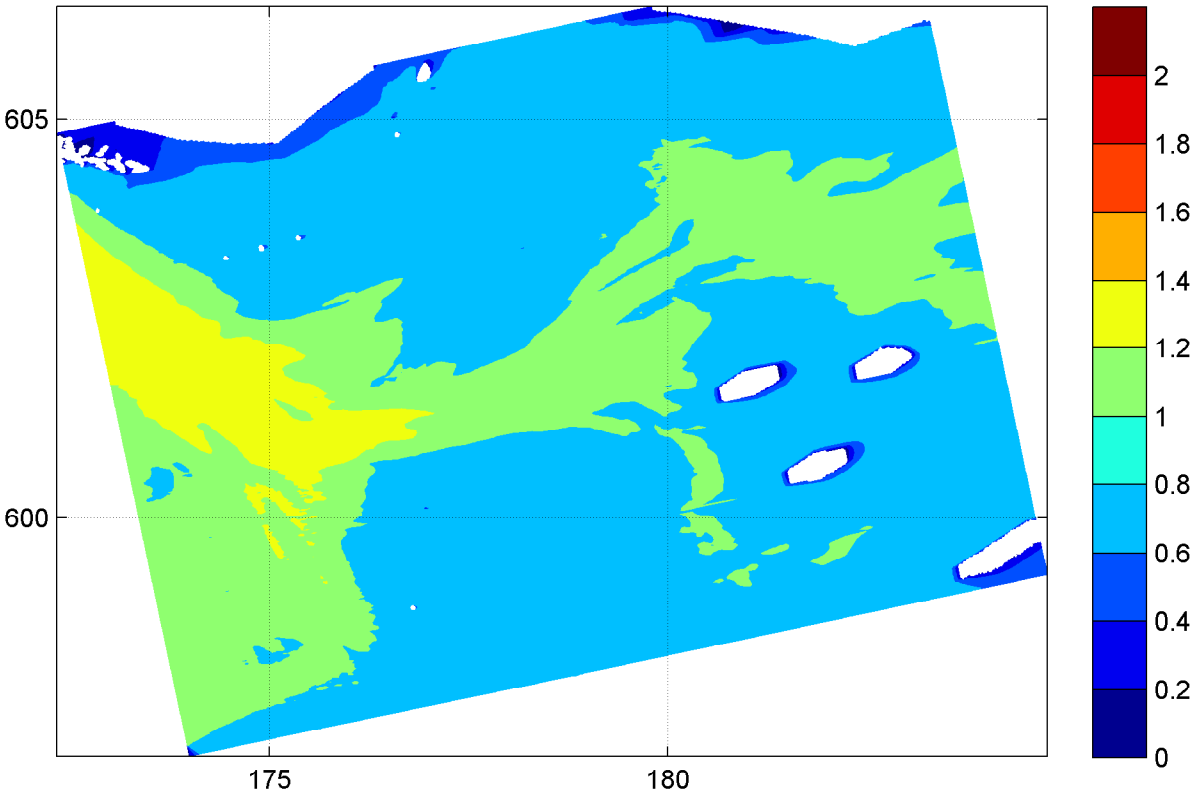

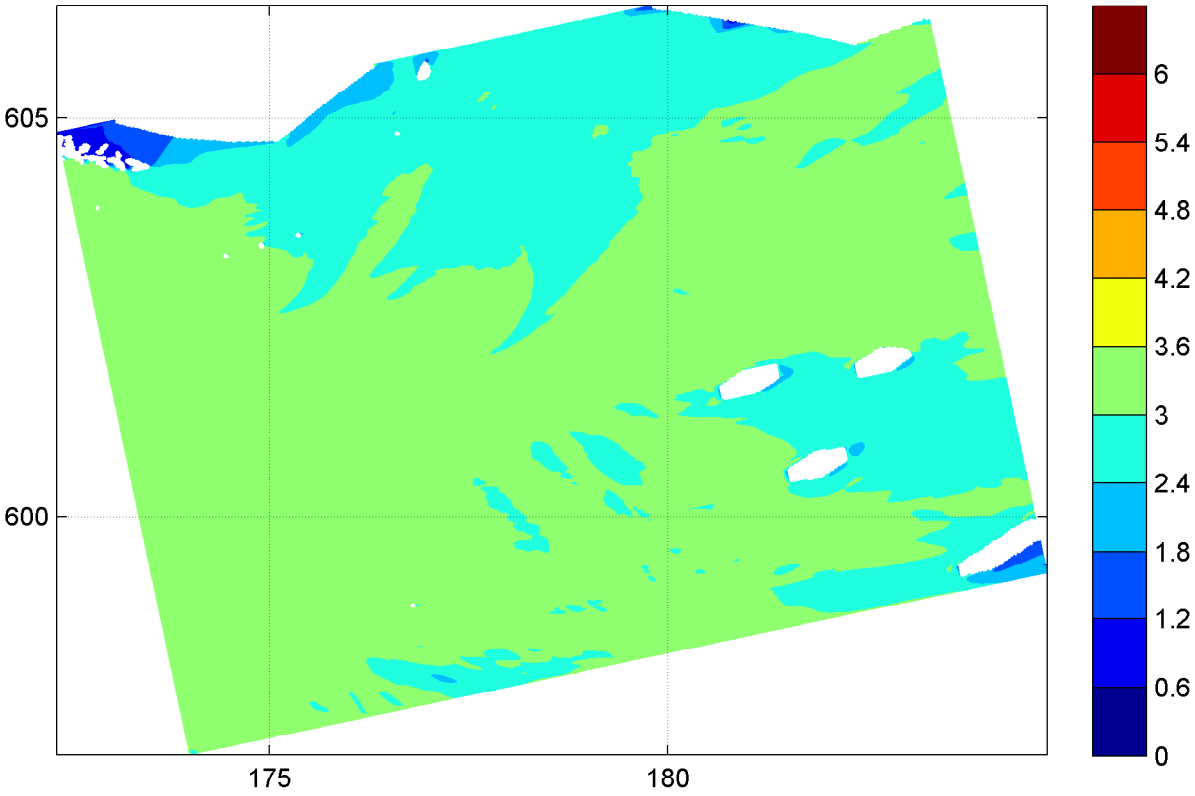

Spatial distribution of wave height H_{m0} [m] (upper panel) and wave period $T_{m-1,0}$ [s] (lower panel) on grid4	20050108	18:00hr
	Hindcast Ameland Inlet	
WL | DELFT HYDRAULICS	H4803.11	Fig. 3.45a

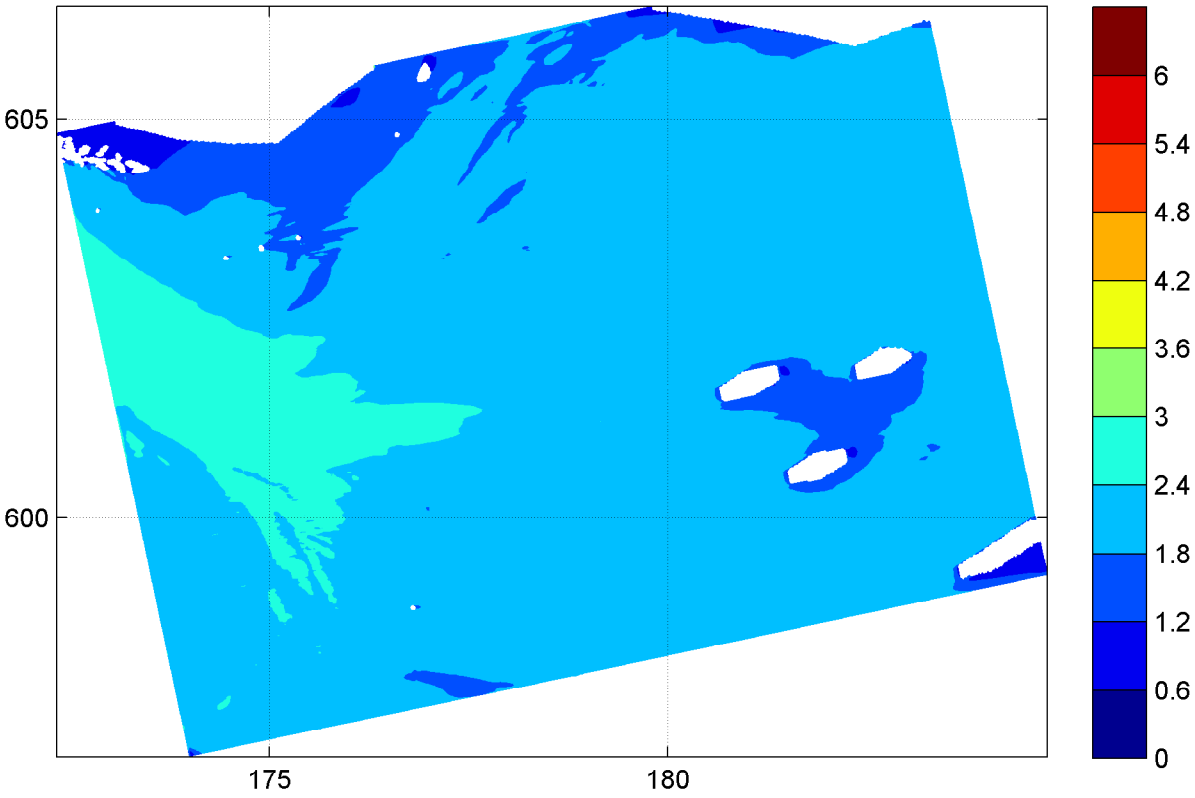

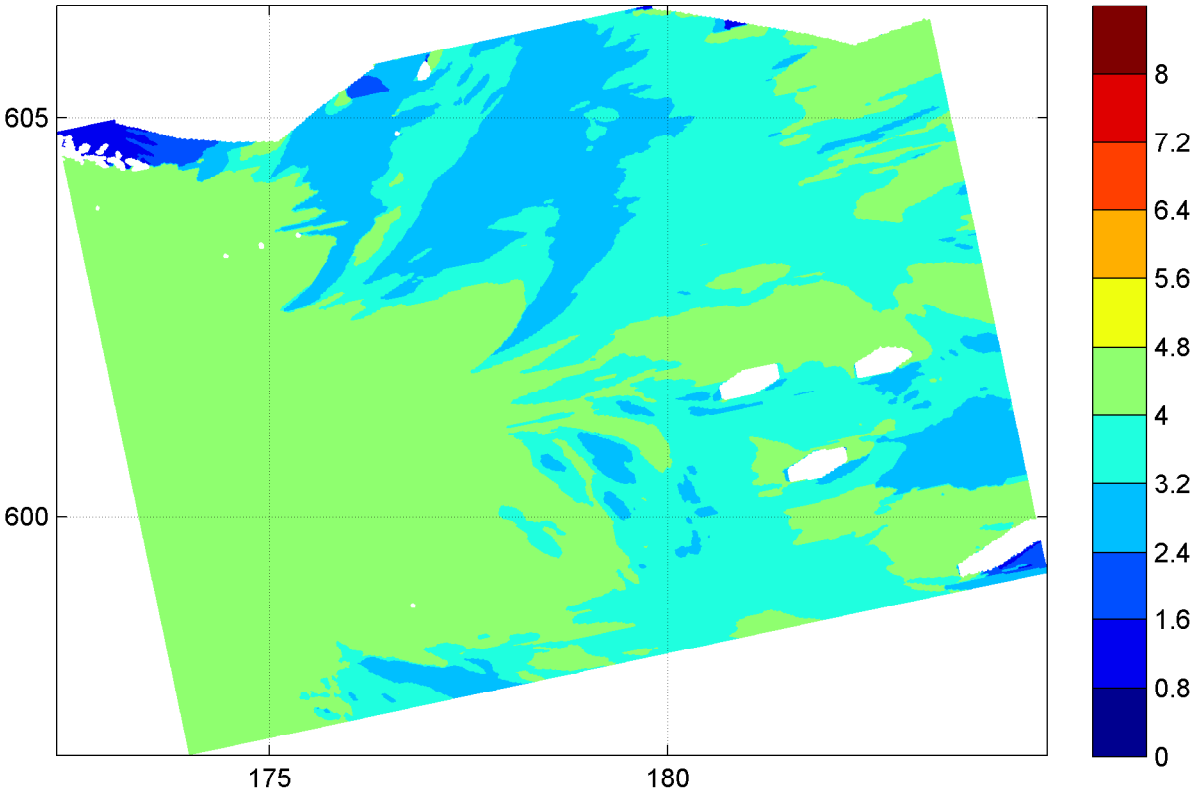

Spatial distribution of wave period T_{m02} [s] (upper panel) and wave period T_p [s] (lower panel) on grid4	20050108	18:00hr
	Hindcast Ameland Inlet	
WL | DELFT HYDRAULICS	H4803.11	Fig. 3.45b

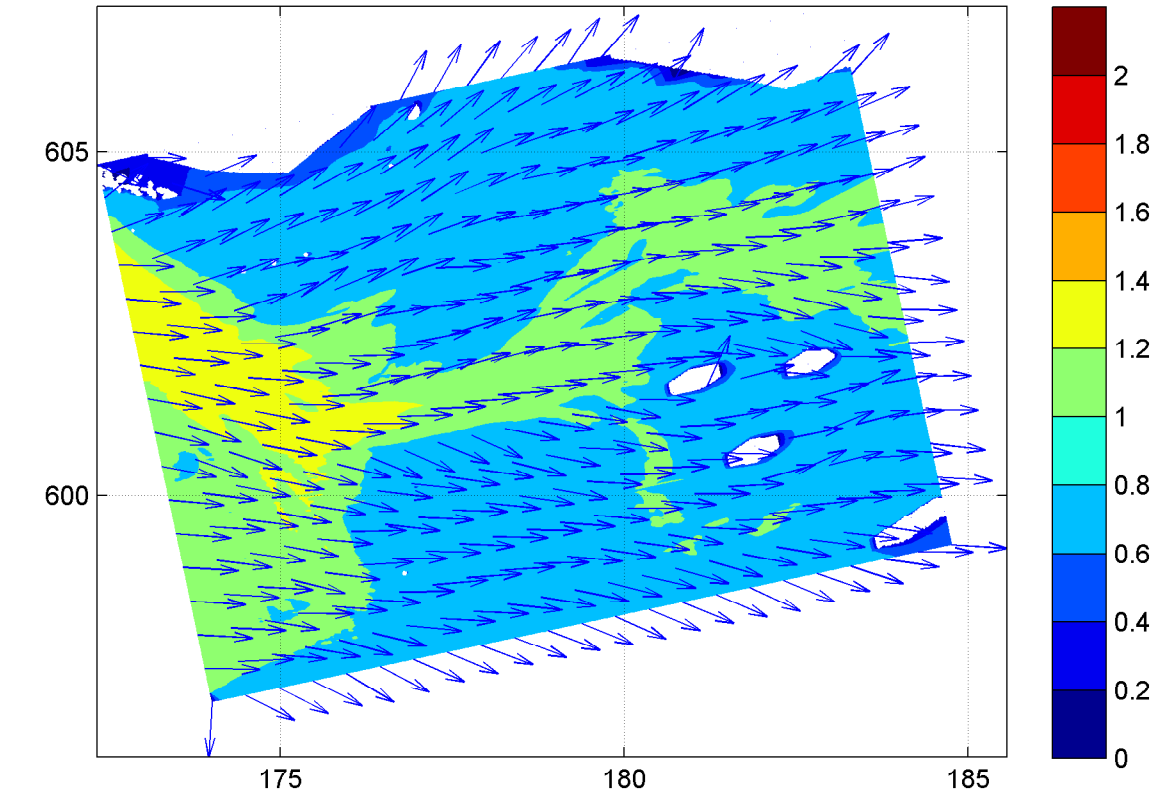

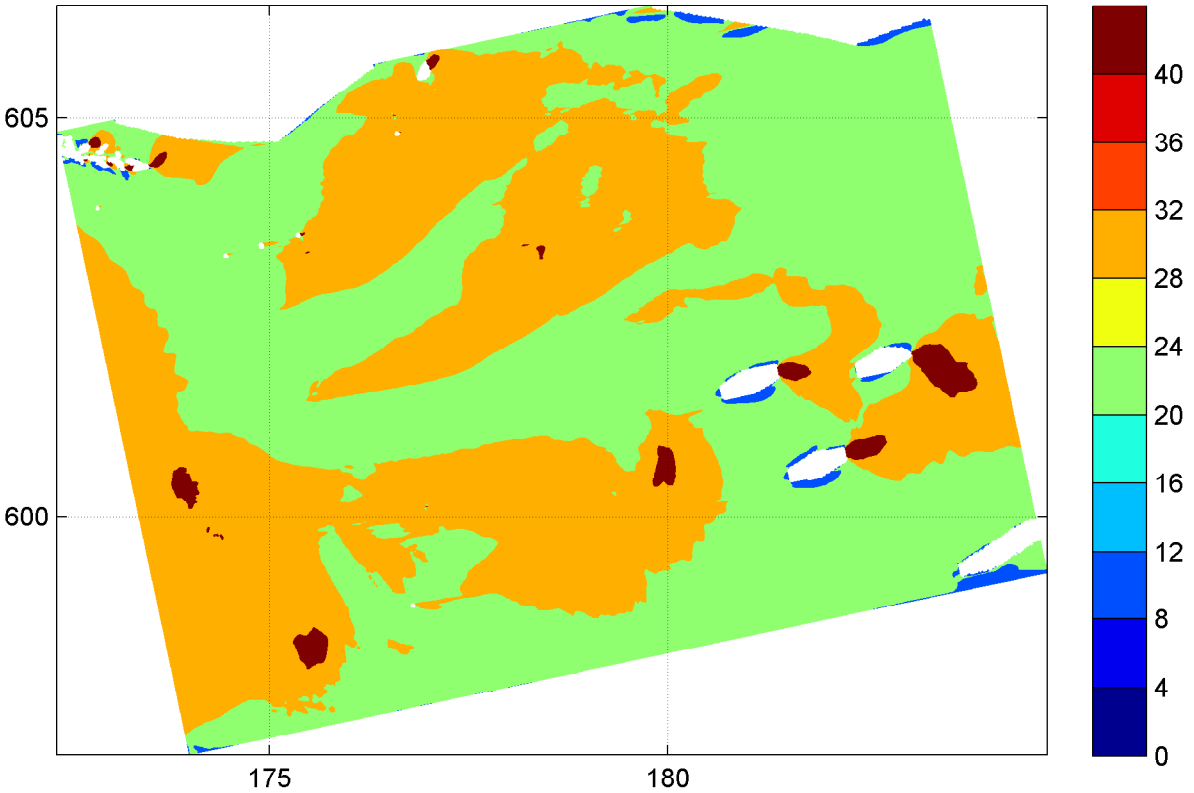

Spatial distribution of wave height [m] and mean wave direction (upper panel) and directional spreading [°] (lower panel) on grid4	20050108	18:00hr
	Hindcast Ameland Inlet	
WL | DELFT HYDRAULICS	H4803.11	Fig. 3.45c

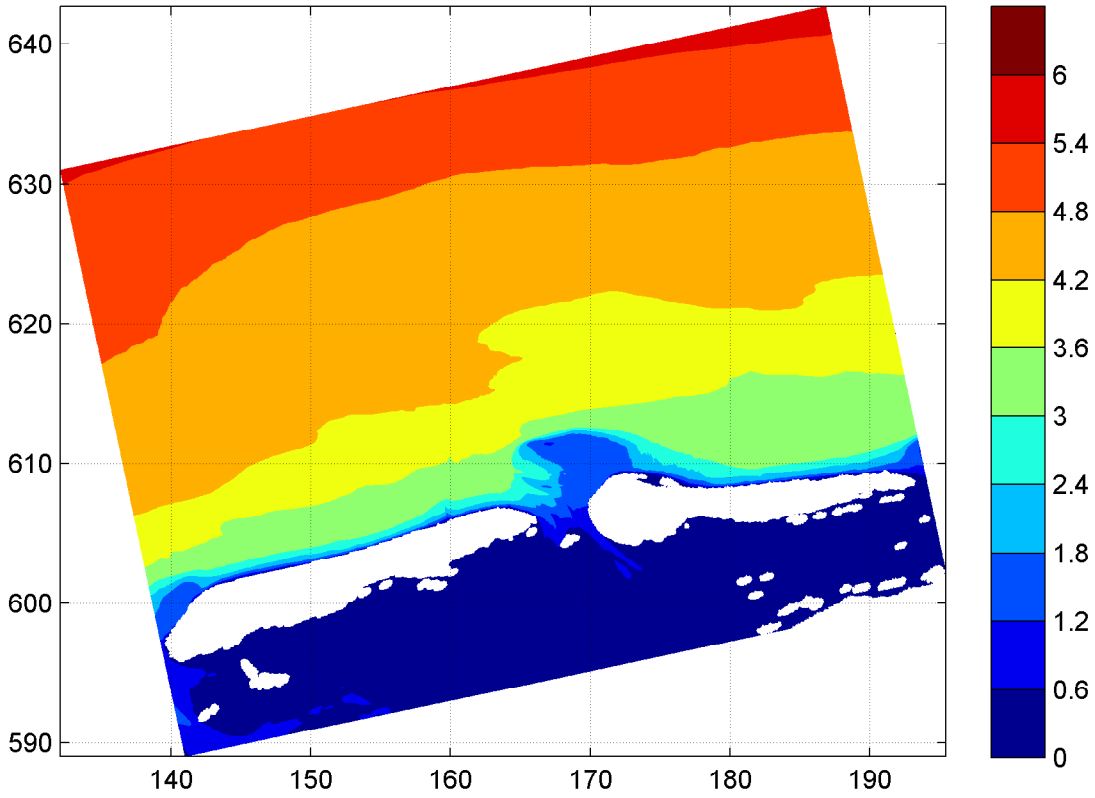

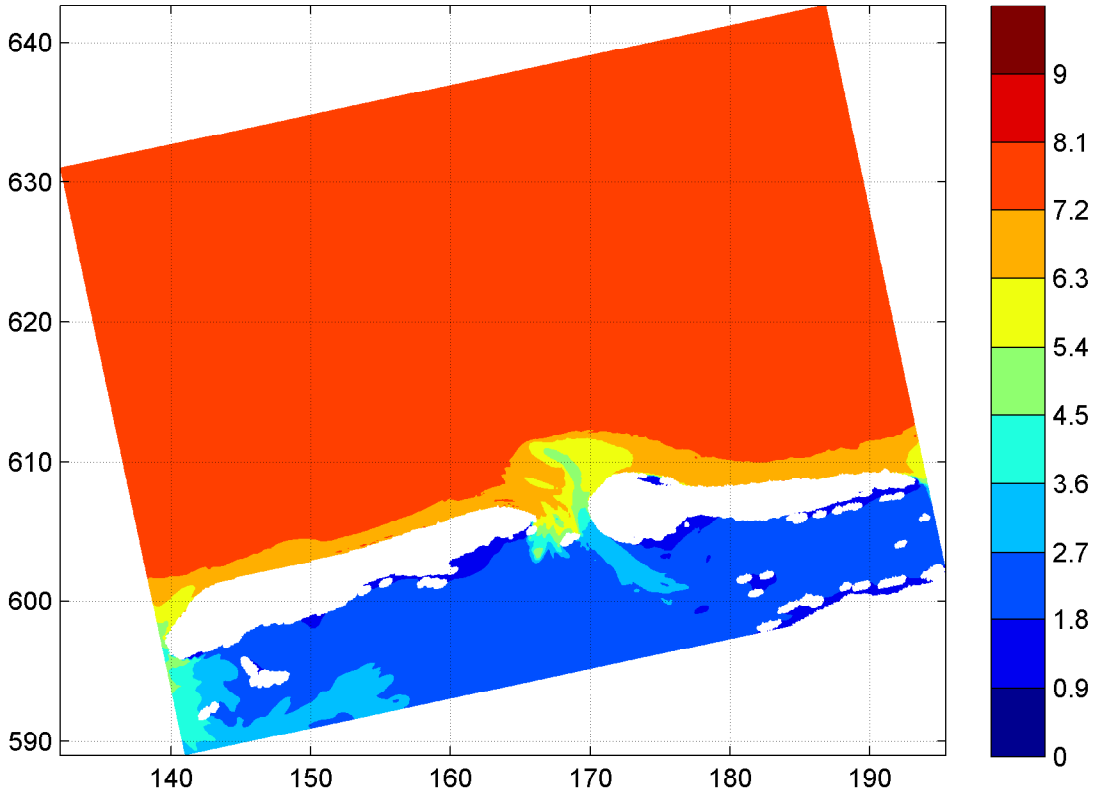

Spatial distribution of wave height H_{m0} [m] (upper panel) and wave period $T_{m-1,0}$ [s] (lower panel) on grid1 uniform water level field and no current	20050102	10:00hr
	Hindcast Ameland Inlet	
WL | DELFT HYDRAULICS	H4803.11	Fig. 3.46a

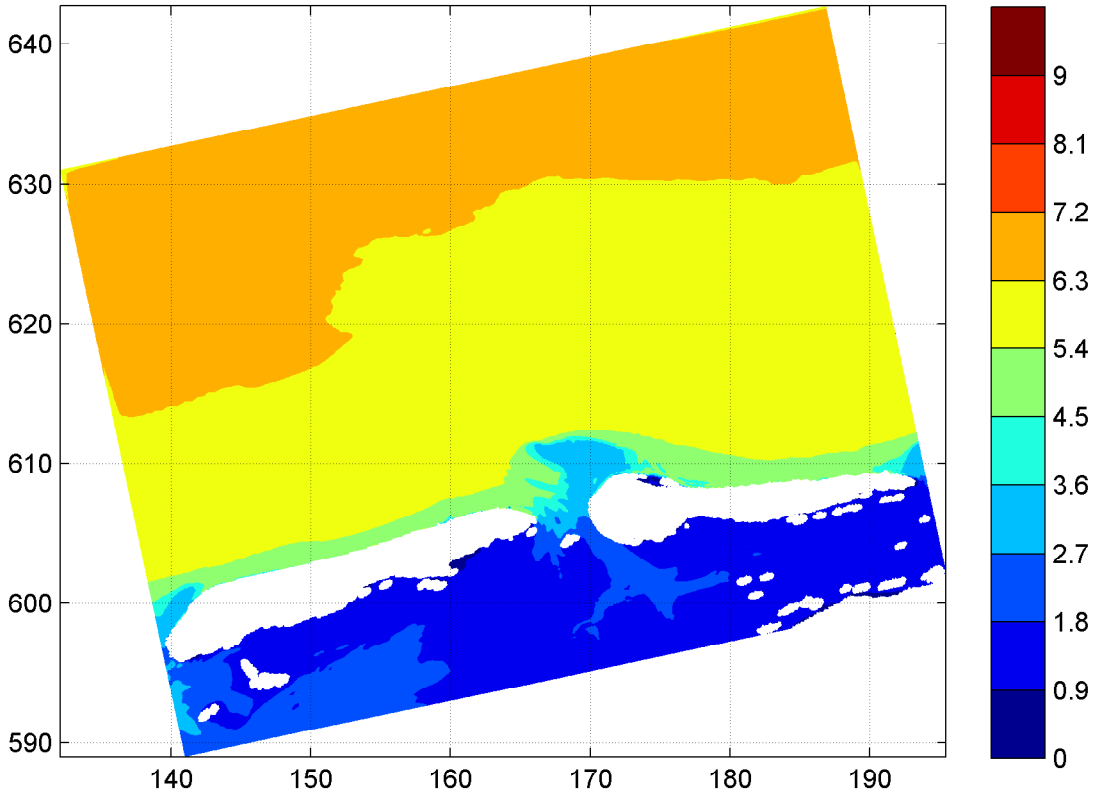

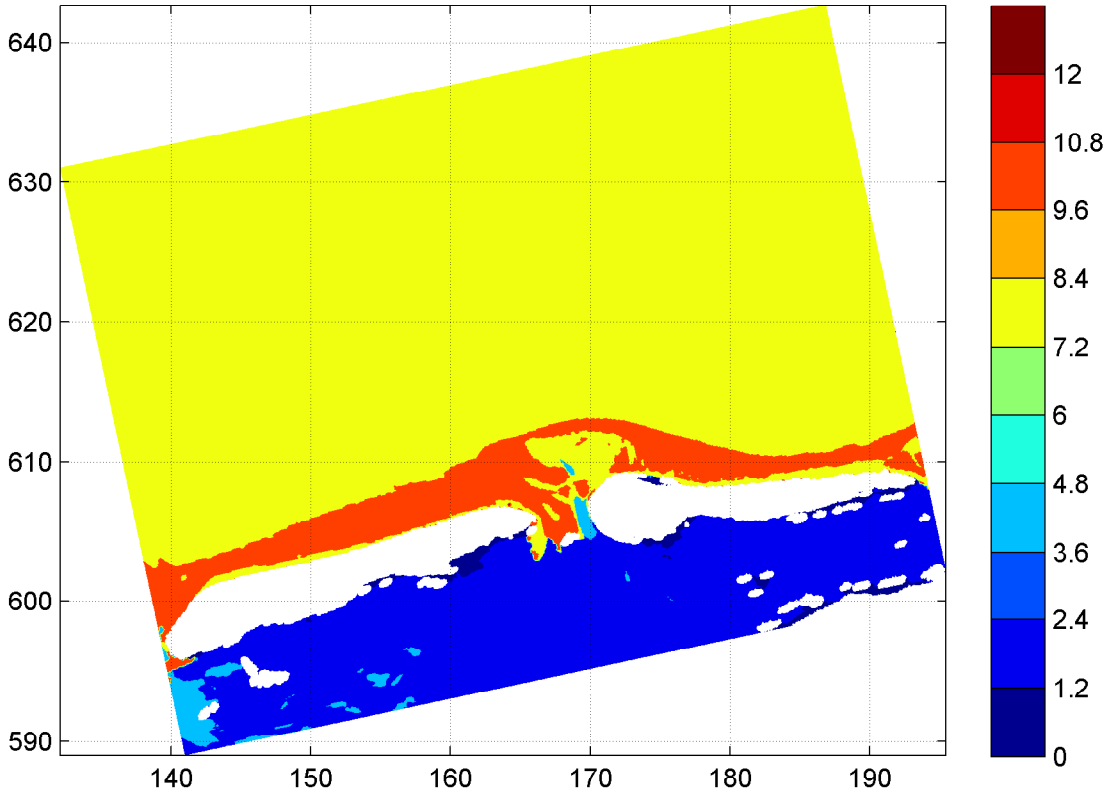

Spatial distribution of wave period T_{m02} [s] (upper panel) and wave period T_p [s] (lower panel) on grid1 uniform water level field and no current	20050102	10:00hr
	Hindcast Ameland Inlet	
WL | DELFT HYDRAULICS	H4803.11	Fig. 3.46b

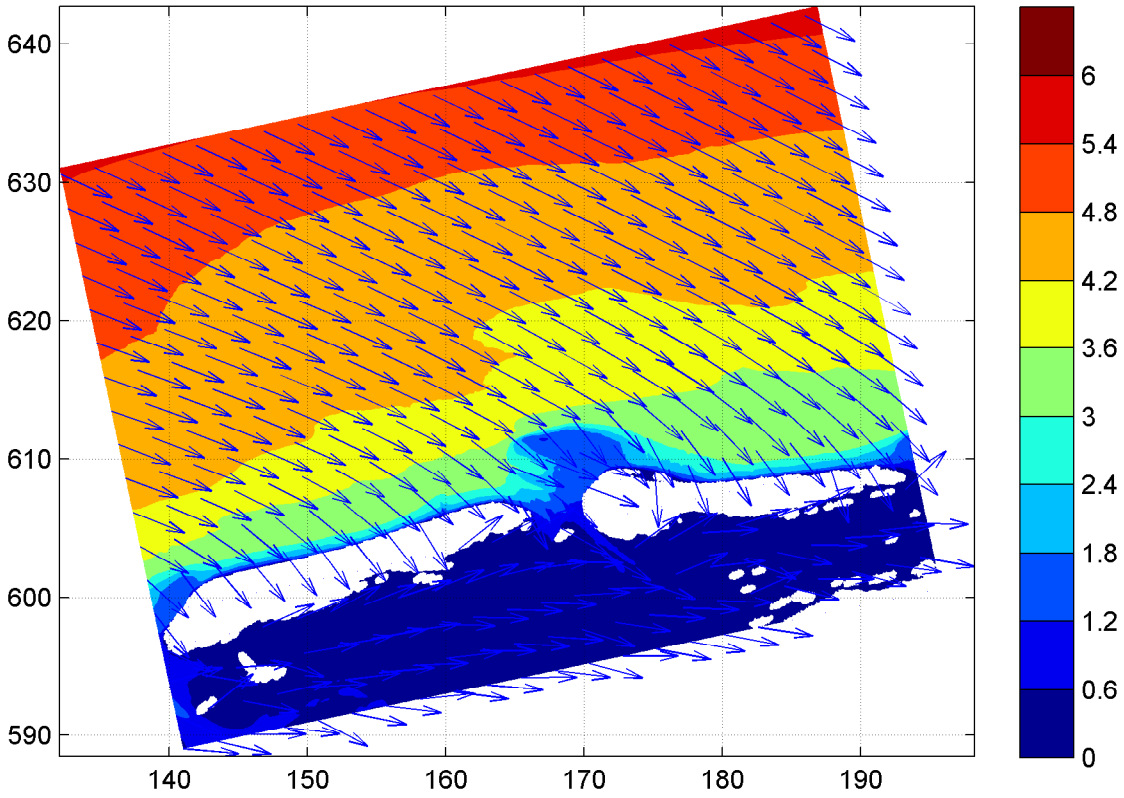

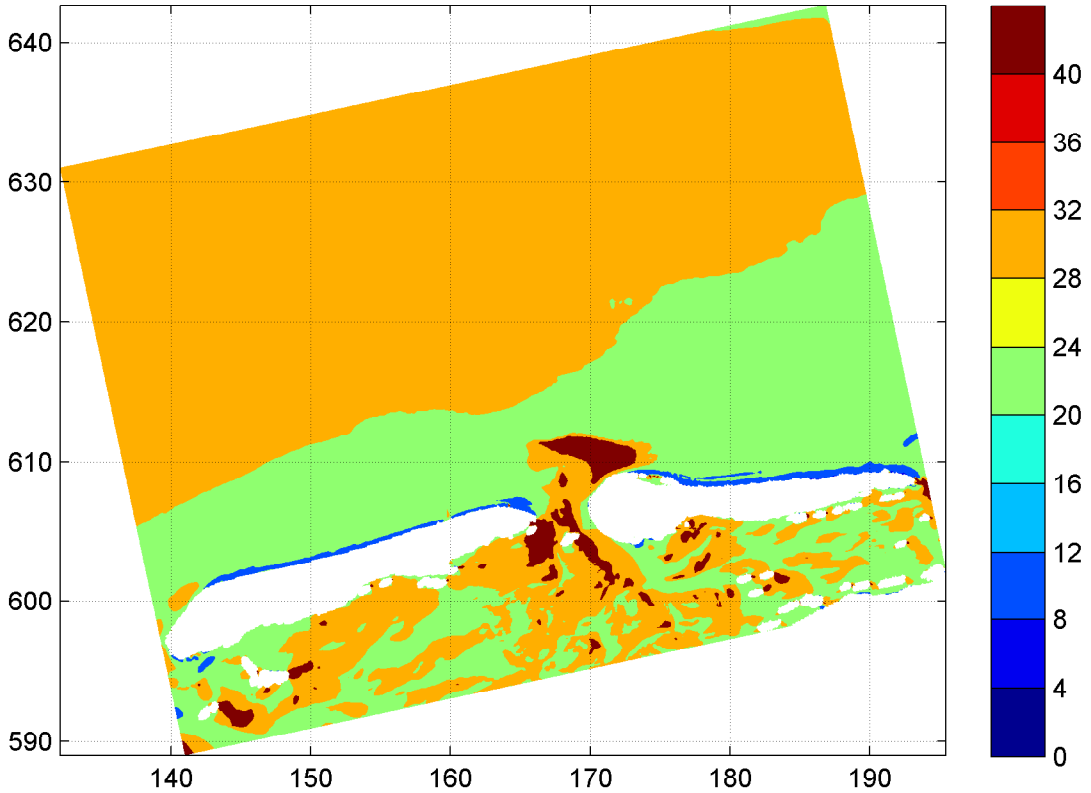

Spatial distribution of wave height [m] and mean wave direction (upper panel) and directional spreading [°] (lower panel) on grid1 uniform water level field and no current	20050102	10:00hr
	Hindcast Ameland Inlet	
WL | DELFT HYDRAULICS	H4803.11	Fig. 3.46c

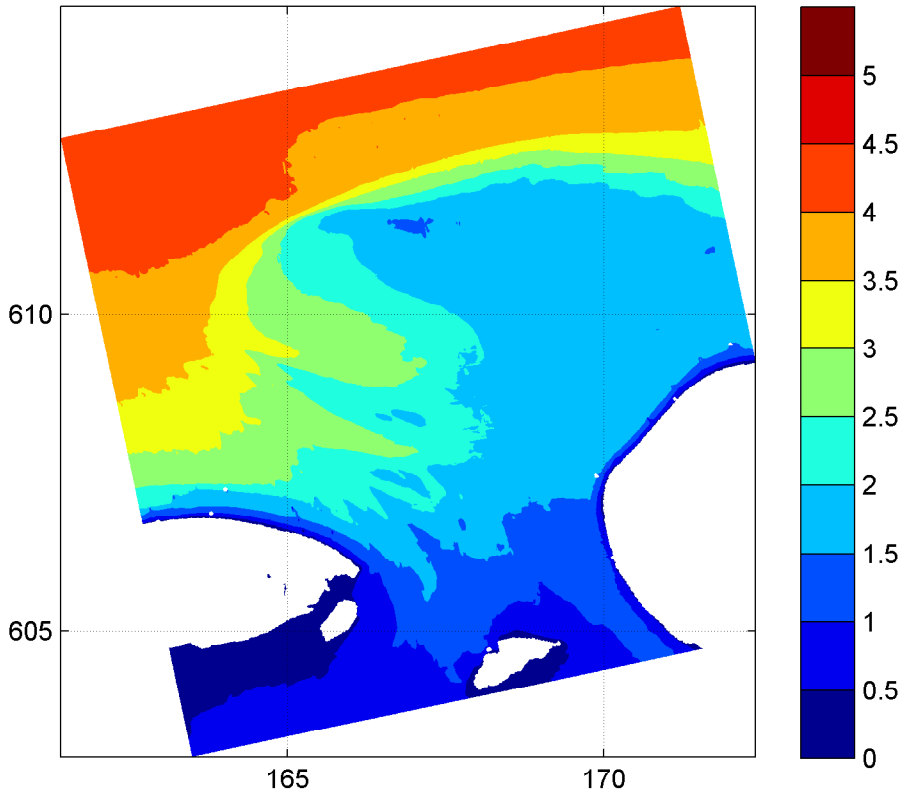

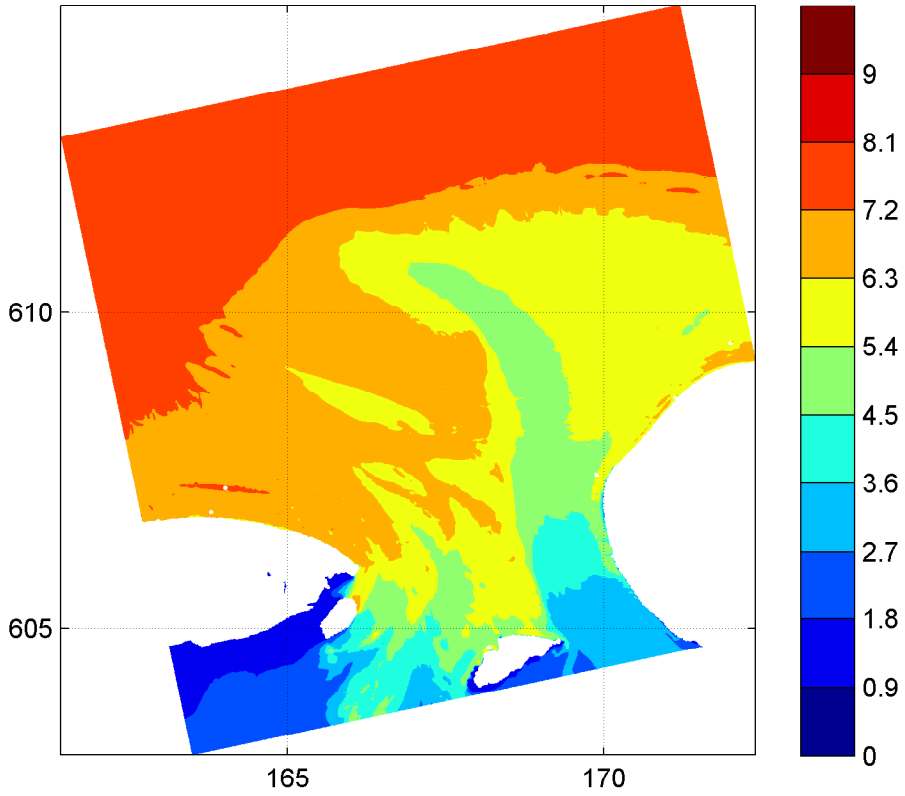

Spatial distribution of wave height H_{m0} [m] (upper panel) and wave period $T_{m-1,0}$ [s] (lower panel) on grid2 uniform water level field and no current	20050102	10:00hr
	Hindcast Ameland Inlet	
WL | DELFT HYDRAULICS	H4803.11	Fig. 3.47a

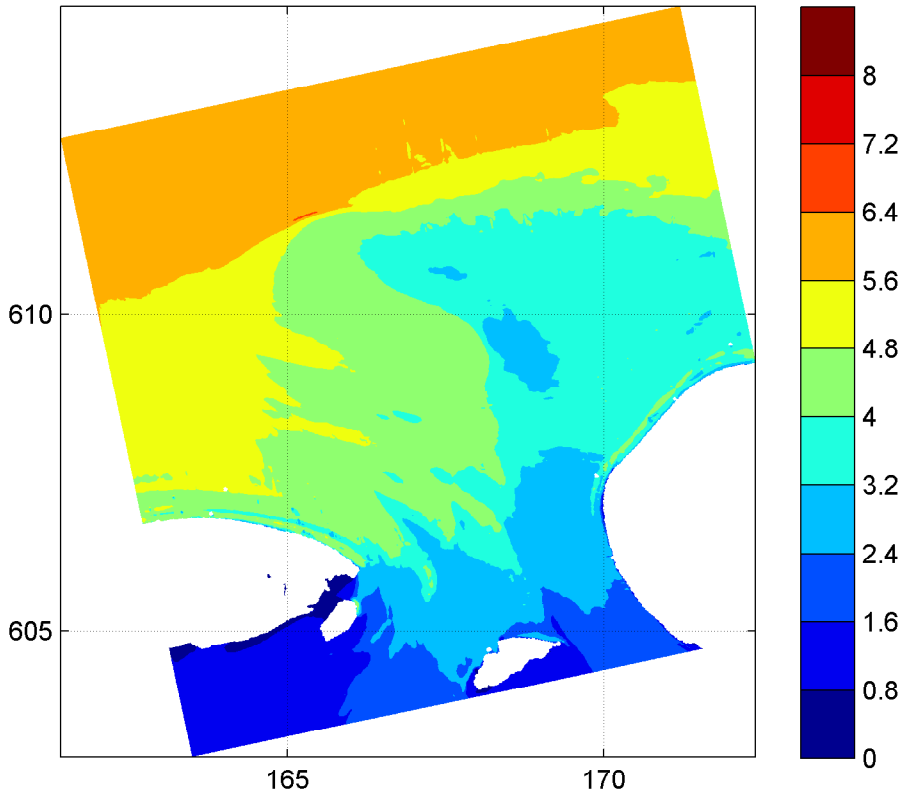

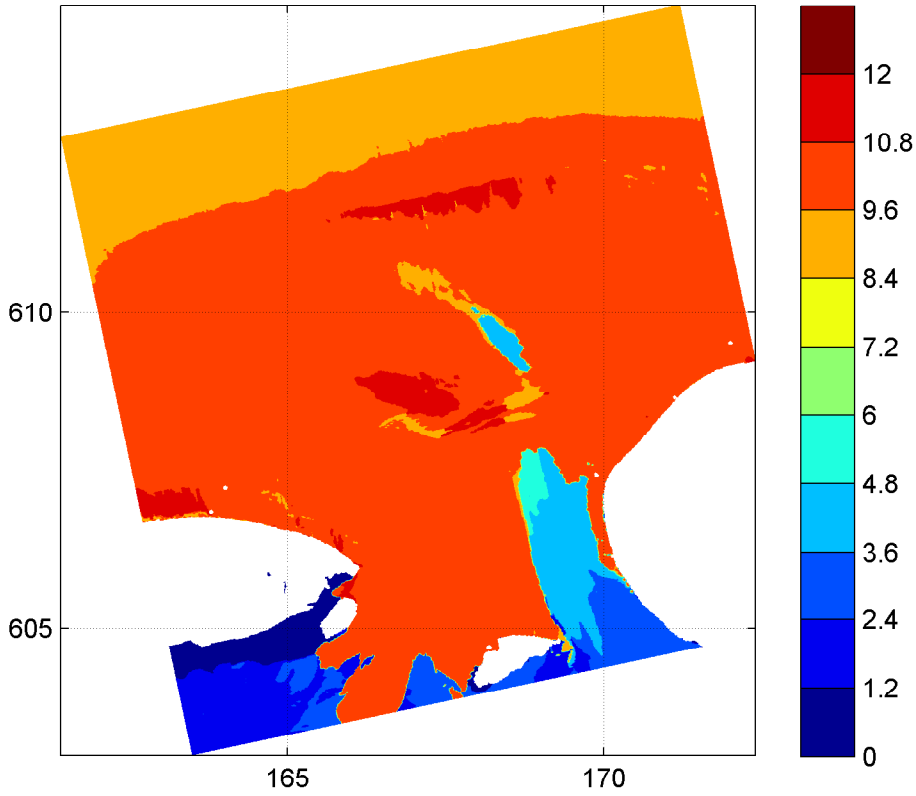

Spatial distribution of wave period T_{m02} [s] (upper panel) and wave period T_p [s] (lower panel) on grid2 uniform water level field and no current	20050102	10:00hr
	Hindcast Ameland Inlet	
WL | DELFT HYDRAULICS	H4803.11	Fig. 3.47b

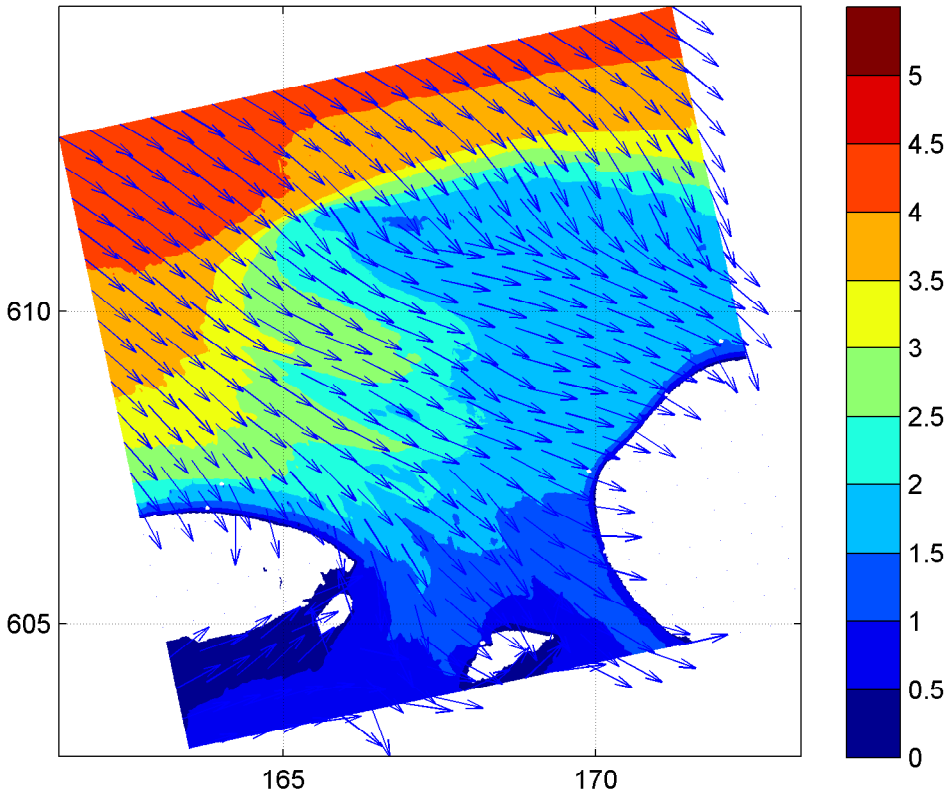

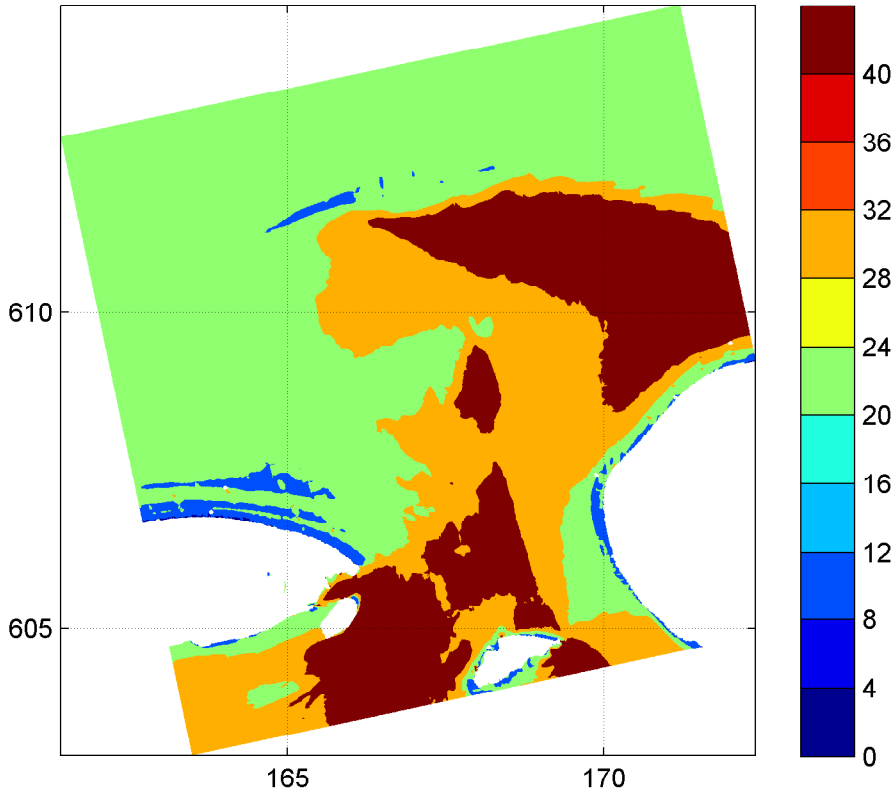

Spatial distribution of wave height [m] and mean wave direction (upper panel) and directional spreading [°] (lower panel) on grid2 uniform water level field and no current	20050102	10:00hr
	Hindcast Ameland Inlet	
WL | DELFT HYDRAULICS	H4803.11	Fig. 3.47c

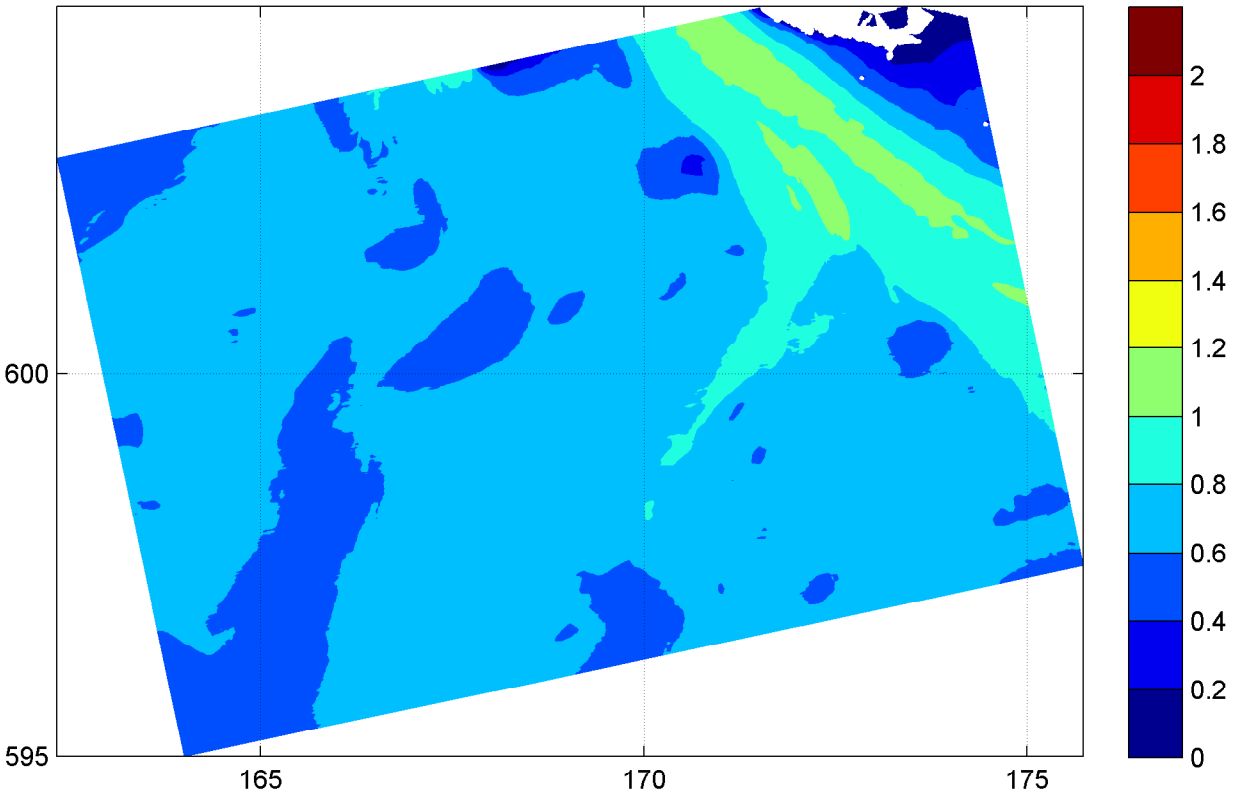

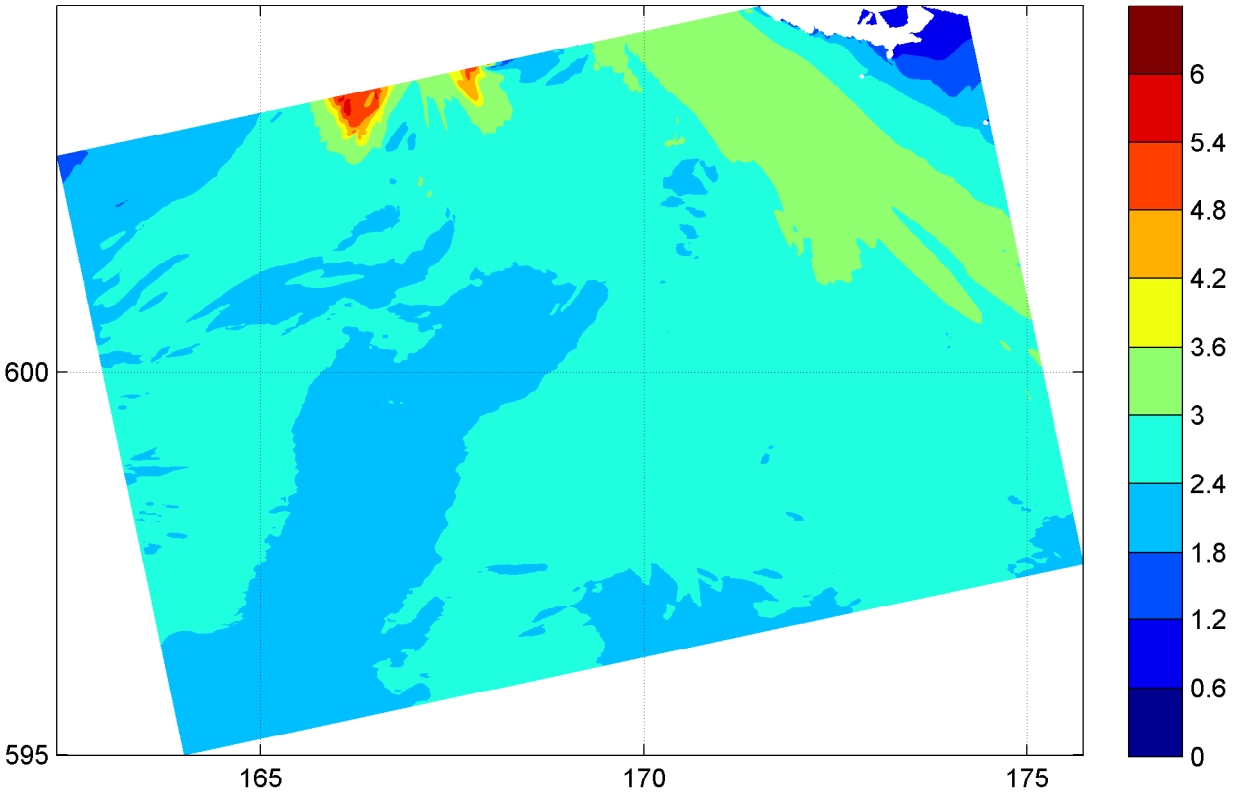

Spatial distribution of wave height H_{m0} [m] (upper panel) and wave period $T_{m-1,0}$ [s] (lower panel) on grid3 uniform water level field and no current	20050102	10:00hr
	Hindcast Ameland Inlet	
WL | DELFT HYDRAULICS	H4803.11	Fig. 3.48a

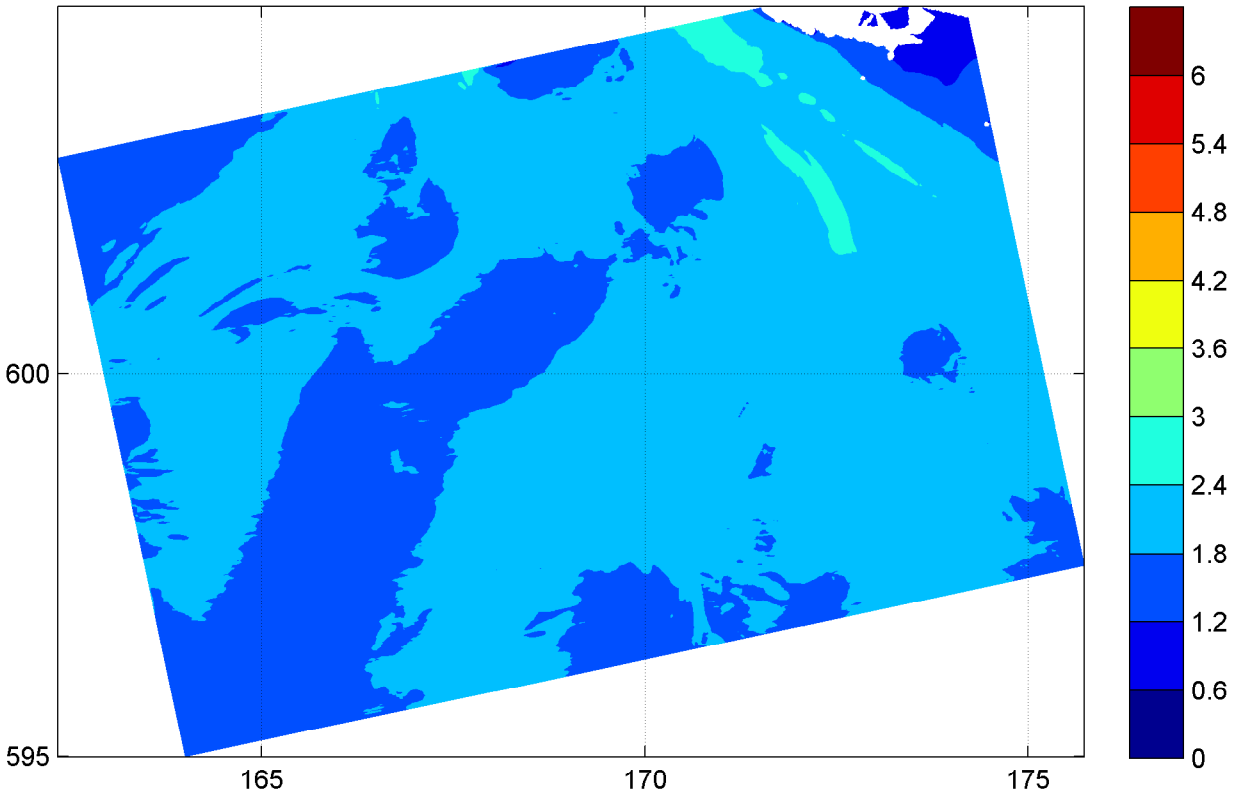

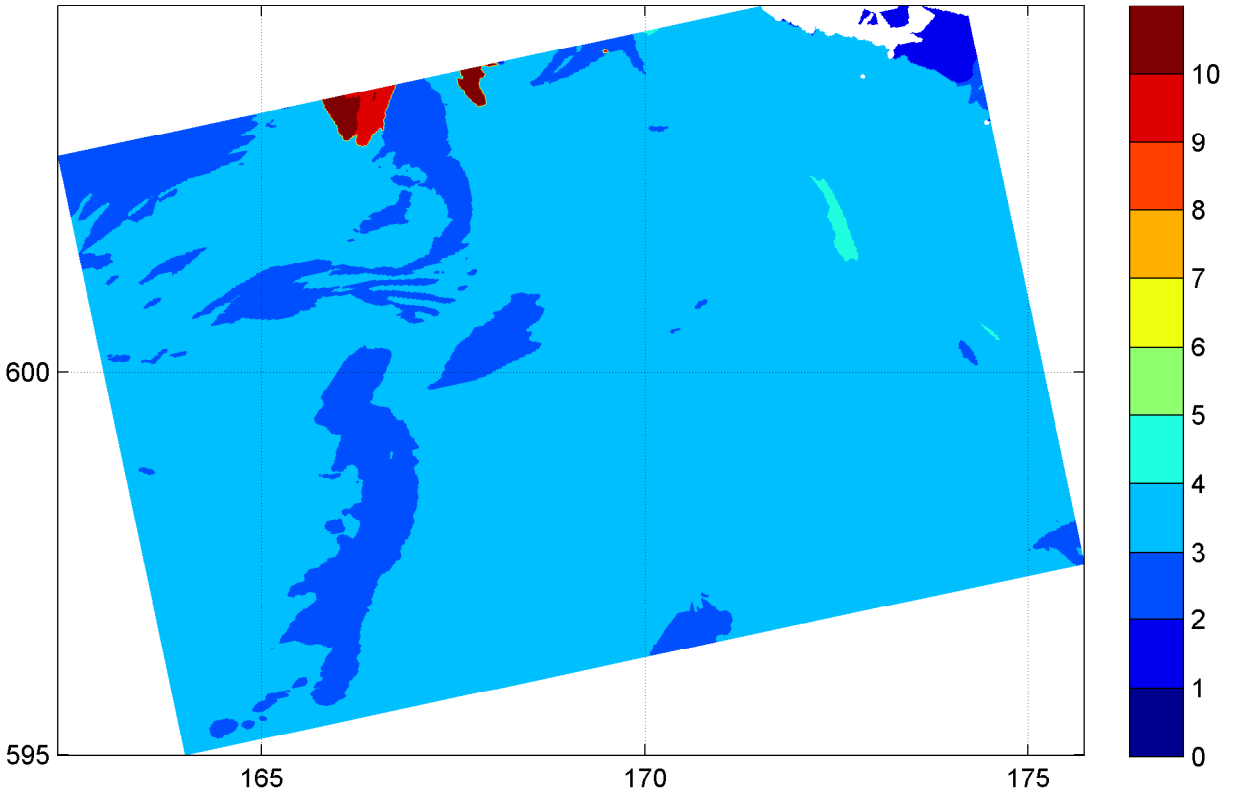

Spatial distribution of wave period T_{m02} [s] (upper panel) and wave period T_p [s] (lower panel) on grid3 uniform water level field and no current	20050102	10:00hr
	Hindcast Ameland Inlet	
WL | DELFT HYDRAULICS	H4803.11	Fig. 3.48b

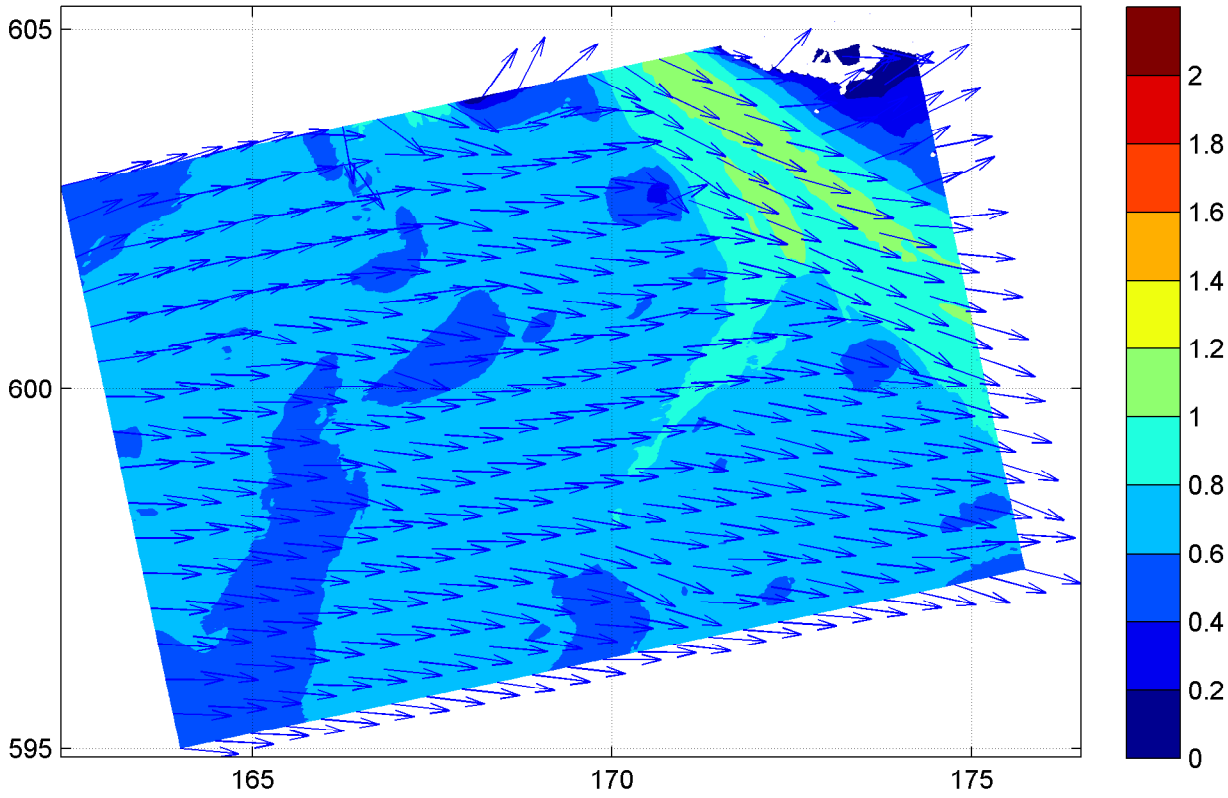

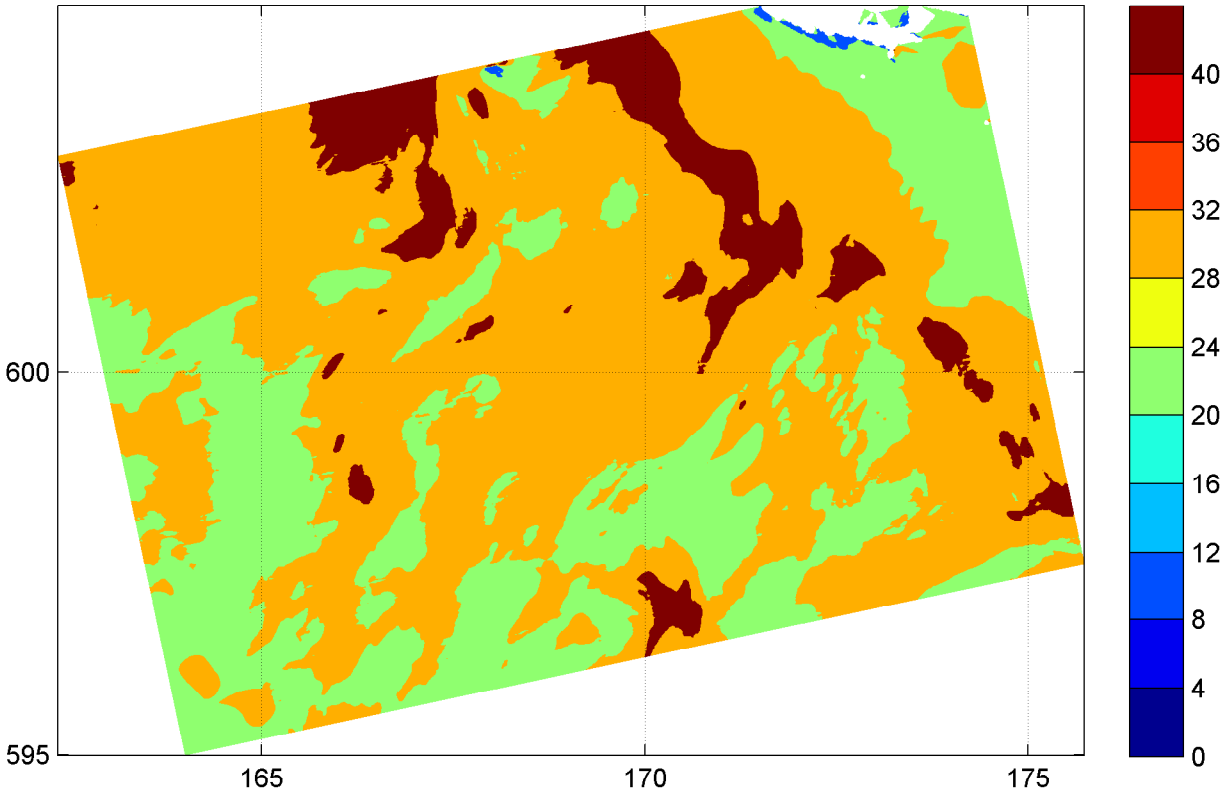

Spatial distribution of wave height [m] and mean wave direction (upper panel) and directional spreading [°] (lower panel) on grid3 uniform water level field and no current	20050102	10:00hr
	Hindcast Ameland Inlet	
WL | DELFT HYDRAULICS	H4803.11	Fig. 3.48c

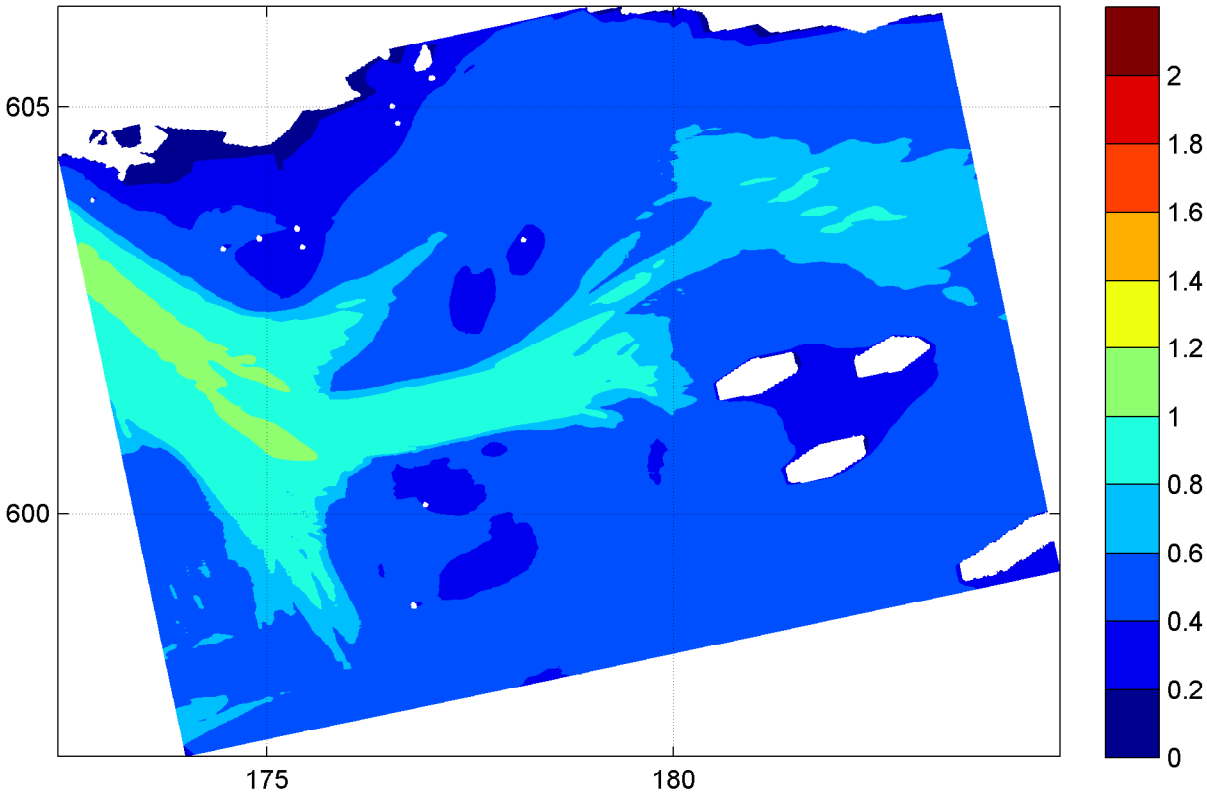

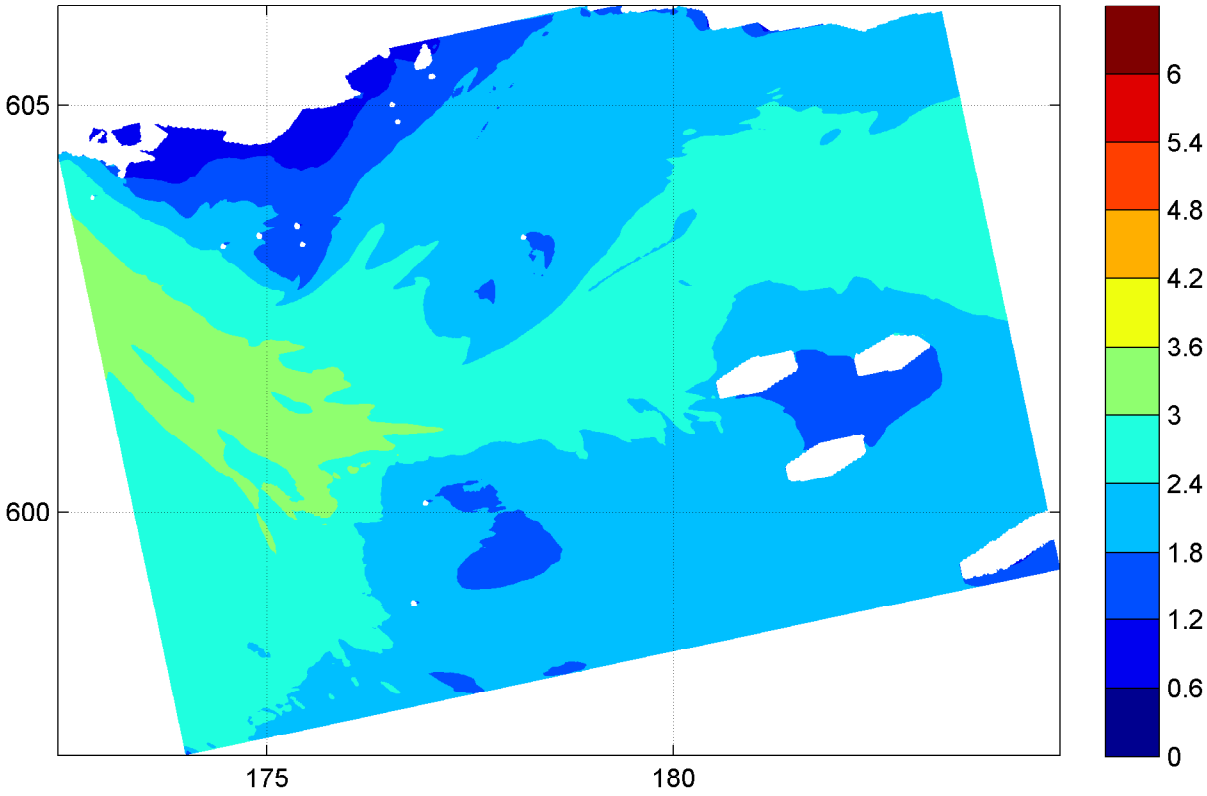

Spatial distribution of wave height H_{m0} [m] (upper panel) and wave period $T_{m-1,0}$ [s] (lower panel) on grid4 uniform water level field and no current	20050102	10:00hr
	Hindcast Ameland Inlet	
WL | DELFT HYDRAULICS	H4803.11	Fig. 3.49a

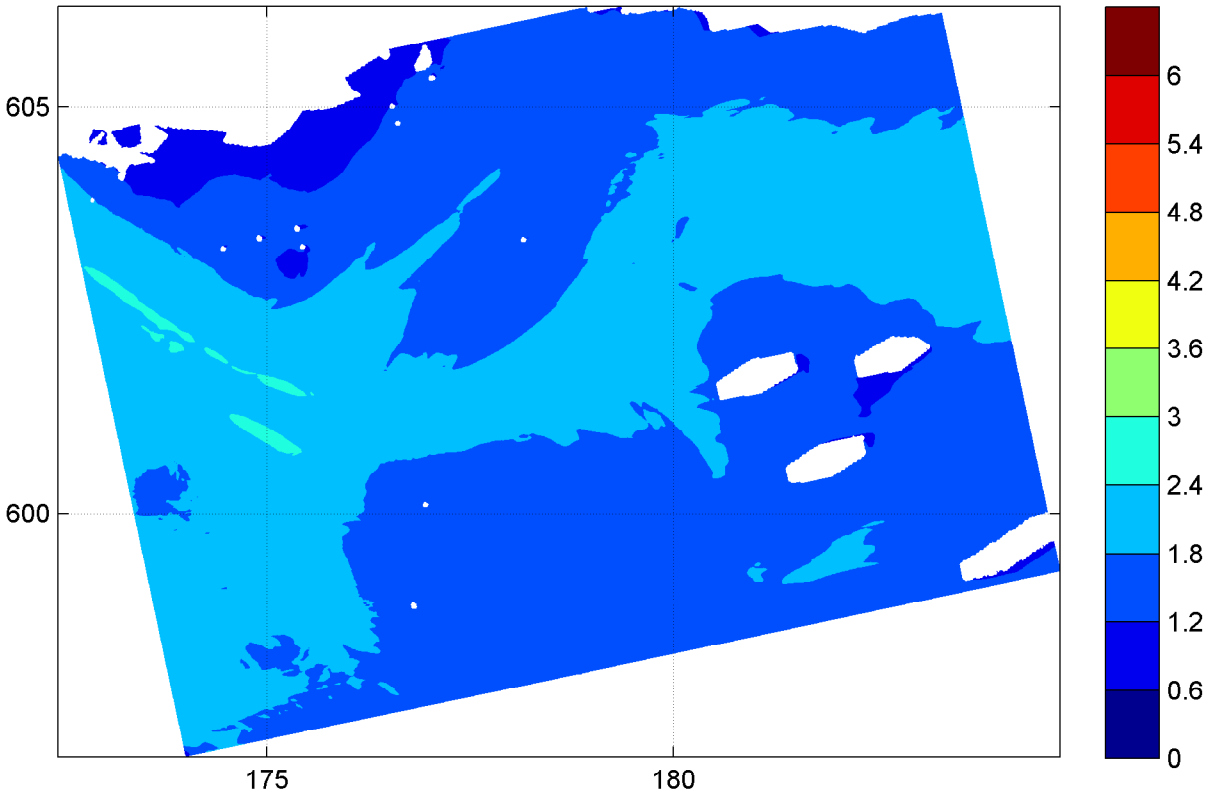

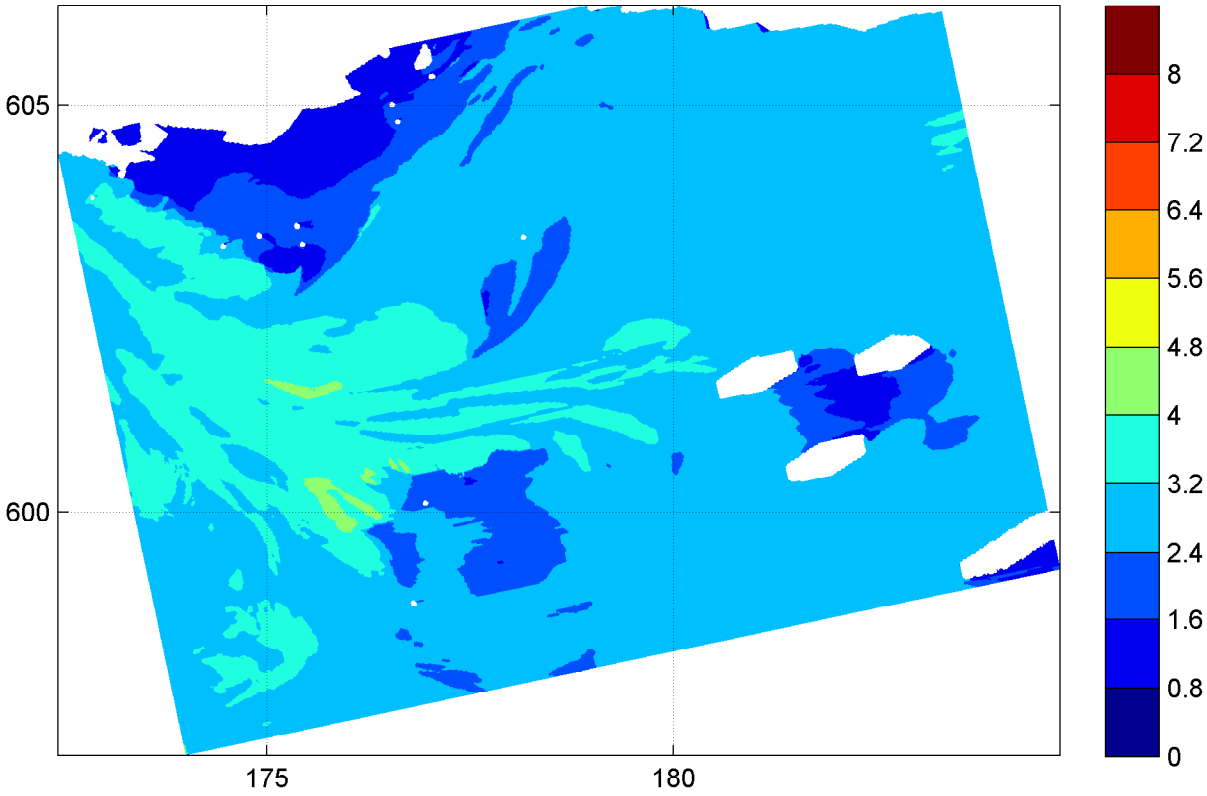

Spatial distribution of wave period T_{m02} [s] (upper panel) and wave period T_p [s] (lower panel) on grid4 uniform water level field and no current	20050102	10:00hr
	Hindcast Ameland Inlet	
WL | DELFT HYDRAULICS	H4803.11	Fig. 3.49b

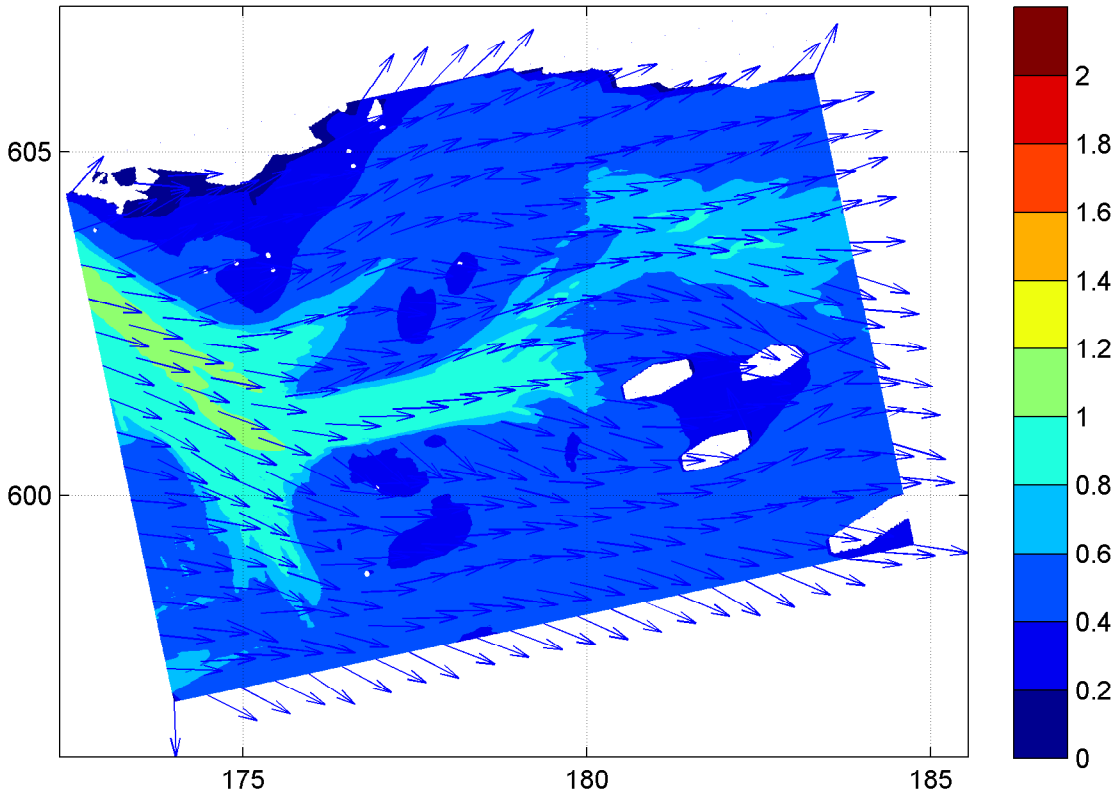

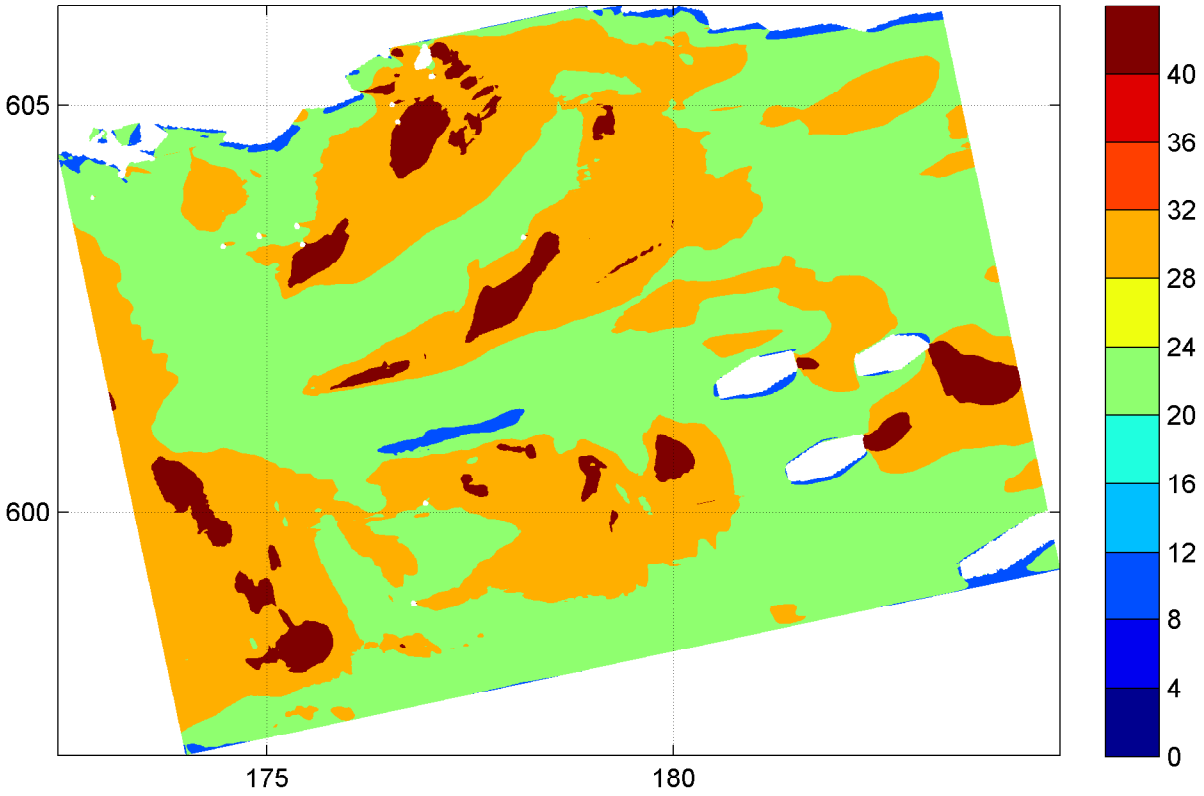

Spatial distribution of wave height [m] and mean wave direction (upper panel) and directional spreading [°] (lower panel) on grid4 uniform water level field and no current	20050102	10:00hr
	Hindcast Ameland Inlet	
WL | DELFT HYDRAULICS	H4803.11	Fig. 3.49c

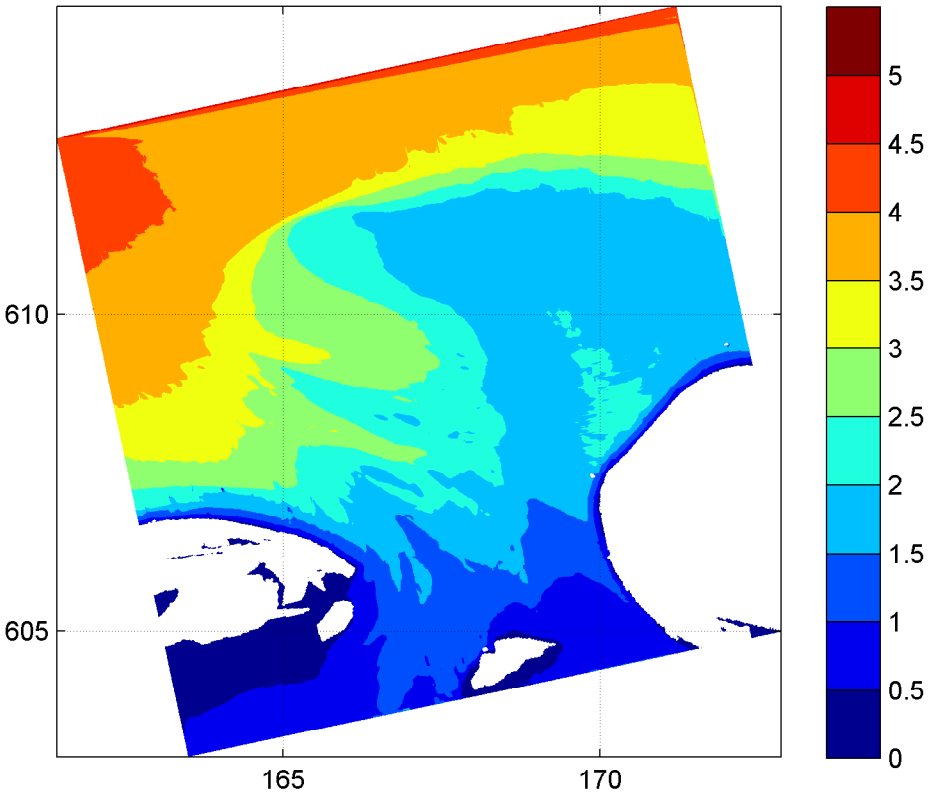

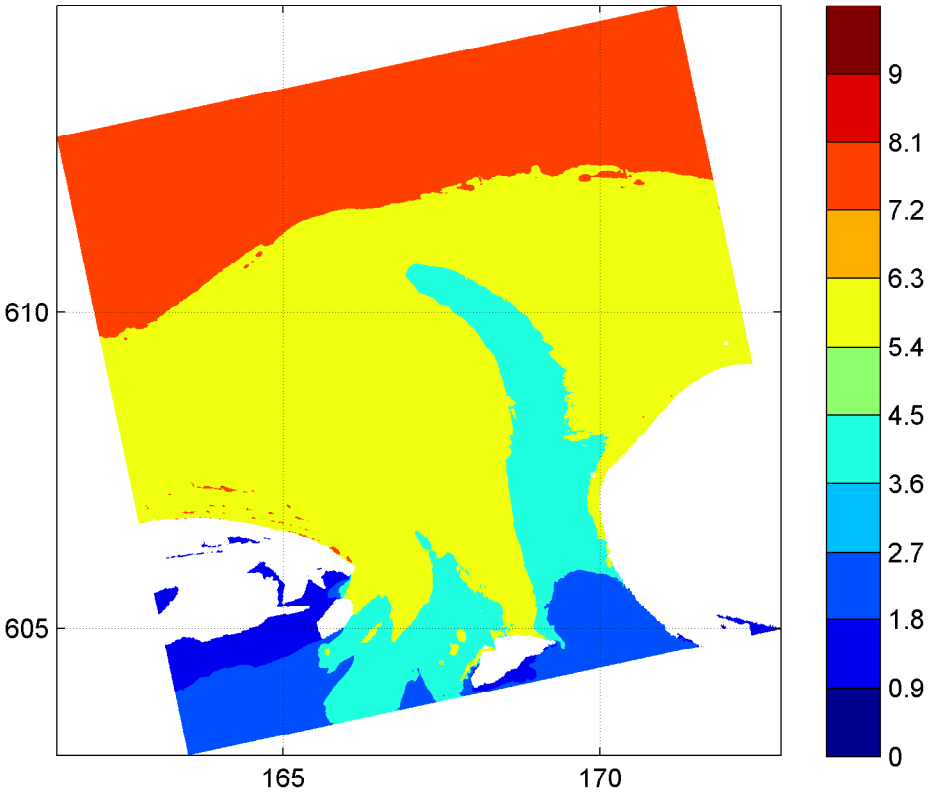

Spatial distribution of wave height H_{m0} [m] (upper panel) and wave period $T_{m-1,0}$ [s] (lower panel) on grid2 WAQUA high resolution	20050102	10:00hr
	Hindcast Ameland Inlet	
WL | DELFT HYDRAULICS	H4803.11	Fig. 3.50a

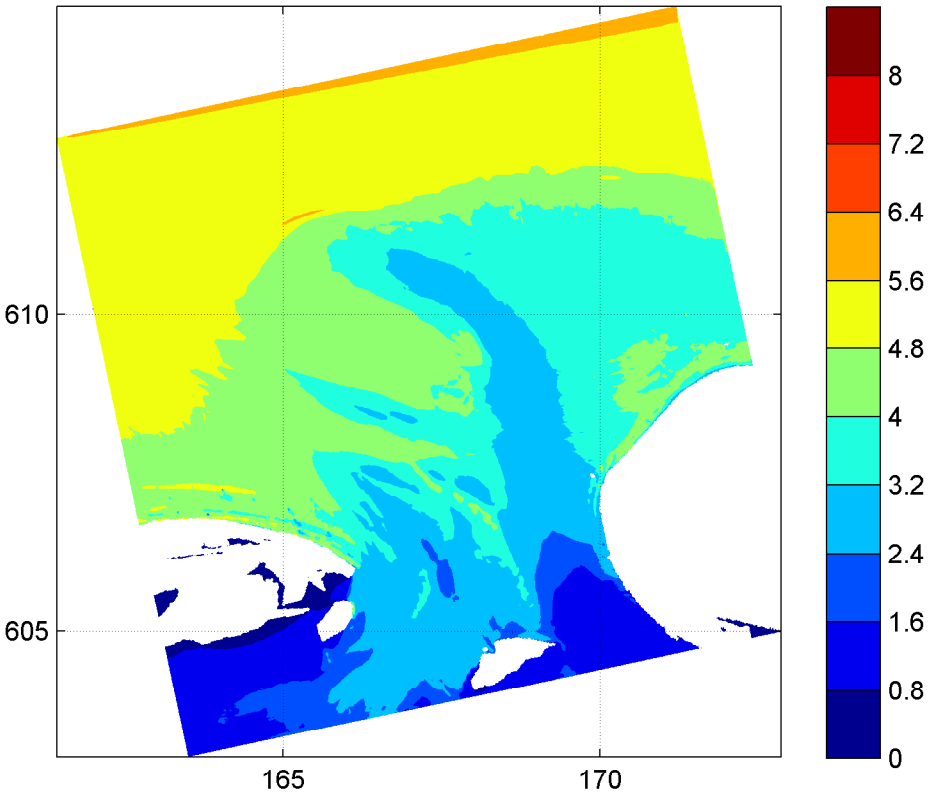

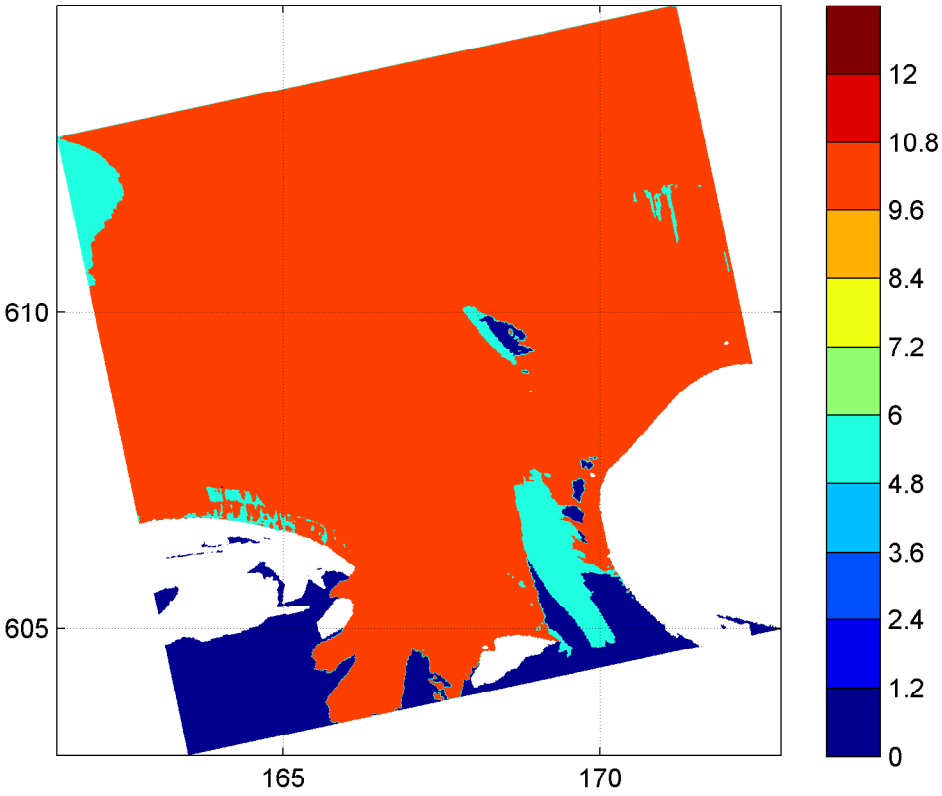

Spatial distribution of wave period T_{m02} [s] (upper panel) and wave period T_p [s] (lower panel) on grid2 WAQUA high resolution	20050102	10:00hr
	Hindcast Ameland Inlet	
WL | DELFT HYDRAULICS	H4803.11	Fig. 3.50b

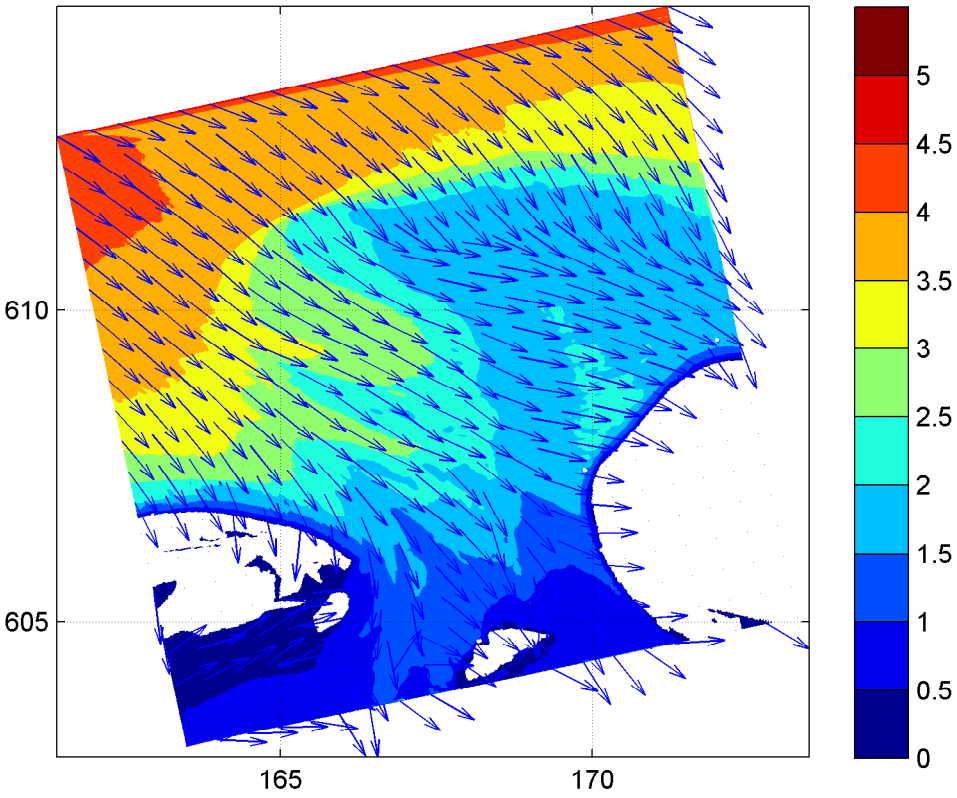

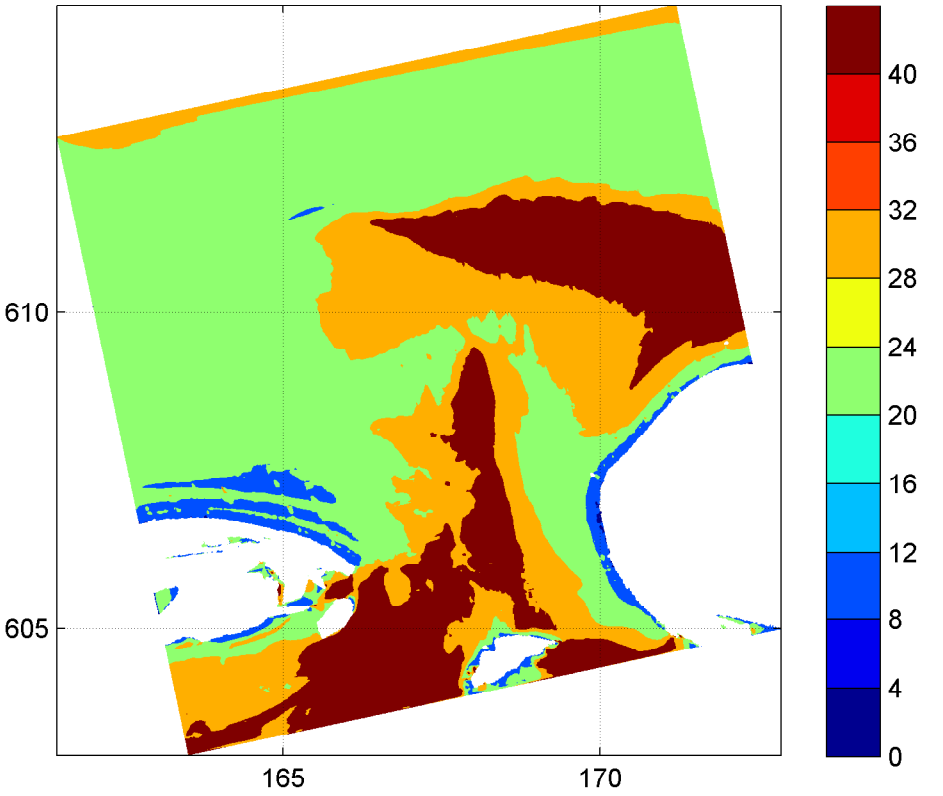

Spatial distribution of wave height [m] and mean wave direction (upper panel) and directional spreading [°] (lower panel) on grid2 WAQUA high resolution	20050102	10:00hr
	Hindcast Ameland Inlet	
WL | DELFT HYDRAULICS	H4803.11	Fig. 3.50c

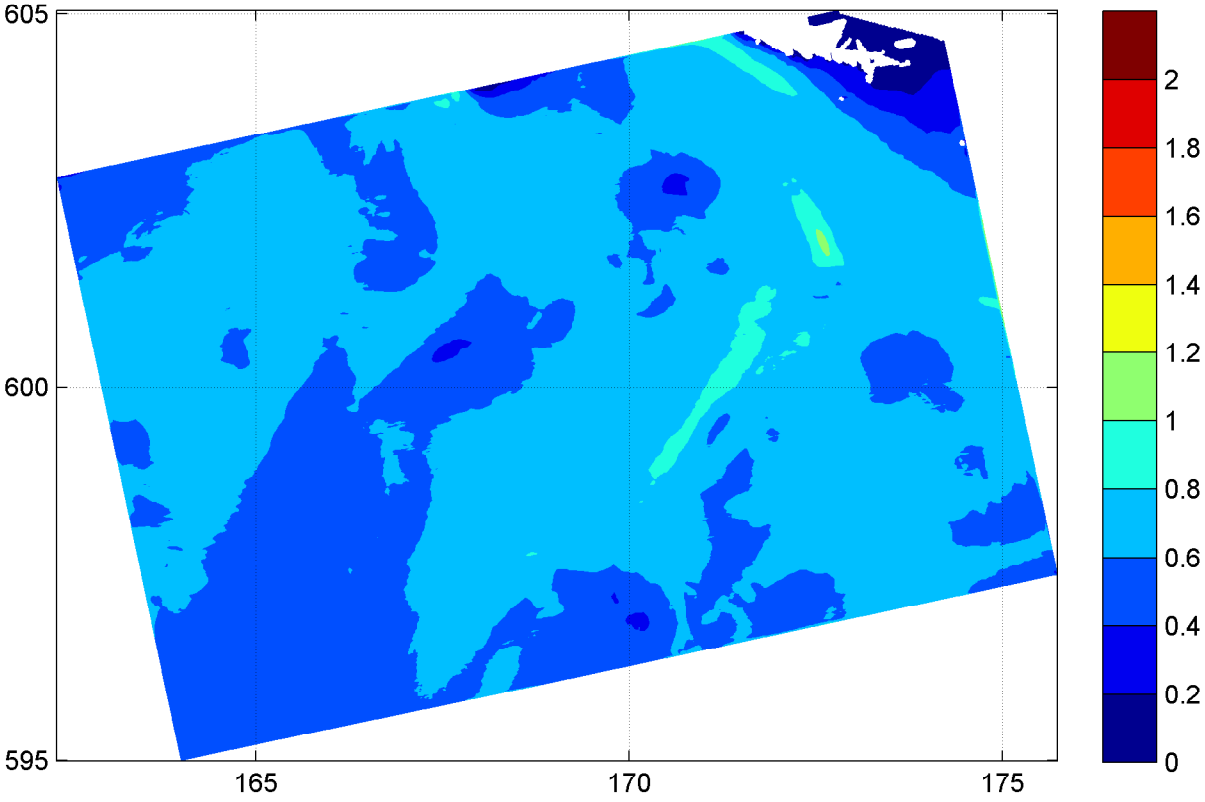

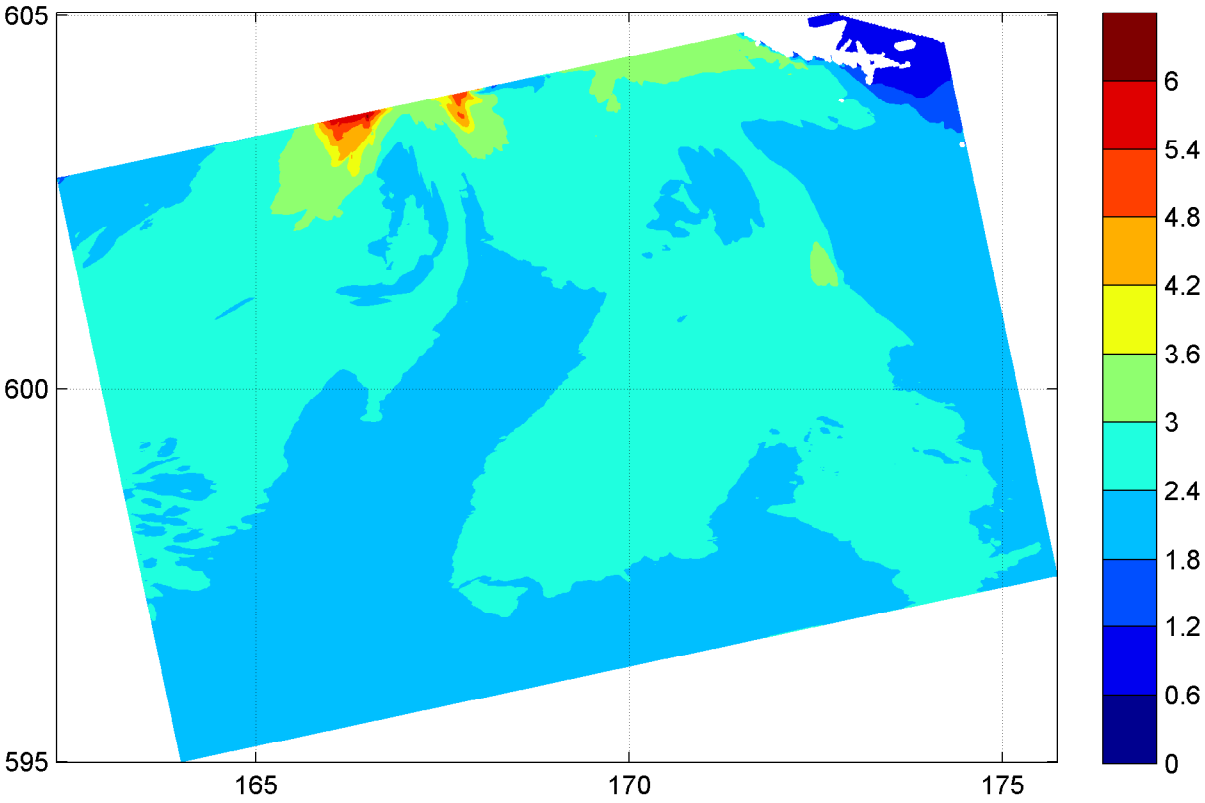

Spatial distribution of wave height H_{m0} [m] (upper panel) and wave period $T_{m-1,0}$ [s] (lower panel) on grid3 WAQUA high resolution	20050102	10:00hr
	Hindcast Ameland Inlet	
WL | DELFT HYDRAULICS	H4803.11	Fig. 3.51a

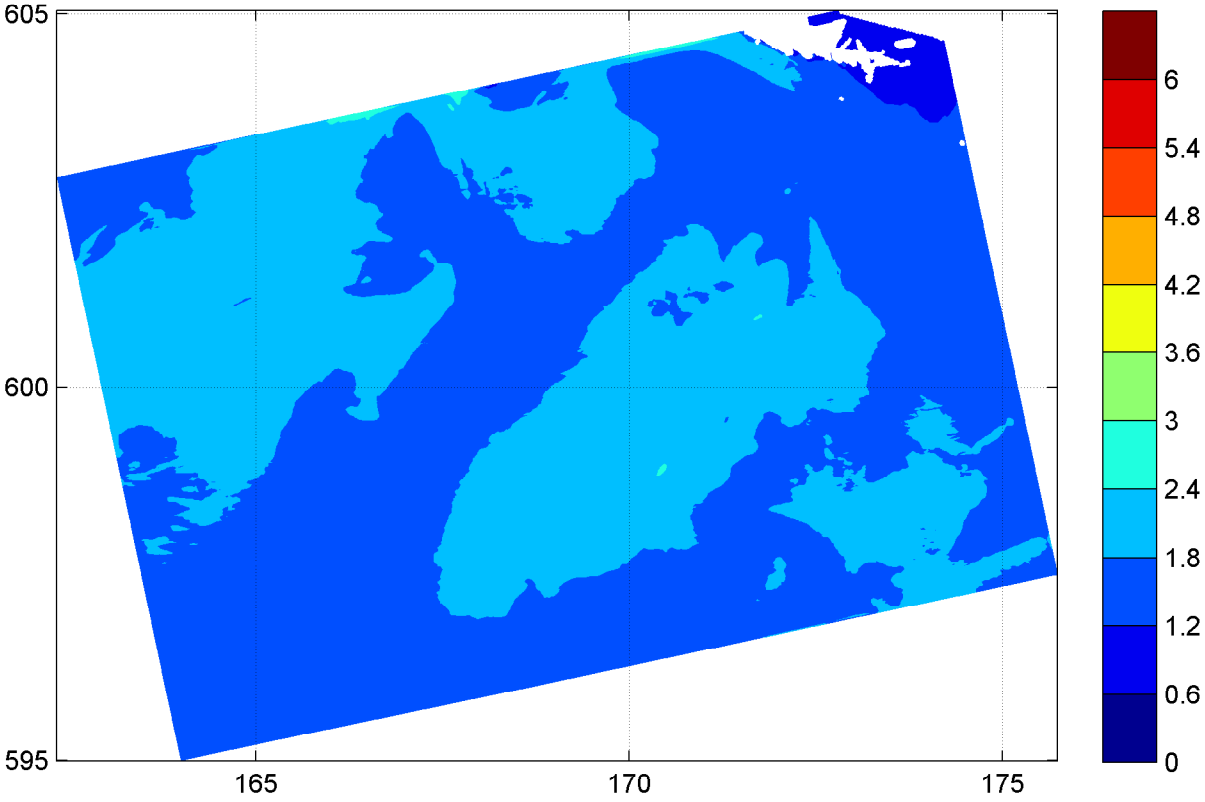

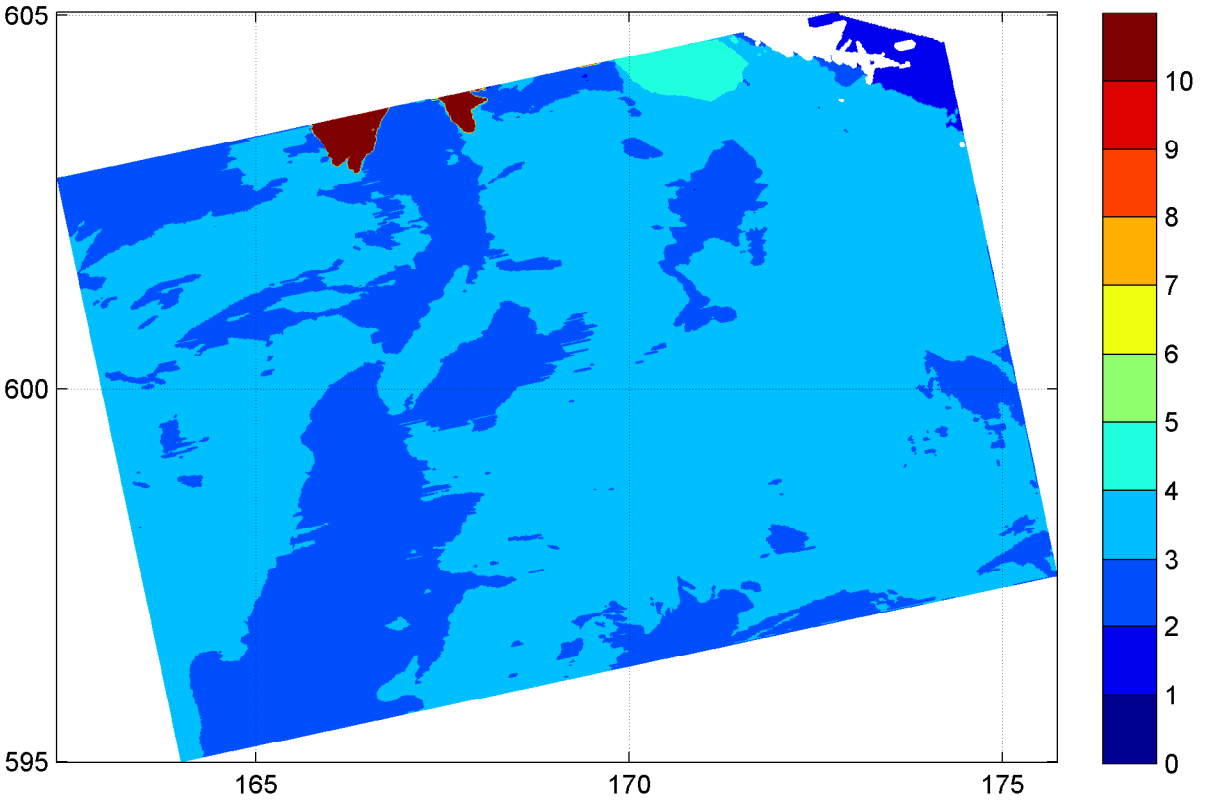

Spatial distribution of wave period T_{m02} [s] (upper panel) and wave period T_p [s] (lower panel) on grid3 WAQUA high resolution	20050102	10:00hr
	Hindcast Ameland Inlet	
WL | DELFT HYDRAULICS	H4803.11	Fig. 3.51b

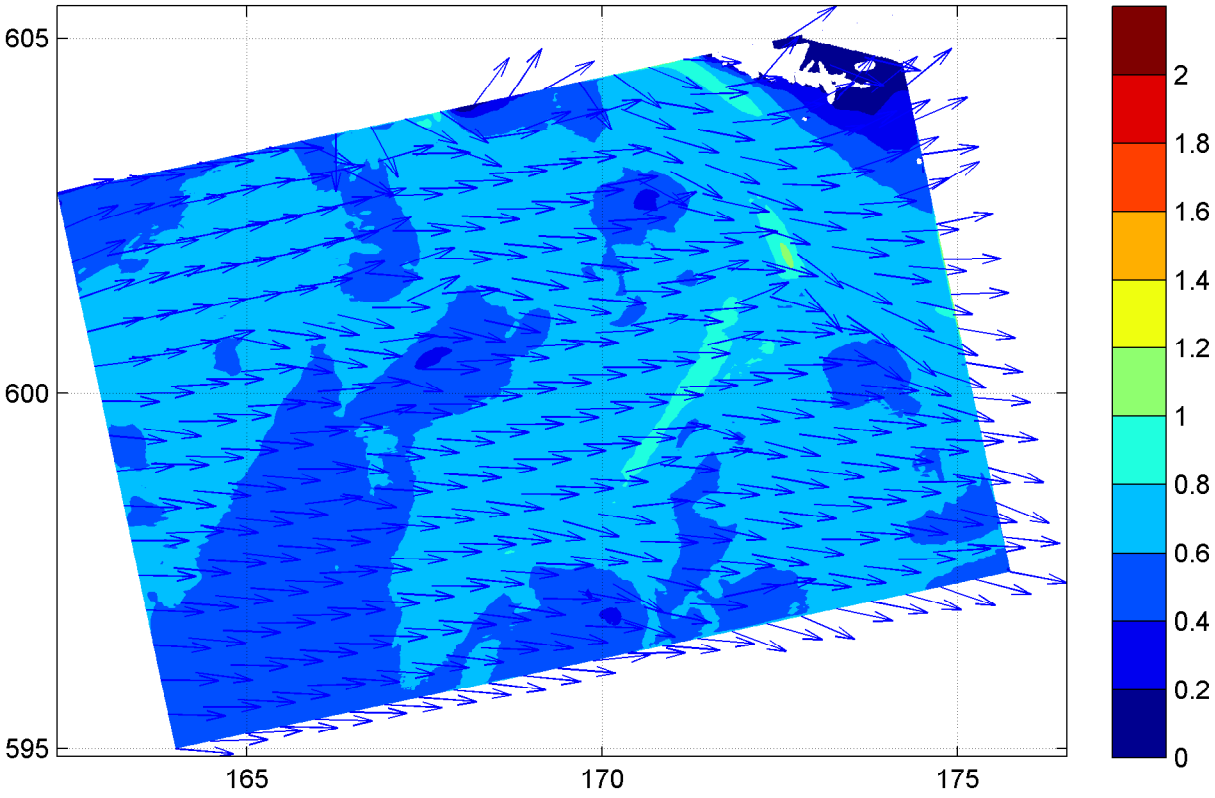

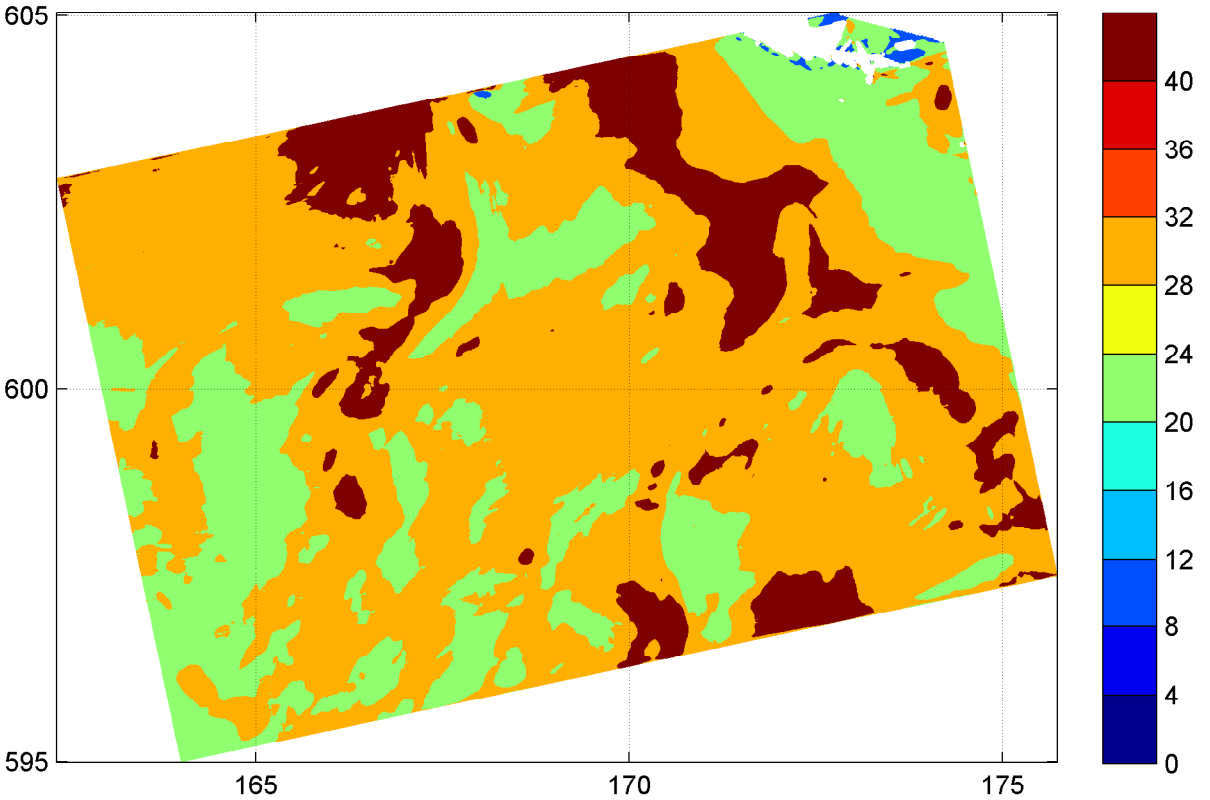

Spatial distribution of wave height [m] and mean wave direction (upper panel) and directional spreading [°] (lower panel) on grid3 WAQUA high resolution	20050102	10:00hr
	Hindcast Ameland Inlet	
WL | DELFT HYDRAULICS	H4803.11	Fig. 3.51c

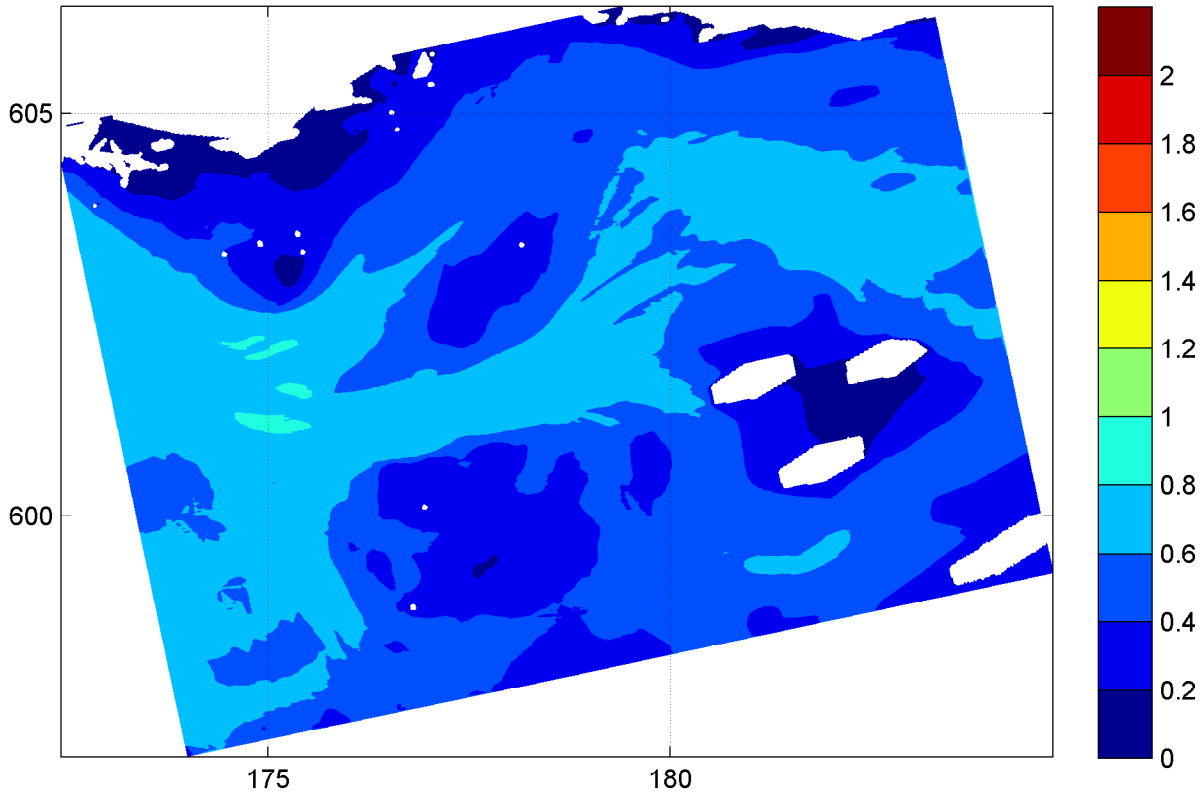

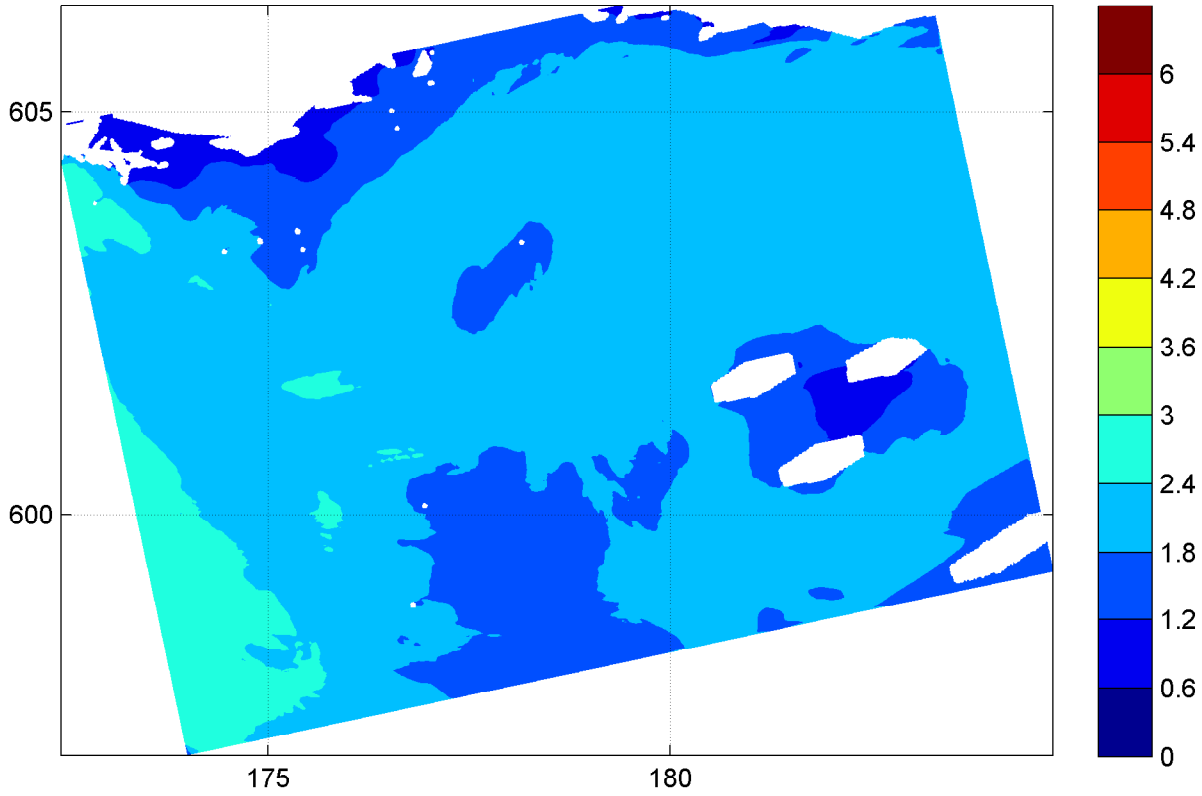

Spatial distribution of wave height H_{m0} [m] (upper panel) and wave period $T_{m-1,0}$ [s] (lower panel) on grid4 WAQUA high resolution	20050102	10:00hr
	Hindcast Ameland Inlet	
WL | DELFT HYDRAULICS	H4803.11	Fig. 3.52a

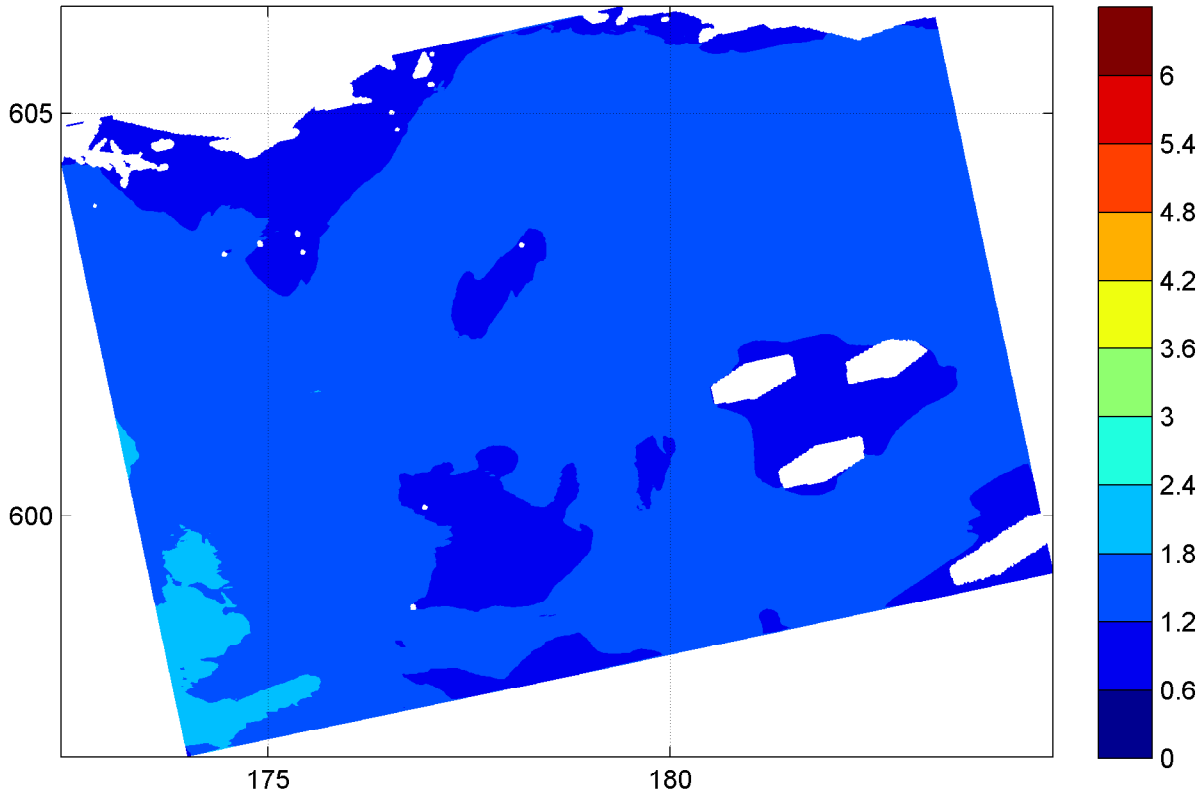

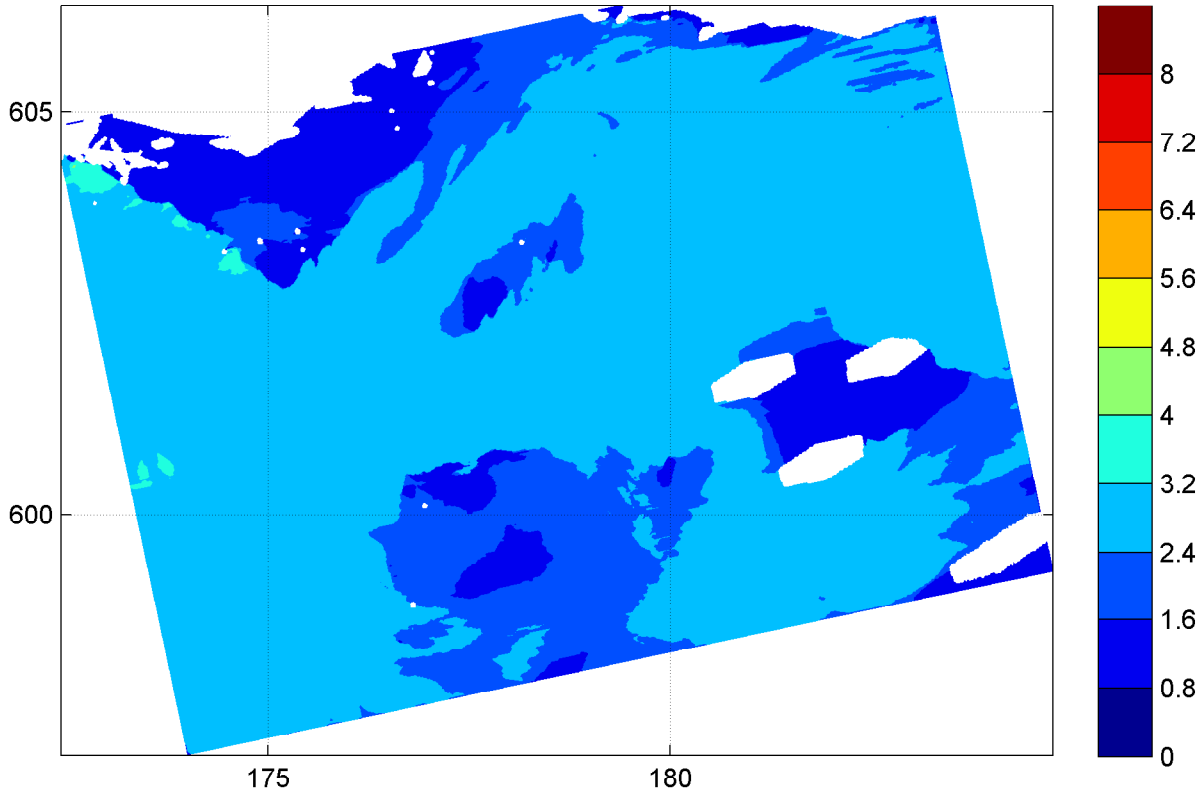

Spatial distribution of wave period T_{m02} [s] (upper panel) and wave period T_p [s] (lower panel) on grid4 WAQUA high resolution	20050102	10:00hr
	Hindcast Ameland Inlet	
WL | DELFT HYDRAULICS	H4803.11	Fig. 3.52b

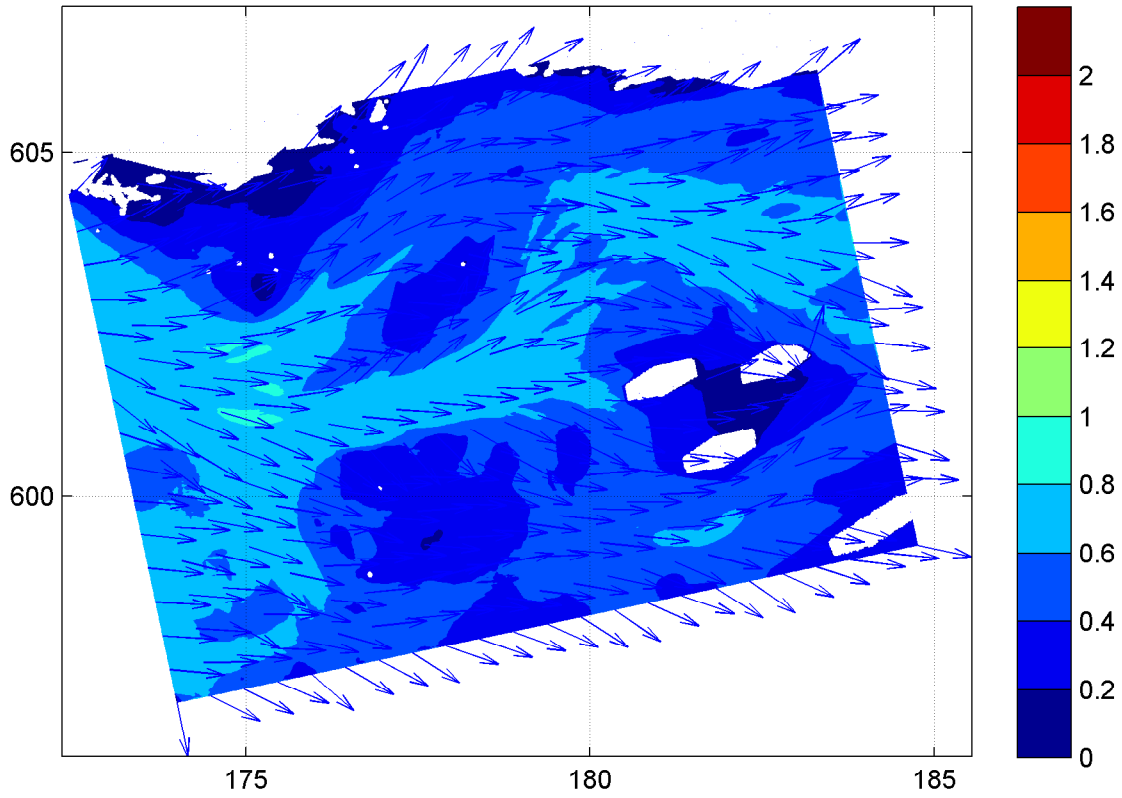

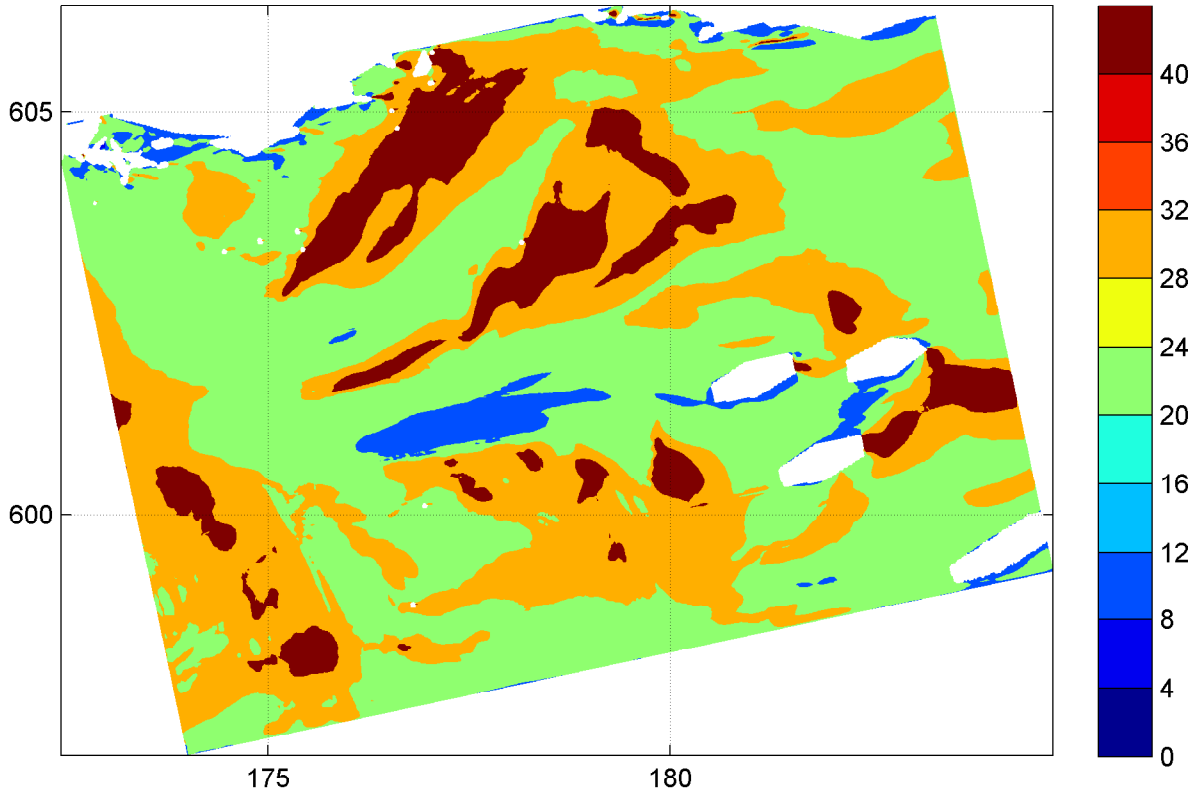

Spatial distribution of wave height [m] and mean wave direction (upper panel) and directional spreading [°] (lower panel) on grid4 WAQUA high resolution	20050102	10:00hr
	Hindcast Ameland Inlet	
WL | DELFT HYDRAULICS	H4803.11	Fig. 3.52c

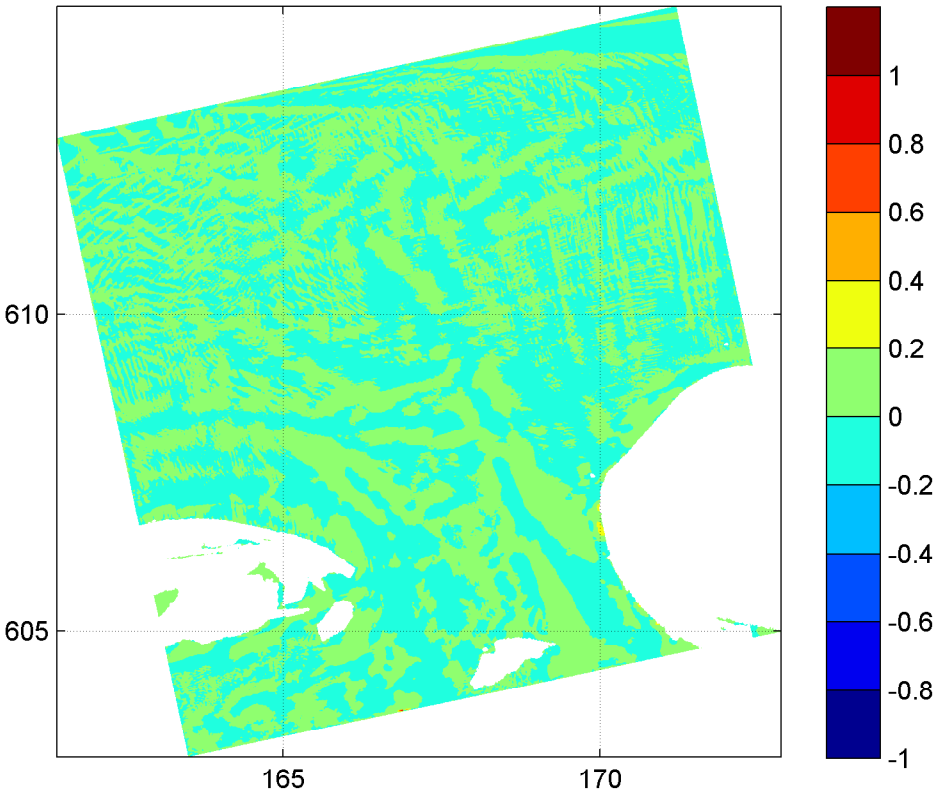

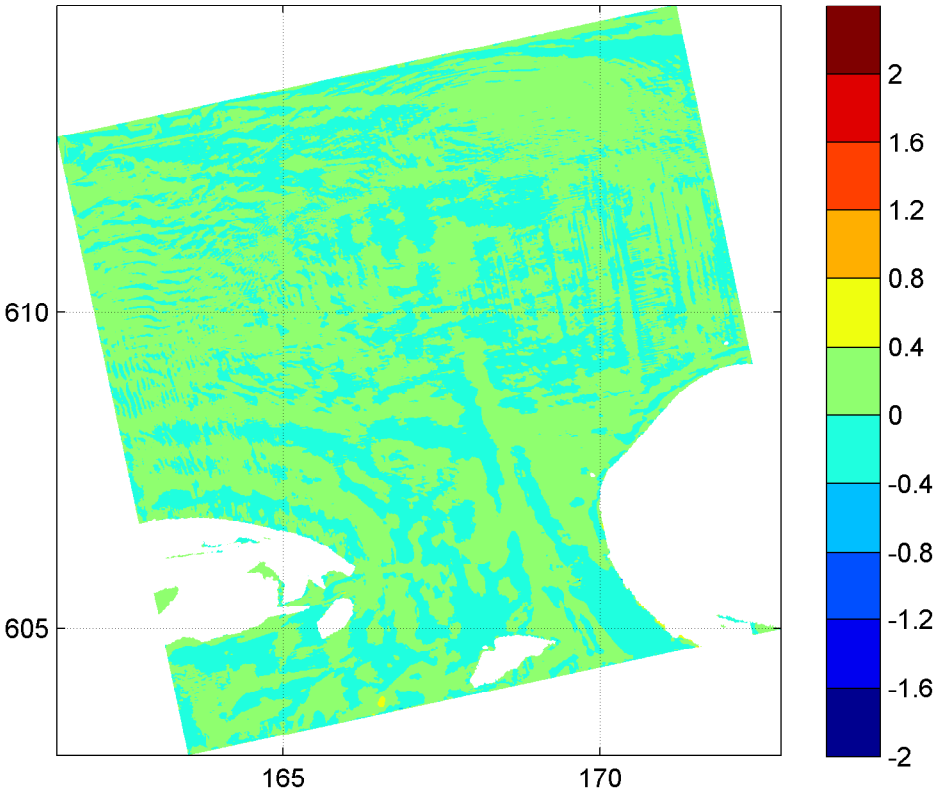

Difference plot of spatial distribution of wave height H_{m0} [m] (upper panel) and wave period $T_{m-1,0}$ [s] (lower panel) on grid2 Difference = results with coarse WAQUA grid - results with fine WAQUA grid	20050102	1000hr
	Hindcast Ameland Inlet	
WL | DELFT HYDRAULICS	H4803.11	Fig. 3.53a

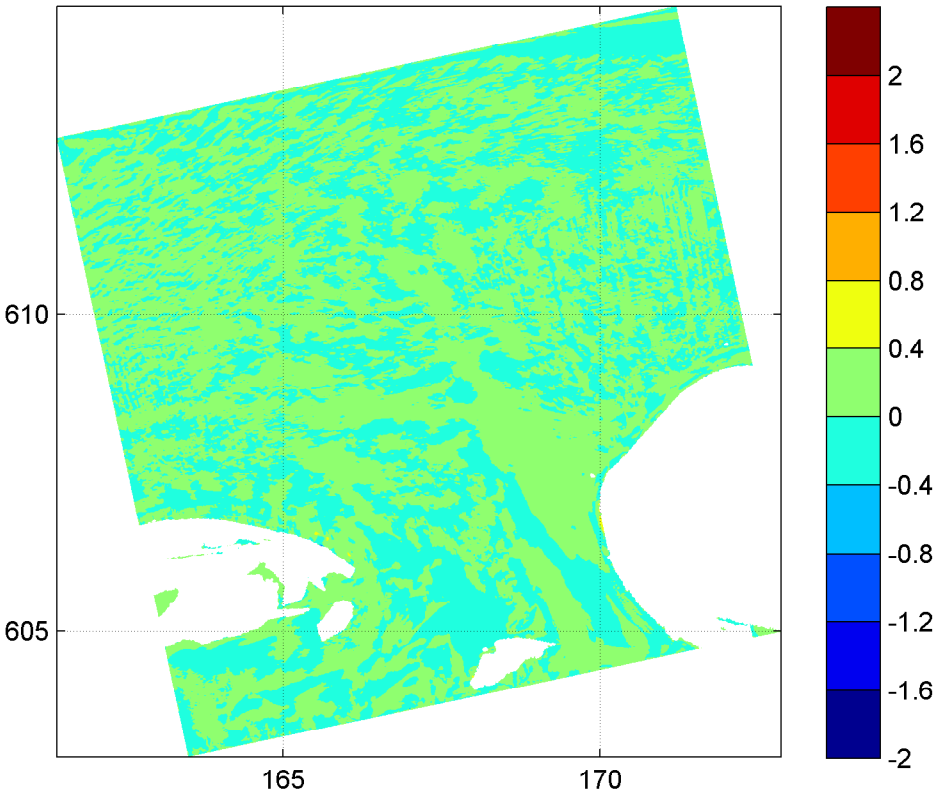

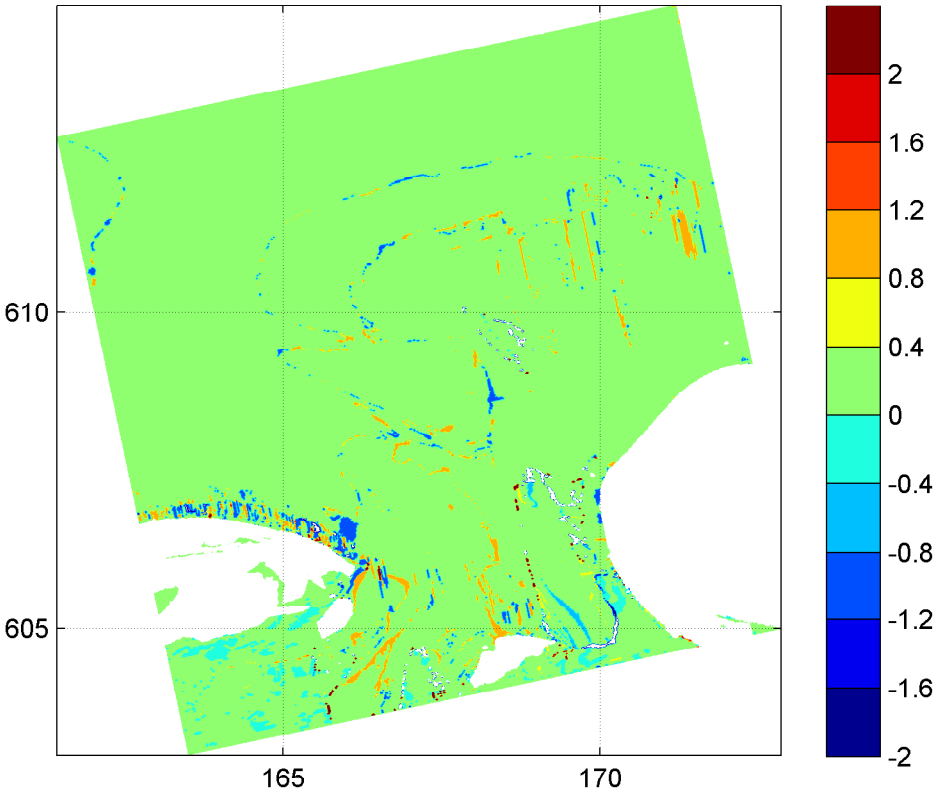

Difference plot of spatial distribution of wave period T_{m02} [s] (upper panel) and wave period T_p [s] (lower panel) on grid2 Difference = results with coarse WAQUA grid - results with fine WAQUA grid	20050102	1000hr
	Hindcast Ameland Inlet	
WL | DELFT HYDRAULICS	H4803.11	Fig. 3.53b

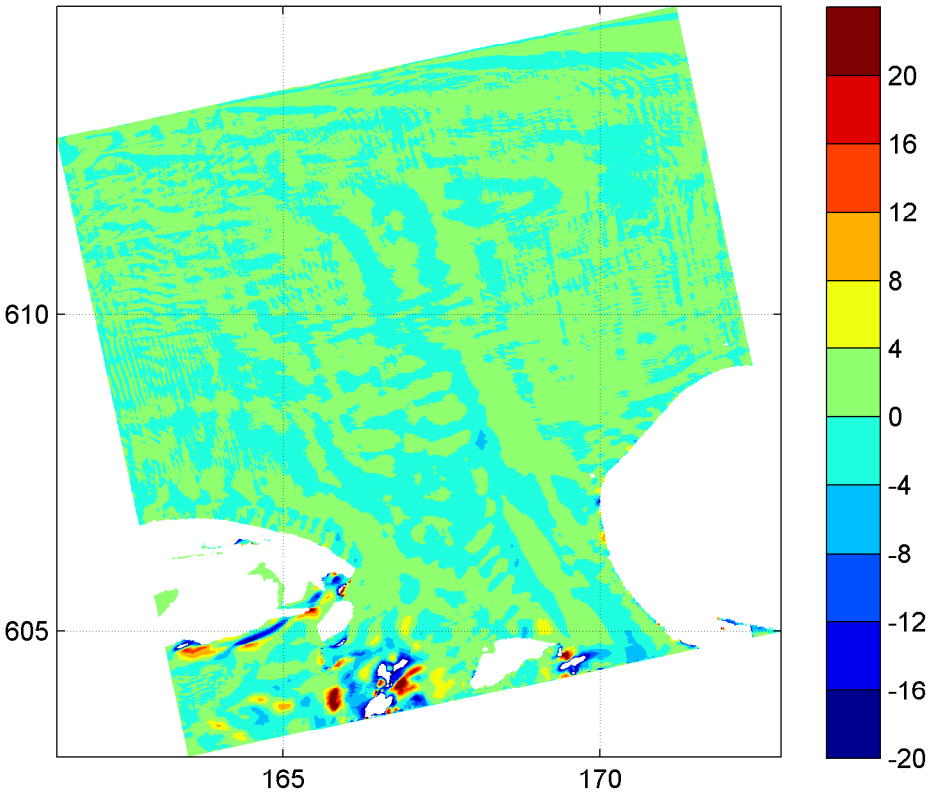

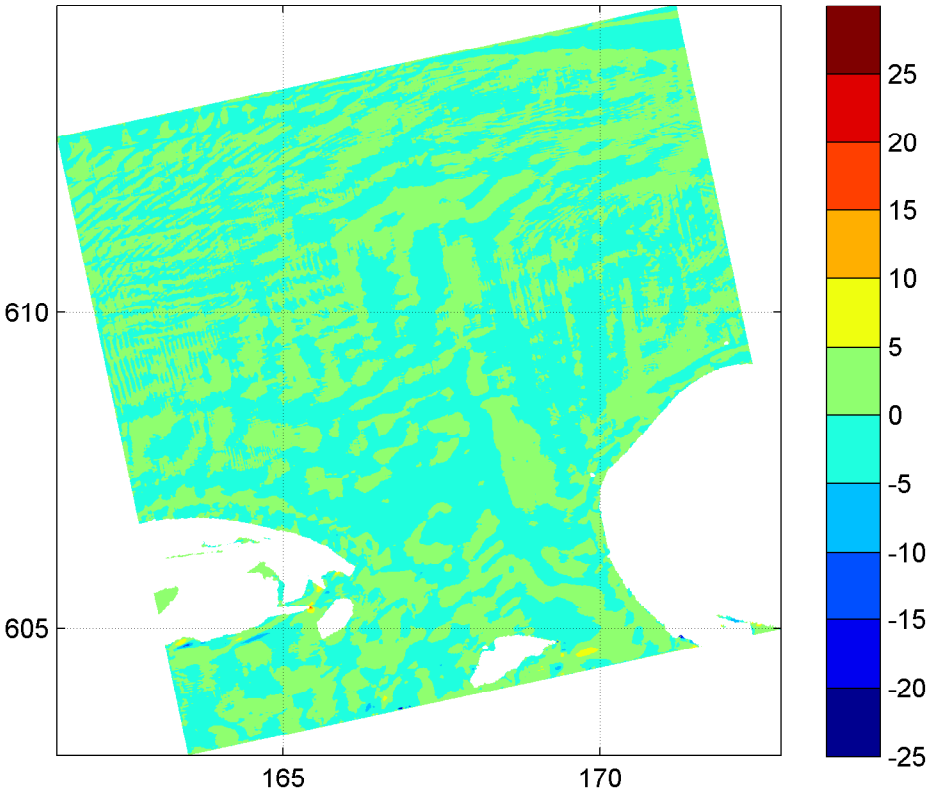

Difference plot of spatial distribution of mean wave direction [°] (upper panel) and directional spreading [°] (lower panel) on grid2 Difference = results with coarse WAQUA grid - results with fine WAQUA grid	20050102	1000hr
	Hindcast Ameland Inlet	
WL | DELFT HYDRAULICS	H4803.11	Fig. 3.53c

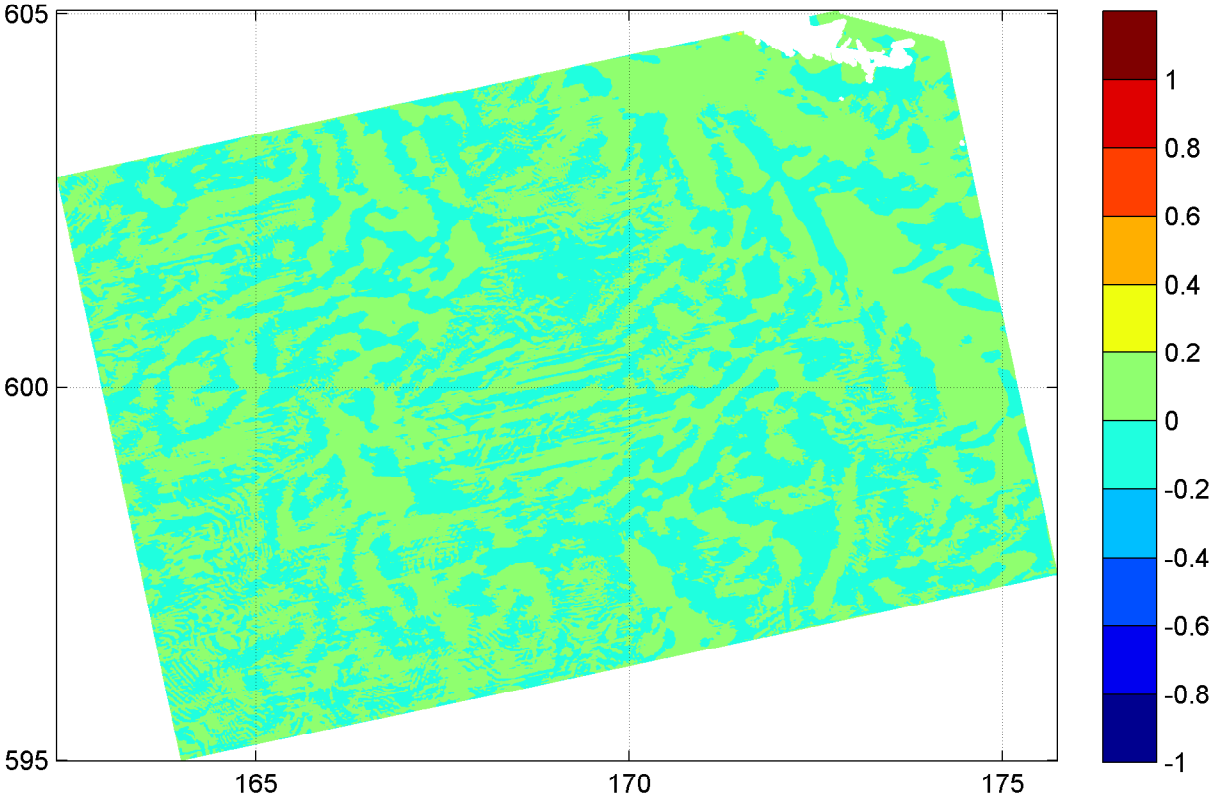

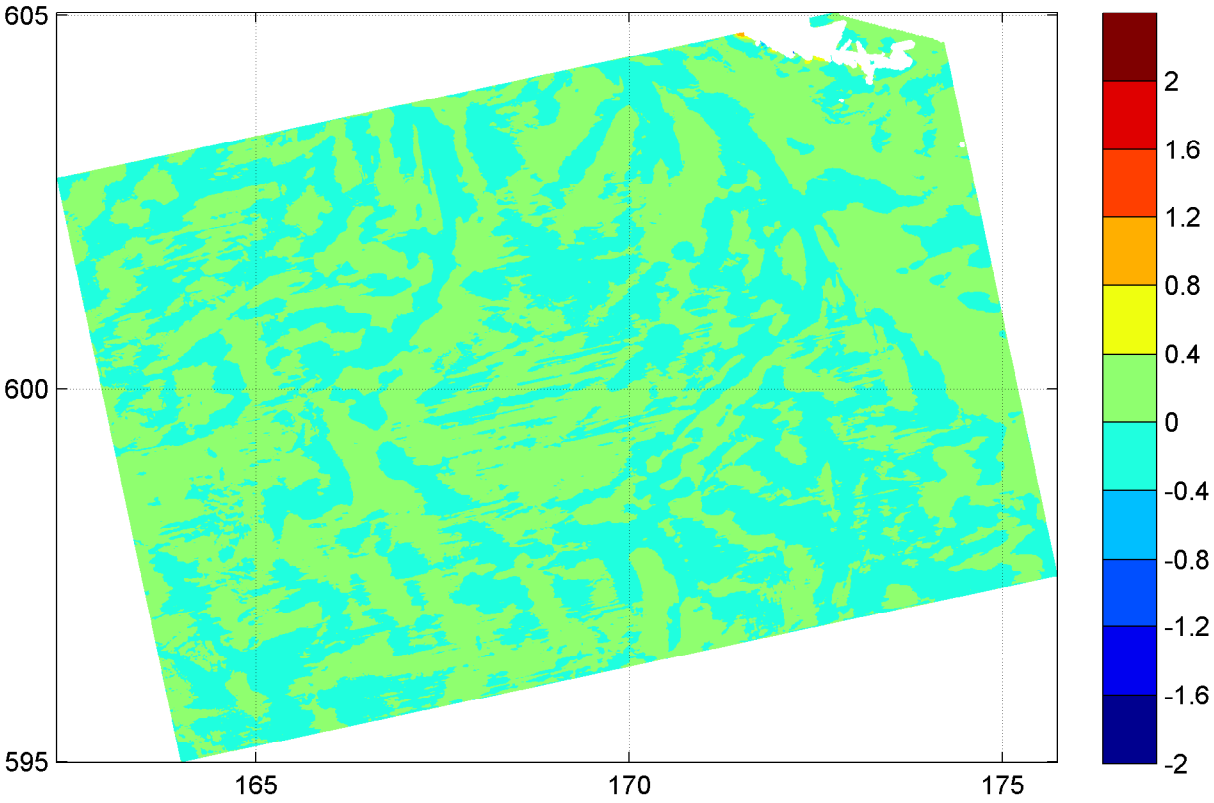

Difference plot of spatial distribution of wave height H_{m0} [m] (upper panel) and wave period $T_{m-1,0}$ [s] (lower panel) on grid3 Difference = results with coarse WAQUA grid - results with fine WAQUA grid	20050102	1000hr
	Hindcast Ameland Inlet	
WL | DELFT HYDRAULICS	H4803.11	Fig. 3.54a

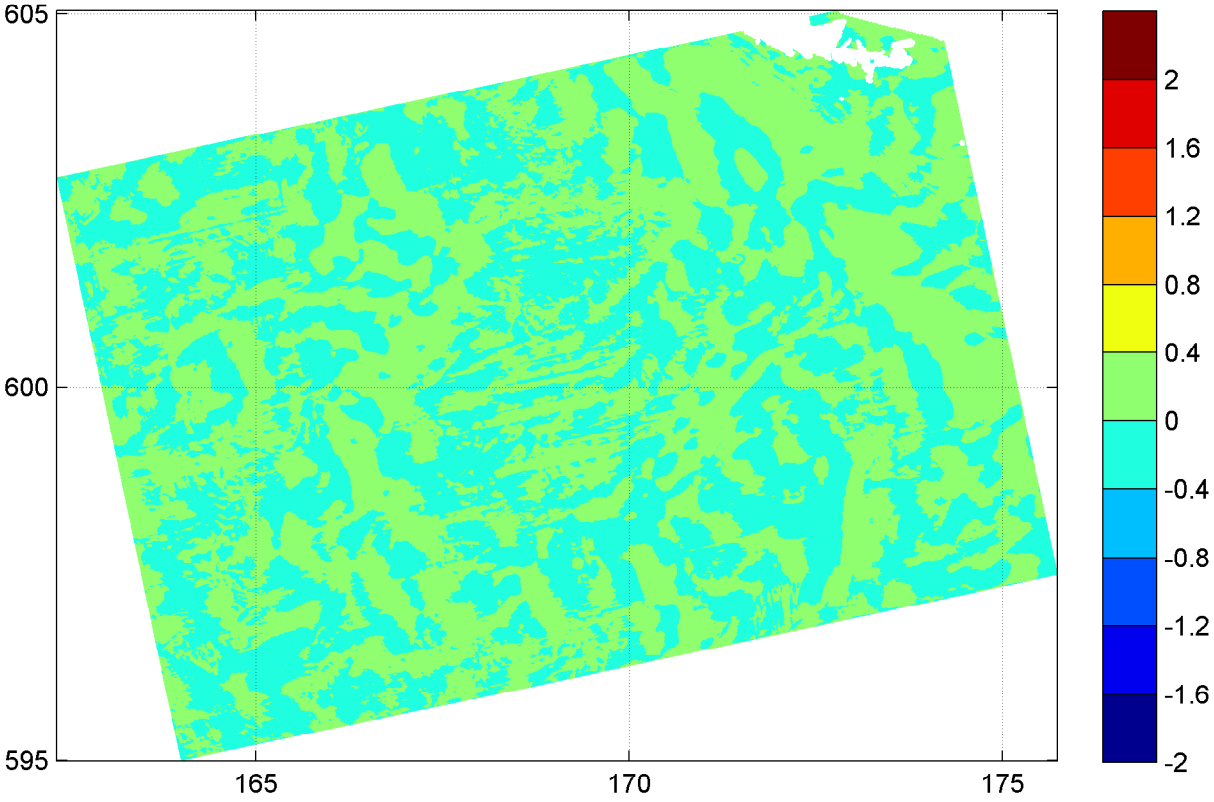

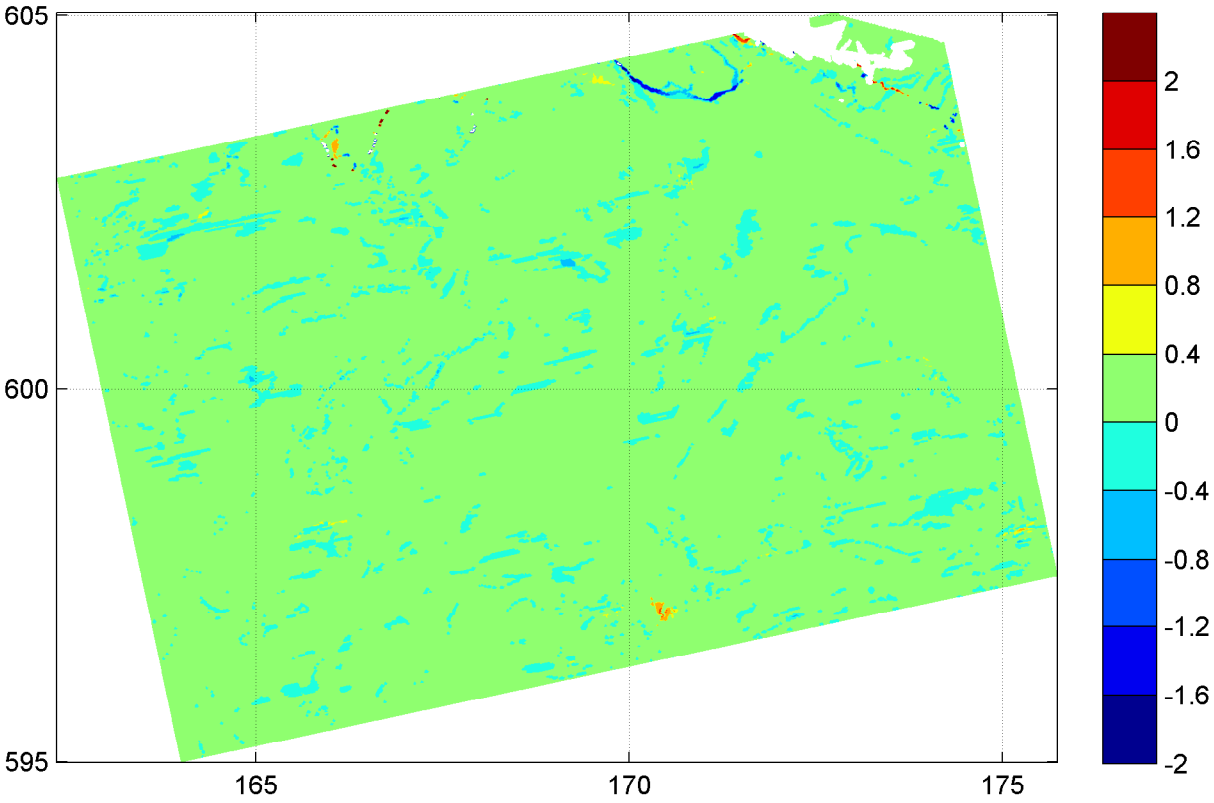

Difference plot of spatial distribution of wave period T_{m02} [s] (upper panel) and wave period T_p [s] (lower panel) on grid3 Difference = results with coarse WAQUA grid - results with fine WAQUA grid	20050102	1000hr
	Hindcast Ameland Inlet	
WL | DELFT HYDRAULICS	H4803.11	Fig. 3.54b

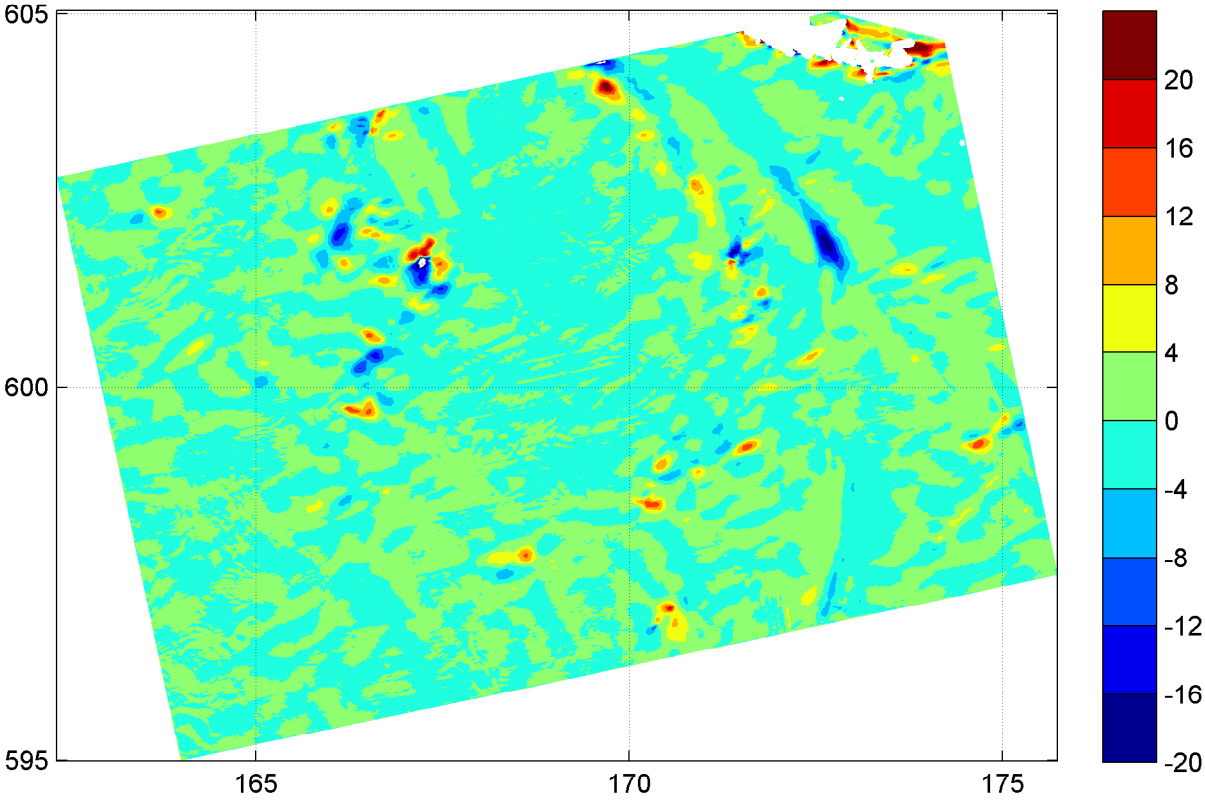

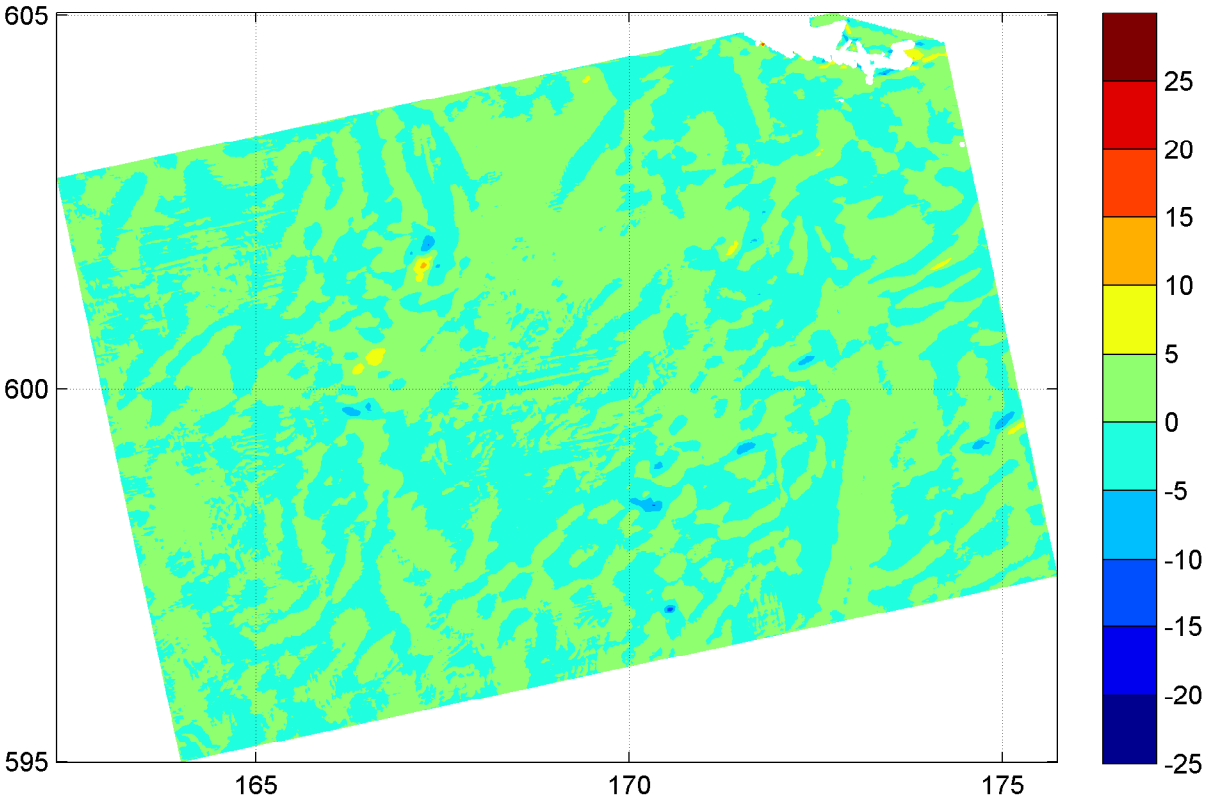

Difference plot of spatial distribution of mean wave direction [°] (upper panel) and directional spreading [°] (lower panel) on grid3 Difference = results with coarse WAQUA grid - results with fine WAQUA grid	20050102	1000hr
	Hindcast Ameland Inlet	
WL | DELFT HYDRAULICS	H4803.11	Fig. 3.54c

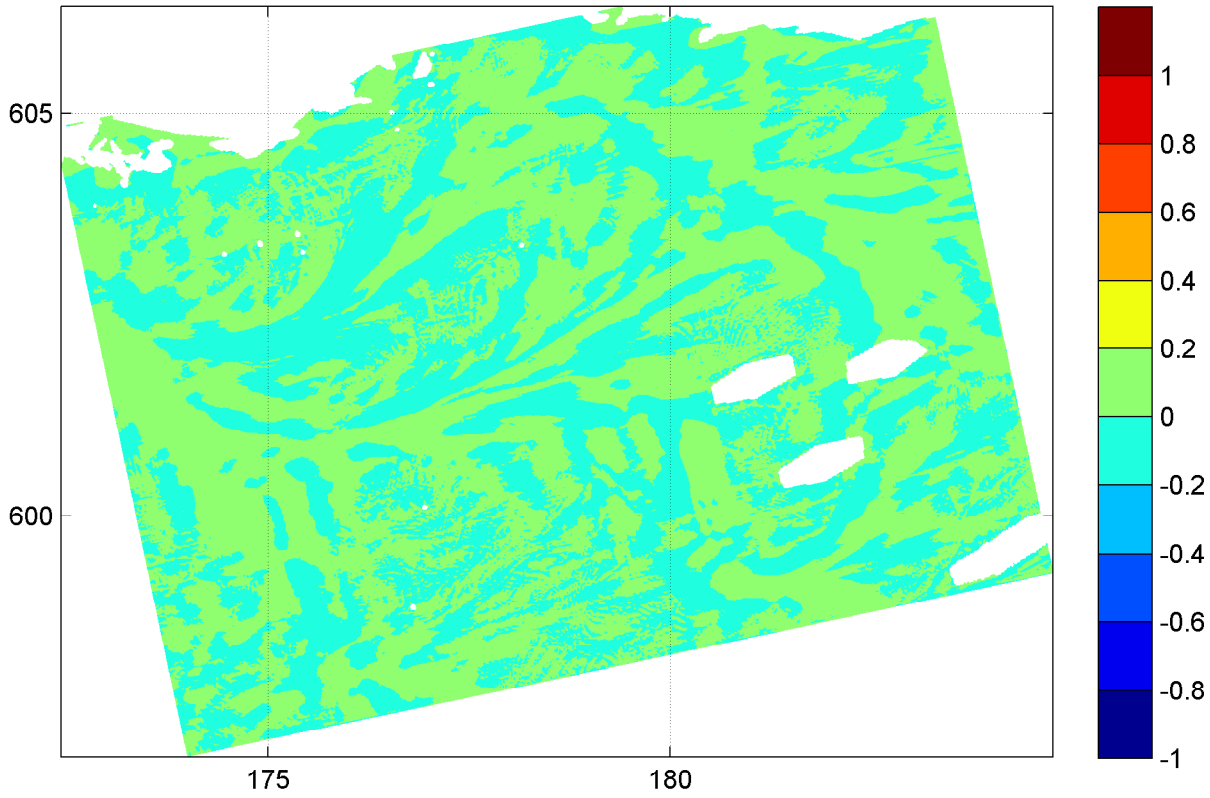

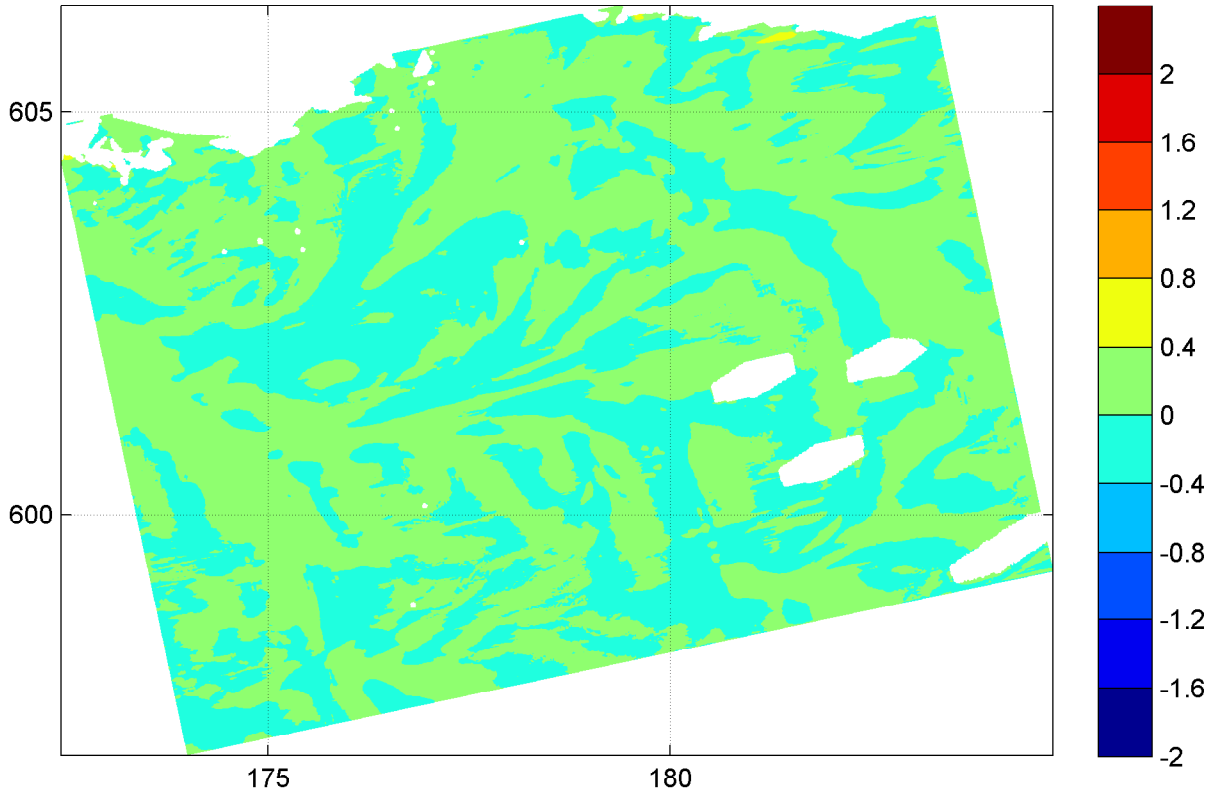

Difference plot of spatial distribution of wave height H_{m0} [m] (upper panel) and wave period $T_{m-1,0}$ [s] (lower panel) on grid4 Difference = results with coarse WAQUA grid - results with fine WAQUA grid	20050102	1000hr
	Hindcast Ameland Inlet	
WL | DELFT HYDRAULICS	H4803.11	Fig. 3.55a

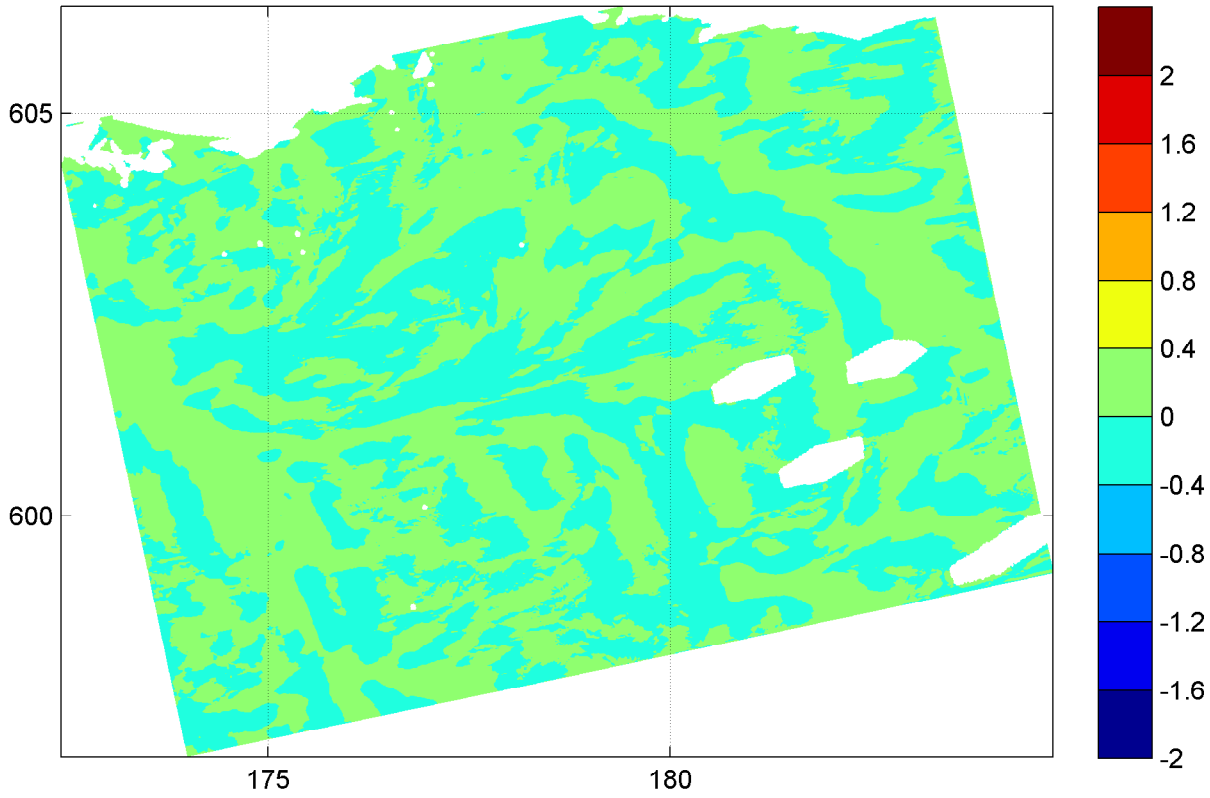

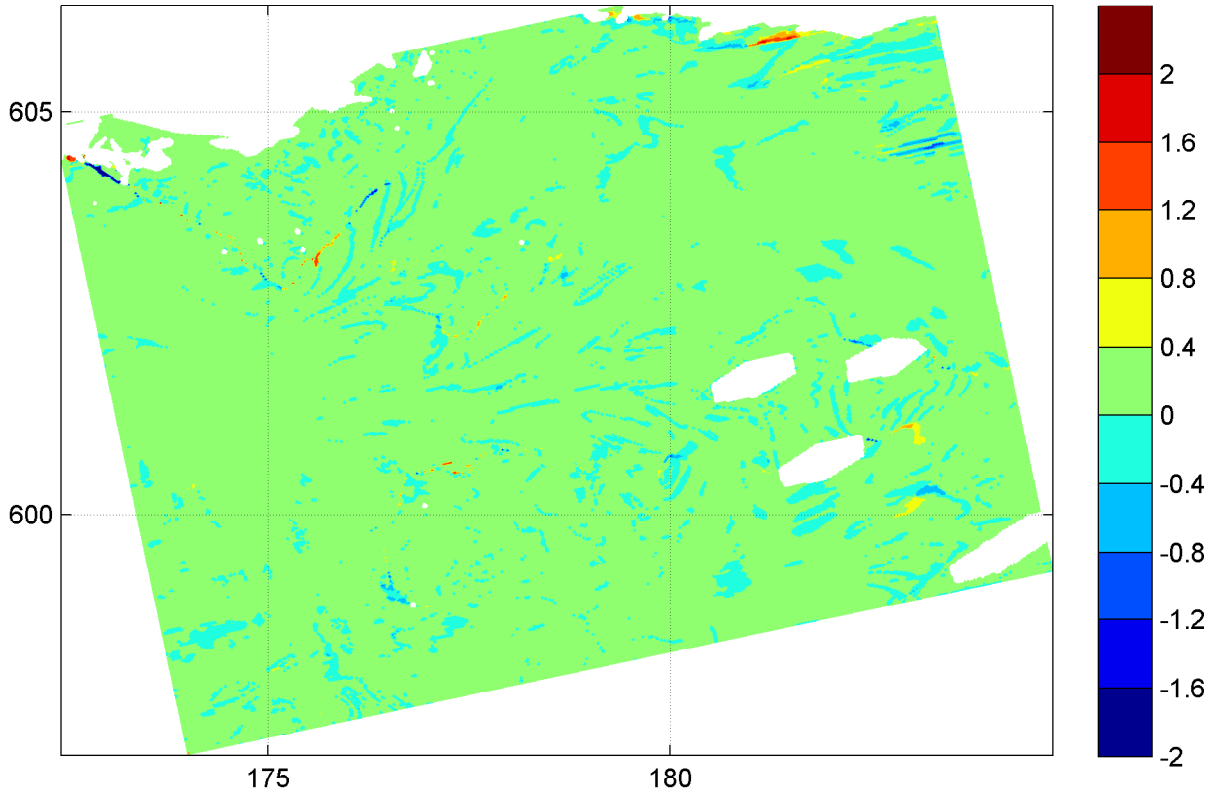

Difference plot of spatial distribution of wave period T_{m02} [s] (upper panel) and wave period T_p [s] (lower panel) on grid4 Difference = results with coarse WAQUA grid - results with fine WAQUA grid	20050102	1000hr
	Hindcast Ameland Inlet	
WL | DELFT HYDRAULICS	H4803.11	Fig. 3.55b

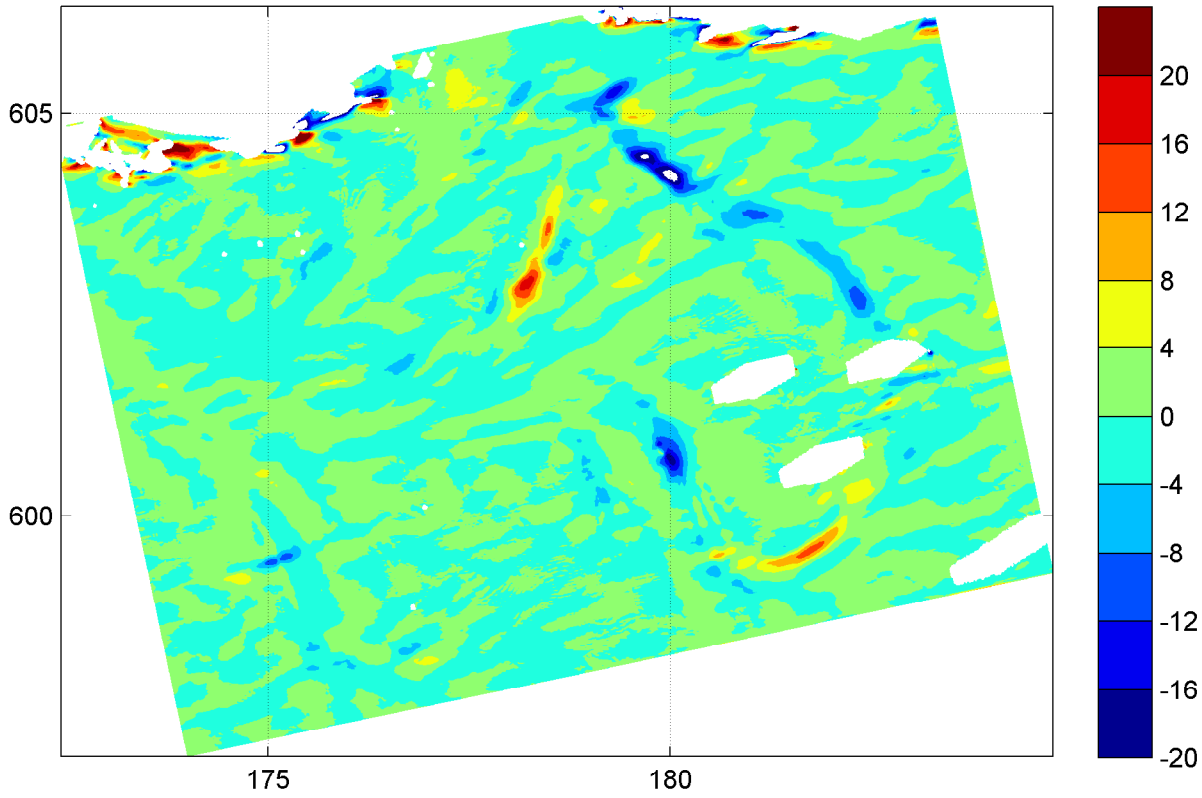

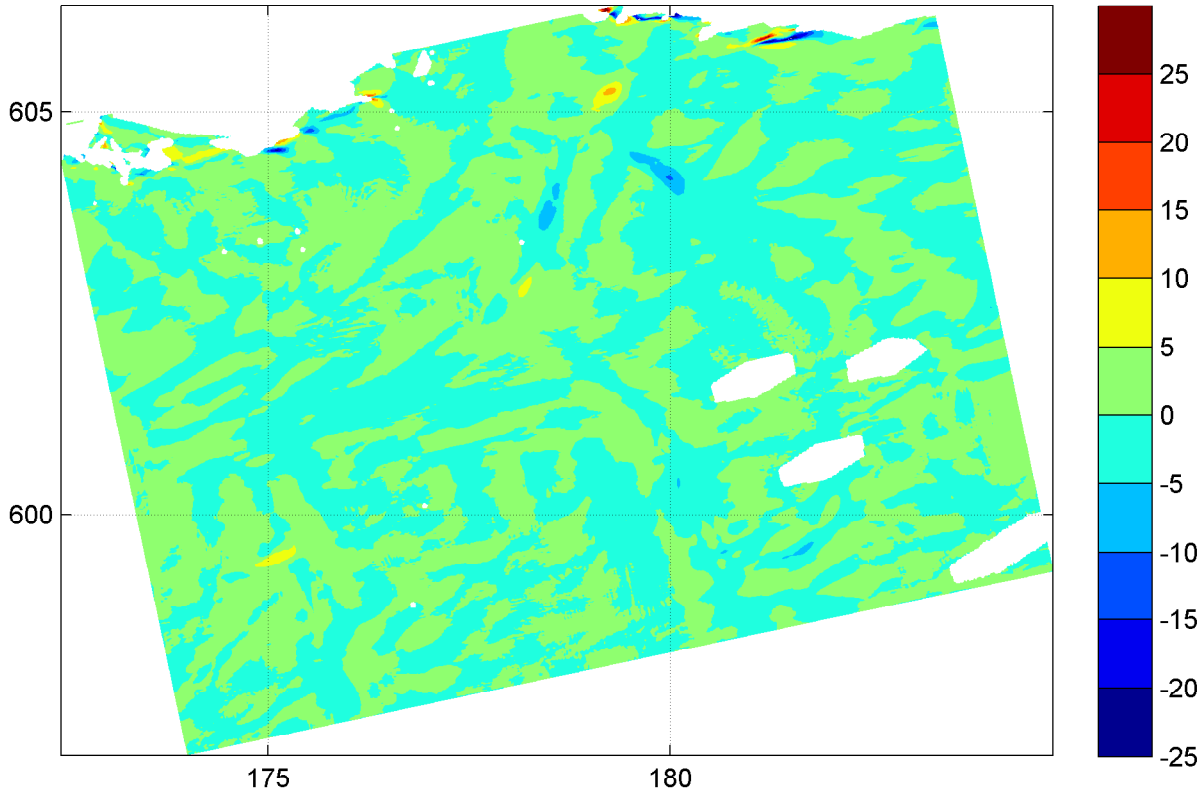

Difference plot of spatial distribution of mean wave direction [°] (upper panel) and directional spreading [°] (lower panel) on grid4 Difference = results with coarse WAQUA grid - results with fine WAQUA grid	20050102	1000hr
	Hindcast Ameland Inlet	
WL | DELFT HYDRAULICS	H4803.11	Fig. 3.55c

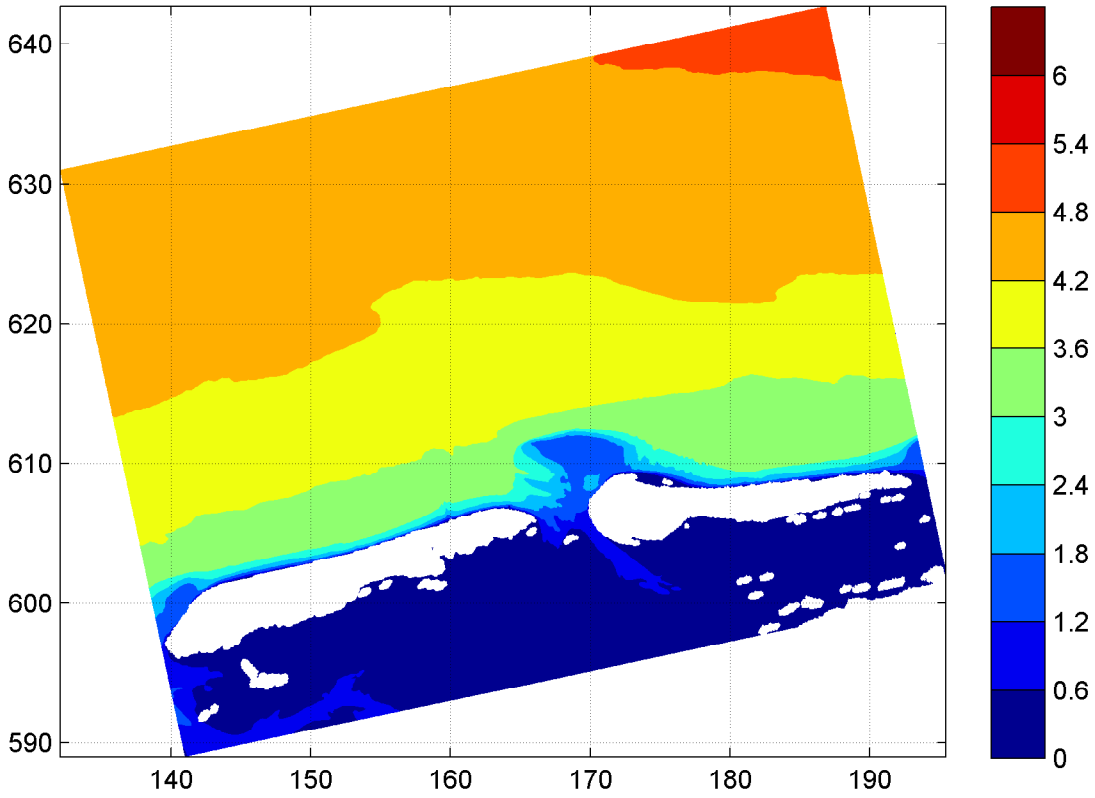

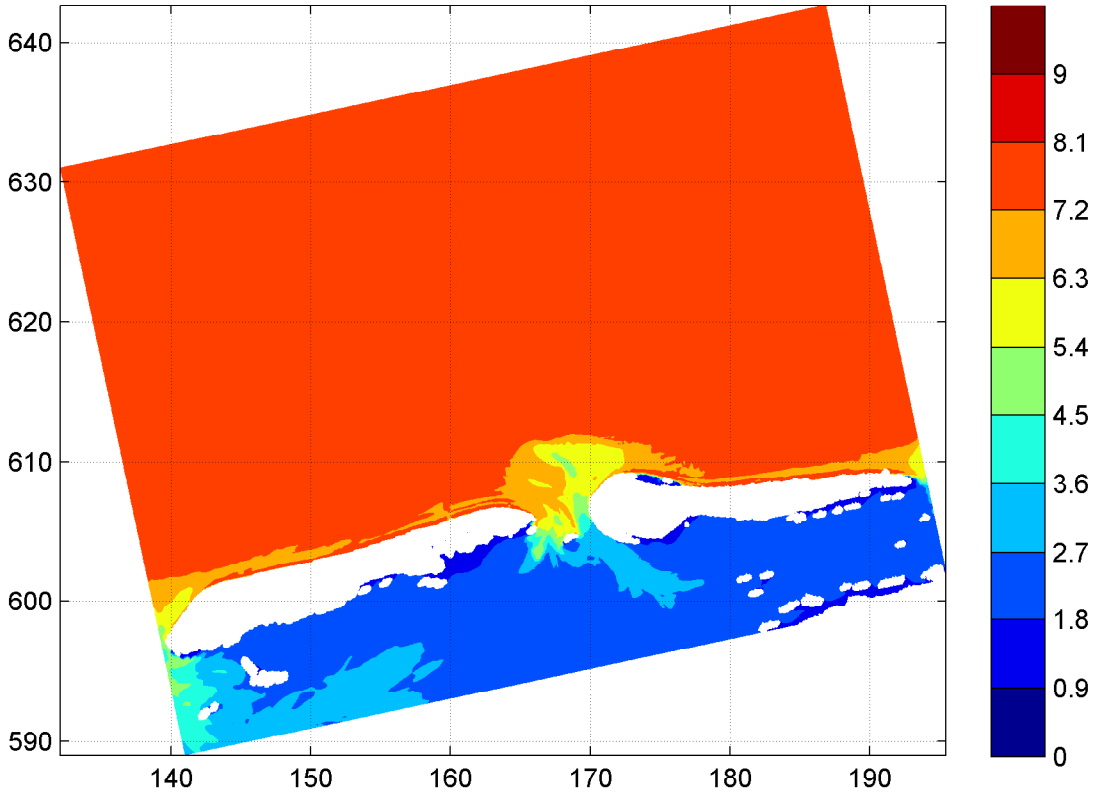

Spatial distribution of wave height H_{m0} [m] (upper panel) and wave period $T_{m-1,0}$ [s] (lower panel) on grid1 uniform water level field and no current	20050102	17:00hr
	Hindcast Ameland Inlet	
WL | DELFT HYDRAULICS	H4803.11	Fig. 3.56a

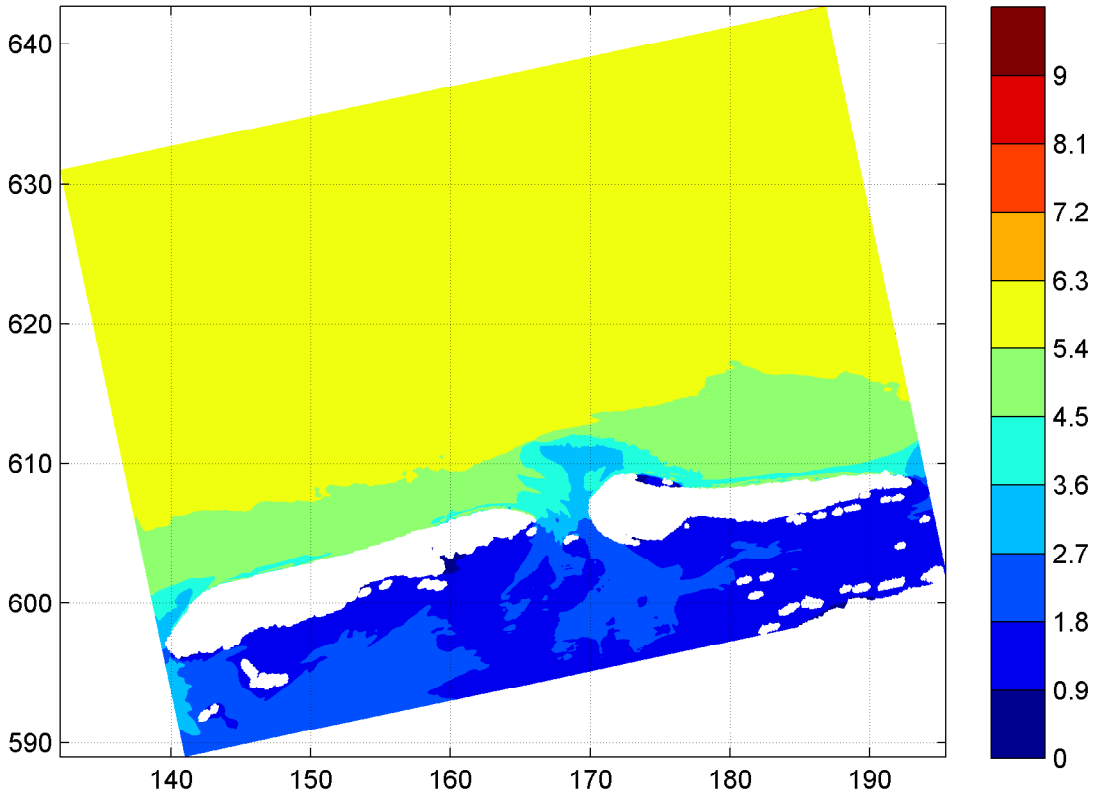

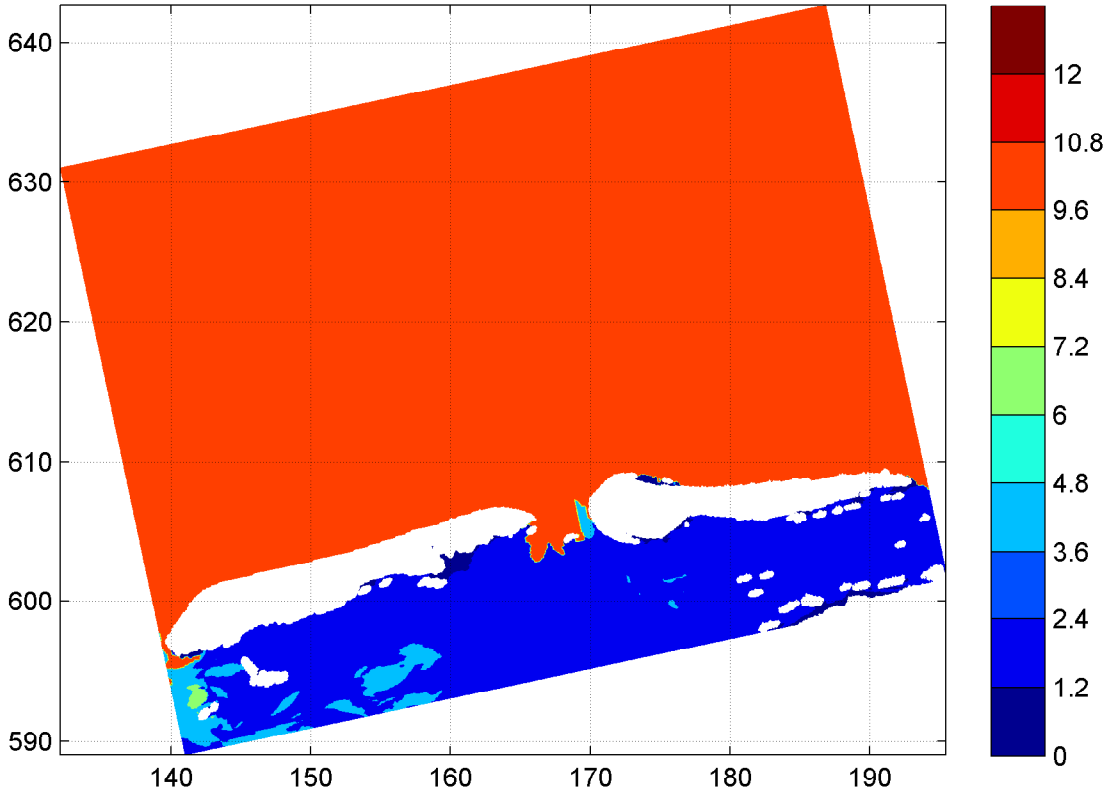

Spatial distribution of wave period T_{m02} [s] (upper panel) and wave period T_p [s] (lower panel) on grid1 uniform water level field and no current	20050102	17:00hr
	Hindcast Ameland Inlet	
WL | DELFT HYDRAULICS	H4803.11	Fig. 3.56b

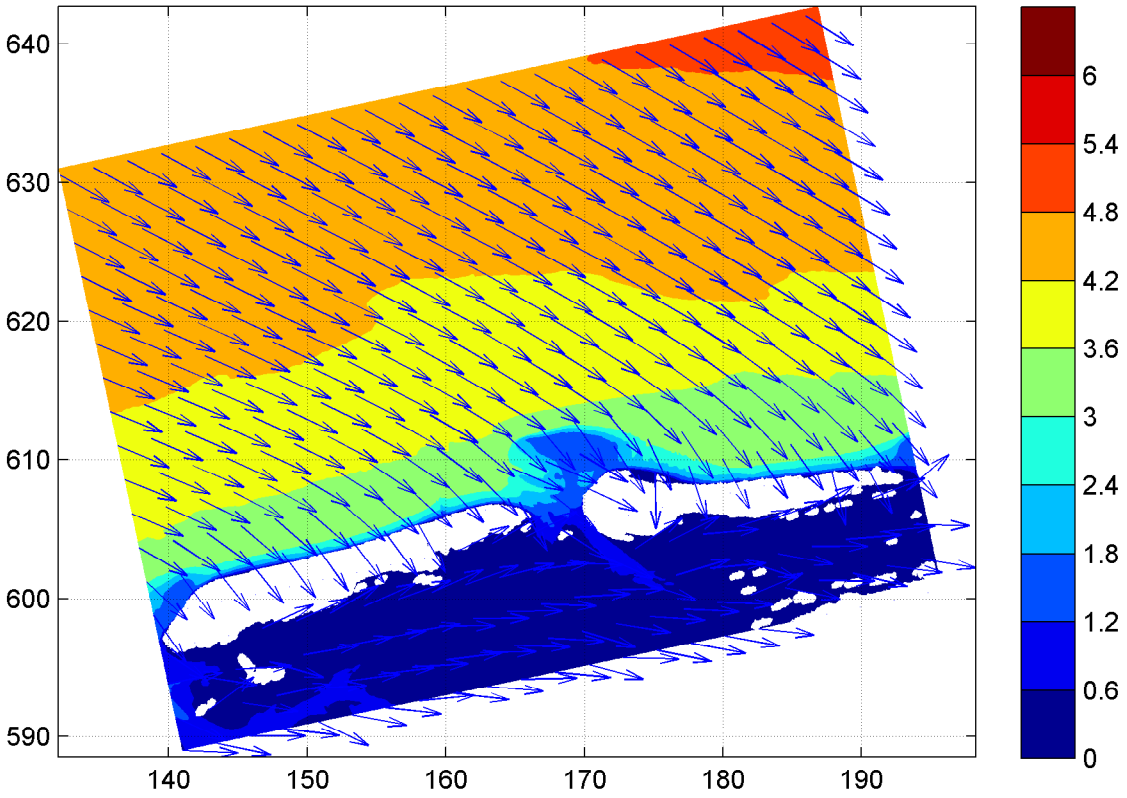

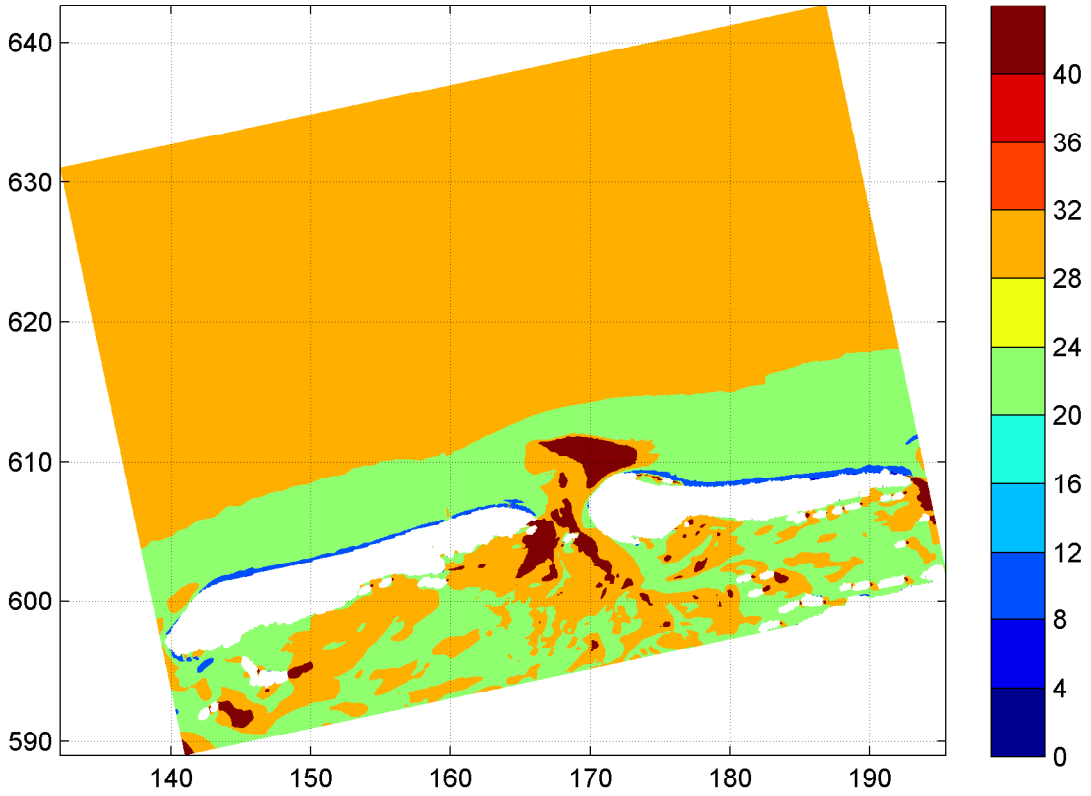

Spatial distribution of wave height [m] and mean wave direction (upper panel) and directional spreading [°] (lower panel) on grid1 uniform water level field and no current	20050102	17:00hr
	Hindcast Ameland Inlet	
WL | DELFT HYDRAULICS	H4803.11	Fig. 3.56c

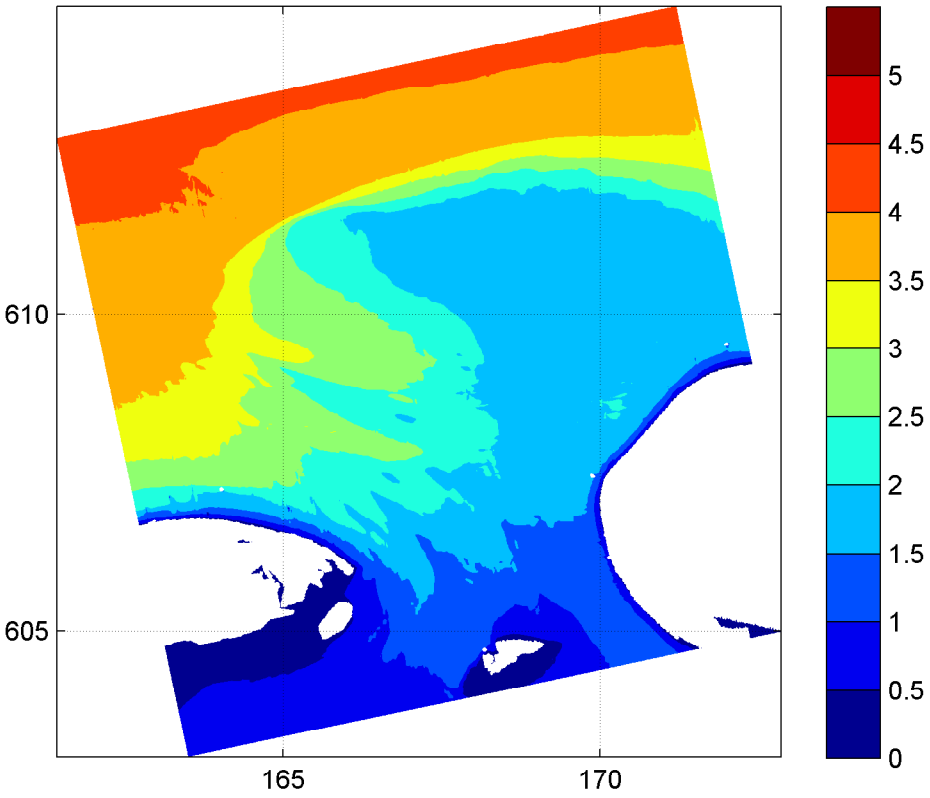

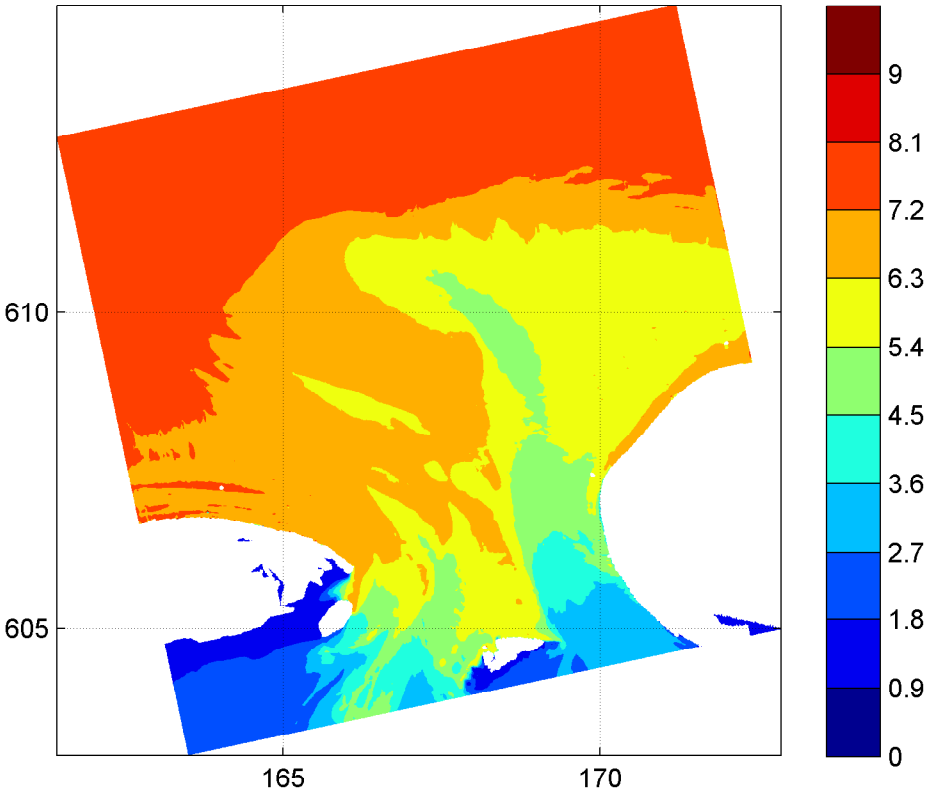

Spatial distribution of wave height H_{m0} [m] (upper panel) and wave period $T_{m-1,0}$ [s] (lower panel) on grid2 uniform water level field and no current	20050102	17:00hr
	Hindcast Ameland Inlet	
WL | DELFT HYDRAULICS	H4803.11	Fig. 3.57a

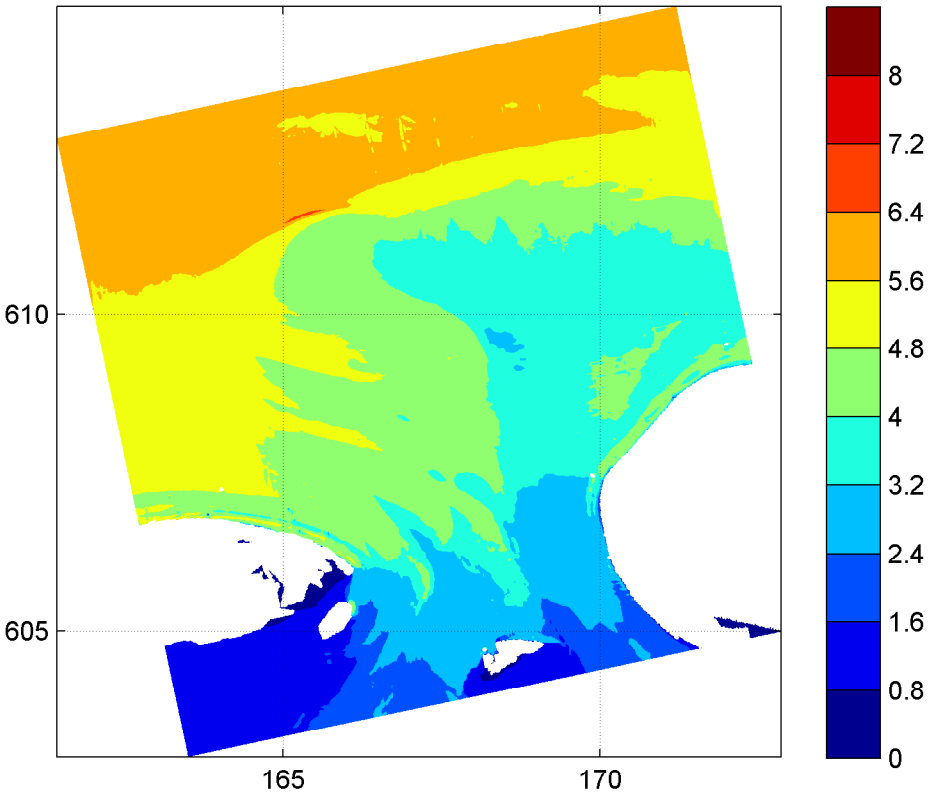

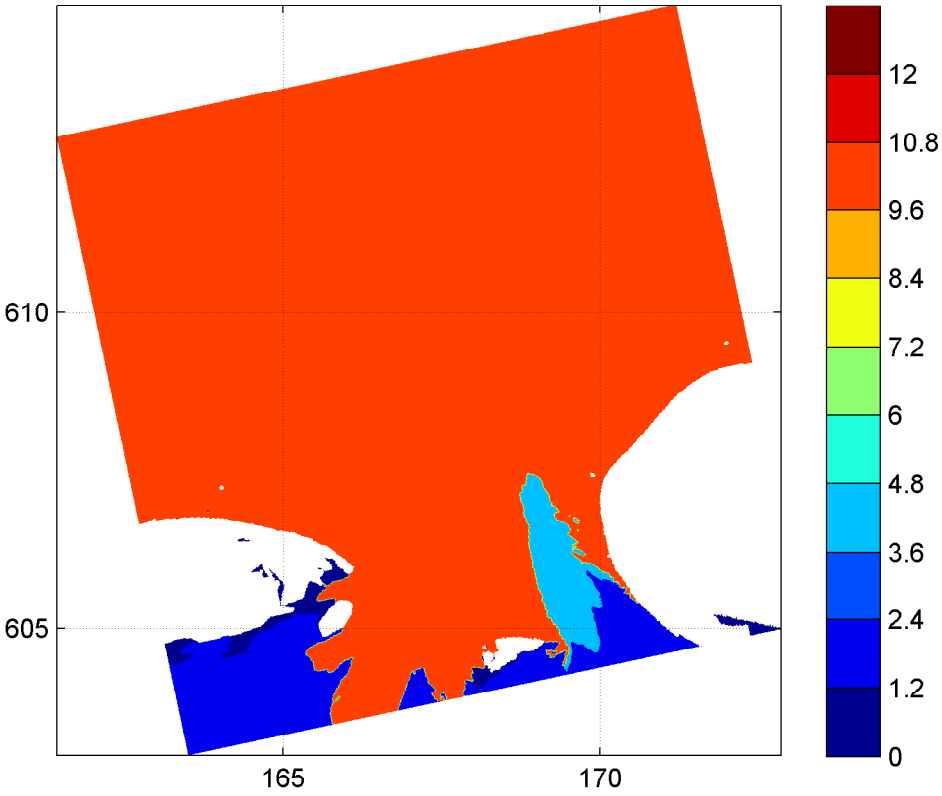

Spatial distribution of wave period T_{m02} [s] (upper panel) and wave period T_p [s] (lower panel) on grid2 uniform water level field and no current	20050102	17:00hr
	Hindcast Ameland Inlet	
WL | DELFT HYDRAULICS	H4803.11	Fig. 3.57b

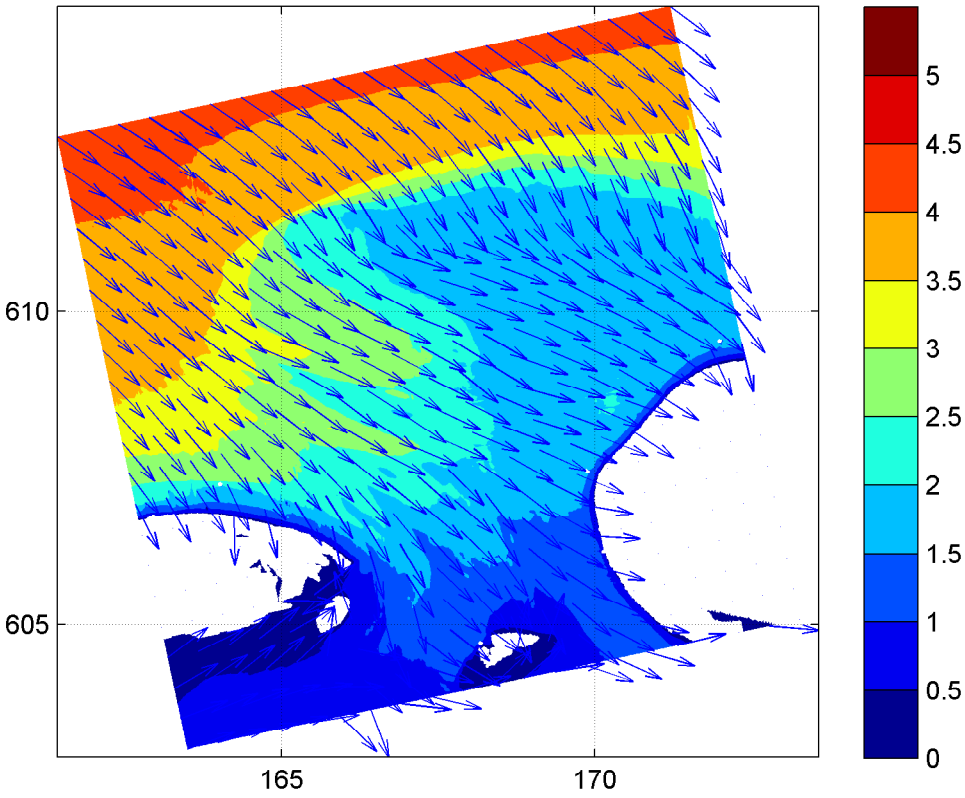

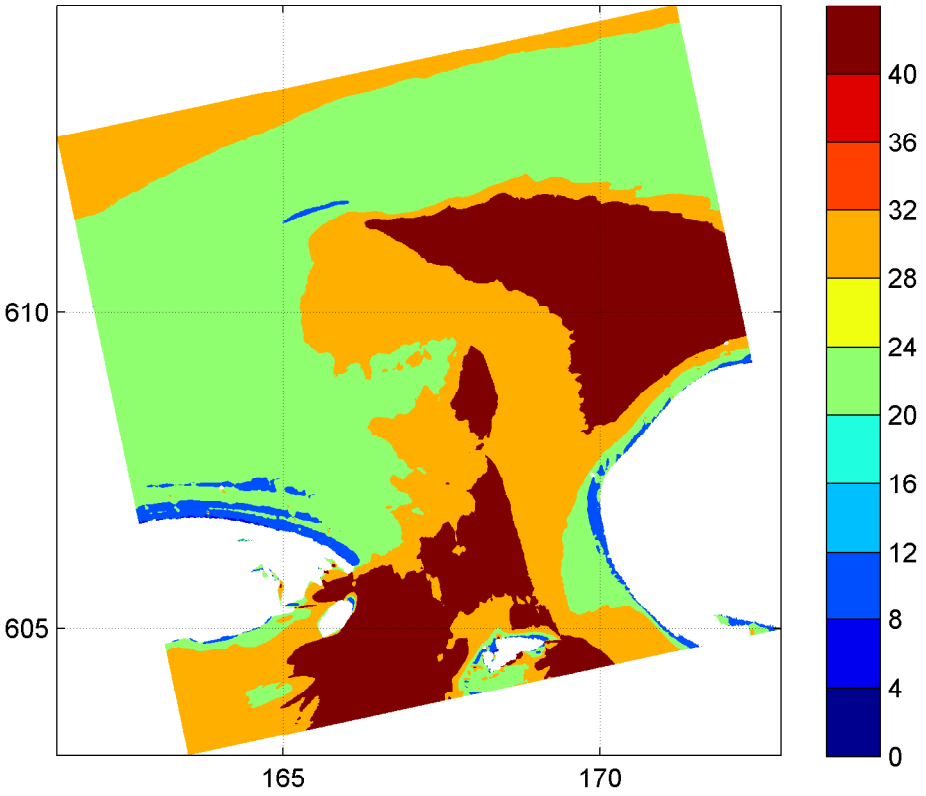

Spatial distribution of wave height [m] and mean wave direction (upper panel) and directional spreading [°] (lower panel) on grid2 uniform water level field and no current	20050102	17:00hr
	Hindcast Ameland Inlet	
WL | DELFT HYDRAULICS	H4803.11	Fig. 3.57c

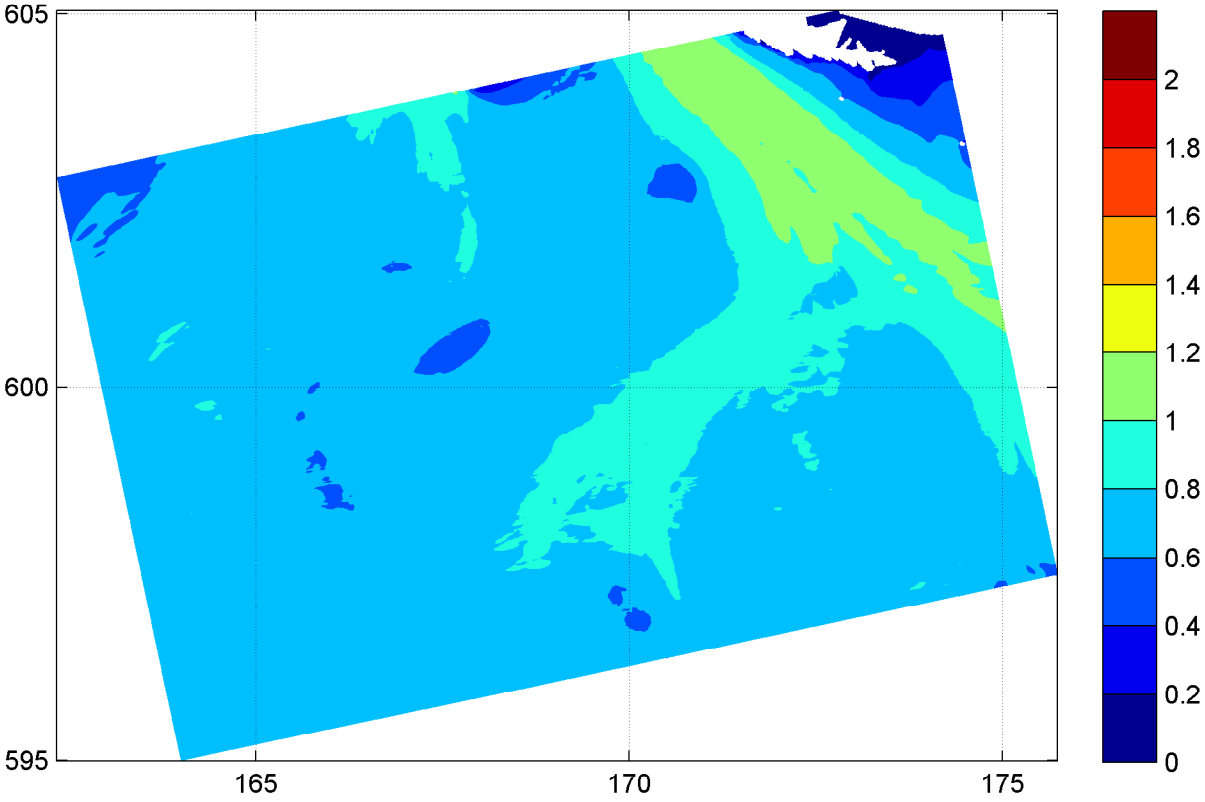

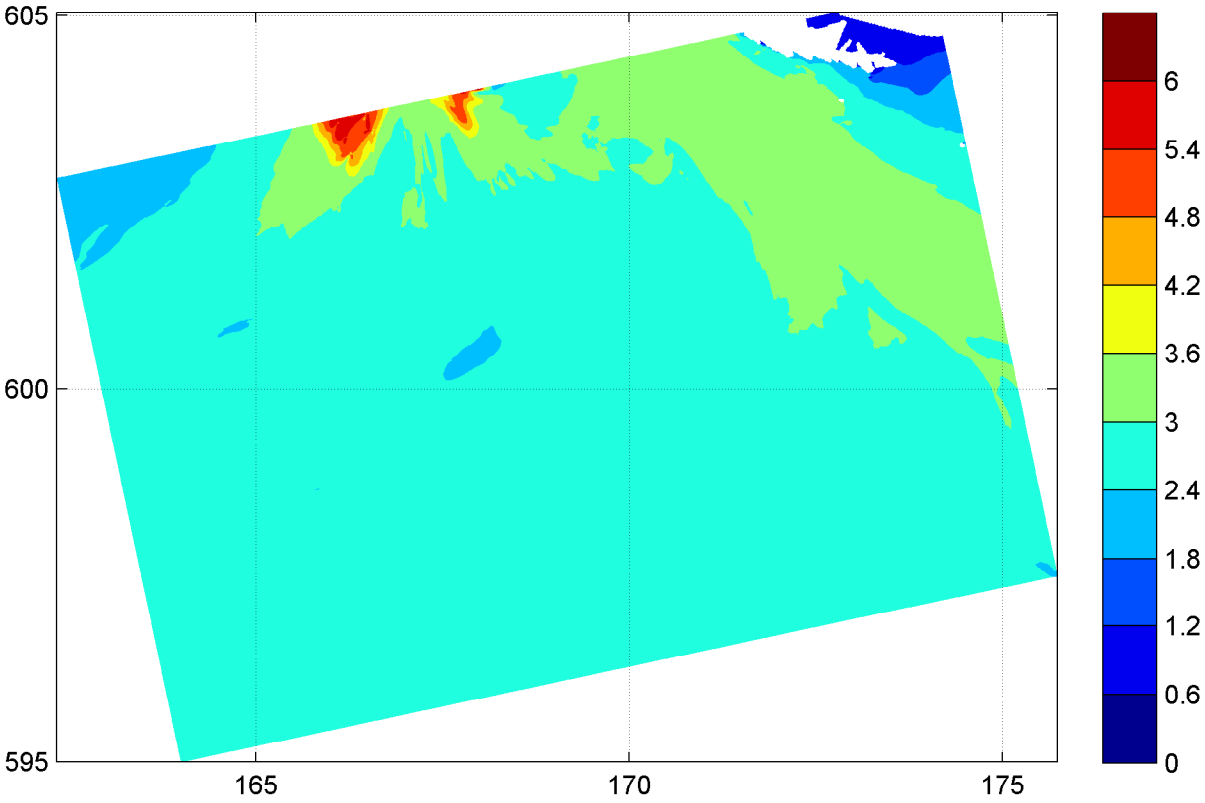

Spatial distribution of wave height H_{m0} [m] (upper panel) and wave period $T_{m-1,0}$ [s] (lower panel) on grid3 uniform water level field and no current	20050102	17:00hr
	Hindcast Ameland Inlet	
WL | DELFT HYDRAULICS	H4803.11	Fig. 3.58a

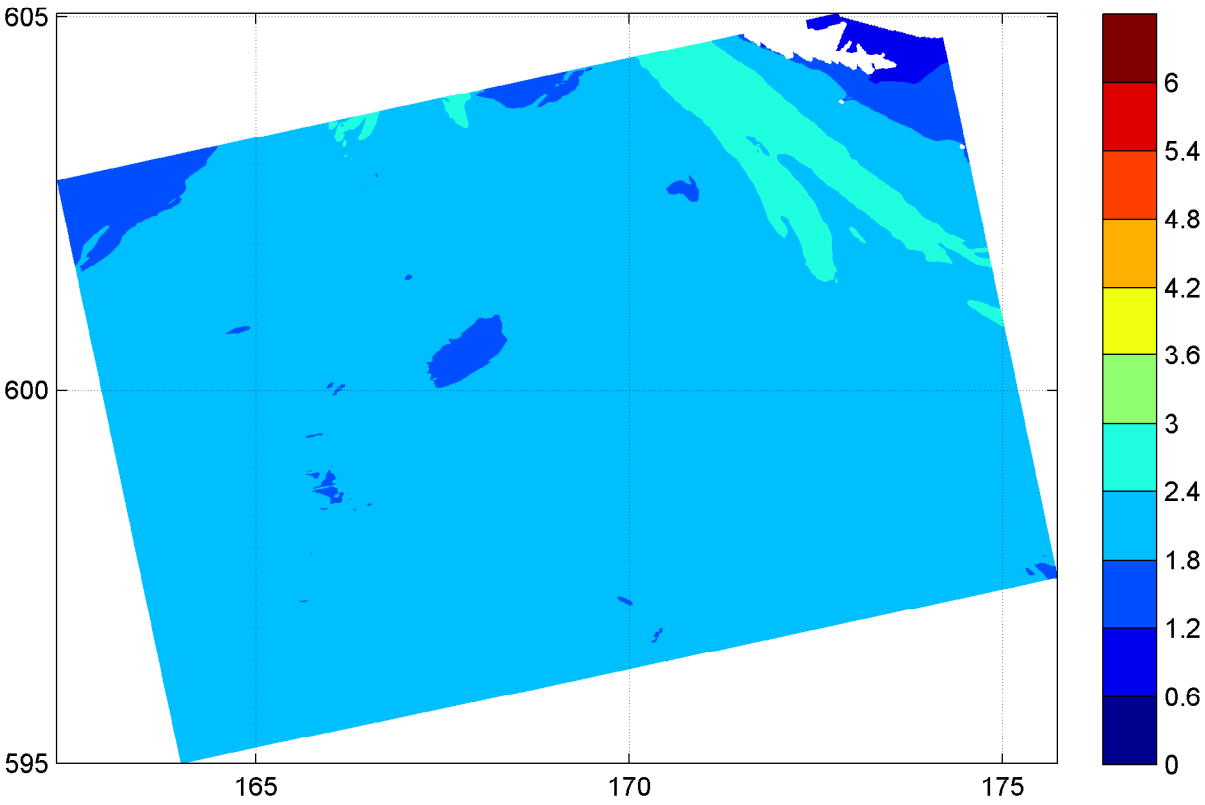

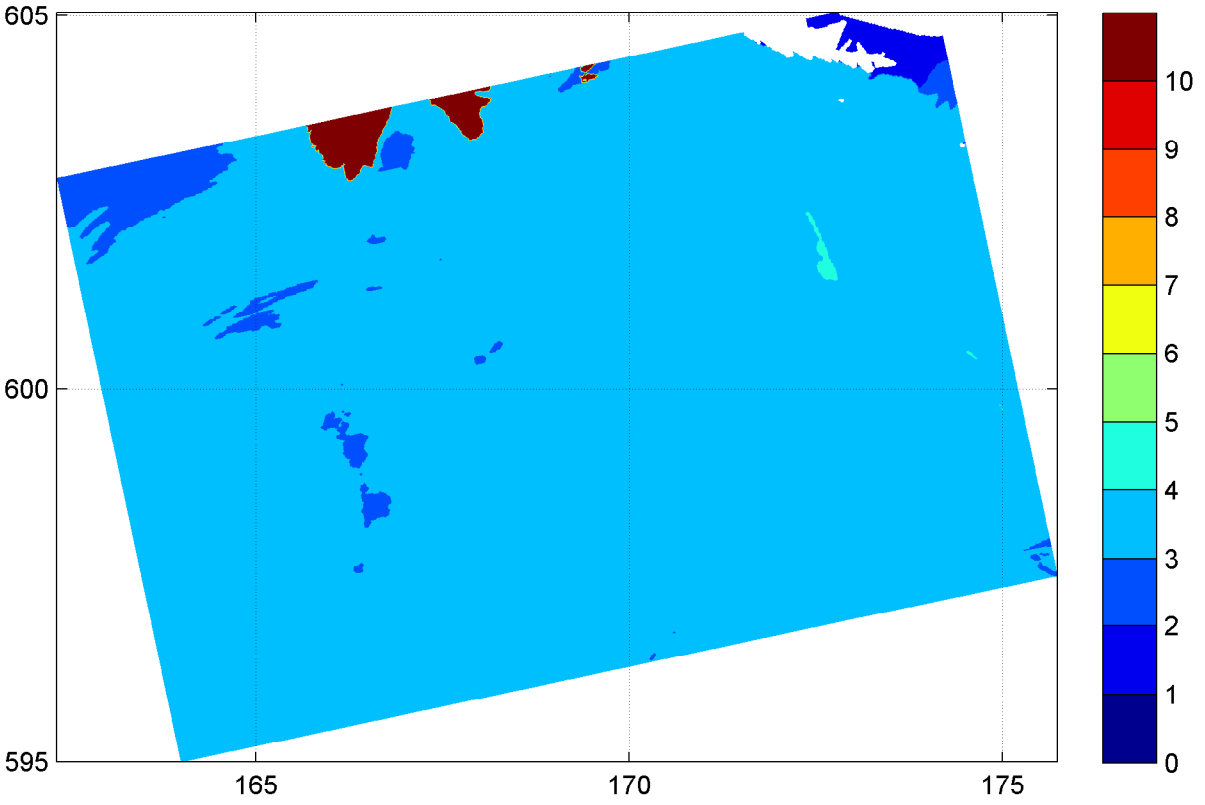

Spatial distribution of wave period T_{m02} [s] (upper panel) and wave period T_p [s] (lower panel) on grid3 uniform water level field and no current	20050102	17:00hr
	Hindcast Ameland Inlet	
WL | DELFT HYDRAULICS	H4803.11	Fig. 3.58b

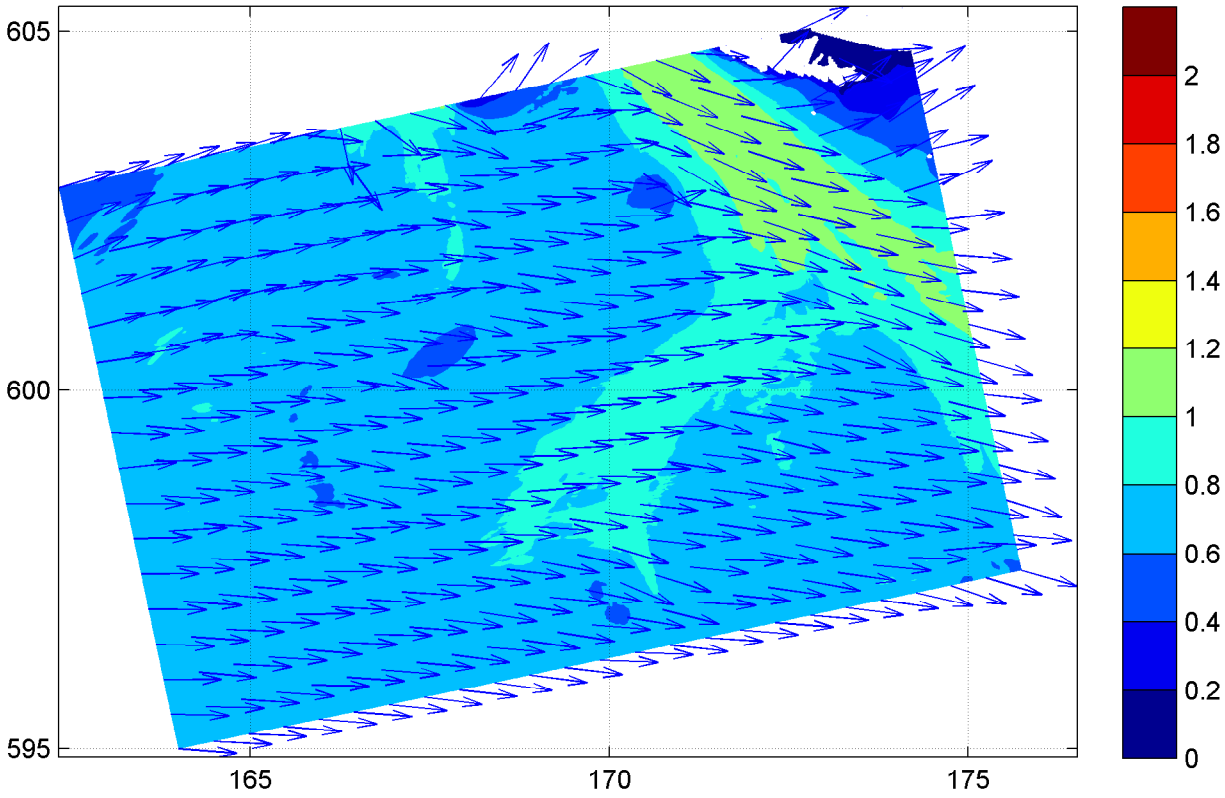

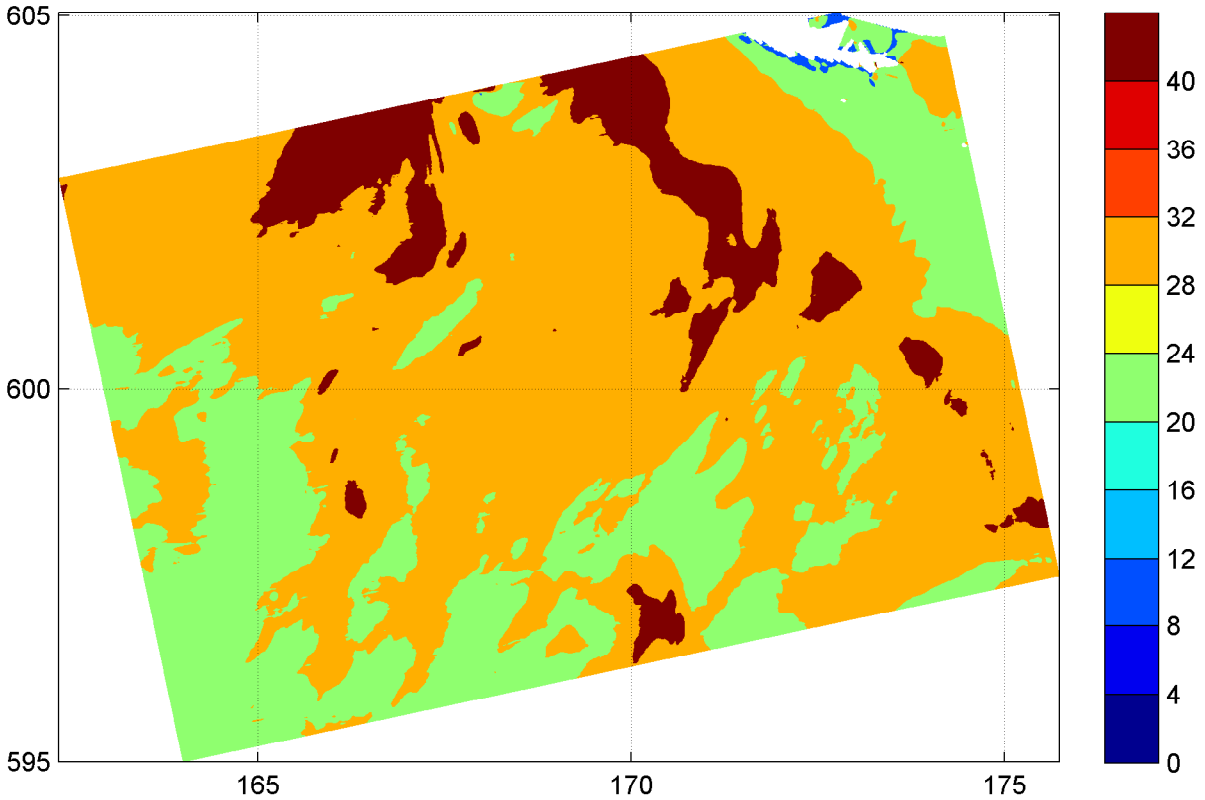

Spatial distribution of wave height [m] and mean wave direction (upper panel) and directional spreading [°] (lower panel) on grid3 uniform water level field and no current	20050102	17:00hr
	Hindcast Ameland Inlet	
WL | DELFT HYDRAULICS	H4803.11	Fig. 3.58c

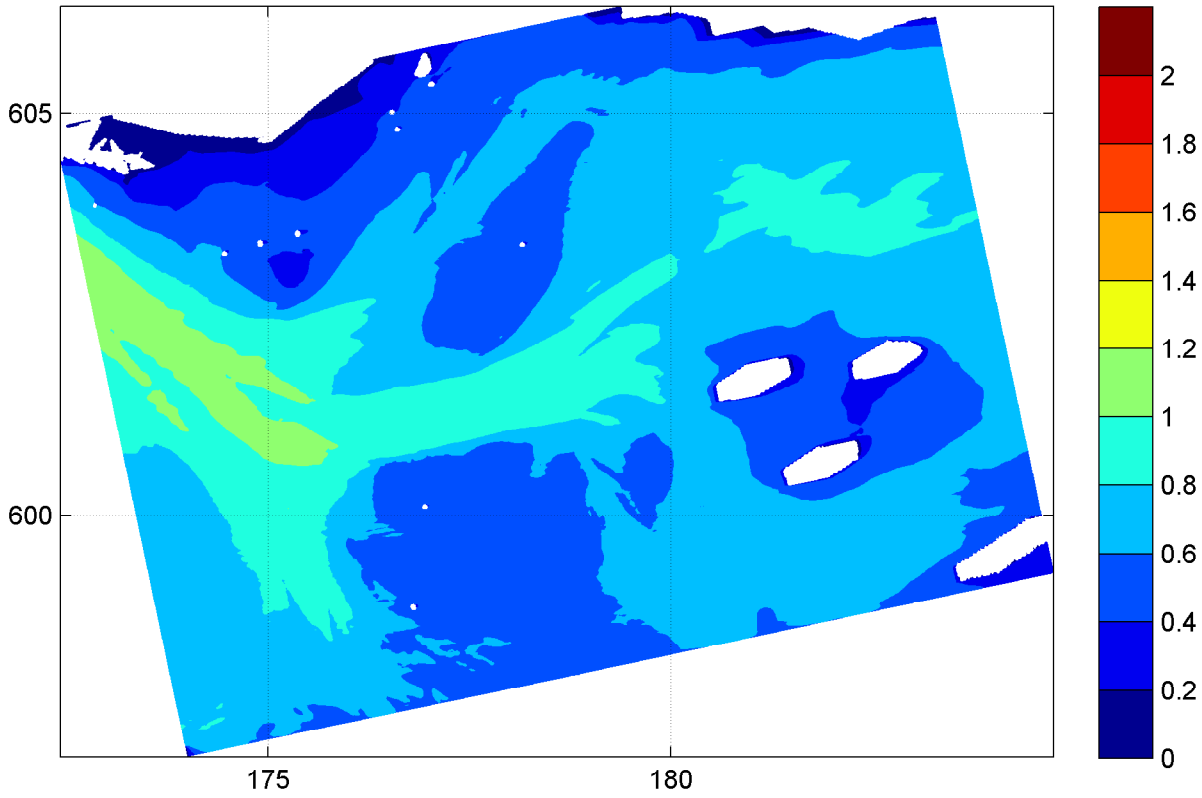

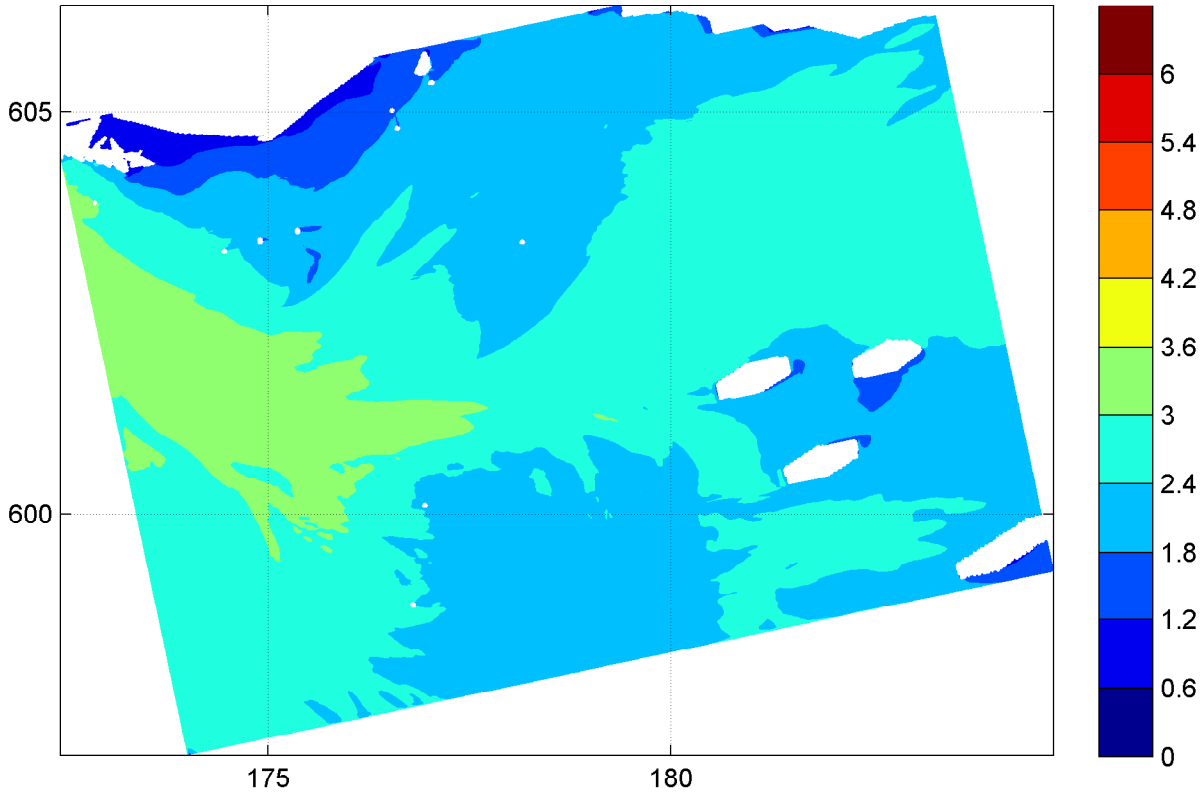

Spatial distribution of wave height H_{m0} [m] (upper panel) and wave period $T_{m-1,0}$ [s] (lower panel) on grid4 uniform water level field and no current	20050102	17:00hr
	Hindcast Ameland Inlet	
WL | DELFT HYDRAULICS	H4803.11	Fig. 3.59a

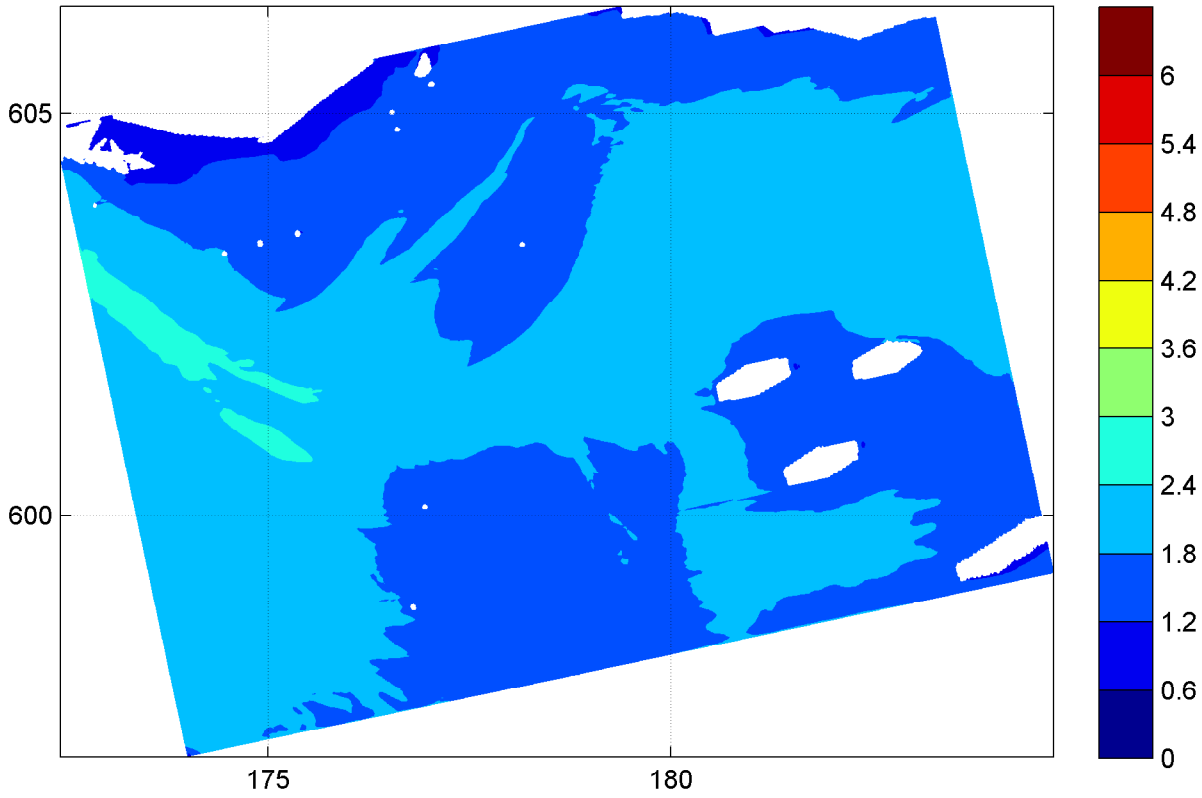

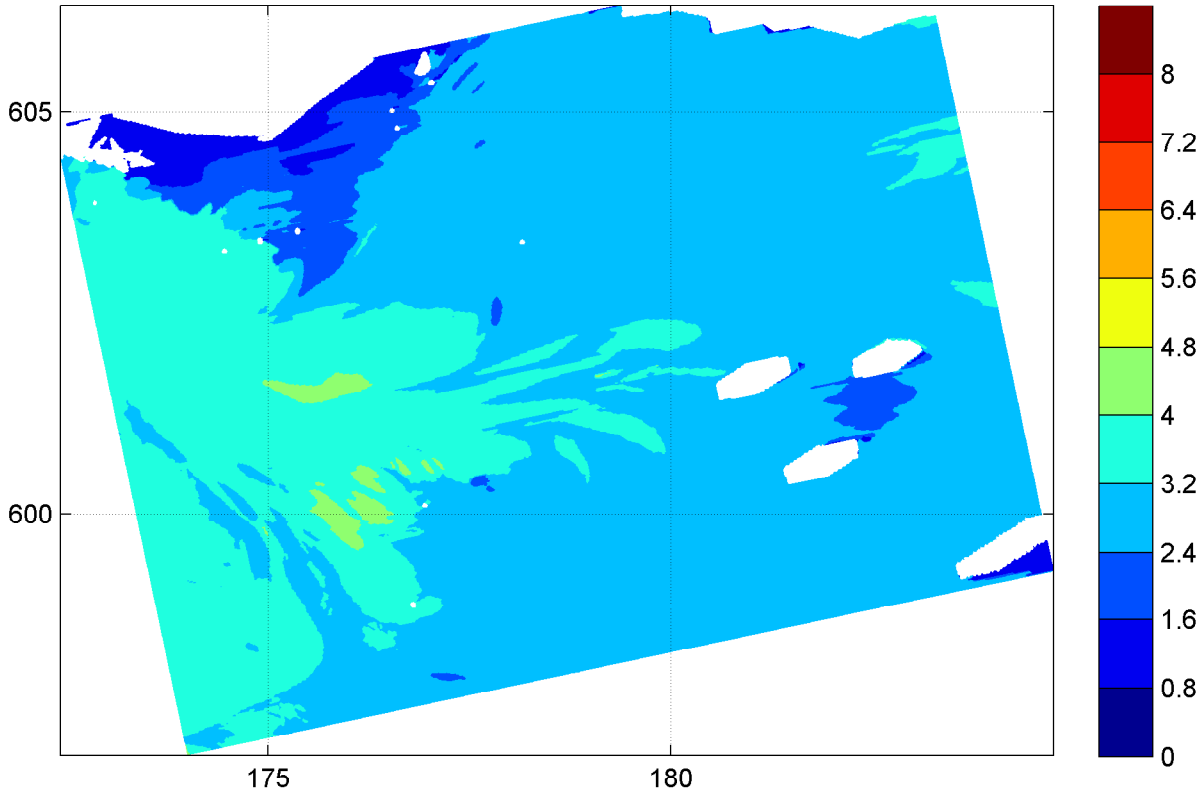

Spatial distribution of wave period T_{m02} [s] (upper panel) and wave period T_p [s] (lower panel) on grid4 uniform water level field and no current	20050102	17:00hr
	Hindcast Ameland Inlet	
WL | DELFT HYDRAULICS	H4803.11	Fig. 3.59b

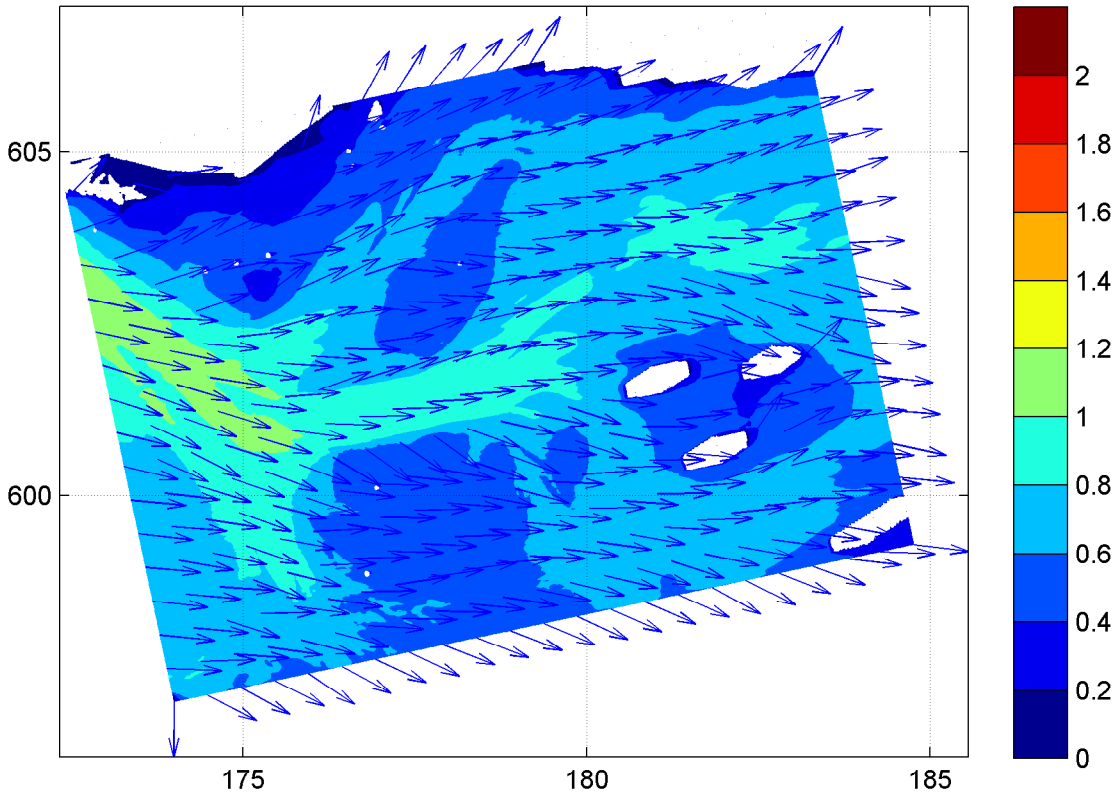

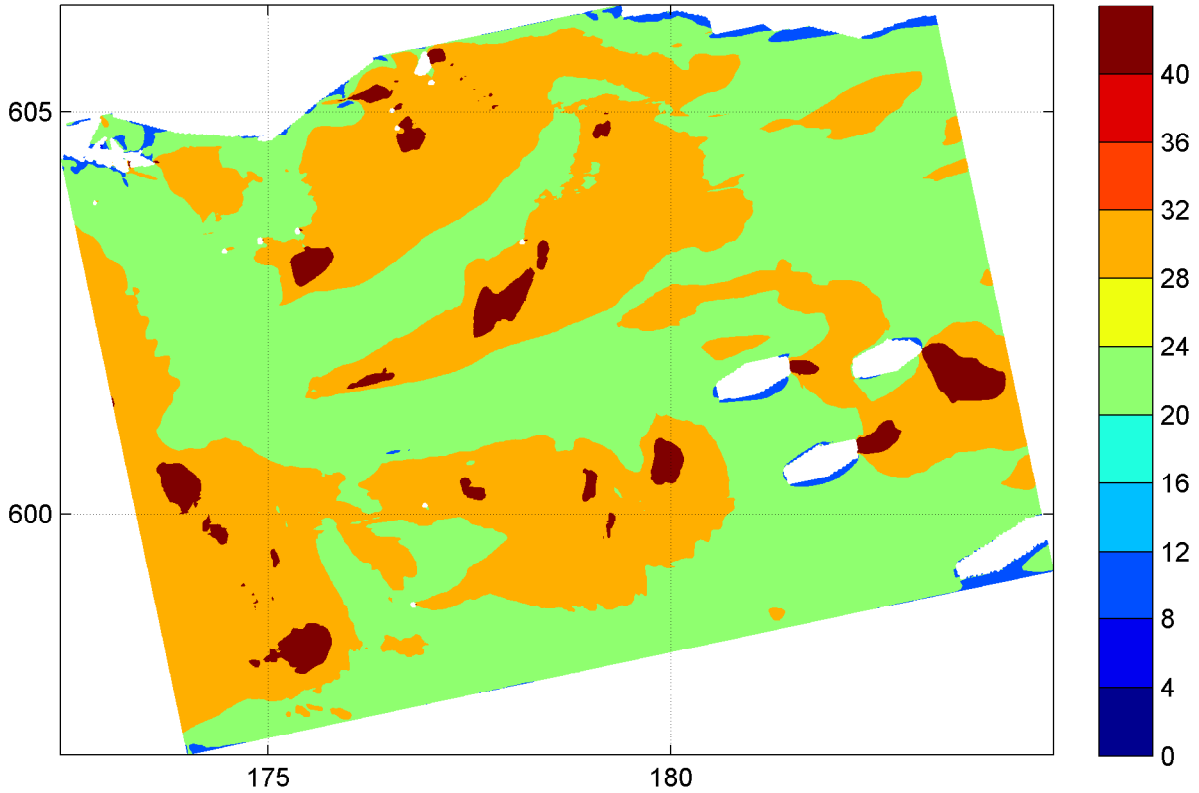

Spatial distribution of wave height [m] and mean wave direction (upper panel) and directional spreading [°] (lower panel) on grid4 uniform water level field and no current	20050102	17:00hr
	Hindcast Ameland Inlet	
WL | DELFT HYDRAULICS	H4803.11	Fig. 3.59c

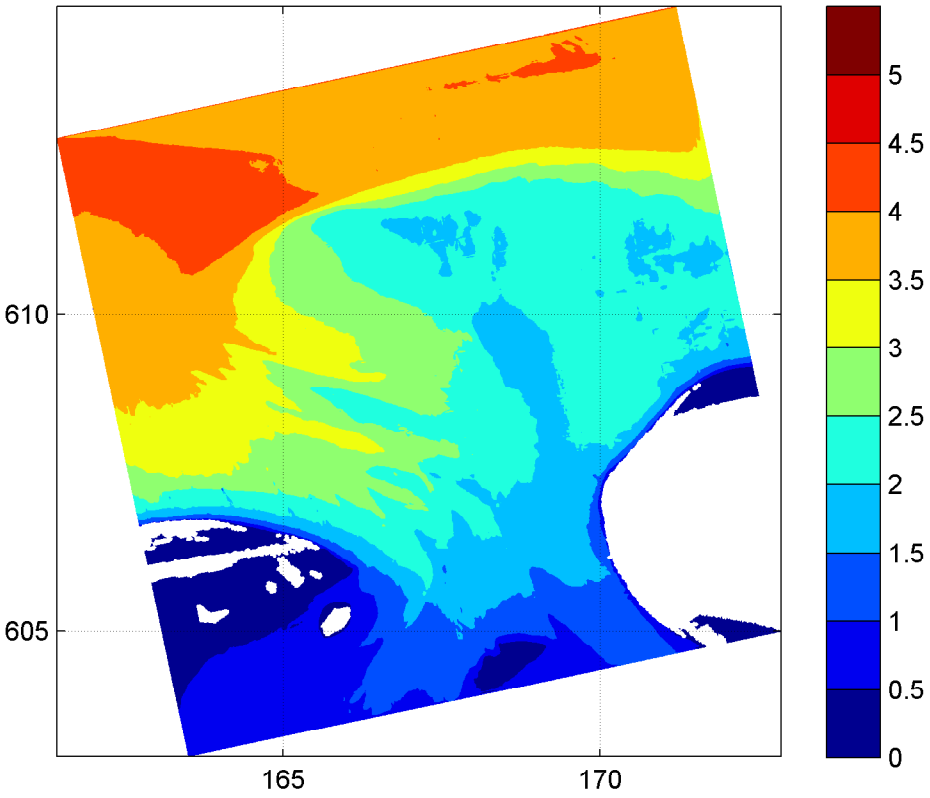

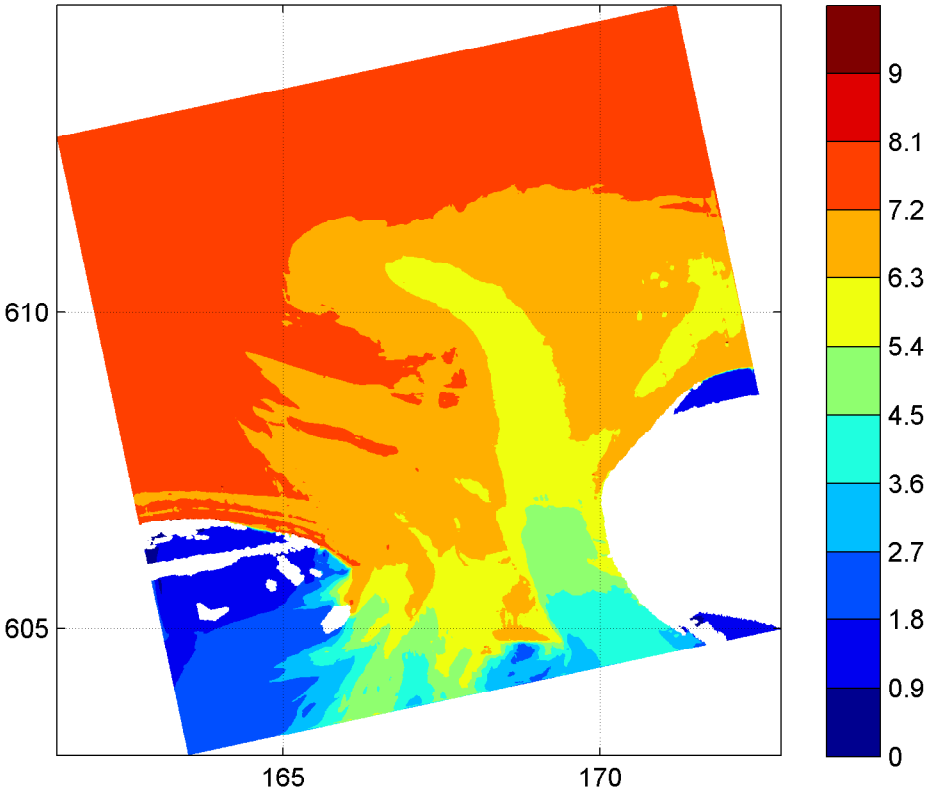

Spatial distribution of wave height H_{m0} [m] (upper panel) and wave period $T_{m-1,0}$ [s] (lower panel) on grid2 WAQUA high resolution	20050102	17:00hr
	Hindcast Ameland Inlet	
WL | DELFT HYDRAULICS	H4803.11	Fig. 3.60a

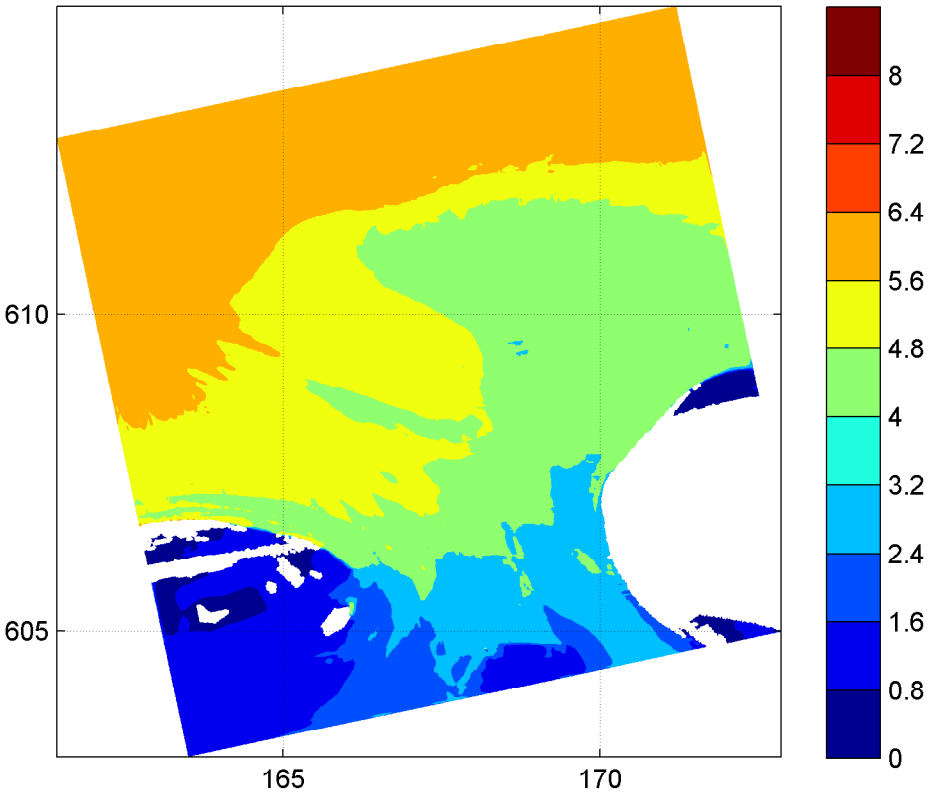

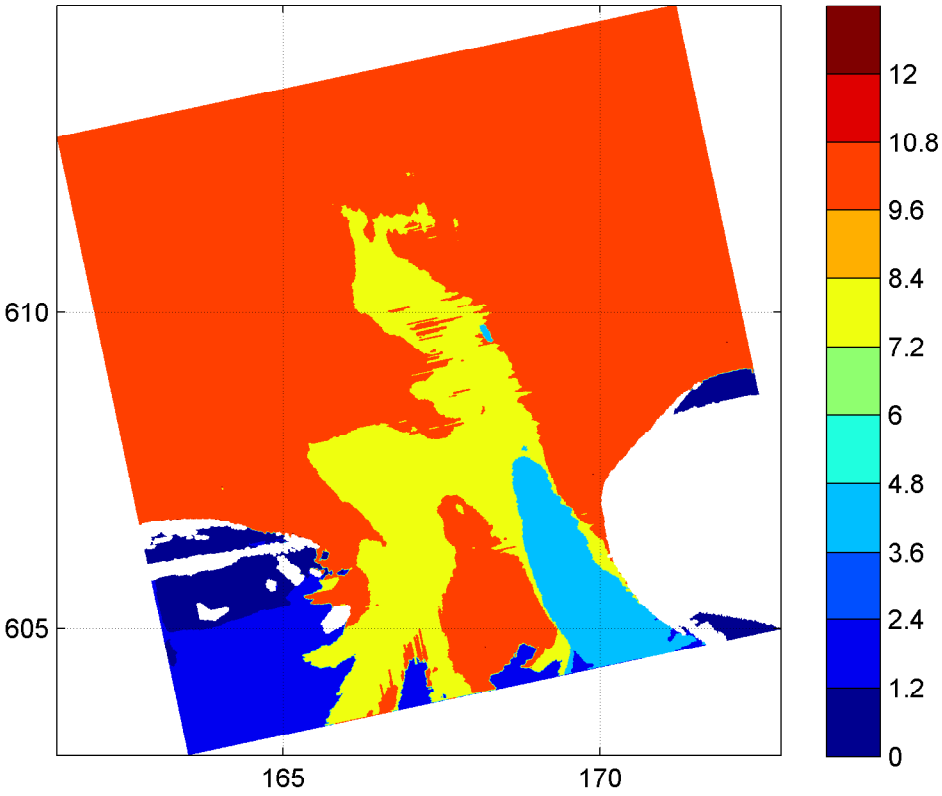

Spatial distribution of wave period T_{m02} [s] (upper panel) and wave period T_p [s] (lower panel) on grid2 WAQUA high resolution	20050102	17:00hr
	Hindcast Ameland Inlet	
WL | DELFT HYDRAULICS	H4803.11	Fig. 3.60b

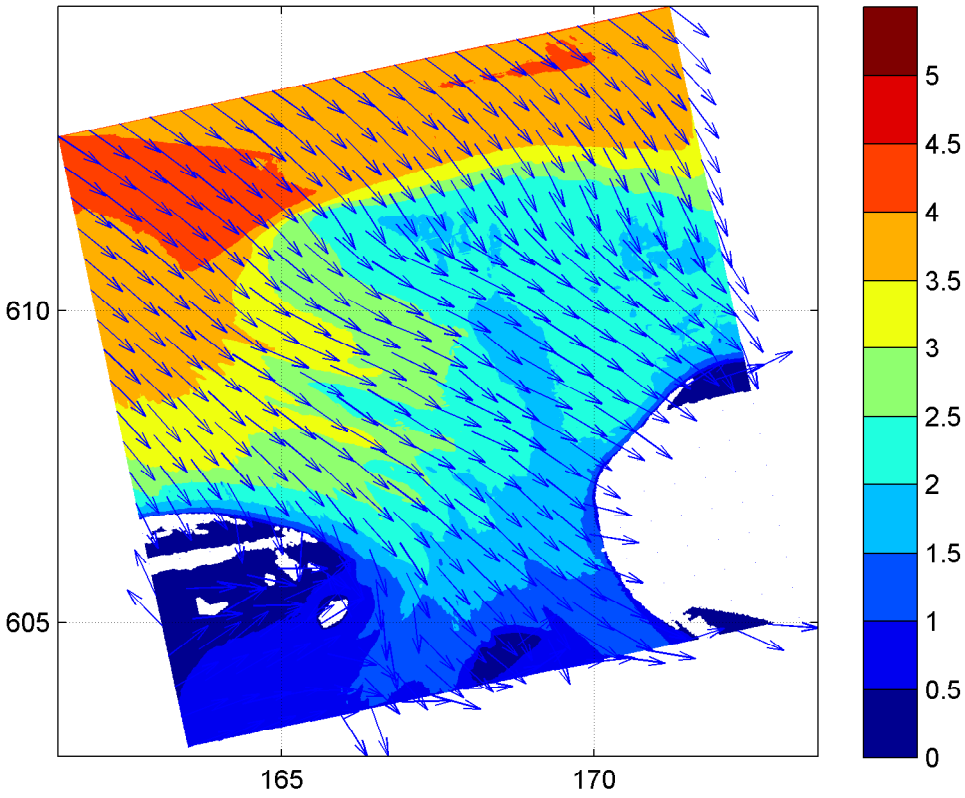

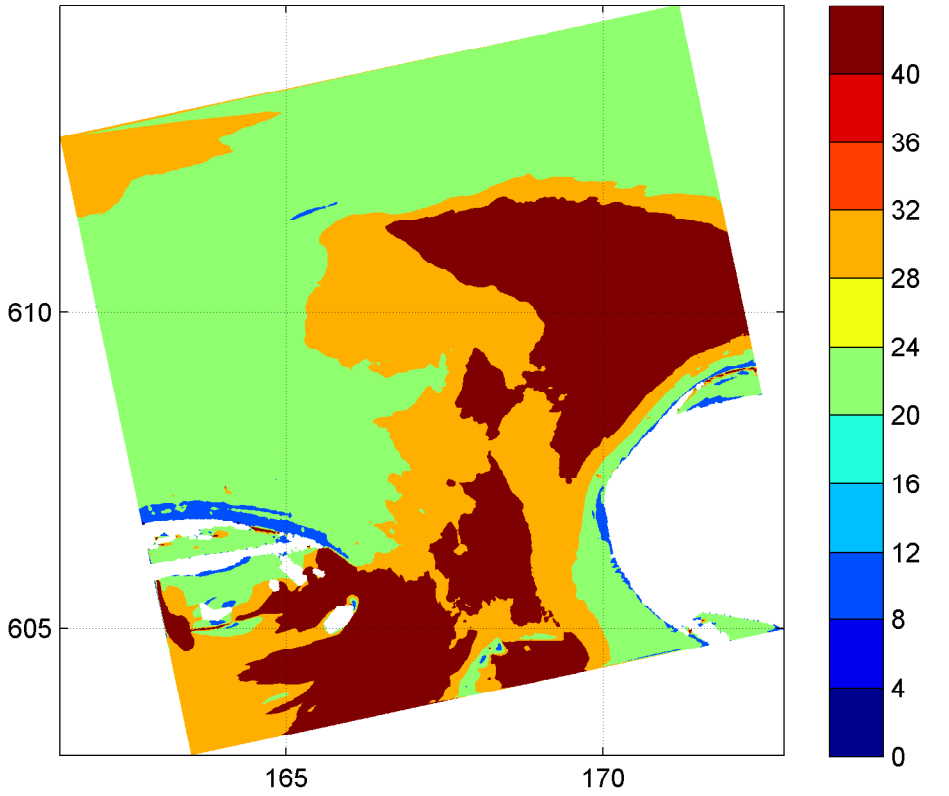

Spatial distribution of wave height [m] and mean wave direction (upper panel) and directional spreading [°] (lower panel) on grid2 WAQUA high resolution	20050102	17:00hr
	Hindcast Ameland Inlet	
WL | DELFT HYDRAULICS	H4803.11	Fig. 3.60c

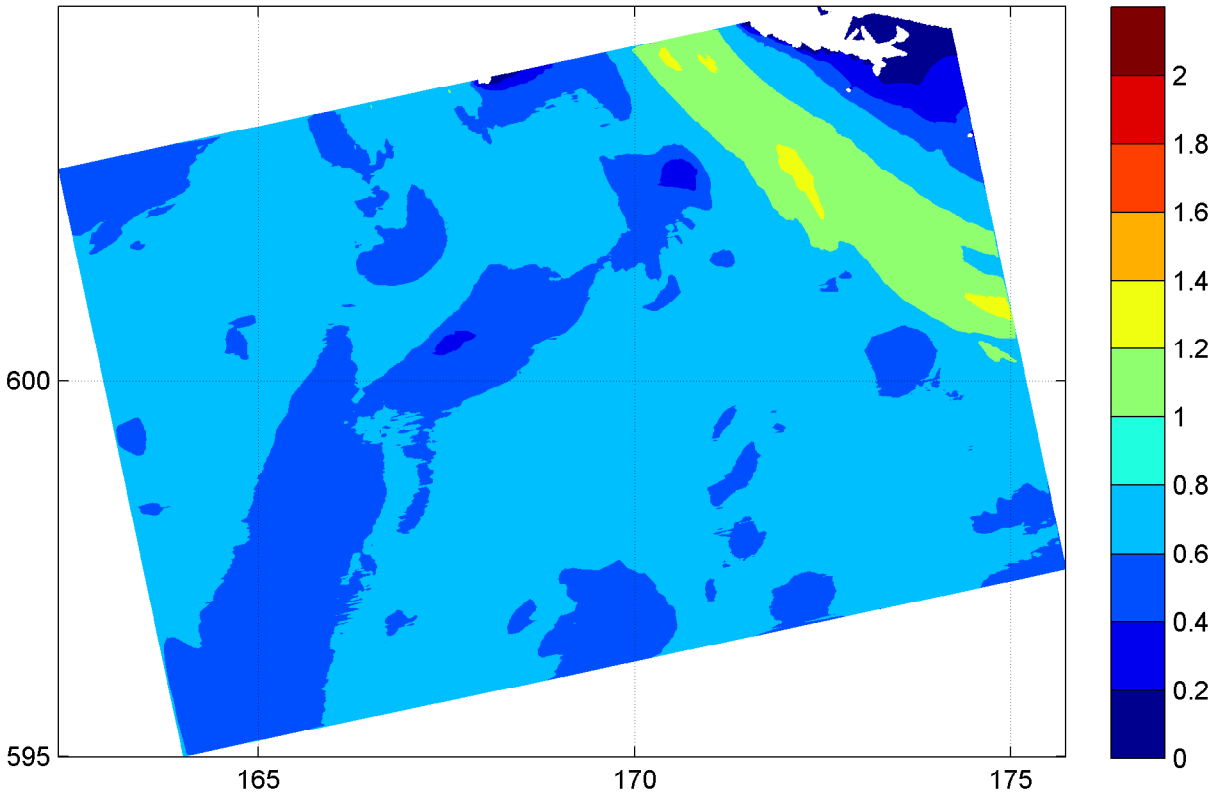

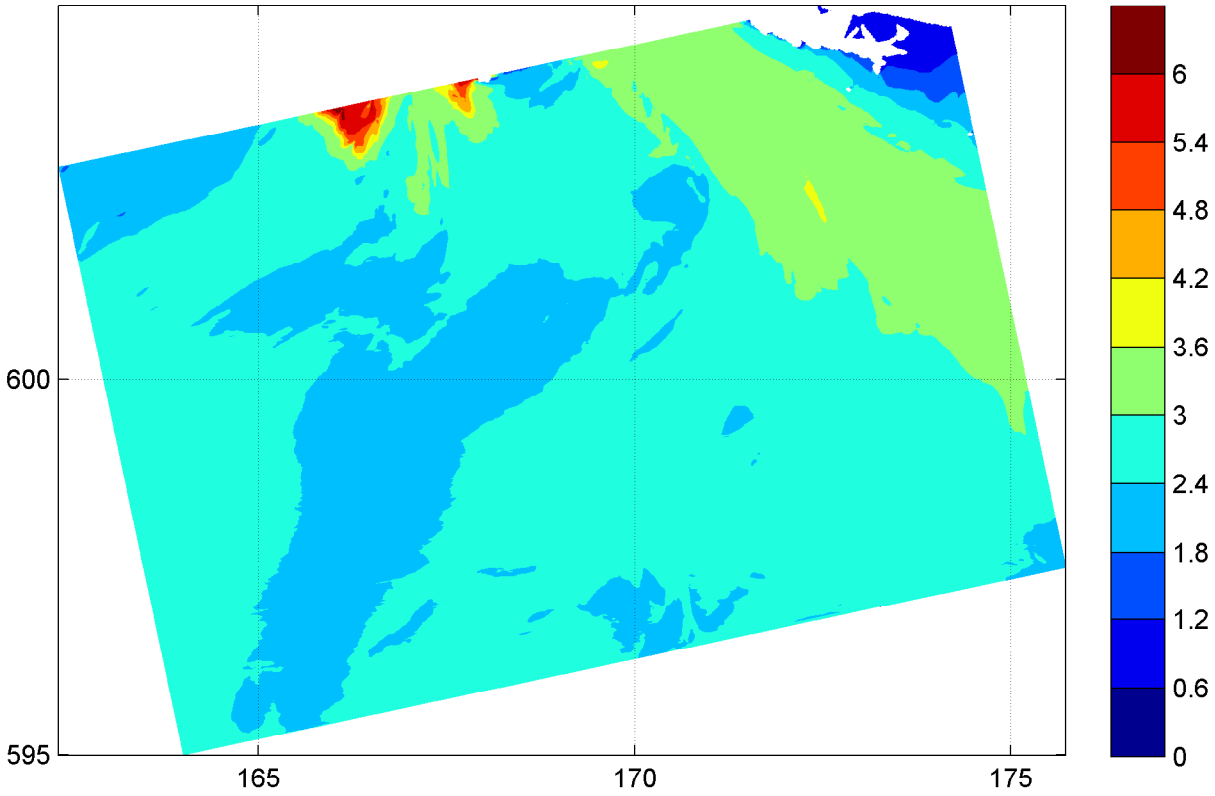

Spatial distribution of wave height H_{m0} [m] (upper panel) and wave period $T_{m-1,0}$ [s] (lower panel) on grid3 WAQUA high resolution	20050102	17:00hr
	Hindcast Ameland Inlet	
WL | DELFT HYDRAULICS	H4803.11	Fig. 3.61a

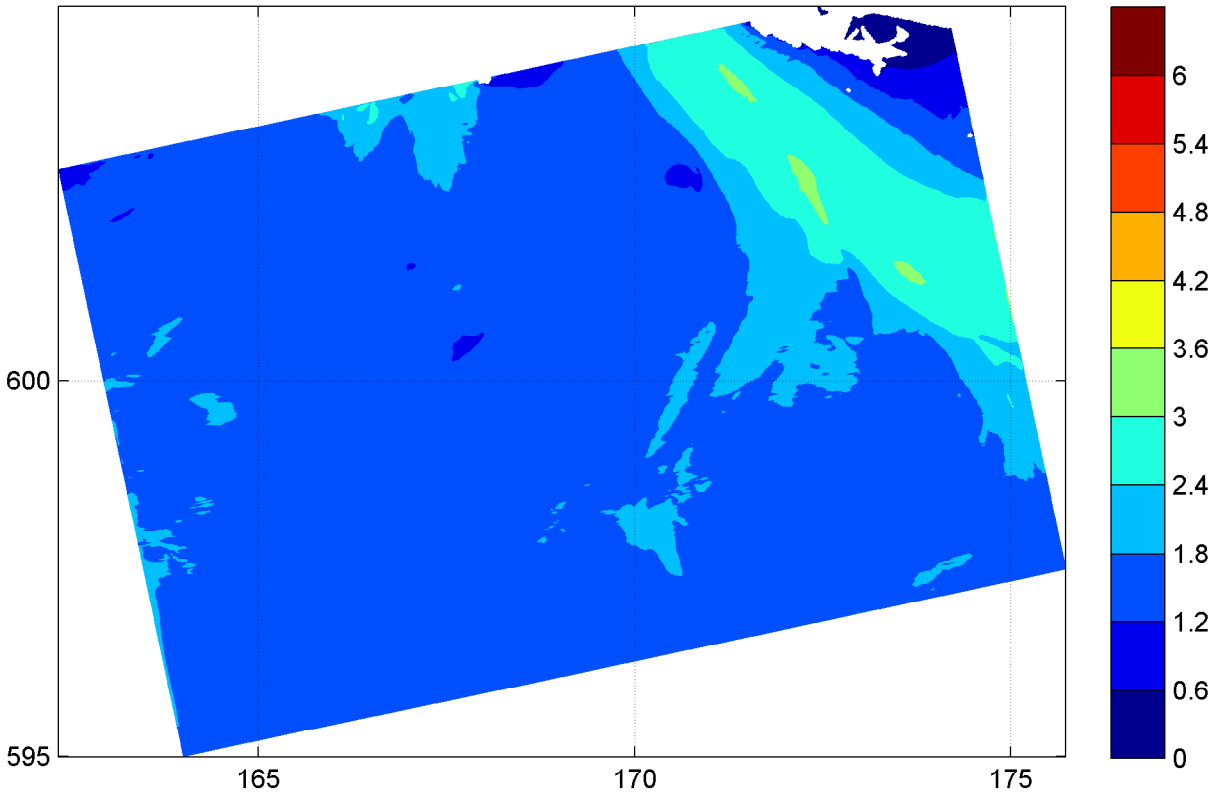

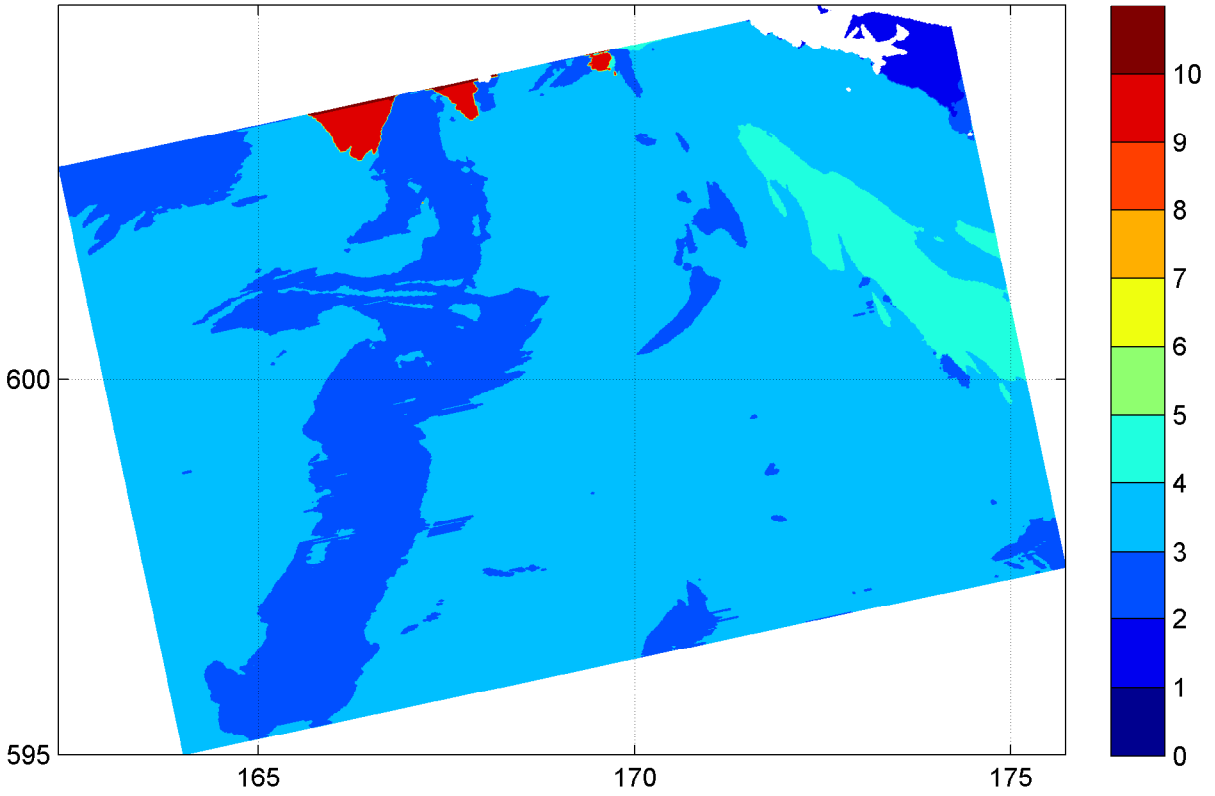

Spatial distribution of wave period T_{m02} [s] (upper panel) and wave period T_p [s] (lower panel) on grid3 WAQUA high resolution	20050102	17:00hr
	Hindcast Ameland Inlet	
WL | DELFT HYDRAULICS	H4803.11	Fig. 3.61b

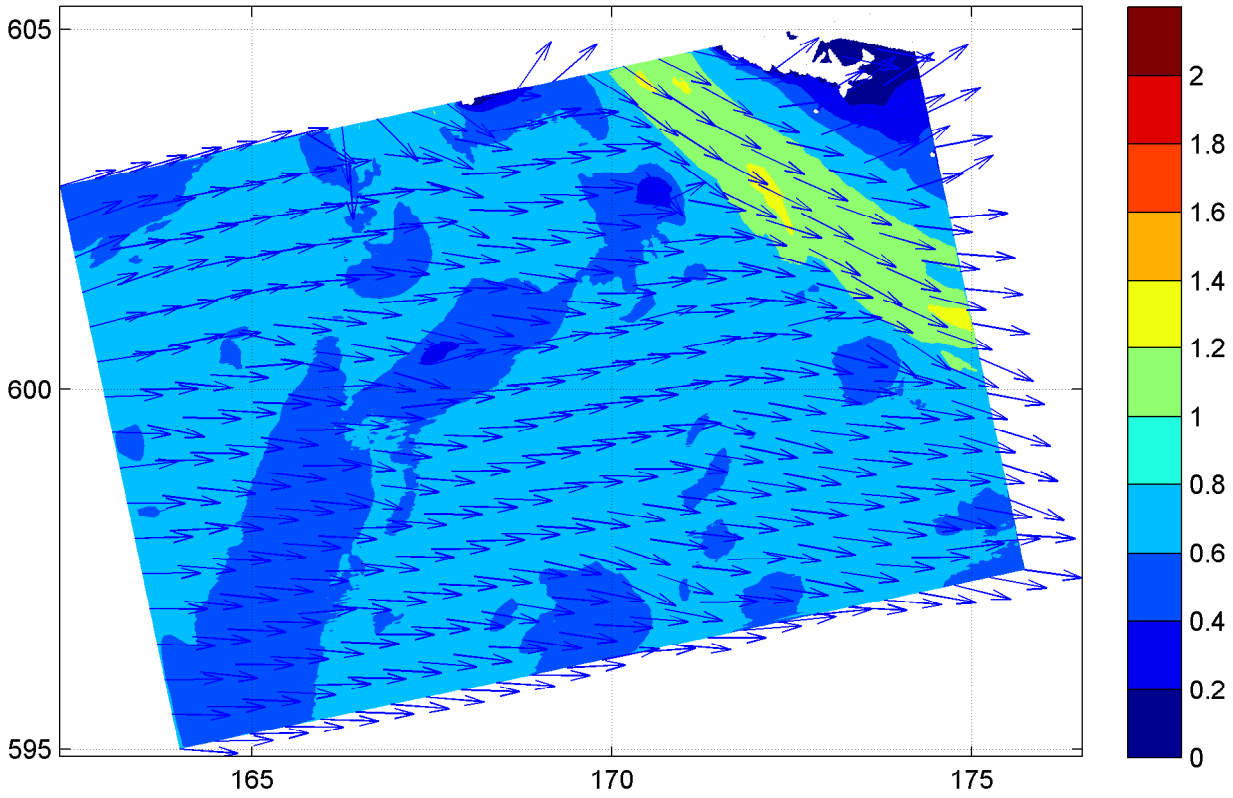

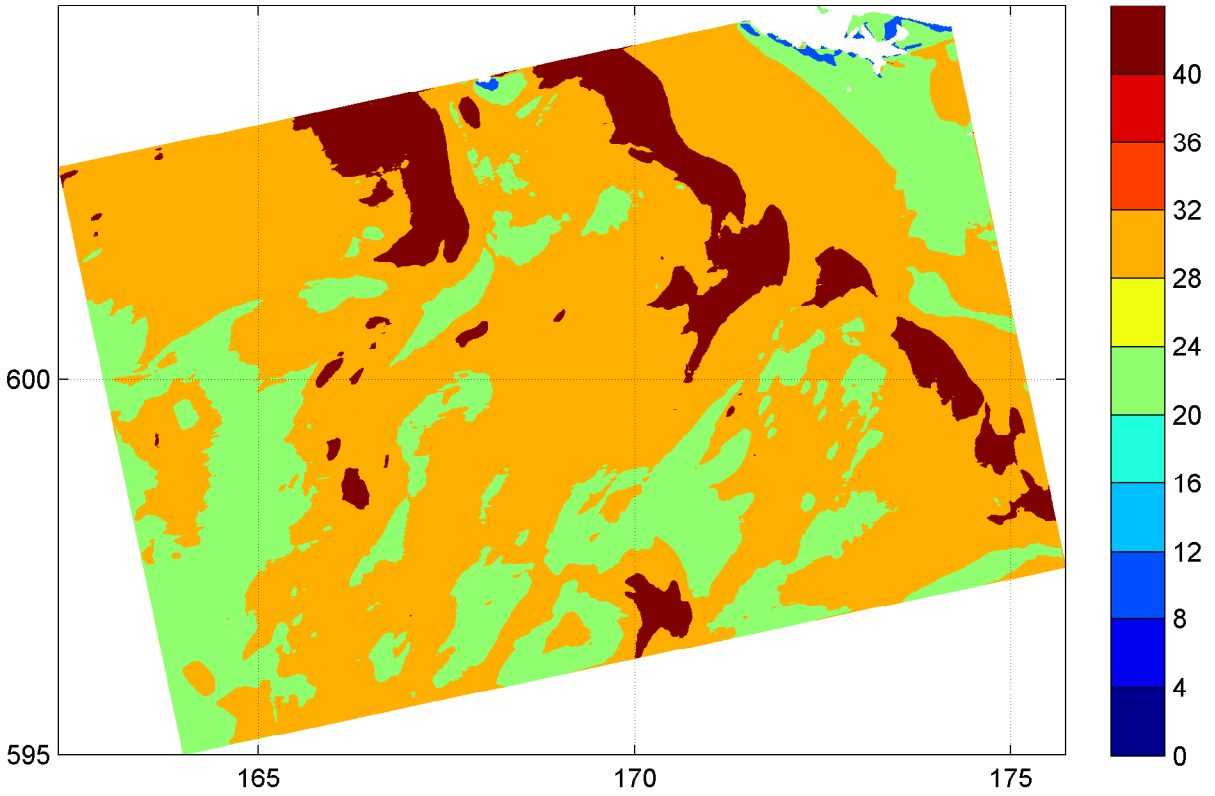

Spatial distribution of wave height [m] and mean wave direction (upper panel) and directional spreading [°] (lower panel) on grid3 WAQUA high resolution	20050102	17:00hr
	Hindcast Ameland Inlet	
WL | DELFT HYDRAULICS	H4803.11	Fig. 3.61c

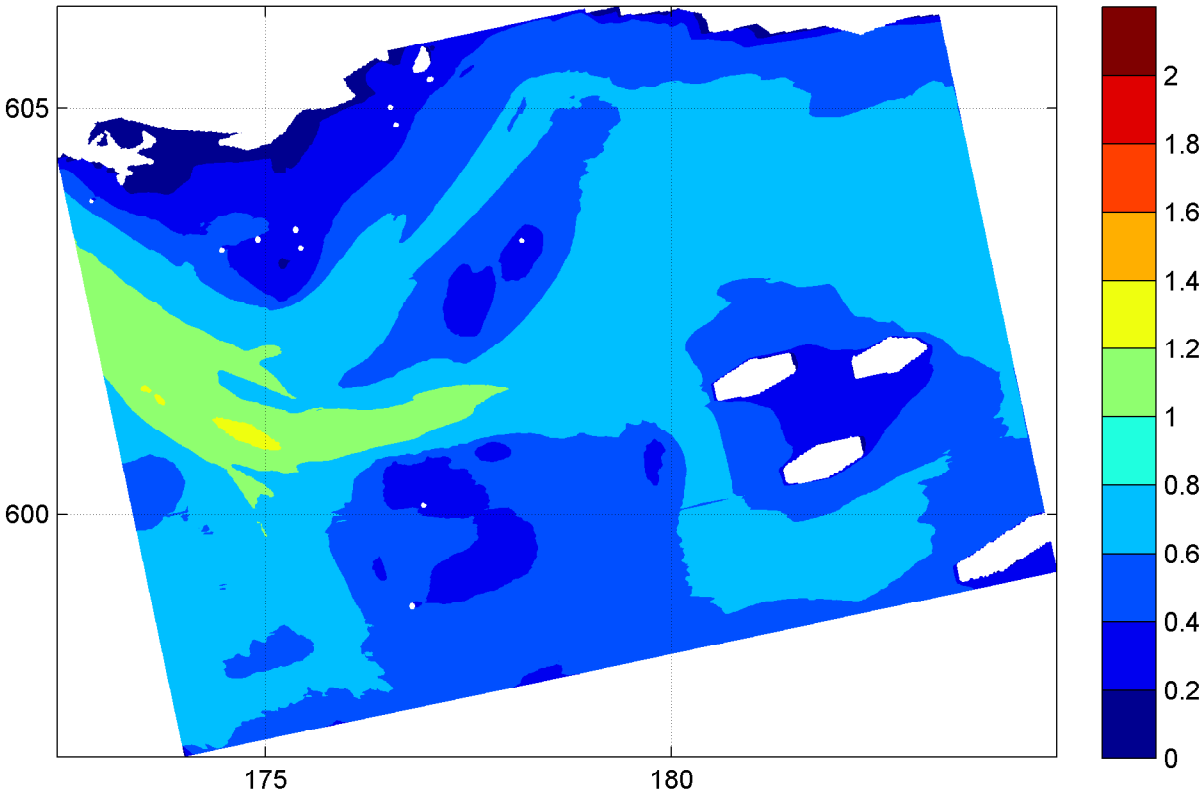

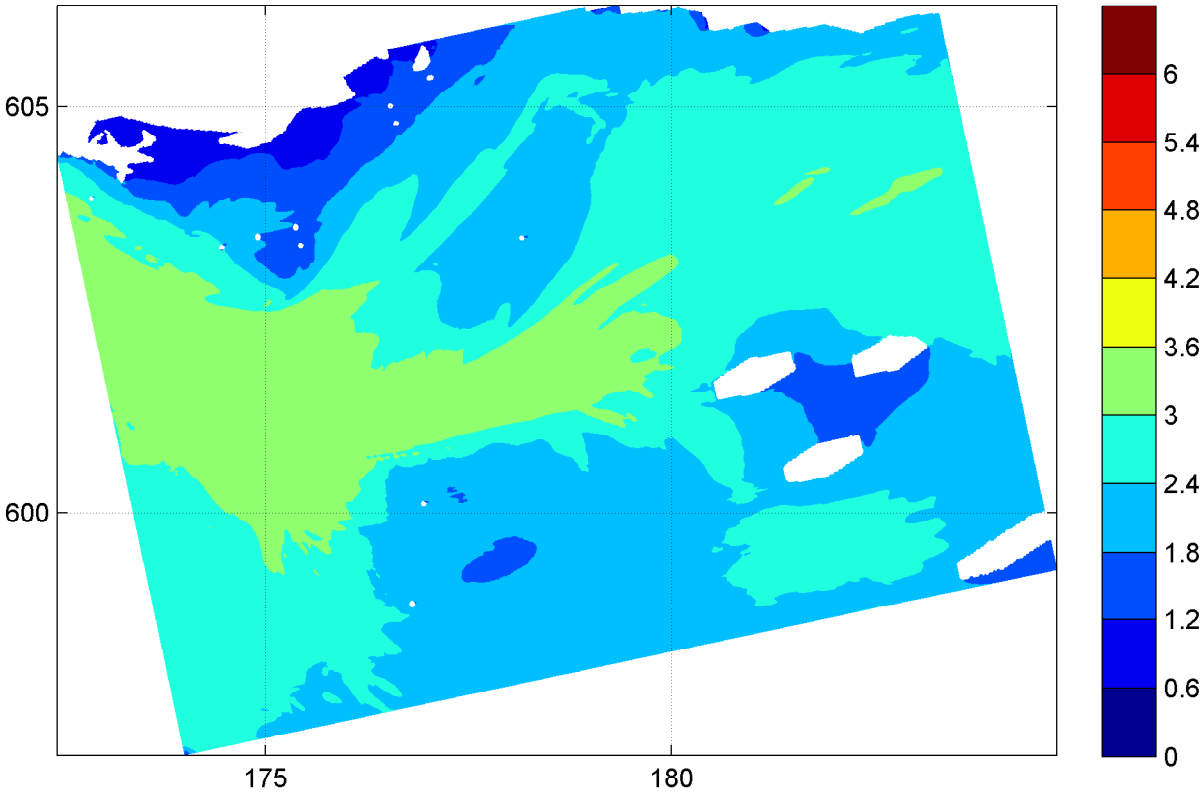

Spatial distribution of wave height H_{m0} [m] (upper panel) and wave period $T_{m-1,0}$ [s] (lower panel) on grid4 WAQUA high resolution	20050102	17:00hr
	Hindcast Ameland Inlet	
WL | DELFT HYDRAULICS	H4803.11	Fig. 3.62a

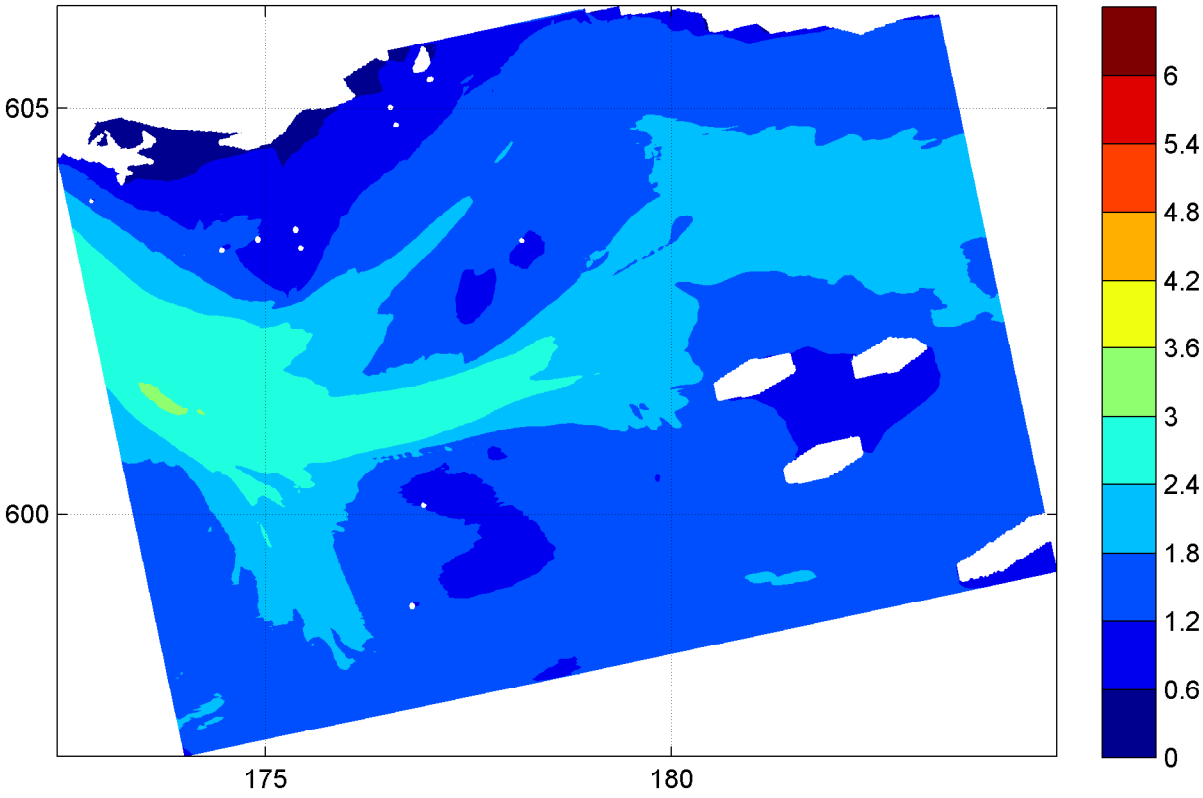

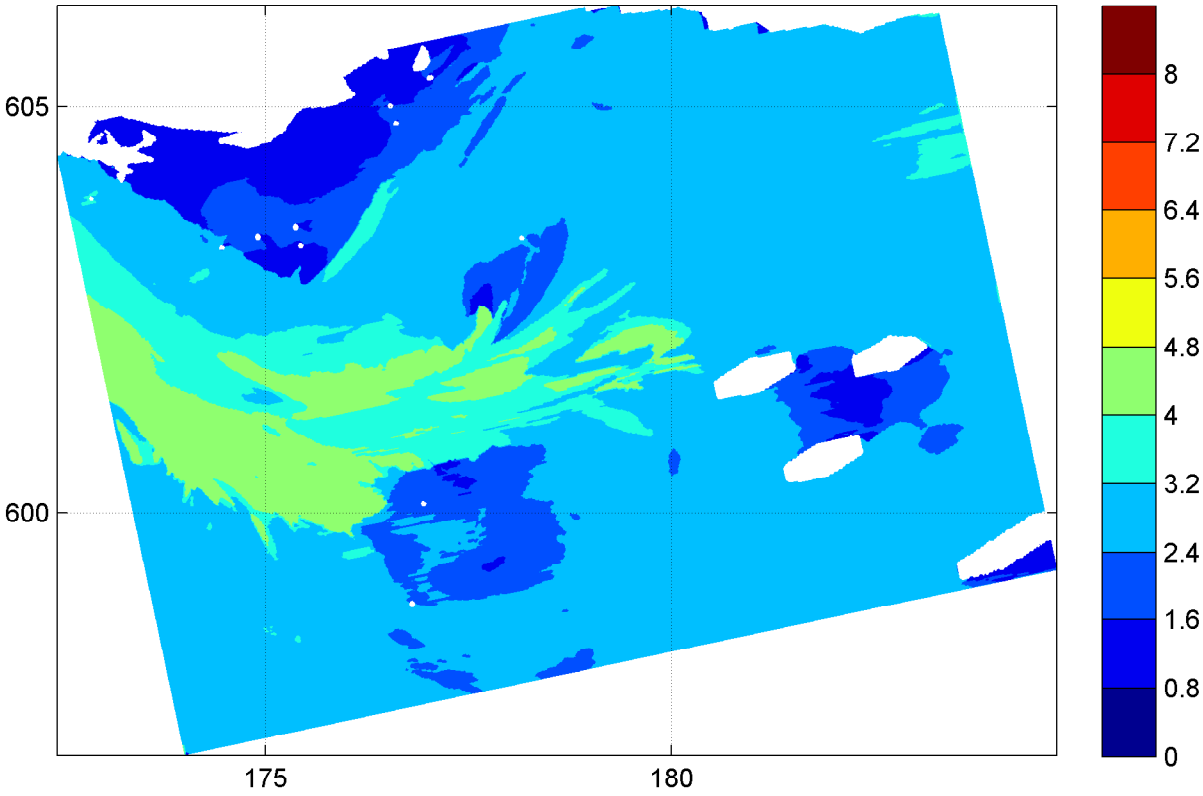

Spatial distribution of wave period T_{m02} [s] (upper panel) and wave period T_p [s] (lower panel) on grid4 WAQUA high resolution	20050102	17:00hr
	Hindcast Ameland Inlet	
WL | DELFT HYDRAULICS	H4803.11	Fig. 3.62b

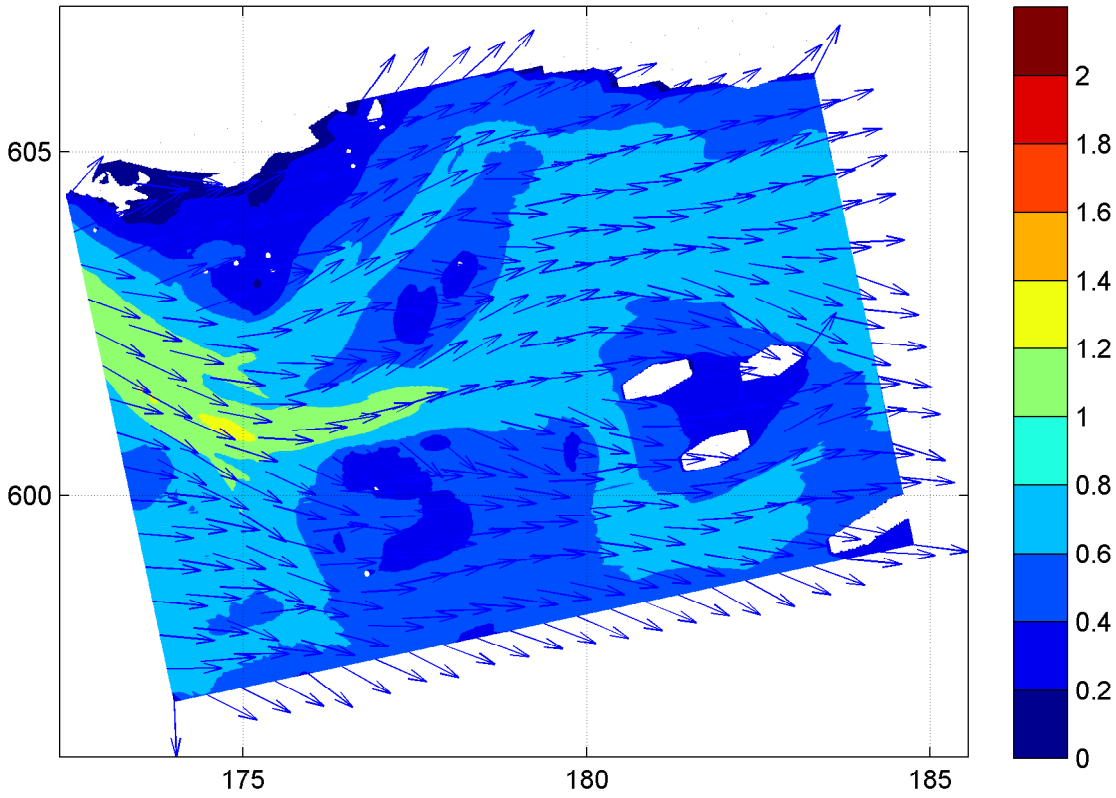

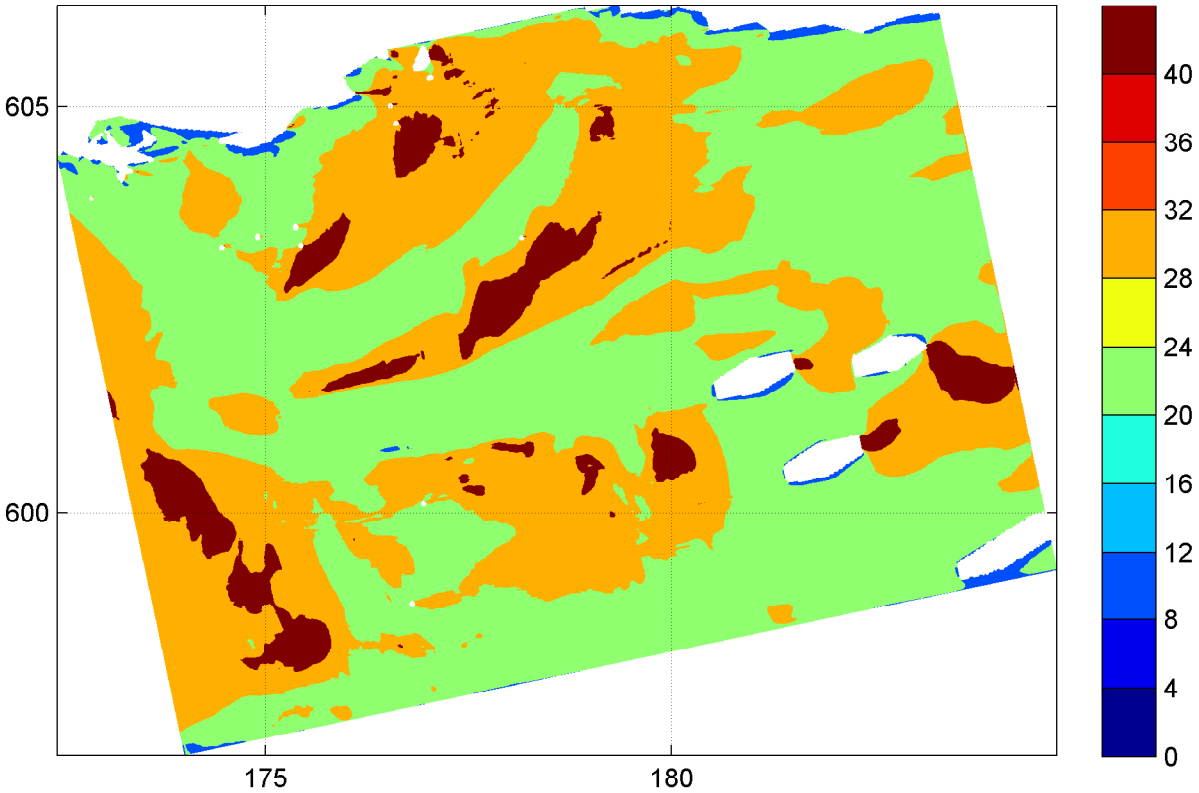

Spatial distribution of wave height [m] and mean wave direction (upper panel) and directional spreading [°] (lower panel) on grid4 WAQUA high resolution	20050102	17:00hr
	Hindcast Ameland Inlet	
WL | DELFT HYDRAULICS	H4803.11	Fig. 3.62c

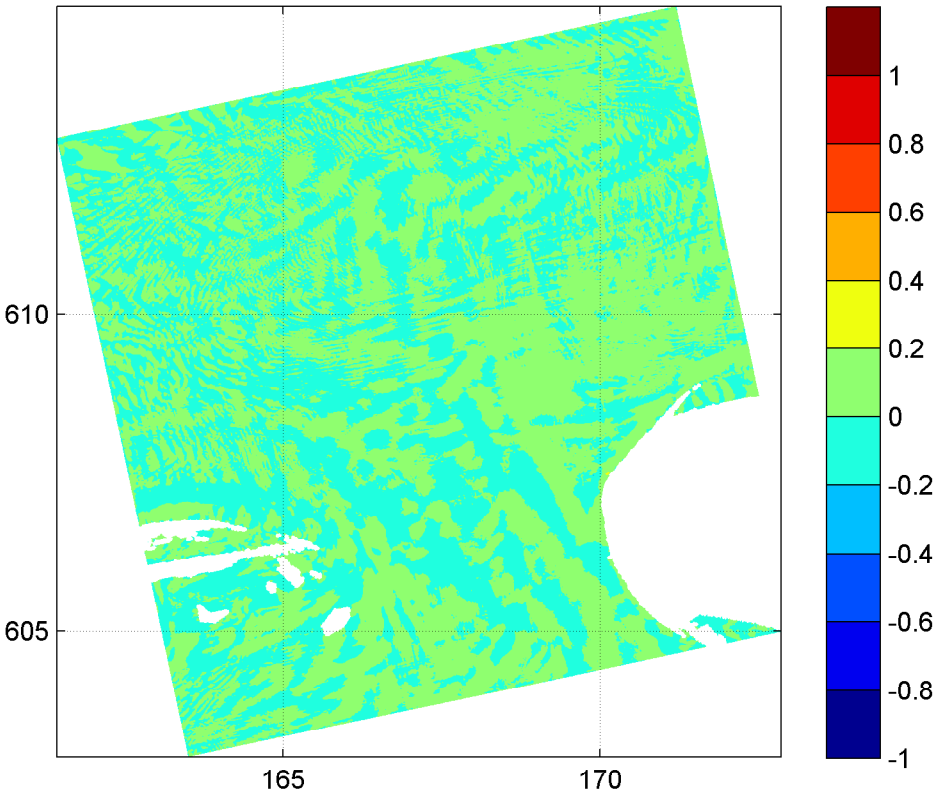

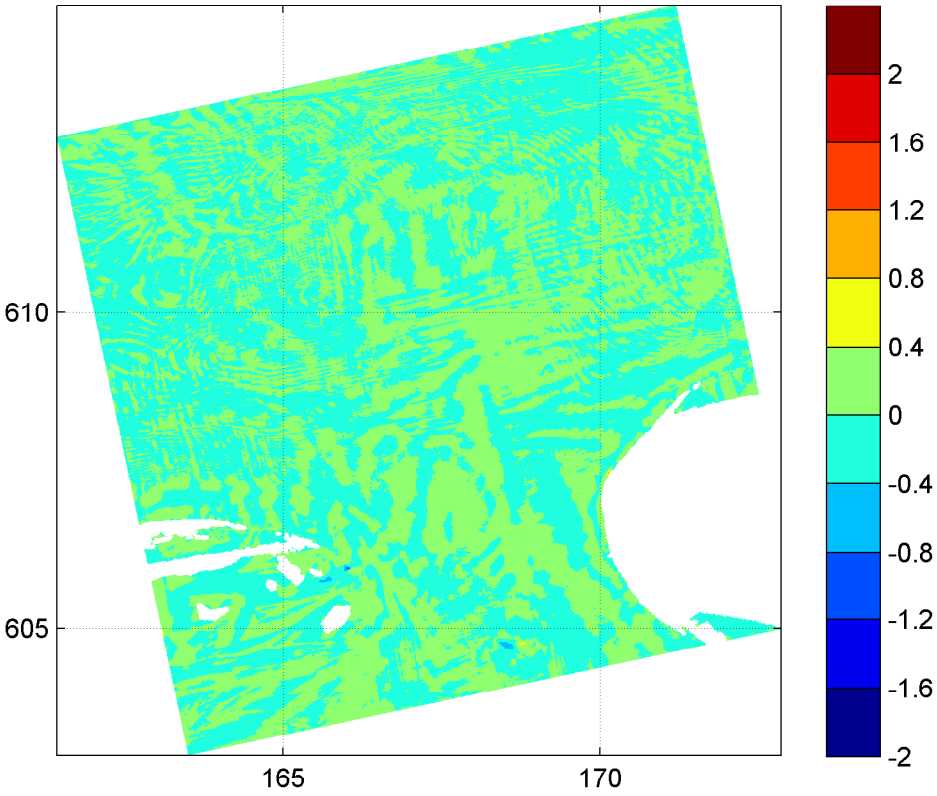

Difference plot of spatial distribution of wave height H_{m0} [m] (upper panel) and wave period $T_{m-1,0}$ [s] (lower panel) on grid2 Difference = results with coarse WAQUA grid - results with fine WAQUA grid	20050102	1700hr
	Hindcast Ameland Inlet	
WL | DELFT HYDRAULICS	H4803.11	Fig. 3.63a

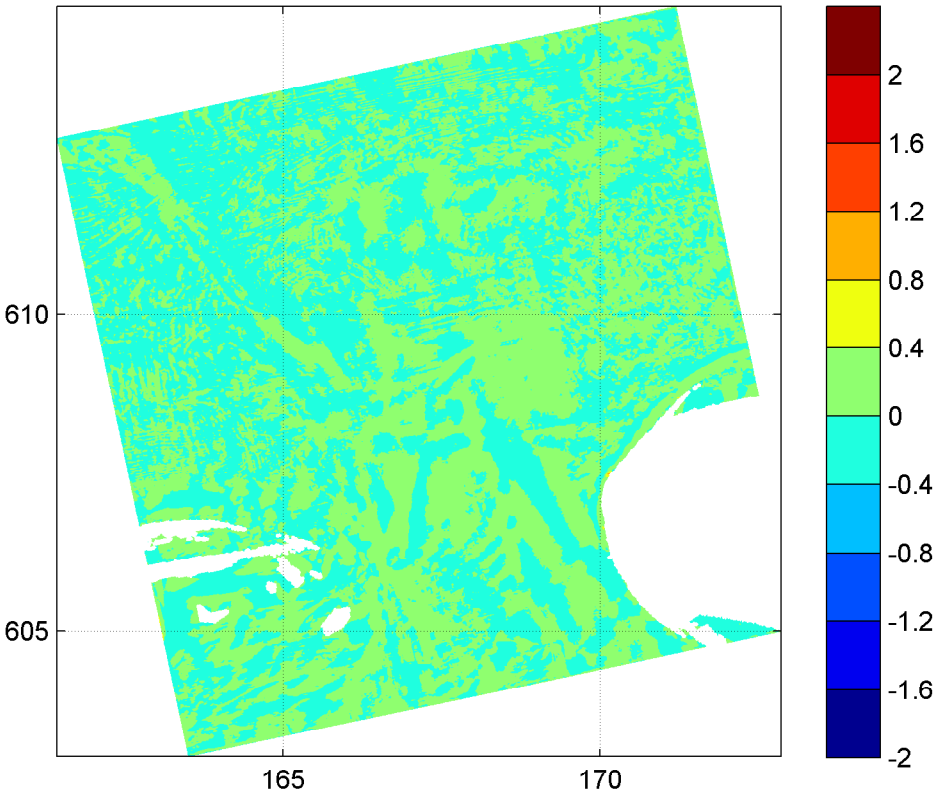

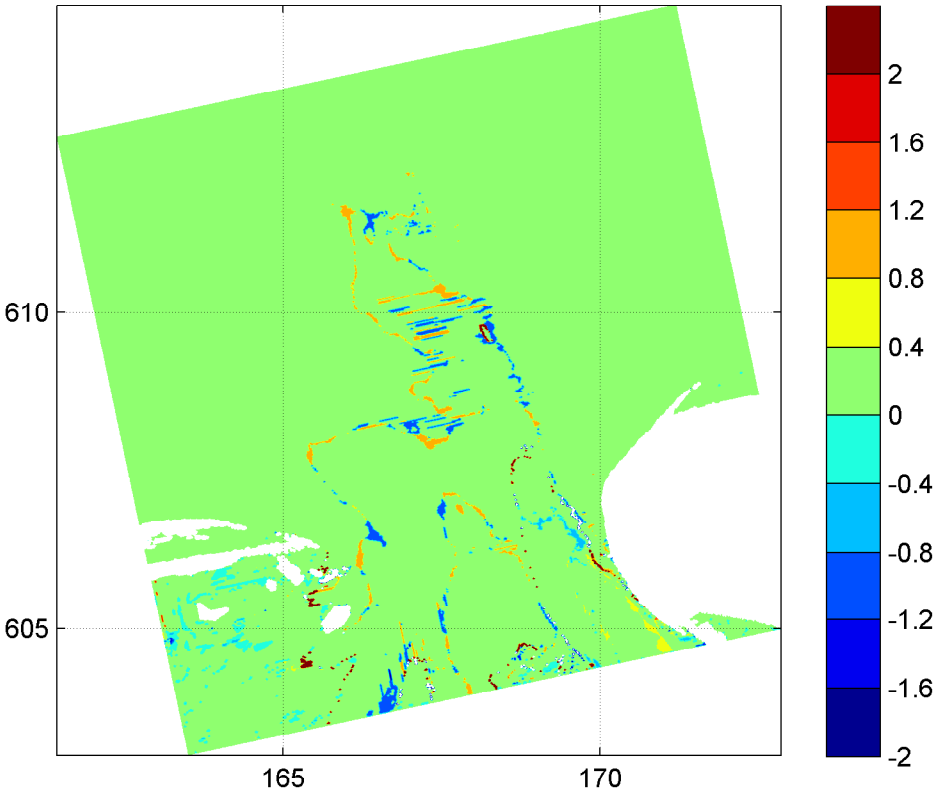

Difference plot of spatial distribution of wave period T_{m02} [s] (upper panel) and wave period T_p [s] (lower panel) on grid2 Difference = results with coarse WAQUA grid - results with fine WAQUA grid	20050102	1700hr
	Hindcast Ameland Inlet	
WL | DELFT HYDRAULICS	H4803.11	Fig. 3.63b

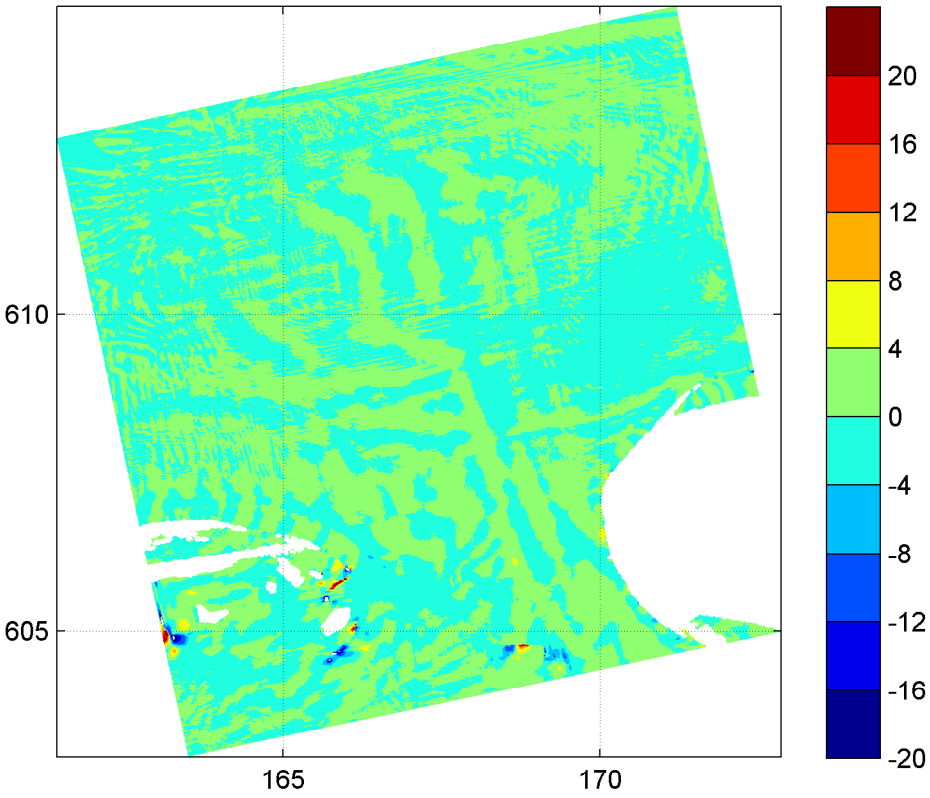

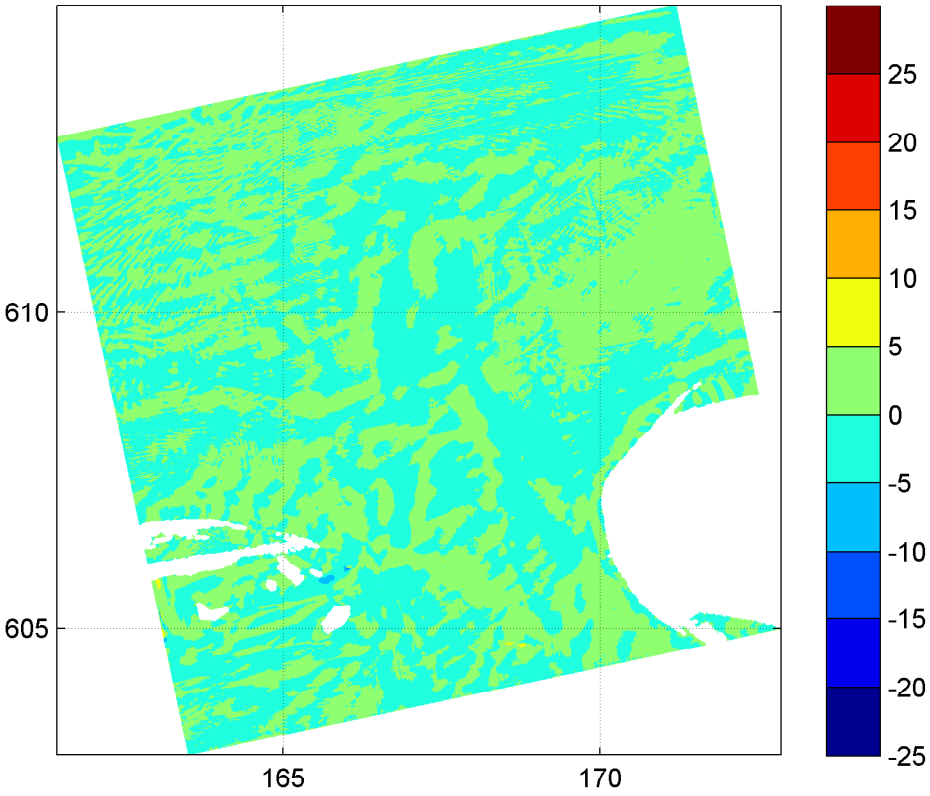

Difference plot of spatial distribution of mean wave direction [°] (upper panel) and directional spreading [°] (lower panel) on grid2 Difference = results with coarse WAQUA grid - results with fine WAQUA grid	20050102	1700hr
	Hindcast Ameland Inlet	
WL | DELFT HYDRAULICS	H4803.11	Fig. 3.63c

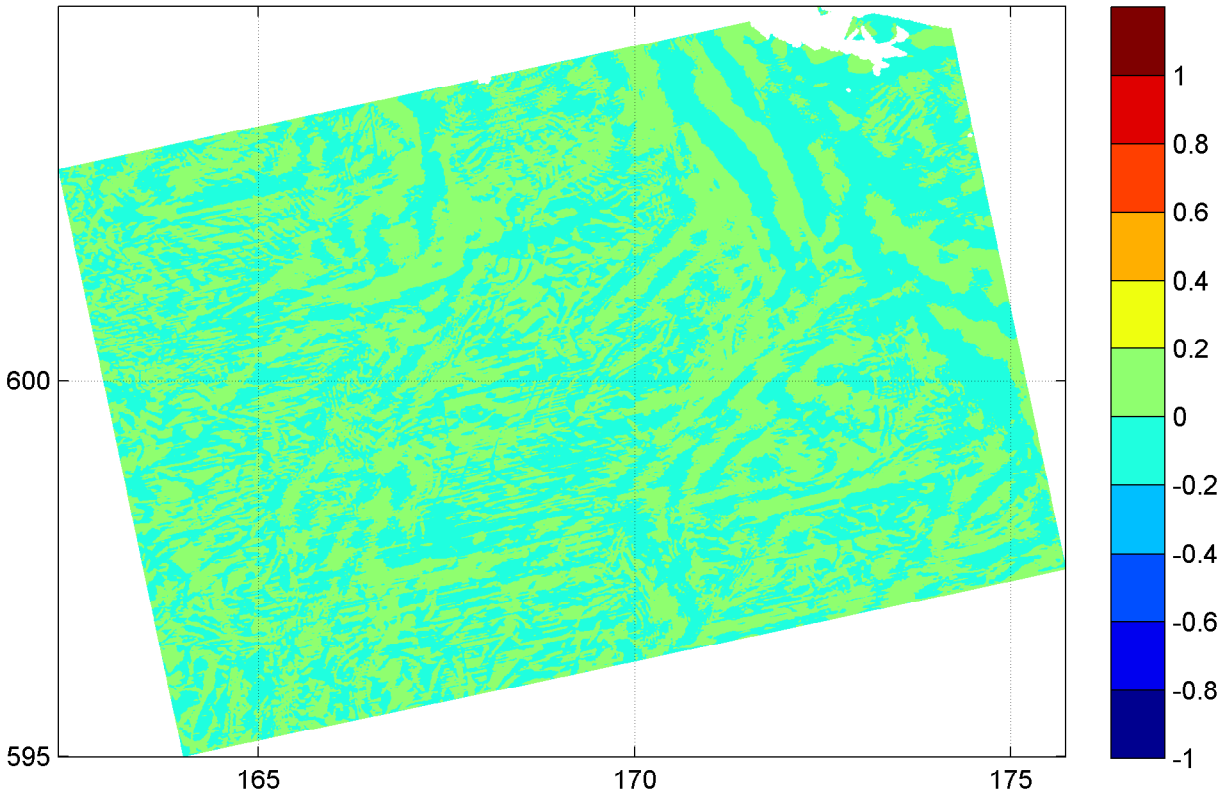

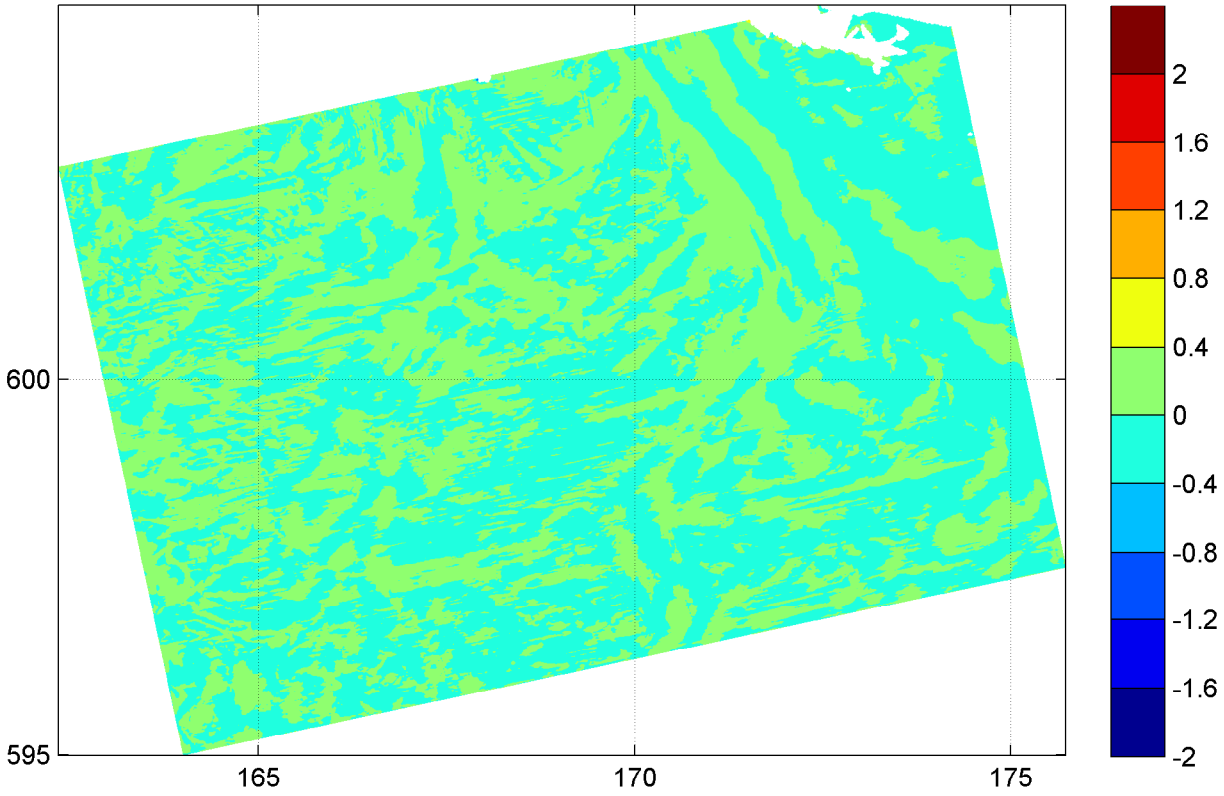

Difference plot of spatial distribution of wave height H_{m0} [m] (upper panel) and wave period $T_{m-1,0}$ [s] (lower panel) on grid3 Difference = results with coarse WAQUA grid - results with fine WAQUA grid	20050102	1700hr
	Hindcast Ameland Inlet	
WL | DELFT HYDRAULICS	H4803.11	Fig. 3.64a

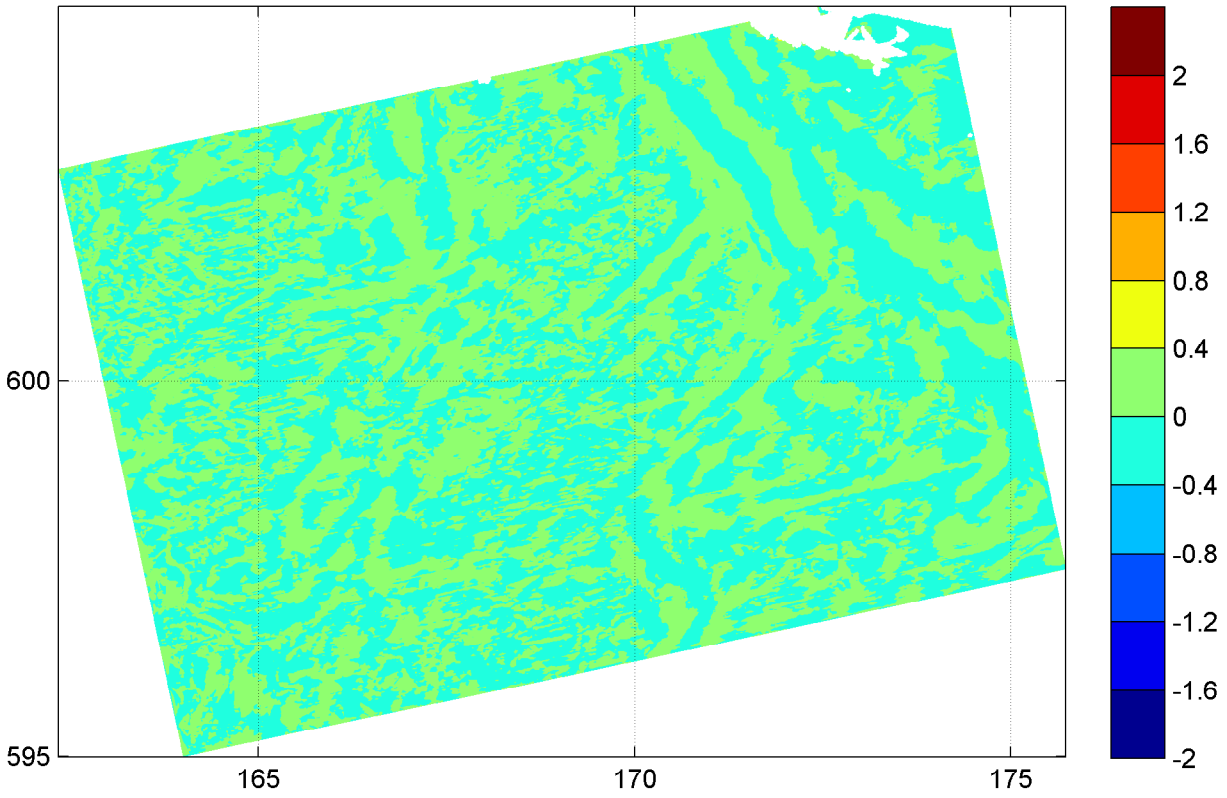

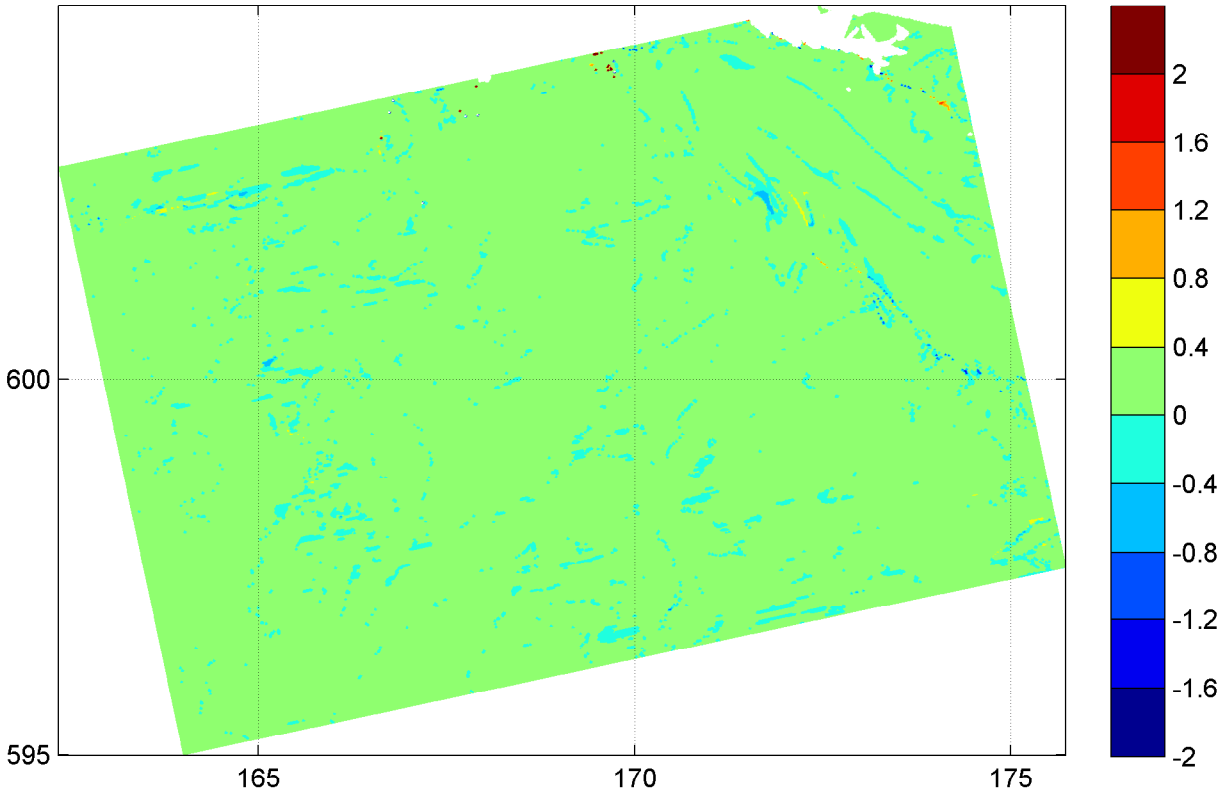

Difference plot of spatial distribution of wave period T_{m02} [s] (upper panel) and wave period T_p [s] (lower panel) on grid3 Difference = results with coarse WAQUA grid - results with fine WAQUA grid	20050102	1700hr
	Hindcast Ameland Inlet	
WL | DELFT HYDRAULICS	H4803.11	Fig. 3.64b

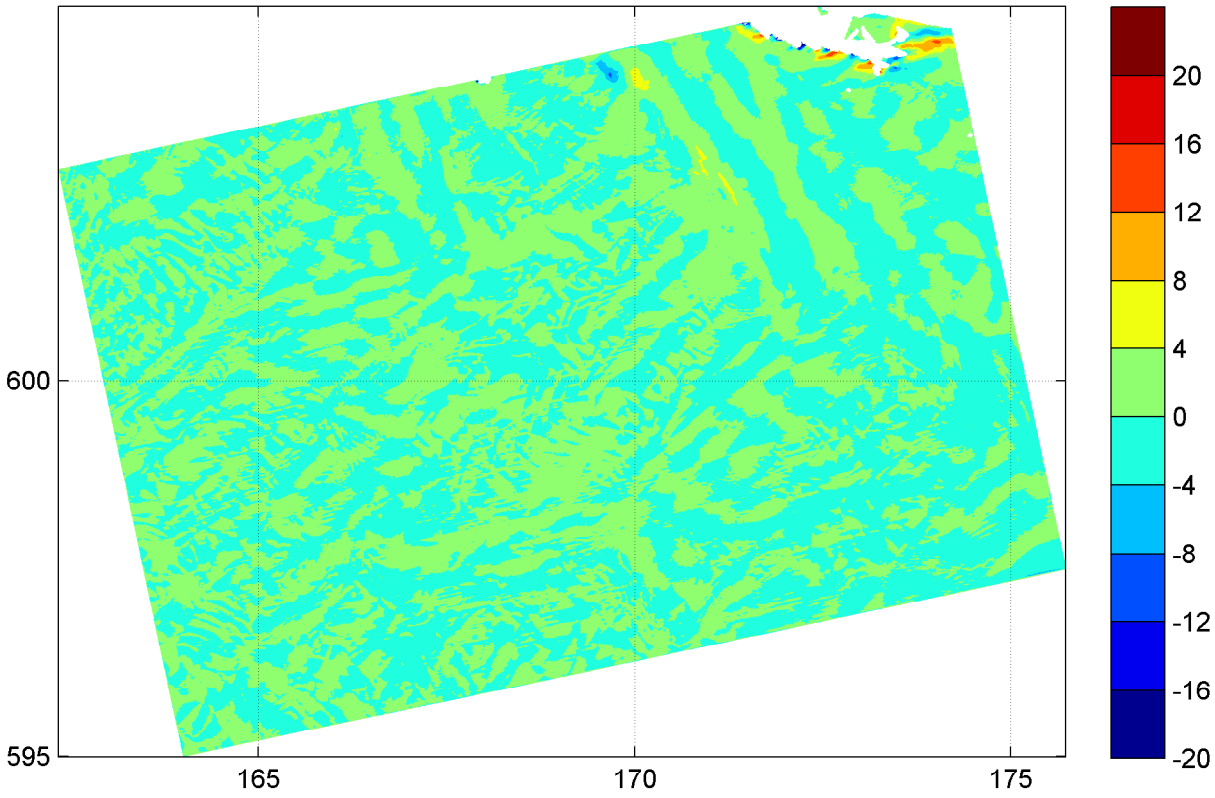

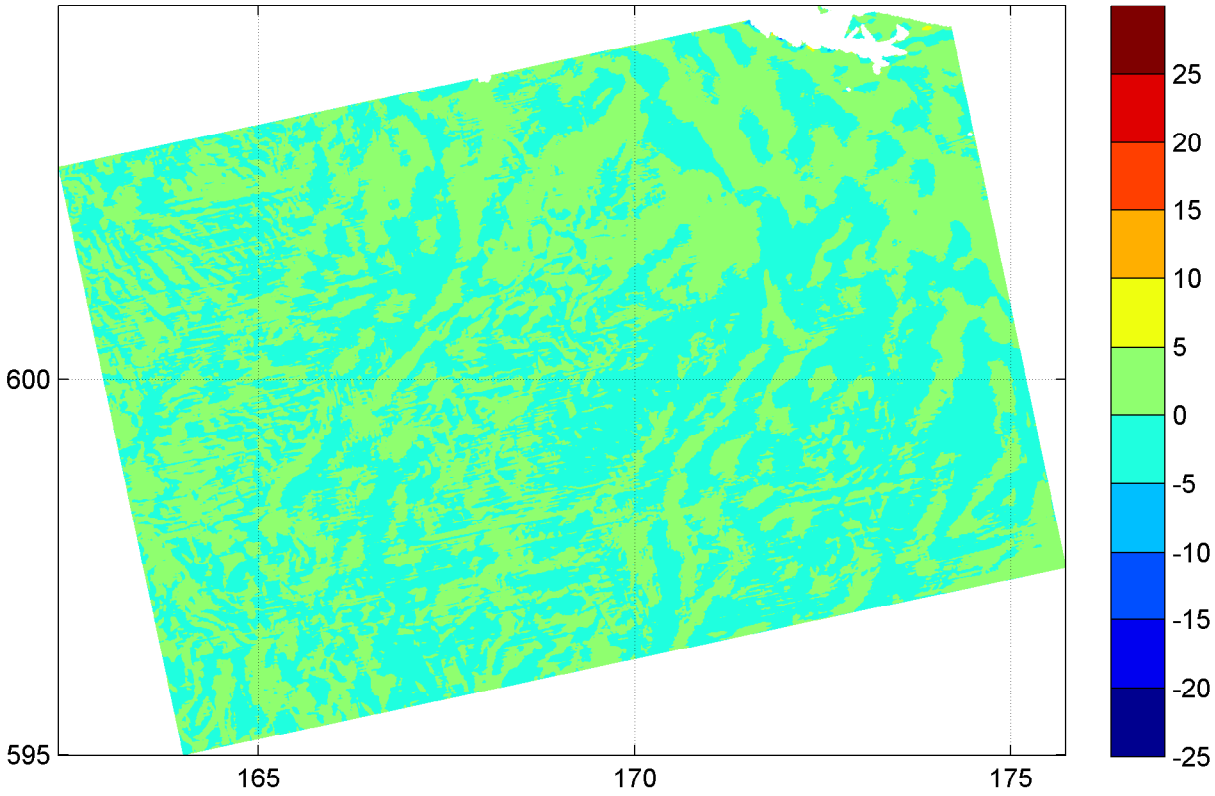

Difference plot of spatial distribution of mean wave direction [°] (upper panel) and directional spreading [°] (lower panel) on grid3 Difference = results with coarse WAQUA grid - results with fine WAQUA grid	20050102	1700hr
	Hindcast Ameland Inlet	
WL | DELFT HYDRAULICS	H4803.11	Fig. 3.64c

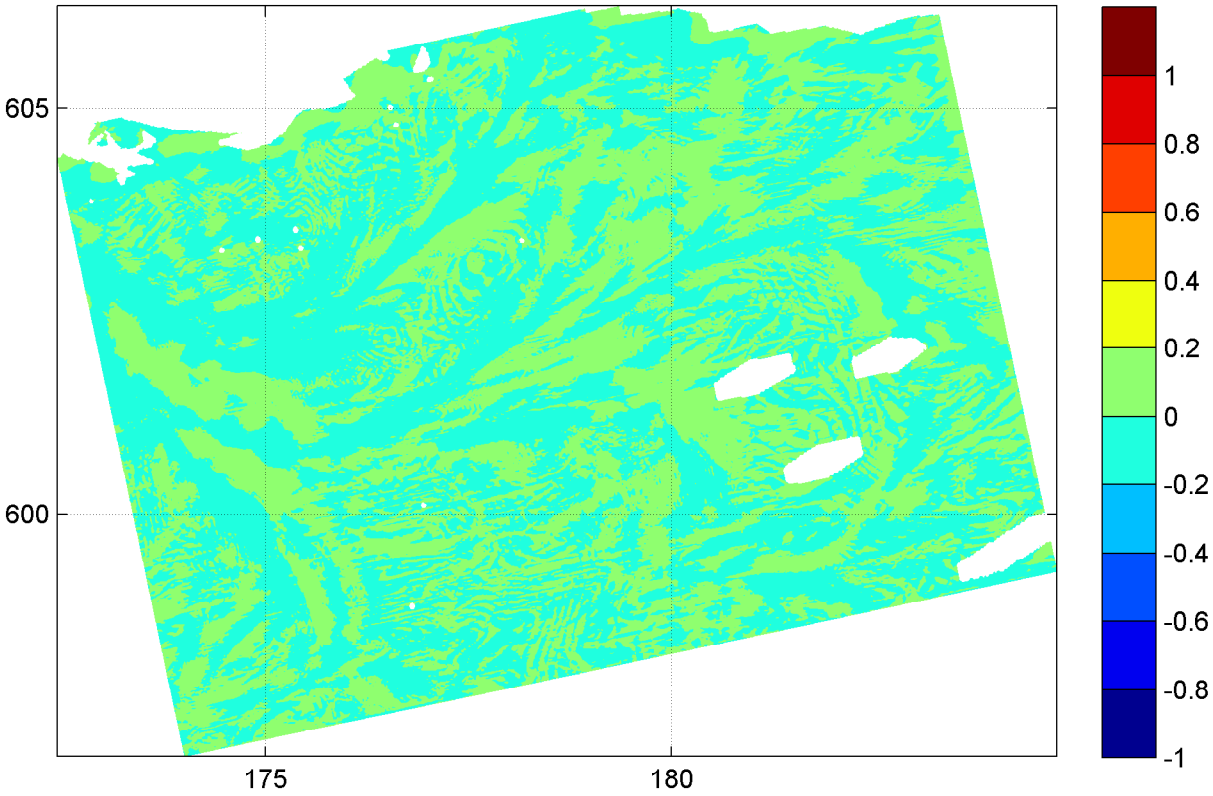

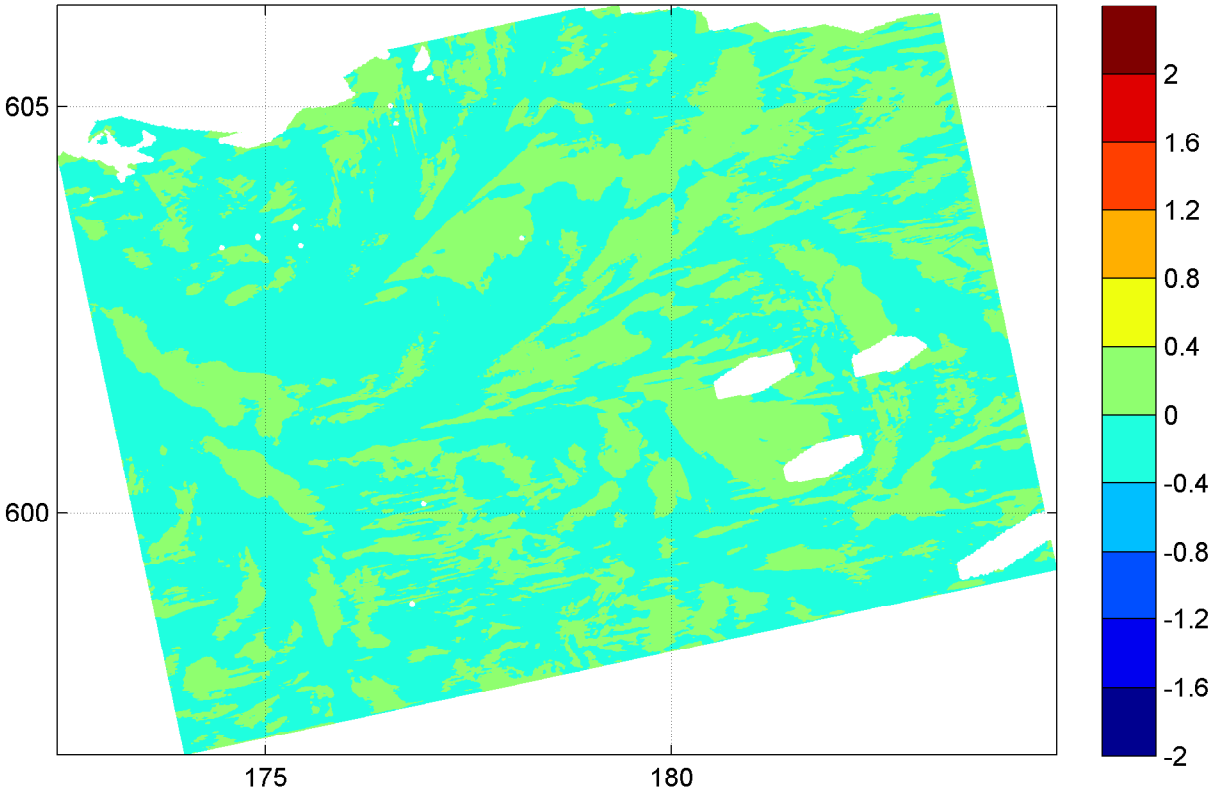

Difference plot of spatial distribution of wave height H_{m0} [m] (upper panel) and wave period $T_{m-1,0}$ [s] (lower panel) on grid4 Difference = results with coarse WAQUA grid - results with fine WAQUA grid	20050102	1700hr
	Hindcast Ameland Inlet	
WL | DELFT HYDRAULICS	H4803.11	Fig. 3.65a

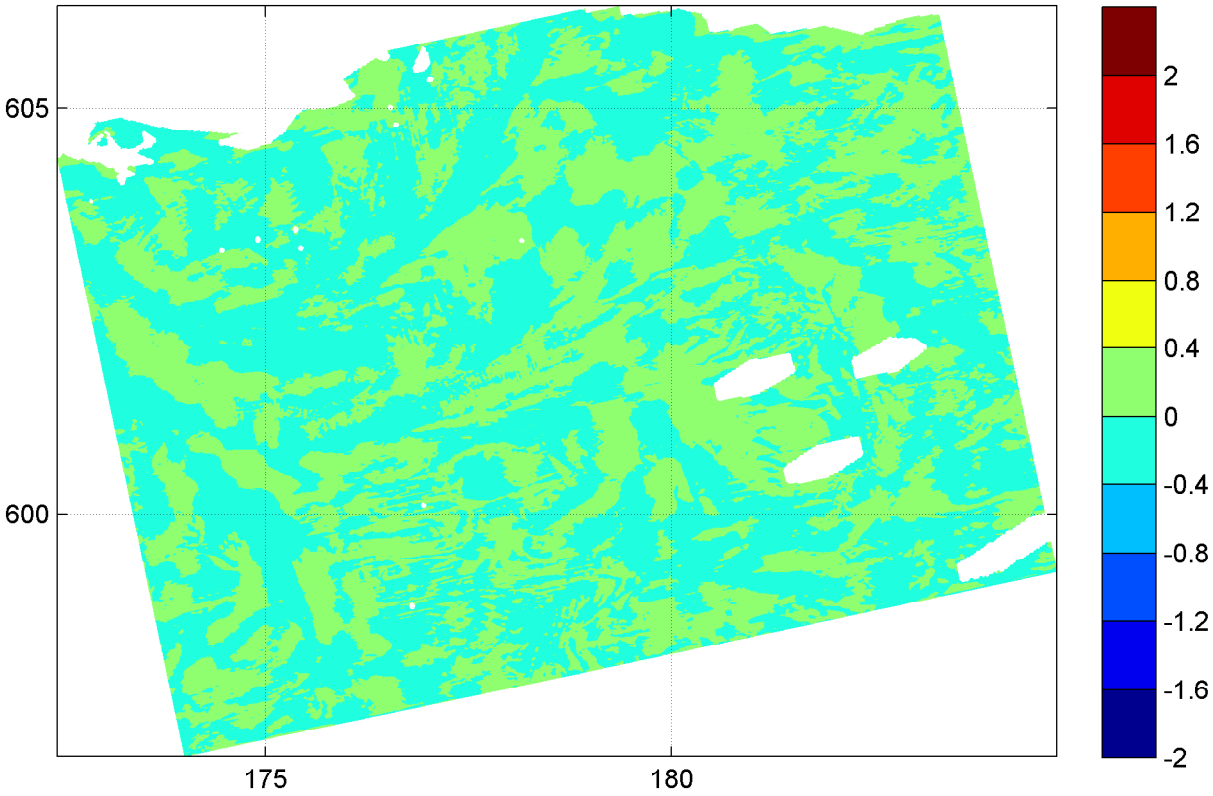

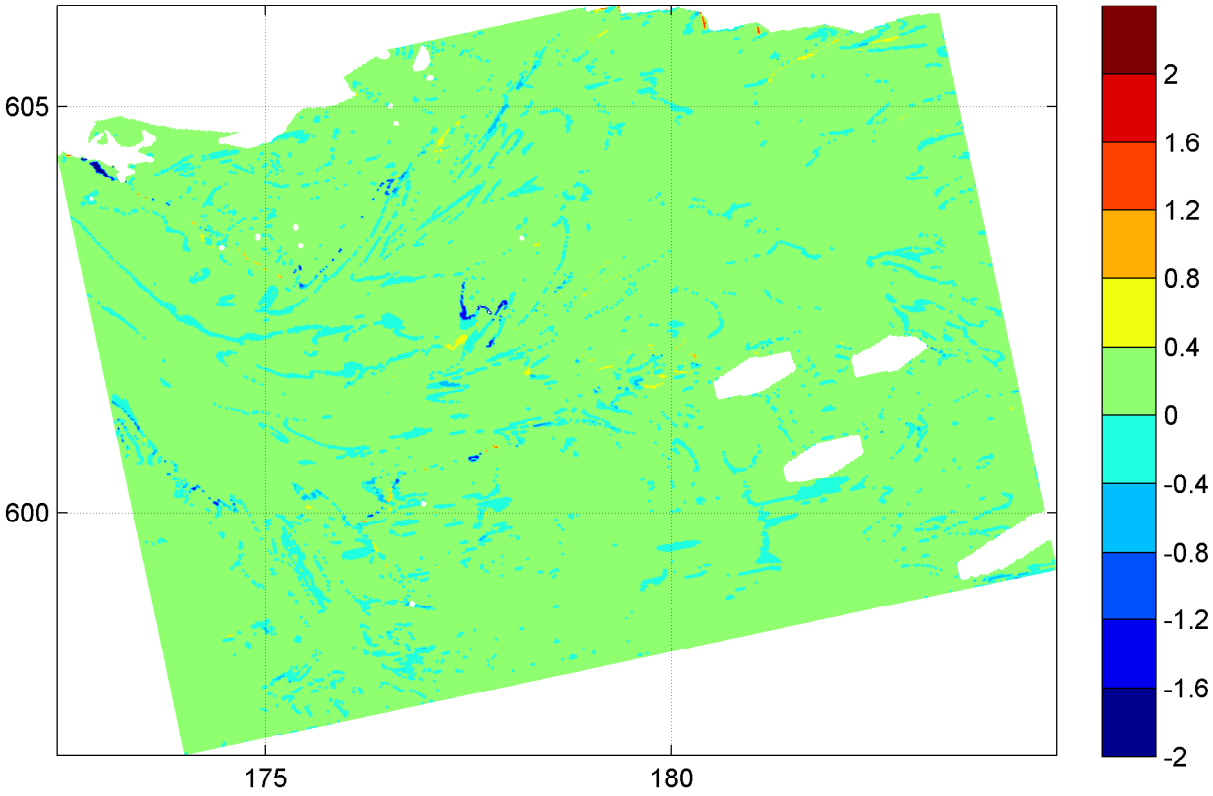

Difference plot of spatial distribution of wave period T_{m02} [s] (upper panel) and wave period T_p [s] (lower panel) on grid4 Difference = results with coarse WAQUA grid - results with fine WAQUA grid	20050102	1700hr
	Hindcast Ameland Inlet	
WL | DELFT HYDRAULICS	H4803.11	Fig. 3.65b

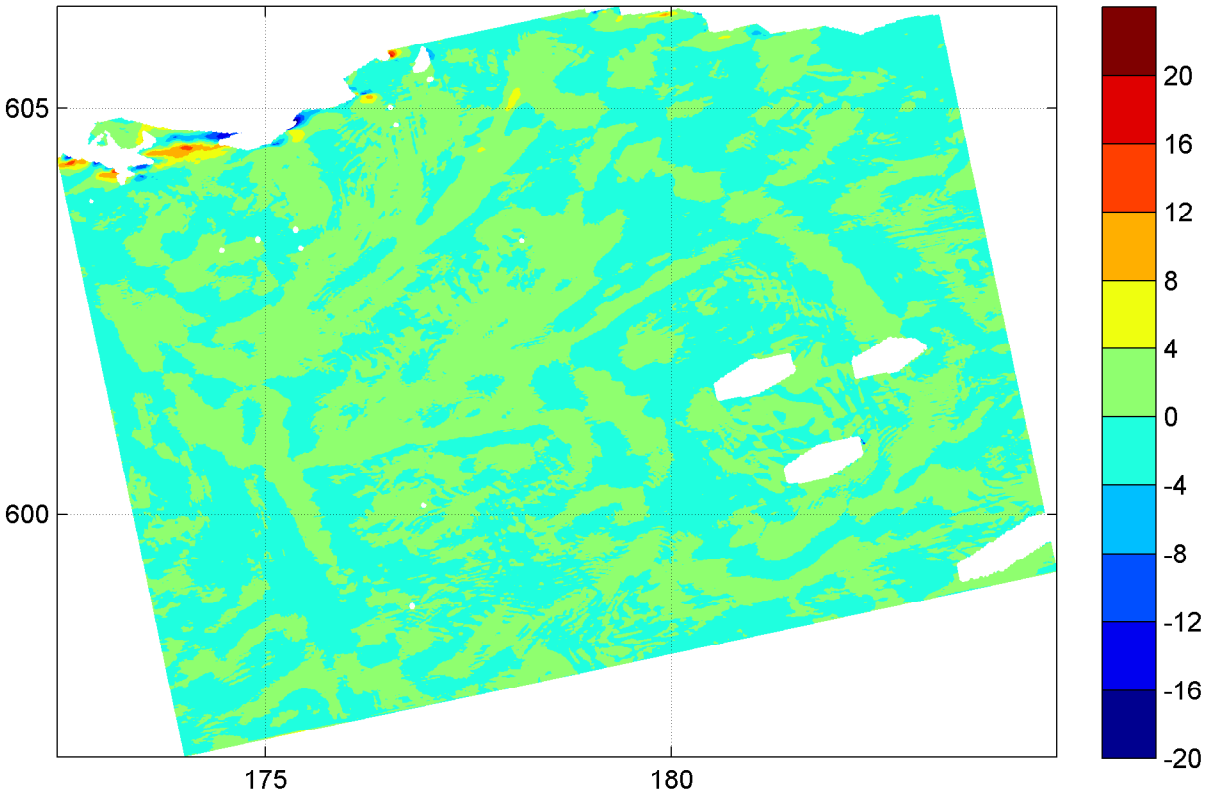

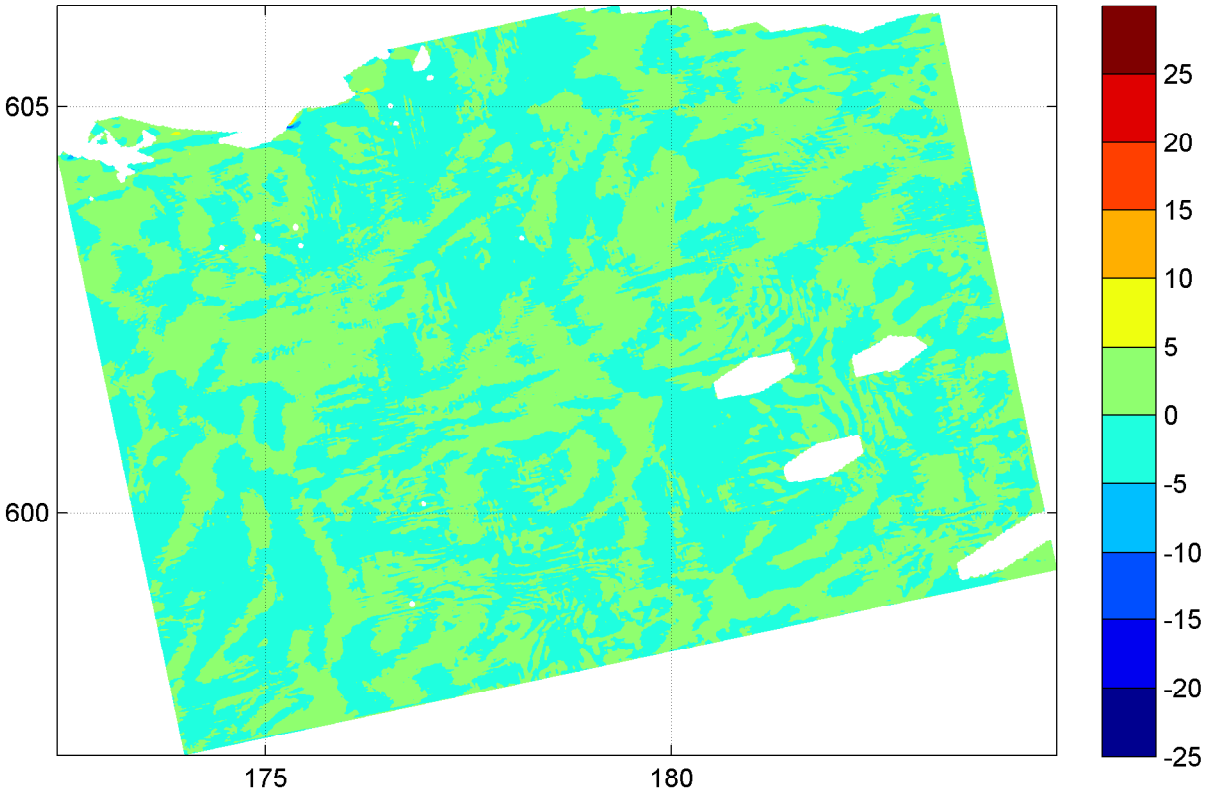

Difference plot of spatial distribution of mean wave direction [°] (upper panel) and directional spreading [°] (lower panel) on grid4 Difference = results with coarse WAQUA grid - results with fine WAQUA grid	20050102	1700hr
	Hindcast Ameland Inlet	
WL | DELFT HYDRAULICS	H4803.11	Fig. 3.65c

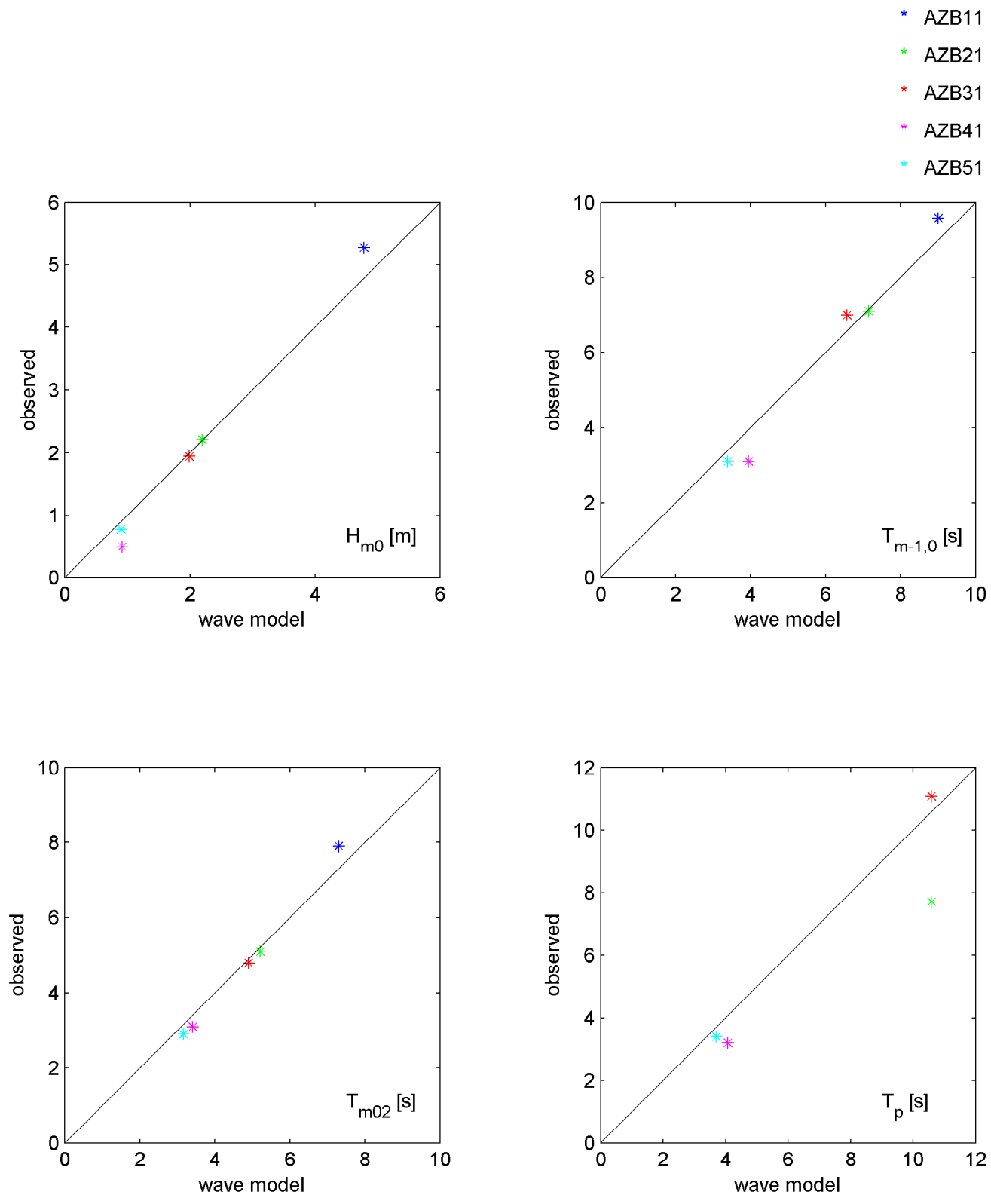

Scatter plot of wave parameters H_{m0} (upper left panel), $T_{m-1,0}$ (upper right panel), T_{m02} (lower left panel) and T_p (lower right panel)	20040208	22:20hr
	Hindcast Ameland Inlet	
WL | DELFT HYDRAULICS	H4803.11	Fig. 3.66

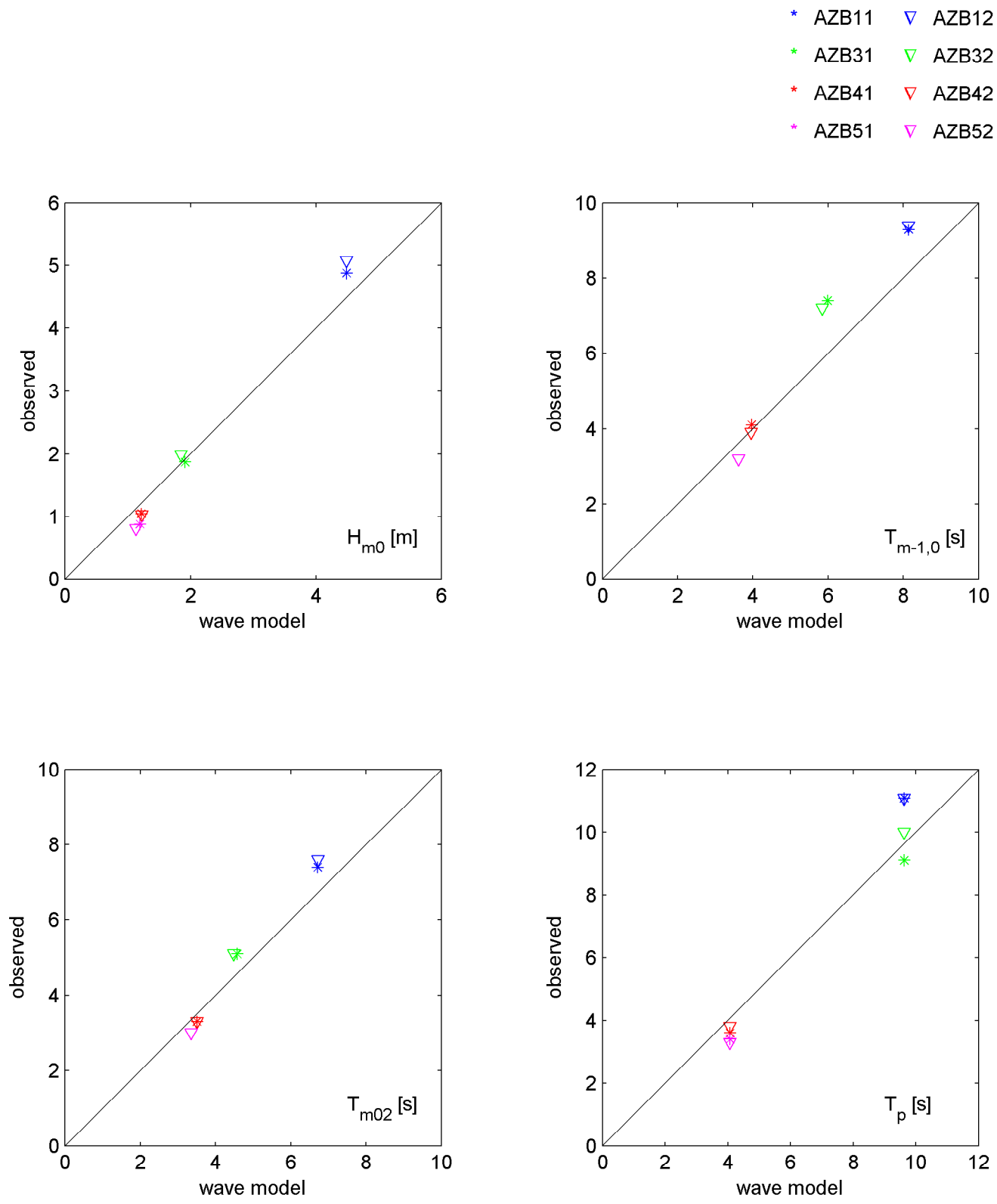

Scatter plot of wave parameters H_{m0} (upper left panel), $T_{m-1,0}$ (upper right panel), T_{m02} (lower left panel) and T_p (lower right panel) uniform wind field	20050102	12:00hr
	Hindcast Ameland Inlet	
WL | DELFT HYDRAULICS	H4803.11	Fig. 3.67

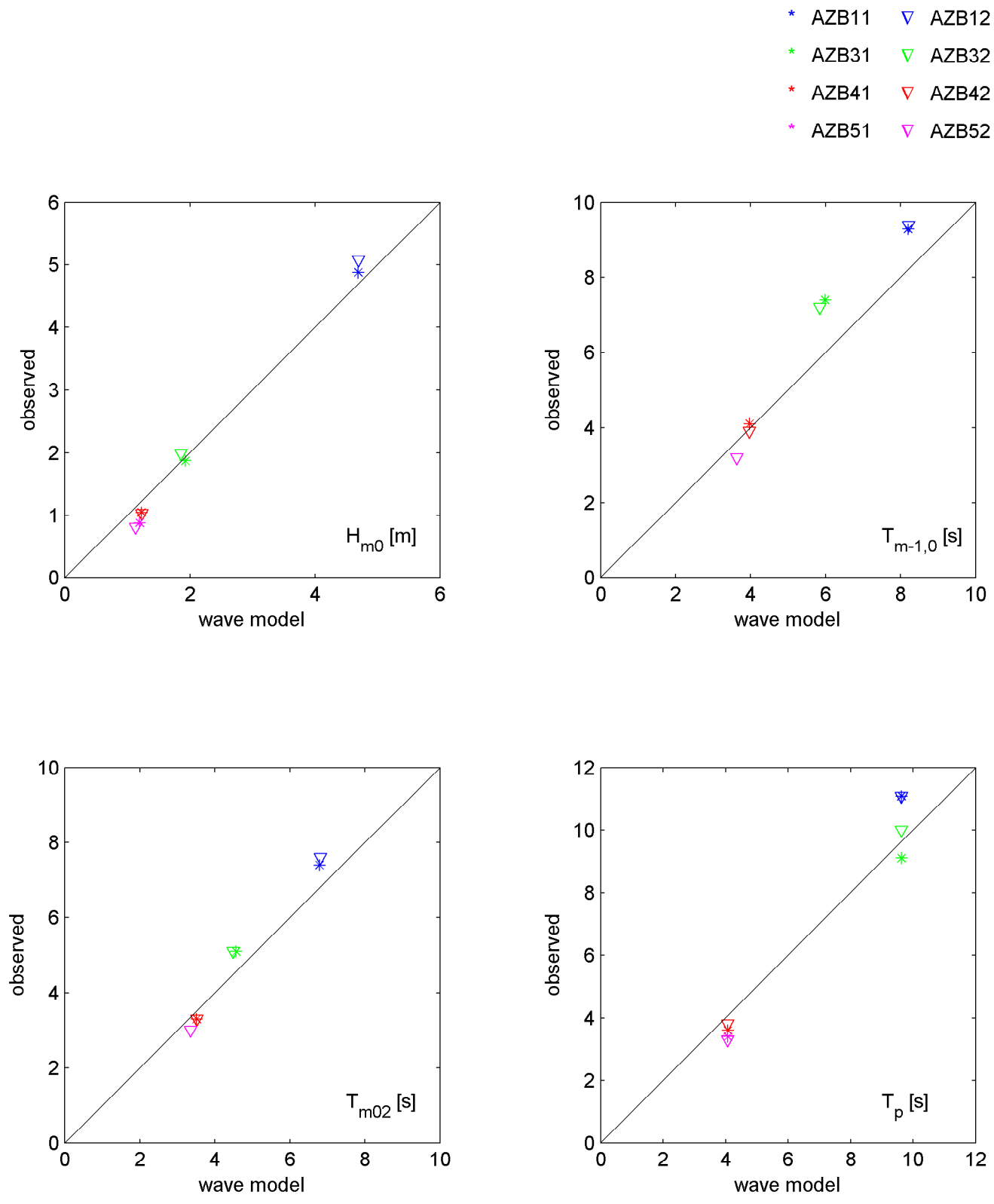

Scatter plot of wave parameters H_{m0} (upper left panel), $T_{m-1,0}$ (upper right panel), T_{m02} (lower left panel) and T_p (lower right panel) HIRLAM wind field	20050102	12:00hr
	Hindcast Ameland Inlet	
WL | DELFT HYDRAULICS	H4803.11	Fig. 3.68

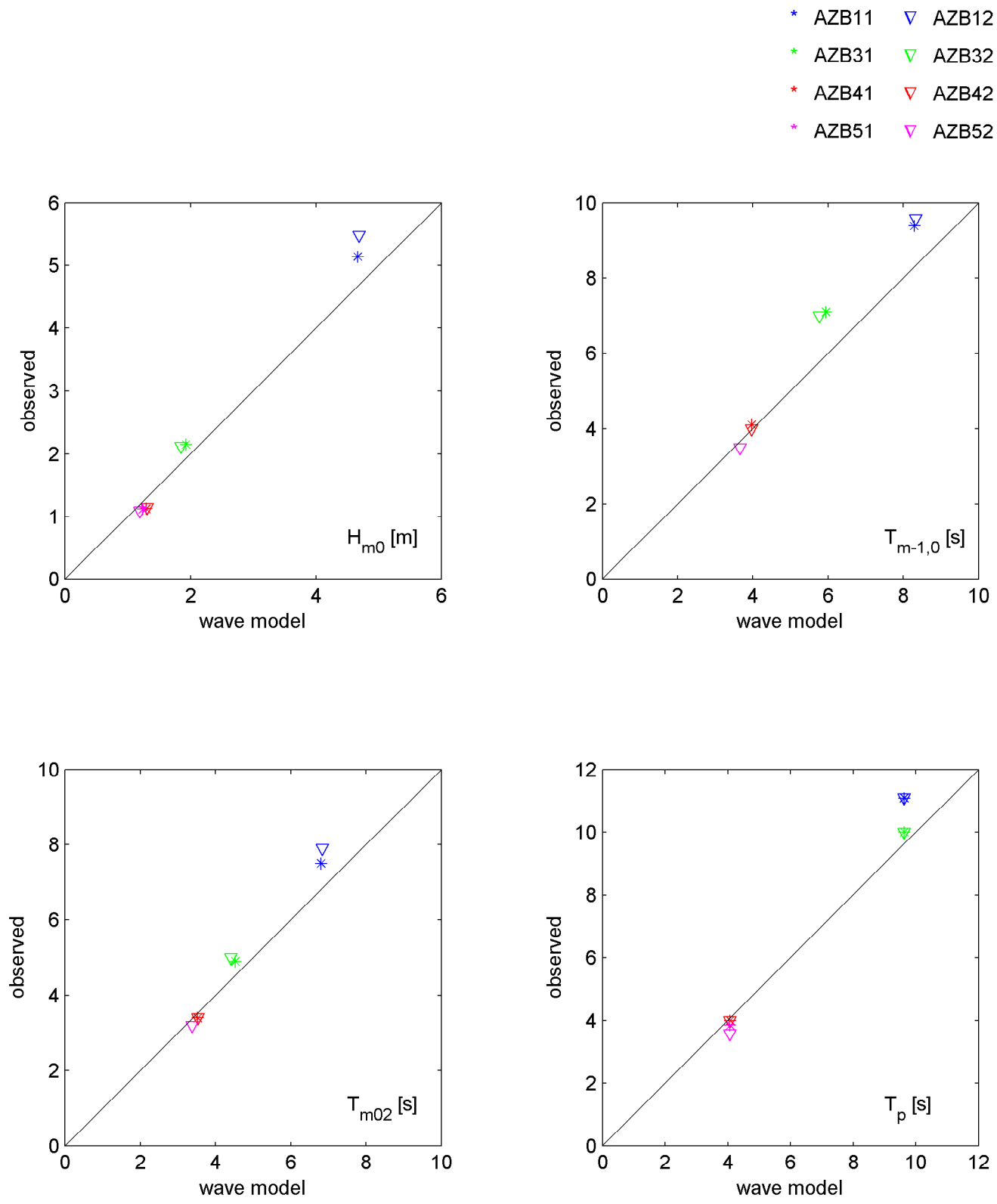

Scatter plot of wave parameters H_{m0} (upper left panel), $T_{m-1,0}$ (upper right panel), T_{m02} (lower left panel) and T_p (lower right panel)	20050108	18:00hr
	Hindcast Ameland Inlet	
WL | DELFT HYDRAULICS	H4803.11	Fig. 3.69

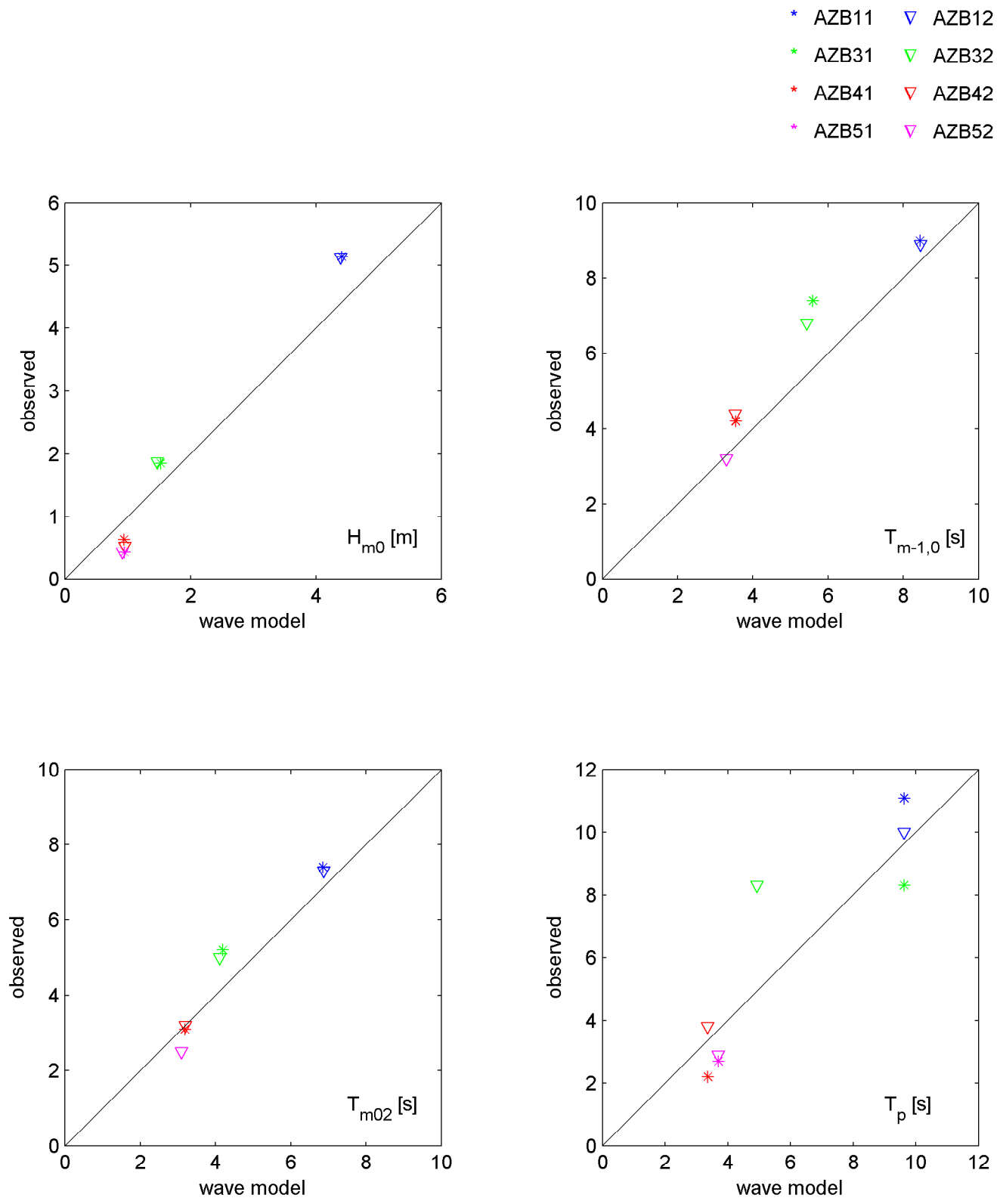

Scatter plot of wave parameters H_{m0} (upper left panel), $T_{m-1,0}$ (upper right panel), T_{m02} (lower left panel) and T_p (lower right panel) uniform water level field and no current	20050102	10:00hr
	Hindcast Ameland Inlet	
WL | DELFT HYDRAULICS	H4803.11	Fig. 3.70

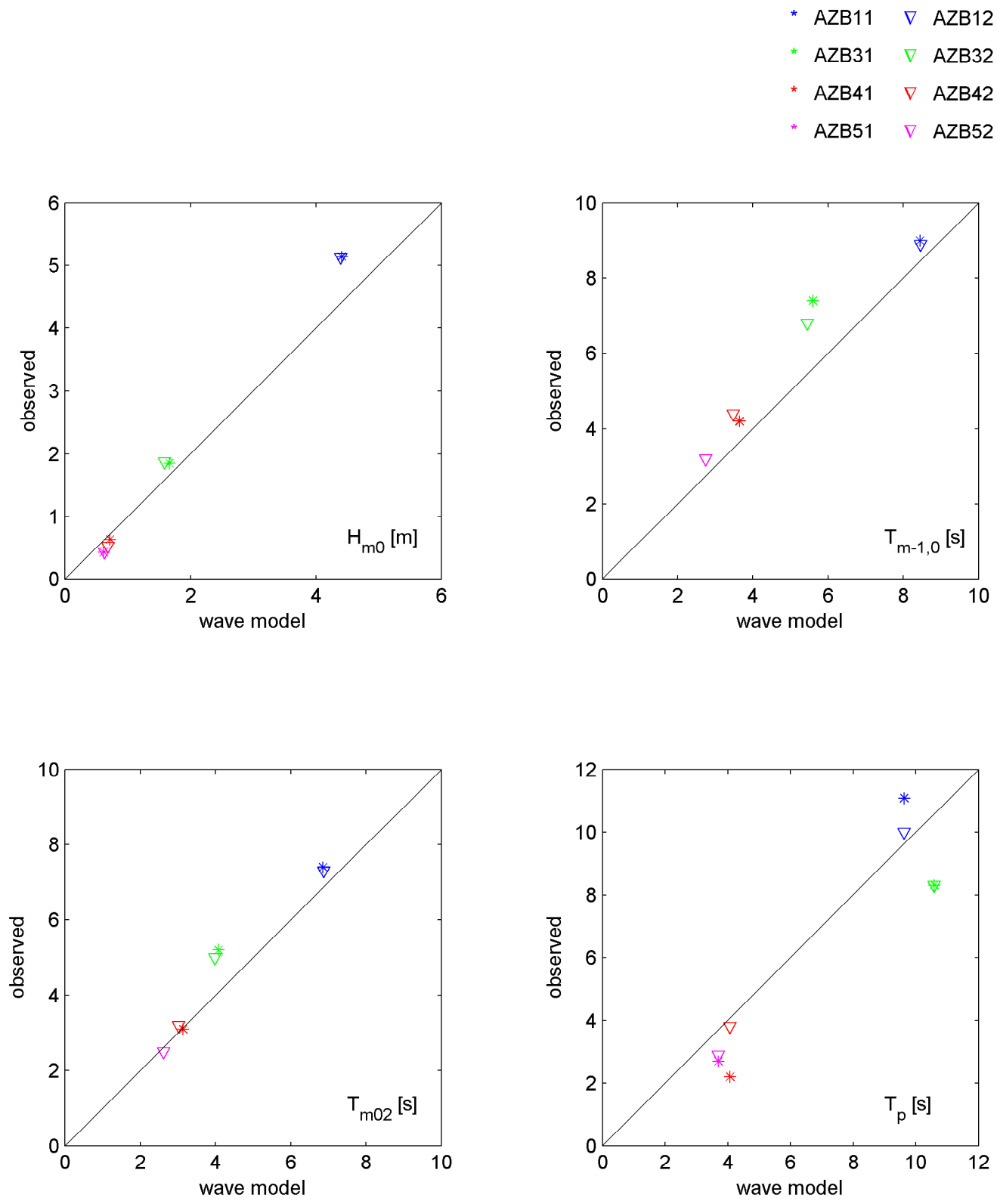

Scatter plot of wave parameters H_{m0} (upper left panel), $T_{m-1,0}$ (upper right panel), T_{m02} (lower left panel) and T_p (lower right panel) WAQUA water level and current; fine WAQUA grid	20050102	10:00hr
	Hindcast Ameland Inlet	
WL | DELFT HYDRAULICS	H4803.11	Fig. 3.71

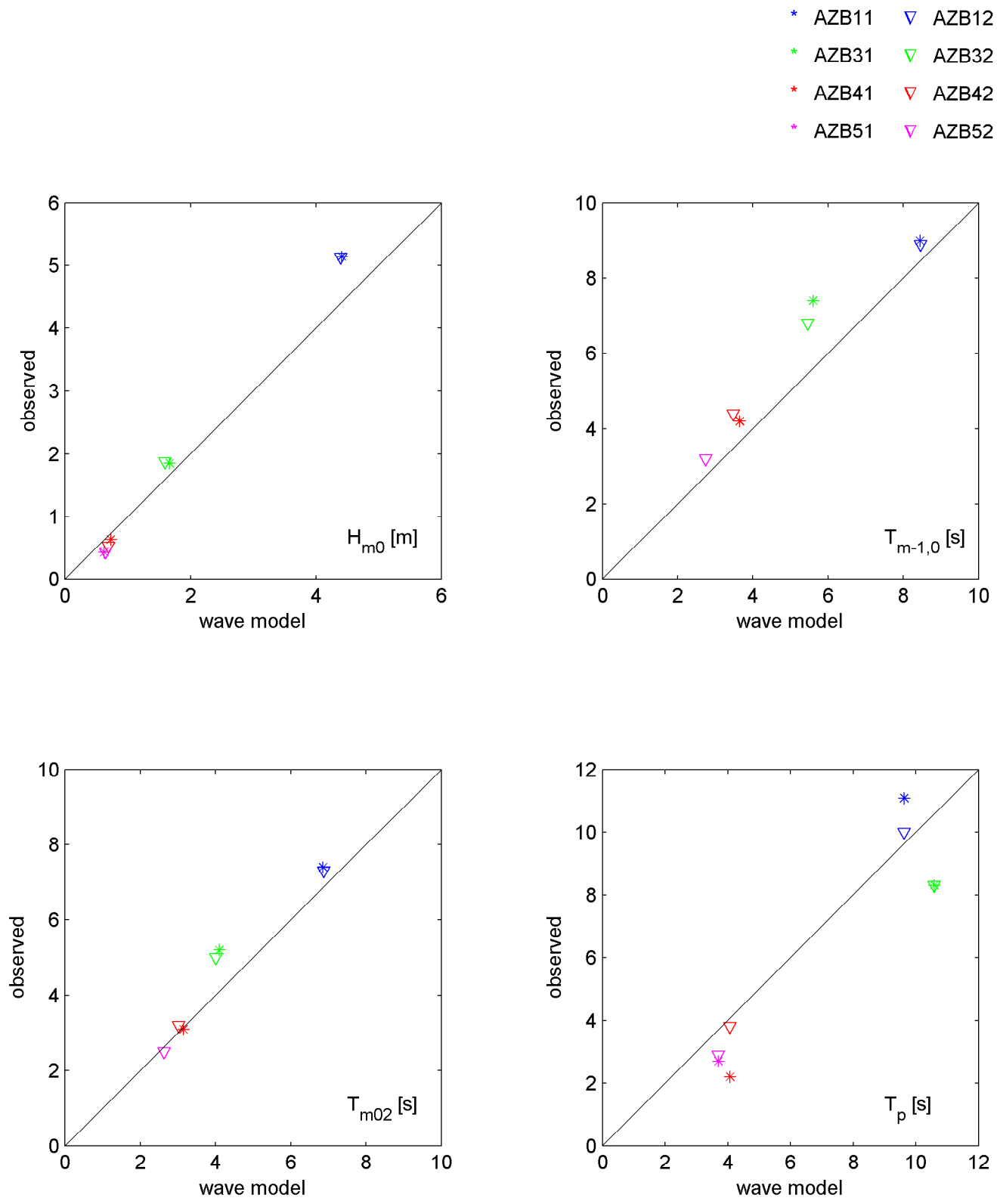

Scatter plot of wave parameters H_{m0} (upper left panel), $T_{m-1,0}$ (upper right panel), T_{m02} (lower left panel) and T_p (lower right panel) WAQUA water level and current; coarse WAQUA grid	20050102	10:00hr
	Hindcast Ameland Inlet	
WL | DELFT HYDRAULICS	H4803.11	Fig. 3.72

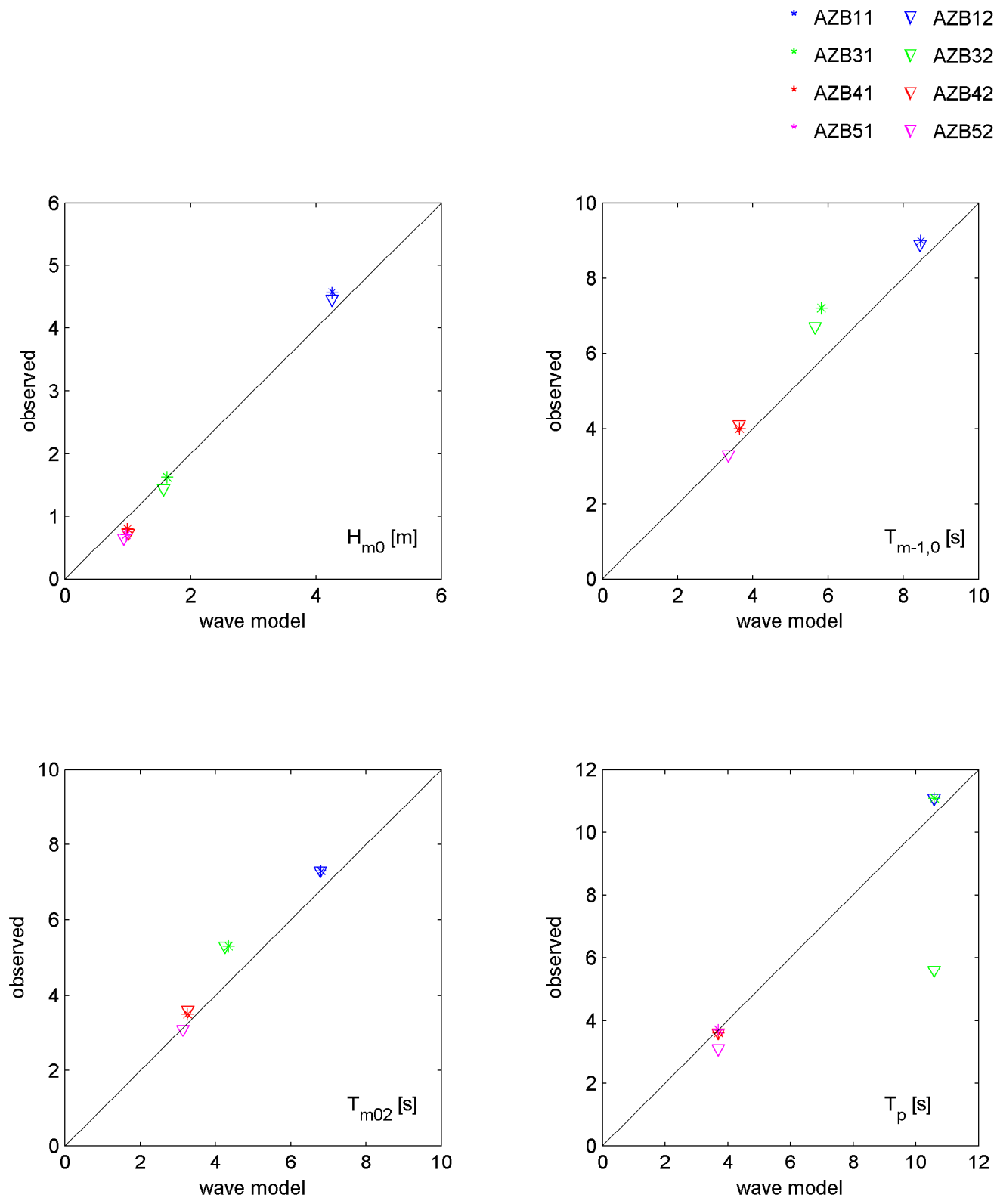

Scatter plot of wave parameters H_{m0} (upper left panel), $T_{m-1,0}$ (upper right panel), T_{m02} (lower left panel) and T_p (lower right panel) uniform water level field and no current	20050102	17:00hr
	Hindcast Ameland Inlet	
WL | DELFT HYDRAULICS	H4803.11	Fig. 3.73

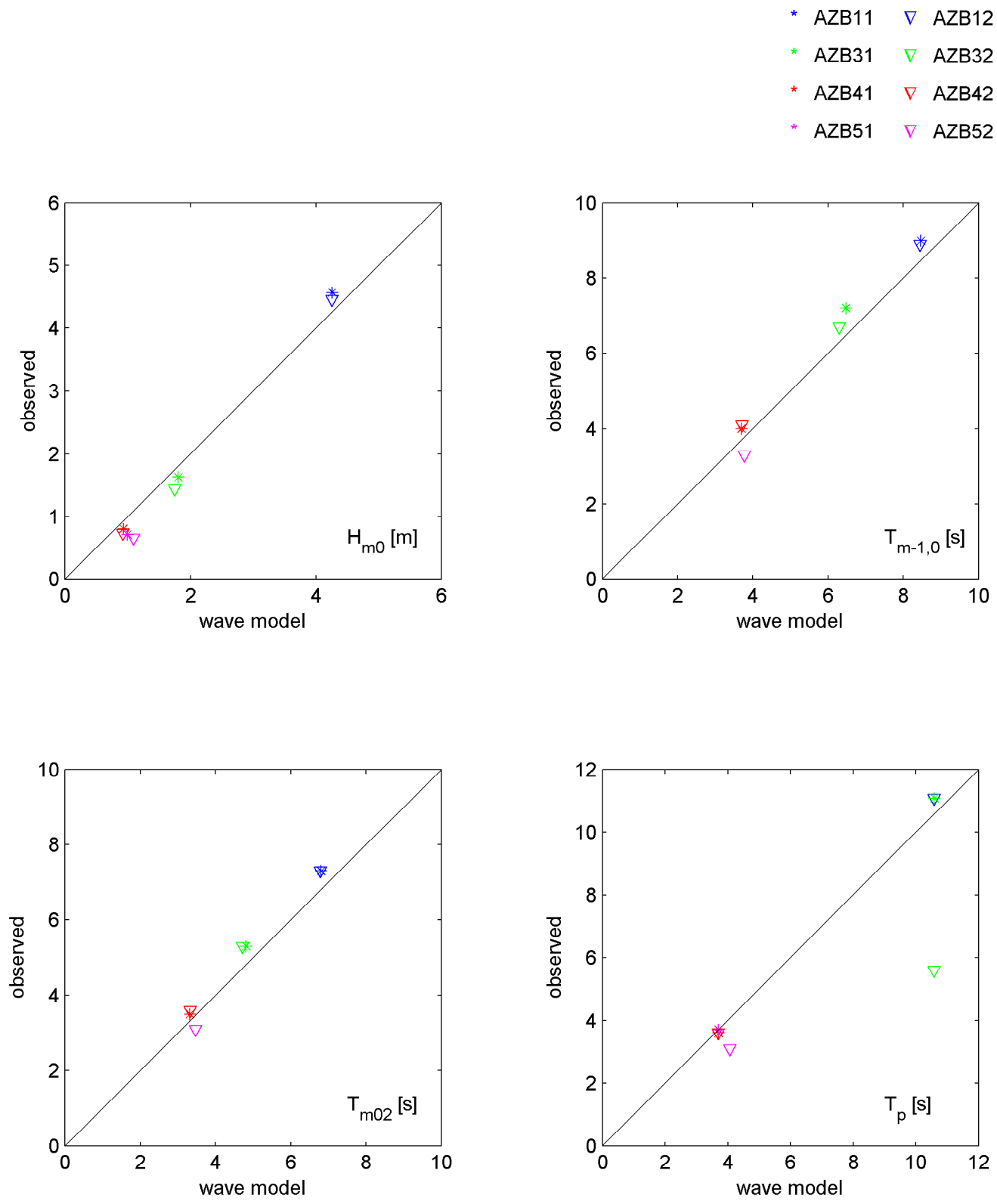

Scatter plot of wave parameters H_{m0} (upper left panel), $T_{m-1,0}$ (upper right panel), T_{m02} (lower left panel) and T_p (lower right panel) WAQUA water level and current; fine WAQUA grid	20050102	17:00hr
	Hindcast Ameland Inlet	
WL | DELFT HYDRAULICS	H4803.11	Fig. 3.74

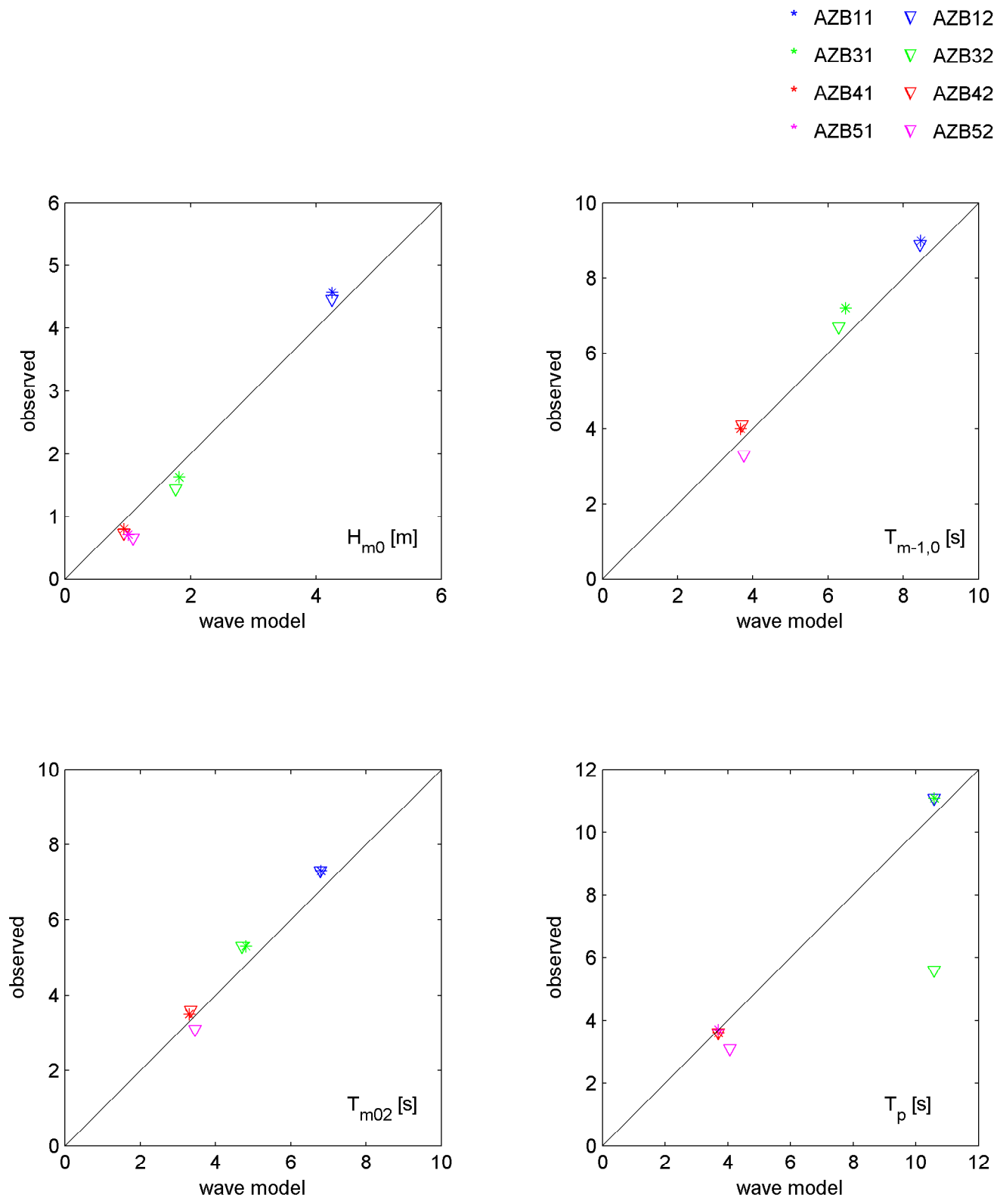

Scatter plot of wave parameters H_{m0} (upper left panel), $T_{m-1,0}$ (upper right panel), T_{m02} (lower left panel) and T_p (lower right panel) WAQUA water level and current; coarse WAQUA grid	20050102	17:00hr
	Hindcast Ameland Inlet	
WL | DELFT HYDRAULICS	H4803.11	Fig. 3.75

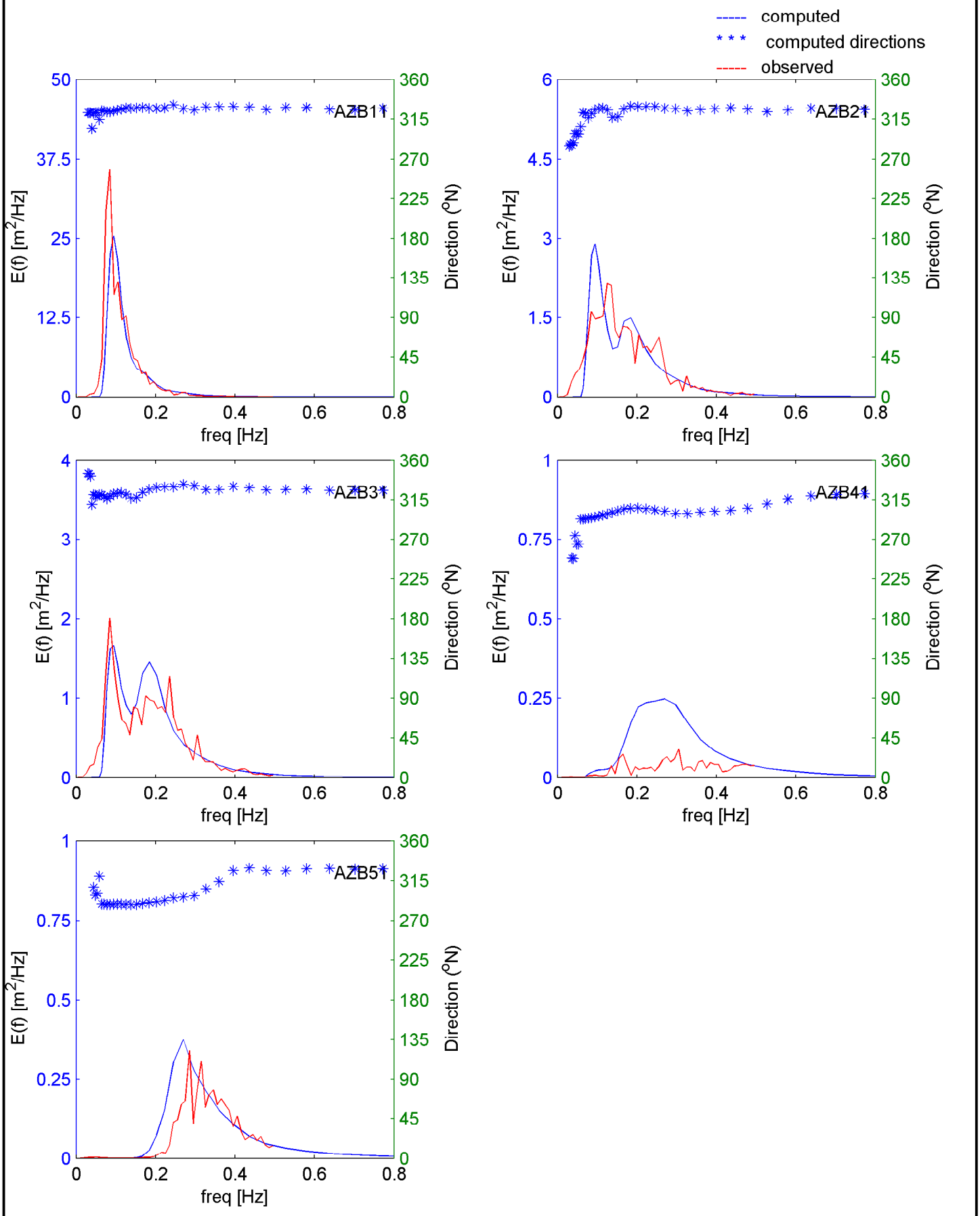

Measured and computed wave energy spectra at AZB11, AZB12, AZB31, AZB41 and AZB51	20040208	22:20hr
	Hindcast Ameland Inlet	
WL | DELFT HYDRAULICS	H4803.11	Fig. 3.76

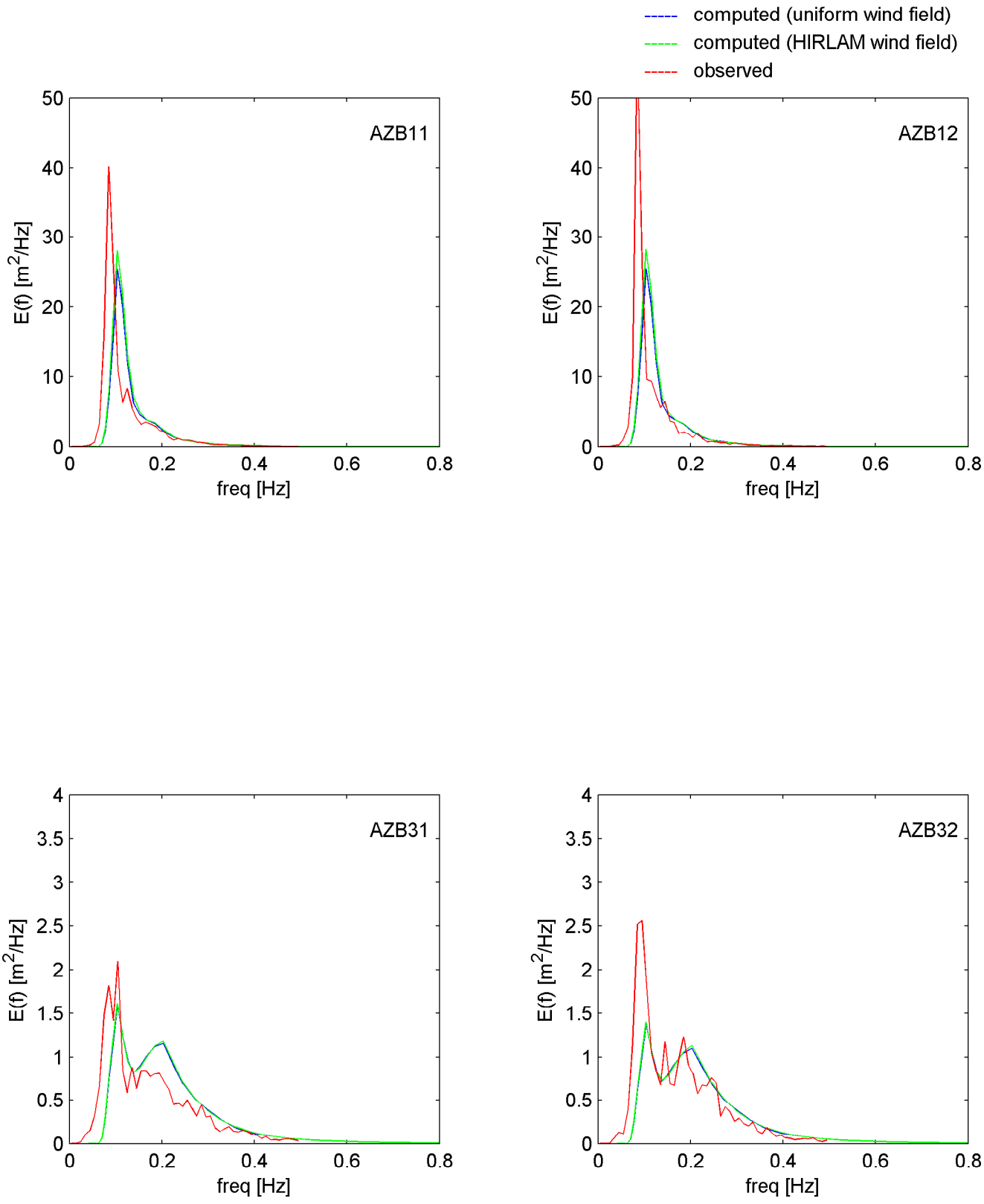

Measured and computed wave energy spectra at AZB11, AZB12, AZB31 and AZB32	20050102	12:00hr
	Hindcast Ameland Inlet	
WL | DELFT HYDRAULICS	H4803.11	Fig. 3.77a

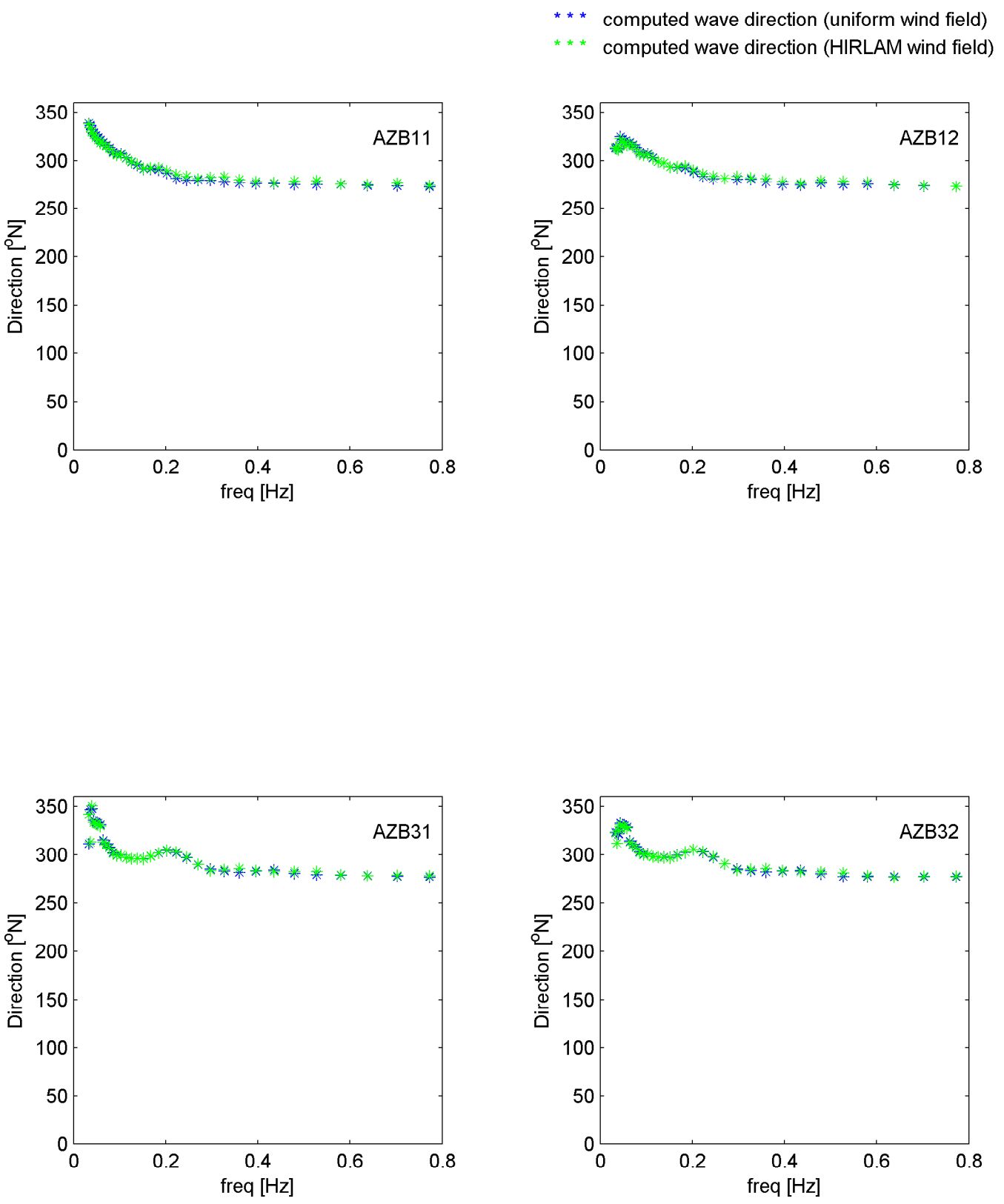

Computed wave directions at AZB11, AZB12, AZB31 and AZB32	20050102	12:00hr
	Hindcast Ameland Inlet	
WL | DELFT HYDRAULICS	H4803.11	Fig. 3.77b

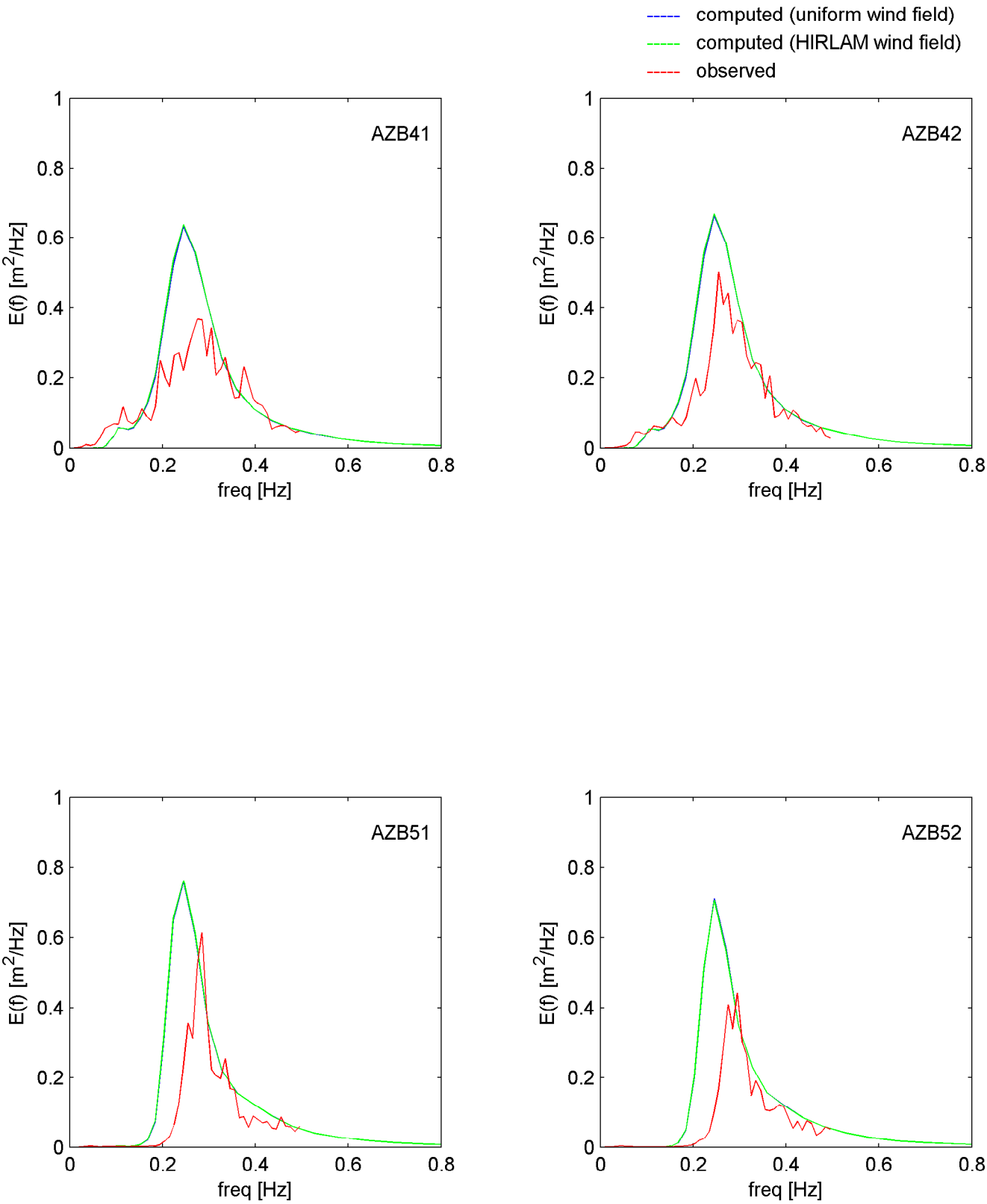

Measured and computed wave energy spectra at AZB41, AZB42, AZB51 and AZB52	20050102	12:00hr
	Hindcast Ameland Inlet	
WL | DELFT HYDRAULICS	H4803.11	Fig. 3.77c

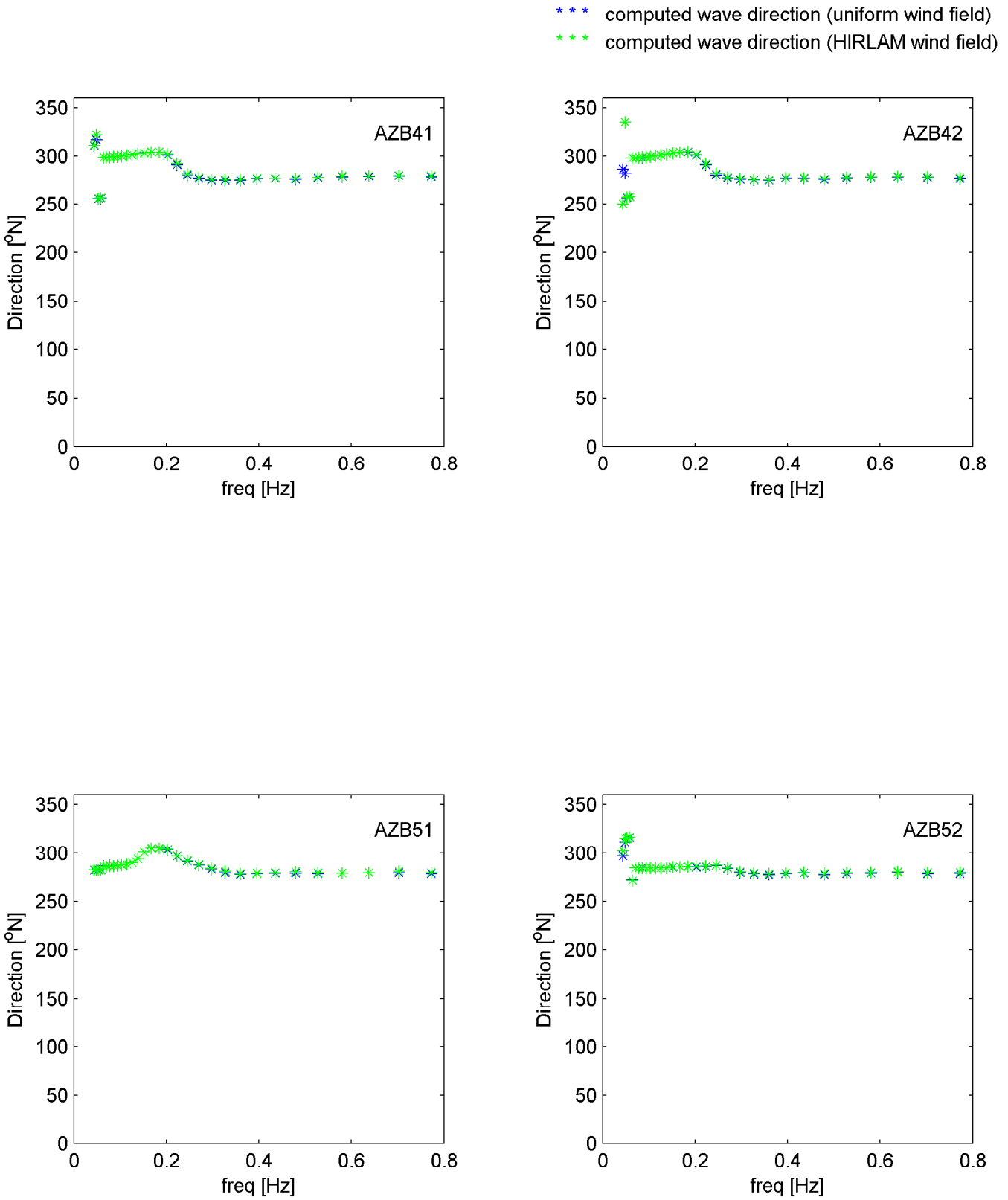

Computed wave directions at AZB41, AZB42, AZB51 and AZB52	20050102	12:00hr
	Hindcast Ameland Inlet	
WL | DELFT HYDRAULICS	H4803.11	Fig. 3.77d

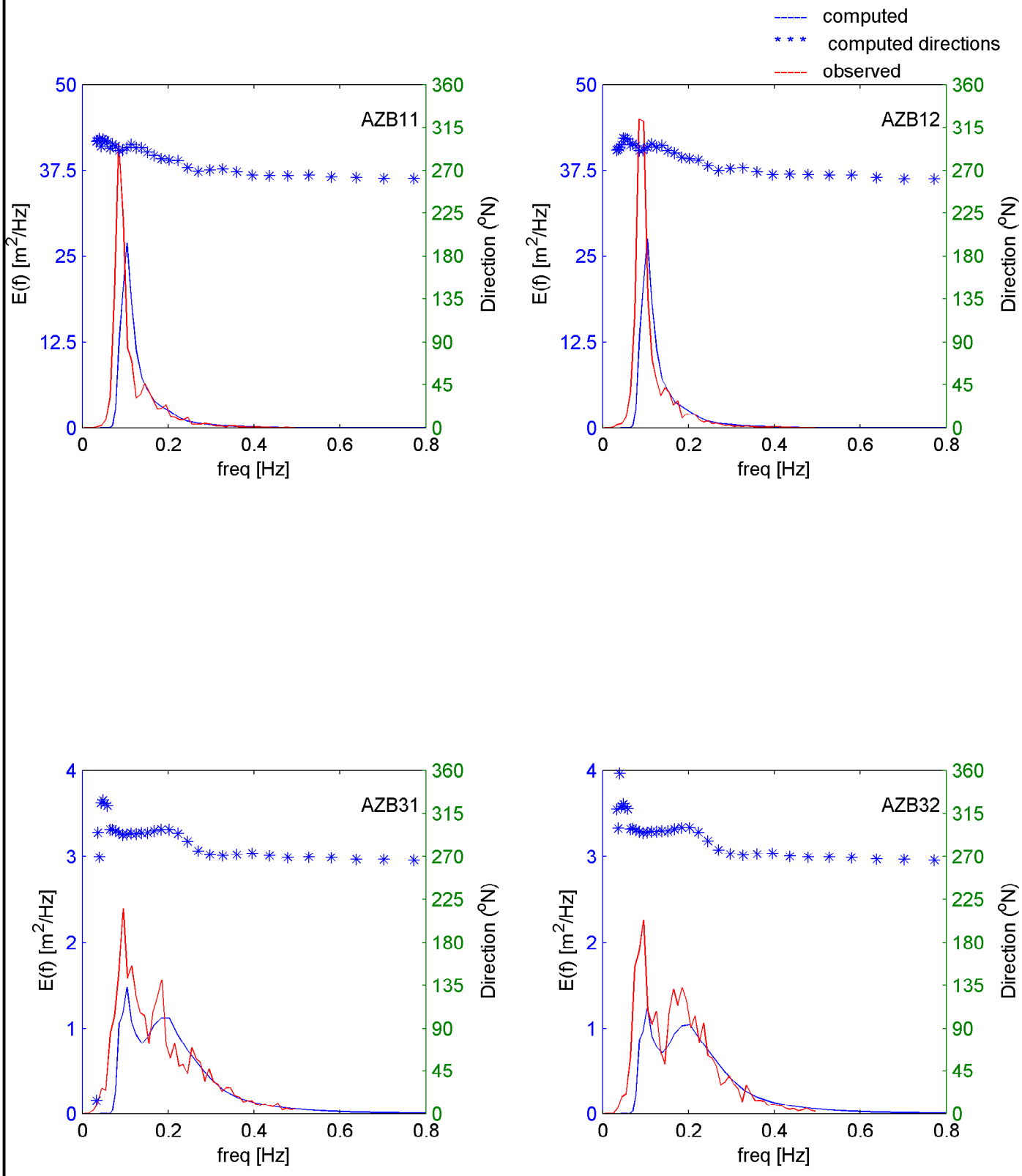

Measured and computed wave energy spectra at AZB11, AZB12, AZB31 and AZB32	20050108	18:00hr
	Hindcast Ameland Inlet	
WL | DELFT HYDRAULICS	H4803.11	Fig. 3.78a

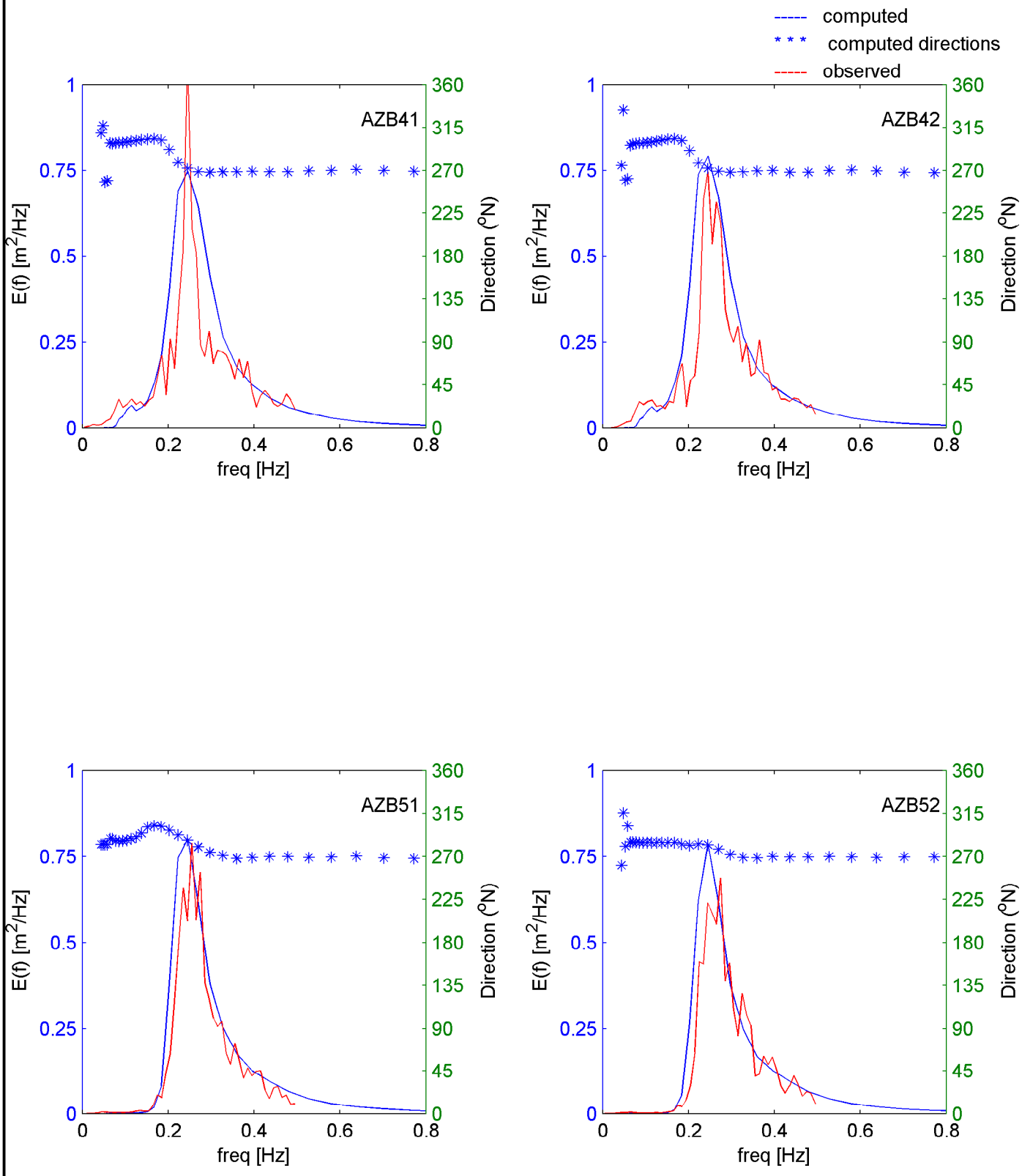

Measured and computed wave energy spectra at AZB41, AZB42, AZB51 and AZB52	20050108	18:00hr
	Hindcast Ameland Inlet	
WL | DELFT HYDRAULICS	H4803.11	Fig. 3.78b

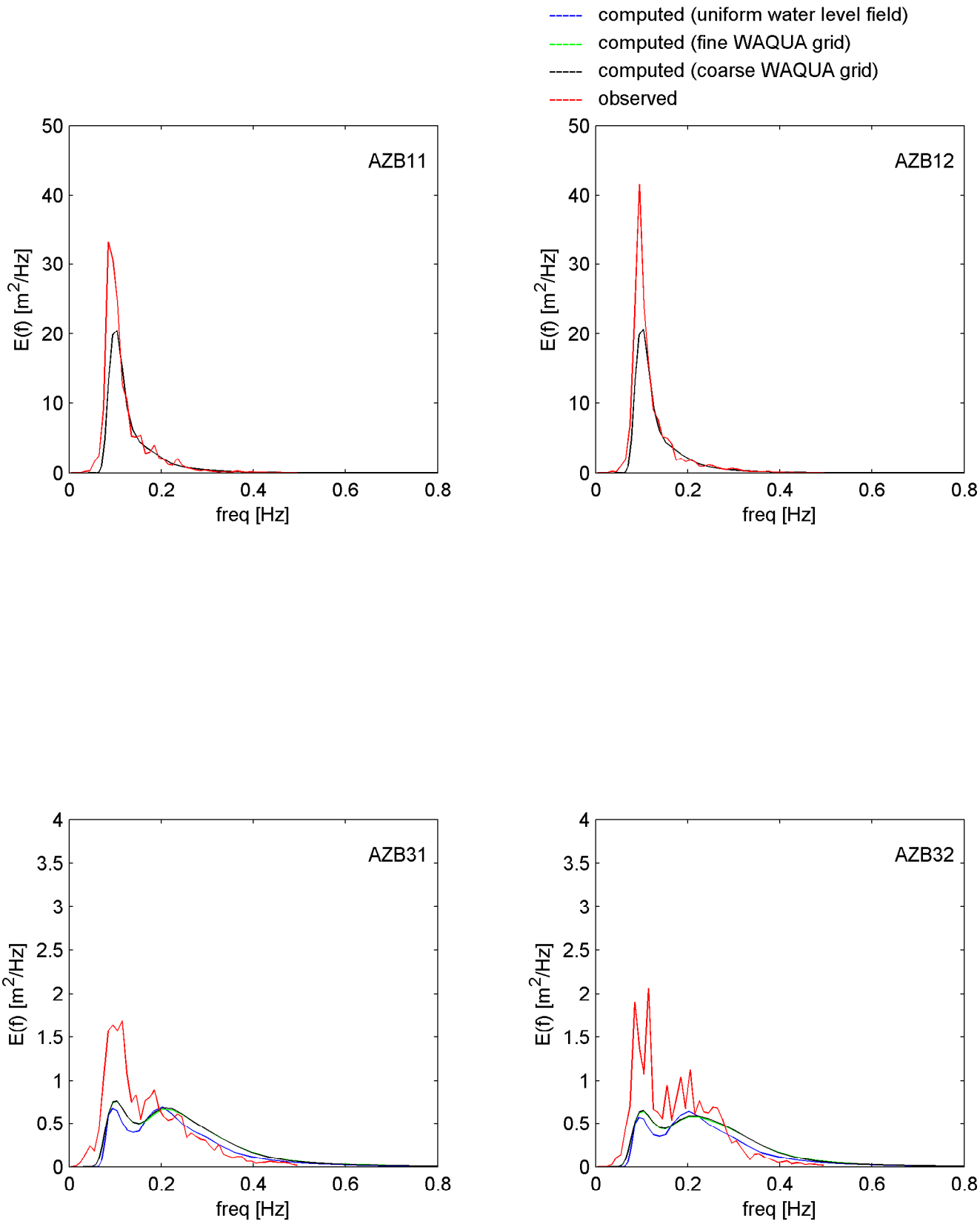

Measured and computed wave energy spectra at AZB11, AZB12, AZB31 and AZB32	20050102	10:00hr
	Hindcast Ameland Inlet	
WL | DELFT HYDRAULICS	H4803.11	Fig. 3.79a

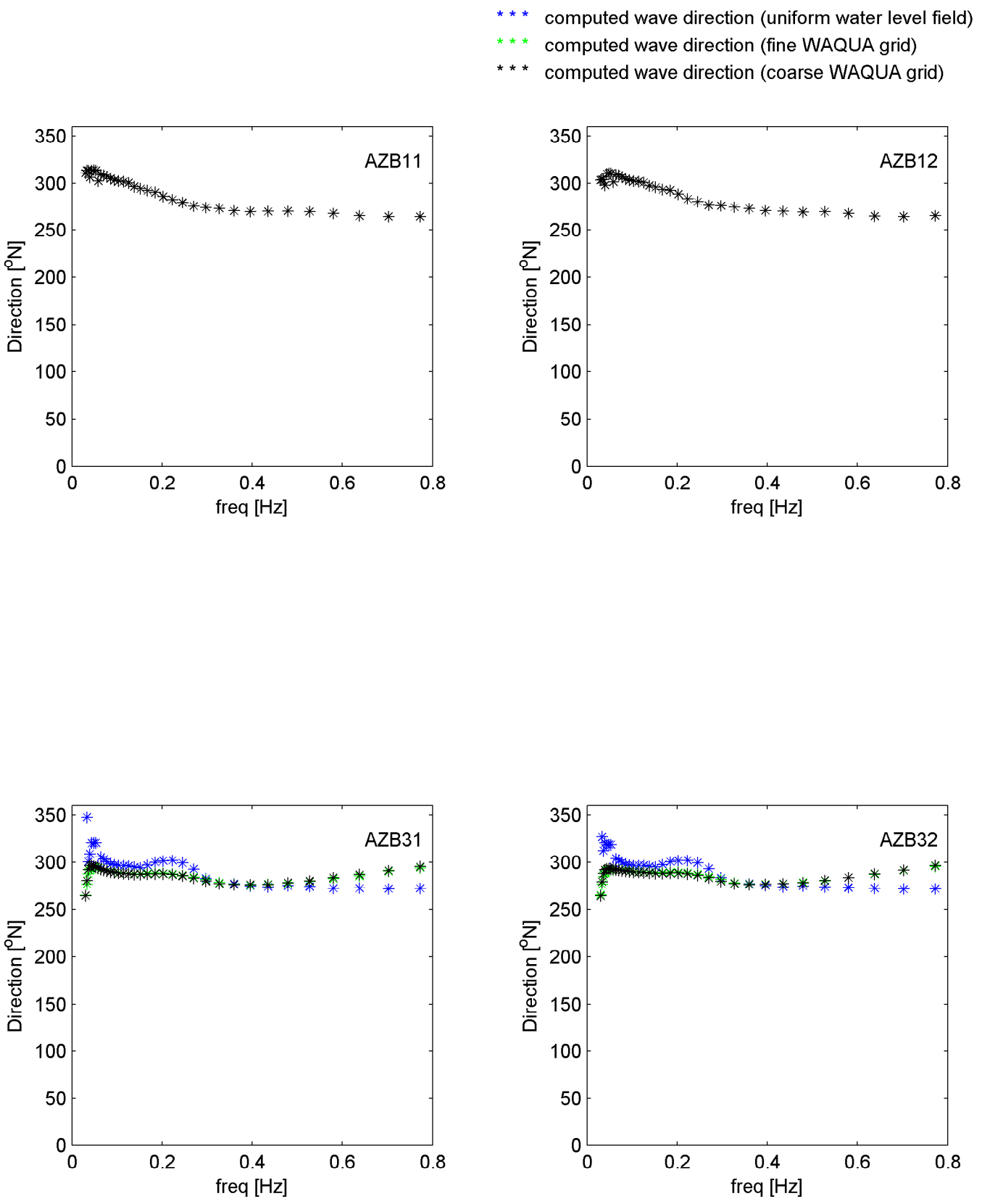

Measured and computed wave energy spectra at AZB11, AZB12, AZB31 and AZB32	20050102	10:00hr
	Hindcast Ameland Inlet	
WL | DELFT HYDRAULICS	H4803.11	Fig. 3.79b

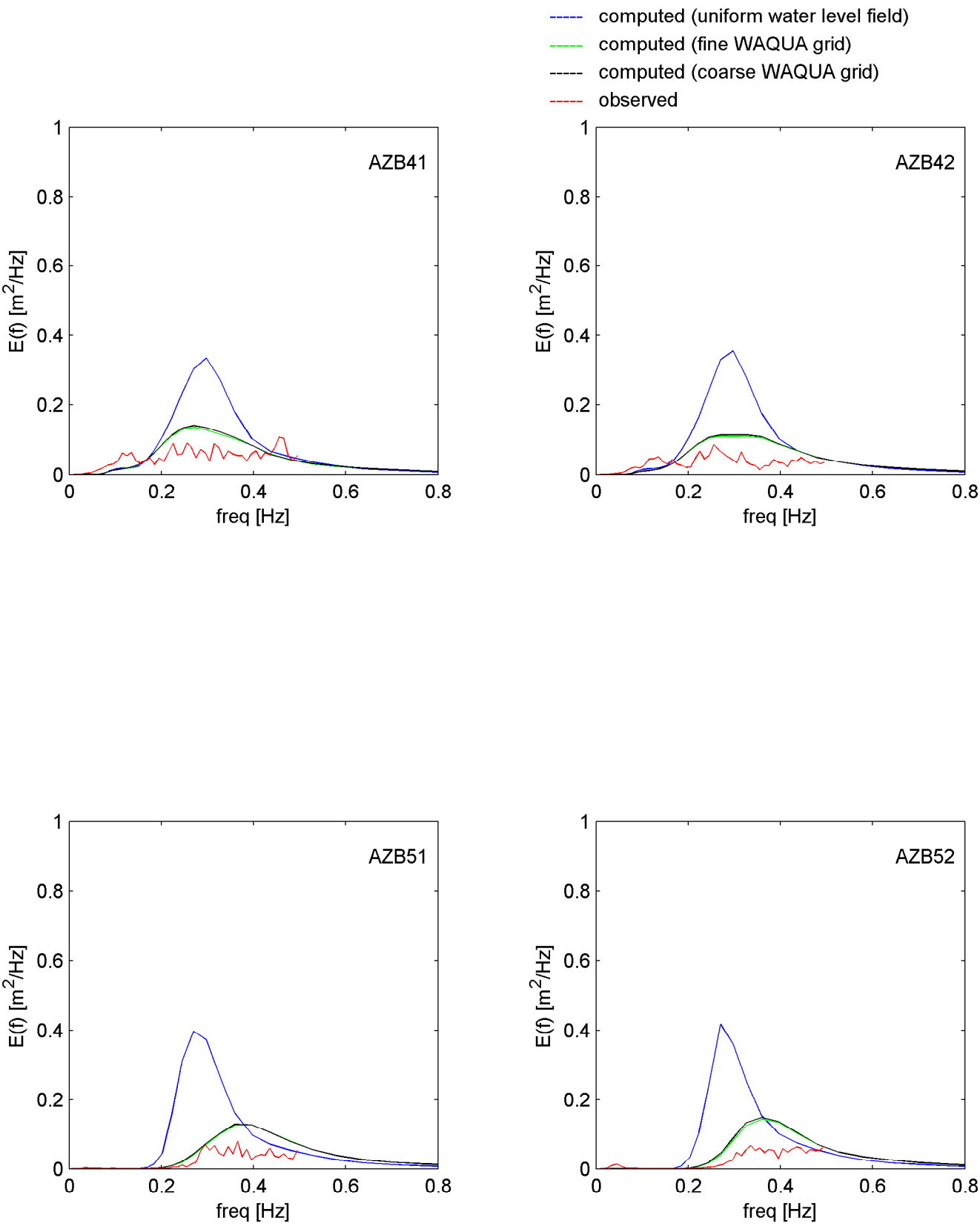

Measured and computed wave energy spectra at AZB41, AZB42, AZB51 and AZB52	20050102	10:00hr
	Hindcast Ameland Inlet	
WL | DELFT HYDRAULICS	H4803.11	Fig. 3.79c

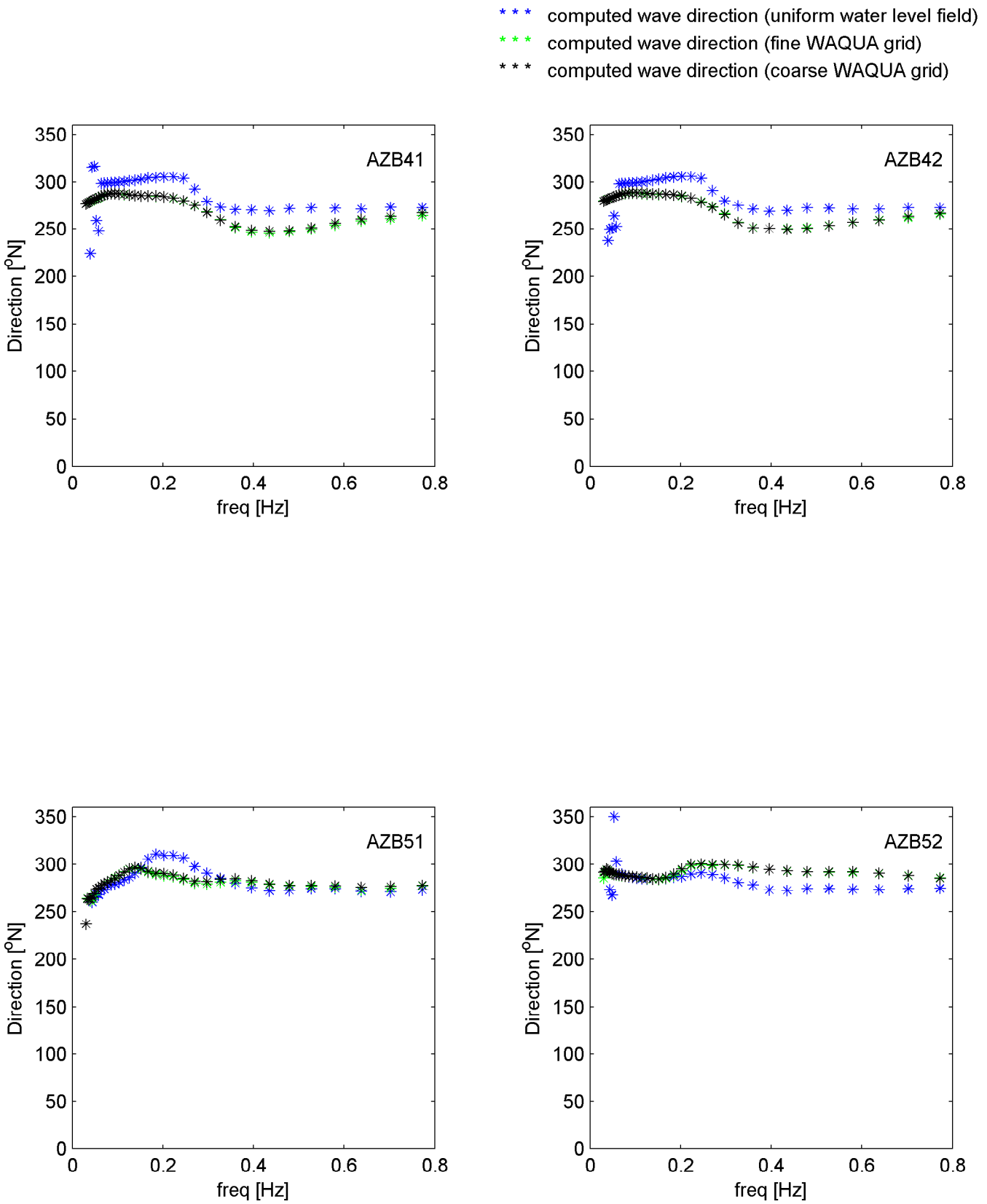

Measured and computed wave energy spectra at AZB41, AZB42, AZB51 and AZB52	20050102	10:00hr
	Hindcast Ameland Inlet	
WL | DELFT HYDRAULICS	H4803.11	Fig. 3.79d

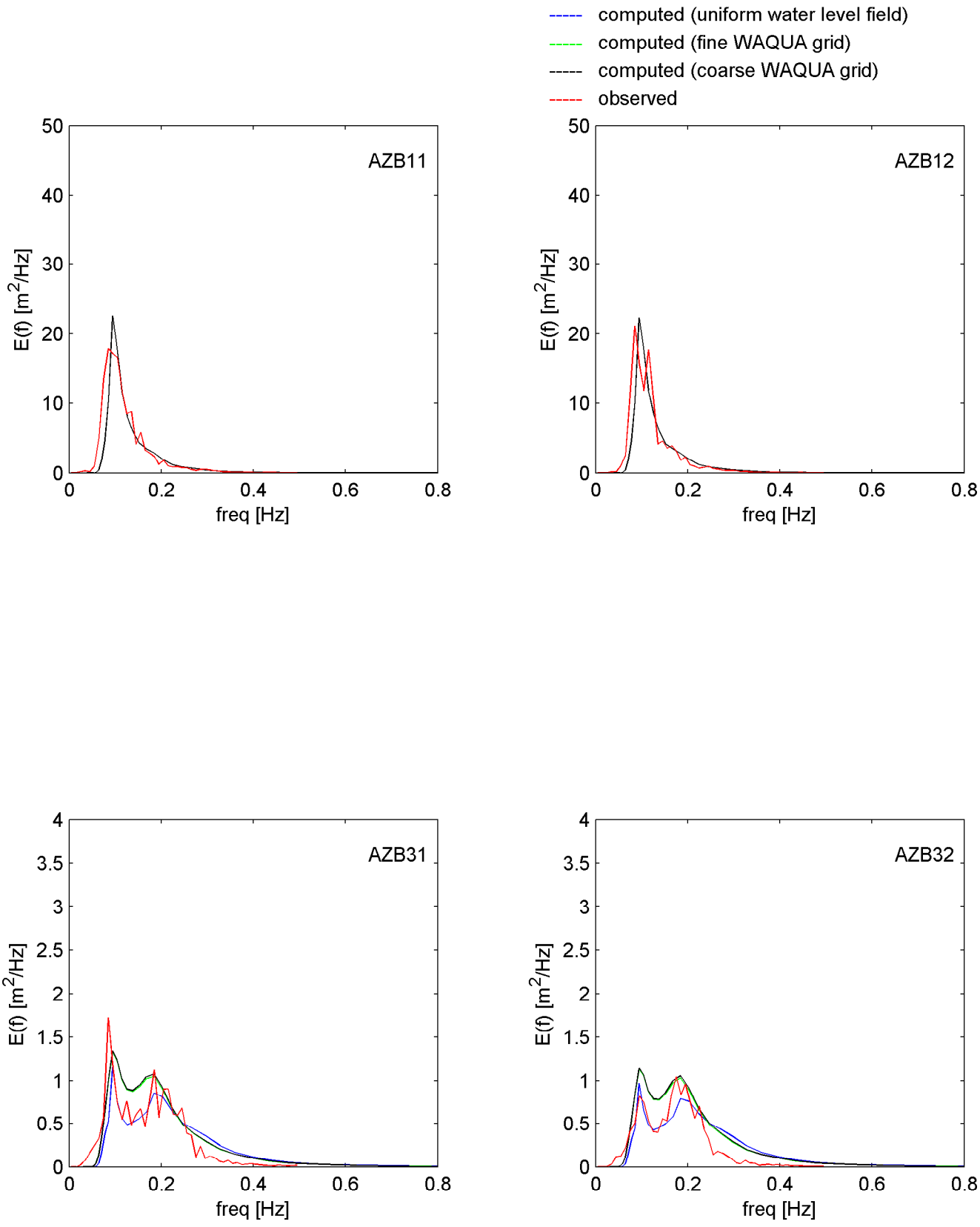

Measured and computed wave energy spectra at AZB11, AZB12, AZB31 and AZB32	20050102	17:00hr
	Hindcast Ameland Inlet	
WL | DELFT HYDRAULICS	H4803.11	Fig. 3.80a

* * * computed wave direction (uniform water level field)
* * * computed wave direction (fine WAQUA grid)
* * * computed wave direction (coarse WAQUA grid)

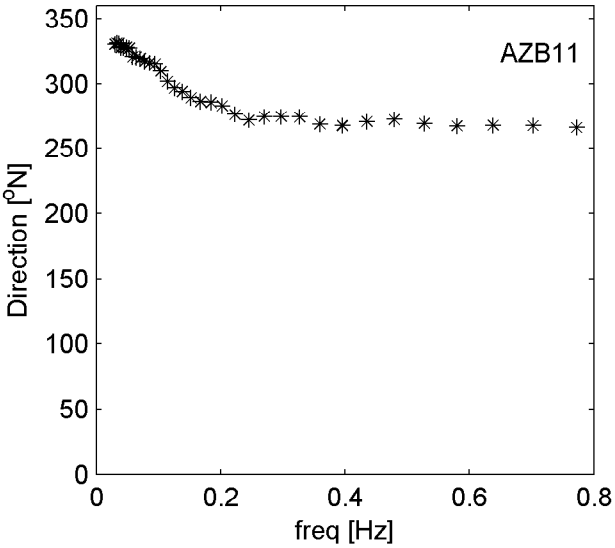

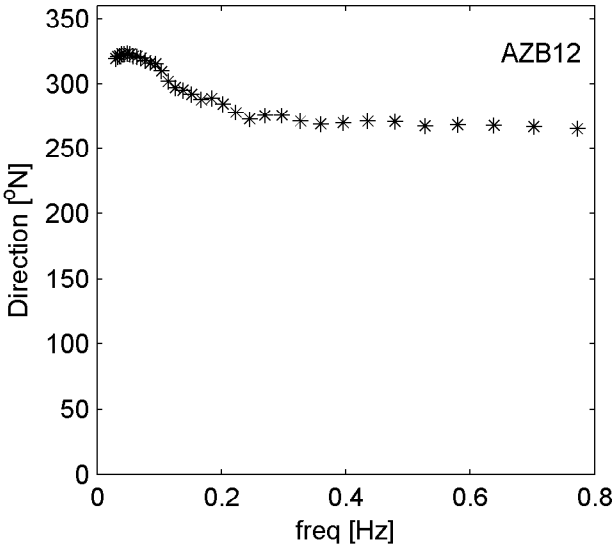

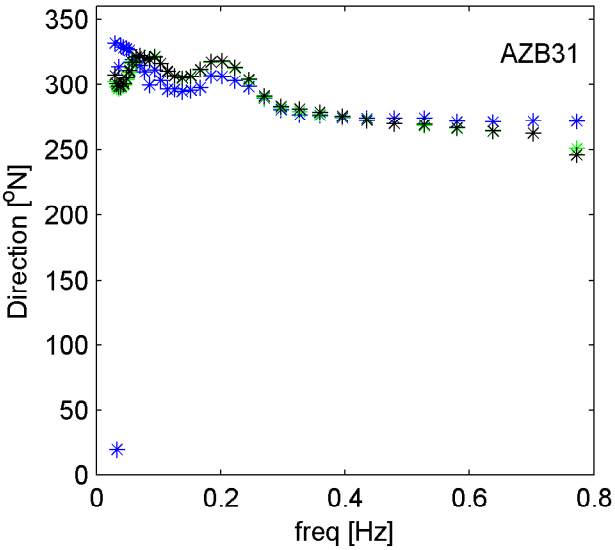

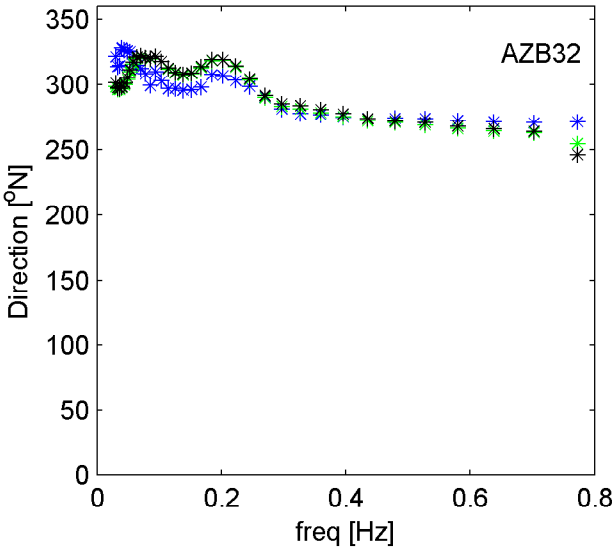

Measured and computed wave energy spectra at AZB11, AZB12, AZB31 and AZB32	20050102	17:00hr
	Hindcast Ameland Inlet	
WL | DELFT HYDRAULICS	H4803.11	Fig. 3.80b

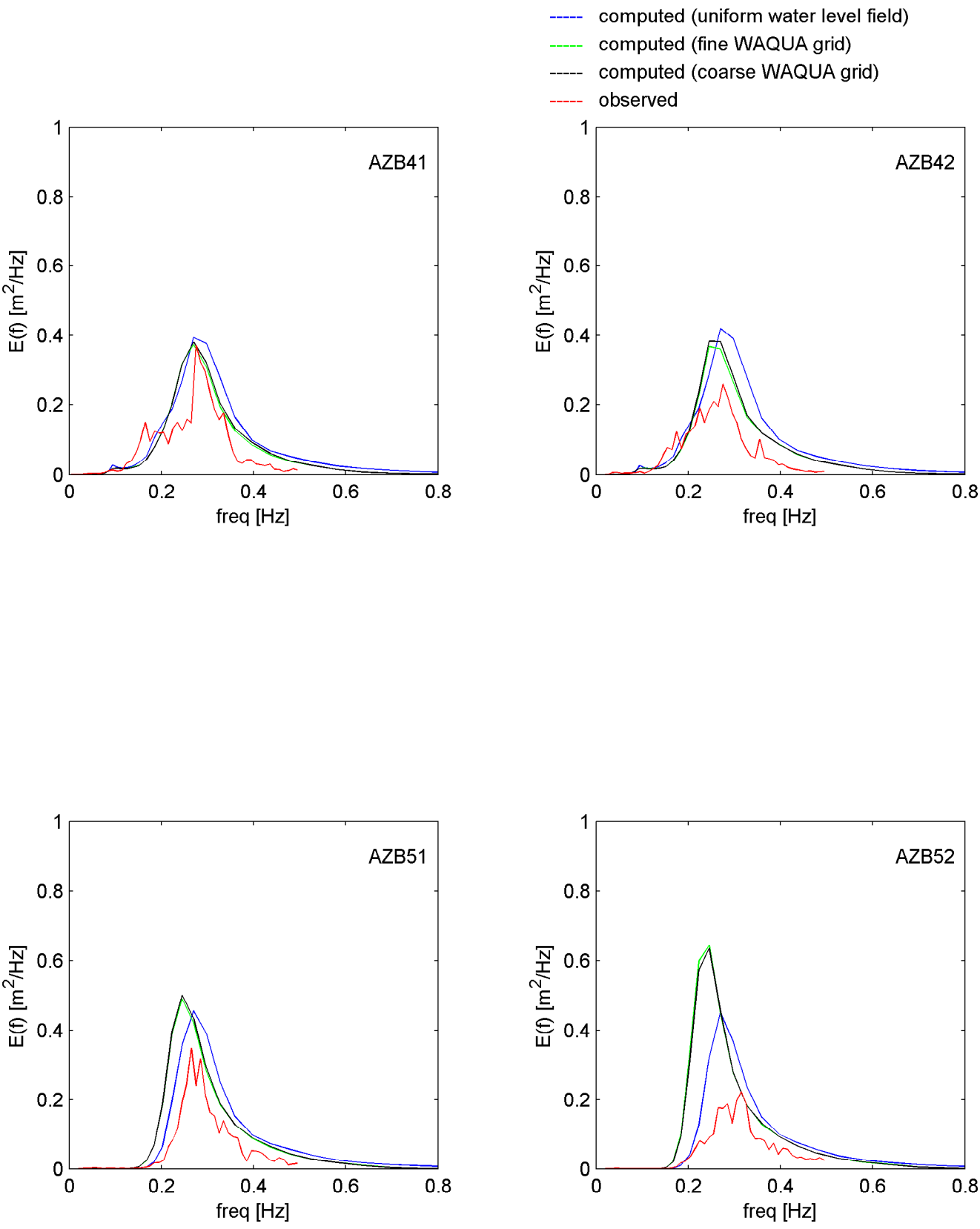

Measured and computed wave energy spectra at AZB41, AZB42, AZB51 and AZB52	20050102	17:00hr
	Hindcast Ameland Inlet	
WL | DELFT HYDRAULICS	H4803.11	Fig. 3.80c

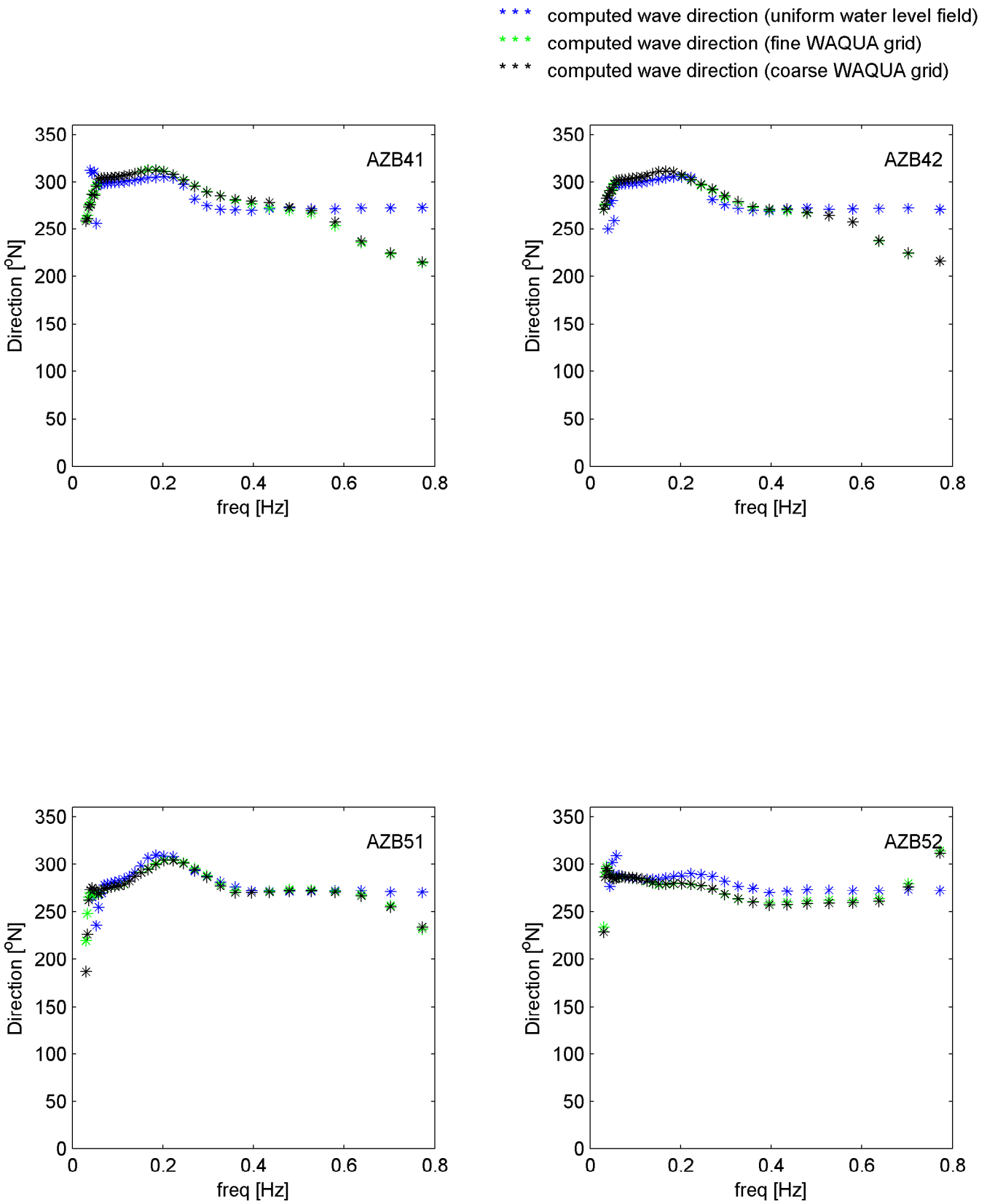

Measured and computed wave energy spectra at AZB41, AZB42, AZB51 and AZB52	20050102	17:00hr
	Hindcast Ameland Inlet	
WL | DELFT HYDRAULICS	H4803.11	Fig. 3.80d

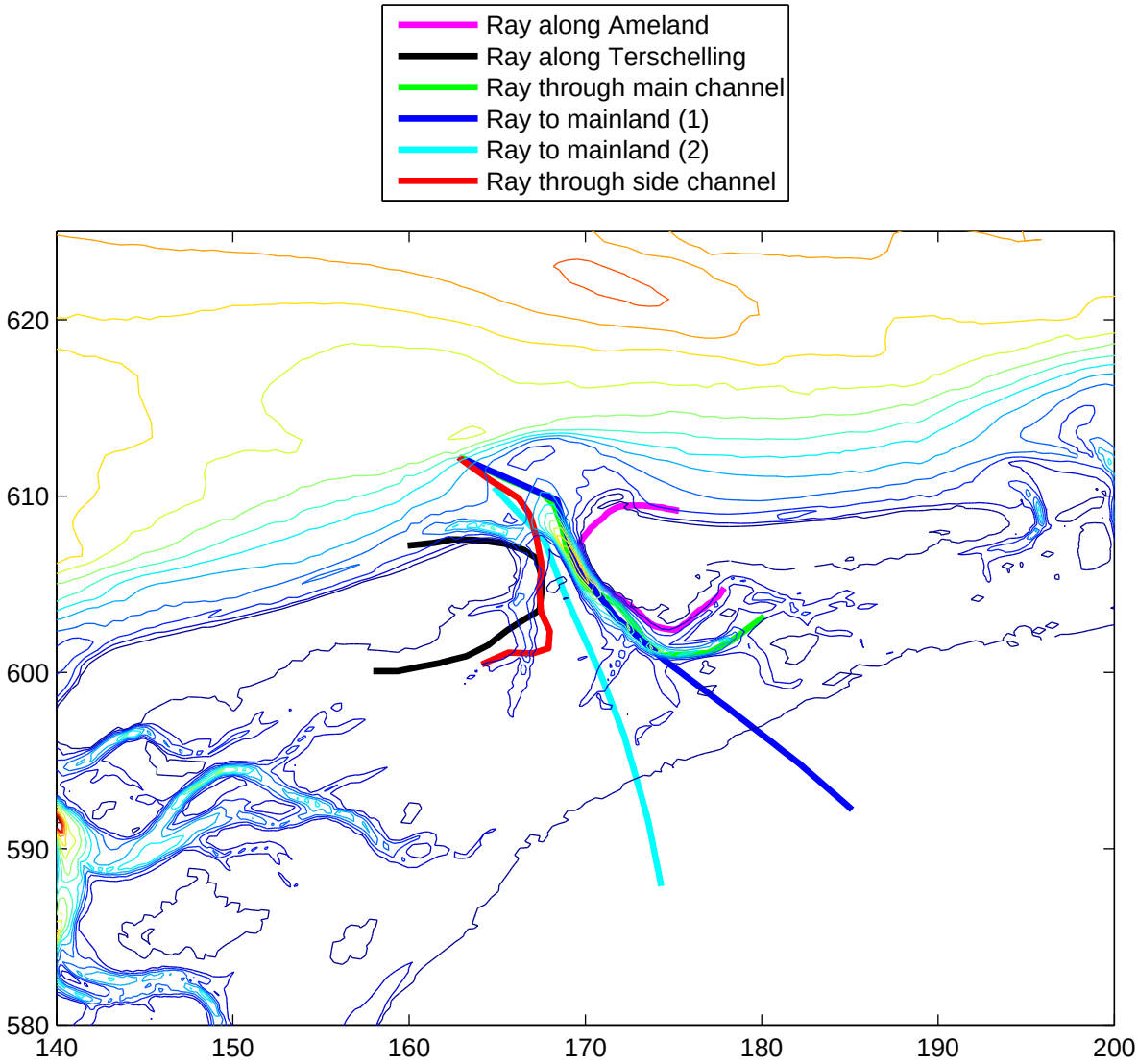

Location of output rays		
	Hindcast Amelander Zeegat	
WL | DELFT HYDRAULICS	H4803.11	Fig. 3.81

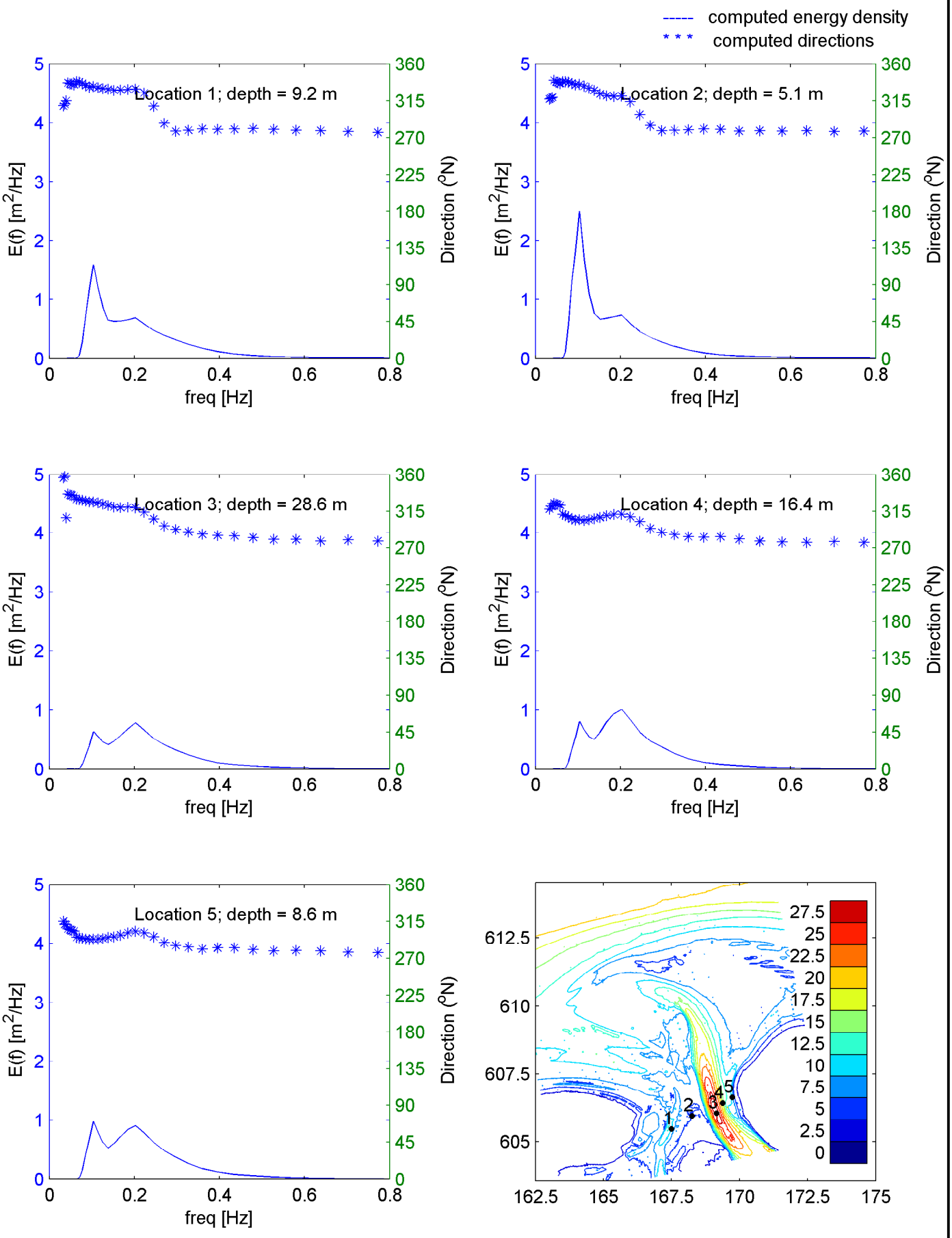

Computed wave energy spectra along transect through channel	20050102	12:00hr
	Hindcast Ameland Inlet	
WL | DELFT HYDRAULICS	H4803.11	Fig. 3.82

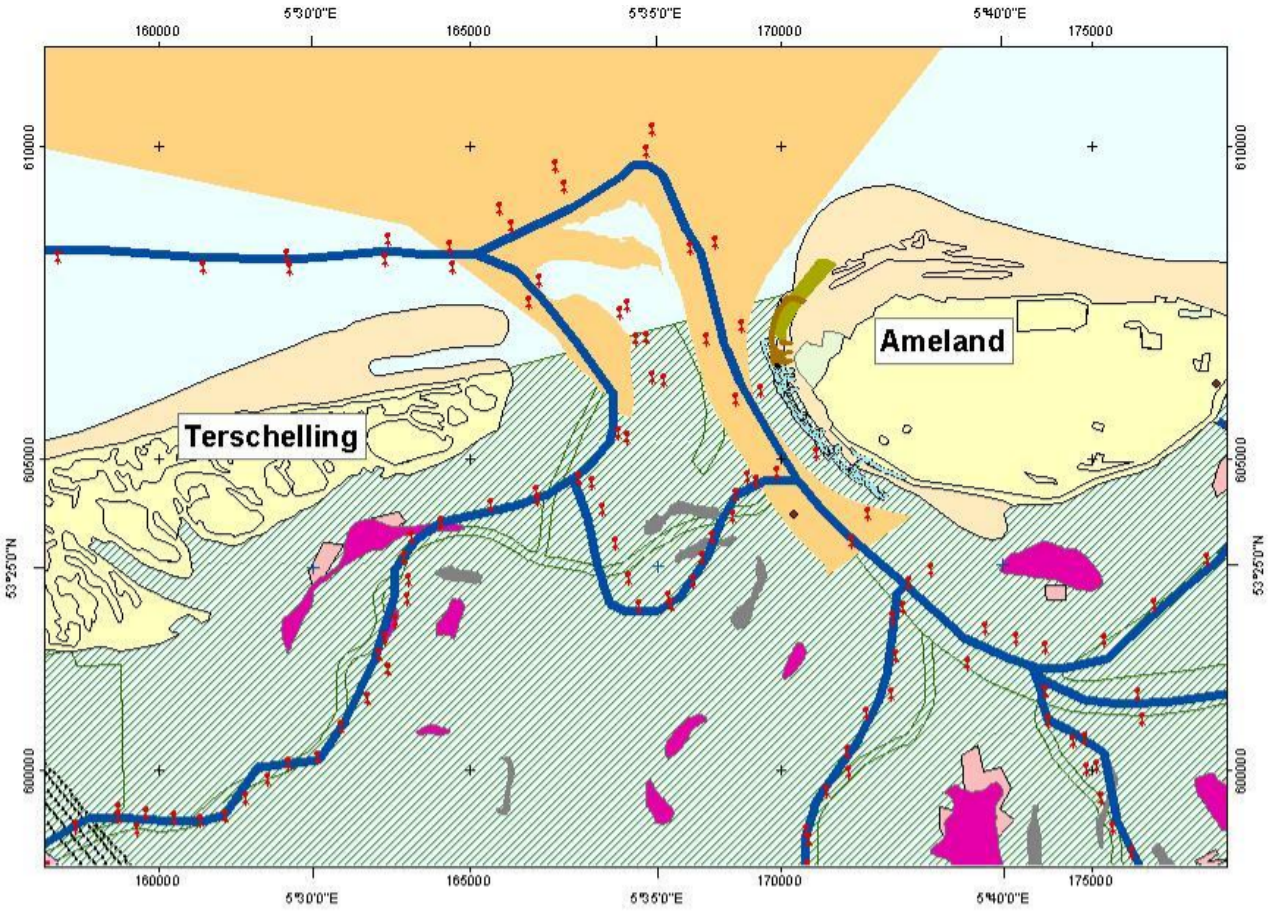

Navigational channels (RIKZ)		
WL | DELFT HYDRAULICS	H4803.11	Fig. 3.83

WL | Delft Hydraulics

Rotterdamseweg 185
postbus 177
2600 MH Delft
telefoon 015 285 85 85
telefax 015 285 85 82
e-mail info@wldelft.nl
internet www.wldelft.nl

Rotterdamseweg 185
p.o. box 177
2600 MH Delft
The Netherlands
telephone +31 15 285 85 85
telefax +31 15 285 85 82
e-mail info@wldelft.nl
internet www.wldelft.nl